



XII. Pracovní setkání fyzikálních chemiků a elektrochemiků

12th Workshop of Physical Chemists and Electrochemists

sborník příspěvků

30. – 31.5.2012

Přírodovědecká fakulta Masarykovy univerzity
Agronomická fakulta Mendelovy univerzity v Brně a
Fakulta elektrotechniky a komunikačních technologií VUT v Brně



středoevropský technologický institut
BRNO | ČESKÁ REPUBLIKA

ORGANIZACE POŘÁDAJÍCÍ KONFERENCI

Přírodovědecká fakulta MU v Brně

Ústav chemie
Kotlářská 2
611 37 Brno
<http://www.sci.muni.cz>

Agronomická fakulta MENDELU v Brně

Ústav chemie a biochemie
Zemědělská 1
613 00 Brno
<http://ucb.af.mendelu.cz>

Fakulta elektrotechniky a komunikačních technologií VUT v Brně

Ústav mikroelektroniky
Technická 3058/10
61600, Brno
<http://www.umel.feec.vutbr.cz>

Středoevropský technologický institut

Vysoké učení technické v Brně
Technická 3058/10
616 00 Brno
<http://www.ceitec.cz>

ORGANIZAČNÍ ZABEZPEČENÍ KONFERENCE

Libuše Trnková

libuse@chemi.muni.cz (Ústav chemie, PřF, MU)

René Kizek

kizek@sci.muni.cz (Ústav chemie a biochemie, AF, MENDELU)

Jaromír Hubálek

hubalek@feec.vutbr.cz (Ústav mikroelektroniky, FEKT, VUT v Brně)

Publikace neprošla jazykovou kontrolou. Jednotlivé příspěvky jsou publikovány tak, jak byly dodány autory. Za věcnou a odbornou správnost jsou plně odpovědni autoři příspěvků. Podrobné informace včetně sborníku příspěvků jsou k dispozici na internetové adrese <http://sci.muni.cz/~labifel/>

ISBN 978-80-7375-618-5

Pracovní setkání bylo podpořeno výzkumnými projekty

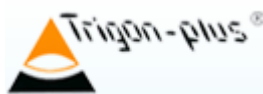


INVESTMENTS IN EDUCATION DEVELOPMENT



Sponzoři pracovního setkání

Organizátoři děkují všem letošním sponzorům za podporu, která umožnila pořádat tuto, již tradiční, akci: METROHM, spol. s. r. o., EPPENDORF Czech & Slovakia, spol. s. r. o., CHROMSPEC, spol. s. r. o., ILABO, spol. s. r. o., MANEKO, spol. s. r. o., MEDESA, spol. s. r. o., PRAGOLAB, spol. s. r. o., SIGMA, spol. s. r. o., TRIGON plus, spol. s. r. o., CLONESTAR Peptide Services, spol. s. r. o., Stargen EU s. r. o., Chromservis s.r.o., Česká společnost chemická, pobočka Brno



SIGMA-ALDRICH



SPOL. S R.O.



Úvodem

Milí přátelé,

pro konání letošního XII. Pracovního setkání fyzikálních chemiků a elektrochemiků (*12th Workshop of Physical Chemists and Electrochemists*) byly zvoleny dva dny na konci května (30. 5. a 31. 5. 2012). Místem konání jsou konferenční prostory s atriem v nové budově Q Univerzity MENDELU v Brně. Naše konference může být považována za jednu z významných akcí v rámci dvou oslav. Brno letos slaví 190 let od narození významného vědce a opata augustiniánského kláštera na Starém Brně Gregora Johana Mendela, který je díky objevu tří základních zákonů dědičnosti považován za otce genetiky. Pod hlavičkou *Mendel 190* si tento významný svátek připomíná různými akcemi (výstavy, konference, přednášky Mendel lectures) nejen univerzita MENDELU, která nese jeho jméno, ale i MASARYKOVA UNIVERZITA. V Mendelově odkazu obě univerzity učí principy genetiky, její základy a rozvoj, uplatňující se jak v říši rostlin a živočichů, tak i v medicíně. Dalším milníkem pro oslavný charakter našeho setkání je 90 let objevu polarografie, za kterým stojí náš nositel Nobelovy ceny v oblasti fyzikální chemie a elektrochemie Jaroslav Heyrovský. Tak jako G.J.Mendel je považován za otce genetiky, J. Heyrovský je považován za otce elektroanalytických metod. Když objevil polarografii, bylo mu pouhých 32 let, kdy za sebou měl úspěšná studia chemie, matematiky a fyziky na Karlově universitě v Praze, a studia u slavných chemiků Sira W. Ramsaye, W. C. McC. Lewise, a F. G. Donnana v Londýně. Jeho metoda, většinou prezentovaná jako analýza roztoků pomocí elektrolýzy, se stala základem pro rozvoj dynamických elektrochemických metod.

Záštitu nad konferencí převzali primátor statutárního města Brna Bc. Roman Onderka, MBA, rektori a děkani vysokých škol, které se na organizaci XII. Pracovního setkání podílely: rektor Masarykovy univerzity Doc. PhDr. Mikuláš Bek, Ph.D. rektor Mendelovy univerzity v Brně Prof. Ing. Jaroslav Hlušek, CSc., dr. h. c., děkan Přírodovědecké fakulty MU Doc. RNDr. Jaromír Leichmann, Dr., **děkan Agronomické fakulty MENDELU Prof. Ing. Ladislav Zeman, CSc.**, děkanka Fakulty elektrotechniky a komunikačních technologií VUT Prof. Ing. Jarmila Dědková, CSc..



středoevropský technologický institut
BRNO | ČESKÁ REPUBLIKA

Na účastníky z České a Slovenské republiky čekají dva konferenční dny naplněné blokem plenárních (6) a vyzvaných přednášek (13), přednášek nadaných studentů (18) v Sekce mladých (SM). Enormní nárůst přednášek, především v SM, nás velice potěšil.

Aby studenti měli dostatek času pro svoje přednášky a diskusi v jazyce anglickém, rozhodli jsme se založit dva SM paralelní bloky, kde přednášky budou hodnoceny dvěma komisemi. Z každého bloku pak budou odměňováni studenti na prvním, druhém a třetím místě. Všichni se mohou těšit na vědecké diskuse, které budou inicializovány nejen přednáškami, ale i prezentacemi velkého počtu posterů. Hodnocení posterů bude probíhat novým způsobem. Autoři plakátových sdělení budou mít možnost se rozhodnout, zda přihlásit svůj poster do soutěže či nikoliv. Potom soutěžící postery budou hodnoceny určenou komisí. Krátká prezentace autora, popř. autorů bude vyžadovat 3 minuty, diskuse 2 minuty.

Všechna abstrakta ve sborníku jsou v jazyce anglickém, mají rozšířenou podobu a obsahují barevné obrázky či grafy. Abstrakta jsou součástí sborníku s ISBN (sborník příspěvků odpovídá kritériím pro hodnocení VaV v kategorii „Článek ve sborníku“). V rámci konference bude vydáno speciální číslo v časopise International Journal of Electrochemical Science s IF 2.808 (ISSN 1452-3981). Běžná cena tzv. open access free, která umožňuje volnou dostupnost publikovaného díla, je 500 Euro. Pro účastníky konference bude snížený poplatek na vložné do časopisu činit 400 Euro. Uzávěrka pro dodání příspěvku je stanovena na 31. 7. 2012. Následně proběhnou recenzní řízení. Vydání speciálního čísla je plánováno na prosinec 2012.

Vítáme všechny účastníky XII. Pracovního setkání fyzikálních chemiků a elektrochemiků a přejeme všem úspěšnou prezentaci, která může být spolu s bohatou diskusí velmi užitečným pomocníkem v jejich dalším bádání.

Organizační a vědecký výbor

doc. RNDr. Libuše Trnková, CSc.

doc. Ing. René Kizek, Ph.D.

doc. Ing. Jaromír Hubálek, Ph.D.

doc. RNDr. Vojtěch Adam, Ph.D.



Technické zabezpečení Pracovního setkání:

Ing. Jiří Sochor, Ph.D.

Mgr. Sylvie Holubová

Mgr. Olga Kryštofová

Mgr. Michal Horák

Kristina Nádeníčková

Martina Rývolová

OBSAH

COMPUTER ANALYSIS OF GROWTH CURVES OF STAPHYLOCOCCUS AUREUS	14
PHOTOINDUCED PROCESSES OF NOVEL SELENADIAZOLOQUINOLONES (AN EPR STUDY)	17
ELECTROCHEMICAL TEMPLATE SYNTHESIS OF NOBLE METAL AND SEMICONDUCTING QUANTUM DOTS	19
ELECTROANALYTICAL METHODS FOR THE GLYCOCONJUGATES DETECTION IN MEDICAL DIAGNOSTICS	21
PHOTODEGRADATION PROCESSES OF QUINOLONES	23
DIRECT VOLTAMMETRIC DETECTION OF INSULIN ON MWCNTS MODIFIED ELECTRODES – PRELIMINARY RESULTS	25
GOLD CD-SENSOR PLATFORM FOR DNA APTAMER ASSEMBLING TOWARDS HUMAN THROMBIN RECOGNITION	28
MULTIWALLED CARBON NANOTUBES - DENDRIMERS PLATFORM FOR APTAMER-BASED BIOSENSOR SENSITIVE TO HUMAN CELLULAR PRIONS	30
ELECTROCHEMICAL FUNCTIONALIZATION OF POROUS-SILICON-BASED CHEMOSENSORS WITH POLYPYRROLE	32
ELECTROCHEMICAL ANALYSIS OF PCR AMPLICONS WITH INCORPORATED 7-DEAZAPURINES	34
HYPHENATION OF ELECTROCHEMISTRY WITH MASS SPECTROMETRY AS A POWERFUL TECHNIQUE TO STUDY PESTICIDES IN ENVIRONMENTAL MATRICES	37
TiO ₂ /GOLD NANOCOMPOSITE FOR BIOSENSING APPLICATIONS	39
INTRACELLULAR SEQUESTRATION OF ELLIPTICINE IN NEUROBLASTOMA CELLS: ROLE OF VACUOLAR-ATPASE	41
PIEZOELECTRIC AND OPTICAL BIOSENSORS FOR DETECTION OF <i>BACILLUS ATROPHAEUS</i>	43
ADVANTAGEOUS ELECTROCHEMICAL FEATURES OF NANOMATERIALS USED IN DEVELOPMENT OF BIOFUEL CELLS	46
SURFACE TENSION OF CYCLOSPORINE SAMPLES	50
DNA LABELLING WITH ELECTROACTIVE MOIETIES AND ITS APPLICATION IN ELECTROCHEMICAL DNA SENSING	52
TIN DIOXIDE SENSOR FOR METHANE DETECTION	54
FISH MERCURY LIVER/MUSCLE RATIO IN COMPARISON WITH MERCURY HEAVILY AND LIGHTLY CONTAMINATED LOCATION	57
ACRIDINE DERIVATIVES AS PROSPECTIVE ANTIOXIDANTS	59
PHOTOLUMINESCENCE STUDY OF LIGHT-INDUCED MODIFICATIONS OF (ELECTRO)CHEMICALLY PREPARED POLYPYRROLE	61
ELECTROCHEMICAL STUDY OF SHORT CYTOSINE OLIGONUCLEOTIDES	64
PROSPECTS OF POLAROGRAPHY - ELECTROLYSIS WITH MERCURY ELECTRODES - FOR THE YEARS TO COME	66

DETERMINATION OF OXIDATIVE STRESS IN GUINEA PIG TREATED BY HALOPERIDOL	68
SURFACE PLASMON RESONANCE BIOSENSORS AND THEIR BIOANALYTICAL APPLICATIONS	70
CHICKEN ANTIBODIES IN WESTERN BLOTS: HOW TO AVOID POTENTIAL KERATIN CROSS-REACTIVITY	71
ELECTRO IMPEDANCE SPECTROSCOPY CHARACTERIZATION OF NANOSTRUCTURED ELECTROCHEMICAL SENSORS	73
MICROTECHNOLOGY TOWARDS SENSORS	75
ANALYSIS OF MICRO RNAS EXPRESSION IN CELL LINES DERIEVED FROM PROSTATE CARCINOMA	77
EPR SPECTROSCOPY OF COPPER COMPLEX SYSTEMS WITH BIOLOGICALLY ACTIVE LIGANDS	80
STUDY OF CONJUGATION OF BOVINE SERUM ALBUMINE WITH CdTE QUANTUM DOTS WITH SPECTROSCOPIC TECHNIQUES	83
ELECTROPHORETIC TECHNIQUES IN THE ANALYSIS OF POLYDEOXYCYTIDYLIC ACIDS	85
REACTIVITY AND MOBILITY OF CU(II) IONS IN HUMIC GELS	87
STRENGTH AND MAGNETISM OF Mn – Pt NANOCOMPOSITES	90
ASSESSMENT OF HEAVY METAL CONTENT IN URBAN SOILS USING DIFFERENT EXTRACTION METHODS	93
THERMODYNAMICS OF THE ANTIOXIDANT ACTION OF MODEL AND NATURAL COMPOUNDS	96
PREPARATION OF PHOTO - CYTOCHROME B ₅ FOR CROSS-LINK WITH CYTOCHROME P450 2B4	100
ELECTROCHEMICAL PREPARATION AND CHARACTERIZATION OF POROUS SILICON	102
STUDY OF CORROSION LAYERS FORMED ON METAL ARTIFACTS USING DOUBLE PULSE LASER-INDUCED BREAKDOWN SPECTROSCOPY	104
COMPARISON OF ELECTROCHEMICAL DETERMINATION OF HEAVY METALS ON PIGE AND CARBON NANOTUBES MODIFIED PIGE	107
RENEWAL OF THREE-DIMENSIONAL NANOCRYSTALLINE DIAMOND BIO-TRANSISTOR BY LOW TEMPERATURE HYDROGENATION	110
CHEMICAL COMPOUNDS ON THE SURFACE OF ICE	113
FREEZING POTENTIAL MEASUREMENTS	115
SIMILARITY OF CYANOBACTERIA BASED ON THE COMPARISON OF WHOLE PROTEIN CODING INFORMATION	116
CHARACTERIZATION OF ELECTROCHEMICAL DNA BIOSENSORS WITH PROTECTIVE MEMBRANES IN SOLUTIONS CONTAINING SURFACE ACTIVE COMPOUNDS	119
STRUCTURE AND EPR SPECTROSCOPY OF COPPER(II) COMPLEXES WITH PHENANTROLINE AND DERIVATIVES OF SALICYCLIC ACID	121

NAD(P)H:QUINONE OXIDOREDUCTASE EXPRESSION IN TRANSGENIC MOUSE MODELS AND ITS INFLUENCING BY CARCINOGENIC ARISTOLOCHIC ACID I	124
THE GROW OF MICROORGANISMS DURING THE RIPENING OF SEMI-HARD CHEESE	129
ELECTROCHEMICAL GROWTH OF POLYPYRROLE ON BORON DOPED DIAMONDS	131
AUTOMATED IMMUNOSEPARATION OF Zn-PROTEINS FROM <i>STAPHYLOCOCCUS AUREUS</i> BY MAGNETIC NANOPARTICLES FOLLOWED BY THEIR ELECTROPHORETIC	134
SELECTIVE FOCUSING AND ANALYSIS OF Na ⁺ , Ca ²⁺ , Mg ²⁺ , Mn ²⁺ , Cd ²⁺ , Zn ²⁺ , Ni ²⁺ , Pb ²⁺ , Cu ²⁺ USING LIGAND STEP GRADIENT FOCUSING IN COMBINATION WITH ITP (LSGF-ITP)	138
PRACTICAL DIFFICULTIES OCCURRING DURING SOLID PHASE PEPTIDE SYNTHESIS	140
STUDY OF ANTIOXIDANT PROFILE OF CATTLE	142
INTERACTION OF CADMIUM WITH GLUTATHIONE	146
INFLUENCE OF MYCORRHIZA ON PRODUCTION OF THIOL COMPOUNDS IN MAIZE EXPOSED TO COPPER	148
PREPARATION OF APOFERRITIN SILVER PHOSPHATE NANOPARTICLES	150
PREPARATION OF METALLOTHIONEIN OLIGONUCLEOTIDE QUANTUM DOTS COMPLEXES	153
ISOLATION AND DETECTION OF NUCLEIC ACID INFLUENZA VIRUSES	156
ELECTROCHEMICAL DETECTION OF IRON IN BLOOD SAMPLES OF MINIPIGS WITH MELANOMA	160
ELECTROCHEMICAL DETERMINATION OF PLATINUM IN BIOLOGICAL SAMPLES	163
ELECTROCHEMICAL DETERMINATION OF RHODIUM IN BIOLOGICAL SAMPLES	166
CHIP CAPILLARY ELECTROPHORETIC STUDIES OF PSA	169
SPECTROMETRIC STUDY OF TAURINE	171
STUDY OF OXIDATIVE STRESS IN <i>STAPHYLOCOCCUS AUREUS</i> BACTERIAL CULTURE TREATED WITH SILVER(I) IONS	174
VOLTAMMETRY OF LAWSONE-COPPER(II)-DNA COMPLEXES	177
EFFECT OF PLATINUM, PALLADIUM AND RHODIUM ON DUCKWEED (<i>LEMNA MINOR</i>)	180
COULOMETRIC DETERMINATION OF SARCOSINE	182
HILIC SEPARATION OF SARCOSINE HYPHENATED TO COULOMETRIC DETECTION	184
ELECTROCHEMICAL DETECTION OF SILVER IONS USING CARBON PASTE ELECTRODE	186
MICROFLUIDIC DETECTION OF QUANTUM DOTS	189

ELEKTROCHEMICAL STUDY OF HYALURONIC ACID-SILVER IONS COMPLEX	192
DETERMINATION OF PLATINUM IN PEA PLANTS (<i>PISUM SATIVUM L.</i>) AND MAIZE (<i>ZEA MAYS L.</i>) USING DIFFERENTIAL PULSE VOLTAMMETRY	195
DEVICE FOR AUTOMATIC CHARACTERIZATION OF SEMICONDUCTOR GAS SENSORS	197
EPR-UV/VIS/NIR SPECTROELECTROCHEMISTRY OF METAL(II) COMPLEXES CONTAINING TETRADENTATE LIGANDS	200
ELECTROCHEMICAL SENSOR WITH PERFORATED SURFACE FOR DETERMINATION OF HEAVY METALS IN WATER	202
PREPARATION AND ELECTROANALYTICAL PROPERTIES OF POROUS FILM ELECTRODES	204
ELECTROANALYSIS OF METHYLXANTHINES ON A GRAPHITE ELECTRODE	207
OPTIMIZATION OF ORDERED SILVER NANOSTRUCTURES PREPARATION	209
ANALYTICAL APPLICATIONS OF NANOSTRUCTURED SILVER LAYERS	211
EXPERIMENTAL STUDY OF GLASS FRIT BONDING	214
SPECTROSCOPIC CHARACTERIZATION OF GOLD NANOPARTICLES	216
EFFECT OF FREQUENCY ON THE C-E CURVES AND TENSAMMETRIC PEAKS OF POLYADENYLIC ACID, OLIGODEOXYNUCLEOTIDES AND CYTOSINE DERIVATIVES	220
THE INFLUENCE OF PLATINUM ON TOBACCO BY-2 CELLS (<i>NICOTIANA TABACUM</i>)	223
EFFECT OF ORGANIC AND INORGANIC FORM OF SELENIUM ON ANTIOXIDANT STATUS OF BREEDING BOARS EJACULATE	225
TREATMENT OF DIFFERENTIAL PULSE VOLTAMMOGRAMS OF TISSUE HOMOGENATES FROM RATS	229
INFLUENCE OF HEAT DENATURATION OF β -SHEET BREAKER PRION PROTEIN ON ELECTROCHEMICAL RESPONSE	234
QUANTUM DOTS AND THEIR INTERACTIONS WITH BIOMOLECULES	237
ELECTROCHEMISTRY OF QUANTUM DOTS	239
ACETYLCHOLINESTERASE BASED ELECTROCHEMICAL BIOSENSOR USING INDOXYLACTATE AS A SUBSTRATE FOR A FAST ASSAY OF NERUOTOXIC COMPOUNDS	242
ELECTROCHEMICAL DETERMINATION OF ENZYMES METABOLIZING ELLIPTICINE AS A TOOL TO EXPLAIN THE MECHANISMS OF ELLIPTICINE TOXICITY TO THYROID CANCER CELLS	244
DOUBLE-PULSE LASER-INDUCED BREAKDOWN SPECTROSCOPY ON LIQUID JETTS FOR DETERMINATION OF NUTRIENT ELEMENTS IN ALGAE	248
LEAD DETECTION ON DIRECT GROWN CNTS BASED WORKING MIKROELECTRODE	251
SYNTHESIS, STRUCTURE, AND OPTO-ELECTRONIC PROPERTIES OF ORGANIC DYES ON DIAMOND	254

CATALYTIC CO-CRACKING OF USED FRYING OILS, MUNICIPAL AND BIO-WASTE.....	256
GEOMETRY-BASED DESCRIPTORS OF SUBSTITUENT EFFECT ON BOND DISSOCIATION ENTHALPIES OF ANILINES, PHENOLS AND THIOPHENOLS.....	258
STEROLS OXIDATION: C–H AND O–H BOND DISSOCIATION ENTHALPIES.....	260
EFFECT OF METALS ON METALLOTHIONEIN CONTENT IN FISH FROM SKALKA AND ŽELIVKA RESERVOIR.....	262
DEVELOPMENT OF NEW FLUOROSENSOR FOR SELECTIVE AND SENSITIVE DETERMINATION OF LN(III) IONS.....	264
COMPARISON OF CHROMATOGRAPHIC AND IMMUNO DETERMINATION OF LACTOFERRIN.....	267
RELATION BETWEEN THIOL CONTENT AND TUMORS OF PROSTATE AND BRAIN.....	269
ELECTROCHEMICAL BEAD-BASED ASSAY FOR LACTOFERRIN.....	272
STUDY OF INTERACTION OF QUANTUM DOTS WITH METALLOTHIONEIN USING DIFFERENTIAL PULSE VOLTAMMETRY.....	275
ELECTROCHEMICAL IMMUNOSENSORS FOR DETECTION OF MICROORGANISMS IN BIOAEROSOLS.....	278
PREPROCESSING AND CLASIFICATION OF ELECTROPHORETIC GEL IMAGE USING DYNAMIC TIME WARPING.....	280
CAPILLARY ELECTROPHORESIS CHIP FOR DNA DETECTION.....	283
OPTIMIZATION OF DNA ISOLATION USING MAGNETIC MICROPARTICLES.....	285
UTILIZATION OF PROTEIN-QUANTUM DOTS INTERACTION FOR VISUALIZATION OF PROTEINS AFTER SDS-PAGE ELECTROPHORESIS.....	288
INTERACTIONS OF BIOTINYLATED OLIGONUCLEOTIDES WITH STREPTAVIDIN-MODIFIED QUANTUM DOTS STUDIED BY CAPILLARY ELECTROPHORESIS WITH UV DETECTION.....	290
H-TERMINATED DIAMOND-CAPPED IMPEDANCE TRANSDUCER: NOVEL MOLECULAR SENSOR.....	293
EXPRESSION LEVELS OF ENZYMES METABOLIZING AN ANTICANCER DRUG ELLIPTICINE DETERMINED BY WESTERN BLOTTING DICTATE ITS CYTOTOXICITY TO NEUROBLASTOMA CELLS.....	296
THE NEW MILLENNIUM WITH NEW CARBON PASTES.....	300
DESING AND FABRICATION OF MEMS LOW POWER HEATING MEMBRANE.....	303
MONITORING THE VIABILITY OF CELL LINE MTF-KO DEPENDING ON THE CONCENTRATION OF Zn ²⁺ USING XCELLIGENCE SYSTEM.....	305
ANALYSIS OF SELECTED REGULATORY GENES IN PROSTATE CANCER CELL LINES.....	307
OPTIMIZATION OF SHEATHLESS AND ELECTRODELESS INTERFACE FOR INORGANIC ION SEPARATION.....	309

CONSTRUCTION OF ELECTROCHEMICAL BIOSENSORS BASED ON NANOMATERIALS.....	311
ELECTROCHEMICAL FABRICATION OF OPTICAL BIOSENSOR FOR DNA DETECTION.....	314
INSTANTANEOUS QUALITATIVE ANALYSIS OF PIGMENTS BY RAMAN SPECTROSCOPY.....	317
ELECTROANALYSIS OF POLYAMINO ACIDS ON MERCURY ELECTRODE.....	319
MULTIMEDIA DATABASE OF THE FRUIT CROP VARIETIES.....	321
MONITORING OF RHEOLOGICAL PROPERTIES OF WINTER WHEAT FLOUR.....	323
ELECTROCHEMICAL DETERMINATION OF LOW CONCENTRATION POTASSIUM IONS IN UREA SOLUTIONS.....	325
INFLUENCE OF LMWOAS ON TRANSPORT OF CADMIUM AND COPPER IONS ACROSS PHOSPHOLIPID BILAYER USING CALCIUM IONOPHORE A23187.....	327
ON-BODY SYSTEM FOR DEHYDRATION DETECTION.....	329
ELECTROCHEMICAL STUDY OF INTERACTION OF 23 FRAGMENTS OF METALLOTHIONEIN WITH CISPLATIN – HIGH THROUGHPUT METHOD.....	331
COULOMETRIC AND PHOTOMETRIC DETERMINATION OF ANTIOXIDANT CAPACITY IN BIOLOGICAL SAMPLE OF HONEYSUCKLE.....	334
APPLICATION OF COPPER SOLID AMALGAM ELECTRODE FOR DETERMINATION OF FUNGICIDE TEBUCONAZOLE.....	337
MODEL PHOSPHOLIPID MEMBRANES AND TRANSPORT OF HAZARDOUS METALS ACROSS THEM.....	339
CHARACTERIZATION OF SILVER NANOPARTICLES.....	341
STUDY OF ELECTROCHEMICAL CORROSION OF A-C:N THIN FILMS.....	344
RARE „REVERSED“ EPR SPECTRA SEEN IN SOME COPPER(II) COMPLEX SYSTEMS.....	347
CHARACTERISATION OF BORON DOPED DIAMOND FOR TRACE METAL DETECTION.....	349
ELECTROCHEMISTRY OF BIOMACROMOLECULES.....	351
ACIDITY FUNCTIONS AND THEIR CONSTRUCTIONS.....	353
BORON DOPED DIAMOND ELECTRODES FOR DETERMINATION OF BIOLOGICAL MOLECULES.....	355
THE ANTICANCER DRUG ELLIPTICINE INDUCES CYTOCHROME B ₅ AND CYTOCHROMES P450 1A1, 1A2 AND 3A IN RAT LIVER, KIDNEY AND LUNG.....	357

PŘÍSPĚVKY

A vertical timeline on a green background with a DNA double helix and leaves. A yellow arrow points downwards through four key milestones, each marked with a portrait and text.

- * 20.7. 1822**
Gregor Johann Mendel
- 1865**
základy moderní genetiky
- * 20.12.1890**
Jaroslav Heyrovský
- 1959**
NOBELOVA CENA

COMPUTER ANALYSIS OF GROWTH CURVES OF STAPHYLOCOCCUS AUREUS

Jaroslav BALOGH¹, Andrea BEZDEKOVA², Jiri SOCHOR², Rene KIZEK², Ivo PROVAZNIK¹

¹ Department of Biomedical Engineering, Faculty of Electrical Engineering and Communication, Brno University of Technology, Technicka 10, 61600 Brno, Czech Republic
² Department of Chemistry and Biochemistry, Faculty of Agronomy, Mendel University in Brno, Zemedelska 1, 613 00 Brno, Czech Republic

ABSTRACT

Growth or inhibition of bacterial organisms is usually represented by growth curves. Analysis of curves requires advanced processing and visualization of measured data. We conducted a series of experiments with *Staphylococcus aureus* and 64 combinations of admixtures – various concentrations of silver ions and hyaluronic acid. We used selected mathematical functions for post-processing and visualization by surface plot with higher informative value. The proposed method can reveal specific parametrical dependences.

INTRODUCTION

The goal of this paper is to present possibilities of detailed study of growth curves of *Staphylococcus aureus*. The most important parameters in analyzing growth or inhibition of microorganisms are amount of organism at specific time, rate of growth and actual course of growth. Measured microorganism was bacteria *Staphylococcus aureus*. It is facultative anaerobic Gram-positive coccil bacterium, frequently found as part of the normal skin flora (about 20 percent of human population are long-term carriers, also animals are). *S. aureus* can cause a range of illnesses, from minor skin infections to life-threatening diseases (pneumonia, meningitis, sepsis, toxic shock syndrome and others). Some strains of *S. aureus* become resistant to most antibiotics (penicillinase-resistant β -lactam antibiotics) and hard to cure. Inhibition of *S. aureus* by admixtures in samples was observed. [5]

EXPERIMENT, DATA AND PROCESSING

Input data

Experiments took continuous 24 hours measurement of relative absorbance, which is directly proportional to amount of *S. aureus* in a sample. We measured absorbance at wavelength 620 nm for 64 combinations of admixtures (eight concentrations of silver ions and eight concentrations of hyaluronic acid, Tab. 1) every 30 minutes at 37°C. With starting relative absorbance at time 0, the experiment produced 64 x 49 real numbers as an output. Relative absorbance at time t_0 which was set to 0 and inhibition of *S. aureus* resulted into negative values down to -0.7. A value of 0.1 was added to all relative absorbances because of presence of *S. aureus* in sample at time t_0 and negative values (absorbance is usually non-negative number). Thus, every value lower than 0.1 means decreased/smaller absorbance than at a beginning of measurement.

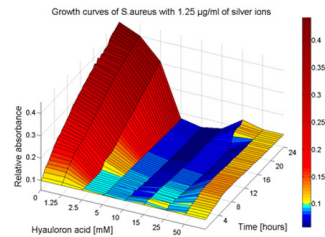
Table 1: Concentrations of admixtures

Substance	Concentrations							
silver ions [$\mu\text{g ml}^{-1}$]	0	1.25	2.5	5	10	15	25	50
hyaluronic acid [mM]	0	0.19	0.39	0.78	1.56	3.12	6.25	12.5

PROCESSED AND VISUALISED DATA

Visualization was provided by a set of relatively simple functions, which return a matrix of values representing particular variables important to interpret results. First of all, the growth curves of *S. aureus* with single admixture were plotted to show behavior in different concentrations of admixture without influence of other substance. 3D surface plot was chosen instead of classical 2D plot, because it provides more informative value and represents “mass” of *S. aureus*. Figure 1 shows information about growth of *S. aureus* influenced by both admixtures.

Figure 1.: Growth curves of *S. aureus* with both admixtures



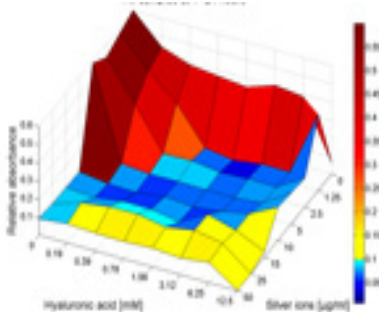
Some growth curves of *S. aureus* with hyaluronic acid represented inhibition of growth, values of relative absorbance were smaller than 0.1 and had descending trend. Customized color map was used, where the blue hues represented values <0.1 , yellow and red hues bigger values (see color map in the Figure 2). Color map applied to surface plot represent standard combination to visualize complex data. All measured data were represented by 8 graphs, one

for every concentration of silver ions.

Post processing

Post processing steps include selected properties. If the target is inhibition of bacteria, the most important value is its amount in time tx, Figure 2 shows relative absorbance of all 64 combinations at time tx= 24 hours.

Figure 2: Relative absorbance at time T=24 hours

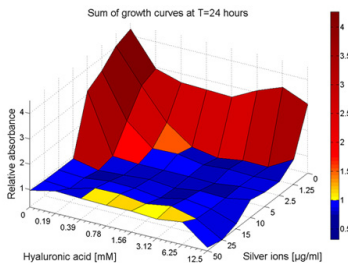


This is not relevant, without knowing shape of every growth curve, which represents every combination and its behavior in time. Additional graph (see Figure 3) represents a sum of relative absorbance Asum of S. aureus throughout whole measurement implied to default absorbance A0 (at time t0) calculated by equation (1):

$$A_{sum} = \sum_{n=1}^{49} (A_n - A_0)$$

Figure 2 shows empirical deviation, when relative absorbance of S. aureus with 12.5 mM of hyaluronic acid and zero concentration of silver ions gives unexpectedly low value. It was clear from classical plots that this growth curve at time t=24 hours is in decline phase. Using equation (1), we get 8x8 matrix (64 combinations of admixtures) representing "amount" of S. aureus in time and information that in particular combination of admixtures there is for example insignificant growth process.

Figure 3: Sum of relative absorbance of S. aureus throughout whole measurement



Measurement errors or significant disharmony in the form of local extremes can be detected by finding minimal and maximal function for every single growth curve. These functions can reveal unwanted process of growth/inhibition. Graph of minimal also helps to find the most inhibited sample.

Growth and inhibition is also represented by rate of growth. Relative rate (RR) is computed by equation (2):

$$A_{sum} = \sum_{n=1}^{49} (A_n - A_0)$$

where Ax and Ax-1 are two following relative absorbances and RR represents growth in percentage. By using this function can be find long growing or inhibiting shape of growth curve.

RESULTS

Plotting post-processed data (set of 16 graphs) represent a number of properties. Growth curves of S. aureus are influenced by admixtures. Therefore, they are not standard bacterial growth curves (Gompertz curve) with lag, logarithmic, stationary and death (decline) phase [6]. About 85 % of curves are monotone (almost logarithmic), only increasing or decreasing. Other 10 % of curves change their growth to inhibition or vice versa, but relative absorbance changes differ against default absorbance about ±0.07. Last 10 % of curves did not reach its maximum (minimum) in 24 hours or had not typical shape. Generally, concentration of silver ions does not affect growth of S. aureus. It only defines how fast it is growing and time of reaching maximum absorbance. The greatest growth was with zero concentration of hyaluronic acid and silver ions, maximal inhibition was at maximum concentrations. However, the dependence was not linear.

CONCLUSION

Data were processed, visualized and interpreted. Surface plot represents most information better than standard 2D plot and it's more comfortable in analysis. Amount of data obtained from just 64 samples in 24 hours and by using just 6 parameters to describe growth tendency is enormous and leads to idea to create expert system for evaluation of results. For example system based on weighted equation with empirically pre-defined weights, where input could be all processed data and weights and output growth curves which fit the best.

ACKNOWLEDGEMENT

This work was supported in part by: GAČR 102/09/H083, GAČR P102/11/1068, NanoCeva TA CR TA01010088.

REFERENCES

- [1] Kahm M., et al: Journal of Statistical Software, 33 (2010), 7, 1-21
- [2] Cheroute-Vialette M., Lebert I., Hebraud M. et al.: International Journal of Food Microbiology, 42 (1998), 71-77
- [3] Zwietering M., et al.: Applied and Environmental Microbiology, 56 (1990), 6, 1875-1881
- [4] Zwietering M., et al: Journal of Applied Microbiology, 72 (1992), 139-145
- [5] Harris L., Foster S., Richards R.,: European Cells and Materials, 4 (2002), 39-60
- [6] Winsor Ch.: Proceedings of the National Academy of Sciences, 18 (1932), 1, 1-8

PHOTOINDUCED PROCESSES OF NOVEL SELENADIAZOLOQUINOLONES (AN EPR STUDY)

Zuzana BARBIERIKOVA*, Ludmila SEKERAKOVA, Jozef LIETAVA, and Vlasta BREZOVA

*Institute of Physical Chemistry and Chemical Physics, Faculty of Chemical and Food Technology, Slovak University of Technology in Bratislava, Radlinskeho 9, SK-812 37 Bratislava, Slovak Republic

*zuzana.barbierikova@stuba.sk

ABSTRACT

Photoinduced reactions of novel 7-substituted 9-ethyl-6-oxo-6,9-dihydro[1,2,5]selenadiazolo-[3,4-*h*]quinolines, as compounds possessing potential photobiological impacts, with perspective of their utilization as photosensitizers, were investigated by means of electron paramagnetic resonance (EPR) spectroscopy. Monochromatic UVA photoexcitation of the selenadiazoloquinolones in dimethylsulfoxide or acetonitrile resulted in the effective generation of reactive oxygen species *via* molecular oxygen activation.

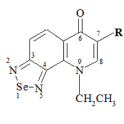
INTRODUCTION

Quinolones represent one of the largest classes of antimicrobial agents used worldwide in medical care [1]. Recent studies of potential phototoxic activity of quinolones, have established that within the photochemical processes occurring during quinolones photoexcitation the reactive oxygen species (ROS) are generated [2]. This specific behavior of quinolones reveals a new field of their applications in targeted therapeutic applications, as photosensitizers, where ROS generation represents a powerful tool for selective cancer cell destruction [3].

Different quinolone derivatives have already been studied in our laboratory and it has been proved that selenadiazoloquinolones behave as photosensitizers, producing superoxide radical anions (O_2^+) and singlet oxygen (O_2) *via* the excited states quenching by molecular oxygen [4]. Such photogenerated species may react with solvent or with selenadiazoloquinolones themselves resulting in their degradation, and we assume that the presence of hydrogen atom at position N-9 can significantly influence their reactivity upon photoexcitation. These findings motivated the synthesis of novel 7-R-9-ethyl-6-oxo-6,9-dihydro[1,2,5]selenadiazolo-[3,4-*h*]quinolones [5], expecting different behavior under irradiation and consequently also enhanced effects in biological systems. An overview of the structure and substituent characterization, along with the abbreviations of the investigated selenadiazoloquinolones are summarized in Table 1.

Table 1: Overview of investigated 7-R-9-ethyl-6-oxo-6,9-dihydro[1,2,5]selenadiazolo[3,4-*h*] quinolones.

R	Abbreviation
H	EQ1
COOC ₂ H ₅	EQ2
COOCH ₃	EQ3
COOH	EQ4
COCH ₃	EQ5



MATERIAL AND METHODS

EPR *in situ* photochemical experiments.

The formation of paramagnetic intermediates upon monochromatic irradiation of the selenadiazoloquinolones was monitored *in situ* using EPR spectrometer EMX Plus (Bruker, Germany). The selenadiazoloquinolone solutions in dimethylsulfoxide (DMSO) or acetonitrile (ACN) containing a spin trapping agent (5,5-dimethyl-1-pyrroline *N*-oxide, DMPO) or/and a hindered amine (4-hydroxy-2,2,6,6-tetramethylpiperidine, TMP) were mixed directly before the EPR measurements, then carefully saturated with air or argon and immediately transferred to a small quartz flat cell optimized for the TE₁₀₂ cavity. The samples were irradiated at 295 K directly in the EPR resonator, and the EPR spectra recorded *in situ* during continuous or after a defined photoexcitation. The irradiation source was an UV LED monochromatic radiator ($\lambda = 365, 385, 400$ nm; Hönle UV Technology).

Steady-state photochemical experiments.

The freshly prepared solutions of the selenadiazoloquinolones were irradiated in a 1-cm quartz cell with an UV LED monochromatic radiator, under air at room temperature and subsequently their UV/vis spectra were taken using UV-3600 UV/vis spectrometer (Shimadzu, Japan).

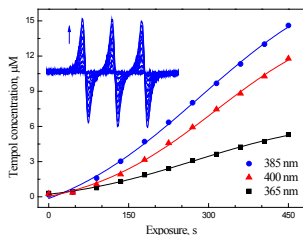
RESULTS AND DISCUSSION

EPR spectroscopy was used to monitor the processes undergoing during the irradiation of 7-R-9-ethyl-6-oxo-6,9-dihydro[1,2,5]selenadiazolo[3,4-*h*]quinolones in DMSO and ACN. EPR spin trapping was applied for the identification of short-lived radicals *via* their trapping by a spin trap, and thus forming a more stable paramagnetic spin adduct. Application of DMPO spin trap confirmed the formation of

$O_2^{\cdot-}$ upon the irradiation of EQ1–5 DMSO solutions. We performed series of experiments, observing EPR spectra upon continuous or 220 s monochromatic excitation at 365, 385, and 400 nm. In both cases well resolved spectra of $^{\cdot}DMPO-O_2^{\cdot-}$ adduct were found, along with $^{\cdot}DMPO-OCH_3$ produced in interactions of $O_2^{\cdot-}$ or photoexcited molecules with solvent.

The detection of $^{\cdot}O_2$ by means of EPR spectroscopy represents an indirect method based on the oxidation of hindered amines by $^{\cdot}O_2$, forming semistable nitroxide radicals. In our experiments ACN and DMSO solutions of investigated compounds were continuously irradiated ($\lambda = 400$ nm) in the presence of TMP and the formation of 4-hydroxy-2,2,6,6-tetramethylpiperidine *N*-oxyl (Tempol) was monitored *in situ*. Immediately after the beginning of the irradiation we observed the increase of three-line signal characteristic for Tempol (inset in Fig.1). Analogous experiments were conducted for other wavelengths of 365 and 385 nm. Figure 1 shows the increase of the Tempol concentration measured in the system EQ2/TMP/ACN under air during the continuous exposure with all three wavelengths.

Figure 1.: Concentration of Tempol produced upon continuous irradiation at different wavelengths (365, 385, and 400 nm) *via* the oxidation of TMP in aerated ACN solutions of EQ2. Inset shows time evolution of the EPR spectrum obtained upon continuous irradiation of EQ2/TMP/ACN/air at 385 nm



Steady state photochemical experiments were conducted in order to detect the effect of irradiation on quinolones. We did not observe any significant changes in electronic absorption spectra of all investigated selenadiazoloquinolones monitored after defined irradiation intervals (0–30 min) for three different irradiation sources 365, 385, and 400 nm.

CONCLUSION

The EPR investigations evidenced that upon the irradiation of investigated selenadiazoloqui-

nonolones, molecular oxygen is effectively activated producing the superoxide radical anions and singlet oxygen. Taking into account the results from steady state photochemical experiments, we propose that the interaction of investigated selenadiazoloquinolones with the photogenerated species and their consecutive degradation is negligible. Consequently, EQ1–5 behave as photosensitizers and their biological impact represent the object of further photobiological investigations.

ACKNOWLEDGEMENT

This study was financially supported by Scientific Grant Agency (VEGA Project 1/0289/12) and Research and Development Agency of Slovak Republic (contract No. APVV-0339-10). Maroš Bella and Viktor Milata are gratefully acknowledged for selenadiazoloquinolones synthesis.

REFERENCES

- [1] Boteva A. A., and Krasnykh O. P.: Chemistry of Heterocyclic Compounds, 45 (2009), 757-785
- [2] Albini A., and Monti S.: Chemical Society Reviews, 32 (2003), 238-250
- [3] Wainwright, M.: Anticancer Agents in Medicinal Chemistry, 8 (2008), 280-291
- [4] Barbieriková Z., Bella M., Kučerák J., et al.: Photochemistry and Photobiology, 87 (2011), 32-44
- [5] Bella M., Schultz M., and Milata V.: ARKIVOC, 5 (2012), 242-251

ELECTROCHEMICAL TEMPLATE SYNTHESIS OF NOBLE METAL AND SEMICONDUCTING QUANTUM DOTS

Marek BEDLEK¹, Radim HRDY^{1,2}, Jana DRBOHLAVOVA^{1,2*}, Jaromír HUBALEK^{1,2}

¹Brno University of Technology, Faculty of Electrical Engineering and Communication, Department of Microelectronics, Technická 3058/10, 616 00 Brno, Czech Republic

²Central European Institute of Technology, Brno University of Technology, Technická 3058/10, 616 00 Brno, Czech Republic

*drbohla@feec.vutbr.cz

ABSTRACT

Luminescent quantum dots (QDs) are increasingly attracting the attention as possible optical detectors of biomolecules, such as proteins, DNA, etc. Large amount of different factors influences the selection of material for QDs synthesis when dealing with substances from living organisms. Hence in this paper, non-toxic and biocompatible titanium dioxide (TiO₂) and gold were chosen as a suitable material for QDs creation employing template based non-lithographic technique. Namely, nanoporous alumina template was used for the fabrication of (i) TiO₂ QDs by anodic oxidation of sputtered Ti film on a silicon wafer and (ii) Au QDs by galvanic deposition from Au containing electrolyte on nickel coated silicon wafer. Self-ordered TiO₂ and Au QDs were characterized by SEM, which confirmed that the size of QDs satisfies the requirement of quantum confinement effect. Fluorescence spectroscopic study was also performed, comparing the emission spectra of annealed and non-annealed QDs and showing that the annealing is essential for achieving desired fluorescence properties of TiO₂ QDs.

INTRODUCTION

Excellent optical properties of QDs (namely high quantum yield, broad absorption spectra and narrow, symmetric fluorescence spectra from UV to NIR, large effective excitation and emission Stokes shifts), long life-time (high resistance to photobleaching) compared to ordinary fluorophores and stability (resistance to photo- and chemical degradation) predestinate them in usage for imaging and as optical probes for detection of peptides, proteins, nucleic acids and other biomolecules [1]. However, main issue is that most QDs are in fact toxic.

Even there is an immense interest in the synthesis of colloidal QDs, the papers concerning the QDs fabrication in deposited form, mainly for *in vitro* biosensing purposes, still lack. Some generally used approach for QDs deposition cover the epitaxial growth and lithographic techniques, which are unfortunately very expensive and time-consuming. Consequently, a need for cheap and reliable method of biocompatible QDs fabrication has arisen.

This paper reports on the anodic oxidation of aluminium layer to create nanoporous template, which serves for QDs arrays fabrication either through the process of anodic oxidation of metal underlayer or by galvanic deposition of metal ions from electrolyte solution. This method is well reproducible, easy, rapid and cheap in comparison with above mentioned techniques. Anodization process was controlled by several factors, most important being choice and concentration of electrolyte, temperature of electrolyte and anodization voltage. All of these parameters influenced

the resulting dimensions, ordering and overall properties of QDs.

MATERIAL AND METHODS

Substrate preparation

Thin layer of titanium (100 nm) or nickel (100 nm) were sputtered on 4" silicon wafer and subsequently 500 nm aluminium layer was deposited by evaporation. Before QDs fabrication, the homogeneity and surface roughness of Ti/Al and Ni/Al layers were observed by scanning electron microscopy (SEM) Mira II MLU (Tescan Mira, Brno, Czech Republic) under following conditions: work distance of 2.5 mm, high vacuum mode (10⁻³ Pa), voltage of 15–20 kV, and spot size of 2.4 nm. The morphology and size of TiO₂ and Au QDs were also observed in SEM.

TiO₂ QDs fabrication

The anodization process took place in 3 M sulphuric acid at 11 °C and under the constant anodization voltage of 5 V, which resulted in the formation of nanoporous alumina template and subsequently of TiO₂ QDs in the case when Ti was deposited under Al. Finally, the alumina template was etched in a mixture of H₃PO₄ (50 ml L⁻¹) and CrO₃ (30 g L⁻¹) and QDs arrays were annealed in vacuum at 500 °C for 1 hour to achieve the transformation of amorphous titania into the crystallographic anatase, which is necessary to reach the desired fluorescence properties.

Au QDs fabrication

To create Au QDs, the anodization of Al was performed under the same conditions, but in two steps to obtain the template as thin as possible and thus to avoid the creation of gold nanowires instead of QDs. In the first step, the anodization was interrupted before the barrier layer came in the contact with nickel layer. The anodized layer was then etched, followed with second anodization of remaining aluminium layer and finally with gold galvanic deposition using 100 ml aqueous solution containing 0.6 g of $K[Au(CN)_2]$ and 0.232 g of H_3BO_3 under various current values and durations to find the optimal conditions.

Optical properties characterization

The QDs arrays were analysed on spectrofluorometer (Horiba, Jobin-Yvon) with laser diode excitation at 350 nm and using photomultiplier (T1 PMT) detector. In the case of TiO_2 QDs, both annealed and non-annealed QDs were characterized.

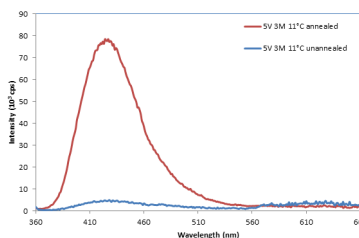
RESULTS AND DISCUSSION

During anodization process, aluminium layer was transformed into nanoporous alumina with pore size of about 5 nm according SEM characterization. As each pore started growing downwards, it was surrounded by so called barrier layer. When barrier layer came in contact with titanium layer, a QD nucleus started growing. Nucleus growth is almost isotropous and continues until nucleus size is about three times the size of the pores [2]. This is very important fact when dealing with QDs fabrication using this method, thus we have to assume that QD size will be at least double of the pore diameter. Anodization was stopped when TiO_2 nucleus growth would start to aim upwards into the pore. The QDs prepared with these conditions were about 10 nm in diameter and therefore satisfied the condition for quantum confinement effect for TiO_2 [3]. Immediately after preparation, QDs do not exhibit intensive fluorescence properties but significant intensity increase (about 16 times higher) was observed after annealing (see Figure 1).

The annealed QDs showed one single Gaussian-like peak with maximum at 425 nm, whereas non-annealed QDs exhibited spectrum without any significant peak. This confirms that the formation of crystalline structure is necessary for achieving intrinsic optical properties of luminescent QDs.

The template for Au QDs was prepared in two step anodization process, which improved the final ordering of created nanostructures. The size of Au QDs was similar to that of TiO_2 QDs. The detailed optical characterization of these QDs is currently in the process.

Figure 1. The comparison of fluorescence spectra between annealed (red line) and non-annealed (blue line) TiO_2 QDs array



CONCLUSION

In this work, we succeeded in the formation of Au and TiO_2 QDs with size of 10 nm and strong photoluminescence peak in the visible range (around 425 nm) employing rapid, inexpensive and reproducible template based method. Such QDs arrays are suitable for biosensing purposes, namely for the detection of various biomolecules such as DNA and proteins after appropriate surface modification and functionalization.

ACKNOWLEDGEMENT

The work has been supported by the grants GACR P102/10/P618, KAN 208130801 and CEITEC CZ.1.05/1.1.00/02.0068.

REFERENCES

- [1] Drbohlavova J, et al., International Journal of Molecular Sciences, 10 (2009), 2, 656-673
- [2] Mozalev A, et al., Electrochimica Acta, 48 (2003), 20-22, 3155-3170
- [3] Drbohlavova J, et al., Nanoscale Research Letters, 7:123 (2012), 1-4

ELECTROANALYTICAL METHODS FOR THE GLYCOCONJUGATES DETECTION IN MEDICAL DIAGNOSTICS

Tomas BERTOK*, Danica MISLOVICOVA, Peter GEMEINER, Jan TKAC

Department of glycobiotechnology, Institute of chemistry, Slovak academy of sciences, Dubravska cesta 9, Bratislava, 845 38, Slovak republic
*chemtobe@savba.sk

ABSTRACT

The modulation of protein function in eukaryotes is relying on a combinatorial potential of saccharidic structures, which greatly exceeds even the potential of amino acids during the polypeptide chain synthesis. Because a majority of human proteins are glycosylated, an analysis of these structures may play an important role during the early diagnostics of some aberrant glycosylation-related diseases [1]. An interaction between biorecognition elements (lectins) and glycoproteins was followed by an electrochemical impedance spectroscopy and differential pulse voltammetry, respectively.

INTRODUCTION

Using so-called self-assembled monolayers (thiolated derivatives of different alkanes with a different chain length), a control of the density (and in some cases orientation) can be provided [2, 3]. These structures may be effectively used for the immobilization of the biorecognition elements. Even if the analyte does not form a redox couple with the biorecognition element (lectins), electroanalytical methods can be used for the analyte detection. Using the electrochemical impedance spectroscopy (EIS), the changes in the impedance were observed (using the Nyquist plot evaluation with R(C[RW]) circuit). Using the differential pulse voltammetry (DPV; with the electrochemical probe immobilized in the SAM layer – in opposite to EIS method, where the electrochemical mediator was present in the measuring solution), the shift in the current response was observed.

MATERIAL AND METHODS

Electrochemical measurements

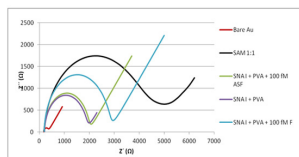
For all measurements, laboratory potentiostat/galvanostat (Metrohm Autolab) was used. For the electrochemical sensor measurements, a three electrode system was chosen, with the modified gold (working) electrode, Ag/AgCl (reference) and platinum (counter) electrode. All incubation steps during the biosensor construction took 30 min, activation of the carboxyl for 15 min, and involved the SAM layer formation, lectin immobilization and blocking of the non-specific interactions (with poly(vinyl alcohol) – PVA). EIS measurements were performed in 0.1M KCl with 5mM $K_3[Fe(CN)_6]/K_4[Fe(CN)_6]$ and DPV assays were run in 20 mM Tris pH 6.5 with addition of 500 mM NaCl. The EIS measurement was done at 200 mV and DPV measurements in the interval from 0 to 400 mV. The

electrochemical probe for the DPV measurement was ferrocenyloctanethiol.

RESULTS AND DISCUSSION

The electrochemical impedance spectroscopy was previously used for the affinity, lectin-based biosensors construction and analyte detection. We proposed a new configuration with the sensitivity for the analyte in a fM range. Differential pulse voltammetry (where the analytical signal was the shift in the current response) was less sensitive working in a nM range. Both of these techniques were previously described many times as a sensitive and simple methods for the detection of different analytes, however, DPV was not used for the glycoconjugate detection. The whole construction process was controlled using atomic force microscopy. For the SNA (*Sambucus nigra* agglutinin) and Con A (*Concanavalin A* from *Canavalia ensiformis*) lectins, the fetuin (a sialylated glycoprotein) [4,5] and invertase (glycoprotein containing mannose in its structure) were chosen as analytes.

Figure 1: A Nyquist plot from the EIS spectra (50 different frequencies) for different stages of the



For the incubation with the planar gold electrode, 20 μ l of the sample was applied in an inverted position. For the SNA lectin, non-specific interactions were revised with asialofetuin.

Figure 2: A calibration curve based on the shift of the ferrocene peak after the analyte binding on the biosensor surface

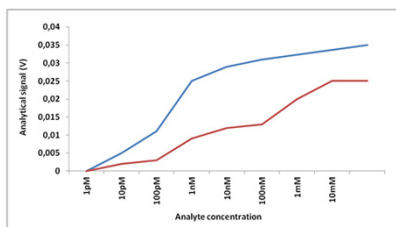
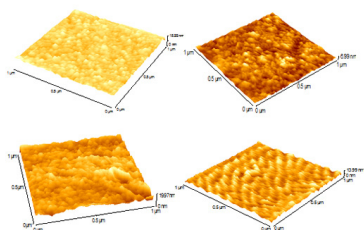


Figure 3: AFM images during the biosensor manufacturing; from upper left to lower right – bare Au electrode, SAM monolayer, immobilized lectin and blocking using PVA



CONCLUSIONS

Using the above described protocol, we managed to prepare a highly sensitive, reliable and easy-to-fabricate lectin based electrochemical biosensor reliably working in low fM concentrations of glycoprotein. The ratio of non-specific to specific interactions was calculated from the slopes of the linear parts of the calibration curves, and they did not exceed 25% [6].

ACKNOWLEDGEMENT

This contribution is the result of the project implementation: Centre of excellence for Glycomics, ITMS 26240120031, supported by the Research & Development Operational Programme funded by the ERDF.

REFERENCES

- [1] Bertók T., Šefčovičová J., Gemeiner P., Tkáč J.: *Chemické Listy*, 106 (2012), 20-26
- [2] Bertók T., Šefčovičová J., Gemeiner P., Tkáč J.: *Chemické Listy*, 106 (2012), 174-181
- [3] Gooding J. J., Darwish N.: *The Chemical Record*, 12 (2012), 92-105
- [4] Shibuya N., Goldstein I. J., Broekaert W. F., et al.: *The Journal of Biological Chemistry*, 262 (1987), 1596-1601
- [5] Broekaert W. F., Nsimba-Lubaki M., Peeters B., Peumans W. J.: *Biochemistry Journal*, 221 (1984), 163-169
- [6] Bertók T., Gemeiner P., Mikula M., et al.: *Analytical and Bioanalytical Chemistry*, (2012) submitted

PHOTODEGRADATION PROCESSES OF QUINOLONES

Miroslava BOBENICOVA*, Andrea CAKLOSOVA, Dana DVORANOVA

Institute of Physical Chemistry and Chemical Physics, Faculty of Chemical and Food Technology, Slovak University of Technology in Bratislava, Radlinského 9, SK-812 37 Bratislava, Slovak Republic

*miroslava.bobenicova@stuba.sk

ABSTRACT

This work is focused on the investigation of the photodegradation processes of synthesized quinolones in alkaline media with/without titanium dioxide applying UV-Vis spectroscopy. The results showed that the decomposition of quinolones upon UVA irradiation is more rapid in the presence of titanium dioxide.

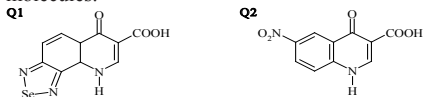
INTRODUCTION

Pharmaceutical compounds and their residues can be found in the wastewaters as undesirable contaminants. The conventional sewage treatment plants are not able to eliminate effectively the pharmaceuticals, so the attention is oriented on the new techniques how to remove them from environment [1-3]. The heterogeneous photocatalysis on titanium dioxide offers the possibility to eliminate the organics effectively *via* oxidation processes up to water and carbon dioxide [3,4]. Our research is focused on the photodegradation processes of novel synthesized quinolones, molecules with potential biological impact, in the reaction systems with/without titanium dioxide.

MATERIAL AND METHODS

Quinolone derivatives (Figure 1) used in the photochemical experiments were synthesized at Institute of Organic Chemistry, Catalysis and Petrochemistry of our faculty.

Figure 1.: Structures of investigated quinolone molecules.



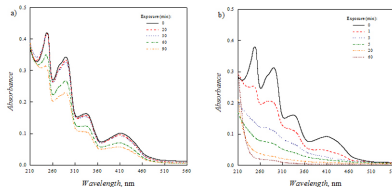
The titanium dioxide (P25 Wacker, 0.5 g L⁻¹) was used for preparation of suspensions. The stock solutions of quinolones were prepared in 1 mM NaOH (Mikrochem, anal. grade) and mixed with redistilled water or titanium dioxide suspension prior to irradiation. Photochemical experiments with quinolones were performed in the photochemical inversion well using 400 W medium pressure mercury lamp ($\lambda_{\text{max}} = 365\text{nm}$; Applied Photophysics, UK) with Pyrex filter ($\lambda > 300\text{ nm}$) at 303 K. Reaction systems were continuously saturated with oxygen. Electronic absorption spectra were recorded on UV-3600 Shimadzu UV-Vis-NIR spectrometer. Samples containing TiO₂ were centrifuged before the

measurement of UV-Vis spectra on centrifuge (Espresso, Thermo Electron Industries, 14 500 rpm).

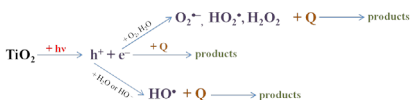
RESULTS AND DISCUSSION

Figure 2 represents the series of electronic absorption spectra of quinolone **Q1** in alkaline media upon UVA irradiation without/with titanium dioxide.

Figure 2.: UV-Vis spectra of **Q1** upon irradiation in (a) 1 mM NaOH and (b) 1 mM NaOH in the presence of TiO₂. Initial concentrations were 25 μM (Q1) and 0.25 g L⁻¹ (TiO₂).



The quinolones due to their extended π -electron system behave as photosensitive molecules, thus upon the UVA photoexcitation in the presence of molecular oxygen the reactive oxygen species (ROS), such superoxide radical anion O₂^{-•}, hydroxyl radical HO[•] or singlet oxygen ¹O₂ are formed [5,6]. On the other hand, heterogeneous photocatalysis on the titanium dioxide is well known for its ability to produce upon ultra-band-gap radiation reactive holes and electrons capable to react directly with organic compounds or produce to HO[•], O₂^{-•}/HOO[•], H₂O₂ and ¹O₂ [3,4]:



Direct irradiation of **Q1** in homogeneous system led to the decomposition of molecule, as is shown in the Fig. 2a, but in the comparison with

heterogeneous suspension (Fig. 2b) the changes in UV-Vis spectra are less significant. The aromatics are sensitive to attack of the ROS generated upon photoexcitation of TiO₂, consequently the irradiation led to the cleavage of aromatic ring; e. g. 20 min. exposure of **Q1** under the given experimental conditions caused the loss of aromatic character, and the corresponding changes were found in UV-Vis spectra. The photogenerated hydroxyl radicals also play an important role in this process as was confirmed by EPR spin trapping technique.

CONCLUSION

This work is focused on the photodegradation processes of quinolones. The results showed that the photocatalytic decomposition of quinolones upon UVA irradiation is more complex and efficient in TiO₂ system in comparison with photoinduced processes in homogeneous solutions and represents an effective way of quinolone elimination from the environment.

ACKNOWLEDGEMENT

Maroš Bella and Viktor Milata are gratefully acknowledged for the synthesis of all investigated quinolone derivatives. This work was financially supported by Scientific Grant Agency (VEGA Project 1/0289/12) and Research and Development Agency of Slovak Republic under the contract No. APVV-0339-10.

REFERENCES

- [1] Oller I et al.: Science of the Total Environment 409 (2011) 4141-4166.
- [2] An T et al.: Journal of Hazardous Materials 197 (2011) 229-236.
- [3] Fujishima A et al.: Surface Science Reports 63 (2008) 515-582.
- [4] Dodd N. et al.: Photochemistry and Photobiology 87 (2011) 632-640.
- [5] Barbieriková Z et al.: Photochemistry and Photobiology 87 (2011) 32-44.
- [6] Barbieriková Z et al.: Journal of Photochemistry and Photobiology A: Chemistry 224 (2011) 123-134.

DIRECT VOLTAMMETRIC DETECTION OF INSULIN ON MWCNTS MODIFIED ELECTRODES – PRELIMINARY RESULTS

Petra BUSINOVA¹, Jan PRASEK¹, Jaromir HUBALEK^{1*}

¹Brno University of Technology, Faculty of Electrical Engineering and Communication, Department of Microelectronics, Technicka 3058/10, 616 00 Brno, Czech Republic

*hubalek@feec.vutbr.cz

ABSTRACT

Direct and rapid insulin detection is very important not for the study of the diabetes mellitus only. Therefore electrochemical determination of insulin could be very attractive. This contribution presents the fabrication of planar carbon working microelectrodes using standard thick film technology and their surface modification with multiwalled carbon nanotubes to promote the electrochemical oxidation of insulin using cyclic voltammetry.

INTRODUCTION

Insulin is a very important polypeptide hormone which controls glucose levels in blood within a narrow concentration range. Its monitoring plays an important role in study of pathophysiology of various disorders especially diabetes. The standard analytical methods for insulin detection include bioassays, immunoassays, and chromatography. These methods are time-consuming and slow and frequently require derivatizations of insulin with isotopes or fluorogenic labels to increase the sensitivity and selectivity [1, 2]. A direct electrochemical measurement of insulin is of considerable interest in the development of fast and sensitive amperometric detectors coupled to flow systems or chromatographic instruments for this hormone. The insulin molecule contains one intrachain and two interchain disulfide bonds. A direct electrochemical detection of insulin relies on either a reduction of some of these bonds at the mercury and silver or oxidation of disulfide bonds at modified electrodes. Direct oxidation of insulin at common electrodes is limited by the slow kinetics and surface fouling onto electrochemical devices. In addition, low sensitivity, reproducibility and stability over a wide range of solution compositions and high overpotential at which the insulin oxidation process occurred are other limitations of unmodified electrodes as an electrochemical sensor for insulin detection [3]. Therefore various chemically modified electrodes have been suggested for promoting the oxidation and detection of insulin. Materials which can promote the electrochemical oxidation of insulin include ruthenium oxide (RuO₂), iridium oxide (IrO₂), ruthenium metallodendrimer and multiwalled carbon nanotubes (MWCNTs) [4].

This work reports on the fabrication of planar MWCNTs thin layer modified carbon working electrodes (WE) using standard thick film tech-

nology suitable for direct voltammetric detection of insulin. Characterization of these microelectrodes and preliminary results of insulin voltammetric detection using these electrodes are presented here.

MATERIAL AND METHODS

Electrodes fabrication

Working electrode substrate was designed as a working electrode of three-electrode planar sensor system [5] deposited on alumina substrate using standard thick-film technology (TFT). Because the output current response depends on the size of the electrode active area, the electrode diameter was designed as large as possible. The diameter of the working electrode was chosen to be 3 mm.

Working TFT microelectrodes were fabricated from polymer thick film pastes on the alumina substrate. The DuPont paste 7102 (DuPont, USA) was used for contact, ESL 243-S (ESL Electroscience, UK) for covering layer and DuPont BQ 221 for WE fabrication.

Electrode modification

The desired amount of MWCNTs was dissolved in 1 mL of *N,N*-dimethylformamide (DMF), and sonicated for 1 h. Then, 2 μ L of the resulting MWCNTs/DMF dispersion (usually containing 2 mg.mL⁻¹ MWCNTs) was cast on the surface of the planar carbon microelectrode. The electrode was allowed to dry at room temperature for at least 2 h.

Voltammetric measurement

Electrochemical detection was carried out in a three-electrode voltammetric cell using 0.05 mol/L⁻¹ phosphate buffer solution (pH 7.4) as a supporting electrolyte against standard Ag/AgCl reference electrode and platinum counter electrode. The cyclic voltammetric (CV) analysis was done using PalmSens potentiostat.

Stock solution of insulin with concentration of 0.50 mmol/L⁻¹ was prepared by dissolving pow-

dered insulin in 0.02M HCl containing 0,02 % (v/v) Tween-80. This stock solution was further diluted with 0.05 M phosphate buffer (pH 7.4) solution to make working solutions with desired concentrations. The pH of the supporting electrolyte solution (7.4) was adjusted using NaOH and HCl.

RESULTS AND DISCUSSION

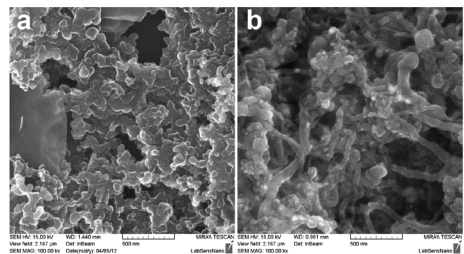
New planar working microelectrodes were fabricated using standard thick film polymer technology. Fabricated electrode is shown in the figure 1.

Figure 1.: Carbon TFT electrode underlay made of special polymer BQ221 paste (DuPont)



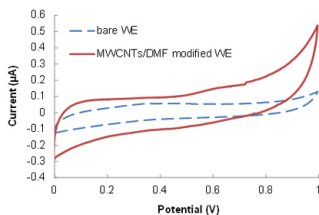
All electrodes were examined optically using SEM. Bare surface of BQ221 carbon electrode is shown in the figure 2a. The electrode surface modified with MWCNTs is shown in the figure 2b. From the figure 2b is clear that the modification was successful and we obtained high porous electrode surface full of free MWCNTs.

Figure 2.: SEM microimages of fabricated electrodes, magnification 100 kx, a) carbon TFT underlay BQ221 (DuPont), b) MWCNTs/DMF modified electrode



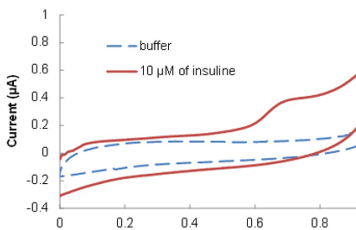
The electrochemical characterization of all electrodes was done using cyclic voltammetry in 0.05 mol/L⁻¹ phosphate buffer solution (pH 7.4) in potential range from 0 to 1 V. Obtained voltammograms for bare carbon TFT underlay and MWCNTs/DMF modified electrode is shown in the figure 3. From the figure 3 is clear that the current response of MWCNTs/DMF electrode is just little bit higher than the signal from bare electrode.

Figure 3.: CV at the bare carbon TFT underlay (DuPont BQ221) and MWCNTs/DMF modified electrode in 0.05 mol/L⁻¹ 1 phosphate buffer solution (pH 7.4) using a scan rate of 50 mV.s⁻¹



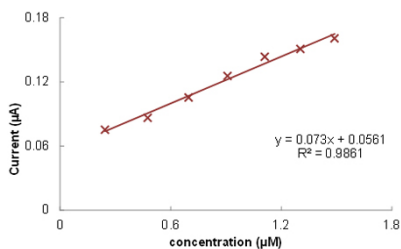
The basic detection of insulin on the MWCNTs/DMF modified electrode was done on sample with higher concentration to check the detection abilities of the electrode. Example of current response to 10 µmol/L⁻¹ addition of insulin into buffer solution is shown in the figure 4. The CV response shown in the figure 4 confirmed that the MWCNTs/DMF modified electrode is able to detect insulin.

Figure 4.: CV response of MWCNTs/DMF modified electrode to buffer solution (dashed line) and to 10 µmol/L⁻¹ insulin solution (continuous line) using a scan rate of 50 mV.s⁻¹



Finally the detection limit and calibration curve of planar thick film modified electrode have been done. Obtained calibration curve is shown in the figure 5. From the figure 5 is clear that we were able to determine insulin from the concentration of 250 nmol/L⁻¹. We obtain linear calibration curve in the range of insulin concentration from 250 nmol/L⁻¹ to 1.6 µmol/L⁻¹. Considering these first results could be concluded that there is high possibility to fabricate special three electrode sensor for fast insulin detection. Next experiments will be focused on fabrication of more sensitive active layer and integration of this working electrode into the three electrode voltammetric sensor.

Figure 5.: Calibration curve of planar thick film MWCNTs/DMF modified electrode obtained for insulin concentrations from 250 nmol/L⁻¹ to 1.6 µmol/L⁻¹ using a scan rate of 50 mV.s⁻¹



CONCLUSION

There was fabricated planar carbon working microelectrodes modified with MWCNTs/DMF to promote the electrochemical oxidation of insulin using cyclic voltammetry. Our experiments confirmed the possibility of electrochemical insulin detection on our working electrode. We were able to determine insulin from the concentration of 250 nmol/L-1. We obtain linear calibration curve in the range of insulin concentration from 250 nmol/L-1 to 1.6 µmol/L-1. Considering these first results could be concluded that there is high possibility to fabricate special three electrode sensor for fast insulin detection.

Next experiments will be therefore focused on fabrication of more sensitive active layer and integration of this working electrode into the three electrode voltammetric sensor.

ACKNOWLEDGEMENT

The work has been supported by NANIMEL GA ČR 102/08/1546 and project SIX CZ.1.05/2.1.00/03.0072.

REFERENCES

- [1] Kivlehan F, Lanyon Y H, Arrigan D W M: *Langmuir*, 24 (2008), 17, 9876-9882
- [2] Zhang M, Mullens C, Gorski W: *Analytical Chemistry*, 77 (2005), 19, 6396-6401
- [3] Salimi A, Noorbakhash A, Sharifi E, et al.: *Biosensors and Bioelectronics*, 24 (2008), 4, 792-798
- [4] Wang J., Musameh M: *Analytica Chimica Acta*, 511 (2004), 33-36
- [5] Prasek J, Policky J: 33rd International Spring Seminar on Electronics Technology, (2010), 478-481

GOLD CD-SENSOR PLATFORM FOR DNA APTAMER ASSEMBLING TOWARDS HUMAN THROMBIN RECOGNITION

Gabriela M. CASTILLO¹*, Libuse. TRNKOVA², Tibor HIANIK¹

¹Department of Nuclear Physics and Biophysics, FMFI UK, Mlynska dolina F1, 842 48 Bratislava, Slovakia

²Department of Chemistry, Faculty of Science, Masaryk University, Kotlarska 2, 611 37 Brno and Central European Institute of Technology (CEITEC), University of Technology, Technicka 3058/10, 616 00 Brno, Czech Republic

*gabriela.castillo@fmph.uniba.sk

ABSTRACT

In this work, we report an aptamer biosensing array for thrombin detection by measuring the electrochemical impedance spectroscopy (EIS) upon aptamer-protein formation at the surface of gold CDtrodes (GCDTs) in the presence of redox couple $[\text{Fe}(\text{CN})_6]^{3-/4-}$ [2]. The biosensor was constructed by self-assembling a thiol-modified thrombin binding aptamer (TBA) onto the GCDT surface followed by the protein addition in a wide range of concentrations ranging from 20 nM to 1 μM . Achieved results reveal that the GCDTs present good versatility and suitable reproducibility for thrombin recognition with a limit of detection (LOD) of 5 nM. Non-specific interaction with similar molecular compounds like bovine serum albumin (BSA) demonstrates an appropriate and specifically target sensor response thanks to the aptamer incorporation as transducer elements. In order to verify the practical application of GCDT aptasensor in complex biological fluids, we have detected thrombin in spiked diluted blood plasma samples. Additionally, individual steps of biosensor assembling were monitored by Scanning electron microscopy (SEM). GCDT response was also satisfactory compared with commercial gold screen printed electrodes (GSPE).

INTRODUCTION

Biosensors based on DNA or RNA aptamers, represent a high sensitive and efficient platform for protein recognition [1]. On the other hand, GCDTs, electrodes fabricated from recordable compact discs that contain a fine gold layer on their surface, emerge as ideal candidates for sensor support due to its low-cost, simple manufacture and disposable character. Among electrochemical aptasensors those for thrombin detection are the best analyzed. This might be due to the properly characterization of thrombin binding aptamers (TBA) that has been made up to date, as well as to the importance that thrombin detection plays in diagnosis purposes. Thrombin is a multifunctional serine protease that takes an essential role in the procoagulant and anti-coagulant functions [3,4]. High concentration of thrombin induces thrombosis while its low content causes an excessive bleeding [4]. The aptasensor as an alternative diagnostic tool for thrombin analysis or blood coagulation with nanomolar detection could gain great interest in the medical research [5].

MATERIAL AND METHODS

Electrochemical determination

Biosensor was constructed by chemisorption of 2 mM thiolated TBA on a clean and dry GCDT surface at 4° C overnight. Before incubation, TBA was denatured at 60° C and then

exposed to cooling on ice bath for 1 min in order to get a proper binding to thrombin. Once the TBA self-assembling monolayer (SAM) was prepared, 100 mM B-Mercaptoethanol (BM) was let interacted during 20 min with the GCDT to facilitate its surface blocking and thus evade any kind of nonspecific adsorption. Modified GCDT was rinsed by binding buffer and immediately exposed to thrombin during 30 min or used directly in electrochemical experiments. The changes in charge transfer resistance R_{ct} were measured following thrombin addition to TBA-BM modified GCDT in a concentration range 20 nM–1 mM. With the aim of testing the specificity of the biosensor, 1 mM of bovine serum albumin (BSA) and 10 times diluted Human Plasma (HP) both prepared in binding buffer, were added to BM-TBA modified GCDT and the changes on R_{ct} were recorded by electrochemical impedance spectroscopy (EIS).

All electrochemical experiments were performed with potentiostat/galvanostat analyzer AUTOLAB PGSTAT 302N connected to 663 V Stand (Eco Chemie-Methrom, Switzerland) in DC mode. Three-electrode system consisting on Pt wire (auxiliary electrode), Ag/AgCl 3 M KCl (reference electrode), and either GCDT or GSPE (working electrode), was used for electrochemical measurements. Fit and data simulation were performed with incorporated software Nova 1.6 Autolab B.V. 2005–2011, distributed by Methrom. EIS measurements were performed using

FRA2 module. AC voltage of amplitude of 0.01 V and DC voltage 0.19 V were applied. The measurements were performed in a frequency range 0.1 Hz to 100 kHz. Binding buffer used in all experiments was composed of 20 mM TRIS, 140 mM NaCl, 1 mM CaCl₂, 1 mM MgCl₂, 5mM KCl, pH 7.4.

RESULTS AND DISCUSSION

The process of sensor fabrication as well as binding of thrombin to TBA can be monitored by EIS. The calculations of electrical parameters of the sensing layer from EIS spectra were made using fitting procedure corresponding to the equivalent Randles circuit (see Figure 1 left-side inset). Here, R_s is the electrolyte resistance, R_{ct} is the charge-transfer resistance, C refers to the capacitance of the electrode solution interface. Constant phase element (CPE) for $n=1$. W element represents the Warburg impedance; it gives information about the diffusion process occurring from the electrode surface to the electrolyte. Figure 1 shows the Nyquist plot of a bare GCDT, modified by TBA without and at the presence of 20 nM of thrombin. As expected, the radius of semicircle which is measure of R_{ct} value increases with surface modification. Fitting the Nyquist plot by Randles equivalent circuit allowed us to determine corresponding values of R_{ct} (see column diagram on Figure 3). It can be seen that R_{ct} increases from 0.798 k Ω at bare to 4.33 k Ω at TBA modified GCDT. To avoiding non-specific adsorption, B-Mercaptoethanol (BM) is added to TBA-SAM and a higher R_{ct} value (5.40 k Ω) is observed from the Nyquist plot, possibly attributed to the improved insulating properties of the sensing layer as well as due to additional negatively charge from dissociated carboxyl terminal groups of BM. Once the thrombin is coupled, TBA folds into a more uniform quadruplex structure creating a condensed layer onto GCDT surface. In addition the negative surface charge also increases due to negatively charged thrombin. This is reflected in further increase of R_{ct} value up to 7.98 k Ω at 20 nM thrombin. On the other hand, when increasing thrombin concentration (20 nM-1 μ M), R_{ct} value also increases as it is seen from increased diameter of semicircles (Fig. 2a) and from calibration plot (Fig. 2b), possibly due to obstruction of electronic communication from the redox markers (increased concentration of thrombin makes the sensor surface more negatively charged which results in repulsion of negatively charged redox marker). See Figure 2.

The sensor revealed satisfactory recovery (approx. 90 %) in a blood plasma with negligible interferences at presence of 1 μ M BSA.

Figure 1: Above: Schematic illustration of GCDT construction and corresponding binding steps occurring at its surface in the presence of the redox couple 1 mM [Fe(CN)₆]^{3-/4-} (a) bare precleaned GCDT; b) TBA onto GCDT surface followed by BM modification ; c) TBA-BM modified GCDT after addition of 20 nM thrombin. Below: SEM images of mentioned binding steps on a GCDT surface. Right-side zoomed scans

correspond to 4 μ m, 2 μ m and 10 μ m respectively

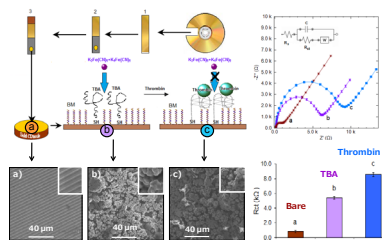
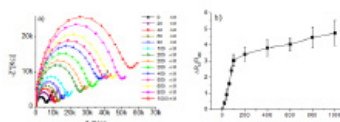


Figure 2: a) Nyquist plot for GCDT modified with TBA at presence of various concentration of thrombin in binding buffer containing 1 mM [Fe(CN)₆]^{3-/4-} (1:1), b) plot of relative charge transfer resistance $\Delta R_{ct}/R_0$ as a function of thrombin concentration:



CONCLUSION

This work was dedicated to present the design and basically simple fabrication of a sensing platform based on a recordable gold compact disc for detecting human α -thrombin using DNA aptamers as receptors. Low cost in fabrication, relative uncomplicated manufactures, and the possibility to assemble numerous GCDTs for running several control experiments (disposableness), are among the principal advantages of this approach. This gold CD sensor also incorporates the high affinity and selectivity properties that aptamers provide as transducer elements in a biosensor response.

ACKNOWLEDGEMENT

This work was supported by Slovak Research and Development Agency (contract No. APVV-0410-10), by Grant Agency VEGA (project No. 1/0785/12) and by CEITEC CZ.1.05/1.1.00/02.0068.

REFERENCES

- [1] Aptamers in Bioanalysis (Ed: M. Mascini), Wiley, Chichester, 2009.
- [2] G. Castillo, L. Trnkova, R. Hrđy, T. Hianik, Electroanalysis (2012), DOI: 10.1002/elan.201200041
- [3] C. A. Holland, A. T. Henry, H. C. Whinna, F. C. Church, FEBS Lett. 2000, 484, 87.
- [4] L. J. Berliner, Thrombin: Structure and Function, Plenum Press, New York 1992.
- [5] T. Hianik, V. Ostatna, M. Sonlajtrnerova, I. Grman, Bioelectrochemistry 2007, 70, 127.

MULTIWALLED CARBON NANOTUBES - DENDRIMERS PLATFORM FOR APTAMER-BASED BIOSENSOR SENSITIVE TO HUMAN CELLULAR PRIONS

Gabriela CASTILLO^{*}, Anna MIODEK², Helene DORIZON², Hafsa KORRI-YOUSSOUFI², Tibor HIANIK¹

¹Department of Nuclear Physics and Biophysics, FMFI UK, Mlynská dolina F1, 842 48 Bratislava, Slovakia

²UMR-CNRS 8182, Institut de Chimie Moléculaire et des Matériaux d'Orsay ICMMO, University Paris-Sud, Bat 420 91405 Orsay, France

*gabriela.castillo@fmph.uniba.sk

ABSTRACT

The aim of this work was to develop a label-free electrochemical aptamer-based nanoarray for in vitro detection of PrP^C as a biomarker of prion disease using multiwalled carbon nanotubes (MWCNTs) as immobilization support. Detection of prions was investigated by cyclic voltammetry (CV) following the redox signal of modified ferrocenyl group anchored in the sensor by means of Poly(amidoamine) dendrimers of 4th generation (PAMAM G4). Individual steps of biosensor formation were characterized by infrared spectroscopy (IR). Aptamer based sensor response was compared with the same array where diethyl amine was attached instead of dendrimer. The nanoarray was tested against non-specific interaction with bovine serum albumin (BSA) and in human serum for prion recognition with satisfactory results.

INTRODUCTION

Prion diseases, a group of fatal brain disorders, result from the transformation of cellular prion (PrP^C) into the pathological isoform (PrP^{Sc}) [1]. PrP^{Sc} aggregates in the nervous system forming amyloid plaques in the neocortex, cerebellum and subcortical nuclei that provokes a rapid degeneration of neuronal tissues [2]. Since prions detection in blood is limited down to picomolar (pM) levels [3], the development of an effective, high-sensitive and reliable approach of recognition is of fundamental importance in the diagnosis and treatment of neurodegenerative diseases, mainly in countries facing ageing problems which are closely related to them.

MATERIAL AND METHODS

Electrochemical determination

Electrochemical experiments were performed with potentiostat/galvanostat analyzer PGSTAT AUTOLAB 1230302 controlled by GPES software connected to a differential electrometer amplifier (Eco Chemie - Methrom, Switzerland). Three electrode system consisting on Pt wire (auxiliary electrode), saturated Ag/AgCl 3M KCl (reference electrode), and gold working electrode - area $2,01 \times 10^{-2} \text{ cm}^2$ (Basi Kenilworth-USA), were used in the electrochemical cell.

Cyclic voltagrams were recorded from $-0,8 \text{ V}$ to $+0,6 \text{ V}$ at scan rate $0,1 \text{ V/s}$.

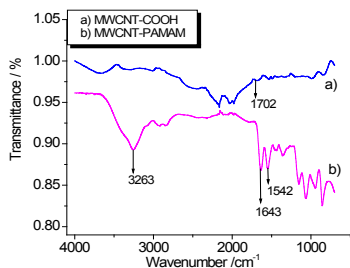
FT-IR Fourier Transform Infrared spectra were acquired using Bruker IFS66 FT-IR spectrometer equipped with a MCT detector and an attenuated total reflectance (ATR) crystal of germanium.

MWCNTs were treated with $\text{H}_2\text{SO}_4:\text{HNO}_3$ (3:1) for incorporating COOH groups. Modified MWCNTs-COOH were linked to PAMAM G4 by EDC-NHS cross-linking chemistry in order to anchor the dendrimer by amide link. Ferrocene group used as redox marker substituted by 2 activated ester (NHP)₂ was covalently attached to the dendrimer and then to biotin group by amide link. Streptavidin-biotin conjugation served as linker with biotinylated aptamer designed for specific prion recognition. All chemicals were of p.a. grade and purchased from Sigma-Aldrich. The recombinant human PrP^C protein (Human PrP^C (103-231)) molecular weight 15.1 kDa was generous gift from Dr. Human Rezaei (INRA Jouy-en-Josas, France).

RESULTS AND DISCUSSION

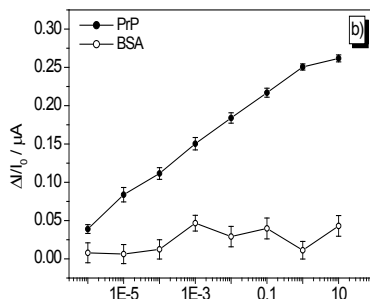
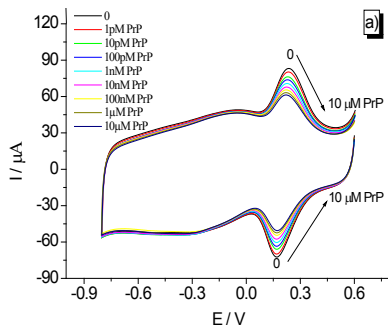
Infrared spectra for MWCNTs-PAMAM G4 conjugates presented on Fig. 1, illustrate absorption peaks of MWCNTs modified by a) COOH groups and b) after addition of PAMAM dendrimers. For a) the absorption peak at 1702 cm^{-1} can be assigned to the C=O bond vibration of acidic group. Spectrum b) shows the large bands at 3263 cm^{-1} which should be assigned to amine group of dendrimers beside bands at 1643 cm^{-1} and 1542 corresponding to amide (-CO-NH-) bound obtained after MWCNTs-dendrimer reaction.

Figure 1.: FT-IR Fourier Transform Infrared spectra for MWCNTs modified by a) COOH and b) PAMAM G4 dendrimers.



Cyclic voltagrams from -0.8 V to $+0.6$ V were recorded for analyzing the biosensor response after addition of Pr^{PrC} prions in PBS buffer solution. From CV presented in Fig. 2a it can be seen well reversible redox waves of the ferrocenyl group with oxidation and reduction peaks corresponding to the potentials 0.24 mV and 0.17 mV, respectively. The current of peaks decreased by increasing Pr^{PrC} concentrations from 1 pM to 10 μ M and reaches up to saturation after 1 μ M. From the calibration plot presented in Fig. 2b, it is possible to observe a linear dependence between absolute value ($\Delta I/I_0$) vs log Pr^{PrC} concentration (closed symbols). **Limit of detection (LOD)** corresponding to $S/N=3$ was found to be 1.30 ± 0.01 pM which can be considered as an acceptable result for practical applications. The sensor was tested also in a human blood serum with satisfactory recovery in average of 74% . The interferences with BSA up to concentrations 10 μ M were negligible. See calibration plot on Fig. 2b (open symbols).

Figure 2.: a) Cyclic voltagrams for prion (Pr^{Pr}) detection. b) Calibration plot of the dependence of reduction peak as a function of Pr^{PrC} and BSA concentrations. Results are mean \pm S.D. obtained from 3 independent experiments.



CONCLUSION

Detection of cellular prions based on an electrochemical nanoarray that includes MWCNTs-PAMAM conjugates linked to artificial receptors aptamers, is presented in this work.

Layer-by-layer sensor arrangement monitored by IR spectroscopy confirms by one side the functionalization of COOH groups on MWCNTs, as well as PAMAM G4 attachment, used as platform for enhancing biosensor signal. By means of CV, high sensitive recognition of cellular prions ranging from 0.1 pM to 10 μ M was achieved either in buffer solution or in human serum. This fact makes of this biosensor a promising tool for detection of protein with future implications on clinical diagnosis.

ACKNOWLEDGEMENT

This work was supported by the Slovak Research and Development Agency (contracts No. APVV-0410-10, SK-FR-0025-09), by France government (PHC Stephanie) and by Grant Agency VEGA (project No. 1/0785/12). This publication is also the result of the project implementation: BIOMAKRO2, ITMS: 26240120027, supported by the Research & Development Operational Program funded by the ERDF and by Centre of Excellence SAS for Functionalized Multiphase Materials (FUN-MAT) and by the Grant of Education and research ministry of French government. We are grateful to Dr. Human Rezaei and Dr. Jasmina Vidic from VIM group of INRA France for generous gift of Pr^{PrC} proteins.

REFERENCES

- [1] M. Sadowski, A. Verma, T. Wisniewski. Prion Diseases. In: Bradley WG, Daroff RB, Fenichel GM, Jankovic J, eds. Neurology in Clinical Practice. Philadelphia: Elsevier Inc; (2004)1613-1630.
- [2] M. Panigaj, A. Brouckova, H. Glierova, E. Dvorakova, J. Simak, J. G. Vostal, K. Holada, Transfusion 51 (2011) 1012-021.
- [3] J. Bratosiewicz-Wasik, T.J. Wasik, P.P. Liberski, Folia Neuropathol. 42 (2004) Suppl A:33-46.

ELECTROCHEMICAL FUNCTIONALIZATION OF POROUS-SILICON-BASED CHEMOSENSORS WITH POLYPYRROLE

Juraj DIAN^{1,*}, Martin KONECNY¹, Gabriela BRONCOVA²

¹Department of Chemical Physics and Optics, Faculty of Mathematics and Physics, Charles University in Prague, Ke Karlovu 3, 121 16 Prague 2, Czech Republic

²Department of Analytical Chemistry, Faculty of Chemical Technology, Institute of Chemical Technology, Technická 5, 166 28 Prague 6, Czech Republic

*dian@karlov.mff.cuni.cz

ABSTRACT

Electrochemical functionalization of porous silicon surface with polypyrrole is presented. Polypyrrole electrodeposition was performed by cyclic voltammetry with Autolab PGSTAT101 system. Prepared samples of polypyrrole functionalized porous silicon were characterized by infrared spectrometry and photoluminescence spectroscopy and subsequently tested for selectivity improvement in gas-phase chemical sensors of organic compounds.

INTRODUCTION

Porous silicon is a silicon-based material with complex nanostructural architecture [1]. Its unique properties, mainly bright visible room temperature photoluminescence, promise many applications in optical devices [2]. Optical sensors of chemical compounds represent one of the most rapidly developing fields in porous silicon research during last decade. For practical purposes one usually needs to detect specific analyte in a mixture of compounds what invokes a need for sensors with increased chemical selectivity. Chemical and electrochemical functionalization of sensor surface is a method for attachment of molecular systems that exhibit molecular recognition properties [3-5]. Polypyrrole electrodeposition on porous silicon surface improves both selectivity as well as operational stability of photoluminescence sensor response of porous silicon [6].

MATERIAL AND METHODS

Electrochemical preparation of samples

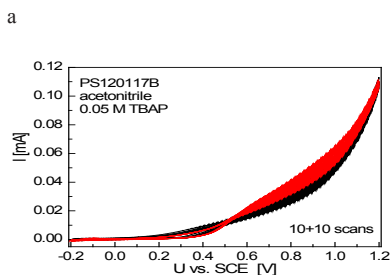
Porous silicon samples were prepared by electrochemical etching of crystalline silicon (p-type, (100), $\rho \approx 10 \Omega \text{cm}$) wafers in HF+ethanol mixture (HF:EtOH=1:2.5) in a teflon cell with two electrodes. Etching procedure was performed with home-build galvanostat ($j=2-5 \text{ mA cm}^{-2}$), silicon wafer was employed as the anode, rotation Pt electrode as the cathode. Polypyrrole electrodeposition in 0.05 M TBAP acetonitrile solution was performed in the same cell with three electrodes setup by means of Autolab PGSTAT101 measuring system and Nova 1.7 software. Cyclic voltammetry was employed for polypyrrole electrodeposition with these parameters: range of potential -0.2 to 1.2 V, scan rate 100 mV/s. Pt electrode was used as the both working and auxiliary electrode, the reference

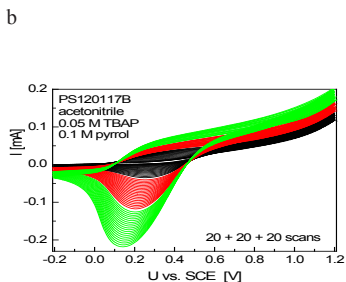
electrode was saturated calomel electrode. Acetonitrile solution was bubbled for 10 min with argon before cycling. Infrared spectra were collected by means of FTIR micro-spectrometer Thermo Nicolet iN10. Photoluminescence spectra were measured using an experimental setup consisting of UV LED ($\lambda=370 \text{ nm}$), 20 cm monochromator (Jobin Yvon HT20), photomultiplier (Hamamatsu R9836), current preamplifier (Stanford SR570) and Lock-in amplifier (Stanford SR830).

RESULTS AND DISCUSSION

The aim of functionalization of porous silicon surface with polypyrrole is improvement of sensor response selectivity and operational stability in photoluminescence detection of organic compounds. Polypyrrole electrodeposition on freshly prepared porous silicon samples was performed using cyclic voltammetry in two steps. At first only base electrolyte (40 ml of 0.05 M TBAP in acetonitrile) was cycled for 10-20 minutes (Fig 1A), afterwards pyrrole was added (268 μl , $\sim 0.1 \text{ M}$ solution) and potential was cycled for 20-30 minutes (Fig 1B).

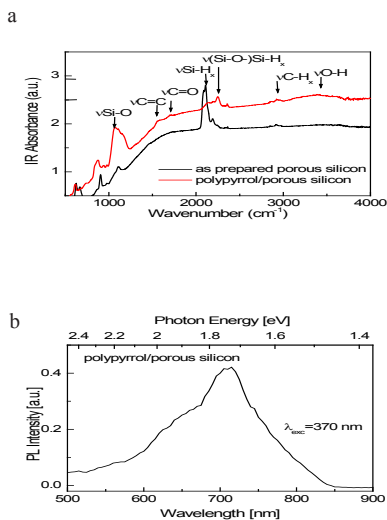
Figure 1: Cyclic voltammograms of porous silicon in: (A) 0.05 M TBAP in acetonitrile, (B) 0.05 M TBAP + 0.1 M pyrrole in acetonitrile





Prepared samples were characterized by means of infrared spectrometry and photoluminescence spectroscopy. From infrared absorption spectrum (Fig. 2A) it follows that Si-H bonds present in freshly prepared porous silicon were partially replaced with Si-O bonds and polypyrrole presence is manifested primarily by appearance of band corresponding to C=C and C=O bond vibration. Photoluminescence spectrum of polypyrrole functionalized porous silicon surface is in Fig. 2B.

Figure 2.: Characterization of polypyrrole functionalized porous silicon – (A) infrared absorption spectrum, (B) – photoluminescence spectrum.



Photoluminescence behavior of functionalized porous silicon in the presence of selected organic compounds (various linear alcohols) in gas phase was measured and compared with as-prepared porous silicon. From the dependence of photoluminescence intensity changes (quenching in most cases, enhancement is several ones) at various concentrations we conclude on possible mechanism in interaction of detected analyte with different chemical termination at porous silicon surface in agreement with previously proposed model [6].

CONCLUSION

Electrochemical preparation porous silicon and functionalization of its surface with polypyrrole is presented. Cyclic voltammetry enabled to control of the polypyrrole layer thickness by means of number of cycles. Samples were characterized by means of infrared spectrometry and photoluminescence spectroscopy and subsequently used for measurement of photoluminescence sensor response in the presence of various concentrations of linear alcohols.

ACKNOWLEDGEMENT

The work has been supported by projects GAČR GA206/09/0375 and TAČR TA01011363.

REFERENCES

- [1] Smith RL, Collins SD: Journal of Applied Physics, 71 (1992), 8, R1-R22
- [2] Canham LT: Applied Physics Letters, 57 (1990), 10, 1046-1048
- [3] Robins EG, Stewart MP, Buriak JM: Chemical Communications 24 (1999), 2479-2480
- [4] Fella S, Ozanam F, Chazalviel JN, et al: Journal of Physical Chemistry B, 110 (2006), 4, 1665-1672
- [5] Haraz FA: Journal of the Electrochemical Society, 153 (2006), 5, C349-C356
- [6] Vrkošlav V, Jelinek I, Broncová G, et al: Materials Science and Engineering C 26 (2007), 5-7, 1072-1076

ELECTROCHEMICAL ANALYSIS OF PCR AMPLICONS WITH INCORPORATED 7-DEAZAPURINES

Zdenka VYCHODILOVA*¹, Hana PIVONKOVA¹, Miroslav FOJTA¹

¹Department of Biophysical Chemistry and Molecular Oncology, Institute of Biophysics Academy of Sciences of the Czech Republic, v.v.i., Kralovopolska 135, 612 65 Brno, Czech Republic
*pannenka@sci.muni.cz

ABSTRACT

In this paper electrochemical behavior of 347 bp long PCR amplicons with enzymatically incorporated 7-deazapurines fully or partly replacing natural purines is described. Samples were measured at hanging mercury drop electrode (HMDE) and pyrolytic graphite electrode (PGE) by adsorptive transfer stripping voltammetry (AdTSV) technique. Electrochemical measurements were done by square wave voltammetry (SWV) and cyclic voltammetry (CV).

INTRODUCTION

7-deazapurines are usually used as basic elements for integration of electrochemically active species into the DNA. Bases are linked through N7 with e.g. sulphur or organometallic groups, osmium and other metal complexes (1-3) which yield specific signal that can be measured electrochemically. One of the metal complexes making linkage to N7 is *cis*-diamminedichloroplatinum(II) (cisplatin) known for its antitumor activity (4). Primarily, intrastrand cross-links between neighboring purine residues are created which can cause conformational changes of the involved DNA. Such bended or unwinded DNA can lose a specific binding site for important nuclear proteins (5) or can be recognized by other set of proteins.

Until 2010 there was no direct electrochemical analysis of long DNA with enzymatically incorporated 7-deazaguanine (G*) or 7-deazaadenine (A*) used as electrochemical label by itself (6). In this paper are shown results of direct analysis of PCR products containing G* or A* in different percentages.

MATERIAL AND METHODS

Amplification reaction was held in solution with following components and amounts: 500 ng template DNA (pT7-7 containing wild type p53 protein sequence, length 347 bp); 0,5 μ M forward and reverse primer; 3 U *Pfu* DNA polymerase; 125 μ M dCTP, dTTP, dATP, dGTP, dA*TP and dG*TP each. We prepared a set of samples with increasing amount of 7-deazaguanine, G* (25, 50, 75, 100 % of G*) or 7-deazaadenine, A* (25, 50, 75, 100 % of A*) replacing natural bases. In control sample only non-modified nucleobases were used (0 G* or A*). PCR conditions (C1000 Thermal Cycler, BioRad): 30 cycles; denaturation step 90 s in 94 °C, annealing step 120 s in 60 °C, extension step 180 s in 72 °C. PCR was followed by purification of amplicons by QIAquick PCR purification kit

and measurement of DNA concentrations using NanoDrop ND-1000 spectrophotometre (NanoDrop Technologies, USA).

Electrochemical measurements of modified nucleobases were performed using Autolab system with VA-Stand 663 Metrohm working station and/or CHI440 Electrochemical Workstation (CHInstruments, Inc., USA). The experiments were done at room temperature in a three-electrode setup (PGE or HMDE as working electrode, Ag/AgCl/3 M KCl as reference, and platinum wire as counter electrode). When measured on HMDE the buffer was 0,3 M ammonium formate pH 6,97. When measured on PGE, the buffer was sodium acetate pH 5. The PCR products were analyzed by using *ex situ* (adsorptive transfer stripping, AdTS) cyclic voltammetry (CV) and AdTS square wave voltammetry (SWV).

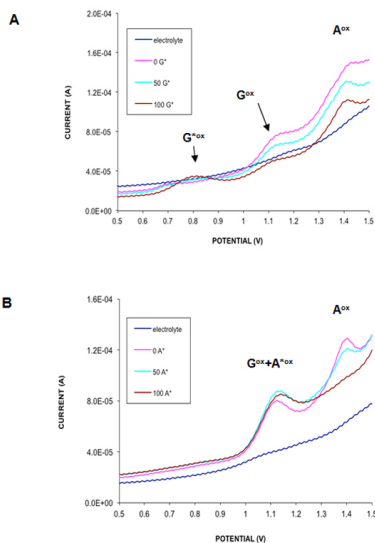
The DNA was accumulated on the electrode surface from 4 μ l aliquots containing 0,2 M NaCl during 60 s. The electrode was rinsed by deionized water and put into the electrochemical cell. CV settings on HMDE: initial potential, 0,0 V; vertex potential, -1,85 V; final potential, 0,0 V; scan rate, 1 Vs⁻¹. SWV settings on PGE: initial potential, 0,0 V; final potential, 1,5 V; frequency, 200 Hz; pulse amplitude, 25 mV.

RESULTS AND DISCUSSION

Polymerase chain reaction (PCR) was used for enzymatic incorporation of 7-deazapurine nucleobases into DNA. These bases were producing electrochemical signal necessary for analysis of electrochemical behavior such modified DNA. AdTS SWV on PGE confirmed that 7-deazapurines are electrochemically oxidized at less positive potentials (see fig. 1), compared to the natural purine nucleobases (6). Standard G^{ox} potential is 1,15 V, standard A^{ox} potential is 1,35 V. Due to increasing amount of 7-deazaguanine (G*) in amplicon chain G^{ox} peak decreased and new G*^{ox} peak appeared at potential 0,8 V (fig. 1A, brown curve). It means that G* can be utilized as quite cheap and reliable label in electrochemistry. In the case of 7-deazaade-

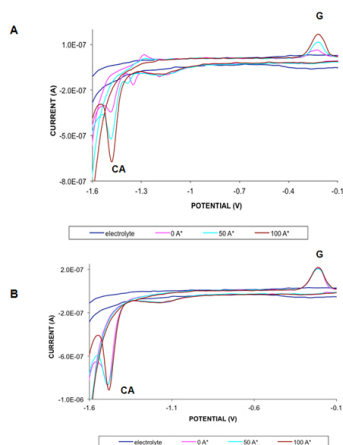
nine (A*) oxidation potential is the same as that of G^{ox} peak at 1,15 V and thus it is not possible to distinguish between these two peaks (fig. 1B).

Figure 1: AdTS SWV on PGE. PCR product with different amount of purine nucleobases replaced by 7-deazapurines were adsorbed on the electrode surface. Time of adsorption: 60 s. Samples were measured in sodium acetate buffer pH 5 (dark blue curve). SWV settings: initial potential, 0,0 V; final potential, 1,5 V; frequency, 200 Hz; pulse amplitude, 25 mV. (A) DNA containing 0, 50 and 100 % of 7-deazaguanines (G*) instead of natural guanines, (B) DNA containing 0, 50 and 100 % of 7-deazaadenines (A*) instead of adenine residues.



Using AdTS CV on HMDE (ds) and singlestranded (ss) DNA molecules containing different amount of G* or A* incorporated into the molecules instead of standard purine nucleobases were studied. When we focused on G peak (at -0,25 V) and CA peak (at -1,5 V) visible on cyclic voltammograms of ss and ds DNAs there were no big differences in their heights in the case of G* incorporation. On the other hand voltammograms of ds molecules with integrated A* showed clearly correlation between the level of modification and peaks heights (see fig. 2A). With higher degree of A* modification G peak increased and CA peak decreased. This suggests that the double helix is unwinding and nucleobases can easily get to electrode surface, the modification make DNA less stable. When AdTS CV of ss A* modified DNA was measured, no differences occurred with different degree of modification (fig. 2B).

Figure 2: AdTS CV on HMDE. Comparison of native ds (A) and denaturated ss (B) PCR products with 7-deazaadenines (A*) nucleobases incorporated into the molecule instead of natural adenines. Samples contain 0, 50 and 100 % of A*. Time of adsorption: 60 s. Samples were measured in 0,3 M ammonium formate buffer pH 6,97. CV settings: initial potential, 0,0 V; vertex potential, -1,85 V; final potential, 0,0 V; scan rate, 1 Vs⁻¹



CONCLUSION

7-deazapurines are well known species in electrochemical labeling. Due to the absence of N7 7-deazapurines are incapable of forming Hoogsteen base pairs and DNA with such modified bases is not able to form multistranded DNA structures. In this work it is shown that using electrochemical methods it is possible to easily analyze DNA with enzymatically incorporated 7-deazapurines fully or partly replacing natural purines .

At carbon electrode both 7-deazapurines yield oxidation peaks at less positive potentials compared to the natural adenine and guanine residues. At mercury electrode 7-deazaguanine does not yield peak G (which is produced by natural guanine) or any other specific signal (natural guanine does). Other electrochemical experiments showed increasing intensities of peak CA and peak G in the case of increasing modification of dsDNA with 7-deazaadenine. This behaviour suggests a lower stability of DNA double helix with a high amount of 7-deazaadenine.

REFERENCES

- [1] H. Cahova, L. Havran, P. Brazdilova, H. Pivonkova, R. Pohl, M. Fojta and M. Hocek. *Angew Chem Int Edit* 47, 2059-2062 (2008).
- [2] P. Horakova, H. Macickova-Cahova, H. Pivonkova, J. Spacek, L. Havran, M. Hocek and M. Fojta. *Org Biomol Chem* 9, 1366-1371 (2011).
- [3] H. Macickova-Cahova, R. Pohl, P. Horakova, L. Havran, J. Spacek, M. Fojta and M. Hocek. *Chem-Eur J* 17, 5833-5841 (2011).
- [4] B. Rosenberg, L. VanCamp, J. E. Trosko and V. H. Mansour. *Nature* 222, 385-386 (1969).
- [5] Y. W. Jung and S. J. Lippard. *J Biol Chem* 278, 52084-52092 (2003).
- [6] H. Pivonkova, P. Horakova, M. Fojtova and M. Fojta. *Anal Chem* 82, 6807-6813 (2010).

HYPHENATION OF ELECTROCHEMISTRY WITH MASS SPECTROMETRY AS A POWERFUL TECHNIQUE TO STUDY PESTICIDES IN ENVIRONMENTAL MATRICES

Jana JAKLOVA DYTRTOVA^{1*}, Michal JAKL², Renata NORKOVA¹

¹Institute of Organic Chemistry and Biochemistry, Academy of Sciences of the Czech Republic, v.v.i., Flemingovo namesti 2, 166 10 Prague 6, Czech Republic; dytrtova@uochb.cas.cz

²Department of Agro-Environmental Chemistry and Plant Nutrition, Faculty of Agrobiolgy, Food and Natural Resources, Czech University of Life Sciences Prague, Kamycka 129, 165 21 Prague – Suchdol, Czech Republic

ABSTRACT

The detection of pesticides in environmental matrices is very complicated analytical procedure. It is a challenge for hyphenation methods to find a competitive alternative to chromatographic methods. Pesticides, such as tebuconazole (triazole fungicide), create in soil solution complexes with cations, which make the direct detection of pesticides impossible. The solution of the problem lies in creation of very stable complex (more stable than others) e.g. copper/tebuconazole and to detect this complex. The copper cations are supplied to the solution continuously from oxidation of copper electrode. The copper/tebuconazole complex is consequently detected using ESI-MS.

INTRODUCTION

Detection of pesticides in environmental matrices such as soil solution or plant tissues is a big challenge for modern analytical methods. Methods with chromatographic separation are widely used, however their detection limit (10^{-6} mol L⁻¹) as well as the time of analysis (tens of minutes) are the limiting factors. Another alternative to chromatographic methods affords hyphenation of electrochemistry (EC) with electrospray ionization mass spectrometry (ESI-MS).

The biggest problem of pesticides analysis in environmental samples is their complexation with many inorganic substances, mainly cations [1]. The total amount of a pesticide is spread into many species and its direct detection is impossible. The EC-ESI-MS method takes advantage of high stability of copper complexes with tebuconazole (**Teb**, a widely used fungicide) to create very stable complex [CuTeb]⁺ with appearance energy 223 kJ mol⁻¹. The presence of Cu²⁺ cation in a solution (in a sample) causes decay of other complexes with **Teb** such as [CTeb]⁺ (where C can be Ca, K, Na, Mg, Cd and Zn) [2].

The detection of electrochemically created [CuTeb]⁺ using ESI-MS is the core of the new presented methods. Using EC-ESI-MS we are able to satisfactorily detect concentrations of **Teb** around $2.5 \cdot 10^{-7}$ mol L⁻¹ without prior pre-concentration. The total time for one measurement is lower than 3 minutes.

MATERIAL AND METHODS

Electrochemical techniques (EC) are very sensitive tool to determination of many organic compounds. The pitfall of EC is their low selectivity. On the other hand they can extend the knowledge about a sample and electrochemical

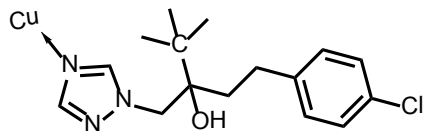
properties. The hyphenation of EC front ESI-MS represents a powerful tool to study electrochemical properties of electroactive compounds together in a sample.

The electrochemical device [3,4] was controlled using computer controlled polarographic/voltammetric analyzer PC-ETP, Polaro-Sensors, Prague, Czech Republic), with 2.3 software (JH IPC, v.v.i., Czech Republic) [5] and POLAR.PRO software v. 5.1 (Polaro-Sensors, Czech Republic). The ESI-MS experiments were performed with a Finnigan LCQ Advantage ion-trap mass spectrometer (ThermoFinnigan, San Jose, CA, USA) fitted with an electrospray ionization source operated in positive and negative-ion mode, with setup followed [6].

RESULTS AND DISCUSSION

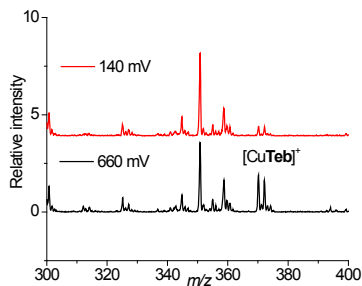
The [CuTeb]⁺ complex (Fig. 1) with *m/z* of leading isotopes 370 was generated in electrochemical cell setup during oxidation of Cu electrode.

Figure 1.: The structure of [CuTeb]⁺ complex



The amount of generated [CuTeb]⁺ depends on inserted potential at Cu electrode (Fig. 2). In higher potentials the amount of generated Cu²⁺ is higher. The Cu²⁺ generated during the Cu electrode oxidation is reduced by **Teb** [7] as well as during electrospray process [8].

Figure 2.: Positive mode spectra of soil solution (25 %) contaminated with tebuconazole (**Teb**) with the addition of acetate buffer (25 %) and methanol (50 %)



The advantage of electrochemical generation of Cu^{2+} instead of addition of some copper salts such as CuCl_2 lies in: (i) in-contamination of the sample with copper counter ion becoming from the salt and (ii) prevention of creation uncharged $[\text{CuXTeb}]^0$ (which are invisible in in ESI-MS spectra) complexes originated from metal salt precursor with an inorganic ligands (such as Cl^-).

The minimal concentration, which was satisfactorily done using this method is $2.5 \cdot 10^{-7} \text{ mol L}^{-1}$ [6], what is almost one order lower concentration than is possible to be measured using chromatographic methods [9]. The total time required to one measurement is less than 3 minutes. The measurements are without prior sample workup.

CONCLUSION

The EC-ESI-MS technique is an alternative method to chromatographic methods. It takes advantageous high stability of copper complexes with triazoles (in this case tebuconazole) to decay complexes with other cations yielding in detection of Cu/tebuconazole complex using ESI-MS. The hyphenated techniques allows to detect tebuconazole in soil solution in concentrations about $2.5 \cdot 10^{-7} \text{ mol L}^{-1}$ without prior preconcentration of the sample in competitively smaller time than chromatographic methods.

ACKNOWLEDGEMENTS

This work was supported by the Academy of Sciences of the Czech Republic (RVO61388963) and by the S grant of MSMT CR.

REFERENCES

[1] Jaklová Dyrtrtová J, Jakl, M, Schröder, D, et al.: Rapid Communications in Mass

Spectrometry, 25 (2011), 1037-42.
 [2] Norková R, Jaklová Dyrtrtová, J, Jakl, M, et al.: Water, Air, & Soil Pollution, in press (2012).
 [3] Jaklová Dyrtrtová J, Jakl, M, Schröder, D. Modern Electrochemical Methods XXX, 24.-28.5.2010 2010, Jetřichovice, pp 89-92.
 [4] Jaklová Dyrtrtová J, Jakl, M, Schröder, D. Modern Electrochemical Methods XXXI, 23.-27.5.2011 2011, Jetřichovice, pp 69-73.
 [5] Navrátil T, Yosypchuk, B, Barek, J: Chemia Analytyczna, 54 (2009), 1, 3-17.
 [6] Jaklová Dyrtrtová J, Jakl, M, Schröder, D, et al.: Analytical Chemistry, submitted (2012).
 [7] Sherif E-S M, Erasmus, R M, Comins, J D: Journal of colloid and interface science, 311 (2007), 1, 144-51.
 [8] Révész Á, Milko, P, Žabka, J, et al.: Journal of Mass Spectrometry, 45 (2010), 11, 1246-52.
 [9] Trösken E R, Bittner, N, Völkel, W: Journal of Chromatography A, 1083 (2005), 1-2, 113-9.

TiO₂/GOLD NANOCOMPOSITE FOR BIOSENSING APPLICATIONS

Matej DZURO¹, Vojtech SVATOS¹, Radim HRDY^{1,2},

Jana DRBOHLAVOVA^{1,2*} and Jaromir HUBALEK^{1,2}

¹Brno University of Technology, Faculty of Electrical Engineering and Communication,
Department of Microelectronics, Technicka 3058/10, 616 00 Brno, Czech Republic

²Central European Institute of Technology, Brno University of Technology, Technicka 3058/10,
616 00 Brno, Czech Republic

*drbohla@feec.vutbr.cz

ABSTRACT

The aim of the work described in this paper is to prepare electrochemically an optical sensor consisting of TiO₂ quantum dots (QDs) using nanoporous Al₂O₃ template in the first step and to modify the surface of QDs with gold layer by evaporation process, again using nanoporous template, in the second step. This easy, cheap and rapid approach provides homogenous and highly ordered distribution of both nanostructures on substrate. The final objective is to characterize the physical parameters and fluorescent properties of TiO₂/Au sensor designed for optical detection of biomolecules such as DNA and proteins.

INTRODUCTION

The big challenge in the production of nanostructured surfaces inheres in the uniformity and the reproducibility of the nanostructures size and their spatial arrangement. The template based nonlitographic methods employing the alumina nanoporous template represent fast, inexpensive and easily reproducible approach of creating the nanostructured surfaces on substrates. Among the various metal and semiconducting nanostructures, QDs gain the outstanding interest of the scientists, due to their unique electronic and optical properties, which make them attractive candidates for optical sensor array regarding their fluorescence effect [1, 2]. Further modification of deposited QDs surface with other fluorescent material, such as noble metals, may enhance the primary luminescence intensity of QDs and provides the suitable affinity to biomolecules used for further functionalization.

In this work, titanium dioxide has been chosen as a material for QDs creation due to its non-toxicity and gold as biocompatible material for QDs luminescence enhancement. The fabrication process lies in anodic oxidation of titanium layer using Al₂O₃ nanoporous template, which also serves for evaporation of gold shell with required thickness after nanopores extension. The combination of both template based and evaporation methods enables to cover even large substrate with desired nanocomposite array.

EXPERIMENT

Titanium and aluminium layer deposition

A high-purity titanium and aluminium layers were sputtered on 4 inch silicon wafer by magnetron sputtering (Leybold-Heraeus Z 550). Two thickness combinations of Ti/Al bilayers were tested: 20 nm/500 nm and 150 nm/250 nm.

Formation of TiO₂ QDs in anodization process

The anodization procedure takes place in the utility model equipment for electrochemical post-processing deposition fabricated in laboratory [3]. Thanks to different anodizing behaviour of Al and Ti layers, the same electrolyte during the whole process can be applied. Sulphuric acid was chosen as an electrolyte since it is known to provide smaller pore diameter in template compared to other commonly used electrolytes. The anodization process ran in constant potential mode under these conditions: 3 M H₂SO₄, at 5 V and 11 °C. Anodization of alumina is performed in two-step process in order to get the homogeneous pore distribution. During the first step of anodization, about 90% of aluminium was oxidized and the alumina template was removed by etching in a mixture of H₃PO₄ (50 ml L⁻¹) and CrO₃ (30 g L⁻¹) at 60 °C for 5 min in the case of 500 nm Al and for 2.5 min in the case of 250 nm Al. The remaining 10% of aluminium was anodized in the second step which resulted in the creation of TiO₂ QDs.

Gold shell evaporation

After the second step of anodization, the nanopores were extended in 5% solution of H₃PO₄ for 5–8 min at 30 °C and finally gold was evaporated. Gold evaporation through thin alumina template provided the gold distribution only in the form of thin shells on TiO₂ QDs surface. Gold evaporation lasted various times in order to achieve the thickness from 2 nm to 10 nm on each sample. After evaporating of gold, the remaining alumina template was etched under the conditions described above.

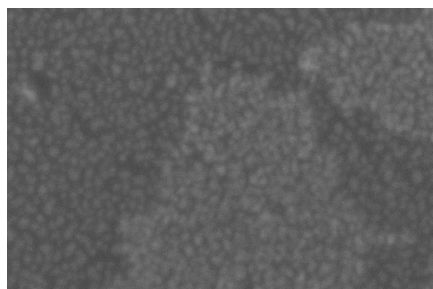
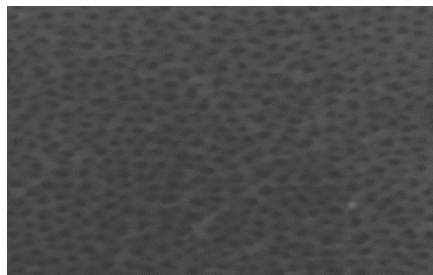
Characterization of physical parameters

The size of TiO₂/gold nanocomposite was estimated using scanning electron microscopy (SEM) Mira II MLU (Tescan Mira, Brno, Czech Republic) under following conditions: work distance of 2.5 nm, high vacuum mode (10⁻³ Pa), voltage of 15–20 kV, and spot size of 2.4 nm. The photoluminescence properties of non-annealed TiO₂/gold QDs array were characterized by fluorescence spectroscopy (Horiba, Jobin-Yvon) with laser diode excitation at 350 nm and using photomultiplier (T1 PMT) detector.

RESULTS AND DISCUSSION

SEM observation of alumina template after pore widening showed the pore size was about 10–15 nm (see Figure 1 left). After gold evaporation and template removing, we found that TiO₂ QDs with diameter of 8–10 nm are covered homogeneously with thin gold shells (see Figure 1 right); however it was difficult to observe the exact gold thickness due to a weak contrast of both materials. Therefore, more precise analysis of gold amount should be done, for example using energy-dispersive X-ray spectroscopy (EDX).

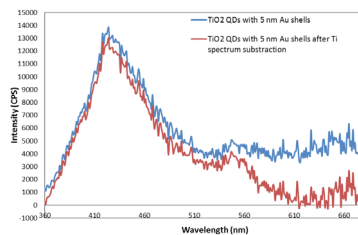
Figure 1. Alumina template with extended nanopores (10–15 nm in diameter) ready for gold evaporation (up) and maps of 2 nm thick gold layer attached on TiO₂ QDs after final template etching (down)



The analysis of fluorescence spectra of non-annealed amorphous TiO₂/gold QDs, repre-

sented in Figure 2, showed no remarkable luminescence intensity (only one small peak is observed at 425 nm), which is in agreement with the requirement of QDs crystallinity for achieving the fluorescence properties. Therefore, further optical characterization will be performed after TiO₂/gold QDs annealing in vacuum, during which amorphous titania is transformed to anatase (at temperature of 500 °C). This crystallographic phase is supposed to show several times higher intensity of luminescence with one narrow and symmetric strong peak in visible range of electromagnetic spectrum.

Figure 2. Photoluminescence spectrum of non-annealed TiO₂/gold QDs with 5 nm Au shells



CONCLUSION

The fabricated self-ordered TiO₂/gold nanocomposite array with TiO₂ QDs size of 10 nm and various gold nanoshell thicknesses represents a promising platform for biosensing applications, namely for optical detection of biomolecules, however further study of optical properties should be performed to observe photoluminescence intensity after TiO₂/gold QDs annealing.

ACKNOWLEDGEMENT

The work has been supported by the grants GACR P102/10/P618, KAN 208130801 and CEITEC CZ.1.05/1.1.00/02.0068.

REFERENCES

- [1] Drbohlavova J, et al., International Journal of Molecular Sciences, 10 (2009), 2, 656-673
- [2] Drbohlavova J, et al.: Nanoscale Research Letters, 7:123 (2012), 1-4
- [3] Hubalek J, et al.: In Proceedings of the Eurosensors XXIII Conference 2009; Lausanne, Switzerland. (2009), 36-39

INTRACELLULAR SEQUESTRATION OF ELLIPTICINE IN NEUROBLASTOMA CELLS: ROLE OF VACUOLAR-ATPASE

Jan HRABETA¹, Jitka POLJAKOVA², Jiri UHLIK³, Marie STIBOROVA²,
Rene KIZEK⁴, Tomas ECKSCHLGAER^{*}

¹Department of Pediatric Hematology and Oncology, 2nd Medical School, Charles University and University Hospital Motol, V Uvalu 84, 15006 Prague 5, Czech Republic

²Department of Biochemistry, Faculty of Science, Charles University, Albertov 2030, 128 40 Prague 2, Czech Republic

³Department of Histology and Embryology 2nd Medical School, Charles University, Plzenska 130, 150 00 Prague 5, Czech Republic

⁴Department of Chemistry and Biochemistry, Mendel University, Zemedelska 1, 613 00 Brno, Czech Republic

*eckschlagertomas@yahoo.com

INTRODUCTION

Neuroblastoma (NBL) is the third most common pediatric cancer and is responsible for approximately 15 % of all childhood cancer deaths [1]. It is a malignant tumor consisting of neuronal crest derived undifferentiated neuroectodermal cells. The clinical hallmark of NBL is heterogeneity. Some of the tumors undergo spontaneous regression or differentiate into benign ganglioneuromas, some are curable with surgery and little or no adjuvant therapy and some progress despite intensive multimodal therapy. This clinical diversity is closely correlated with the molecular biological features of the tumor. Approximately 40% of NBL are in the high risk neuroblastoma (HR-NBL) group, and therapeutic improvements in the past decade have not substantially improved their outlook compared with other pediatric malignancies. Chemotherapy is ultimately ineffective in curing HR-NBL, because drug-resistance arises in most of patients despite intensive therapy. Recent studies have provided a link between increased metastatic potential and drug-resistant phenotypes, indicating that in addition to the development of drug resistance, chemotherapy of tumors may cause changes in their biological characteristics. Treatment of older children with disseminated NBL continue to be great challenges for pediatric oncologists. To achieve suitable treatment, drugs are used in combinations. Over the last 40 years the prognosis for most childhood cancers has improved, but not for HR-NBL even though a delivering intensive therapy, suggesting the need for development of new therapies [1]. One of the future possibilities in therapy of HR NBL seems to be ellipticine /ELLI/.

ELLI exhibit antitumor activities. The main reasons for the interest in ellipticine clinical purposes are its efficiency against several types of cancer, limited toxicity particularly lack of hematotoxicity. ELLI arrests cell cycle progression by regulating the expression of cyclinB1 and Cdc2 and by phosphorylation of Cdc2. ELLI induces apoptosis by the generation of free radicals, the activation of Fas/Fas ligand system,

the regulation of Bcl-2 family proteins, by increase of wild-type p53, and the initiation of the mitochondrial apoptosis pathway. ELLI also uncouples mitochondrial oxidative phosphorylation. However, the precise molecular mechanism responsible for these effects has not yet been explained. It was suggested that the prevalent mechanisms of its antitumor activity is intercalation and topoisomerase II inhibition. We have demonstrated that ELLI covalently binds to DNA after enzymatic activation, suggesting a third possible mechanism of action [2].

The development of resistance to cytostatic agents is a major cancer therapy problem and has been the focus of many research efforts [3]. Tolerance to one agent is often accompanied by cross-resistance to a variety of others, often unrelated compounds. The behavior may be explained by a selection of subclones of cells within the original tumor that have the ability to survive the cytotoxic effects of anticancer drugs [3]. At the cellular level, a number of resistance mechanisms can operate. These mechanisms include drug efflux via membrane pumps (ABC transporters such as P-glycoprotein), drug metabolism, including inactivation or failure to activate a prodrug, alteration in the abundance of the target protein, for example the topoisomerase II enzyme, mutation of the target protein and/or inactivation of pathways leading to cell death, such as apoptotic signaling [4]. Vacuolar (H⁺)-ATPases is the enzyme complex reside within many intracellular compartments, including trans-Golgi network, endosomes, lysosomes, secretory granules, and have been also identified in the plasma membrane of certain cells. These proteins cover a number of functions in a variety of normal as well as tumor cells in processes such as receptor-mediated endocytosis, intracellular targeting of lysosomal enzymes, protein processing and degradation, and the coupled transport of small molecules. V-ATPases have a important role in tumor metastasis,

chemoresistance and cancer progression [5]. Chemoresistance may be related to acidification of intracellular compartments of cancer cells and V-ATPase-dependent ion trapping of the cationic form of drugs in acidic vesicles as lysosomes. Role of V-ATPase and lysosomal compartment in metabolism and toxic action of ellipticine is not known. The aim of our work was to study the relationship between ELLI sequestration and chemoresistance in NBL and possibility to influence this mechanism.

MATERIAL AND METHODS

Cell lines: The UKF-NB-4 line was established from recurrent bone marrow metastases of HR-NBL. This line was kindly provided by Dr. J. Cinatl Jr. (Johann Wolfgang Goethe University, Frankfurt am Mein, Germany). The ELLI resistant line designated UKF-NB-4^{ELLI} we established by incubation of UKF-NB-4 with increasing concentrations of ellipticine. Lines were grown in IMDM (Lonza Inc, Allendale, USA) supplemented with 10% fetal calf serum (PAA Laboratories, Pasching, Austria). Medium for UKF-NB-4^{ELLI} contained 2.5 μ M ELLI. The drug-resistance of UKF-NB-4^{ELLI} to ELLI was verified using the MTT test. The resistant lines showed 2.7 times increase in resistance to ellipticine measured as IC₅₀ [4].

Western blotting: Protein concentrations were assessed using a DC protein assay kit (Bio-Rad, Hercules, USA). 40 μ g of protein was subjected to SDS-PAGE electrophoresis. After migration, proteins were transferred to a nitrocellulose membrane and incubated with non-fat milk (Bio-Rad, Hercules, USA). The membranes were exposed to antibodies to LC3 (Novus Biologicals) and actin (SigmaAldrich) as control overnight at 4°C. Membranes were washed and exposed to goat anti-rabbit anti-IgG (H+L) – HRP conjugate secondary (Bio-Rad, Hercules, USA), and the antigen-antibody complex was visualized using chemiluminescence (Immun-Star HRP Substrate, Bio-Rad, Hercules, USA). Subcellular localization of ELLI was detected by confocal microscopy, as lysosomal marker was used LysoTracker Red (LifeTechnologies, Carlsbad, USA). Ultrastructure of vacuoles was evaluated by electron transmission microscopy.

RESULTS AND DISCUSSION

ELLI treatment is a causes of significant and concentration-dependent cytoplasmic vacuolization of the NBL cells. The vacuoles were detectable already 30 minutes after the treatment and ELLI was concentrated to the vesicular structures in cytoplasm. Electron microscopy verified that vacuoles have not typical morphological signs of autophagosomes. This finding was proved by Western blotting detection of LC3, that did not find increased LC3 II form. We detected ELLI in those vacuoles by fluorescent confocal

microscopy. Staining with LysoTracker verified that those vacuoles are lysosomes. Vacuolization and intravesicular ellipticine-associated fluorescence was abolished by co-treatment with the specific V-ATPase inhibitor bafilomycin A1 [6] and lysomotropic agents chloroquine. V-ATPase plays a pivotal role in acidification and protein degradation in the lysosomes [5]. Chloro-quine and bafilomycin pretreatment increased the efficiency of ellipticine in both tested cell lines UKF-NB-4 and UKF-NB-4^{ELLI}. The significance of lysosomal sequestration was also suggested by findings of overexpression in UKF-NB-4^{ELLI} in comparison with UKF-NB-4 [4].

CONCLUSIONS AND FUTURE DIRECTIONS

ELLI is sequestered to the vesicular structures probably of lysosomal origin, this sequestration may be one of the mechanisms that cause chemoresistance. Specific V-ATPase inhibition or using of lysosomotropic drug chloroquine increased ELLI efficiency. One may speculate that drug sequestration may play role in resistance to other anticancer drugs. Inhibition of sequestration of drugs could thus increase the effectiveness of chemotherapy.

ACKNOWLEDGMENT.

This work was supported from GACR grant No. P301/10/0356

REFERENCES:

- [1] Maris JM. Recent advances in neuroblastoma. *N Engl J Med.* 2010; 362: 2202-11
- [2] Stiborova M, Poljakova J, Martinkova E, et al. Ellipticine cytotoxicity to cancer cell lines - a comparative study. *Interdiscip Toxicol.* 2011; 4: 98-105.
- [3] Raguz S, Yague E. Resistance to chemotherapy: new treatments and novel insights into an old problem. *Br J Cancer.* 2008; 99: 387-91
- [4] Procházka P, Libra A, Zemanová Z, Hřebáčková J, Poljaková J, Hraběta J, Buněk M, Stiborová M, Eckschlager T, Mechanisms of ellipticine-mediated resistance in UKF-NB-4 neuroblastoma cells. *Cancer Sci.* 2012;103:334-41
- [5] Nishi T, Forgac M. The vacuolar (H⁺)-ATPases--nature's most versatile proton pumps. *Nat Rev Mol Cell Biol.* 2002 Feb;3(2):94-103.
- [6] Bowman EJ, Siebers A, Altendorf K. Bafilomycins: a class of inhibitors of membrane ATPases from microorganisms, animal cells, and plant cells. *Proc Natl Acad Sci U S A.* 1988; 85: 7972-7976.

PIEZOELECTRIC AND OPTICAL BIOSENSORS FOR DETECTION OF *BACILLUS ATROPHAEUS*

Zdenek FARKA^{1*}, David KOVAR^{1,2}, Petr SKLADAL^{1,2}

¹Department of Biochemistry, Faculty of Science, ² CEITEC MU, Masaryk University, Kotlářská 2, 611 37 Brno, Czech Republic

*farka@mail.muni.cz

ABSTRACT

Interactions of antibodies with the bacterium *Bacillus atrophaeus* were studied using piezoelectric (PZ) and surface plasmon resonance (SPR) based biosensors, with the aim of future development of biosensor for *Bacillus* species. Antibodies were covalently immobilised on gold surfaces of PZ crystal resonators and SPR chips. QCM Analyzer and Biacore 3000 were used for real-time and label-free measurements of immunocomplexes. Concentrations of *B. atrophaeus* below 10⁵ CFU ml⁻¹ were successfully detected.

INTRODUCTION

Biosensor can be defined as an analytical device with sensitive biological element which is in close contact or a tightly linked part of physicochemical transducer. Biological part provides either biocatalytical (e.g. enzyme) or bioaffinity (e.g. antibody) recognition.

Piezoelectric biosensors are based on the piezoelectric effect – alternating current applied on the crystal causes high-frequency vibrations; for biosensing, the thickness shear vibrations represented by the quartz crystal microbalance (QCM) system are mostly used thanks to robust performance and simple construction of the driving electronics [1].

Optical biosensors are based on the measurements of light intensity or changes of advanced optical properties of biomaterials. In recent years, the intrinsic sensing represented by surface plasmon resonance has been receiving increasing attention [2].

This contribution is devoted to study of interactions between antibodies [3] and *Bacillus atrophaeus*. It is a gram-positive sporulating non-pathogenic bacterium similar to *Bacillus anthracis* which is a well-known pathogen causing anthrax. This is why *B. atrophaeus* is being widely used as a safe model microorganism for development and optimisation of detection methods for *B. anthracis* [4].

MATERIAL AND METHODS

To obtain sufficient amounts of spores of *Bacillus atrophaeus* (ATCC 9372; received from Czech Collection of Microorganism), the cultivation procedure [5] was optimised. The aliquot of frozen suspension containing spores was mixed with the cultivation medium and after 6 hours, the culture was sterilely inoculated to the sporulation medium enriched with Ca²⁺ and Fe²⁺ ions. Sporulation was prolonged from 1 to 3 weeks. The obtained spores were purified using gradient centrifugation in sucrose solution [6]. Amount and purity of spores was checked using phase contrast with the optical microscope

Olympus BX41.

QCM Analyzer manufactured by Keva (Brno, Czech Republic) was used for PZ measurements. PZ biosensor was created by immobilisation of anti *Bacillus* antibodies (GenWay, LSBio, and Tetracore) on the gold surface of 10 MHz PZ crystal (ICM, Oklahoma City, USA) activated by protein A [7]. After placing into the flow-through cell, this biosensor followed affinity interactions in real-time [8]. Solutions were transported through the cell and binding interactions were represented by changes of signal (resonance frequency and resistance of the PZ crystal). Optimal flow rate was 17 µl min⁻¹ and 50 mM phosphate buffer pH 7.0 (PB) was used as the carrier.

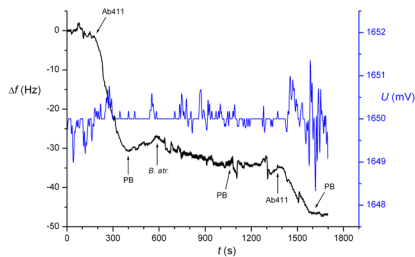
Optical measurements were carried out using Biacore 3000. Its measuring system is formed by a glass prism and a layer of gold which is in contact with the 4-channel microfluidic cell [9]. Chips CM5 and buffers HBS-P were used. The carboxymethylated dextran sensing surface was activated using the mixture of EDC (1-ethyl-3-(3-dimethylaminopropyl)carbodiimide) and NHS (N-hydroxysuccinimide) and antibody dissolved in acetate buffer was bound. Spores and cells were injected and the association and dissociation phases of the immunoaffinity interaction were measured, flow rate was 5 µl min⁻¹. Immunosensing surface was regenerated using 50 mM HCl for 1 min.

RESULTS AND DISCUSSION

Interactions of 7 antibodies with *B. atrophaeus* ATCC 9372 were studied using both techniques. Initially, antibodies were bound to PZ crystals through the covalently linked protein A, the oriented attachment of IgG is obtained in this way. Only 2 out of 7 antibodies were specific against the chosen *Bacillus* strain. The interacting antibodies were Ab151 (LS-C103151) and Ab411 (LS-C103411), both supplied from LSBio. To improve sensitivity, the sandwich assay was used. In Fig. 1, the surface-bound Ab411 cap-

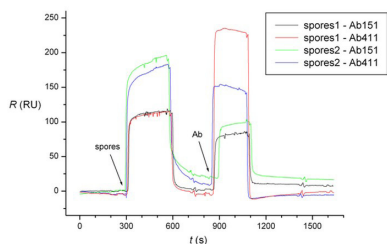
tured *B. atrophaeus* spores and the second layer of Ab411 formed the sandwich immunocomplex.

Figure 1.: Interactions of *B. atrophaeus* and Ab411 in sandwich assay measured by QCM. Resonant frequency Δf and resistance represented by the AGC signal U are shown.



Evidently, the rather low signal due to the direct binding of the microbial spores was nicely enhanced by the secondary antibody, which also caused increased change of resistance. Further measurements were carried out using Biacore 3000; this was anticipated to be more sensitive than much cheaper QCM Analyzer. Antibodies were covalently immobilised to SPR chips using EDC/NHS. Afterwards, interactions between *B. atrophaeus* (both spores and native cells) and antibodies were studied. Sandwich assay of *B. atrophaeus* spores can be seen in Fig. 2. Antibody Ab411 was immobilised on the chip, *B. atrophaeus* was captured and then 2 different antibodies (Ab151 and Ab411) were allowed to form the sandwich complex.

Figure 2.: Binding interactions of *B. atrophaeus* and Ab411 in sandwich assay (with Ab151 or Ab411) measured by SPR.



Cultivation and purification of spores was optimised. It can be seen in Fig. 2 that the optimised procedure (spores2) gives better results than the commonly recommended procedure (spores1). Antibodies Ab151 and Ab411 again formed sandwich. Sensitivity increased with Ab151. Unfortunately with Ab411 the signal dropped. The most probable reason is that free antibody has higher affinity to *B. atrophaeus* than immobilised one and it is able to remove the spores out of the sensor surface.

Interactions of spores and native cells with antibodies were also compared, the Ab-spores complexes exhibiting higher stability which agrees with assumptions. The SPR experiments with Biacore 3000 confirmed interaction of *B. atrophaeus* only with Ab151 and Ab411. Furthermore, the results obtained with Biacore 3000 seem not significantly better compared to the QCM Analyzer; however, the automated operation of this system is a convenient advantage.

CONCLUSION


It was found out that *B. atrophaeus* ATCC 9372 binds only to antibodies Ab151 (LS-C103151) and Ab411 (LS-C103411) and that these antibodies are specific against bacterial spores. Interactions depend on the method of bacterial cultivation and purification. Sandwich assay was a good choice to improve sensitivity. Assumption that Biacore 3000 would be a better option for our measurements was unfortunately not true. Detection of spores under concentration of 105 CFU ml⁻¹ seems possible and promising for detection of *B. anthracis*.

ACKNOWLEDGEMENT

The work has been supported by the Ministry of Defence of Czech Republic (projects no. OVVTUO2008001 and OSVTUO2006003).

REFERENCES

- [1] Abad J M, Pariente F, Hernández L, Abruña J D, Lorenzo E: *Anal. Chem.*, 70 (1998), 2848–2855
- [2] Homola J: *Chem. Rev.*, 108 (2008), 462–493
- [3] Killard A J, Deasy B, O’Kennedy R, Smyth M R: *Trends Anal. Chem.*, 14 (1995), 257–266
- [4] McGovern J P, Shih W Y, Rest R, Purohit M, Pandya Y, Shih W H: *Analyst*, 135 (2008), 649–654
- [5] Nicholson W, Setlow P, In: *Molecular Biological Methods for Bacillus*, Harwood C R, Cutting S M (Eds.), Wiley, Chichester, New York (1990), 391–450

- 
- [6] Zhao J, Krishna V, Moudgil B, Koopman B: Separation and Purification Technology, 61 (2008), 341–347
 - [7] Storri S, Santoni T, Minunni M, Mascini M: Biosens. Bioelectron., 19 (1998), 347–357
 - [8] Skládal P, Pohanka M, Pavliš O: Sensors, 7 (2007), 341–353
 - [9] Shankaran D R, Gobi K V, Miura N: Sens. Acutators B, 121 (2007), 158–177

ADVANTAGEOUS ELECTROCHEMICAL FEATURES OF NANOMATERIALS USED IN DEVELOPMENT OF BIOFUEL CELLS

Jaroslav FILIP*, Peter GEMEINER, Jan TKAC

Department of Glycobiotechnology, Institute of Chemistry, Slovak Academy of Sciences, Dubravská cesta 9, 845 38, Bratislava, Slovakia

*Jaroslav.Filip@savba.sk

ABSTRACT

In enzymatic biofuel cells, supplied fuel is oxidized and a depolarizer reduced on an anode and a cathode surface, respectively. Thus an electrical energy is obtained in the same way as in conventional fuel cells, but relevant reactions are catalyzed by immobilized enzymes. In this work different nanomaterials were tested for construction of conductive electrode interfaces providing high surface area for adsorption of sufficient amount of fructose dehydrogenase (bioanode) and bilirubin oxidase (biocathode). It was concluded that gold nanoparticles-based bioanode and biocathode can be used for a construction of high-performance enzymatic electrodes, nevertheless power output of fructose/dioxygen biofuel cell consisted of these electrodes ($27 \mu\text{W}\cdot\text{cm}^{-2}$) was not as high as in the case of a device constructed from electrodes based on carbon nanomaterials ($50 \mu\text{W}\cdot\text{cm}^{-2}$; carbon nanotubes and KetjenBlack dispersed in chitosan). After the performed optimization, further experiments can be done in order to achieve high loading of biocatalysts on electrodes and to elucidate basic principles of the enzyme adsorption and catalytic activity.

INTRODUCTION

In order to achieve lower dependence on fossil fuels and more effective usage of renewable resources, devices able to harness an electrical energy from renewable substrates employing biocatalysts are developed. In the case of so called enzymatic biofuel cells (BFC), enzymes immobilized on the surface of two electrodes – bioanode and biocathode – are responsible for a substrate oxidation (anode) and a reduction of final electron acceptor (oxygen at a cathode), exactly in the same manner as in conventional (i. e. anorganic catalysts-based) fuel cells.

Progress in nanotechnology is crucial for a development of effective systems where immobilized enzymes are able to effectively exchange electrons involved in either substrate oxidation or depolarizer reduction with an electrode surface. Nanomaterials offer high active surface area and good electron conductivity, which are desired features for effective enzymatic electrodes.

In our work, different nanomaterials were employed in a construction of electrode interfaces for an enzyme immobilization. Fructose dehydrogenase (FDH) and bilirubin oxidase (BOD) were chosen as an anodic and a cathodic biocatalyst, respectively, because both enzymes are known to exchange electrons with electrode directly, without any mediator needed. The enzymes were immobilized on gold nanoparticles (AuNP) and spherical carbon nanoparticles KetjenBlack (KB); also some hybrid nanointerfaces were tested with very satisfying results.

MATERIAL AND METHODS

Preparation of electrodes

In a typical experiment, glassy carbon (GCE) or polycrystalline gold (AuE) electrode were cleaned according to the protocols published previously [1,2] and modified by deposition of several μl of nanomaterial dispersions. Single wall CNT and KB were dispersed in chitosan (0.1% in 0.3% acetic acid), whereas AuNP were deposited from their aqueous dispersion. After the dispersion dried out, obtained modified electrode was incubated with a buffer solution of a relevant enzyme (overnight incubation, at 4°C). Subsequently, an abundant enzyme solution was washed out with distilled water.

Electrochemical measurements

All measurements were conducted using a potentiostat/galvanostat Autolab PGSTAT 128N (Ecochemie, Utrecht, Netherlands). An Ag/AgCl/3M KCl and Pt disc electrodes served as the reference and auxiliary electrodes, respectively. Nanoparticles-modified GCE and AuE and electrodes incubated with enzymes were used as working electrodes in three-electrode configuration and tested separately using cyclic voltammetry (CV). For biofuel cell tests, only biocathode and bioanode were connected to the potentiostat; an open circuit potential was determined using chronopotentiometry and E-i characteristics were determined using chronoamperometry.

RESULTS AND DISCUSSION

For a construction of enzyme-immobilizing electrode nanointerfaces, spherical gold nanoparticles are very often used because of their

good conductivity and a facile and adjustable preparation [3]. In our group we have optimized a protocol for assembling of high surface area electrode nanointerface (as described by Murata et al., 2009 [4]) based on commercially available AuNP ($d=20$ nm, Sigma Aldrich). As received AuNP dispersion was concentrated by centrifugation (10000 RPM, 30 min, 98 % of supernatant discarded) prior its deposition on AuE surface. The deposition was performed dropwise (3 μ l of AuNP in one deposition step, dried in air, typically 4 steps) and after the last deposition step AuE||AuNP electrode was treated by CV (in 100 mM H_2SO_4 , potential window -200 to $+1500$ mV, scan rate 100 mV.s $^{-1}$) in order to check a real electroactive surface area. Interestingly, this step seemed to have quite a significant positive influence on a desired bioelectrocatalytical performance of AuNP-based bioanode and biocathode, most probably because of a restructuring of nanoparticle film (it is known that gold surface undergo an oxidation and a reduction in an applied potential window [1]), which led to an enhanced interconnection of single nanoparticles or their conglomerates and higher overall conductivity of the nanointerface. „CV-activated“ AuE||AuNP electrodes were incubated with FDH and BOD solutions in order to accomplish a construction of the bioanode and the biocathode, respectively. For bioanode, a mercaptoethanol (ME) monolayer was assembled on AuE||AuNP surface before an enzyme incubation according to a protocol published previously [2,5]. After the incubation and washing out of an unbound enzyme, both bioanode and biocathode were tested for a biocatalytical activity towards their respective substrates. Obtained background-corrected cyclic voltammograms are shown in Fig.1 (red curves); bioanode clearly exhibited an oxidative wave in the presence of 200 mM fructose with beginning at ca -120 mV and a current density of 625 $\mu A.cm^{-2}$ reached at 400 mV. Similarly, on the biocathode a reduction wave was observed in an aerated buffer with beginning at 500 mV and a current density of 450 $\mu A.cm^{-2}$ reached at 0 mV. In the next step, electrodes were assembled into a membraneless biofuel cell configuration and basic performances of such equipment were revealed. An open circuit potential of 746 mV and maximum power density of 27 $\mu W.cm^{-2}$ at 300 mV was detected. A plot of a current density and a power output versus BFC potential is shown in Fig. 2A.

Besides metals such as gold, carbonaceous nanomaterials are also very often employed for an effective immobilization of electrocatalytical enzymes. Carbon nanotubes („1D“ carbon) are known to poses excellent electrochemical properties (high electron conductivity, high active surface area and even surface catalytical activi-

ty [6,7]); on the other hand, spherical carbon nanoparticles such as KB („0D“ carbon) are known to adsorb some enzymes very effectively. A crucial step in fabrication of carbon nanomaterial-based interfaces is to disperse the nanoparticles in an appropriate matrix. For this purpose, chitosan was used preferentially because of its low cost and zero toxicity of dissolving agent (acetic acid versus N-methylpyrrolidone typically used for dissolving of highly fluorinated polymers, which are, nevertheless, very advantageous materials for KB binding [8,9]). We have performed an optimization of electrode nanointerface preparation that was based on KB dispersed in chitosan (KB/CHI) and was stable in an electrolyte solution and suitable for adsorption of BOD. Details of procedure are listed elsewhere [10] and Fig. 1 (black dashed lines) shows a background-corrected CV obtained with GCE||KB/CHI||BOD biocathode. The reduction wave starts at ca 400 mV, which is more negative than for AuNP-based biocathode. It may be suggested that, in KB/CHI matrix the enzyme is preferentially oriented towards a nanoparticle surface in such a way that its active site with a lower redox potential is involved in direct electron transfer instead of so called T1 site, which is suggested to have the highest E_0 and which is involved in a withdrawal of electrons from natural substrates or from an electrode surface (see [11] and references within). Current density reached value of 98 $\mu A.cm^{-2}$ at 0 mV. Interestingly, KB/CHI nanointerface was absolutely unsuitable for an immobilization of FDH – prepared bioanode did not exhibit any catalytic activity towards 200 mM fructose (data not shown).

In the next step the way was sought to increase overall conductivity of KB-based interface. A series of experiments proved that it is possible to gain overall bioelectrocatalytical performance by integration of CNTs into KB/CHI matrix which was performed by deposition on a GCE surface of a chitosan solution obtaining 4.3 mg.ml $^{-1}$ KB and 0.67 mg.ml $^{-1}$ CNT (experiment details listed elsewhere [10]). Such modified electrode denoted to as GCE||KB-CNT/CHI was capable of adsorption of FDH and BOD, as well. Fig. 1 (black solid lines) shows background-corrected CVs of GCE||KB-CNT/CHI||FDH and GCE||KB-CNT/CHI||BOD in presence of 200 mM fructose and dioxygen (secured by an electrolyte aeration), respectively. For bioanode, the voltammogram is different when compared to the one for electrode without a CNT integrated; it is rather similar to AuNP-based bioanode, so it can be suggested that in both cases FDH is oriented towards the surface in the same way. Current density reached a value of 450 $\mu A.cm^{-1}$ at 400 mV, what is lower in comparison to the AuNP-based bioanode,

exhibiting very small capacitive current (i. e. an active surface area). Taking this into account, it is obvious that carbon nanoparticle-based interface provides lower amount of active FDH adsorbed per unit of active surface area. The difference is caused by a controlled FDH immobilization due to the ME monolayer on AuNP surface.

GCE||KB-CNT/CHI||BOD configuration turned out to be effective for a dioxygen reduction as can be seen in Fig. 1. A beginning of a reduction process is at 540 mV, significantly higher than in the configuration without integrated CNT. Apparently, CNTs may be responsible for a better enzyme orientation or just for a better connection between an enzymatic redox sites and the electrode surface.

Optimized GCE||KB-CNT/CHI||FDH and GCE||KB-CNT/CHI||BOD were consequently used for an assembling of biofuel cell with measured OCP of 655 mV and maximum power output of 50 $\mu\text{W}\cdot\text{cm}^{-2}$. Dependence of current density and power output on potential applied to BFC is in the Fig. 2B. Overall performances better than at AuNP-based BFC are quite unexpected because of the lower catalytic current densities obtained for separated KB/CNT-CHI based bioelectrodes. There may be possible explanation relied on a good proton conductivity of chitosan, which enhances overall charge transfer between the electrodes, nevertheless such significant difference would be subjected to a further investigation.

Figure 1: Background-corrected CVs of Au-E||AuNP-based bioanode and biocathode (red solid lines), GCE||KB/CHI||BOD (black dashed line) and GCE||KB-CNT/CHI-based bioanode and biocathode (black solid line). 100 mM acetate buffer pH 6.0, containing 200 mM fructose (anode) or aerated with air (cathode), for background CVs no fructose was added (anode) and deaeration with N_2 was secured (cathode). CVs were run at scan rate of 10 $\text{mV}\cdot\text{s}^{-1}$.

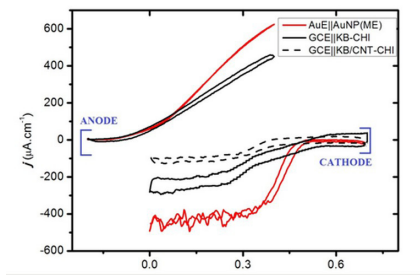
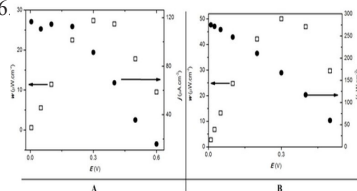


Figure 2: Current and power density versus potential applied plots obtained for Au-E||AuNP-based (A) and GCE||KB-CNT/CHI-based (B) BFC. Measurements were done in an aerated 100 mM acetate buffer pH 6.



CONCLUSIONS

Spherical gold nanoparticles (AuNP) and two different carbon nanomaterials (CNT and spherical nanoparticles KB) were employed in construction of electrode nano-interfaces. After optimization of the fabrication protocols, fructose dehydrogenase and bilirubin oxidase were immobilized on such prepared interfaces, with a bioanode and a biocathode of fructose/dioxygen biofuel cells being assembled. Each prepared bioanode and biocathode was investigated separately using CV in the absence and presence of 200 mM fructose (for bioanode) or dioxygen (for biocathode; secured by aeration of an electrolyte during the measurement) and finally fundamental operational performances were investigated for AuNP and KB-CNT/CHI-based biofuel cells. It was revealed that, AuNP-based bioanode and biocathode reached higher current densities (625 and 450 $\mu\text{A}\cdot\text{cm}^{-2}$, respectively) than KB-CNT/CHI-based ones (450 and 280 $\mu\text{A}\cdot\text{cm}^{-2}$, respectively), however BFC constructed from AuNP-based electrodes reached maximum power density of only 27 $\mu\text{W}\cdot\text{cm}^{-2}$ whereas the latter electrodes were assembled into BFC with a 50 $\mu\text{W}\cdot\text{cm}^{-2}$ power output. Regardless of surprisingly low power output of AuNP-based BFC, gold and carbon nanoparticles were successfully assembled into an effective electrode interface with enzymatic biocatalysts immobilized on their surfaces. As a further direction of research in this field, complexes of nanomaterials (especially graphene) with enzymes will be tested in order to achieve higher loading of active catalytic units per electrode and thus to obtain higher power outputs of membraneless biofuel cells based on direct

electron transfer.

ACKNOWLEDGEMENT

The financial support from SAV-FMEHP-2008-04-04 and from VEGA 2/0127/10 was acknowledged. This contribution/publication was the result of the project implementation: Centre for materials, layers and systems for applications and chemical processes under extreme conditions—stage II, supported by the Research and Development Operational Program funded by the ERDF.

REFERENCES

- [1] Tkac J, Davis J J: *J. Electroanalytical Chemistry*, 621 (2008), 1, 117-120
- [2] Filip J, et al., proceedings of Student Scientific Conference, Faculty of Nature Sciences, Comenius University in Bratislava, (2010), 140-145
- [3] Murata K, Kajiya K., Nukaga M, et al.: *Electroanalysis*, 22 (2010), 2, 185-190
- [4] Murata K, Kajiya K, Nakamura N, et al.: *Energy & Environmental Science*, 2 (2009), 12, 1280-1285
- [5] Murata K, Suzuki M, Kajiya K, et al.: *Electrochemistry Communications*, 11 (2009), 3, 668-671
- [6] Tkac J, Ruzgas T: *Electrochemistry Communications*, 8 (2006), 5, 899-603
- [7] Filip J, Šefčovičová J, Tomčík P, et al.: *Talanta*, 84 (2011), 2, 355-361
- [8] Habrioux A, Napporn T, Servat K, et al.: *Electrochimica Acta*, 55 (2010), 26, 7701-7705
- [9] Miyake T, Oike M, Yoshino S, et al.: *Chemical Physics Letters*, 480 (2009), 1-3, 123-126
- [10] Filip J, Gemeiner P, Tkac J: Proceedings of Chemical-Technological Conference Aprochem (2011), article number 185
- [11] Opallo M, Bilewicz R: *Advances in Physical Chemistry*, 2011 (2011), Article ID 947637

SURFACE TENSION OF CYCLOSPORINE SAMPLES

Petra FISEROVA¹, Tomas ANDRYSEK², Libuse TRNKOVA^{1,3}

¹Department of Chemistry, Faculty of Science, Masaryk University, Kotlarska 2, CZ-611 37 Brno, Czech Republic

²Technology & Scientific manager in TEVA Czech Industries s.r.o., Ostravska 305/29, CZ-74770 Opava - Komarov, Czech Republic

³Central European Institute of Technology – CEITEC, Brno, University of Technology, Technicka 3058/10, 616 00 Brno, Czech Republic

*libuse@chemi.muni.cz

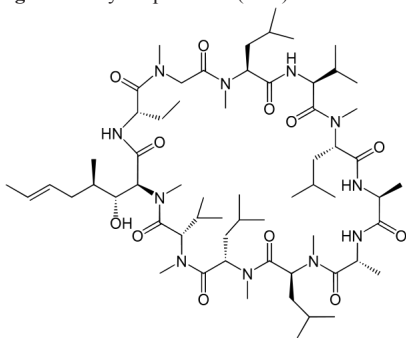
ABSTRACT

The company Teva Czech Industries s.r.o. is an important producer of pharmaceuticals. One of them is the immunosuppressive preparation based on cyclosporine A which is targeted to patients after transplantations. The aim of this investigation was to determine the effect of water and lubrication components on surface tension behavior of some cyclosporine samples before and after encapsulation.

INTRODUCTION

The company Teva Czech Industries s.r.o., originally known as Galena, is an important traditional producer of pharmaceuticals [1]. All products comply with recognized quality standards and are exported to many countries of the world including the USA and Western Europe. The company successful operation is accomplished by approximately 1500 employees and in 2006 the company became a part of the multinational group TEVA. The immunosuppressive preparation is focused on the products with cyclic polypeptide – cyclosporine A (Fig.1). Drug products with this substance influence the organism's auto-immune reactions and they are necessary for patients after transplantations. Discovered in the lab of Sandoz in Switzerland in 1972, cyclosporine A (CsA) has since revolutionized transplant medicine [2].

Figure 1: Cyclosporine A (CsA)



One of the possible characteristics of these samples is the surface tension [3-4], which can be well and relatively easily measured by means of tensiometer.

MATERIAL AND METHODS

Samples have been measured by digital tensiometer Sigma 700/701 [5]. Due to this type we are able to measure surface and interfacial tension. Also we have two possibilities of probe – we can use Du Nouy Ring, made of platinum and iridium, or only platinum probe called Wilhelmy Plate. Offered temperature period is from -10 to 100 degrees Celsius. Tensiometer can be controlled by computer, including software gserve, which helps us to generate graphs, results of measuring and import them to different systems for treatment of data.

Figure 2: Sigma tensiometer 700/701



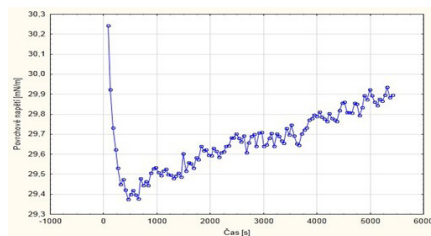
This type of tensiometer is able to use several methods, which are studying surface and interfacial tension, dynamic contact angles, powder wettability, single fiber wettability, adsorption behavior of solids, critical micelle concentration – CMC, surface free energy of solids. In our case, only surface tension method has been used yet.

RESULTS AND DISCUSSION

The first experiment consists in the calibration of tensiometer by using redistilled (Millipore) water. In the second experiment the surface tension of clear solution of CsA samples with the volume (10 cm³) was measured. After addition of a CsA sample to redistilled water the surface tension decreases nearly 2.5 times. The final step was measuring of small portion of sample (0.1 g), added to 20 cm³ of redistilled water. In this experiment, decreasing of surface tension in time was observed (Fig.3).

We are disposing of nine samples, which contains of cyclosporine A (CsA), polyglycerol-3-oleate, polyglycerol-10-oleate, ethanol; d,l-alpha-tocopherol and Cremophor RH40, in some of them is allowance of lubricant – miglyol or paraffin oil, in different concentrations, some of them are before and after encapsulation. Specifically, our sample (S1) is filling of capsule after encapsulation, mixed with 20 cm³ of distilled water. (Fig.3)

Figure 3: Surface tension of sample S1 (CsA), mixed with 20 cm³ distilled



Opposite case is small portion of sample in 20 cm³ of ethanol, where it is not possible to observe changes of surface tension in time. As we suppose, creation of micelles take place in water, so if we will continue with utilizing of graph, we can find value of critical micelle concentration.

CONCLUSION

Purpose of project was to characterize samples, and find out, how the surface tension and other qualities will change after adding water or several types of lubricant substances with different concentration. So far we studied the influence of water addition on the surface tension of CsA

sample and we found that this parameter is subject to temporal change. Therefore, this study will require further experiments, including the definition of qualities of lubricate material, which is used nowadays, and the comparison with substances which can substitute.

Due to results and graphs of samples mixed with the water, is prospectively possible to compile values of Critical Micelle Concentration, influence of lubricant substances, or effect of encapsulation on cyclosporine oral solution.

ACKNOWLEDGEMENT

This research was supported by the following Projects: (a) CEITEC – Central European Institute of Technology Project CZ.1.05/1.1.00/02.0068, and (b) OPVK project (NanoBioMetalNet) CZ.1.07/2.4.00/31.0023. Acknowledgement belongs also to the company TEVA Czech Industries s.r.o. Opava - Komárov which provided samples and purpose of project.

REFERENCES

- [1] <http://www.ivax-cz.com/web/structure/4.html>
- [2] Tedesco D., Haragsim L.: Journal of Transplantation, Volume 2012, Article ID 230386, 7 pages, Hindawi Publishing Corporation (2012)
- [3] Atkins, P. W. Fyzikálna chémia, 6. vyd. Bratislava : Slovenská technická univerzita v Bratislave, 1999. 308 s. ISBN 80-227-1238-8.
- [4] Kellö, V., Tkáč, A. Fyzikálna chémia, 3.vyd. Bratislava: Vydavateľ'stvo technickej a ekonomickej literatury Bratislava (2009)
- [5] <http://sci.muni.cz/~labifel/?q=vybaveni>

DNA LABELLING WITH ELECTROACTIVE MOIETIES AND ITS APPLICATION IN ELECTROCHEMICAL DNA SENSING

Miroslav FOJTA

Central European Institute of Technology, Masaryk University, Kamenice 753/5, CZ-625 00
Brno, Czech Republic
fojta@ibp.cz

ABSTRACT

Natural nucleobases are electrochemically active, producing analytically useful oxidation and reduction signals at carbon- or mercury-based electrodes, respectively. Electroactive labels are used in electrochemical nucleic acids sensing to improve selectivity and sensitivity of the biosensors and bioassays. Covalent DNA labelling offers a better discrimination between complementary strands forming the DNA double helix in DNA hybridization assays. Moreover, redox coding of particular nucleobases can be utilized in electrochemical DNA sequencing and single nucleotide polymorphism typing. Besides classical synthesis of modified nucleic acids via solid phase phosphoramidite methodology, more facile and versatile approaches have been introduced, based on either chemical modification of natural DNA components (such as thymine bases with oxoosmium complexes), or enzymatic incorporation of modified nucleotides using deoxynucleotide triphosphate conjugates bearing electroactive labels.

INTRODUCTION

Nucleic acids (NA) exhibit an inherent electrochemical activity conferred by electrochemical reducibility or oxidizability of the nucleic acids constituents [1]. The intrinsic NA electroactivity and specific surface activity have been utilized in many label-free NA assays. At the mercury and some amalgam electrodes, both redox and tensammetric responses of the NAs are strongly sensitive to the accessibility of nucleobase residues, providing information about DNA structure and events resulting in structural changes (such as DNA double helix unwinding, enzymatic digestion, DNA damage leading to formation of DNA strand breaks etc). Despite generally less pronounced structure sensitivity of NA oxidation signals measured at the carbon electrodes, oxidation of G has been perhaps the most popular way to label-free NA electrochemical analysis. Many electrochemical sensing systems have been proposed to detect DNA hybridization – formation of duplex DNA of two complementary single strands, of which one is specifically designed as a probe of known nucleotide sequence to capture and detect the complementary target strand featuring the analyte. In general, in the DNA hybridization assays and other sequence-specific DNA sensing techniques it is necessary to distinguish between the probe and target DNA strands or between the single stranded probe and the hybrid duplex, or to identify sites and types of nucleobase substitutions. It seems that more reliable distinction among the probe/target/hybrid duplex DNA, and particularly recognition of single nucleotide substitutions, can be attained through application of redox active labels rather than through label-free DNA electrochemistry [2].

NUCLEIC ACIDS LABELING WITH OXOOSMIUM COMPLEXES.

Introducing oxoosmium tags into nucleic acids is based either on the reaction of osmium tetroxide complexes (Os(VIII),L) with pyrimidine (predominantly thymine) nucleobases, or on the reaction of osmate(VI) complexes (Os(VI),L) with terminal ribose residues in ribonucleotides. Facile modification of base-unpaired thymines within oligo- and polynucleotide chains under physiological conditions and distinct electrochemical properties of the Os,L-labeled DNA render the Os(VIII),L reagents useful for various modes of electrochemical DNA sensing [3]. Polarographic or voltammetric studies of the oxoosmium-modified DNAs with mercury-based electrodes revealed three reversible faradaic processes within potential region between 0.0 and -1.0 V, and a catalytic process around -1.2 V. At the carbon and gold electrodes, the reversible faradaic current signals due to the Os,L DNA adducts can be observed. A concept of reporter probes (RP) bearing easily detectable osmium tags has been elaborated to analyze DNA sequences via molecular hybridization and, quite recently, also to monitor DNA-protein interactions. Moreover, the oxoosmium tags, owing to DNA structure selectivity of the reaction with thymine, have successfully been applied to detect DNA damage and thymine residues within single base mismatches [3].

ENZYMATIC INCORPORATION OF LABELLED NUCLEOTIDES

Modified DNA can be synthesized enzymatically via incorporation of modified nucleotides by DNA polymerases or terminal deoxynucleotidyl transferases (TdT) [4]. A number of labelled dNTPs are commercially available, including those bearing luminophores (e.g., fluorescein, TAMRA) or affinity tags (biotin, digoxigenin). Albeit the palette of commercially available dNTPs bearing electroactive labels is still rather limited, it is being continuously expanded owing to progress in the methodology of synthesis of base-modified dNTPs, involving C7-substitutions of 7-deazapurines, C8-substitutions of purines and C5-substitutions of pyrimidines [4]. These efforts have resulted in application of several electroactive DNA tags (such as ferrocene, nitro- and aminophenyl, $[M(bpy)_3]^{3+/2+}$ complexes of Ru or Os, anthraquinone etc.) producing specific electrochemical signals due to their reversible or irreversible reduction or oxidation at different potentials. Diversity in electrochemical properties of these labels offers their facile distinction from one another, as well as from intrinsic DNA responses related to reduction or oxidation of natural nucleobases. Simple nucleobase analogues, such as 7-deazapurines (commercially available as dNTPs), are applicable as specific electroactive tags as well since these bases exhibit substantially lower overpotentials of electrochemical oxidation, compared to their natural counterparts [5]. The enzymatic DNA labelling strategy has been applied in a number of biological applications, including DNA hybridization, PCR monitoring, SNP typing and DNA-protein interaction studies.

CONCLUSION

Labelling of DNA with electrochemically active moieties proved to be a convenient way to development of electrochemical bioassays applicable in analyzing nucleotide sequences, detecting DNA damage and in DNA-protein interaction studies. Through combinations of various labels differing in redox potentials, highly specific electrochemical analysis of DNA sequences can be attained.

ACKNOWLEDGEMENT

Financial support from The Czech Science Foundation GACR (project P206/12/G151) and GA ASCR (IAA400040901) is gratefully acknowledged.

REFERENCES

- [1] Paleček E., Bartošik M.: Chem Rev 112 (2012), published ASAP - DOI: 10.1021/cr200303p.
- [2] Fojta, M, Havran, L, Pivonkova, H, Horakova, P, Hocek, M. Curr Org Chem 15 (2011) 2936-2949.

- [3] Fojta, M.; Kostecka, P.; Pivonkova, H.; Horakova, P.; Havran, L. Curr Anal Chem, 7 (2011), 35-50.
- [4] Hocek M., Fojta M. Chem. Soc. Rev. 40 (2011), 5802-5814
- [5] Pivonkova, H.; Horakova, P.; Fojtova, M.; Fojta, M.: Anal. Chem. 82 (2010), 6807-6813

TIN DIOXIDE SENSOR FOR METHANE DETECTION

Imrich GABLECH¹, Zdenek PYTLICEK¹, Jan PRASEK^{1,2}, Jaromir HUBALEK^{1,2*}

¹Department of Microelectronics, Faculty of Electrical Engineering and Communication, Brno University of Technology, Technicka 3058/10, 616 00 Brno, Czech Republic

²Central European Institute of Technology, Brno University of Technology, Technicka 3058/10, 616 00 Brno, Czech Republic

*hubalek@feec.vutbr.cz

ABSTRACT

This paper reports on characterization of tin dioxide (SnO₂) sensors for methane detection in the air atmosphere and determination of the optimal temperature range to achieve high sensitivity. There were done two measurement of our SnO₂ thick film sensor on two different temperatures (240 °C and 380 °C) and compared with commercial sensor Figaro TGS 822. It was found that the sensitivity of our SnO₂ sensor is the same at both temperatures we tested. In comparison of our SnO₂ sensor with the commercial sensor Figaro TGS 822 was found that our SnO₂ sensor has not a very high sensitivity for lower concentrations, but the saturation level is higher. It means that our SnO₂ sensor is able to determine accurately the higher concentrations than the commercial sensor. We were able to determine methane in the concentration range from 50 to 4000 ppm.

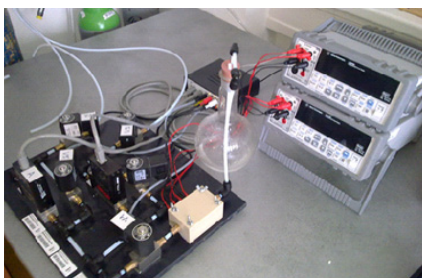
INTRODUCTION

Nowadays number of applications and places with gasses presence is increasing (e.g. natural gas, mine gas). Most of these gasses contain methane which is extremely flammable and explosive even in low concentrations in the air (from 4.4 to 15 volume percent) [1]. Therefore it is very important to detect methane in low concentrations. In general the heated gas sensors with the active layer based on SnO₂ semiconducting material are used for gas detection. This type of sensors has very high sensitivity to methane and it is able to detect many other gasses. These sensors are usually implemented with a selective membrane to ensure the selectivity of the sensors to detect selected gas. Sensors with the membranes are used in houses where it is very important to detect just the methane and not to detect other gasses (e.g. ethane), which often cause false warnings. Oxygen anions (O²⁻, O₂⁻) are generated due to oxygen chemisorption. These anions drain away free electrons from semiconductor which cause active layer conductivity decreasing [2]. In the case of methane presence in the air, the conductivity increases due to reaction with oxygen chemisorbed anions. The increasing of conductivity is dependent on concentration and reactivity of methane. The methane reactivity is temperature dependent. Heater is necessary to reach activation energy of chemical reactions which improves sensitivity of the sensor and its ability to detect the gas as soon as possible. Heating elements allow setting the operating temperature very precisely. These elements are placed under the active layer and they could be fabricated by thick film technology on the alumina substrate or by lithography on silicon microhotplates. Alumina substrates are used due to their high temperature resistance and low coefficient of thermal expansion [3].

EXPERIMENTAL

All measurements were done on station for gas measurement (figure 1.), which is equipped with two mass controllers for accurate regulation of two different gases and with chamber for two gas sensors in TO-8 package. Agilent U3603A multifunctional device was used for as power supply. The communication system between measuring devices, sensors and valves was controlled in LabView interface.

Figure 1.: Station for gas sensors characterization

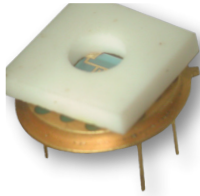


The tested sensor (figure 2) is equipped with platinum heater meander. The heater was fabricated using standard thick film technology from platinum paste ESL 5545 (ESL, Electrosience, UK) and its temperature resistivity coefficient is 3020 ppm/°C. The heater resistivity was determined by monitoring various values of current in dependence on input voltage.

The sensor sensitivity was investigated on several values of methane concentrations (50, 100, 200, 300, 500, 1000, 1500, 2000, 2500, 3000, 3500 and 4000 ppm) in synthetic air. Sensitivity was determined at constant gas flow (400 ml/

min) for two selected temperatures 240 °C and 380 °C.

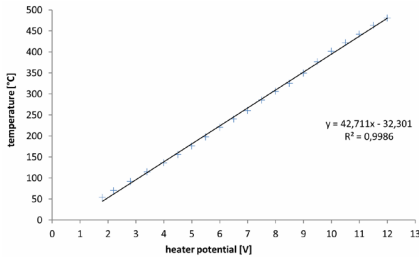
Figure 2.: tin dioxide sensor in TO12 package



RESULTS AND DISCUSSION

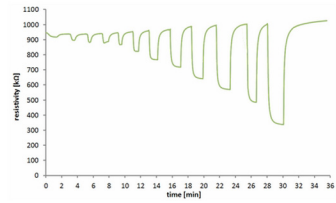
The temperature dependence of heating element on applied voltage is shown in the figure 3. From the figure 3 is clear that the temperature increases linearly with applied voltage so the temperature is possible to be set precisely. The voltage range from 1.8 V to 12 V corresponds to temperature range from 50 to 480 °C.

Figure 3: Temperature dependence of heating element on applied voltage



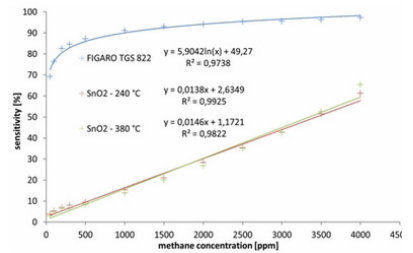
The resistivity response of measured SnO₂ gas sensor at 380 °C is shown in the figure 4. Figure 4 depict the effect of methane on the resistance of the sensor active layer, which decreases with increasing concentration. Resistivity values were measured for the concentration levels 50, 100, 200, 300, 500, 1000, 1500, 2000, 2500, 3000, 3500 and 4000 ppm. From the figure 4 is clear, that the resistivity response of our SnO₂ sensor at 380 °C to concentrations changes occurs within few seconds and the resistivity is stabilized in about two minutes.

Figure 4.: The resistivity response course of measured SnO₂ gas sensor at 380 °C



From obtained resistivity responses at 240 and 380 °C two sensitivity curves of SnO₂ sensor were plotted out and compared with measured values obtained with commercial sensor Figaro TGS 822 as is shown in the figure 5.


Figure 5.: Sensitivity characteristics of Figaro TGS 822 and SnO₂ thick film sensor for CH₄ detection



From the figure 5 is clear, that there was almost no difference of our SnO₂ sensor sensitivity at both measured temperatures. The comparison with the Figaro TGS 822 sensor indicates that SnO₂ sensor has not a very high sensitivity for lower concentrations, but the saturation level is higher. It means that our SnO₂ sensor is able to determine accurately the higher concentrations than the commercial sensor.

CONCLUSION

In this paper was characterized SnO₂ thick film sensor and compared with commercial sensor Figaro TGS 822. It was found that the sensitivity of our SnO₂ sensor is the same at both temperatures of 240 °C and 380 °C we tested. It means that the sensing temperature of 240 °C is enough. The higher temperature leads just to sensors life time reduction and increases the power consumption. In comparison of our SnO₂ sensor with the commercial sensor Figaro TGS 822 was found that SnO₂ sensor has not a very high sensitivity for lower concentrations, but the saturation level



is higher. It means that our SnO₂ sensor is able to determine accurately the higher concentrations than the commercial sensor. We were able to determine methane in the concentration range from 50 to 4000 ppm.

ACKNOWLEDGEMENT

The work has been supported by GA ĀR 102/09/1601, project KAN 208130801 (NANOSEMED), and project CZ.1.05/1.1.00/02.0068 (CEITEC).

REFERENCES

- [1] Beck U, Hertwig A, Kormunda M, et al.: Sensors and Actuators B: Chemical, 160 (2011), 1, 609-615
- [2] Quaranta F, Rella R, Siciliano P, et al.: Sensors and Actuators B: Chemical, 58 (1999), 1-3, 350-355
- [3] Riva R, De Angelis L.: Sensors and Actuators B: Chemical, 28 (1995), 1, 25-29

FISH MERCURY LIVER/MUSCLE RATIO IN COMPARISON WITH MERCURY HEAVILY AND LIGHTLY CONTAMINATED LOCATION

Lenka GAJDOVA¹, Kamila KRUIKOVA^{1*}, Renata KENSOVA¹,
Zdenka SVOBODOVA¹

¹Department of Veterinary Public Health and Toxicology, Faculty of Veterinary Hygiene and Ecology, University of Veterinary and Pharmaceutical Sciences Brno, Palackeho 1/3, 612 42 Brno, Czech Republic

*h10023@vfu.cz

ABSTRACT

The aim of our study was to split Czech locations on mercury heavily and lightly contaminated sites based on results of total mercury liver/muscle ratio in fish. Muscle and liver of 165 fishes were analyzed on total mercury content and then the total mercury liver/muscle ratio was calculated. Total mercury liver/muscle ratio for both predators and non-predators was assessed for five sites in the Czech Republic. Significantly higher ratio was found out for both predators and non-predators from the Skalka Reservoir in comparison with other studied sites (Lužnice, Otava, Jordán, Berounka). Obtained results showed that Skalka Reservoir is still heavily contaminated by mercury. Obtained results confirmed that total mercury liver/muscle ratio can be used for assessment of mercury contamination, when this ratio is higher than value 1.0 it means that location is mercury heavily contaminated.

INTRODUCTION

It is historically confirmed, that consumption of fish with elevated mercury levels caused severe human intoxication (e.g. Minamata disease). From this fact it is necessary to monitor and evaluate mercury contamination of the aquatic ecosystem. Studies have shown that repeated or continuous exposure to any form of mercury can result in the accumulation of mercury in the body. The target organs for mercury accumulation are muscle, liver and kidney. In fact, higher accumulation of mercury in liver may be considered the primarily signal of metal exposure [1].

MATERIAL AND METHODS

Fish sampling

A total of 165 fishes belong to 13 fish (5 predators and 8 non-predators) species were collected during the 2011 on the other 5 locations and also in 2003 in the Skalka Reservoir. In this project, the fishes from the following localities on the Czech rivers: Berounka, Lužnice, Otava, and on the Czech Reservoirs Skalka and Jordán were sampled. Fishes were sampled using electrofishing mainly in the spring. Fish species described by their absolute and relative frequencies are shown in the Tab. 1.

Mercury analysis and calculation of THg liver/muscle ratio

The total mercury content in the muscle and liver of fishes was determined by cold vapor atomic absorption spectrometry using AMA 254 (Altec Ltd., Czech Republic) analyzer. The method does not require any sample preparation. Limit of detection of THg was 1 µg/kg. The limit of detection was set as a sum of the triple

standard deviation of a blank and a blank mean value. The accuracy of THg values was validated using standard reference material BCR-CRM 464 (Tuna Fish, IRMM, Belgium). The total mercury concentration in fish muscle and liver was given in mg/kg fresh weight and then THg liver/muscle ratio was calculated. THg liver/muscle ratio is ratio of liver to muscle Hg concentrations and is calculated as follows: [THg in liver (mg/kg)/THg in muscle (mg/kg)].

Table 1: Number of sampled fishes from the Czech rivers and reservoir (2003 and 2011)

Fish species	Latin	Berounka Cernotice	Lužnice Subšlab	Otava Strakonice	Skalka 2011	Skalka 2003	Jordán	TOTAL
PREDATORS								
asp	<i>Aspius aspius</i>	4	4	0	5	3	4	59 (35.7%)
barbel	<i>Barbus barbus</i>	0	0	0	0	1	0	20 (12.1%)
perch	<i>Percis fluviatilis</i>	0	0	5	5	0	4	14 (8.5%)
pike	<i>Esox lucius</i>	5	5	4	5	0	0	319 (11.5%)
pikeperch	<i>Stizostedion heringaceus</i>	0	0	0	5	0	0	5 (3.0%)
NON-PREDATORS								
rudd	<i>Scardinus erythrophthalmus</i>	14	18	19	27	13	15	106 (64.2%)
big head	<i>Aristichthys nobilis</i>	0	0	0	4	0	0	4 (2.4%)
breach	<i>Abramis brama</i>	5	5	4	5	5	5	29 (17.5%)
carp	<i>Cyprinus carpio</i>	4	3	0	4	0	5	16 (9.6%)
roach	<i>Rutilus rutilus</i>	5	5	5	5	3	5	28 (16.9%)
tench	<i>Tinca tinca</i>	0	0	5	0	0	0	5 (3.0%)
chub	<i>Leuciscus cephalus</i>	0	5	5	4	0	0	14 (8.5%)
silver bream	<i>Abraamis hypnatus</i>	0	0	0	5	0	0	5 (3.0%)
TOTAL		36(3)	36(27)	36(48)	36(47)	36(17)	36(15)	36(15)
		(13.9%)	(16.4%)	(16.5%)	(28.4%)	(10.3%)	(13.9%)	(100%)

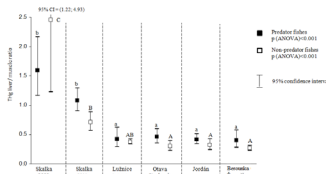
RESULTS AND DISCUSSION

This study included both predator and non-predator fish which were compared. Dataset consists of 165 fish was remitted to the correlation among THg muscle, liver, liver/muscle ratio and the main characteristics of fish (age and weight). No correlation both for predators and non-predators was found for THg liver/muscle ratio and age (or weight) so no conversion on age or weight was needed. The THg liver/muscle ra-

tio according to locality and food preference of fishes and their statistical differences ($p < 0.001$) among locations are showed in the Fig. 1. The statistically highest THg liver/muscle ratio was found in Skalka Reservoir in 2003 followed by Skalka Reservoir in 2011. Value of THg liver/muscle ratio for fish from the Skalka Reservoir (both for 2003 and 2011) exceed value 1 which means that the preference of mercury accumulation is especially to the liver. The liver plays an important role in storage, detoxification and transformation of pollutants especially in metals [2]. High THg liver/muscle ratio confirmed a highly contaminated location which Skalka Reservoir absolutely still is. The historical mercury contamination of Skalka reservoir via waste water from Germany chemical plant is still persisting and it should be monitored in the future. Mercury accumulation preferentially to the liver in contaminated locations confirmed also Abreu et al. (2000) [3]. In their study, three locations of Lagoon Ria de Aveiro in Portugal was assess from the THg liver/muscle ratio. Mercury was determined in the liver and muscle of sea bass (*Dicentrarchus labrax*) as a top predator species from contaminated and un-contaminated locations. THg liver/muscle ratio in contaminated site Largo do Laranjo was 2.0 while in non-contaminated sites in Muranzel and Costa Nova was 0.9 and 0.4, respectively. Surface water in the Largo do Laranjo are contaminated by the industrial mercury. Per contra, significantly lower THg liver/muscle ratio was detected in Berounka-Černošice, Jordán Reservoir, Otava-Strakonice and Lužnice-Soběslav locations for both predators and non-predators in comparison with Skalka (2003 and 2011) excepting non-predators in Lužnice-Soběslav. The THg liver/muscle ratios in all locations with exception Skalka Reservoir were about 0.4 which correspond with lightly contaminated locations. The statistical analysis between predators and non-predators within given locality using independent t-test was done. The statistical differences was observed in Berounka-Černošice ($p = 0.033$) and Skalka 2011 ($p = 0.045$). In the both cases, higher THg liver/muscle ratio was found for predator fish species. The same holds true for data published by Havelková et al. [4] even the THg liver/muscle ratio was adjusted on age. According Berzas Nevado et al. [5] THg liver/muscle ratio varied substantially among species and also among sampling point. In their study, samples of non-predator carp taken from contaminated sites had relatively high ratio (mean=2.2) in comparison with control site. However, this tendency was not observed in THg liver/muscle ratio for catfish from the same sites. In our study, no significant differences between predator and non-predator fish were found out in the other locations (with exception Skalka

and Berounka which are mentioned above). So THg liver/muscle ratio of both predator and non-predator fish can be used for evaluation of the locality contamination.

Figure 1: THg liver/muscle ratio according to locality and food preference of fishes from the Czech rivers and reservoirs study



a, b– homogeneous group of predator fishes computed using Tukey post hoc test; the same letters denote groups without statistically significant differences

A, B, C–homogeneous groups of non-predator fishes computed using Tukey post hoc test; the same letters denote groups without statistically significant difference

CONCLUSION

In conclusion, a comparison between total mercury contamination in muscle and liver showed differences in mercury accumulation in fish from lightly and heavily contaminated sites. When the THg liver/muscle ratio is higher (or about) than value 1, fish come from mercury heavily location. On the other hand, mercury accumulated to the muscle of fish entail lightly contaminated location (THg liver/muscle ratio lower than 1).

ACKNOWLEDGEMENT

The work has been supported by a project “Veterinary aspects of food safety and quality” MSM 6215712402.

REFERENCES

- [1] P Olsson, P Kling and C Hogstrand (1998). Metal metabolism in Aquatic Environment, eds. W. J. Langston and M.J. Bebianno, pp 321-350
- [2] DW Evans, DK Dodoo, PJ Hanson. Marine Pollution Bulletin 26 (1993), 329–334
- [3] AN Abreu, E Pereira, C Vale et al.: Marine Pollution Bulletin, 4 (2000), pp 293-297
- [4] M Havelková, L Dušek, D Neméthová et al.: Sensors, 8 (2008), 4095-4109
- [5] JJ Berzas Nevado, RC Rodriguez Martin-Doimeadios, FJ Guzmán Bernardo et al.: Archive of Environmental Contamination and Toxicology, 61(2011), 642-652

ACRIDINE DERIVATIVES AS PROSPECTIVE ANTIOXIDANTS

Lukas GALA^a, Ladislav DRAJNA^b, Jan IMRICH^b, Marian VALKO^a

^aSlovak University of Technology in Bratislava, Faculty of Chemical and Food Technology, Institute of Physical Chemistry and Chemical Physics, Department of Physical Chemistry, SK-81237 Bratislava, Slovakia

^bPavol Jozef Safarik University in Kosice, Faculty of Science, Institute of Chemistry, Department of Organic Chemistry, SK-04154 Košice, Slovakia

ABSTRACT

Neurological disorders such as Alzheimer's disease (AD) and Parkinson's disease (PD) represent a serious threat for humans. The primary target in studies of Alzheimer disease has been centered on aggregation of Amyloid beta (A β). Recently, a common denominator for both AD and PD has been found to be enhanced oxidative stress in brain due to the breakdown metabolism of redox active metals such as copper and iron. One of the possible therapeutical approaches is to use acridines (derivatives of acridines) which have metal-chelating properties as well as they inhibit enzyme cholinesterase. In this short contribution we report the free radical-scavenging properties of a series of newly prepared derivatives of acridines which are believed to suppress the level of oxidative stress in brain.

INTRODUCTION

AD is an age-related neurodegenerative disorder characterized by a progressive loss of cognitive abilities, such as, memory, language skills, attention, speech, depression and disorientation. For two decades, the primary target in studies of Alzheimer disease has been centered on Amyloid beta (A β). A β is a peptide of 39–43 amino acids that appear to be the main constituent of amyloid plaques in the brains of Alzheimer's disease (AD) patients [1]. The AD brain is under extensive oxidative stress as documented by protein oxidation and lipid peroxidation. Moreover, A β has been found to induce protein oxidation and lipid peroxidation both in vitro and in vivo. Thus, A β , central to the pathogenesis of AD, is likely also to be central to the oxidative stress under which the AD brain exists. The main features of enhanced oxidative stress in the AD brain involve increased brain content of Cu and Fe capable of stimulating free radical generation, increased protein and DNA oxidation in the AD brain, enhanced lipid peroxidation in the AD brain, decreased levels of cytochrome c oxidase in the brain in AD, and advanced glycation end products (AGEs), carbonyls, malondialdehyde, peroxynitrite, and heme oxygenase-1 (OH-1) [2]. Acridines were one of the first synthesized cholinesterase inhibitors approved for the treatment of Alzheimer's disease. Acridines is another class of compounds affecting amyloid beta aggregation of lysozyme, thus having a potential importance in the treatment of Alzheimer's disease. If increased pools of copper (and iron) are not appropriately chelated they can participate in the formation of harmful free radicals including the hydroxyl radical, enhancing thus oxidative stress in brain. Properly chelated copper ions in the brain may reduce cata-

lytic activity of copper ions to participate in the formation of free radicals. The aim of our work is to study the free radical scavenging activity of a series of newly prepared acridines using the ABTS method.

MATERIAL AND METHODS

Materials

For the evaluation of the antioxidant activity was used 2,2'-azino-bis(3-ethylbenzothiazoline-6-sulfonic acid) diammonium salt (ABTS, obtained from Sigma-Aldrich). Potassium persulfate and DMSO were obtained from Fluka. All derivatives of acridine were synthesized in our laboratory and the details will be published elsewhere. The following ligands were prepared:

4-(2,3,4,6-tetra-*O*-acetyl- β -glukopyranozyl)-1-(1,2,3,4-tetrahydroakridin-9-yl) tioseminkarbazid (**L1**)

4-(2,3,4,6-tetra-*O*-acetyl- β -*D*-manopyranozyl)-1-(9,10-dihydroakridin-9-yliden) tioseminkarbazid (**L10**)

2'-(9,10-dihydroakridin-9-yliden)hydrazono-3'-(2,3,4,6-tetra-*O*-acetyl- β -*D*-galaktopyranozyl)-1',3'-tiazolidin-4'-on (**L11**)

[2'-(9,10-dihydroakridin-9-yliden) hydrazono-3'-(2,3,4,6-tetra-*O*-acetyl- β -glukopyranozyl)-4'-oxotiazolidin-5-yliden] acetate (**L13**)

4-(2,3,4,6-tetra-hydroxyl- β -glukopyranozyl)-1-(9,10dihydroakridin-9-yliden) tiosemikarbazid (**L15**)

Spectroscopy

The free radical scavenging activity of taci-nes was determined using a UV/vis spectrometer Shimadzu UV-3600 (Shimadzu, Kyoto, Japan).

ABTS assay

All tacrines were dissolved in DMSO at 1 mM. Free radical scavenging activity of all drugs was studied using ABTS method. Free radical scavenging activity of the drugs was assessed spectrophotometrically by the formation of the ABTS^{•+} (2,2'-azinobis-(3-ethylbenzothiazoline-6-sulfonic acid)) radical cation (ABTS^{•+}) [3]. ABTS^{•+} was formed by reacting ABTS stock solution with potassium persulfate and allowing the mixture to stand in the dark at 8°C for 18 h before use. For the study of free radical scavenging activity of tacrines, the ABTS^{•+} solution was diluted with distilled water to reach the final concentration of ABTS^{•+} 80 μM. Time decay of absorbance of the ABTS^{•+} (2950 μL, concentration 80 μM) in the presence of tacrines (50 μL, concentration 1 mM) was measured at 730 nm.

The TEAC (Trolox Equivalent Antioxidant Capacity) method is one of the most commonly used methods for the evaluation of the total antioxidant activity (TAA) of various substances [4]. The TEAC method is based on the ability of substances to scavenge the stable radical cation ABTS^{•+} and a TEAC value is calculated for all substances by comparing their scavenging capacity to that of Trolox (6-hydroxy-2,5,7,8-tetramethylchromane-2-carboxylic acid) a water soluble analogue of vitamin E. The percentage inhibition of absorbance at 730 nm was calculated and plotted as a function of concentration of Trolox. An equal amount of DMSO was added to the control.

RESULTS

The Figure 1. shows the time decay of absorbance for all five acridines. The upper line (in black) is ABTS reference. The most profound free radical scavenging activity was observed for the ligands L15 and L1. Conversely, the least free radical scavenging activity was noted for the L11 and L13.

Figure 1.; Time decay of the absorbance of ABTS^{•+} in the presence of tacrines.

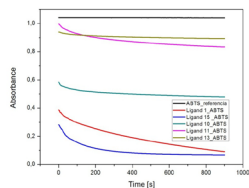


Table 1. shows the calculated values of TEAC for all studied ligands.

Table 1. TEAC values for the acridines.

Sample	TEAC
Ligand 1 +ABTS	2,2687
Ligand 10 +ABTS	1,3478
Ligand 11 +ABTS	0,5096
Ligand 13 +ABTS	0,3653
Ligand 15 +ABTS	2,3220

The structure vs. free radical scavenging activity of all studied drugs assessed by ABTS test in combination with other experimental techniques will be the subject of our next study.

ACKNOWLEDGEMENTS

VEGA Projects #1/0856/11 and # 1/0289/12 and Research and Development Agency of the Slovak Republic (Contracts No. VVCE-0004-07).

REFERENCES

- [1] K. Jomova, D. Vondrakova, M. Lawson, M. Valko: Metals, oxidative stress and neurodegenerative disorders. *Mol. Cell. Biochem.* 345; 91-104 (2010).
- [2] A. Antosova, B. Chelli, E. Bystrenova, K. Siposova, F. Valle, J. Imrich, M. Vilkova, P. Kristian, F. Biscarini, Z. Gazova: Structure-activity relationship of acridine derivatives to amyloid aggregation of lysozyme. *Biochim. Biophys. Acta* 1810; 465-474 (2011).
- [3] A. Stasko, V. Brezova, S. Biskupic, P. Rapta: *J. Food Nutr. Res.* 46; 145-149 (2007).
- [4] R.L. Prior, X.L. Wu, K.J. Schaich.; *Agr. Food Chem.* 53; 4290-4302 (2005).

PHOTOLUMINESCENCE STUDY OF LIGHT-INDUCED MODIFICATIONS OF (ELECTRO)CHEMICALLY PREPARED POLYPYRROLE

Pavel GALAR^{1*}, Petr MALÝ¹, Jan CERMAK², Bohuslav REZEK², Alexander KROMKA²

¹Faculty of Mathematics and Physics, Charles University in Prague, Ke Karlovu 3, 121 16 Prague 2, Czech Republic

²Institute of Physics ASCR v.v.i., Cukrovarnicka 10, 162 00 Prague 6, Czech Republic

*pavel.galar@seznam.cz

ABSTRACT

Permanent modifications of polypyrrole (PPy) after UV light irradiation were studied by photoluminescence (PL), optical absorption and X-ray photoelectron spectroscopy (XPS). PPy samples were prepared by electrochemical anodic oxidation and chemical oxidation. Influence of light exposure on polymer properties was studied under ambient condition, low pressure and after polymer annealing from 300K to 520K. The main demonstration of the polymer modification was up to an order of magnitude increase in the PL spectral band at 535 nm, small increase in the light transmittance interval in the range 300 - 780 nm, and quenching of carboxyl functional group. All of these changes were almost independent of polymer preparation conditions. We interpret our results in terms of light induced modification of functional groups on the polymer surface.

INTRODUCTION

From the time they have been discovered conductive polymers received great attention primarily because of their electrical, optical and mechanical properties. One of the representative conducting polymer is polypyrrole showing high electrical conductivity, biocompatibility and good stability in ambient conditions [1]. During the years the main synthesis methods – the chemical oxidative and electrochemical polymerization have been extended by many others such as matrix assisted pulsed laser evaporation [2,3]. PPy properties are widely tunable by the variation of preparation conditions [4]. All these characteristics make PPy good candidate for many applications in electronics, optoelectronics, photovoltaic and biomedicine [5,6].

One of the most fundamental weaknesses of each conductive polymer is its vulnerability to UV light [7,8]. Light induced modifications have a major impact on function of photovoltaic and optoelectronic devices. On the other hand, once sufficiently understood, these modifications could become a useful tool for intentional alteration of PPy properties.

In this paper we present the study of UV light induced modifications on PPy. We focus on elucidating the origin of observed changes and on development of a precise and simple method for their monitoring. For this purpose we use photoluminescence spectroscopy as a tool sensitive to material properties and defects.

MATERIAL AND METHODS

Preparation

PPy was electrochemically grafted from solu-

tion of pyrrole (240mM; Aldrich) and NaCl (100 mM) in deionised water. The electrochemical deposition was performed in galvanostatic regime, applying the current from 500nA to 10 μ A for 120 to 300 s by a potentiostat (Autolab PGSTAT302) on the counter electrode (Pt) [9]. As the substrates gold, platinum and surface conductive H-terminated monocrystalline diamond (MCD) was used.

Chemically prepared PPy was synthesized by long-term natural oxidation of pyrrole in the above solution and subsequently deposited by a drop on a spectrally pure quartz glass or MCD surface.

Experimental details

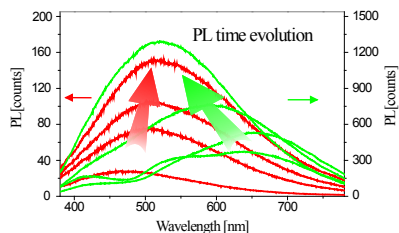
The PL spectra were measured by the grating spectrograph with CCD camera (Andor DV420A) and corrected for the spectral sensitivity of the whole setup. The 325 nm (3.82 eV) line of a He-Cd laser (Omnichrome T2056-MA03, Melles Griot) was used for both the PPy sample irradiation and PL excitation. For the low pressure measurements we used a cryostat chamber and a cascade of oil and turbomolecular pump. Thermal annealing of the samples was carried out on a commercial hotplate.

RESULTS AND DISCUSSION

PPy layers prepared by electrochemical grafting on MCD were irradiated by light of wavelength 325 nm and intensity 5 W/cm². Fig.1 shows that after the exposure a new broad band with maximum about 535 nm (2.31 eV) appeared and increased in the PL spectra. This new band can be interpreted as dipole-allowed transition between valence and polaron band or recombination of trapped electron-hole pair (polaron-ex-

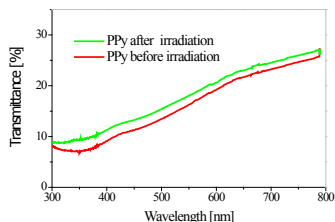
citon) [10,11]. The increase of the PL band intensity continues for the next 1 to 3 hours depending on the excitation intensity. The speed of the PL changes was also dependent on exposition light intensity and was rising with increasing intensity. This phenomenon was observed only if the irradiation intensity was from the interval 100 mW/cm² to 10 W/cm². The light intensity > 10 W/cm² caused destruction of the polymer. Photo-induced PL changes were permanent and independent of deposition conditions or used substrates. The same behaviour was observed also for PPy prepared by chemical oxidation (see also Fig.1). It is noteworthy that initial PL spectra of electrochemically and chemically prepared PPy are different in the beginning, but after irradiation they converge to the same spectral shape.

Figure 1: The time evolution of normalized PL spectra of PPy during light irradiation (325 nm and 5W/cm² for 2 hours): red curve - electrochemically prepared PPy on MCD, green curve - chemically prepared PPy on pure quartz glass.



Increased PL after UV irradiation could be interpreted as a specific defect creation. High efficiency of non-radiative recombination, that is typical for this type of conjugated polymers, is directly linked to the conjugation length of polymer chain [11,12]. This occurs through rapid inter-chain motion of excited charge carriers to recombination centre and charge delocalization. During UV irradiation conjugation length of PPy is being systematically reduced which can result in a significant increase of photoluminescence. In case of polaron-exciton, UV modification of the polymer chain can stimulate suitability of polaron-exciton generation at the expense of polarons. Moreover a reduction of the polymer conjugation length would be expected to decrease polymer absorption [8,13]. This phenomenon was indeed measured as shown in Fig.2.

Figure 2: Transmittance of electrochemically prepared PPy layer on MCD before and after UV irradiation (325 nm and 5W/cm² for 2 hours)



Presence of air proved to be an important parameter for the occurrence of PPy modifications. Fig.3 shows photo-induced PL changes of electrochemically grafted PPy on gold substrate that was measured in various ambient. Under the atmospheric air pressure there was up to an order of magnitude increase of PL band with the maximum at around 535 nm. After lower air pressure in the order of 0.01 Pa the induced PL changes were minimal and very soon saturated.

The possible thermal origin of the observed modifications was excluded by study of thermal annealing of the PPy layers. The layers were electrochemically deposited on gold substrate. Annealing was carried out at temperatures 370, 420, 480 and 530 K. The excitation light intensity 100 mW/cm² was intentionally chosen below the photo-induction threshold so that only changes in PL spectrum due to the annealing are monitored. The results are shown in Fig. 4 from which it is clear that no changes are observed up to the annealing temperature of 520 K when the thermal degradation of PPy starts. The burning temperature of PPy is about 200 K higher [14]. These results exclude cross-linking of the PPy chains, chain scissoring and most likely even thermo-initiated oxidation of the polymer as possible origins of the photo-induced PPy modification.

Figure 3: Comparison of electrochemically prepared PPy on gold substrate PL changes after three hours of irradiation by UV light (325 nm, 5 W/cm²) in air under atmospheric pressure and in 0.01 Pa vacuum.

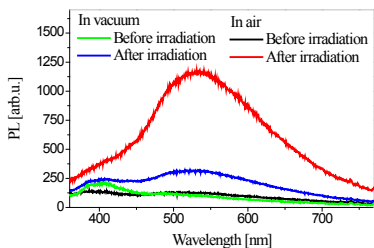
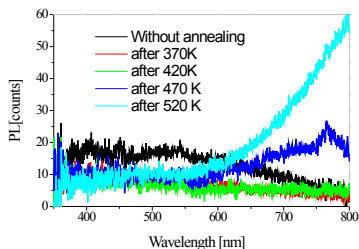


Figure 4. PL spectra of electrochemically prepared PPy on gold substrate that was annealed for 2 hours at various temperatures from 370 K to 520 K.



Evidence of changes in functional groups of PPy after the light exposure is provided by XPS analysis of our samples (Table 1). XPS measurements show that at least carboxyl functional group is being quenched during light irradiation. Increase of C-O-H and C=O groups suggest that photo-induced oxidation is being to the certain extend involved during irradiation [16]. Presented results can be interpreted as follows: UV light starts after exceeding an intensity threshold generate specific free-radicals. These radicals aren't thermal-initiated and they oxidize at the presence of the air. Among others these modifications reduce conjugation length of polymer chain and cause strong increase of photoluminescence.

Table 1. XPS analysis of electrochemically prepared PPy on gold substrate carbon bonds (at. %) before and after UV modification

	C1s C=C	C1s C-C/ C=C*-N	C1s C-N/ C-O	C1s C=O	C1s COO
Before irradiation	57,973	10,412	10,989	8,821	11,080
After adonation	63,648	7,594	16,11	12,648	0

CONCLUSION

We have shown that PPy is modified by the UV light exposure. XPS measurements have proved that C-O-O-H functional group is being quenched and C-O-H and C=O is created during irradiation, but likely other functional groups are affected, too. Presented modifications are highly dependent on presence of air and can't be induced thermally. Photo-induced changes likely cause decrease of conjugation length of polymer chains which result in increase of radiative recombination of excited charge carriers. The greatest advantage of the light-induced PPy modification is that it works in almost the same way on PPy prepared by different methods and under various conditions.

ACKNOWLEDGEMENT

The work was supported by Charles University in Prague grant SVV-2012-265306, by GAUK 151910/2012 and by GACR P108/12/G108. For XPS analysis authors would like to thank M.Omastková and M.Mičušik from Slovakian Academy of Science.

REFERENCES

- [1] Vernitskaya T.V, Efimov O.N.: Russian Chemical Review, 66 (1997), 5, 443- 457
- [2] Stejskal J, Omastová M, Prokeš J, et al.: European Polymer Journal, 43 (2007), 2331-2341
- [3] Vršata M, Kopecký D, Myslík V, et al.: Synthetic Metals, 160 (2010), 1081 - 1085
- [4] Stevens G.C, Cheung M, Bloor D.: Journal of Materials Science, 25 (1990), 3814 - 3837
- [5] Gaponik N.P, Talapin D. V, Rogacha A. L.: Journal of Materials Chemistry, 10 (2000), 2163-2166
- [6] Smela E.: Advanced Materials 15 (2003), 5, 481- 494
- [7] Fang Q, et al.: Sensors and Actuators A, 99 (2002), 74 - 77
- [8] Tada K, Onoda M.: Journal of Applied Physics, 86 (1999), 6, 3134 - 3141
- [9] Čermák J, Rezek B, Kromka A, et al.: Diamond & Related Materials, 18 (2009), 1098 - 1101
- [10] Bredas J.L, Scott J.C, Yakushi K and Steet G.B.: Physical Review B, 30 (1984), 2, 1023 - 1025

ELECTROCHEMICAL STUDY OF SHORT CYTOSINE OLIGONUCLEOTIDES

Libor GURECKÝ¹, Zdenka BALCAROVA¹, Iveta PILAROVA^{1,2,3}, Libuse TRNKOVA^{1,3,4*}

¹Department of Chemistry, Faculty of Science, Masaryk University, Kotlarska 2, CZ-611 37 Brno, Czech Republic

²Central European Institute of Technology – CEITEC, Masaryk University, Zerotinovo namesti 617/9, CZ-601 77 Brno, Czech Republic

³Department of Pathological Physiology, Faculty of Medicine, Masaryk University, Kotlarska 2, CZ-611 37 Brno, Czech Republic

⁴Central European Institute of Technology – CEITEC, Brno University of Technology, Technicka 3058/10, CZ-616 00 Brno, Czech Republic

*libuse@chemi.muni.cz

ABSTRACT

Cytosine-rich oligodeoxynucleotides (C-rich ODNs) play diverse roles in the regulation of protein expression at both transcriptional and translational levels. A repetitive C sequence can be responsible for some diseases. It is commonly known that C-rich ODNs form the stable i-motif structure, interesting due to a crucial role in the process of genetic information transfer. The aim of this contribution is to find out the relationship between the structure of homo-ODNs in buffered solutions with the same ionic strength ($I = 0.18 \text{ M}$) but with a different number of cytosines (dC_x ; $x = 3, 4, 5, 6, 9$). Using linear sweep voltammetry (LSV) and elimination voltammetry with linear scan (EVLS), electrochemical reduction signals studied on a mercury electrode reflect the conformational changes of the C-rich ODN chain.

INTRODUCTION

Cytosines, as pyrimidine components of DNA, participate in the processes of energy transfer, cell signaling, and are an essential building block of DNA together with other pyrimidine and purine bases [1]. According to pH and ionic strength the cytosine-rich oligonucleotides (C-rich ODNs) are capable of forming i-motif (intercalated motif) structures with two parallel-stranded C–C⁺, where one cytosine must be hemiprotonated at the N₃ position, and base-paired duplexes intercalate into each other in an antiparallel orientation [2]. For the monitoring of these DNA conformers, spectroscopic methods (circular dichroism and UV/VIS) [3] are very often applied, but lately the application of electrochemical methods has been significantly increasing [4]. Earlier, electrochemical reduction and oxidation of cytosine on mercury and graphite electrodes were studied by means of linear sweep voltammetry (LSV) and cyclic voltammetry (CV) [5,6]. Nowadays, great attention has been devoted to the study of the redox and adsorption behavior of homo- and hetero-oligodeoxynucleotides containing cytosine [7-9].

The aim of this research is to detect the influence of the secondary structure of oligodeoxynucleotides (ODNs) on reduction signals. Electrochemical analyses of ODNs are compared with circular dichroism (CD) spectral results.

MATERIAL AND METHODS

Chemicals:

ODNs, 5'-CCC-3' (dC_3) and 5'-C CCC-3' (dC_5) were purchased from Thermo Fisher Scientific, Ulm, Germany; 5'-CCC CC-3' (dC_5), 5'-CCC CCC-3' (dC_6), 5'-CCC CCC CCC-3' (dC_9) from Integrated DNA Technologies, Inc., USA. The exact concentrations of ODNs studied were determined by UV spectroscopy. The concentration of monitored cytosine-rich ODNs was $10 \mu\text{M}$. The solutions of homo-ODNs were added into the phosphate-acetate buffer (supporting electrolyte; pH 3-7.5) with adjusted ionic strength $I = 0.18 \text{ M}$ (NaCl).

Linear sweep voltammetry (LSV)

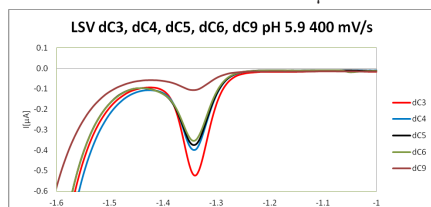
The voltammetric experiment was performed using the electrochemical analyzer AUTOLAB PGSTAT 20 (Ecochemie, Utrecht, The Netherlands) in connection with GPES software. Electrochemical measurements were carried out in a three-electrode system. HMDE with an effective area of 0.4 mm^2 was used as a working electrode. Ag/AgCl/3M KCl was used as a reference electrode and platinum wire as an auxiliary electrode. The experimental conditions were as follows: potential range from -1 V to -1.7 V , time of adsorption 0 s , and scan rate from 50 mV/s to 800 mV/s . The results from LSV will be used for elimination voltammetry with linear scan (EVLS).

RESULTS AND DISCUSSION

We studied five short homodeoxyoligonucleotides (homo-ODNs) containing cytosine (C): dC₃, dC₄, dC₅, dC₆, and dC₉ using LSV. The voltammetric study of homo-ODNs at HMDE at the same pH value buffers provided different dependences on the number of C in ODNs chains. As follows from Fig. 1, the height of the reduction peaks of the ODNs studied decreased with the increasing number of cytosines in the chains. Based on this fact, it can be stated that dC₃ is not able to form the i-motif structures, but dC₄, dC₅, dC₆, and dC₉ can form them.

Via the C reduction signals we determined that the prolongation of the ODN chain supports the formation of more non-canonical bonds in the hemiprotinated (C+-C) pair ("i-motif"). Using elimination voltammetry with linear scan (EVLS) [9] the strong adsorption of ODNs on the mercury electrode surface influenced by an "i-motif" was confirmed.

Figure 1: Linear voltammetric (LSV) curves of C-rich homo-ODNs (dC_x, x= 3,4,5,6, and 9) measured at 400 mV/s and pH 5.9. The concentration of ODNs was 10 μM



CONCLUSION

Using voltammetry (LSV and EVLS) we investigated the dependences of the structure of short homo-ODNs on their reduction behavior at different pH. Besides pH and the ionic strength of buffer solutions, the number of cytosines in the ODN chain plays a key role not only for their electrochemical reduction but also for their adsorption on electrode surfaces. We can conclude that electrochemical results reflect the ODN conformational polymorphism represented by the i-motif.

ACKNOWLEDGMENTS

This research was supported by the following projects: (a) CEITEC – Central European Institute of Technology Project CZ.1.05/1.1.00/02.0068, (b) OPVK Project (NanoBioMetalNet) CZ.1.07/2.4.00/31.0023, and (c) 106/09/H035 of the GA CR.

REFERENCES

[1] Bloomfield V A, Crothers D M, and Tinoco I: *Nucleic Acids: Structures, Properties, and Functions*, Sausalito: University Science

Books (2000).
 [2] Leroy J L, et al.: *Biochemistry*, 32 (1993) 6019-6031.
 [3] Simonsson T, Pribylova M, and Vorlickova M.: *Biochem. Biophys. Res. Commun.*, 278 (2000) 158-166.
 [4] Palecek E., Bartosik M.: *Chem. Rev.* 2 (2012) in press.
 [5] Dryhurst G.: *Electrochemistry of Biological Molecules*, Academic Press, New York (1977).
 [6] Trnkova L., Friml J., Dracka O.: *Bioelectrochemistry*, 54 (2001) 131.
 [7] Trnkova L.: Jelen F., Postbieglova I.: *Electroanalysis*, 15 (2003) 1529-1535.
 [8] Trnkova L., Jelen F., Postbieglova I.: *Electroanalysis*, 18 (2006) 662-669.
 [9] Trnkova L., in: V. Adam and R. Kizek (Eds.), *Utilizing of Bio-electrochemical and Mathematical Methods in Biological Research*, Research Signpost, Kerala, India, Ch. 4 (2007) 51.

PROSPECTS OF POLAROGRAPHY - ELECTROLYSIS WITH MERCURY ELECTRODES - FOR THE YEARS TO COME

Michael HEYROVSKY*

J. Heyrovský Institute of Physical Chemistry, Academy of Sciences of the Czech Republic,
Dolejškova 3, 182 23 Prague 8, Czech Republic

*heyrovsk@jh-inst.cas.cz

The mercury drop by its physical and chemical essence represents an ideal universal instrument in electrochemical research. Polarography in its narrow sense - electrolysis with dropping mercury electrode - now after 90 years of many-sided development serves as an experimental and theoretical base for further advancement of polarography in wider sense including research with stable mercury electrodes, mostly in form of hanging mercury drops.

Electrolysis with hanging mercury drop offers many experimental possibilities which have not yet been quite fully exploited. Electrochemical polarization of a hanging mercury drop can be done either by applying electrical voltage - voltammetry [1], or electrical current - chronopotentiometry [2], by single pulse or by repeated pulses.

On surface of the hanging mercury drop electrode at a certain constant potential the product of cathodic or anodic reaction or of adsorption of the studied compound can be accumulated within a certain time and the product then subjected to opposite electrode reaction or desorption; from the thus obtained experimental curve the studied compound can be identified and quantitatively determined. This method, considerably increasing sensitivity of electrochemical analysis, is known as "stripping" - cathodic [3], anodic [4] or adsorptive [5].

Electrochemically inactive substances can be transformed into electrochemically active by an appropriate chemical reaction - in case of organic macromolecules, e.g., this has been successfully achieved by compounds of osmium (VI) [6, 7] or (VIII) [8]. Similar result can be achieved by an appropriate modification of the surface of mercury electrode [9].

Apart from substances electrochemically reducible or oxidizable on mercury electrodes are electrochemically active also substances able to catalyze evolution of hydrogen, either in presence of cobalt compounds in solution by the "Brdička reaction" [10], or without it by the "presodium catalysis" [11]. Cobalt is not the

only element which can spur catalytic activity of particular compounds [12, 13].

As the kinetics of electrode reactions in voltage-controlled electrolysis differ from those in current-controlled electrolysis, the voltammetric curves differ from the chronopotentiometric curves of identical solutions. The derivative chronopotentiometric curves of solutions of hydrogen catalysts yield the well developed "presodium peak H" [14]. Catalytically active are many macromolecular organic compounds, the inactive ones can be transformed into active by appropriate reactions. The method of "constant current derivative stripping chronopotentiometry" offers many possibilities to follow biologically important molecules in nanomolar and lower concentrations [15 - 21].

The electrochemical activity of mercury can be modified to a certain extent by the use of some of amalgam electrodes which maintain the main advantages of mercury electrodes [22-23].

The area of electrochemistry opened by polarography ninety years ago is still fertile, though no more only by dropping mercury electrode.

ACKNOWLEDGEMENT

This contribution could have been prepared thanks to financial support by GA ČR project No P206/11/1638 and P208/12/1645 and by GA AV ČR project No IAA 400400806.

REFERENCES

- [1] Kemula W.: *Advances in Polarography*, Vol.1 (1959), 103-143
- [2] Delahay P., Berzins T.: *J. Am. Chem. Soc.*, 75 (1955), 2486-2493
- [3] Ball R.G., Manning D.L., Menis O.: *Anal. Chem.* 32 (1960), 621-623
- [4] Kemula W., Strojek J.W.: *J. Electroanal. Chem.* 12 (1966), 1-8
- [5] Kalvoda R.: *Electroanalysis* 12 (2000), 1207-1210
- [6] Trefulka M., Bartošik M., Paleček E.: *Electrochem. Communic.* 12 (2010), 1760-1763
- [7] Paleček E., Trefulka M.: *Analyst* 136 (2011), 321-326
- [8] Fojta M., Billová S., Havran L., Pivoňková

- H., Černocká H., Horáková P., Paleček E.:
Anal.Chem.80 (2008), 4598-4605
- [9] Ostatná V., Černocká H., Paleček E.:
Bioelectrochemistry 84 (2012),
- [10] Heyrovský M.: Electroanalysis 12 (2000),
935-939
- [11] Mader P., Veselá V., Dorčák V., Heyrovský
M.: Collect.Czech.Chem.Comm. 66
(2001), 397-410
- [12] Banica F.G., Ion A.: Collect.Czech.Chem.
Commun. 65 (2000), 995-1013
- [13] Heyrovský M.: Collect.Czech.Chem.
Commun. 66 (2001), 67-80
- [14] Tomschik M., Havran L., Fojta M., Paleček
E.: Electroanalysis 10 (1998), 403-409
- [15] Brázdová M., Kizek R., Havran L., Paleček
E.: Bioelectrochemistry 55 (2002), 115-
118
- [16] Masařík M., Sobiecka A., Kizek R., Jelen F.,
Pechan Z., Hoyer W., Jovin T.M.,
Subramaniam V., Paleček E.: Electroanalysis
16 (2004), 1172-1181
- [17] Dorčák V., Paleček E.: Electroanalysis 19
(2007), 2405-2412
- [18] Ostatná V., Kuralay F., Trnková L., Paleček
E.: Electroanalysis 20 (2008), 1406-1413
- [19] Ostatná V., Paleček E.: Electrochim.Acta 53
(2008), 4014-4021
- [20] Dorčák V., Paleček E.: Anal.Chem. 81
(2009), 1543-1548
- [21] Paleček E., Ostatná V.: Chem.Comm. 2009,
1685-1687
- [22] Yosypchuk B., Barek J.: Crit.Rev.Anal.
Chem. 39 (2009), 189-203
- [23] Yosypchuk B., Fojta M., Barek J.:
Electroanalysis 22 (2010), 1967-1973

DETERMINATION OF OXIDATIVE STRESS IN GUINEA PIG TREATED BY HALOPERIDOL

Marian HLAVNA^{1,2}, Tibor STRACINA³, Jiri SOCHOR⁴, Ondrej ZITKA⁴, Jaromir GUMULEC¹, Marketa SZTALMACHOVA^{1,2}, Petr BABULA², Vojtech ADAM⁴, Rene KIZEK⁴, Marie NOVAKOVA³, Michal MASARIK¹

¹Department of Pathological Physiology, Faculty of Medicine, Masaryk University, Kamenice 5, 625 00 Brno, Czech Republic

²Department of Natural Drugs, Faculty of Pharmacy, University of Veterinary and Pharmaceutical Sciences, Palackeho 1-3, CZ-612 42 Brno, Czech Republic

³Department of Physiology, Faculty of Medicine, Masaryk University, Kamenice 5, 625 00 Brno, Czech Republic

⁴Department of Chemistry and Biochemistry, Faculty of Agronomy, Mendel University in Brno, Zemědělská 1, 613 00 Brno, Czech Republic

ABSTRACT

Aim of our study was to investigate level of oxidative stress caused by haloperidol as a highly potent neuroleptic drug in animals. We treated *Cavia porcellus* (guinea pig) with haloperidol and we used several approaches for determination of oxidative stress level from plasma and erythrocyte. We were concerned also on comparison results obtained by these methods to figure out the best approach for oxidative stress monitoring.

INTRODUCTION

Haloperidol is an older antipsychotic used in the treatment of schizophrenia and in the treatment of acute psychotic states and delirium. Due to its strong central antidopaminergic action, it is classified as a highly potent neuroleptic [1]. It is used in several diagnoses such as psychosis, manic phases, hyperactivity, aggressively, and acute delirium and in some cases it is used in long-term treatments. However, the usage of typical neuroleptic drugs has been limited by the side effects and toxicity produced by them [2-4]. Therefore is essential to know all possible risks which bring together treatment with these drugs. We decided to measure and compare level of oxidative stress from plasma and erythrocytes from 17 guinea pigs (10 treated and 7 untreated). We were concerned on superoxide dismutase detection, FRAP method, glutathione reductase and reduced and oxidized glutathione GSH:GSSG ratio measurement as a relevant oxidative stress pointer.

MATERIAL AND METHODS

Animals

Animals were obtained from Velaz, Czech republic. Animals were 4 months old and were treated for 3 weeks in total dose 4200 mg of haloperidol per 100g of animal.

Determination of low-molecular-mass thiols and haloperidol

High performance liquid chromatography with electrochemical detection (HPLC-ED) system consisted of two solvent delivery pumps operating in the range of 0.001-9.999 ml/min (Model

582 ESA Inc., Chelmsford, MA), Zorbax Eclipse AAA Column (4.6 × 150mm 3.5-micron particle size; Varian Inc., CA, USA), and a CoulArray electrochemical detector (Model 5600A, ESA, USA). The sample (30 µl) was injected using autosampler (Model 540 Microtiter HPLC, ESA, USA). HPLC-ED experimental conditions were as follows – mobile phases compositions: A: 80 mM trifluoroacetic acid and B: methanol. They were mixed in gradient from 3 % B in the 1st min, 10 % B in the 2nd to the 6th min and 98 % B from the 7th min of the separation; flow of the mobile phase was 0.8 ml/min, temperature of the separation was 40 °C; working electrodes potential was 900 mV; detector temperature was 30 °C; each measurement was done in triplicates. Retention time of the reduced glutathione (GSH) was 5 min. GSH concentration was calculated from a calibration curve (0.5 – 100 µM). The signal was quantified as a sum of current responses from all working electrodes. In the case of real sample measurements, the shift of the retention time was of about ± 2 %.

Determination of antioxidant activity

For determination of antioxidant activity a BS-400 automated spectrophotometer (Mindray, China) was used. It is composed of cuvette space tempered to 37±1 °C, reagent space with a carousel for reagents (tempered to 4±1 °C), sample space with a carousel for preparation of samples and an optical detector. Transfer of samples and reagents is provided by robotic arm equipped with a dosing needle (error of dosage up to 5 % of volume). Cuvette contents are mixed by an auto-

matic mixer including a stirrer immediately after addition of reagents or samples. Contamination is reduced due to its rinsing system, including rinsing of the dosing needle as well as the stirrer by MilliQ water. For detection itself, the following range of wave lengths can be used - 340, 380, 412, 450, 505, 546, 570, 605, 660, 700, 740 and 800 nm. Experimental details on all used spectrometric assay are described in the following paper [5].

This study was approved by the Committee for Ethics of Faculty of Medicine, Masaryk University, Brno.

RESULTS AND DISCUSSION

We treated 17 guinea pigs by haloperidol and measured oxidative stress from plasma and isolated erythrocytes. As you can see in Fig.1 haloperidol was present in plasma of treated animals while was undetectable in animals without treatment. In animals treated by haloperidol was significantly increased superoxide dismutase (SOD) and glutathione reductase, which is clear evidence about ROS and oxidative stress. Our findings are in concordance with previous studies [6, 7]. SOD was increased also in isolated erythrocytes and also ratio between reduced and oxidized glutathione (GSH:GSSG) was shifted to oxidative stress state.

Figure 1.: Oxidative stress measurement from plasma. In first graph is haloperidol detected in plasma of treated and untreated animals. Untreated animals had undetectable amounts of haloperidol in plasma

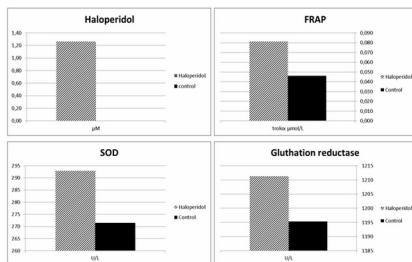
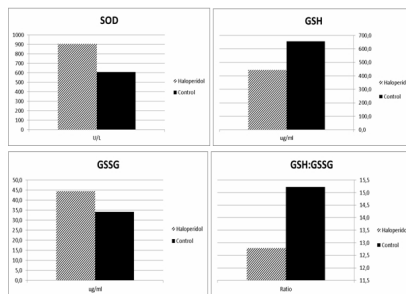


Figure 2.: Oxidative stress measurement from isolated erythrocytes.



CONCLUSION

The present study demonstrates that administration of haloperidol causes significant oxidative stress, which was able to measure by FRAP and was evident in Glutathione reductase and significantly decreased GSH and GSH:GSSG ratio in treated animals.

ACKNOWLEDGEMENT

The work has been supported by MUNI/A/0846/2011, NanoBioMetalNet CZ.1.07/2.4.00/31.0023.

REFERENCES

- [1] Janssen, P.A., et al., Pimozide, a chemically novel, highly potent and orally long-acting neuroleptic drug. 3. Regional distribution of pimozide and of haloperidol in the dog brain. *Arzneimittelforschung*, 1968. 18(3): p. 282-7.
- [2] Ikemura, M., et al., The blood concentration and organ distribution of haloperidol at therapeutic and toxic doses in severe fatty liver disease. *Leg Med (Tokyo)*, 2012. 14(3): p. 147-53.
- [3] Maxa, J.L., et al., Possible toxic encephalopathy following high-dose intravenous haloperidol. *Ann Pharmacother*, 1997. 31(6): p. 736-7.
- [4] Tsujimoto, A., et al., Toxic haloperidol reactions with observation of serum haloperidol concentration in two children. *Dev Pharmacol Ther*, 1982. 4(1-2): p. 12-7.
- [5] Sochor, J., et al., Fully Automated Spectrometric Protocols for Determination of Antioxidant Activity: Advantages and Disadvantages. *Molecules*, 2010. 15(12): p. 8618-8640.
- [6] Polydorou, M., et al., Haloperidol- and clozapine-induced oxidative stress in the rat brain. *Pharmacol Biochem Behav*, 2004. 78(4): p. 751-6.
- [7] Heiser, P., et al., Effects of antipsychotics [and vitamin C on the formation of reactive oxygen species. *J Psychopharmacol*, 2010. 24(10): p. 1499-504.

SURFACE PLASMON RESONANCE BIOSENSORS AND THEIR BIOANALYTICAL APPLICATIONS

Jiri HOMOLA

Institute of Photonics and Electronics, Chaberská 57, Prague, Czech Republic
homola@ufe.cz

ABSTRACT

This paper reviews the present state of the art in the development of surface plasmon resonance (SPR) biosensors and presents selected results of research into SPR sensors at the Institute of Photonics and Electronics, Prague.

INTRODUCTION

Label-free photonic biosensors represent a disruptive technology that enables the direct observation of molecular interaction in real-time and rapid, sensitive and label-free detection of chemical and biological species with potential applications in a wide number of important areas including medical diagnostics, environmental monitoring, food safety and security. Optical biosensors based on surface plasmon resonance represent the most advanced and mature label-free photonic biosensor technology [1, 2].

SPR BIOSENSORS

Since their conception in the nineties, SPR biosensors have made great advances in terms of the method, instrumentation and applications. This paper review advances in the development of optical platforms for SPR sensors based on propagating surface plasmons on continuous metallic films and localized surface plasmons on metallic nanostructures and describes selected implementations of SPR sensors (e.g. high-performance biosensors based on SPR imaging of surface plasmons on gold films [3] and arrays of gold nanorods [4], compact SPR sensors for the use in the field [5]). Fluidic aspects of SPR biosensing and advanced microfluidic concepts for SPR biosensors are also discussed [6, 7]. Finally, examples of SPR biosensors for the detection of chemical and biological analytes related to medical diagnostics, environmental monitoring, food safety and security are provided.

ACKNOWLEDGEMENT

This work was supported by Praemium Academiae of the Academy of Sciences of the Czech Republic, the Czech Science Foundation (contracts P205/12/G118) and by the Ministry of Education, Youth and Sports (contracts OC09058 and LH11102).

4. REFERENCES

- [1] J. Homola, Surface plasmon resonance based sensors, Springer, Berlin (2006).
- [2] J. Homola, Chemical Reviews, 108 (2008), 462-493.
- [3] M. Piliarik, H. Šípová, P. Kvasnička, N. Galler, J. R. Krenn, J. Homola, Optics Express, 20 (2012), 672-680.
- [4] M. Piliarik, L. Párová, J. Homola, Biosensors & Bioelectronics 24 (2009), 1399-1404.
- [5] M. Piliarik, M. Vala, I. Tichý, J. Homola, Biosensors & Bioelectronics 24 (2009), 3430-3435.
- [6] T. Špringer, M. Piliarik, J. Homola, Analytical and Bioanalytical Chemistry, 398 (2010), 1955-1961.
- [7] H. Šípová, D. Vrba, J. Homola, Analytical Chemistry, 84 (2012), 30-33.

CHICKEN ANTIBODIES IN WESTERN BLOTS: HOW TO AVOID POTENTIAL KERATIN CROSS-REACTIVITY

Jitka KRIZKOVA, Iva MACOVA, Marie STIBOROVA, Petr HODEK*

Department of Biochemistry, Faculty of Science, Charles University in Prague, Hlavova 2030, 128 40, Prague 2, Czech Republic

*hodek@natur.cuni.cz

ABSTRACT

Chicken antibodies (IgY) are increasingly being used as a primary antibody in the Western blotting immunodetection, offering several advantages compared to the common mammalian antibodies. The presence of additional bands in the region of 45-70 kDa, vertical streaks, and spots on the membrane, caused by human keratins, made the evaluation of the developed blots hardly possible. In this study, we describe a method how to eliminate the cross-reactivity of IgY with human keratins.

1. INTRODUCTION

Western blotting is an essential electrochemical method widely used for protein transfer and immunodetection of various antigens. Chicken antibodies (IgY) are frequently used as a primary antibody in this immunodetection technique. The chicken antibodies, which are purified from egg yolks, offer several advantages compared to the common mammalian antibodies (for review see Hodek et al. [1]). However, in some particular cases the application of IgY could cause severe problems. In our research, the chicken antibodies are employed for the determination of microsomal cytochromes P450 (CYPs), the enzymes involved in the metabolism of xenobiotics (e.g. drugs, carcinogens) and endogenous substrates (e.g. steroids). Our difficulties with the chicken antibodies were manifested by the presence of additional bands in the region of 45-70 kDa, vertical streaks, and spots in the developed blots identified as keratins. In this study, we describe a cost-effective method for the prevention of keratin-originated interferences during Western blotting immunodetection, when using the chicken antibodies.

MATERIALS AND METHODS

Microsomal fractions

Microsomal fractions were prepared by differential centrifugation according to van der Hoeven and Coon [2] from the liver of rats treated with hesperidin (Sigma-Aldrich, USA). The electrophoretical separation of microsomal CYP proteins was carried out on 7.5% SDS-polyacrylamide gel according to the standard protocol of Laemmli [3]. Microsomal samples (7.5 micrograms of protein) were applied on each well. Following the electrophoresis, the separated proteins were electro-transferred to an Immobilon-P membrane (Millipore Corp., USA) using the Whatman Biometra® Fastblot B 32 (Whatman, USA). To prevent non-specific

binding of proteins, the membrane was blocked in 5% non-fat dried milk dissolved in PBS containing 0.3% Triton X100 overnight at 4°C.

Saturation of primary antibody

The primary chicken antibody against rat CYP1A1/2 (0.25 mg per ml PBS containing 0.3% Triton X100) was incubated with human keratins of *Stratum corneum* (pieces of keratinized layer of human skin from the soles, 0.01 g per ml) overnight at 4°C. After filtration, the neutralized antibody was diluted (30 µg per ml) and used for the detection of CYP1A1/2 on the blot. The membrane was then incubated with anti-chicken IgG conjugated with alkaline phosphatase (1:1500 dilution) and proteins were visualized by Sigmafast BCIP/NTB substrate for alkaline phosphatase.

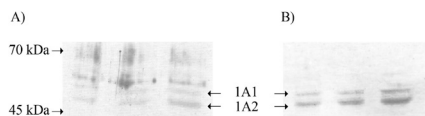
RESULTS AND DISCUSSION

To overcome keratine-originated interference, all chemicals were tested for the keratine contaminations. Keratine was found mainly in 2-mercaptoethanol, the chemical, which is frequently used for reduced SDS-PAGE. All attempts to purify this chemical were inefficient. Thus, our effort was focused on primary IgY antibody, which reacts with keratine. The primary IgY antibody was pretreated with solutions of human keratine to saturate the anti-keratin antibody prior to its binding to keratins present in the course of the Western blotting procedure. The results presented in Figure 1A clearly demonstrate the interferences caused by keratins (region 45-70 kDa), when the untreated primary antibody against rat CYP1A1/2 was used to probe the membrane with transferred microsomal proteins. No keratin bands or streaks (see Figure 1B) were found after the application of the keratin-saturated primary antibody on the Western blots.

CONCLUSION

The described procedure suggests a simple and effective method how to prevent the occurrence of interfering bands caused by the presence of human keratins during Western blotting, when using the primary chicken antibody. As shown, the cross-reactivity of IgY with human keratins can be completely eliminated by using the chicken antibody saturated with pieces of keratinized human skin (dispensable human material).

Figure 1. Western blots of rat liver microsomal samples. Separated proteins (7.5 µg of protein/well) were electro-transferred to the PVDF membrane and reacted with the primary chicken antibody (against CYP1A1/2) pre-incubated without (A) or with (B) human keratins. The visualization was done by BCIP/NTB substrate.



ACKNOWLEDGEMENT

This work was supported from grant P303/12/G163 of The Grant Agency of the Czech Republic.

REFERENCES

- [1] Hodek, P., Koblas, T., Rýdlová, H., Kubičková, B., Šulc, M., Hudeček, J., Stiborová, M. (2004) Chicken egg yolk as an excellent source of highly specific antibodies against cytochromes P450. *Collect. Czech. Chem. Commun.* **69**, 659-673
- [2] van der Hoeven, T.A., Coon, M.J. (1974) Preparation and properties of partially purified cytochrome P-450 and reduced nicotinamide adenine dinucleotide phosphate-cytochrome P-450 reductase from rabbit liver microsomes. *J. Biol. Chem.* **249**, 6302-6310
- [3] Laemmli, U.K. (1970) Cleavage of structural proteins during the assembly of the head of bacteriophage T4. *Nature* **227**, 680-685

ELECTRO IMPEDANCE SPECTROSCOPY CHARACTERIZATION OF NANOSTRUCTURED ELECTROCHEMICAL SENSORS

Radim HRDY^{1,2*}, Hana KYNCLOVA¹, Jana DRBOHLAVOVA^{1,2}, Jana CHOMOUCKA^{1,2}, Petra BUSINOVA^{1,2}, Jan PRASEK^{1,2} and Jaromir HUBALEK^{1,2}

¹Department of Microelectronic, Faculty of Electrotechnology and Communications, Brno University of Technology, Technická 3058/10, 616 00 Brno, Czech Republic

²Central European Institute of Technology, Brno University of Technology, Technicka 3058/10, 616 00 Brno, Czech Republic

*hrdy@feec.vutbr.cz

ABSTRACT

The aim of this paper is optimization and following characterization of gold nanostructured electrochemical sensors suitable for biological and heavy metal ions detection. The EIS (electro impedance spectroscopy) measurements of surfaces, with various geometry of nanoparticles, have showed the high dependence between the rate of nanomachining and active electrochemical surfaces area.

INTRODUCTION

Electrochemical high resolutions detection of heavy metals ions or DNA fragments can be improved by nanomechanized surface of electrochemical sensors. The main idea of using nanoparticles is enlarging the active surface of working electrodes and gaining some special new abilities such as higher selectivity and signal stability [1]. However, the simply growing metal nanowires on electrodes are not always the right way to obtain the improved system [2]. According to previous papers, it is known the long nanowires covered surface has not as improved parameter of detection as flat electrodes without nanoparticles. The responses of nanomachined sensors to analyst are usually worse which is caused by the interactions with ions only with the top part of nanowires [3]. One of the solutions is the change of nanowires geometry and concurrently the parameters and form of diffusion layer.

EXPERIMENTS

Nanosurface fabrication

A thin aluminum film (1 μm) was deposited on surface. Subsequently, the thin porous anodic alumina template was obtained by one-step anodization process under potentiostatic voltage (40 V) in 0.3 M oxalic acid at 17 °C. The counter electrode was gold electrode. The metal used for experiments on the nanostructure growth was gold (component of electrolyte: 6 g/L of $\text{K}[\text{Au}(\text{CN})_2]$ and 2.32 g/L of H_3BO_3). The current density of deposition over the total area of nanopores was usually 0.25 mA/cm² for Au nanostructures. The filled template was dissolved in 5% H_3PO_4 .

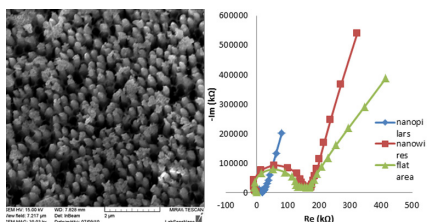
Sensors measurement


Measuring system Metrohm $\mu\text{Autolab III}$ with FRA2 module was used for the EIS characterizations of sensors. Samples were measured in 10 ml of potassic sulfate of various concentrations (0.1 μM – 10 mM). The frequency range was set on 1 Hz – 1 MHz and the amplitude was 60 mV. A three electrodes cell with Pt auxiliary electrode and Ag/AgCl/3M KCl the reference electrode were used for the measurements.

RESULTS AND DISCUSSION

Three types of electrodes have been prepared and two of them with different length of gold nanowires, one with long deposition with fully filled nanoporous template. The second one was deposited in lower current density and shorter time creating the very short nanopillars, fig. 1, where the ratio of diameter to length has an importance. This is more visible on EIS spectra fig 2. Both of nanomachined samples have a similar diffusion part, which means the same angle in comparison with surface without nanoparticles. The angle close to 90° indicates the added capacitance of a nanolayer.

Figure 1, 2.: Short nanorods, EIS spectrum of nanorods, nanowires and particle less surface





However, the remaining part of the long deposited nanowires surface is very similar as the flat surface. The value of double layer capacity and charge transfer resistance are equal. On the other hand, the short nanorods have ten times less impedance than the rest of them that has shown the fact that the real electrochemical surface area has increased.

CONCLUSION

The important fact of the sensors area increasing has been shown. The direct proportion of nanowire length and area enlarging has limits. The simple deposition of nanowires on electrodes does not cause increasing the active electrochemical area.

ACKNOWLEDGEMENT

The work has been supported by project GA ČR 102/08/1546 (NANIMEL), project KAN 208130801 (NANOSEMED), and project CZ.1.05/1.1.00/02.0068 (CEITEC).

REFERENCES

- [1] Hrdy R, Voroztzova M, Hubalek J, et al.: *Act. Metal*, 306 (2008), 13-6, 1335-1532
- [2] Hubalek J Hrdy R, Voroztzova M, , et al.: *Sensors*, 36 (20011), 1-1, 1876-6196
- [3] Hrdy R, Voroztzova M, Hubalek J, et al.: *X. Pracovní setkání fyzikálních chemiků a elektrochemiků*, 87 (20010), 3-1.1978-80-7375-396-2

MICROTECHNOLOGY TOWARDS SENSORS

Jaromir HUBALEK^{1,2}, Vojtech ADAM^{1,2}, Rene KIZEK^{1,2}

¹Department of Microelectronics, Faculty of Electrical Engineering and Communication, Brno University of Technology, Technická 10, 616 00 Brno, Czech Republic

²Central European Institute of Technology, Brno University of Technology, Technická 10, 616 00 Brno, Czech Republic

*hubalek@feec.vutbr.cz

ABSTRACT

Nowdays microtechnology brings many solutions in integration several systems on a chip. Chips are approaching into our life very rapidly facilitate our daily activity. MEMS chips present possibility to measure physical values, provide chemical or biological analysis. The work present review of current technology possibilities and levels.

INTRODUCTION

Microtechnologies have developed a lot towards others application behind microelectronics and today offers many techniques for fabrication several structures using many different materials not common in microelectronics. Especially fabrication of microsensor has got long history now. For microsensors a special MEMS technology was developed. This technology was mainly used for electromechanical transducers useful in physical sensors preparation. During last two decades the technology was advanced for optical applications, biomedical and pharmaceutical applications as chemical micro-sensors, micro-biosensors, and arrays or assays.

MEMS TECHNOLOGY

This technology is based on silicon technology for microelectronics extended by micromachining techniques based on wet or dry etching of materials containing Si. The technique use anisotropic etching of silicon monocrystal. Isotropic is used also for silicon but functions with all, in technology, used inorganic materials. Combination of photolithography and etching can be fabricated several shapes of devices as membranes, cantilevers or movable system (linear or angular). Thin films with specific properties deposited on formed device provide transformation of mechanical movement into electrical signal and vice versa. Examples of common MEMS are accelerometer, gyroscope, pressure or force sensor, etc. Today's effort in optical measuring instruments miniaturization brought Optical MEMS (MOEMS) assuring optical signal transmitting. [1]

C-MEMS

This technology is powerful approach to build up carbon devices where necessary techniques involved in fabrication are only photolithography and burning. In the technology patterned

photoresist is pyrolyzed in inert environment at high temperature to carbonize organic material that resists is prepared from. As C-MEMS the fractal 3D carbon microelectrode arrays were fabricated. [2].

BIOMEMS

Among the new technologies with an increasingly broader impact in biology, medicine and pharmacy is a lab-on-a-chip (LOC) where electrophoretic microfluidic systems for separation and analysis are miniaturized as one of the first BioMEMS without any electromechanical systems. These devices are extremely attractive for clinical applications, bringing the bedside analysis through point-of-care analyzers capable of comprehensive diagnostics poised to reshape the delivery of health care. Microfabricated devices for sample preparation would open new possibilities by allowing comprehensive genomic and proteomic analyses. On-chip blood sample preparation would lead to gentler, faster, and more consistent manipulation of living cells, and therefore to more accurate and better quality extracted information.

The mean-square displacement of a particle from its origin is proportional to time, and that surface area to volume is proportional to the scale of the microchannel. As the scale decreases, surface area to volume increases, while time for diffusion decreases. In LOC devices, the channel size of 150–250 μm means diffusion across the channel may occur in seconds. Today valves, pumps, mixing chambers etc. are already integrated which really brings the LOC system as BioMEMS among powerful analytical tools. [3]

Microfabrication in area of Biomedical applications was already advanced from non-living systems as genes on a chip or labs on a chip towards in-vivo application. Today a new generation of microdevices that incorporates living cells is emerging, fueled by recent advances in the understanding of cellular behaviour in microenvironments. These emerging devices are

expected to become key technologies in the 21st century of medicine, with a broad range of applications varying from diagnostic, tissue-engineered products, cell-based drug screening tools, and basic molecular biology tools. [4]

CONCLUSION

Microtechnology knows many techniques to miniaturize huge amount of systems for measurements of whatever. MEMS technology brings many solutions for fabrication of analyzers integrating methods utilized in medicine, diagnosis and pharmacy and open the laboratory methods for easy using by no specialist during day life. MEMS can be powerful tool for analysis that helps progressing point-of-care and saving many human lives.

ACKNOWLEDGEMENT

The work has been supported by the project MAS No. 120228 supported by ENIAC JU and the project SIX No. CZ.1.05/2.1.00/03.0072.

REFERENCES

- [1] Tai-Ran Hsu, MEMS & Microsystems: Design, Manufacture, and Nanoscale Engineering, 2nd edition, Wiley (2008) p. 576
- [2] Chunlei Wang, et al., Electrochem. Solid-State Lett., Volume 7, Issue 11, pp. A435-A438 (2004)
- [3] Steven S. Saliterman, Fundamentals of BioMEMS and Medical Microdevices, 1st edition, SPIE Publications, 2006, p. 608
- [4] Blood on a Chip, BioMEMS Resource Centre, Massachusetts General Hospital, Boston, USA, 2005-2007 [<http://www.biomemsrc.org/biomemsrc/research-core-blood.htm>]

ANALYSIS OF MICRO RNAS EXPRESSION IN CELL LINES DERIVED FROM PROSTATE CARCINOMA

Kristyna HUDCOVA^{1,2}, Martina RAUDENSKA¹, Marian HLAVNA¹, Jaromir GUMULEC¹, Marketa SZTALMACHOVA^{1,3}, Veronika TANHÄUSEROVA¹, Petr BABULA⁴, Vojtech ADAM³, Rene KIZEK³, Michal MASARIK^{1*},

¹Department of Pathological Physiology, Faculty of Medicine, Masaryk University, Kamenice 5, 625 00 Brno, Czech Republic

²National Center for Biomolecular Research, Faculty of Science Masaryk University, Kamenice 5, 625 00 Brno, Czech Republic

³Department of Chemistry and Biochemistry, Faculty of Agronomy, Mendel University in Brno, Zemedelska 1, CZ-613 00 Brno, Czech Republic

⁴Department of Natural Drugs, Faculty of Pharmacy, University of Veterinary and Pharmaceutical Sciences, Palackeho 1-3, CZ-612 42 Brno, Czech Republic

*masarik@med.muni.cz

ABSTRACT

MiRNAs constitute a large class of single-stranded RNA molecules of 19 to 25 nucleotides that are involved in post-transcriptional gene silencing. MiRNAs not only regulate various developmental and physiologic processes but also are involved in cancer development and can play a role as an important biomarkers. The aim of this study was to determinate the expression levels of selected miRNA in the non-tumor PNT1A line in comparison with tumor lines 22Rv1, PC-3, and LNCaP. We used the *TaqMan* Gene Expression Assays and quantitative RT-PCR. We observed significantly higher ($p < 0.01$) expression of miRNA 23a in all tumor lines compared to non-tumor PNT1A. Significantly higher ($p < 0.01$) expression of miRNA 224 in 22Rv1 line compared to others and significantly higher ($p < 0.01$) expression of miRNA 375 in all tumor lines in comparison with non-tumor PNT1A.

INTRODUCTION

MicroRNAs (miRNAs) are small, phylogenetically conserved, noncoding RNAs that are estimated to regulate at least 30% of all protein encoding genes [1]. Mature miRNAs are involved in post-transcriptional gene silencing. They arise from intergenic or intragenic (both exonic and intronic) genomic regions that are transcribed as long primary transcripts. In recent years, miRNAs have received attention as potential cancer diagnostic markers and therapeutic targets. Deregulated miRNAs expression were reported in various human cancers including prostate cancer [2].

Furthermore, miRNA expression profiles have been shown to classify different cancers and identify cancer tissue origins [3]. On the other hand, it is well described that prostate cancer cells have without exceptions altered ability to uptake and to accumulate Zn(II) ions compared to healthy prostate tissue [4]. In the light of above mentioned facts, it is highly expectable that altered Zn(II) metabolism will have a great impact on prostate cancer tumorigenesis. Zinc (II) homeostatis and metabolism in healthy and tumour tissues as well are maintained mainly by metallothioneins (MTs). Metallothioneins are a family of low-molecular-mass (6-10 kDa) proteins characterized by a high cysteine content and a high binding capacity for post-transition metal ions. In this study we focused on

miRNAs which have a sequential homology with metallothionein genes (*MT2A*, *MT1A*). Our previous study have provided evidence of the association between metallothionein (MT) expression and prostate tumor progression. On mRNA level, significantly increased expression of *MT2A* (2.4-fold) and insignificantly (1.9-fold) elevated *MT1A* in tumor line 22Rv1 compared to non-tumor PNT1A were determined. Contrary to mRNA, significantly ($p = 0.01$) reduced level of MT protein in tumor lines was determined [5]. **Due to these facts, post-transcriptional gene silencing can be involved and different levels of miRNA s in tumor and non-tumor lines, can be expected.**

MATERIAL AND METHODS

Cell lines and cell culture growing

The **PC-3** was derived from a advanced androgen independent bone metastasis of a grade IV prostatic adenocarcinoma from a 62 year old male Caucasian.

The **22Rv1** has been derived from a human prostatic carcinoma xenograft, CWR22R. This represents one of very few available cell lines representative of this disease. This cell line expresses prostate specific antigen.

The **LNCaP** cells line is a cell line derived from a needle human prostate adenocarcinoma cells of a 50-year old caucasian male in 1977, where cells were taken from a needle aspiration

biopsy of a metastatic lesion in the left supraclavicular lymph node.

The PNT1A primary culture was obtained from the prostate of a 35-year-old male at post-mortem. The cells contain the SV40 genome and express large T protein. They present the phenotype of differentiated luminal prostatic cells with the expression of cytokeratin 8 and 18 (markers for luminal glandular epithelia) and vimentin. PNT1A cells are non-tumorigenic in nude mice.

RNA isolation and reverse transcription

Total RNAs were extracted from 200- μ l liquid cell suspension with PBS using High Pure RNA Isolation Kit (Roche, Switzerland). The extracted RNA was eluted from High Pure Filter Tube with 100 μ l Elution Buffer. Concentration and purity of RNA were determined spectrophotometrically using NanoDrop ND-1000 Spectrophotometer (Thermo Scientific, Wilmington, DE, USA). The samples were stored at -80°C.

The isolated RNA was used for complementary DNA (cDNA) synthesis using TaqMan® Small RNA Assay (Applied Biosystems). For each 15 μ l reaction 5 μ l of RNA, 3 μ l of specific RT primer and 7 μ l of RT master mix were combine (program of the thermal cyclor were 30 min at 16°C, 30 min at 42°, 5 min at 85°C and then held at 4°C).

RT-PCR

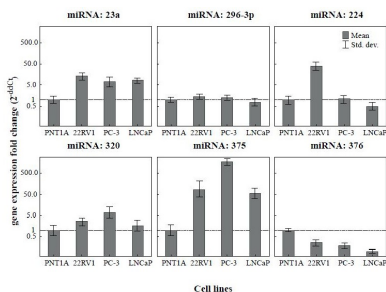
We used the *TaqMan* Gene Expression Assays to RT-PCR in 20 μ l reaction. Reaction mixture contained 4 μ l cDNA (product from RT reaction), 10 μ l of TaqMan® Universal PCR Master Mix, 1 μ l of specific probe TaqMan® Small RNA Assay and 5 μ l nuclease-free water. Reaction was incubated at 50°C for 2 min, 95°C for 10 min and followed by 40 cycles in programme 95°C for 15 s and 60°C at 1 min. For the relative expressions evaluation $2^{-\Delta CT}$ method and a reference expression of *Hnu24* gene were used.

RESULTS AND DISCUSSION

We selected six miRNAs (23a, 296-3p, 224, 320, 375, and 376) according to the homology of their sequences with MT1A and MT2A. For evaluation was used the program Targetscan (<http://www.targetscan.org>). Furthermore, we performed a measurement of miRNA expression levels in four different cell lines (PNT1A, 22Rv1, PC-3, and LNCaP). The differences in particular miRNA expressions is shown in Fig. 1. We observed significantly higher ($p < 0.01$) expression of miRNA 23a in all tumor lines compared to non-tumor PNT1A, significantly higher ($p < 0.01$) expression of miRNA 224 in 22Rv1 line compared to others, significantly higher ($p < 0.01$) expression of miRNA 375 in all tumor lines in comparison with non-tumor PNT1A, marginally lower ($p < 0.05$) expression of miRNA 376 in all tumor lines in comparison with non-tumor PNT1A, marginally higher ($p < 0.05$) expression of miRNA 320 in PC-3 line compared to others,

and no differences between cell lines were observed in expression of miRNA 296-3p.

Figure 1: miRNA levels in cell lines



Porkka et al. found that miRNA 23a and miRNA 23b are significantly decreased in human prostate cancer as compared with BPH (benign prostatic hyperplasias) tissue [6]. We ascertained the increased level of miRNA 23a in cancer tissue as compared with normal prostatic tissue in this study. The expression of miRNA 23a is in correlation with zinc levels in prostate tissue, because in addition to zinc(II) levels in normal prostatic tissue, its levels are increased in benign prostate hyperplasias (BPH), and significantly decreased in prostate cancer [4]. Profiling miRNA expression in hepatocellular carcinoma by Wang et al. revealed miRNA 224 up-regulation [7]. We observed specific up-regulation of miRNA 224 in 22Rv1 line compared to others. The 22Rv1 line has been derived from a primary human prostatic tumor thus one may speculate that this increasing of miRNA 224 level can be use for diagnosis of primary prostatic tumors. In primary prostate cancer tissue, Szczyrba et al have previously found by miRNA sequencing that miR-375 was up-regulated [8]. We found that up-regulation is not specific for primary prostatic cancer, but is occurring in all tumor lines in our study.

CONCLUSION

Accordingly, miRNAs are interesting candidate targets for therapeutic intervention, and there is increasing focus on miRNA-based therapeutics for cancer. An advantage of miRNA analysis is that their small size reduces their susceptibility to degradation in archived tissue and allows for application of miRNA profiling both on diagnosis and prognosis. Thus, miRNAs will likely serve as valuable cancer diagnostic marker.

ACKNOWLEDGEMENT

The work has been supported by NanoBioMetalNet CZ.1.07/2.4.00/31.0023

REFERENCES

- [1] He L, Hannon GJ.: MicroRNAs: small RNAs with a big role in gene regulation. *Nat Rev Genet.*, 5 (2004), 522–531 [PubMed: 15211354]
- [2] Porkka KP, Pfeiffer MJ, Waltering KK, et al.: MicroRNA expression profiling in prostate cancer. *Cancer Res.*, 67 (2007), 6130–6135 [PubMed: 17616669]
- [3] Gaur A, Jewell DA, Liang Y, et al.: Characterization of microRNA expression levels and their biological correlates in human cancer cell lines. *Cancer Res.*, 67 (2007), 2456–2468 [PubMed: 17363563]
- [4] Costello LC, Franklin RB.: Zinc is decreased in prostate cancer: an established relationship of prostate cancer. *J Biol Inorg Chem.*, 16 (2011), 3-8. [PubMed: 21140181]
- [5] Gumulec J, Masarik M, Krizkova S, et al.: Evaluation of alpha-methylacyl-CoA racemase, metallothionein and prostate specific antigen as prostate cancer prognostic markers. *Neoplasma.*, 59 (2012), 191-201 [PubMed: 22248277]
- [6] Porkka KP, Pfeiffer MJ, Waltering KK, et al.: MicroRNA Expression Profiling in Prostate Cancer. *Cancer Res.*, 67 (2007), 6130–6135. [PubMed: 17616669]
- [7] Wang Y, Lee AT, Ma JZ, Wang J, et al.: Profiling microRNA expression in hepatocellular carcinoma reveals microRNA-224 up-regulation and apoptosis inhibitor-5 as a microRNA-224-specific target. *J Biol Chem.*, 283(2008), 13205-15 [PubMed: 18319255]
- [8] Szczyrba J, Nolte E, Wach SG, et al.: Downregulation of Sec23A protein by miRNA-375 in prostate carcinoma. *Mol Cancer Res.*, 9(2011), 791-800 [PubMed: 21593139]

EPR SPECTROSCOPY OF COPPER COMPLEX SYSTEMS WITH BIOLOGICALLY ACTIVE LIGANDS

Lucia HUSARIKOVA*, Zuzana REPICKA, Ladislav MARTISKA,
Dusan VALIGURA, Marian VALKO, Milan MAZUR

Faculty of Chemical and Food Technology, Slovak University of Technology in Bratislava,
Radlinského 9, SK-812 37 Bratislava, Slovakia

*lucia.husarikova@stuba.sk

ABSTRACT

The chemical environments of Cu^{2+} ions in four copper complex systems with different Cu^{2+} salts ($\text{Cu}(\text{ac})_2$ and CuSO_4), 5-chlorosalicylic acid (5-ClSalH) and different biologically active ligands ($\text{N,N}'$ -diethylnicotinamide = denia and 3-pyridylmethanol = ronicol): $[\text{Cu}(\text{ac})_2(\text{aq}) + 2(5\text{-ClSalH}(\text{solv})) + x\text{denia}(\text{l})]$, $[\text{Cu}(\text{ac})_2(\text{aq}) + 2(5\text{-ClSalH}(\text{solv})) + x\text{ron}(\text{l})]$, $[\text{CuSO}_4(\text{aq}) + 2(5\text{-ClSalH}(\text{solv})) + x\text{denia}(\text{l})]$ and $[\text{CuSO}_4(\text{aq}) + 2(5\text{-ClSalH}(\text{solv})) + x\text{ron}(\text{l})]$, where $x = 0, 2, 4, 6, 8$, were studied by EPR spectroscopy in the frozen water/methanol solutions. When $x > 0$, the ^{14}N superhyperfine splitting was well resolved in the perpendicular part of the 2nd derivative axially symmetric Cu^{2+} EPR spectra for all mentioned complex systems.

INTRODUCTION

EPR spectroscopy is a useful tool for the study of copper complexes formed in the solutions among Cu^{2+} ions with various ligands [1, 2]. When Cu^{2+} ions are bound to nitrogen containing ligands, the ^{14}N superhyperfine splitting may appear in the Cu^{2+} EPR spectra. In this case EPR technique can provide additional information about the nitrogen donor atoms coordinated with the Cu^{2+} ions [1, 3, 4]. The chemical environments of Cu^{2+} ions in the following copper complex systems: i) $[\text{CuSO}_4(\text{aq}) + 2(5\text{-ClSalH}(\text{solv})) + x\text{ron}(\text{l})]$, $[\text{Cu}(\text{ac})_2(\text{aq}) + 2(5\text{-ClSalH}(\text{solv})) + x\text{ron}(\text{l})]$ [5] and ii) $[\text{CuSO}_4(\text{aq}) + 2(5\text{-ClSalH}(\text{solv})) + x\text{denia}(\text{l})]$, $[\text{Cu}(\text{ac})_2(\text{aq}) + 2(5\text{-ClSalH}(\text{solv})) + x\text{denia}(\text{l})]$ [6], where $x = 0, 2, 4, 6, 8$, were separately studied in the frozen water/methanol solutions by EPR spectroscopy. Consequently, the general comparisons of all the above mentioned four copper complex systems could not be done in our previous studies [5, 6]. Therefore, main object of this contribution is to deal with such together summary, including the effects of the varying Cu^{2+} salts ($\text{Cu}(\text{ac})_2$ or CuSO_4) containing anions of different basicity, varying biologically active ligand (ronicol or denia) concentration and finally varying ligand-to-metal ratio x , on the formation of resulting copper complex systems in the solutions.

MATERIAL AND METHODS

Sample preparation - Four copper complex systems with varying ligand-to-metal ratio x , $[\text{Cu}(\text{ac})_2(\text{aq}) + 2(5\text{-ClSalH}(\text{solv})) + x\text{denia}(\text{l})]$, $[\text{Cu}(\text{ac})_2(\text{aq}) + 2(5\text{-ClSalH}(\text{solv})) + x\text{ron}(\text{l})]$, $[\text{CuSO}_4(\text{aq}) + 2(5\text{-ClSalH}(\text{solv})) + x\text{denia}(\text{l})]$ and $[\text{CuSO}_4(\text{aq}) + 2(5\text{-ClSalH}(\text{solv})) + x\text{ron}(\text{l})]$, where $x = 0, 2, 4, 6, 8$, were prepared in water-methanol (1:3) solutions as follows: Copper acetate ($\text{Cu}(\text{ac})_2$) or copper sulphate (CuSO_4) with 5-chlorosalicylic acid (5-ClSalH) and two biologically active ligands, either 3-pyridylmethanol (ron = ronicol) or $\text{N,N}'$ -diethylnicotinamide (denia), were mixed in respective molar ratios.

Water solution of appropriate copper(II) salt was mixed with methanolic solution of 5-chlorosalicylic acid (to obtain stoichiometric composition shown above and simultaneously water/methanol ratio 1:3). The resulting solution was then stirred carefully to homogenize, then diluted by water/methanol mixture (1:3) in the ratio 1:1 and poured into EPR capillaries. For further information, see our previous papers [5, 6].

EPR measurement - After synthesis was finished, the 1st derivative Cu^{2+} EPR spectra of prepared copper complex systems were measured in a standard TE102 rectangular cavity of an EMX X-band (≈ 9.4 GHz) EPR spectrometer (Bruker, Germany) in frozen water/methanol solutions at temperature of 98 K. For instrumental parameters set up, see Ref. [5]. Bruker programs, WinEPR [7] and SimFonia [8], were used for processing and calculation of EPR spectra. The averaged g-factor, $g = (2g_{\perp} + g_{\parallel})/3$, [9], the geometric parameter, $G = (g_{\perp} - 2) / (g_{\parallel} - 2)$ [10, 11] and the empirical factor, $f = g_{\parallel} / A_{\parallel}$ [12], were calculated from spin Hamiltonian parameters. More experimental details are given in Refs. [5, 6].

RESULTS AND DISCUSSION

In this section, we show the original experimental Cu^{2+} EPR spectra of the above mentioned four copper complex systems, but measured in the frozen diluted water/methanol solutions, which were not presented in our previous papers [5, 6].

The experimental 1st-derivative Cu^{2+} EPR spectra of two complex systems $[\text{Cu}(\text{ac})_2(\text{aq}) + 2(5\text{-ClSalH}(\text{solv})) + x\text{ron}(\text{l})]$ or $x\text{denia}(\text{l})]$, where $x = 0, 2, 4, 6, 8$, measured in the frozen diluted water/methanol solutions at temperature of 98 K are illustrated in Fig. 1. In the case of the first Cu^{2+} salt ($\text{Cu}(\text{ac})_2$), the same results were obtained for both ligands: (i) when $x = 0$ was resolved perpendicular ^{14}N superhyperfine splitting.

The experimental 1st-derivative Cu²⁺ EPR spectra of two complex systems [Cu(ac)₂(aq) + 2(5-ClSalH(solvv)) + xron(l) or xdenia(l)], where x = 0, 2, 4, 6, 8, measured in the frozen diluted water/methanol solutions at temperature of 98 K are illustrated in Fig. 1. In the case of the first Cu²⁺ salt (Cu(ac)), the same results were obtained for both ligands: (i) when x = 0 evolved perpendicular ¹⁴N superhyperfine splitting.

Figure 1. Experimental 1st-derivative Cu²⁺ EPR spectra of copper complex systems [Cu(ac)₂(aq) + 2(5-ClSalH(solvv)) + xron(l) or xdenia(l)], where x = 0, 2, 4, 6, 8, measured in frozen diluted water/methanol solutions at temperature of 98 K.

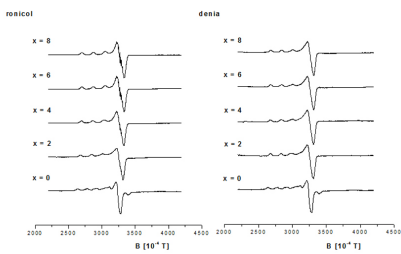
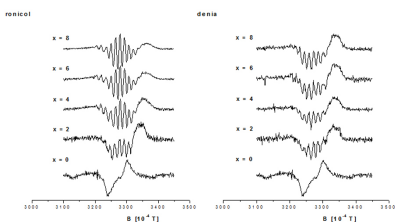


Figure 2: Nitrogen superhyperfine splitting in perpendicular region of experimental 2nd-derivative Cu²⁺ EPR spectra of copper complex systems [Cu(ac)₂(aq) + 2(5-ClSalH(solvv)) + xron(l) or xdenia(l)], where x = 0, 2, 4, 6, 8, measured in frozen diluted water/methanol solutions at temperature of 98 K.



The spin Hamiltonian parameters are (within experimental error) very similar to those obtained for given non-diluted stock solutions. See corresponding tables in Ref. [5] for ronicol and in Ref. [6] for denia. Comparing ronicol and denia containing systems, the both g-factor (g_{\perp} , g_{\parallel}) values are systematically higher and parallel hyperfine splitting (A_{\parallel}) values systematically lower for denia containing systems. The ¹⁴N superhyperfine splitting are constant for both ligands, $A_{\perp}^N = 1.45$ mT.

Figure 2 shows details of ¹⁴N superhyperfine splitting in perpendicular region of expansion of the experimental 2nd-derivative Cu²⁺ EPR spect-

ra of the above mentioned copper complexes. The resolution of superhyperfine lines increased (for ronicol more progressively) when the concentration of both ligands increased from x = 2, 4, 6 to 8. No superhyperfine splitting was monitored when x = 0.

Analogously, but for the second Cu²⁺ salt (CuSO₄), Fig. 3 illustrates the experimental 1st-derivative Cu²⁺ EPR spectra of two complex systems [CuSO₄(aq) + 2(5-ClSalH(solvv)) + xron(l) or xdenia(l)], where x = 0, 2, 4, 6, 8, measured in the frozen diluted water/methanol solutions at 98 K. Again, for this copper salt, the same results were obtained for both ligands: (i) when x = 0, single axially symmetric Cu²⁺ EPR spectra were observed, (ii) when x = 2, composite EPR spectra were obtained and (iii) when x > 2, single axially symmetric Cu²⁺ EPR spectra were recorded. All the EPR spectra (including composite spectra) exhibited well resolved parallel and unresolved perpendicular hyperfine splitting, and when x > 0, non-resolved parallel and well resolved perpendicular ¹⁴N superhyperfine splitting. As for the first copper salt, also in this case, the spin Hamiltonian parameters are (within experimental error) very similar to those presented for given non-diluted stock solutions. See corresponding tables in Ref. [5] for ronicol and in Ref. [6] for denia. And again, comparing ronicol and denia containing systems, the g-factor values are systematically higher and parallel hyperfine splitting values are systematically lower, for denia containing system, and nitrogen superhyperfine splitting values are identical ($A_{\perp}^N = 1.45$ mT) for both ligands. Likewise in this case, the details of ¹⁴N superhyperfine splitting in perpendicular region of expansion of the experimental 2nd-derivative Cu²⁺ EPR spectra are shown in Fig. 4. Also for this copper salt: (i) when x = 0 no superhyperfine splitting was monitored and (ii) when the concentration of both ligands increased from x = 2, 4, 6 to 8, the resolution of superhyperfine lines increased (but again, for ronicol more progressively).

The trends in the spin Hamiltonian parameter values are very similar for all the copper complex systems under investigation. The anisotropic g-factors (g_{\perp} , g_{\parallel}) and their averaged (g_{av}) values decreased (eventually remained constant), when ligand concentration increased. G-parameter values

Figure 3: Experimental 1st-derivative Cu²⁺ EPR spectra of copper complex systems [CuSO₄(aq) + 2(5-ClSalH(solvv)) + xron(l) or xdenia(l)], where x = 0, 2, 4, 6, 8, measured in frozen diluted water/methanol solutions at temperature of 98 K

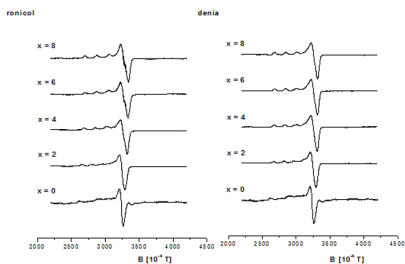
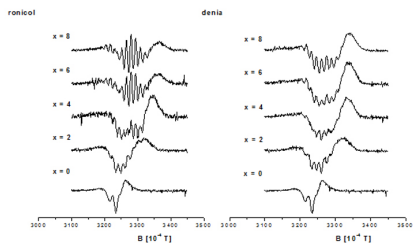


Figure 4. Nitrogen superhyperfine splitting in perpendicular region of experimental 2nd-derivative Cu²⁺ EPR spectra of copper complex systems [CuSO₄(aq) + 2(5-ClSalH(sol)) + xron(l) or xdenia(l)], where x = 0, 2, 4, 6, 8, measured in frozen diluted water/methanol solutions at temperature of 98 K.



varied from minimal (4.0) to maximal (5.6) values and f-factor values varied from minimal (131 cm) to maximal (217 cm) values. However, comparing ronicol and denia containing systems, the G-parameters are systematically higher and f-factors are systematically lower for ronicol containing system for both copper salts. For more information, see our previous papers [5, 6].

CONCLUSION

Summarizing results presented herein and referred in our previous papers [5, 6], it is obvious that

(i) the unpaired electron on the Cu²⁺ ion is localized in the $d_{x^2-y^2}$ orbital, which is indicated by ($g_{\parallel} > g_{\perp} > 2.0023$) relation, (ii) the resolution and signal intensity of the ¹⁴N superhyperfine splitting increased when the ligand concentration increased.

ACKNOWLEDGEMENT

This work was supported by the Slovak Research and Development Agency under the contract Nos. (APVV-0202-10 and APVV-0339-10) and Scientific Grant Agency of the Slovak Republic (Projects VEGA 1/0856/11 and 1/0289/12).

REFERENCES

[1] Della Lunga G., Basosi R.: J. Magn. Reson.,

A 114 (1995) 174-178

- [2] Pogni R., Baratto M.C., Diaz A., Basosi R.: J. Inorg. Biochem., 79 (2000) 333-337
- [3] Basosi R., Della Lunga G.: Appl. Magn. Reson., 11 (1996) 437-442
- [4] Della Lunga G., Pazzato M., Baratto M.C., Pogni R., Basosi R.: J. Magn. Reson., 164 (2003) 71-77
- [5] Martiška L., Husáriková L., Repická Z., Valigura D., Valko M., Mazúr M.: Appl. Magn. Reson., 39 (2010), 423-435
- [6] Martiška L., Husáriková L., Repická Z., Valigura D., Valko M., Mazúr M.: Appl. Magn. Reson., 40 (2011), 405-411
- [7] Thiele H., Etsling J., Such P., Hofer P., WIN-EPR Bruker Analytik GmbH, Bremen and Rhenstetten, Germany, (1992)
- [8] Weber R.T., WIN-EPR SimFonia, Software version 1.2, EPR Division, Bruker Instruments, Inc., Billerica, USA (1995)
- [9] Weil J.A., Bolton J.R., Wertz J.E.: Electron Paramagnetic Resonance: Elementary Theory and Applications, Wiley-Interscience, New York, (1994)
- [10] Hathaway B.J. and Billing B.J.: Coord. Chem. Rev., 5 (1970) 143-207
- [11] Hathaway B.J., Tomlinson A.A.G.: Coord. Chem. Rev., 5 (1970) 1-43
- [12] Sakaguchi U., Addison A.W.: J. Chem. Soc. Dalton Trans., 4 (1979) 600-608

STUDY OF CONJUGATION OF BOVINE SERUM ALBUMINE WITH CdTe QUANTUM DOTS WITH SPECTROSCOPIC TECHNIQUES

Jana CHOMOUCKA^{1,2*}, Jana DRBOHLAVOVA^{1,2}, Marketa RYVOLOVA^{1,2}, Ana MIHAJLOVIĆ¹, Jaromir HUBALEK^{1,2}

¹LabSensNano, Department of Microelectronics, Faculty of Electrical Engineering and Communication, Brno University of Technology, Technicka 3058/10, 616 00 Brno, Czech Republic

²Central European Institute of Technology, Brno University of Technology, Technicka 3058/10, 616 00 Brno, Czech Republic

*chomoucka@feec.vutbr.cz

ABSTRACT

In this paper, water soluble CdTe quantum dots modified with different ligands (3-mercatoacetic acid, thioglycolic acid and glutathione) were prepared by a simple one step method using Na₂TeO₃ and CdCl₂. Preliminary results showed that subsequent modification of QDs surface with bovine serum albumin (BSA) resulted in quenching of fluorescence depending on the biomolecules concentration.

INTRODUCTION

Semiconductor nanocrystals, also known as quantum dots (QDs), are nano-scale inorganic particles in the size range of 1–10 nm. Due to their quantum confinement, QDs show unique and fascinating optical properties, such as sharp and symmetrical emission spectra, high quantum yield (QY), good chemical and photo-stability and the size dependent emission wavelength tenability [1]. So far, QDs have been linked with bio-recognition molecules such as proteins, peptides and nucleic acids, and have been successfully used in biological and medical fields such as immunoassay, DNA hybridization, cell imaging and potential photodynamic therapy. QDs bioconjugation is of great importance in biological applications. In general, QD bioconjugation approaches reported are mainly based on bifunctional linkage (such as 1-ethyl-3-(3-dimethylaminopropyl) carbodiimide hydrochloride, EDC), electrostatic attraction, and biotin–avidin interaction. However, no matter what conjugation approach is used, QD bioconjugates need to be purified and characterized.

Bovine serum albumin (BSA) has been one of the most extensively studied proteins, particularly because of its structural homology with human serum albumin. It has been often used as coating reagent to modify the surface of nanoparticles due to its strong affinity to a variety of nanoparticles, such as gold nanoparticles, silica nanoparticles, and QDs. Up to now, QDs modified by BSA have been applied to ion sensors, fluorescence resonance energy transfer, and chemiluminescence resonance energy transfer. Moreover, due to the increasing extension of nanotechnology in biological sciences, it is imperative to develop a detailed understanding

how biological entities, especially proteins, may interact with nanoscale particles [2].

MATERIAL AND METHODS

Synthesis of CdTe QDs and bioconjugation

The procedure to synthesize 3-mercaptopropionic acid (MPA)-capped CdTe QDs, glutathione (GSH)-capped CdTe QDs and thioglycolic acid (TGA)-capped CdTe QDs was adapted from the work of Wang et al. [3]. Sodium telluride was used as the Te source. Due to the fact that sodium telluride is air stable, all of the operations were performed in the air avoiding the need of inert atmosphere. The synthesis of CdTe QDs and their subsequent coating were as follows: 114 mg of the CdCl₂·2.5 H₂O was diluted with 25 mL of water. During constant stirring, 65 μL MPA (56 μL TGA or 150 mg GSH), 25 mg of sodium citrate, 2 mL of Na₂TeO₃ solution (c = 0.01 mol/L), and 10 mg of NaBH₄ were added into water-cadmium(II) solution. Dropwise addition of 1 M NaOH was used to adjust the pH to 10 under vigorous stirring. The mixture was kept at 95°C under the reflux cooling for 4 hours. BSA can readily conjugate to CdTe QDs by electrostatic attraction. Two hundred and fifty microliters QDs (2 mg/ml) were added to the mixture of 137.5 μL BSA (12 mg/ml) and 92.5 μL phosphate buffered saline (PBS) and stand for 2 h at room temperature. The mixture contents were 1 mg/ml QDs and 3.3 mg/ml BSA. The reaction solution was stored in the refrigerator at 4°C [4].

Characterization of CdTe QDs

Photoluminescence spectra were measured at room temperature with Infinite M200 Pro, Tecan, quantum yield with Quanta j, HORIBA Jobin Yvon.

RESULTS AND DISCUSSION

In this paper, we selected three kinds of mercaptan ligands such as MPA, TGA, GSH for the preparation of water soluble CdTe QDs. The emission spectra of a typical CdTe QD used in study were measured (excitation at 380 nm). The emission spectrum displays that the emission peak is at 620 nm in the case of MPA-capped CdTe QDs, 506 nm in the case of GSH-capped CdTe QDs and 540 nm in the case TGA-capped CdTe QDs. All spectra is characterized by good symmetry and narrow spectral width. The QY of CdTe QDs was 11,5% (CdTe-MPA), 10,5% (CdTe-GSH) and 7% (CdTe-TGA).

Figure 1: Fluorescence spectra of CdTe QDs

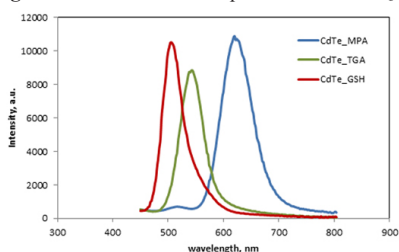
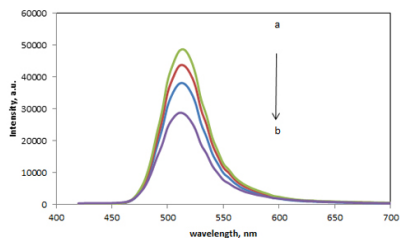


Figure 2: Fluorescence intensity of GSH capped BSA-CdTe QDs at various concentrations of BSA: a = 3 mg/ml BSA, b = 6 mg/ml BSA, c = 8 mg/ml BSA and d = 12 mg/ml BSA



Since CdTe QDs were prepared in aqueous phase using MPA, GSH or TGA as a stabilizer, the thiol groups of ligand linked to the surface of CdTe QDs by thiol group-Cd coordination, and the functional carboxylic group is free, which can be easily coupled to biomolecules with amino groups, such as proteins, peptides or amino acids.

As shown in Figure 2., the emission of CdTe QDs decreases progressively with increasing concentration of BSA.

CONCLUSION

In this work the synthesis of CdTe QDs with three different mercaptan ligands is shown. In the next stage, QDs were conjugated with BSA and the luminescence quenching test was performed showing that biomolecules concentration has strong influence on luminescence intensity decrease.

ACKNOWLEDGEMENT

The financial support from the grant GAAV KAN 208130801 (NANOSEMED) and project CZ.1.05/1.1.00/02.0068 (CEITEC) is highly acknowledged.

REFERENCES

- [1] Drummen, G: International Journal of Molecular Sciences 11 (2010) 154-163
- [2] Liang J, Cheng Y, Han H: Journal of Molecular Structure 892 (2008) 116-120
- [3] Wang H, Han H: Journal of Colloid and Interface Science 351 (2010) 83-87
- [4] Huang X, Weng J, Sang F, et al.: Journal of Chromatography A, 1113 (2006) 251-254

ELECTROPHORETIC TECHNIQUES IN THE ANALYSIS OF POLYDEOXYCYTIDYLIC ACIDS

Miroslava BITTOVA^{1*}, Katerina JELINKOVA¹, Vendula ROBLOVA¹,
Libuse TRNKOVA^{1,2}

¹Department of Chemistry, Faculty of Science, Masaryk University, Kotlarska 2, CZ-611 37 Brno, Czech Republic

²Central European Institute of Technology – CEITEC, Brno University of Technology, Technicka 3058/10, CZ-616 00 Brno, Czech Republic

*bittova@sci.muni.cz

ABSTRACT

Electrophoretic techniques such as capillary zone electrophoresis and one-dimensional polyacrylamide gel electrophoresis were applied in the separation of polydeoxycytidylic acids between 3 and 18 nucleotides in chain length (dC3-dC18). In capillary zone electrophoresis (CZE), the electrophoretic behavior of homo-oligonucleotides in hydrophilic coated capillary (CEP) and polyethyleneimine coated capillary (PEI) was followed under various experimental conditions. One-dimensional polyacrylamide gel electrophoresis was chosen as a supplemental method in the characterization of electrophoretic properties of polydeoxycytidylic acids.

INTRODUCTION

The electrophoretic behavior of oligonucleotides in free solutions depends on the charge-to-mass ratio, which is in case of DNA almost constant and independent of fragment length [1]. This fact makes separation of oligonucleotides in free solution very difficult and requires the presence of a sieving agent such as linear polyacrylamide (LPA), polyethylene glycol (PEG), hydroxyethyl cellulose (HEC), etc. Although polyacrylamide gel filled capillaries are most often used in the separation of oligonucleotides, their usability is limited due to low reproducibility and lifetime. More suitable for routine analysis is the addition of replaceable polymers into the background electrolyte, which can be easily flushed from the capillary and/or renewed [2].

The aim of this work was electrophoretic characterization of polydeoxycytidylic acids in various separation systems in relation to their different lengths.

MATERIAL AND METHODS

All analyses were done using a CE 3D (Agilent Technologies) capillary electrophoresis instrument with a diode-array detector. CEP (capillary electrophoresis phase) coated capillary (75 μm , 25/33.5 cm length) and fused-silica capillary (75 μm , 41.5/50 cm length), consequently coated with polyethyleneimine according to a previous procedure, were used [3]. Acetate, phosphate-acetate, MES or TBE as buffers were used and hydroxyethyl cellulose (HEC) as a sieving matrix were tested. One-dimensional polyacrylamide gel electrophoresis was carried out using PROTEAN II xi Cell equipment (Bio-Rad). All electrophoretic runs were carried out in 20% polyacrylamide

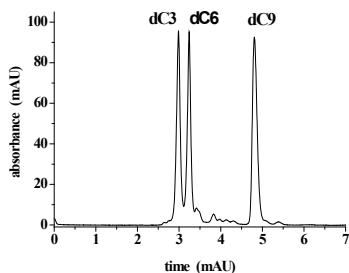
gel and as a separation electrolyte, TBE or Britton-Robinson buffer with various pH was used. All experiments were done without denaturation agents.

RESULTS AND DISCUSSION

Electro-osmotic flow suppression in a CEP coated capillary allows separation of analytes only in relation to their charge-to-mass ratio. In the separation system without any sieving agent, only a poor resolution of studied oligonucleotides was observed (phosphate-acetate buffer pH 3.5). A slight improvement of the separation was recorded only after HEC was added. As expected, higher pH resulted in increasing electrophoretic mobilities of the analytes and caused impairment of separation efficiency.

A PEI coated capillary is characterized with amine groups on the inner capillary wall, which are positively charged at pH above 8. At alkali pH, slightly negative charges can be observed. Analyses in a PEI coated capillary were done using TBE buffer pH 9.4 with the addition of HEC, and a satisfying separation of the selected polydeoxycytidylic acids was obtained [Fig. 1]. Surprisingly, in comparison with a CEP coated capillary, an opposite separation order of the analytes in the PEI coated capillary at the same electric polarity was observed. This fact was related to the distribution of the charge in the oligonucleotide structure and additive interactions with background electrolyte components.

Figure 1: Separation of selected polydeoxycytidylic acids using CZE. PEI coated capillary 8.5 cm eff., TBE buffer pH 9.4+0.01% HEC, voltage +12 kV, inject. 50 mbar/5 sec, 270 nm



CONCLUSION

Capillary zone electrophoresis provides a useful and effective tool in the analysis of homo-oligonucleotides such as polydeoxycytidylic acids. Suitably selected capillary modification in combination with properly chosen separation conditions allows separate analytes in order by request. However, also in polydeoxycytidylic acid analysis, the presence of a sieving agent is required.

ACKNOWLEDGMENT

The work was supported by the CEITEC – Central European Institute of Technology Project CZ.1.05/1.1.00/02.0068 and by the project MUNI/A0992/2009.

REFERENCES

- [1] McKeown AP, Shaw PN, Barrett DA.: Electrophoresis, 22 (2001), 1119-1126.
- [2] Quesada MA, Mencher S, in: Mitchelson KR, Cheng J: Capillary electrophoresis of nucleic acids. Vol. 1, Humana Press, New Jersey, 2001, 193.
- [3] Nutku MS, Berker FBE: Turkish Journal of Chemistry, 27 (2003), 1, 9-14.

REACTIVITY AND MOBILITY OF CU(II) IONS IN HUMIC GELS

Michal KALINA*, Martina KLUČAKOVÁ, David LANG, Jakub GRUNT, Petr SEDLÁČEK

Centre for Materials Research CZ.1.05/2.1.00/01.0012, Faculty of Chemistry, Brno University of Technology, Purkynova 118, 612 00 Brno, Czech Republic
*xckalina@fch.vutbr.cz

ABSTRACT

The mobility of Cu(II) ions in humic gels with respect to their reactivity and concentration dependence is investigated in this work. Two various methods: instantaneous planar source and constant source were used in order to study their diffusion at very low and very high Cu(II) concentrations, respectively. It was confirmed, that the higher concentration gradient in method of constant source supports mobility of Cu(II) ions, which corresponds with higher values of computed diffusion coefficients. The diffusion coefficient was more influenced by concentration change in case of gel prepared from $\text{Na}_3\text{P}_3\text{O}_{10}$ as a result of less stable complexes formed in the gel with Cu(II) ions.

INTRODUCTION

Humic acids (HA) are natural ubiquitous organic compounds, which can be found in soils, waters, sediments and coal. Their main role is in binding, transport and biological uptake of different nutrients and contaminants in nature [1]. Their high affinity toward heavy metals is well known and studied. In previous works [2,3,4] easy diffusion and sorption experiments in humic hydrogels were described as a suitable approach for the study of reactivity and mobility of metals in humic acids. The aim of this work was the deeper exploration of these interactions between the HA and metals.

MATERIAL AND METHODS

The first part of the work was focused on the study of the mobility of Cu(II) ions in humic hydrogels. The whole work procedure of isolation of HA from South-Moravian lignite and characterization of the material can be found elsewhere [2,3]. In this work two different humic hydrogels were utilized. For the preparation of gel A humic acids were dissolved in 0.5M NaOH and acidified to the pH close to 1. Gel B was prepared by dissolving of HA in 0.1M $\text{Na}_3\text{P}_3\text{O}_{10}$ and acidifying to the pH close to 1.

These gels were packed in cylindrical tubes and used for the diffusion experiments. Chosen methods of diffusion were instantaneous planar source and constant source [2,3]. The main aim of this setting was to determine the diffusion coefficient of Cu(II) ions in both gels and to investigate the influence of the concentration on the diffusion process. The first method, instantaneous planar source, was used for the study in the range of very low concentration. On the other hand, constant source was used for the study of Cu(II) diffusion at high concentration.

On the deeper study of the reactivity of Cu(II) ions and HA the second part of the work was

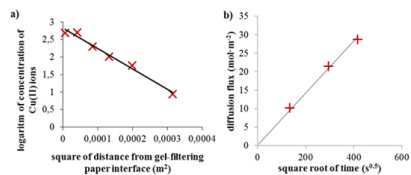
focused. Both prepared humic hydrogels were used for sorption experiments of Cu(II) ions from the solution. The chosen starting ratios of CuCl₂ concentration in solution/gel were: 0.001, 0.005, 0.01, 0.05 and 0.1M.

The diffused Cu(II) ions were extracted from the slices of the gels after diffusion with 1M HCl. This extraction solution was also used for extraction of sorbed Cu(II) ions from the samples of humic hydrogel in order to determine desorbed amounts and investigate the stability of prepared complexes. The Cu(II) ions concentrations in all solutions (from diffusion and from sorption experiments) were determined by the means of UV-VIS spectroscopy. All the experiments were carried at laboratory temperature (25±1 °C).

RESULTS AND DISCUSSION

The first part of experiments were focused on mobility study of Cu(II) ions in two different humic hydrogels (Gel A and Gel B).

Figure 1: a) Linearized concentration profiles of Cu(II) ions (results from instantaneous planar source); b) Dependence of diffusion flux on the square root of duration of diffusions (results from constant source diffusion).



From measured values of absorbance of solutions the concentrations profiles and the dependences of diffusion flux on the square root of duration of diffusions were determined. Figure 1 a) shows example of the linearized concentration profile, which was used for the determining of the diffusion coefficient of Cu(II) ions in humic hydrogel for the case of instantaneous planar source diffusion experiment. Figure 1 b) represents the example of the dependence of diffusion flux of Cu(II) ions on the square root of duration of diffusion experiment for the constant source diffusion experiment.

All determined diffusion coefficients for both used hydrogels and both setting of diffusion experiments are summarized in Table 1. We can see that diffusion process in the gel A (prepared from HA dissolved in NaOH) is less dependent on the change of concentration than in the case of gel B (prepared from HA dissolved in Na₂P₂O₇). Simultaneously we can observe that the differences between both gels increases with growing Cu(II) concentration. The concentration gradient, which is driving force of the diffusion, is very high in case of the method of constant source (the source of Cu(II) ions is their saturated solution). Therefore the structure of both gels and its influence on metal ions mobility is stronger in comparison of method of instantaneous source, which utilizes only very short initial pulse of Cu(II) ions.

Table 1. Determined diffusion coefficients of Cu(II) ions

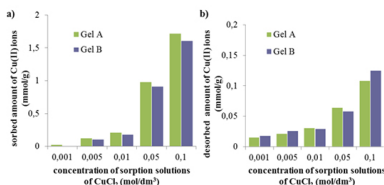
Type of gel	Diffusion coefficients (m ² ·s ⁻¹)	
	Instantaneous planar source	Constant source
Gel A	4.24·10 ⁻¹⁰ ± 4.89·10 ⁻¹¹	8.27·10 ⁻¹⁰ ± 1.87·10 ⁻¹¹
Gel B	3.96·10 ⁻¹⁰ ± 3.67·10 ⁻¹¹	10.66·10 ⁻¹⁰ ± 4.23·10 ⁻¹²

effective values of diffusion coefficients

In the second part of the work the sorption experiments from the solution of CuCl₂ were used for the deeper study of the reactivity between copper and HA. Figure 2 a) shows the sorbed amount of Cu(II) ions on 1 g of humic hydrogel and Figure 2 b) comparison with amount of Cu(II) ions desorbed from 1 g of humic hydrogels into acidic solution. From the comparison of sorbed amounts of Cu(II) on Gel A and Gel B is obvious that Gel A has a little higher sorption affinity for Cu(II) ions than Gel B. On the other hand, the complexes prepared from Gel B are less stable because the desorbed amounts are higher in this case. It seems that the bond strength of Cu(II) ions

in Gel B is lower, which causes their higher mobility resulting in higher value of diffusion coefficient computed from data obtained from method of constant source (while values of diffusion coefficient determined for both gels at low concentrations are comparable).

Figure 2: Comparison of a) sorbed amount and b) desorbed amount of Cu(II) ions on humic hydrogels in dependence on the starting concentration of sorption solution.



From obtained data were constructed the Freundlich isotherms:

$$a = k \cdot c_q^m \quad (\text{Eq. 1})$$

where a represents sorbed amount of Cu(II) ions on 1 g of humic gel, c_q is equilibrium concentration of sorbed Cu(II) ions, k and m are empirical constants.

Table 2. Calculated k and m parameters of Freundlich isotherm

Type of gel	k (mmol ⁻¹ ·dm ^{3m} ·g ⁻¹)	m
Gel A	0,0505	0,816
Gel B	0,0313	0,896

CONCLUSION

The main objective of presented work was to describe the interactions and mobility of Cu(II) ions in two different humic hydrogels. The results showed that mobility of Cu(II) ions in Gel B can be more influenced by the concentration than in Gel A. The "classical" humic hydrogel A (HA dissolved in NaOH and precipitated with HCl) has higher sorption affinity towards Cu(II) ions. The presented combination of diffusion and sorption experiments showed to be very suitable for the study of reactivity of metals with model humic matrices.

ACKNOWLEDGEMENT

This work was supported by the project "Centre for Materials Research at FCH BUT" No. CZ.1.05/2.1.00/01.0012 from ERDF and by Czech Science Foundation, project P106/11/P697.



REFERENCES

- [1] Avena, M.J, Knoopal, L.K, van Riemsdijk, W.: J. Colloid Interface Sci. 217 (1999), 37-48.
- [2] Sedláček, P, Klučáková, M.: Collect. Czech. Chem. C., 74 (2009), 9, 1323 – 1340.
- [3] Sedláček, P, Klučáková. M.: Geoderma, 153 (2009), 1–2, 286 – 292.
- [4] Klučáková, M., Omelka, L.:Chem. Papers, 58 (2004), 170–175.

STRENGTH AND MAGNETISM OF Mn – Pt NANOCOMPOSITES

Tomas KANA^{1*}, Mojmír SOB^{2,3,1}

¹Institute of Physics of Materials, Academy of Sciences of the Czech Republic, Žitkova 22, 616 62 Brno, Czech Republic

²Central European Institute of Technology, CEITEC MU, Masaryk University, Kamenice 5, 625 00 Brno, Czech Republic

³Department of Chemistry, Faculty of Science, Masaryk University, Kotlářská 2, 611 37 Brno, Czech Republic

*kana@ipm.cz

ABSTRACT

Using ab initio electronic structure calculations, we have analysed Mn atoms dissolved in a platinum matrix, forming thus intermetallics MnPt₃, MnPt₇ and MnPt₁₅ that can be considered as prototypes of natural Mn–Pt nanocomposites. On the whole, manganese addition makes the resulting Mn–Pt compound softer but increases its resistance to shape deformation. With increasing Mn content, both tensile and compressive theoretical strength is enhanced. In agreement with experiment, our calculations confirm the antiferromagnetic (AFM) ground state of the MnPt₇ structure with spins directions altering along the [100] crystallographic direction (AFM [100]). In addition, we have proposed and studied three prototypes of linear MnPt₁₅ nanocomposites consisting of Mn nanochains in the Pt matrix. Again, AFM [100] ordering was found in the ground state of MnPt₁₅.

INTRODUCTION

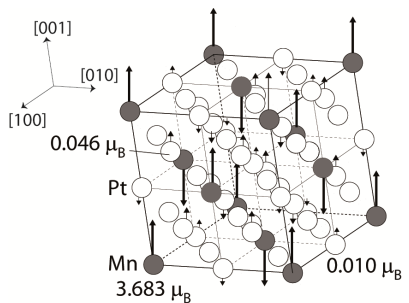
The recent findings of structure transitions in Fe, Ni [1] and Mn [2] nanowires stimulated our interest in ab initio simulation of tensile tests of nanocomposite metallic materials. Among others, our aim was to study Mn–Pt compounds and nanocomposites, in particular the recently found ordered MnPt₇ structure, and find the relation between their mechanical and magnetic properties. Another interesting topic are the MnPt₁₅ compounds proposed in this work, which represent natural nanocomposites with Mn chains oriented along the [100], [110] and [111] directions. It turns out that some of these configurations are stabilized by antiferromagnetic ordering and magnetic moments of manganese atoms may be coupled through the platinum atoms.

MATERIALS AND METHODS

For the ab initio total-energy calculations, we employed the full-potential linearized augmented-plane wave (FLAPW) method implemented in the WIEN2k code [3]. Exchange-correlation energy was determined within the local density approximation (LDA) [4]. The spin-orbit coupling was not included and our calculations were restricted to collinear magnetic ordering. The values of calculated magnetic moments at individual atoms correspond to electrons inside the muffin-tin spheres.

RESULTS AND DISCUSSION

First, we have calculated the elastic constants c_{11} , c_{12} and c_{44} of elemental Pt and performed ab initio tensile tests along the $\langle 100 \rangle$ and $\langle 111 \rangle$ directions. Our values of maximum tensile stress $\sigma_{\max,0}$ and the corresponding strain $\epsilon_{\max,0}$ were in a good agreement with previous results [5, 6]. The same calculations were carried out for the ferromagnetic compound MnPt₃ and for the novel antiferromagnetic compound MnPt₇ (see Fig. 1). For MnPt₁₅, we have found the antiferromagnetic ground-state, similarly as it was found experimentally for the Pt–8.8 at. % Mn alloy [7]. **Figure 1:** The antiferromagnetic (AFM [100]) ordering of the MnPt₇ structure corresponding to its ground state.



The effect of manganese addition to platinum matrix consists in its softening – the bulk modulus B and elastic constants c_{11} and c_{12} are redu-

ced. On the other hand, the Mn-doped structures are more resistant against shape deformation and exhibit an increase in the Young moduli E_{100} , E_{111} and shear moduli c_{44} and $(c_{11}-c_{12})/2$ (see Fig. 2). The maximum tensile stress $\sigma_{\max,0}$ in the directions $\langle 100 \rangle$ and $\langle 111 \rangle$ slightly increases (by up to 7 %) with increasing Mn content (Fig. 3). On the other hand, maximum compressive stress $\sigma_{\max,0} \langle 100 \rangle$ grows quite strongly with increasing Mn content. Its increase amounts to 46 % when comparing MnPt_7 to Pt and even to 111 % when comparing MnPt_3 to Pt. The increase in the compressive stress $\sigma_{\max,0} \langle 111 \rangle$ is intermediate (by 7.7 % when comparing MnPt_7 to Pt and by 12.8 % when comparing MnPt_3 to Pt).

Figure 2.: Variation of elastic properties of Mn-Pt compounds with increasing Mn content

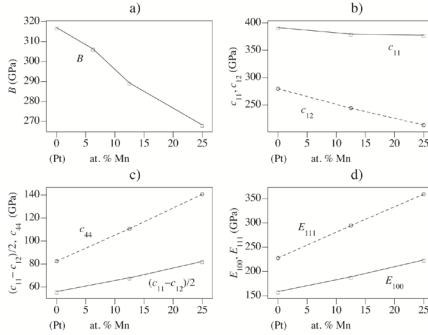
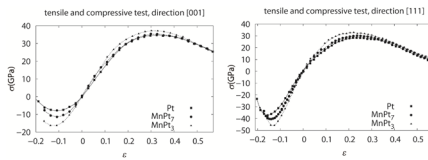


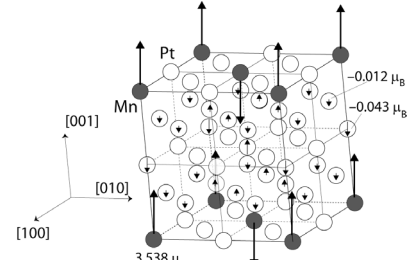
Figure 3.: Variation of tension (compression) stress σ with the deformation ϵ for Pt, MnPt_7 , and MnPt_3 .



In addition, we modeled the preferential occupation of Mn atoms in the Pt matrix and confirmed the experimental result that they prefer the positions at the corners and at the centers of faces of the $2 \times 2 \times 2$ Pt supercell. Our model structures denoted as MnPt_{15} have 6.25 at. % of Mn and can be regarded as natural linear nanocomposites. We found that the “base-centered” structure with the stripped Mn-Pt nanochains along the $[110]$ direction has the lowest energy among these three

structures and is stabilized by antiferromagnetic ordering (see Fig. 4) [8]. An alternative ferromagnetic ordering has the total energy only by 3.3 meV/atom higher.

Figure 4.: The antiferromagnetic ordering of the MnPt_{15} structure in the “base-centered” ground-state structure [8]. The Mn–Pt nanochains embedded in the Pt matrix are oriented along the $[110]$ direction.



CONCLUSION

In summary, we have studied the effect of Mn addition in platinum and found an increase of Young moduli E_{100} , E_{111} and shear moduli $(c_{11}-c_{12})/2$ and c_{44} . Both the maximum tensile and compressive stresses $\sigma_{\max,0}$ increase with increasing Mn content. An increase of compressive stress $\sigma_{\max,0}$ in the $\langle 100 \rangle$ direction is most remarkable. On the other hand, the manganese atoms act as softening agent in the Pt matrix, reducing the lattice constant a , bulk modulus B and the values of elastic constants c_{11} and c_{12} .

We have modeled several systems with various concentrations of Mn atoms in Pt matrix, in particular the recently found MnPt_7 nanocomposite, and determined the antiferromagnetic ordering as its ground state. A similar antiferromagnetic ordering has been found in our model MnPt_{15} structure. This is in agreement with experimental finding, as an antiferromagnetic ordering has been determined in the Pt–8.8 % Mn alloy with manganese concentration similar to MnPt_{15} .

ACKNOWLEDGEMENTS

This research was supported by the Ministry of Education of the Czech Republic (Projects No. COST OC10008 and No. COST LD12037), the Grant Agency of the Czech Republic (Project No. P108/12/0311), the Grant Agency of the Academy of Sciences of the Czech Republic (Project No. IAA100100920), by the Project CEITEC–Central European Institute of Technology (CZ.1.05/1.1.00/02.0068) from the European Regional Development

Fund and by the Academy of Sciences of the Czech Republic (Institutional Project No. RVO:68081723). The access to the MetaCentrum computing facilities provided under the program LM2010005 "Projects of Large Infrastructure for Research, Development, and Innovations" funded by the Ministry of Education of the Czech Republic is highly appreciated. We are also grateful for the access to the computing facilities of the Institute for Theoretical Computer Science in Plzeň provided under the Research Project No. MSMT 1M0545.

REFERENCES

- [1] Zelený M, Šob M, Hafner J: Phys. Rev. B, 79 (2009), 134421
- [2] Zelený M., Šob M. and Hafner J. Phys. Rev. B, 80 (2009), 144414
- [3] Blaha P, Schwarz K, Madsen G K H, Kvasnicka D, Luitz J: WIEN2k, An Augmented Plane Wave Plus Local Orbitals Program for Calculating Crystal Properties (Vienna University of Technology, 2007
- [4] Ceperley D M, Alder B. J: Phys. Rev. Lett, 45 (1980), 566
- [5] Černý M, Pokluda J: Phys. Rev. B, 76 (2007), 024115
- [6] Černý M, Pokluda J: Phys. Rev. B, 82 (2010), 174106
- [7] Takahashi M, Yoshimi S, Ohshima K, Watanabe Y: Phys. Rev. B, 61 (2000), 3528
- [8] Káňa T, Šob M: to be published

ASSESSMENT OF HEAVY METAL CONTENT IN URBAN SOILS USING DIFFERENT EXTRACTION METHODS

Andrea KLECKEROVA*, Hana DOCEKALOVA, Josef HEDBAVNY

Department of Chemistry and Biochemistry, Faculty of Agronomy, Mendel University in Brno, Zemedelska 1, 613 00 Brno, Czech Republic

*Andrea.klr@seznam.cz

ABSTRACT

The aim of this work was to investigate heavy metals content in urban polluted soils by using different leaching methods. The soil samples were collected from the topsoil of three sampling sites of Brno city in April 2011. The sampling site Opuštěná Street represented the heavily polluted locality with high traffic density situated in the city centre. Sampling site Videňská Street belongs to medium polluted locality that is situated close to frequented roads. Relatively clean locality is represented by Šrámkova Street, which is situated in peripheral city district with smaller traffic density. Four extracting methods (with deionised water, 2 mol.l⁻¹ nitric acid, 0.43 mol.l⁻¹ acetic acid and 0.05 mol.l⁻¹ ethylenediaminetetraacetic acid) were used for determination of heavy metals content, such as cadmium, lead, nickel and copper. The highest values of metal contents (Cd: 0.75 ± 0.01 mg.kg⁻¹, Pb: 78.20 ± 3.62 mg.kg⁻¹, Ni: 16.58 ± 0.07 mg.kg⁻¹, Cu: 44.13 ± 2.37 mg.kg⁻¹, Hg: 0.230 ± 0.004 mg.kg⁻¹) were found in the soil samples from Opuštěná Street by using nitric acid method.

INTRODUCTION

The different kinds of elemental soil analysis are used for the determination of 'total', 'pseudo-total' and 'extractable' soil contents. Firstly, it is the determination of the 'total' element contents in the soil by the methods that use solid samples, such as X-ray fluorescence spectrometry (XRF), DC arc optical emission spectrometry (DCAOES), neutron activation analysis (NAA), and glow discharge mass spectrometry (GDMS), or by various methods where solutions prepared by acid dissolution involving hydrofluoric acid or by fusion (LiBO₂)/dissolution procedures are used [1]. Secondly, digestion in strong acids such as nitric acid, hydrochloric acid or mixture such as aqua regia ('pseudo-total' analysis) that do not dissolve the silicate matrix can give an estimate of the maximum amounts of elements that are potentially mobilisable with changing environmental conditions [1, 2]. Leaching with 2 mol.l⁻¹ nitric acid is used in Czech Republic for determination of risk elements in soils. Maximum tolerable levels of these elements are presented in Regulation No. 13/1994 of the Ministry of Environment Czech Republic [3].

Single extractants can be in their role of releasing elements from particular soil phases with which they are bound or associated [4]. The water-soluble metals can be determined from the saturation paste extract of a soil or by extracting soil with deionised water at a certain soil – water ratio [5]. This phase contains the water soluble species made up of free ions and ions complexed with soluble organic matter and other constituents. It constitutes the most mobile and potentially the most available metal and metalloid speci-

es. The concentration of trace element nutrients or pollutants in the soil solution is very low and only accessible to the most sensitive analytical techniques [4].

Exchangeable fraction includes weakly adsorbed metals retained on the solid surface by relatively weak electrostatic interaction, metals can be released by ion-exchange processes [4, 6]. Acetic acid (2.5% v/v) dissolves the exchangeable species but releases, in addition, more tightly bound exchangeable forms [1].

Complexing extractants such as ethylenediaminetetraacetic acid (EDTA) or diethylenetriaminepentaacetic acid (DTPA) can, by virtue of their strong complexing ability, displace metals from insoluble organic or organometallic complexes in addition to those sorbed on inorganic soil components [7, 8]. Most of the heavy metals present in the carbonate phase are dissolved by sodium acetate to pH 5 with acetic acid or EDTA and acetic acid [1].

Determination of 'pseudo-total' and 'extractable' soil content was the main purpose of this study. Deionised water, 2 mol.l⁻¹ nitric acid, 0.43 mol.l⁻¹ acetic acid and 0.05 mol.l⁻¹ EDTA were used to determine the content of cadmium, lead, nickel and copper.

MATERIAL AND METHODS

The soil samples were collected from the topsoil of three sampling sites of the Brno city in April 2011. The sampling site Opuštěná represents the heavily polluted locality with high traffic density situated in the city centre. Sampling site Videňská belongs to medium polluted locality that is situated close to frequented roads. Relatively clean locality is represented by Šrámkova Street, which are situated in peripheral city

district with smaller traffic density. The soils were sampled from a depth horizon of 0-10 cm, ten samples at every sampling place, which represented an area of 3sq.m. For characterization of soils, a fine soil fraction of particle size below 2 mm was obtained by sieving the air-dried raw sample. Each sample of soil was measured three times and the standard deviation was observed from these three measurements.

Mercury in soil samples was determined by atomic absorption spectrometry using the AMA 254 (Altec, s.r.o.). Cadmium, lead, nicker and co-per concentrations were determined by electrothermal atomic-absorption spectrometer (SpektrAA-30, Varian).

Leaching with deionised water

A portion of 50 g of the soil was shaken with 50 ml of high purity water in a cleaned plastic tube for two hours and the mixture was then let to incubate for 24 hours. After centrifugation, the supernatant was immediately filtered through filter (Millipore). The leachate was collected in PP bottle a stabilized by acidifying with 50 µl of concentrated Suprapure grade nitric acid.

Leaching with ethylenediaminetetraacetic acid (EDTA)

Sample portion of about 5 g was admixed to 5 ml of 0.05 mol.l⁻¹ EDTA (pH = 7.00 ± 0.05) in extraction bottle. The mixture was then shaken for 1 hour at ambient temperature (25°C). The extract was immediately filtrated and the filtrate was collected in PE bottle. Content of elements extractable by EDTA was determined according to the recommendation of the Community of Bureau of Reference (BRC) [9].

Leaching with acetic acid

Sample portion of about 5 g was shaken in an extraction bottle at ambient temperature (25°C) with 200 ml of 0.43 mol.l⁻¹ acetic acid (Merck) for 16 hours. The extract was immediately filtered and the filtrate was collected in PE bottle. Extraction of elements soluble in acetic acid was performed according to the recommendation of the Community of Bureau of Reference (BRC) [9].

Leaching with nitric acid

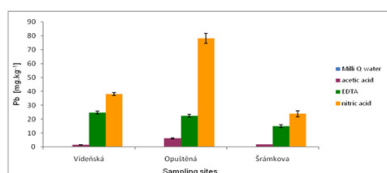
Sample portion of about 7 g was shaken in an extraction PE-bottles at ambient temperature (25°C) with 7 ml of 2 mol.l⁻¹ Suprapure grade nitric acid (Penta) for 16 hours. The extract was immediately filtrated and the filtrate was collected in PE bottle [10].

RESULTS AND DISCUSSION

The highest content of lead in soil was found at the sampling site Opuštěná. The average amount

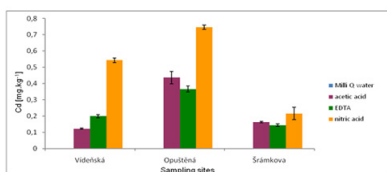
of lead in soil was 78.23 ± 3.62 mg.kg⁻¹. This content was determined by using nitric acid method. This content expresses maximum amount of element that is potentially mobilisable. Approximately half the levels of lead in soil were detected at sampling location Videňská with application of nitric acid as leaching method. The lowest lead concentration (nitric acid: 23.87 ± 2.18 mg.kg⁻¹, EDTA: 14.98 ± 0.66 mg.kg⁻¹, acetic acid: 1.86 ± 0.08 mg.kg⁻¹, deionised water: 0.0020 ± 0.0008 mg.kg⁻¹) was measured in soil samples collected at sampling site Šrámkova (Fig. 1).

Figure 1.: Average content of lead in soil



The highest content of cadmium in soil was found at the sampling site Opuštěná (nitric acid: 0.75 ± 0.01 mg.kg⁻¹, EDTA: 0.36 ± 0.02 mg.kg⁻¹, acetic acid: 0.43 ± 0.03 mg.kg⁻¹, deionised water: 0.0010 ± 0.0004 mg.kg⁻¹). Significantly lower amounts of cadmium than other collector sites were detected at the sampling site Šrámkova, the average content of cadmium in soil was by using nitric acid 0.22 ± 0.03 mg.kg⁻¹. Obtained results were summarized in (Fig. 2.). Higher content of exchangeable fraction of cadmium was found in samling sites Opuštěná and Šrámkova than in sampling site Videňská where was more insoluble organic complexes, which were determined by using EDTA method.

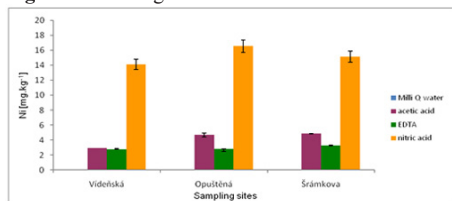
Figure 2.: Average content of cadmium in soil



The highest nickel content in soil was found at the sampling site Opuštěná. The average concentration of nickel was at this site: nitric acid: 16.58 ± 0.07 mg.kg⁻¹, EDTA: 2.77 ± 0.06 mg.kg⁻¹, acetic acid: 4.67 ± 0.26 mg.kg⁻¹, deionised water: 0.0200 ± 0.0004 mg.kg⁻¹. The the highest nickel content in soil was found by using nitric acid method. Obtained results are

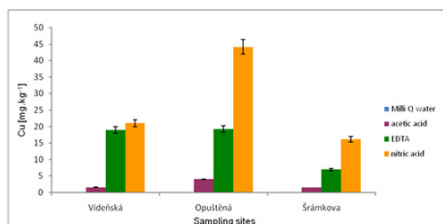
summarized at Fig. 3. Higher content of exchangeable species of nickel was determined in all sampling sites by using acetic acid method.

Figure 3: Average content of nickel in soil



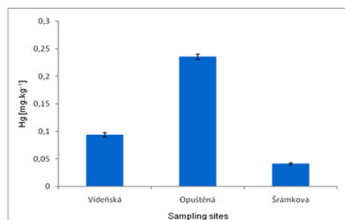
The highest copper content in soil was found at the sampling site Opuštěná (nitric acid: 44.13 ± 2.37 mg.kg^{-1} , EDTA: 19.26 ± 0.64 mg.kg^{-1} , acetic acid: 4.01 ± 0.02 mg.kg^{-1} , deionised water: 0.120 ± 0.007 mg.kg^{-1}). Approximately half the levels of copper in soil were detected at sampling location Vídeňská with application of nitric acid as leaching method. The lowest copper concentrations were measured in soil samples collected at sampling site Šrámkova. (Fig. 4). Higher content of chelating-bound species of copper was found in all sampling sites by using EDTA as extracting method than it was by determination of nickel content.

Figure 4: Average content of copper in soil



The highest content of mercury in soil was found at the sampling site Opuštěná. The average concentration of mercury was at this site 0.230 ± 0.004 mg.kg^{-1} . At the sampling site Vídeňská was recorded the second highest content of mercury in the soil, 0.090 ± 0.004 mg.kg^{-1} . Significantly lower amounts of mercury than other collector sites were detected at the sampling site Šrámkova, the average content of mercury in soil was 0.040 ± 0.001 mg.kg^{-1} . Obtained results were summarized in (Fig. 5).

Figure 5: Average content of mercury in soil



CONCLUSION

All measurements were compared with extracting method by using 2 mol.l^{-1} nitric acid which is used in Czech Republic for determination of risk elements in soils. Maximum tolerable levels of these elements are presented in Regulation No. 13/1994 of the Ministry of Environment Czech Republic. Levels of cadmium, nickel, copper and mercury in studied Brno urban soil samples were not exceed the maximum tolerable levels in this regulation. Average content of lead in sampling site Vídeňská (78.23 ± 3.62 mg.kg^{-1}) exceeded the maximum tolerable levels defined by the Czech legislation (Regulation No. 13/1994 of the Ministry of Environment Czech Republic) (limit of lead content in soil is 70 mg.kg^{-1}).

ACKNOWLEDGEMENT

The work has been supported by Grant Agency of the Czech Republic, Project No. P503/10/2002).

REFERENCES

- [1]Ure A.M.: Science of the Total Environment, 1996. **178**(1–3): p. 3-10.
- [2]Sabieně N., Brazauskienė D.M.: Ekologija, 2004. **1**: p. 36–41.
- [3]Regulation No. 13/1994 of the Ministry of Environment Czech Republic 1994: Czech Republic.
- [4]Rao C., Sahuquillo J., Sanchez L.: Water, Air, & Soil Pollution, 2008. **189**(1): p. 291-333.
- [5] Svete P., Milacic R., Pihlar B.: Annali di Chimica, 2000. **90**(5-6): p. 323-334.
- [6]Krishnamurti G.S.R., Huang P. M., Van Rees K. C. J., et al.: Analyst, 1995. **120**(3): p. 659-665.
- [7]Berrow M.L., Mitchell R. L.: Earth Sciences, 1980. **71**(2): p. 103-121.
- [8]Ure A.M., Davidson C. M.: Chemical speciation in the environment. 2001, Glasgow: Blackie.
- [9]Ure A.M., Muntau H., Griepic B.: Int. J. Environ. Anal. Chem., 1993. **61**: p. 135-151.
- [10]Zbiral J.: Analýza půd I., 2002, Brno: ÚKZÚZ

THERMODYNAMICS OF THE ANTIOXIDANT ACTION OF MODEL AND NATURAL COMPOUNDS

Erik KLEIN^{1*}, Vladimír LUKES¹, Jan RIMARCIK¹, Adam VAGANEK¹, Jozef LENGYEL^{2,3}, Michal ILCIN¹, Lenka ROTTMANNOVA¹

¹Institute of Physical Chemistry and Chemical Physics, Slovak University of Technology in Bratislava, Radlinského 9, SK-812 37 Bratislava, Slovakia

²J. Heyrovský Institute of Physical Chemistry, v.v.i., Academy of Sciences of the Czech Republic, Dolejškova 3, CZ-182 23 Prague 8, Czech Republic

³Department of Physical Chemistry, Institute of Chemical Technology, Technická 5, CZ-166 28 Prague 6, Czech Republic

*erik.klein@stuba.sk

ABSTRACT

This contribution presents short overview of our research in the field of thermodynamics of primary antioxidant action. Reaction enthalpies corresponding to three known mechanisms of radical scavenging by antioxidants have been studied using quantum chemical calculations.

INTRODUCTION

Oxidative processes represent an essential part of aerobic life. Oxidation involves electron transfer between molecules or electron-rich species to an oxidizing agent. This transfer can give rise to highly reactive radicals. If these radicals are not effectively scavenged, they lead to various diseases and ageing of organisms [1].

An antioxidant is a substance that inhibits or prevents the oxidation of another molecule. Antioxidants are often classified either as primary, or secondary [2]. Primary (chain-breaking) antioxidants inhibit oxidation processes. Secondary antioxidants convert products formed during the oxidation, such as hydroperoxides, to more stable non-radical species. Non-toxicity represents one of the key properties of antioxidants. Thus, recent research is strongly focused on naturally occurring compounds. Besides, human diet contains various substances showing antioxidant activities. Most important representatives of dietary antioxidants are vitamin C, tocopherols and tocotrienols (components of vitamin E), flavonoids and carotenoids. Moreover, sterols also may show an antioxidant effect [3].

Phenolic compounds represent the most important group of natural antioxidants. They can act through several mechanisms. Corresponding reaction enthalpies represent one of important characteristics of antioxidants. In the majority of papers on antioxidant action of phenolic compounds (ArOH), one-step hydrogen atom transfer (HAT) mechanism

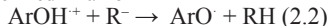


is studied. In eq. 1, R[·] represents a scavenged radical. From the thermodynamics point of view, HAT is governed by phenolic O–H bond dissociation enthalpy (BDE). However, two-step

mechanisms of phenoxy radical, ArO[·], formation can also take place. In the first step of Single Electron Transfer – Proton Transfer (SET-PT) mechanism, electron transfer to a radical, R[·], occurs

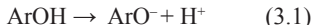


In the second step, proton is transferred to the formed R⁻ anion



This mechanism is described by ionization potential (IP) and proton dissociation enthalpy (PDE) from ArOH^{·+} radical cation formed in the first step. However, low IP values also enhance the probability of superoxide radical anion formation through the direct transfer of an electron to surrounding O₂ [4, 5].

Few years ago, another two-step mechanism has been discovered. It was named Sequential Proton-Loss Electron-Transfer (SPLET) [6, 7]. Reaction kinetics experiments proved that vitamin E, flavonoids and other phenols can react with dpph[·] (2,2-diphenyl-1-picrylhydrazil radical) and other electron deficient radicals by two different and nonexclusive mechanisms, HAT and SPLET [6–8]. SPLET can be described as follows



The reaction enthalpy of the first step corresponds to the proton affinity (PA) of the phenoxide anion, ArO⁻. The reaction enthalpy of the second step, eq. 3.2, has been denoted as electron transfer enthalpy, ETE [9]. Since SPLET was discovered in 2003–2004, the majority of published works is devoted only to the O–H BDEs and IPs. In the case of flavonoids

(polyphenolic compounds), there is also another mode of their antioxidant action: metal-chelation of copper and iron cations, which are able to accelerate the oxidation [1,2].

In our papers, the main attention was paid on the large sets of primary antioxidants model compounds (anilines, phenols and thiophenols), as well as naturally occurring phenolic compounds (tocopherols, chromans, flavonoids). All three mechanisms, i.e. HAT, SET-PT and SPLET, were studied for mono-substituted phenols, thiophenols, tocopherols, chromans and flavonoids. In the case of mono-substituted anilines, N–H bond dissociation enthalpies have been studied. Homolytic cleavage of O–H and selected C–H bonds in terms of corresponding BDEs was studied for most common phytosterols and cholesterol for experimentally determined oxidation attack sites.

COMPUTATIONAL PROCEDURE

All calculations were performed using Gaussian 03 program package [10]. The gas-phase geometry of each compound, radical or ionic structure was optimized using DFT method with B3LYP [11] functional without any constraints (energy cut-off of 10^{-5} kJ mol⁻¹, final RMS energy gradient under 0.01 kJ mol⁻¹ Å⁻¹). Calculations were performed usually in 6-311++G** basis set [12]. This approach was found to be suitable for BDE, IP, PDE, PA and ETE calculations, because it gives results in accordance with available experimental values of studied reaction enthalpies for phenols and thiophenols. Moreover, it describes the effect of various electron-donating and electron-withdrawing substituents reliably. The application of identical computational approach in works related to model compounds and naturally occurring substances has two advantages: (i) All results are fully comparable (they are not affected by the employment of different calculation methods and/or basis-sets). (ii) Agreement between experimental and computed reaction enthalpies for simple model molecules (such as anilines, phenols and thiophenols) allows assuming that used computational approach will provide reliable predictions also for other compounds (such as tocopherols, tocotrienols, polyphenols). For naturally occurring compounds, often no experimental values are available, yet. Integral Equation Formalism Polarized Continuum Model (IEF-PCM) method [13, 14] was used for the investigation of the effect of solvents with various polarities on studied reaction enthalpies. All enthalpies were calculated for 298.15 K.

BRIEF SUMMARIZATION OF SELECTED RESULTS

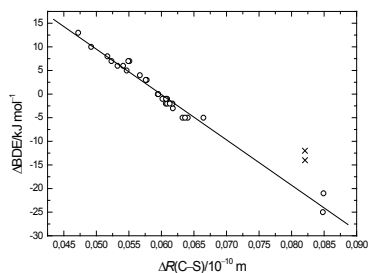
Model compounds: phenols and thiophenols

In the case of *para*- and *meta*-substituted phe-

nols [9, 15, 16, 17] and thiophenols [18, 19], we have quantified the effect of various electron-donating and electron-withdrawing groups on the enthalpies of homolytic and heterolytic O–H and S–H bonds cleavage in the gas-phase and several solvents. Obtained results were confronted with available experimental data. Approximately linear Hammett-type dependences were found for all reaction enthalpies. These enable estimation of a reaction enthalpy from the Hammett constant of a substituent and *vice versa*. In studied environments, thermodynamically favored reaction pathway was determined. In the gas-phase and non-polar benzene, HAT is preferred, while in polar solvents (ethanol, DMSO and water), SPLET is thermodynamically favored mechanism. Solvents attenuate substituent effect on IP, PDE, PA and ETE. On the contrary, substituent induced changes in O–H and S–H BDEs are in slightly wider range.

For substituents placed in *meta* positions, linearity of found Hammett-type dependences is usually worse in comparison to *para*-substituted molecules. Therefore, their applicability for prediction of changes in BDEs using Hammett constants ρ_m may be limited.

Figure 1: Dependence of gas-phase Δ BDE on $R(C-S)$ for 28 *para*- and *meta*-substituted thiophenols, two points (x) were omitted from regression.



For *para*- and *meta*-substituted phenols, we tried to find a structure-based descriptor of substituent effect [16]. We have found linear dependences of O–H BDE on the phenolic C–O bond length, $R(C-O)$, and its shortening after hydrogen atom abstraction, $\Delta R(C-O) = R(C-O, \text{molecule}) - R(C-O, \text{radical})$. We have confirmed that analogous linear dependences exist also for thiophenols [19], Fig. 1. Our recent calculation results for *para*- and *meta*-substituted anilines [20] show that N–H BDE values can be correlated with aniline C–N bond length, $R(C-N)$ or its shortening after hydrogen atom

abstraction, $\Delta R(C-N)$, too. Moreover, in the case of thiophenols [19] and anilines [20], one equation can describe substituent induced changes in BDEs for both, *para* and *meta*, positions. For phenols, *meta*- and *para*-substituted molecules have to be treated separately [16].

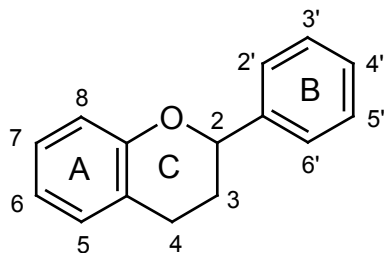
Tocopherols and chromans

Gas-phase reaction enthalpies related to the individual steps of HAT, SET-PT and SPLET were calculated for four tocopherols and seven chromans [21]. For α -tocopherol and one of the chromans, reaction enthalpies in water were computed. It was found that water causes severe changes in the energetics of SET-PT and SPLET mechanisms, which include charged species ($ArOH^+$ radical cation and ArO^- anion). From the thermodynamics point of view, entering SPLET mechanism represents the most probable process in water. Again, it was confirmed that a solvent does not influence phenolic O–H BDEs significantly; the differences between gas-phase and solution phase BDE values usually do not exceed 10 kJ mol^{-1} .

Flavonoids

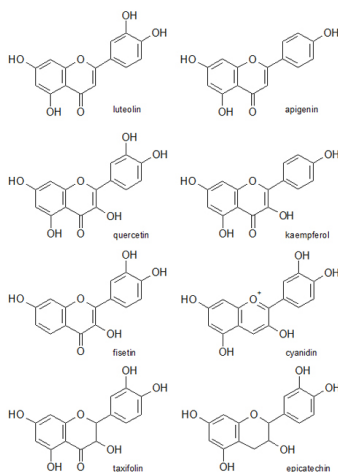
Although numerous experimental reports on antioxidant action of flavonoids have been published, still no experimental reaction enthalpies related to HAT, SET-PT and SPLET are available. Theoretical works provide O–H BDE, IP, and PA values for the most “popular” flavonoids, but they were obtained using different (semiempirical, DFT or *ab initio*) quantum chemical methods. Therefore, published enthalpies are not compatible. Moreover, some used methods may provide less reliable results.

Figure 2.: Atom numbering and rings denotation in flavonoids.



Recently, for eight flavonoids (Fig. 2), all three mechanisms of phenolic antioxidant action are being studied in the gas-phase [22], non-polar benzene and polar water. Selected group of flavonoids enables to evaluate the effects of various structural features, such as presence of certain hydroxy groups (3'-OH, 3-OH, 5-OH), C2=C3 double bond and C4=O keto group in the molecules on investigated reaction enthalpies.

Figure 3.: Studied flavonoids.



Lowest gas-phase O–H bond dissociation enthalpies (HAT) and proton affinities (SPLET) have been found usually for 4'-OH groups at ring B. In the second step of SET-PT mechanism, formation of radicals at 4'-OH position is again favored, as it can be expected from the thermodynamic cycle. For apigenin in water, the lowest PA was obtained for 7-OH, while the lowest BDE was found for 4'-OH group. These results are in accordance to experimental work of Musialik et al. [6], where it was found that in ionization supporting solvents, SPLET runs in ring A from ionized 7-OH group of quercetin and HAT/SET-PT occurs from 3',4'-dihydroxy moiety. Contrary to the gas-phase, in water all PAs are significantly lower than corresponding BDEs. The study of the solvent effect on individual BDEs, IPs, PDEs, PAs and ETes for the remaining seven flavonoids is under progress.

Sterols

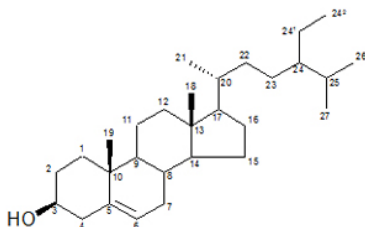
Phytosterols, as components of human diet, received much attention because of their cholesterol-lowering and reported antioxidant properties [3]. Sterols having double bond between C5 and C6 atoms (Fig. 4) in sterol nucleus are called Δ^5 -sterols. Another group of sterols, Δ^7 -sterols, has double bond between C7 and C8 car-

bons [3]. We have performed the first theoretical study of sterols oxidation in terms of O–H and C–H BDEs. For seventeen

Δ^5 - and Δ^7 -sterols, BDEs were calculated for reported sites of oxidation attack [23]. Obtained results indicate that Δ^7 -sterols are more susceptible to oxidation attack in comparison to

Δ^5 -sterols. In sterol nuclei, the lowest BDE was found for C7–H bond in Δ^5 -sterols and for C14–H in Δ^7 -sterols. Homolytic cleavage of hydroxyl O–H bond requires larger energy in comparison to studied C–H bonds. We have shown that C–H bonds with lowest BDE values actually correspond to the dominant sites of oxidation attack. Recently, the study of sterols with more than one C=C double bond in nucleus is under progress.

Figure 4: Atom numbering in sterols



CONCLUSION

Although studied reaction enthalpies represent important characteristics of antioxidants, it should be noted that the activity of an antioxidant is also affected by the reaction kinetics, environment (e.g. polar / non-polar solvent or cellular environment, pH), its concentration and the presence of other compounds in the system. Increased amount of antioxidant may not result in its higher efficiency. Excessive, as well as insufficient, amount of antioxidants in living systems can be even harmful. Discovery of new and more effective antioxidants based on naturally occurring compounds represents one of the main aims of current research. Equally important aim is to define optimum concentrations in systems, where individual antioxidants are employed.

ACKNOWLEDGEMENT

This work has been supported by the Slovak Grant Agency VEGA (Project No. 1/0137/09) and the Science and Technology Assistance Agency (Project LPP-0230-09).

REFERENCES

[1] Craft B D, Kerrihard A L, Amarowicz R, Pegg R B: *Comprehensive Reviews in Food Science and Food Safety*, 11 (2012), 148-173

[2] Gugumus F: *In Oxidation inhibition in organic materials*. (vol. 1), Boca Raton: CRC Press, 1990

[3] Moreau R A, Whitaker B D, Hicks K B: *Progress in Lipid Research*, 41 (2002), 457-500

[4] Wright J S, Johnson E R, DiLabio G A: *Journal of American Chemical Society*, 123 (2001), 1173-1183

[5] Pratt D A, DiLabio G A, Brigati G, Pedulli G F, Valgimigli L: *Journal of American Chemical Society*, 123 (2001) 4625-4626

[6] Musialik M, Kuzmicz R, Pawlowski T S, Litwinienko G: *Journal of Organic Chemistry*, 74 (2009), 2699-2709

[7] Musialik M, Litwinienko G: *Organic Letters*, 7 (2005), 4951-4954

[8] Staško A, Brezová V, Biskupič S, Mišík V, *Free Radical Research*, 41 (2007), 379-390

[9] Klein E, Lukeš V: *Journal of Physical Chemistry A*, 110 (2006), 12312-12320

[10] Pople J A, et al.: *GAUSSIAN 03, Revision A.1*, Gaussian, Inc., Pittsburgh, PA, 2003

[11] Becke A D: *Journal of Chemical Physics*, 98 (1993), 5648-5652

[12] Binkley J S, Pople J A, Hehre W J: *Journal of American Chemical Society*, 102 (1980), 939-947

[13] Cancès E, Mennucci B, Tomasi J: *Journal of Chemical Physics*, 107 (1997) 3032-3037

[14] Cancès E, Mennucci B: *Journal of Mathematical Chemistry*, 23 (1998), 309-326

[15] Klein E, Lukeš V: *Chemical Physics*, 330 (2006), 515-525

[16] Klein E, Lukeš V: *Journal of Molecular Structure (Theochem)*, 767 (2006), 43-50

[17] Klein E, Rimarčík J, Lukeš V: *Acta Chimica Slovaca*, 2 (2009), 37-51

[18] Rimarčík J, Lukeš V, Klein E, Rottmannová L: *Computational and Theoretical Chemistry*, 967 (2011), 273-283

[19] Rottmannová L, Vagánek A, Rimarčík J, Lukeš V, Klein E: *Acta Chimica Slovaca*, 5, (2012), 33-37

[20] Vagánek A, Rimarčík J, Lukeš V, Klein E (2012) to be published

[21] Klein E, Lukeš V, Ilčin M: *Chemical Physics* 336 (2007), 51-57

[22] Vagánek A, Rimarčík J, Lukeš V, Klein E: *Computational and Theoretical Chemistry*, submitted

[23] Lengyel J, Rimarčík J, Vagánek A, Fedor J, Lukeš V, Klein E: *Food Chemistry*, 133 (2012), 1435-1440

PREPARATION OF PHOTO - CYTOCHROME b_5 FOR CROSS-LINK WITH CYTOCHROME P450 2B4

Monika KOBEROVA, Tomas JECMEN, Miroslav SULC, Vera CERNA, Jiri HUDECEK, Marie STIBOROVA, Petr HODEK*

Department of Biochemistry, Charles University in Prague, Hlavova 2030, 128 40 Prague 2, Czech Republic,

*hodek@natur.cuni.cz

ABSTRACT

To study the enigmatic role of cytochrome b_5 in a cytochrome P450 monooxygenase multienzyme system, the cytochrome b_5 analogue having methionine residues substituted with photolabile diazirine derivatives (photo-cytochrome b_5), was expressed and purified. Reaction mixture containing cytochrome P450 2B4 (CYP2B4) and photo- b_5 was photolyzed and separated on SDS-PAGE. The analysis (high resolution LC-FT-ICR mass spectrometry) of tryptic peptides of formed cross-links revealed several covalent oligomers composed of CYP2B4 and photo-cytochrome b_5 in 1:1, 1:2, and 2:1 molar ratios. The amount of oligomers formed was markedly increased by the presence of the CYP2B4 substrate diamantane in the reaction mixture showing that this substrate increases the binding affinity between cytochromes P450 and cytochrome b_5 .

INTRODUCTION

Cytochrome b_5 (cyt b_5) is considered to be a facultative constituent of a cytochrome P450 monooxygenase multienzyme system (MFO system). This protein is composed of two functional domains, a soluble heme-containing core, and a short hydrophobic C-terminal tail, which anchors the protein into the microsomal membrane. Cyt b_5 has been shown to stimulate, inhibit or have no effect on cytochrome P450-mediated reactions. These effects might be attributed to two roles of cyt b_5 : i) the direct electron transfer from cyt b_5 to cytochrome P450 (CYP) and/or ii) the induction of conformational changes of CYP facilitating the substrate binding and/or its metabolism. However, the mechanism of cyt b_5 action has not been fully explained yet. To elucidate the protein-protein interactions in the MFO system, the novel approach based on the chemical cross-linking of these proteins in the membrane environment was designed and tested.

MATERIAL AND METHODS PREPARATION OF CYTOCHROME b_5 WITH INCORPORATED PHOTO-METHI- ONINE

Bacterial strain *E. coli* BL21 (DE3) Gold was transformed by expression vector pET22b containing the gene for rabbit cyt b_5 . Transformed bacteria were cultivated in a LB medium at 37°C. After washing by PBS, bacteria were transferred into DMEM-LM with addition of photo-methionine (pMet) (0.4 mM) and Leu (1.6 mM). Protein production was induced by IPTG (1 mM) and terminated after 1 hour. Membrane fraction of bacteria was isolated by differential

centrifugation and solubilized by detergents Brij 35 and sodium cholate. Expressed photo- b_5 was purified using DEAE-Sepharose CL6B column chromatography. The incorporation of pMet was verified by MALDI-TOF analysis. CYP2B4 was isolated from phenobarbital-induced rabbit liver microsomes as described elsewhere [1]

Covalent cross-linking

CYP2B4 (2 μ M) and photo-cyt b_5 (13.5 μ M) were reconstituted in DLPC lipids (300 μ M) in the presence/absence of a CYP2B4 substrate – diamantane (50 μ M). Photo-cyt b_5 was activated by UV-irradiation (photolyser Oriel equipped with Hg-Arc lamp emitting 254 nm) for 3 min. A photolyzed reaction mixture was separated on SDS-PAGE and formed cross-links analyzed using high resolution LC-FT-ICR mass spectrometry after their digestion with trypsin.

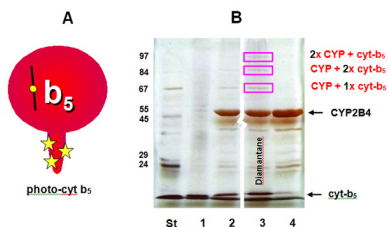
RESULTS AND DISCUSSION

Tandem mass spectrometry of photo-cyt b_5 and cyt b_5 revealed that the highest content of pMet was after 1 hour of its production. Under these conditions, more than 30% exchange of Met for pMet in the resulting photo-cyt b_5 was achieved. Using these conditions the large-scale production was carried out and photo-cyt b_5 was successfully purified. After photoactivation three hetero-crosslinks were detected on SDS-PAGE. The analysis of their tryptic peptides revealed three covalent CYP-cyt b_5 oligomers composed of CYP2B4 and cyt b_5 in 1:1, 1:2, and 2:1 molar ratios. The amount of oligomers formed was markedly increased by the presence of diamantane (CYP2B4 substrate) in the reaction mixture (see Fig. 1). This observation is in

agreement with the experimental evidence that the CYP substrate enhances the binding affinity between CYP and cyt b_5 . It appears that CYP and cyt b_5 have a rather complex interaction; in addition to interactions described for their cytosol-exposed regions [2], our data show that they interact also in the microsomal membrane by their membrane anchors. To our best knowledge this protein-protein interaction was directly proved for the first time. Thus, the obtained data in conjunction with our previous results of chemical cross-linking will allow refining *in silico* models of CYP - b_5 interactions.

[3] S.-Ch. Im, L. Waskell, *Arch. Biochem. Biophys.*, **507**, 144-153 (2011).

Figure 1. Photocross-linking of photo-cyt b_5 and CYP2B4. Scheme depicts a possible location of photo-Met (asterisks) in the membrane exposed C-terminal domain of cyt b_5 (Panel A). Photolysed reaction mixture containing CYP2B4 and photo-cyt b_5 was separated on SDS-PAGE (Panel B). Violet frames mark newly formed protein bands composed of CYP2B4 and cyt b_5 after photoactivation. For all samples 15% separation gel was used. **St** – standard Mw, **1** – photo-cyt b_5 (control), **2** – CYP2B4 + photo-cyt b_5 , **3** – CYP2B4 + photo-cyt b_5 + diamantane, **4** – CYP2B4 (control).



CONCLUSION

Recombinant photo-cyt b_5 was successfully prepared (~30% incorporation photo-methionine) and proved to covalently link through its photoactivated diazirine to CYP2B4 in the membranous environment.

ACKNOWLEDGEMENT

The financial support from grants 305/09/H008, P207/12/0627, P301/10/0356 and 303/09/0472 of The Grant Agency of the Czech Republic is highly acknowledged.

REFERENCES

- [1] J.B. Schenkman, I. Jansson, *Drug Metab. Rev.*, **31**, 351-364 (1999).
- [2] M. Sulc, P. Hodek, M. Stiborova, *Gen. Physiol. Biophys.*, **29**, 175-185 (2010).

ELECTROCHEMICAL PREPARATION AND CHARACTERIZATION OF POROUS SILICON

Martin KONECNY¹*, Juraj DIAN¹

¹Department of Chemical Physics and Optics, Faculty of Mathematics and Physics, Charles University in Prague, Ke Karlovu 3, 121 16 Praha 2, Czech Republic

*konecmar@seznam.cz

ABSTRACT

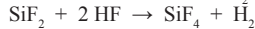
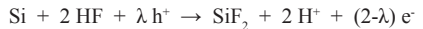
We present the most common methods for preparation of porous silicon by means of the electrochemical etching of crystalline silicon in hydrofluoric acid and ethanol mixture. Although porous silicon is a material with many applications in various fields, the detailed mechanism of its electrochemical formation is not clarified yet. Present models are based on experimental observations that the etching of crystalline silicon results in its partial dissolution and a release of hydrogen. Results of porous silicon electrochemical preparation in electrolyte of various HF concentration and gravimetric characterization are presented.

INTRODUCTION

Porous silicon is prepared by etching of crystalline silicon hydrofluoric acid. There are two ways, chemical and electrochemical. Electrochemical method is due to its simplicity and reproducibility more used. The properties of the porous layers are dependent on many factors. We can modify the properties of resulting porous silicon by the type of silicon substrate (doping, concentration of impurities, crystallographic orientation), by the preparation conditions (composition of the etching electrolyte, current density, etching time) and storage of the prepared sample. Porous silicon is formed in the presence of fluoride ions during the dissolution at constant anodic current. For the anodic oxidation a two electrode setup is usually used; silicon substrate is connected as the anode and the platinum electrode as the cathode we use as an electrolyte the mixture of hydrofluoric acid and ethanol in a Teflon cell.

The first models of the electrochemical etching of crystalline silicon in hydrofluoric acid on the surface of silicon assumed formation of Si-F bonds. More detailed study found that in fact Si-H bonds are formed [1]. The complete mechanism of electrochemical etching of porous silicon is not known yet [2]. There are several models of possible mechanism for porous silicon formation. Probably the most accurate description enable models by Turner [3] and by Lehmann and Gösele [4]. These two models are based on the fact that the etching process itself requires fluoride ions and the positive charge carriers – holes (h⁺) – and that during this process there is a release of hydrogen.

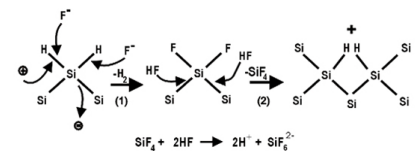
According to Turner the etching runs by the following sequence of reactions:



In one step, the number of exchanged charges is equal to one and leads to formation of Si-H bonds.

Illustrative model by Lehmann and Gösele assumes the oxidation of surface Si bonds by a hole capture followed by electron separation, which leads to etching silicon in the exchange of two charge carriers, as shown in Fig 1. [5]

Figure 1: Model dissolving mechanism of silicon fluoride ions



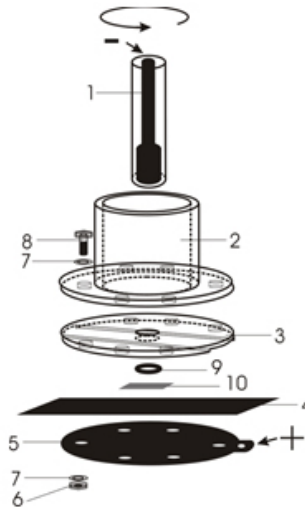
MATERIAL AND METHODS

Electrochemical preparation

Porous silicon samples were prepared by electrochemical etching of crystalline silicon (ON semiconductor Rožnov, p-type, (100), $\rho \approx 10 \text{Wcm}$, thickness 0.5 mm). Wafers were etched in various HF (50%) + ethanol (96%) mixtures (2:1, 1:1, 1:2, 1:2.5 and 1:3) in a Teflon cell with two electrodes (Fig. 2). Etching procedure was performed in galvanostatic mode with home-build galvanostat for current densities of 2, 5 and 10 mA cm⁻² and etching times of 10, 30 and 60 minutes. Silicon wafer was employed as the anode, rotation Pt electrode as the cathode (6 mm diameter, rotation speed around 20 rpm). After etching porous silicon samples (diameter of the etched area was around 10 mm)

were rinsed with distilled water and ethanol and placed in the evacuated desiccator.

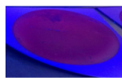
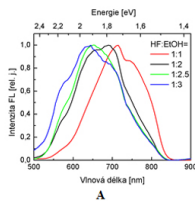
Figure 2.: Diagram of etching cell [6]



RESULTS AND DISCUSSION

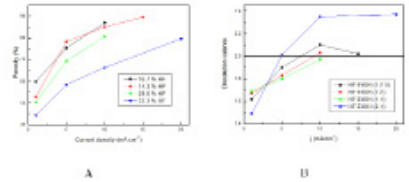
Typical porous silicon samples prepared at above-mentioned experimental conditions exhibit bright visible photoluminescence at room temperature. Photoluminescence properties are presented in Fig. 3.

Figure 3.: (A) -Spectrum of photoluminescence of porous silicon, (B) – visible (red) photoluminescence from porous silicon sample under UV light excitation.



B

Figure 4.: (A) – Porosity of porous silicon as a function of current density for various HF concentrations of etching electrolyte, (B) – Dissolution valence of silicon for as a function of HF concentration



CONCLUSION

Porous silicon samples were prepared by means of electrochemical etching. Characteristics of dissolution reaction like dissolution valence and of prepared samples like porosity and thickness were determined.

ACKNOWLEDGEMENT

The work has been supported by projects GAČR GA206/09/0375 and TAČR TA01011363.

REFERENCES

- [1] Gerischer H, Lübke M: Journal of the Electrochemical Society, 135 (1988),11, 2782-2786
- [2] Föll H, Christophersen M, Carstensen J, et al.: Materials Science and Engineering R, 39 (2002), 4, 93-141
- [3] Turner D.R.: Journal of the Electrochemical Society, 105 (1958), 402
- [4] Lehman V, Gösele U: Applied Physics Letters, 58 (1991), 8, 856-858
- [5] Dian J, Jelinek I: Chemická listy 104, (2010), 12, 1140-1147
- [6] Vrkoslav V: Diploma thesis, Faculty of Science, Charles University in Prague, 2003
- [7] Halimaoui A: in Porous Silicon Science and Technology (Vial JC, Derrien J, Eds.), Chapter 3, Springer Verlag, 1995

STUDY OF CORROSION LAYERS FORMED ON METAL ARTIFACTS USING DOUBLE PULSE LASER-INDUCED BREAKDOWN SPECTROSCOPY

Veronika KONECNA^{1*}, Lubomír PROKES², Martin HLOZEK³, Ales HRDLICKA², Jozef KAISER¹, David PROCHAZKA¹, Radomir MALINA¹, Karel NOVOTNY², Jan NOVOTNY¹, Pavel PORIZKA¹, Michal PETRILAK¹,

¹X-ray micro CT and nano CT research group, CEITEC - Central European Institute of Technology, Brno University of Technology, Technická 2, 616 69 Brno, Czech Republic

²Department of Chemistry, Faculty of Sciences, Masaryk University
Kotlářská 2, 611 37 Brno, Czech Republic

³Methodical Centre of Conservation, Technical Museum in Brno, Purkyňova 105, 612 00 Brno, Czech Republic

* veronika.konecna@seznam.cz

ABSTRACT

This work is focused on study of corrosion layers using double pulse laser-induced breakdown spectroscopy. Used artifacts from various locations were made from copper, copper alloy and silver. The qualitative contents of contaminant elements in the corrosion layer of the surface, which was created due to soil conditions, was estimated on the basis of the measured results. The elemental composition of the alloy itself, from which the artifact was made in the past, was also determined. The work also deals with depth profiles examination that allows estimating of the changes of element representation from the corrosion layer on the surface down to the metal core. The measured data were processed by statistical analysis.

INTRODUCTION

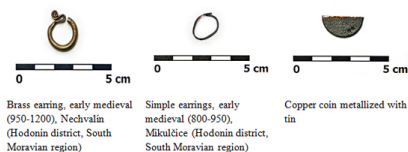
Corrosion products in conservation and restoration practice are usually undesirable phenomena on the surface of metals. Nevertheless they can be a valuable source of information for determination of the origin, function, or dating the artifact [1]. They allow us to reconstruct the story of an artifact from the time of its creation until the moment of excavation [2]. The aim of this work is an inspection of corrosion products on metal objects from archaeological sites by laser-induced breakdown spectroscopy (LIBS). The purpose of the exploration is an identification of the elements present in the corrosion layers created on metal artifacts. LIBS method provides information concerning not only the surface of the object (corrosion products), but also provides insight into the depth including the identification of the chemical composition of the object itself [3]. This method is combined with X-ray fluorescence (XRF).

EXPERIMENTAL

Archaeological samples

For measurement, several sets of archaeological samples were chosen. All objects were made of copper alloy or silver of different chemical composition of the alloy, the type of corrosion layers and location (see tab. 1).

Table 1: Archaeological samples



EXPERIMENTAL

DP LIBS Instrumentation

Analyses were performed by double pulse LIBS technique in orthogonal arrangement. The primary pulse came from Nd: YAG laser (Solar LQ-529a) with a flat beam profile (532 nm). This pulse impacted the sample perpendicularly. Secondary pulse came from Nd: YAG laser (Quantel Brilliant B, 1064 nm) with a Gaussian profile and reached the primary microplasma under normal direction to the primary beam 2 mm above the sample surface. The sample was placed in an interaction vacuum chamber (Tescan LM) on the motorized translation stage movable in three axes. The emitted radiation was analyzed using a spectrometer (Andor Mechelle 5000, wavelength range from 200 to 975 nm) equipped with an iCCD camera (Andor Istar). Time synchronization of all components was provided by a digital delay generator (Stanford Research Systems 545).

X-ray fluorescence Instrumentation

Samples were also subjected to X-ray fluorescence analysis (XRF): handheld X-ray ana-

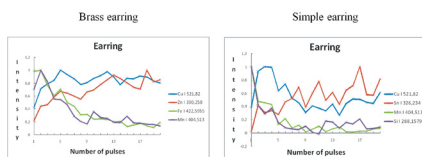
lyzer Niton XL3t GOLDD + (X-ray tube with Au anode (50 kV) and Ag anode in a version for the analysis of light elements), detector SDD (Silicon Drift Detector). Scanned area was 1 cm², the penetration depth app. 0.1 mm below the surface. The analysis is strongly affected by the surface of the material. The yielded results depend on the surface position. The work is mainly focused on acquisition of depth profiles for monitoring of changes in elemental composition of layers created on the surface of artifacts due to adverse conditions. The measured results can be divided into two groups of elements. The intensities increase with depth for the first group of elements, from which the sample is made (e.g. Cu, Ag, Sn). On the contrary, the intensities of the group of corrosion elements decrease with depth (e.g., Mg, Na, Ca, K, Si).

RESULTS AND DISCUSSION

LIBS analysis of brass earring sample has confirmed the expected increasing intensity of spectral lines of copper and zinc. The same behavior was also seen by the spectral lines of tin and lead (not shown). Silver, however, had the opposite trend, and thus it is not the part of the alloy. It came on the surface in the form of impurity or subject could have been silver plated in the past. The corrosion elements are also created by sodium, potassium, silicon, magnesium, calcium, manganese, as well as by iron and aluminum, because the intensity of their lines gradually decreases.

The depth profile of earrings created by LIBS shows that the intensity of spectral lines of copper, which is contained in the alloy, is not very different from elements that are naturally contained in the corrosion layer. The intensity of emission line of copper increases sharply to the third pulse and then decreases sharply. Tin emission line is detected by the device after the second pulse and its intensity gradually increases with increasing depth. It is possible to deduce from the measured data that the sample is plated with a thin layer of copper on the surface. The core is probably composed of an alloy of tin and copper. The intensity of the emission from the corrosion layer elements, consisting of calcium, magnesium, sodium, potassium, manganese, silicon, iron and aluminum, decreases with an increasing number of pulses.

Figure 1.: Graph of depth profile of copper samples

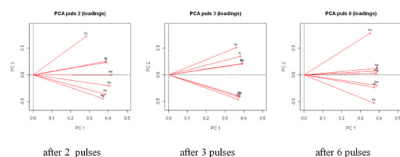


Statistical analysis was carried out with matrix-similar samples. To assess the relationship between the individual samples, elements present in all samples were selected. Optical emission spectra from the first to the sixth pulse were processed because they contained representative information about the elements in the corrosion layer. The classical method of principal components (PCA – Principal Component Analysis) was applied.

Plot Components Loadings

The Plot Components Loadings shows that there is a correlation between calcium and magnesium, eventually sodium and potassium. Iron correlates more with alkaline earth metals (magnesium, calcium). Sodium and potassium carbonate can be part of crusts and patina. Iron is fixed similarly. Sodium and potassium are mobile elements that normally do not form insoluble compounds (see fig. 2).

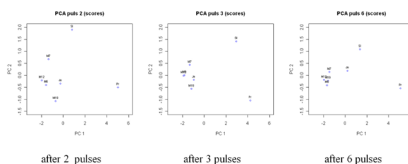
Figure 2.: Graph of component weights (loadings) of copper samples



Principal Component Scores

Principal Component Scores indicate that the samples from Mikulčice (M) and a needle (Je) show a certain degree of similarity in comparison with an ingot (SI) and a ring (Pr). With a higher number of pulses there is a tendency of Mikulčice samples to be closer to each other, while the needle tends to be away from them (see fig. 3).

Figure 3.: Diagram of the component scores of copper artefacts



CONCLUSIONS

Based on the results of analysis of individual subjects, the information about the elemental constituents of the corrosion layers formed on

the surface of artifacts was obtained. Contamination elements identified in the majority of objects were sodium, calcium, magnesium, potassium, manganese, silicon, aluminum and iron. Furthermore, it was possible to identify elements in the alloy artifact. Depth profiling enables to resolve whether the detected elements belong to the corrosion layer or to the alloy. It was also possible to estimate the thickness of plating by the number of applied laser pulses. X-ray fluorescence was used as a comparative method. XRF equipment that was available did not allow in principle to analyze cores of artifacts, and therefore it was associated with the LIBS analysis. The results obtained by statistical evaluation indicate this approach as a very promising.

ACKNOWLEDGEMENT

We acknowledge the Ministry of Education, Youth and Sports of the Czech Republic for bestowing the research projects ME08002 and ME10061 and the support of Brno University of Technology on the frame of grant FSI-S-11-22 (Application of advanced optical methods). This work was also supported by the project "CEITEC - Central European Institute of Technology" (CZ.1.05/1.1.00/02.0068) from European Regional Development Fund.

REFERENCES

- [1] CRONYN, J. M.: The Elements of Archeological Conservation. Routledge, 1990, London
- [2] STAMBOLOV, T.: The Corrosion and Conservation of Metallic Antiquities and Works of Art., Central Research Laboratory for Objects of Art and Science. 1985, Amsterdam
- [3] CREMERS, D., RADZIEMSKI, L.: Handbook of Laser-Induced Breakdown Spectroscopy. Chichester, UK, John Wiley and Sons Ltd, 2006

COMPARISON OF ELECTROCHEMICAL DETERMINATION OF HEAVY METALS ON PIGE AND CARBON NANOTUBES MODIFIED PIGE

Zuzana KOVACOVA, Silvia STEFANOVA, Lubomir PIKNA*

Department of Chemistry, Faculty of Metallurgy, Technical University in Košice, Letná 9, 042 00 Košice, Slovak Republic

*lubomir.pikna@tuke.sk

ABSTRACT

The aim of this paper is to compare the electrochemical determination of heavy metals with paraffin impregnated graphite electrode (PIGE) and modified PIGE with carbon nanotubes by cyclic voltammetry and anodic stripping voltammetry.

INTRODUCTION

Carbon nanotubes (CNT) have become the subject of intense researches in the last decades because of their unique properties and the promising applications in any aspect of nanotechnology. Carbon nanotubes have received considerable attention in the field of electrochemical sensing, due to their unique structural, electronic and chemical properties, for instance, unique tubular nanostructure, large specific surface, excellent conductivity, modifiable sidewall, high conductivity, good biocompatibility, and so on [1].

Mercury electrodes, namely the hanging mercury drop and the mercury film electrode, have been commonly used for electrochemical determination. However, because of its high toxicity, mercury should be replaced by less toxic or, preferably, non-toxic electrode materials [2].

In general, carbon electrodes have a number of advantages over metal electrodes such as a larger available potential span, lower cost and higher adsorption capacity. The glassy carbon electrode (GCE) is always the favorite choice due to its great inertness to chemical attack, high electro-conductivity and high purity. PIGE is also a very useful carbon electrode with the advantage of low background current, low noise and fast base-line stabilization. Li and col. from a comparison of the amperometric and electro-generated chemiluminescent (ECL) results concluded that the low-cost PIGE exhibited better ECL responses and sensitivity than the GCE and presented excellent stability in aqueous solution [3].

MATERIAL AND METHODS

Basic graphite electrodes with the diameter of 4 mm were impregnated with paraffin in vacuum for 2 hours to fill all the pores. Then the electrodes were stripped of the excess paraffin from the surface and left to cool down. The contact surface was polished with emery, filter and smo-

oth paper to a mirror-like finish and rinsed with distilled water. This was provided before each measurement because of surface regeneration.

A multi-walled carbon nanotubes (MWCNT) (Sigma-Aldrich, outer diameter 40 – 60 nm, inner diameter 5–10 nm, length 0,5 – 500 μm , purity 95+%) were used for modification of PIGE surface. Firstly CNT were purified and carboxylated under reflux in the mixture of concentrated sulphuric and nitric acid for 6 hours then washed with distilled water and dried at room temperature. Then the CNT suspension was made by dispersing CNT in nitric acid (1mg CNT:1ml nitric acid) and sonicated (ultrasonic bath UC 005 AJI TESLA) for 20 min. For electrode modification the aliquots of CNT suspension were dropped onto the prepared PIGE surface and left to dry at the room temperature. Modified electrodes (PIGE/MWCNT) were electrochemically cleaned before each measurement by immersing in nitric acid and 5 cyclic voltammograms were recorded.

All electrochemical measurements were carried out on a PC-controlled potentiostat ECASTAT 120 P (Istran, Bratislava). A three electrode system was used: PIGE as a working electrode, Ag/AgCl/3 mol dm^{-3} KCl as a reference electrode and Pt electrode as an auxiliary electrode. We engaged two electrochemical methods: cyclic voltammetry (CV) and anodic stripping voltammetry (ASV).

Conditions of CV were: scan rate 50 mV/s, potential range from 0,9 to -0,9 V. Conditions of ASV were: polarization before measurement and potential range were chosen according to metal anodic peak position, time of adsorption 90 s, polarization after measurement 0,6 V, time 120 s, current range 3 mA and scan rate 50 mV/s.

The standard solutions of Cd(II), Cu(II), Hg(II) and Pb(II) of concentration 10^{-4} mol dm^{-3} were prepared.

As a supporting electrolyte, 0,2 mol dm^{-3} acetic buffer (pH 5) was used. Passing nitrogen through the cell provided removing oxygen

from the buffer and good stirring after addition of analyte.

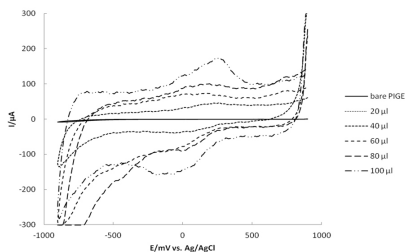
All solutions were prepared with distilled water.

RESULTS AND DISCUSSION

Different authors dispersed CNT in different solutions and used different volumes of the CNT suspension for electrode modification. Zhang and col. prepared CNT suspension in double-distilled water and dropped 20 μl [4], Goyal and Bishnoi dispersed CNT in N_2 , N-dimethylformamide and dropped 40 μl [5], Rezaei and col. added CNT to HNO_3 and casted 300 μl [6] on the electrode surface.

In our experiment CNT in nitric acid suspension and different volumes of CNT suspension (20-100 μl) for the modification of the electrode were used. A total suspension volume on the electrode surface was pipetting of sequential additions of 20 μl and after each addition it was left to dry. More CNT suspension on the electrode surface had higher current response, as can be seen in Fig. 1. With the volume of 100 μl we can observe both cathodic and anodic peak in spite of the fact there was nothing more than just an electrolyte. In spite of 20 μl seems well, this volume was not enough to cover whole electrode surface. Therefore, optimal volume 40 μl of CNT suspension was chosen. It refers to 3.18 $\mu\text{g mm}^{-2}$ density of carbon nanotubes on the electrode surface.

Figure 1: Cyclic voltammograms of supporting electrolyte provided on PIGE modified with different volumes of CNT suspension.



For heavy metals (Cd, Cu, Hg, Pb) determination, cyclic voltammetry (CV) and anodic stripping voltammetry (ASV) were used. Tab. 1 presents the highest current responses measured by these two methods performed on PIGE and PIGE/MWCNT for each metal ion.

Concentration of each heavy metal in the electrolyte was $.5.66 \times 10^{-6}$ mol.dm $^{-3}$ for CV and 4.76×10^{-7} mol dm $^{-3}$ for ASV. Comparing the results, current responses obtained by CV on PIGE/MWCNT are 63 times higher than that on PIGE, in average. ASV was used because simi-

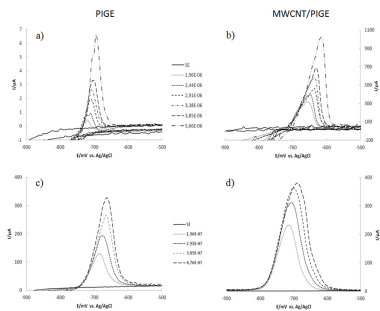
lar current responses could be obtained for 10 times lower concentrations. Current responses obtained by ASV on PIGE/MWCNT are 1.9 times higher than that on PIGE, in average.

Table 1: Comparison of the highest current responses of Cd(II), Cu(II), Hg(II), Pb(II) for modified and unmodified PIGE obtained from both electrochemical methods

Analyte	CV $I_{\text{max}} [\text{A}], c = 5.66 \times 10^{-6} \text{ mol dm}^{-3}$		ASV $I_{\text{max}} [\text{A}], c = 4.76 \times 10^{-7} \text{ mol dm}^{-3}$	
	PIGE	PIGE/MWCNT	PIGE	PIGE/MWCNT
Cd	$6.71 \cdot 10^{-6}$	$1.02 \cdot 10^{-3}$	$3.26 \cdot 10^{-2}$	$3.81 \cdot 10^{-2}$
Cu	$2.90 \cdot 10^{-5}$	$1.05 \cdot 10^{-3}$	$2.25 \cdot 10^{-2}$	$2.80 \cdot 10^{-2}$
Hg	$4.93 \cdot 10^{-5}$	$6.92 \cdot 10^{-4}$	$1.04 \cdot 10^{-2}$	$3.32 \cdot 10^{-2}$
Pb	$2.24 \cdot 10^{-5}$	$1.18 \cdot 10^{-3}$	$3.43 \cdot 10^{-2}$	$4.51 \cdot 10^{-2}$

Fig. 2 illustrates current responses of Cd(II) provided on PIGE and PIGE/MWCNT obtained by both CV and ASV. We can clearly see higher peaks with PIGE/MWCNT on the right side of the figure. Comparing them, current responses obtained by CV resulted in 328 times higher responses on PIGE/MWCNT than that on PIGE, in average. Current responses obtained by ASV on PIGE/MWCNT are 1.5 times higher than that on PIGE, in average. Measurements realized by CV started with concentration of cadmium 1.96×10^{-6} mol dm $^{-3}$ and standard addition was 50 μl . On the other hand, ASV measurements started with just 1.96×10^{-7} mol dm $^{-3}$ and standard addition was only 10 μl . Records in Fig. 2 illustrate that increase in current response is comparable in both CV and ASV.

Figure 2: Cyclic voltammograms on PIGE (a) and on PIGE/MWCNT (b) and stripping voltammograms on PIGE (c) and on PIGE/MWCNT (d) of supporting electrolytes (SE) and different concentrations [mol dm $^{-3}$] of Cd(II).



CONCLUSION

Methods used in this experiment - CV and ASV - are quite simple and relatively fast. Carbon electrodes are more environment-friendly than mercury electrode and modified ones have excellent properties and are very good for determination of heavy metals. The preparation of PIGE and than its modification by CNT is effortless and cheap. Procedure of PIGE modification presented in this paper provides stabile electrode and offers better current responses then the bare PIGE.

ACKNOWLEDGEMENT

The work was supported by Grant Agency of Slovak Republic VEGA, project No. 1/0236/11.

REFERENCES

- [1] Hu C, Hu S: Journal of Sensors, 2009 (2009), Article ID 187615
- [2] Jorge E O, Neto M M M, Rocha M M: Talanta, 72 (2007), 1392-1399
- [3] Li F, Lin X-Q, Cui H: Journal of Electroanalytical Chemistry, 534 (2002), 91-98
- [4] Zhang X, Wang S, Jia L, Xu Z, Zeng Y: J. Biochem. Biophys. Methods 70 (2008), 1203-1209
- [5] Goyal R N, Bishnoi S: Electrochimica Acta, 56 (2011), 2717-2724
- [6] Rezaei B, Zare S Z H: Sensors and Actuators B, 134 (2008), 292-299

RENEWAL OF THREE-DIMENSIONAL NANOCRYSTALLINE DIAMOND BIO-TRANSISTOR BY LOW TEMPERATURE HYDROGENATION

Marie KRATKA^{1*}, Neda NEYKOVA^{1,2}, Egor UKRAINTSEV¹, Alexander KROMKA¹ and Bohuslav REZEK¹

¹ Institute of Physics ASCR, Cukrovarnicka 10/112, 162 00 Prague 6, Czech Republic

² Czech Technical University in Prague, Faculty of Nuclear Sciences and Physical Engineering, Trojanova 13, 120 00 Prague 2, Czech Republic

*kratka@fzu.cz

ABSTRACT

We employ directly grown microscopic (20 μm and 5 μm) solution-gated field-effect transistors (SGFET) as a biosensor with H-terminated surface acting as a gate insulator towards solution and generator of surface conductivity at the same time. Reactive ion etching and photolithographic processing of a nucleation layer is used to define SGFET patterns. Diamond microstructures are then grown by microwave plasma enhanced chemical vapor deposition on Si/SiO₂ substrates. The area between contacts was covered with photoresist (thickness 3-4 μm) to insulate it from the solution. We show that such 3D transistors including the encapsulation can be easily renewed (cleaned from cell medium proteins) by low temperature hydrogen plasma treatment in linear antenna microwave reactor.

INTRODUCTION

Common diamond field-effect transistors (FETs) based on hydrogen terminated diamond surface conductivity are prepared by diverse technological steps including lithography, lift-off, selective oxidation, encapsulation, deposition of contacts etc. [1, 2]. This is complicated for renewal of device when used as a biosensor because proteins and other organic molecules are persistent on the surface [1]. It was shown by atomic force microscopy (AFM) that proteins in this medium create thin inter-layer on the diamond which remains on diamond surface even after phosphate buffered saline (PBS) and water rinsing [3].

A direct growth of diamond structures via patterning of nucleation/seeding layer can represent an alternative solution [4 - 6].

Therefore, we employ nanocrystalline diamond (NCD) films to fabricate directly grown FET microchannels (20 μm and 5 μm). We show that such 3D transistors including the encapsulation and gold contacts can be easily recycled (re-hydrogenated) just by low temperature hydrogenation process performed in linear antenna reactor [7] and that this process cleans diamond surfaces from proteins.

MATERIAL AND METHODS

Fabrication of directly grown NCD channels

Directly grown NCD FET channels were prepared by photolithographic processing with two polymer layers and by reactive ion etching through photolithographic mask [8].

Afterwards, growth of NCD thin films was performed in a microwave plasma CVD system

(AIXTRON P6) from a methane/hydrogen gas mixture. Process parameters were as follows: microwave power 2.5 kW, 1% methane in hydrogen, total gas pressure 50 mbar, substrate temperature 800°C, and total growth time 3 h [8]. The surfaces of diamond films were hydrogenated in pure H plasma at 600°C for 10 min.

Preparation of SGFETs

Source and drain gold contacts were prepared by thermal evaporation (10 nm of Ti and 50 nm of Au) followed by lift-off technique. The area between contacts was covered with positive photoresist OFPR (thickness 3-4 μm) and deep UV curing of resist for hardening and biocompatibility was applied.

Low temperature hydrogenation

Commonly used relatively high substrate temperatures ($T \geq 600^\circ\text{C}$) during diamond growth and hydrogenation lead to partial or complete damage of the metal electrodes or other electronic parts [9]. Thus, 3D transistors including the encapsulation (resist OFPR), gold contacts and with adsorbed proteins on diamond surface were exposed to hydrogen plasma using low temperature in linear antenna plasma system (Roth and Rau). The main advantage of this system is a larger distance between the high-density plasma region and the sample surface (50-100 mm) [10, 11]. Hydrogen termination at 200°C performed in linear antenna plasma system is efficient to induce hydrogen-terminated conductive surfaces and no damage of polymer-based passivating layer (SU8) as well as Au contacts was observed [11]. In our case samples were exposed

to hydrogen plasma at the following conditions: microwave power 1000 W, vacuum pressure 0.3 mbar, 100 sccm of hydrogen flow, and processing time 30 min. The substrate temperature was 200°C.

AFM study of protein layer

Study of protein layer was performed using AFM on monocrystalline diamond (MCD). To check the effectiveness of low temperature hydrogen termination fetal bovine serum (FBS) was adsorbed on the surface of MCD from 15% FBS solution for 10min. The thickness of protein layer was measured in air using contact mode nanoshaving [12, 13]. Then, the low temperature hydrogen termination was performed and the protein thickness was measured again using the same method.

RESULTS AND DISCUSSION

After application of FBS, the SGFET conductivity decreased as reflected by the shift of transfer characteristics by -50 mV. This shift is permanent even after rinsing by diverse solution. This is in full agreement with our results on conventional planar SGFETs where a thin protein layer remains on diamond surfaces in spite of sample rinsing [1, 2].

AFM results in Figure 1 show that low temperature hydrogen termination in linear antenna plasma removed this FBS protein layer from the monocrystalline diamond surface successfully (unlike the solutions). Only < 1 nm thin layer (probably some hydrocarbons) remains on the surface and should be taken into account in future experiments.

Figure 1. AFM study of protein layer before and after low-T hydrogenation

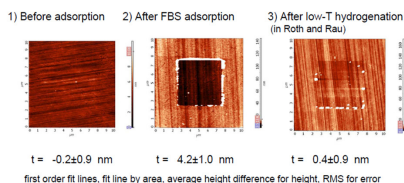
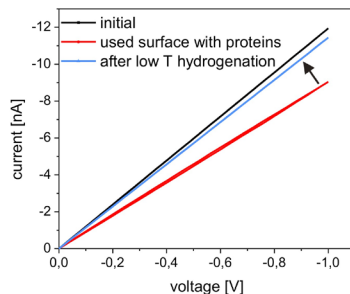


Fig. 2 shows I(V) characteristics of pristine device, after adsorption of FBS and after low temperature hydrogenation in linear antenna plasma system. It is evidenced that the H-terminated surface was refreshed after low temperature hydrogen plasma treatment and the SGFET channel conductivity is recovering towards the initial values.

The quality of encapsulation resist layer and

contacts remains similar based on optical microscope inspection. Yet, profilometry measurements showed that resist thickness decreased after low-T hydrogenation in the linear plasma system from 3.2 μm to 2.3 μm (etching rate 30 nm/min). This may be limitation for repeated device renewal. Nevertheless, the resist material still leaves room for optimization.

Figure 2. I (V) characteristics of three-dimensional diamond transistor channel in pristine state, after protein adsorption, and after low-T hydrogenation



CONCLUSION

Low temperature hydrogen termination in linear antenna plasma successfully removed FBS proteins from the diamond surface, refreshed H-termination and kept the similar quality of covering resist layer and Au contacts. Thus such 3D transistors including the encapsulation and gold contacts can be easily recycled (re-hydrogenated) just by low temperature hydrogenation process performed in linear antenna reactor (200°C, 30 minutes).

ACKNOWLEDGEMENT

Technical support of Jitka Libertínová, Oleg Babchenko, Zdeňka Poláčková, Karel Hruška, Vlastimil Jurka, Antonín Fejfar, Antonín Brož and Marie Kalbacova is gratefully appreciated. This research was financially supported by the projects P108/12/0996 (GACR), P108/12/G108 (GACR), doctoral project 202/09/H041, SVV-2011-263304 and by the Fellowship J.E. Purkyně (BR, AK).

REFERENCES

- [1] Rezek B, Krátká M, Kromka A, Kalbacova M: Biosens. Bioelectron. 26 (2010) 1307-1312
- [2] Krátká M, Kromka A, Ukraintsev E, Ledinský M, Brož A, Kalbacova M, Rezek B: Sens. Actuators B (2012), accepted, doi:10.1016/j.snb.2012.02.049
- [3] Rezek B, Ukraintsev E, Michalíková L,

- 
- Kromka A, Zemek J, Kalbacova M: Diam. Relat. Mater. 18 (2009) 918-922
- [4] Kromka A, Babchenko O, Rezek B, Ledinský M, Hruška K, Potměšil J, Vaněček. M: Thin Solid Films 518 (2009) 343-347
- [5] Kozak H, Kromka A, Babchenko O, Rezek B: Sensor Lett. 8 (2010) 482-487
- [6] Babchenko O, Verveniotis E, Hruška K, Ledinský M, Kromka A, Rezek B: Vacuum 86 (2012) 693-695
- [7] Kromka A, Babchenko O, Izak T, Hruška K, Rezek B: Vacuum 86 (2012) 776-779
- [8] Babchenko O, Izak T, Ukraintsev E, Hruška K, Rezek B, Kromka A: phys. stat. sol. (b) 247 (2010) 3026-3029
- [9] Neykova N, Babchenko O, Kozak H, Kromka A, Hruska K, Vanecek M: 15th International Conference on Applied Physics of Condensed Matter (2009, 24-26 June), Bystra, Liptovsky Jan, Slovak Republic, p.256-261 ISBN 978-80-554-0057-0
- [10] Kromka A, Babchenko O, Izak T, Potocky S, Davydova M, Neykova N, Kozak H, Remes Z, Hruška K, Rezek B: Nanocon 2011, Brno (21. – 23. 9. 2011)
- [11] Neykova N, Kozak H, Ledinský M, Kromka A: Vacuum 86 (2012) 603-607
- [12] Rezek B, Shin D, Nebel C E: Langmuir 23 (2007) 7626-7633
- [13] Ukraintsev E, Rezek B, Kromka A, Brož A, Kalbacova M: phys. stat. sol. (b) 246 (2009) 2832-2835

CHEMICAL COMPOUNDS ON THE SURFACE OF ICE

Jan KRAUSKO¹, Dominik HEGER^{1,2}

¹Department of Chemistry, Faculty of Science, Masaryk University, Kamenice 5/A, 62500 Brno, Czech Republic

²Research Centre for Toxic Compounds in the Environment, Faculty of Science, Masaryk University, Kamenice 3, 62500 Brno, Czech Republic

ABSTRACT

Microenvironment of 1-methylnaphthalene (1-MN) on the surface of ice grains was studied by fluorescence spectroscopy an environmental scanning electron microscopy (ESEM). Experimental observations and results of molecular dynamics (MD) simulations, DFT and CC2 calculations were compared.

INTRODUCTION

Ice surface is an environment with unique properties significantly different from those of aqueous solution. Impurities present in a solution (prior to freezing) are expelled from the ice lattice [1] to the boundaries of ice grains.

Freezing-induced aggregation of methylene blue[2] and enhanced protonation of cresol red [3] was observed in frozen aqueous solutions. It was reported that similar effect occurs in the frozen aqueous solutions of inorganic compounds [4; 5] and accelerates reactions in troposphere.

Photochemical transformations of organic compounds in ice lead to products different from those produced by irradiation of solution [6; 7] Their toxicity is higher, which poses an environmental threat[8; 9]. Understanding the fate of organic compounds on the ice surface is essential.

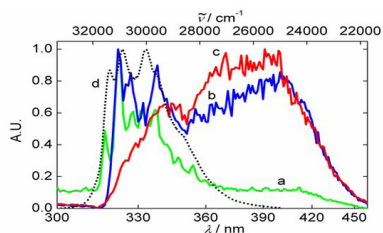
PREPARATION OF SAMPLES AND METHODS OF MEASUREMENT

1-MN was deposited on the surface of artificial snow grains from vapors at 238 K. Amount of 1-MN deposited on snow was dependent on duration of deposition and was determined by UV-Vis spectroscopy (in melted snow). The specific surface area of this snow (produced by spraying very fine droplets of pure water from a nebulizer into liquid nitrogen) was $1.1 \times 10^4 \text{ cm}^2 \text{ g}^{-1}$. AMIN-CO –Bowman Series 2 Spectrofluorometer was employed for fluorescence measurements. Amount of 1-MN deposited on snow was dependent on duration of deposition and was determined by UV-Vis spectroscopy (in melted snow). The specific surface area of this snow (produced by spraying fine droplets of pure water from a nebulizer into liquid nitrogen) was $1.1 \times 10^4 \text{ cm}^2 \text{ g}^{-1}$. Surface coverage by 1-MN was calculated for each sample.

RESULTS AND DISCUSSION

Fluorescence emission spectra of samples with different surface loading ($\text{mol} \cdot \text{kg}^{-1}$) and spectrum of neat 1-MN at 77 K are shown (Figure 1). Samples with low surface loading exhibited dominant emission bands of monomer (318 nm, 323 nm, 327 nm, 332 nm, 338 nm, 344 nm, 350 nm), while samples with higher surface loading showed bands of monomer as well as bands of excimer (360 nm, 400 nm, 430 nm). Bands of excimer were clearly dominant at highest surface loading.

Figure 1. Fluorescence emission spectra of neat 1-MN (dotted line – d) and 1-MN deposited on the surface of artificial snow. Surface loading: 5×10^{-6} (green line - a), 7×10^{-5} (blue line – b) and 9×10^{-5} (red line – c). Measured at 77 K.



CONCLUSION

Weak excimer fluorescence was observed for a loading of $5 \times 10^{-6} \text{ mol kg}^{-1}$, which is 2-3 orders of magnitude below monolayer coverage. However, formation of excimers is favored at higher surface loadings ($5 \times 10^{-5} \text{ mol kg}^{-1}$), albeit still being below monolayer coverage. The calculations of excited states of monomer and associated moieties suggested that a parallel-displaced arrangement is responsible for the excimer emission observed experimentally [10].

REFERENCES

- [1] PETRENKO, V. F.; WHITWORTH, R. W. *Physics of ice*. Oxford: Oxford University Press, 1999.
- [2] HEGER, D.; JIRKOVSKY, J.; KLAN, P. Aggregation of methylene blue in frozen aqueous solutions studied by absorption spectroscopy. *Journal of Physical Chemistry A*, 2005, vol. 109, no. 30, p. 6702-6709.
- [3] HEGER, D.; KLANOVA, J.; KLAN, P. Enhanced protonation of cresol red in acidic aqueous solutions caused by freezing. *Journal of Physical Chemistry B*, 2006, vol. 110, no. 3, p. 1277-1287.
- [4] TAKENAKA, N.; DAIMON, T.; UEDA, A. et al. Fast oxidation reaction of nitrite by dissolved oxygen in the freezing process in the tropospheric aqueous phase. *Journal of Atmospheric Chemistry*, 1998, vol. 29, no. 2, p. 135-150.
- [5] TAKENAKA, N.; UEDA, A.; DAIMON, T. et al. Acceleration mechanism of chemical reaction by freezing: The reaction of nitrous acid with dissolved oxygen. *Journal of Physical Chemistry*, 1996, vol. 100, no. 32, p. 13874-13884.
- [6] KLAN, P.; ANSORGOVA, A.; DEL FAVERO, D. et al. Photochemistry of chlorobenzene in ice. *Tetrahedron Letters*, 2000, vol. 41, no. 40, p. 7785-7789.
- [7] KLAN, P.; DEL FAVERO, D.; ANSORGOVA, A. et al. Photodegradation of halobenzenes in water ice. *Environmental Science and Pollution Research*, 2001, vol. 8, no. 3, p. 195-200.
- [8] KLAN, P.; HOLOUBEK, I. Ice (photo)chemistry. Ice as a medium for long-term (photo)chemical transformations - environmental implications. *Chemosphere*, 2002, vol. 46, p. 1201-1210.
- [9] KLAN, P.; KLANOVA, J.; HOLOUBEK, I. et al. Photochemical Activity of Organic Compounds in Ice Induced by Sunlight Irradiation: The Svalbard Project. *Geophysical Research Letters*, 2003, vol. 30, no. 4, p. art. no. 1313.
- [10] HEGER, D.; et al. *The Journal of Physical Chemistry A*, Washington : American Chemical Society, 115, 41, 11412-1142 s. ISSN 1089-5639. 2011.

FREEZING POTENTIAL MEASUREMENTS

Lubica KRAUSKOVA¹, Dominik HEGER^{1,2}, Zdenek ROUBAL³, Pavel FIALA³

¹Department of Chemistry, Faculty of Science, Masaryk University, Kamenice 5/A8, Brno 602 00, Czech Republic

²Research Centre for Toxic Compounds in the Environment, Faculty of Science, Masaryk University, Kamenice 3, 625 00 Brno, Czech Republic

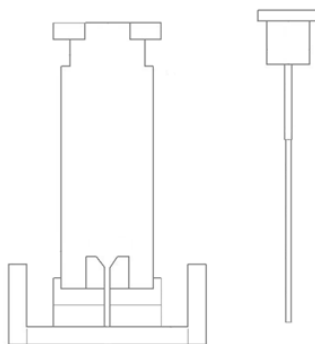
³Department of Theoretical and Experimental Electrical Engineering, Brno University of Technology, Kolejní 2906/4, Brno 612 00, Czech Republic

ABSTRACT

When a dilute aqueous solution of salt is frozen rapidly, cations and anions are not equally incorporated into the ice lattice. The charge separation generates large potential difference between ice and unfrozen solution during freezing, as large as tens or even hundreds of volts [1]. The freezing potential is a strictly nonequilibrium effect. It is dependent on salt species and concentration, ice growth rate, ice crystal orientation, and time [2]. In general, results of previous workers correspond as regards sign but differ as regards magnitude [3].

This phenomenon was discovered more than 60 years ago [4] but remains poorly understood. Such a large electric potential might participate in denaturation of proteins and damage of cells when biological and biochemical samples are frozen [5]. Thus, understanding of the freezing potential might be applied in the field of cryopreservation. The goal of our work is to measure the freezing potential under various conditions and compare the results with pH changes and enzyme denaturation during freezing.

For the purpose of measuring the freezing potential, a special apparatus was constructed (Figure 1). A sample was put into a glass tube with two platinum electrodes. One of the electrodes was at the bottom of the tube; the latter was placed in the solution near a water-level. The sample was cooled from the bottom. When the ice front got beyond the bottom electrode, an abrupt change in potential was observed. The freezing potential of various solutes has been measured and the results will be discussed.



REFERENCES

- [1] Workman, E.J.; Reynolds, S.E.: Electrical Phenomena Occurring during the Freezing of Dilute Aqueous Solutions and Their Possible Relationship to Thunderstorm Electricity. *Physical Review*, 1950. 78(3), p. 254.
- [2] Wilson, P.W.; Haymet, A.D.J.: Workman-Reynolds freezing potential measurements between ice and dilute salt solutions for single ice crystal faces. *Journal of Physical Chemistry B*, 2008. 112(37), p. 11750-11755.
- [3] Rastogi, R.P.; Tripathi, A.K.: Effect of Nonionic Solutes on the Freezing Potential of Dilute Ionic Aqueous-Solutions. *Journal of Chemical Physics*, 1985. 83(3), p. 1404-1405.
- [4] Workman, E.J.; Reynolds, S.E.: A Suggested Mechanism for the Generation of Thunderstorm Electricity. *Physical Review*, 1948. 74(6), p. 709.
- [5] Sola, M.I.; Corti, H.R.: Freezing Induced Electric Potentials and Ph Changes in Aqueous-Solutions of Electrolytes. *Anales De La Asociacion Quimica Argentina*, 1993. 81(6), p. 483-498.
- [6] Roubal, Z.; Szabó, Z.; Steinbauer, M.; Heger, D.; Kubásek, R.: The design of high-impedance and high-voltage input amplifier for measurement of electropotentials on solid-liquid phase boundary. *PIERS Proceedings*, 2011.

SIMILARITY OF CYANOBACTERIA BASED ON THE COMPARISON OF WHOLE PROTEIN CODING INFORMATION

Vladimira KUBICOVA¹, Ivo PROVAZNIK¹

¹ Department of Biomedical Engineering, Faculty of Electrical Engineering and Communication, Brno University of Technology, Kolejni 4, 612 00 Brno, Czech Republic

*kubicova@feec.vutbr.cz

ABSTRACT

We present a method for determination of the similarity among cyanobacteria by comparing coding information in whole genome. This method is based on comparing orthologous genes of the analysed organisms. The number of the orthologous genes can be found by Needleman-Wunsch algorithm. There are two ways how to analyse orthologous genes: first is to rate the significance of diagonal plot, second is to count the number of genes with defined score. We constructed distance tree from number of orthologous genes with score more than 0.8. This distance tree was compared with two distance trees presented in literature.

INTRODUCTION

Cyanobacteria are aquatic and photosynthetic bacteria living in the water. They are small, unicellular and often grow in colonies. Cyanobacteria are still highly studied organism. One of the main reasons is that cyanobacteria have played a significant role in Earth history as primary producers and the ultimate source of atmospheric oxygen. Until now, however, how and when the group diversified has remained unclear. Another reason is that plastids or chloroplasts are descendants of an ancestral cyanobacterium and we still do not know which cyanobacteria was the most similar to the plastid ancestor.

Phylogenetic trees of cyanobacteria family have been determined by various methods and described in literature. Comparison of the bacterial 16S rRNA gene sequence has emerged as a preferred genetic technique because 16S rRNA is highly conserved between different species of bacteria [1]. Many authors have studied the relationships based on 16S rRNA and their results are similar or slightly different [2, 3, 4]. Determination of relationship based on the comparison of gene families is presented in [5] and [6].

Similarities among cyanobacteria can be searched by comparing coding information in their whole genomes. It may provide for more accurate results and reveal inaccuracies in phylogenetic relationship based on observing a single gene (16S rRNA) or family of genes. We propose a method of comparing the cyanobacteria based on searching orthologous genes.

MATERIAL AND METHODS

Four cyanobacteria were chosen for the study: *Nostoc punctiforme*, *Nostoc sp. PCC 7120*, *Ana-*

beana variabilis, and *Trichodesmium erythraeum*. Complete genomes of these organisms were downloaded from NCBI (National Centre for Biotechnology Information) databases. NCBI identification numbers, size of genomes in base pairs, and numbers of coding regions of the relevant sequences are listed in Table 1.

Table 1: Cyanobacteria sequences used in the study.

No.	Organism	NCBI ID	Genome length [bp]	Number of coding regions
1.	<i>Nostoc punctiforme</i>	NC_010628	8 234 322	6 086
2.	<i>Nostoc sp. PCC 7120</i>	NC_003272	6 413 771	5 365
3.	<i>Anabeana variabilis</i>	NC_007413	6 365 727	5 043
4.	<i>Trichodesmium erythraeum</i>	NC_008312	7 750 108	4 451

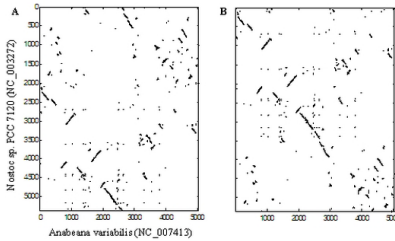
We used global alignment of each pair of coding regions to compare these genomes. Coding regions were represented by amino acid sequences, which are the result of translation. Needleman–Wunsch algorithm [7] with the BLOSUM50 scoring matrix was used as an alignment algorithm.

The overall score of global alignment by Needleman–Wunsch algorithm is affected by the length of the sequences. Long sequences tend to higher (or lower) scores than shorter sequences. Therefore, the overall scores were normalized by dividing by the score obtained using global alignment the second sequence with itself [8]. The maximum normalized score is equal to 1 and occurs in the case of identical sequences. After the determination of normalized score between every coding region, numbers of orthologous genes corresponded with normalized score were determined.

Most of prokaryotic genomes are circular and

the beginning of linear sequences stored in databases is arbitrary. Thus, first step of the proposed analysis method is to find fiducial points in all sequences to obtain the “corresponding beginnings”. This technique is explained in the example of comparison the *Nostoc* sp. PCC 7120 and *Anabeana variabilis*. The Fig. 1 A

Figure 1: Coding region with normalized score > 0.8 ; axis represents the order of coding region in genome; A: without change in order of coding regions, B: rotation of the first 2 000 coding regions in *Nostoc* sp. PCC 7120



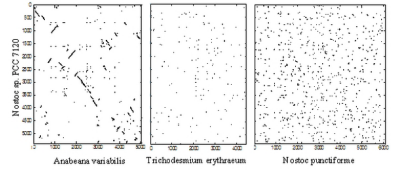
depicts the normalized score between the coding regions, which is higher than 0.8. We applied rotation of the first 2 000 coding regions in *Nostoc* sp. PCC 7120 and obtained a result shown in Fig. 1 B. In this figure, we can see diagonal lines, which represent relative ordering of genes on chromosomes between two organisms. Thus, we found that the order of first coding region in *Anabeana variabilis* corresponds to 2001th coding region in *Nostoc* sp. PCC 7120.

RESULTS AND DISCUSSION

We can analyze the obtained data in two ways. First, we can rate the significance of diagonal lines. Second, we can count number of genes (coding parts) with defined normalized score – number of orthologous genes.

Each diagonal line is created by a group of genes with the same order in both organisms. The diagonal lines depicted on Fig. 1. B can only be seen for closely related organisms. We compared *Nostoc* sp. PCC 7120 sequence with other organism sequences and the results are depicted on Fig. 2. By analyzing the diagonal lines we state that the most related sequence to *Nostoc* sp. PCC 7120 is *Anabeana variabilis*. In other plots of normalized scores greater than 0.8, we cannot see diagonal lines and thus the relationship among those organisms cannot be determined.

Figure 2: Comparison of orthologous genes between *Nostoc* sp. PCC 7120 and other organisms



We analyzed a number of orthologous genes between each pair of chosen organisms. Dependence of the number of the genes on the normalized score is depicted in Fig.3. The values in this figure correspond with number of genes greater than normalized score. The distribution of genes among chosen organisms is similar.

To evaluate the relationship between organisms, we constructed distance tree using clustering with the Unweighted Pair Group Method with Arithmetic Mean (UPGMA) from orthologous genes with normalized score greater than 0.8. Result of this method is depicted in Fig. 4 as a dendrogram. The analyzed organisms were included in studies [5] and [6] with resulting trees showed in Fig. 5. The tree on Fig. 5 A is based on plastid-encoded proteins and considers

Figure 3: Dependence of the number of genes on normalized score between pair of organisms (numbers in legend corresponds with Tab. 1), values on axis y corresponds with number of genes greater than normalized score on axis x

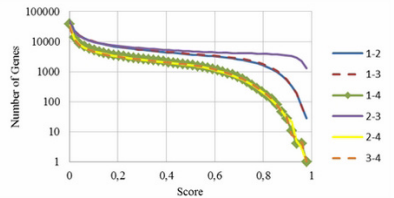


Figure 4: Distance tree from orthologous genes with score > 0.8

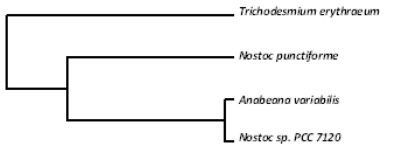
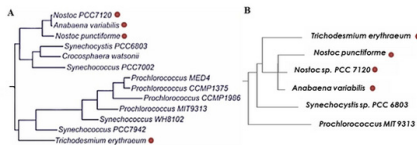


Figure 5: Related distance trees presented in [5] and [6]. Red dots indicate the organisms analyzed in this paper. A: tree based on plastid-encoded proteins [6], B: tree constructed by hidden Markov model from sequences of proteins of known structure [5]



Anabaena variabilis and Nostoc sp. PCC 7120 as most related organisms among chosen for analysis. Another tree on Fig. 5 B is constructed by a hidden Markov model (HMM) from sequences of proteins of known structure. According this tree, Nostoc punctiforme is closely related to Anabaena variabilis and Nostoc sp. PCC 7120. Overall, our distance tree is more similar to the tree created by comparing the plastid-encoded proteins (Fig. 5 A).

CONCLUSION

We presented a method to find fiducial points in sequences to obtain “corresponding beginnings” of circular genomes. This method is suitable only for organisms closely related with the nearly same order of orthologous genes. This condition is met e.g. for Nostoc sp. PCC 7120 and Anabaena variabilis. We found that the order of the 1st coding region in Anabaena variabilis corresponds with the 2001th coding region in Nostoc sp. PCC 7120.

We counted the number of genes for different values of normalized score and from the number of genes with score > 0.8 we calculated the distance tree by UPGMA method. The distance was compared with other two trees presented in literature. The distribution of organisms by our method is similar as the distribution in trees presented in literature. We assume that the presented method based on comparing the coding information in whole genome is suitable for comparison of relationship. Our method is - in principle - more accurate than methods based on comparison of few selected genes.

ACKNOWLEDGEMENT

This work was supported in part by: GAČR 102/09/H083, GAČR P102/11/1068.

REFERENCES

[1] Clarridge J E: Impact of 16S rRNA Gene Sequence Analysis for Identification of Bacteria on Clinical Microbiology and Infectious Diseases. *Clinical Microbiology Reviews* 3 (2004), 840–862.
 [2] Nelissen B, Van de Peer Y, et al: An early origin of plastids within the cyanobacterial divergence is suggested by evolutionary trees based on complete 16S rRNA sequences. *Molecular Biology and Evolution* 12 (1995), 1166–1173.
 [3] Turner S, Pryer KM et al: Investigating deep

phylogenetic relationships among cyanobacteria and plastids by small subunit rRNA sequence analysis. *The Journal of Eukaryotic Microbiology*. 46 (1999), 327–338.

[4] Honda D, Yokota A, Sugiyama J: Detection of seven major evolutionary lineages in cyanobacteria based on the 16S rRNA gene sequence analysis with new sequences of five marine *Synechococcus* strains. *Journal of Molecular Evolution* 48 (1999), 723–739.
 [5] Gough J, Karplus K, Hughey R. and Chothia C: Assignment of Homology to Genome Sequences using a Library of Hidden Markov Models that Represent all Proteins of Known Structure. *Journal of Molecular Biology* 313 (2001), 903–919.
 [6] Rodríguez-Ezpeleta N, Brinkmann H et al: Monophyly of primary photosynthetic eukaryotes: green plants, red algae, and glaucophytes. *Current Biology* 15 (2005), 1325–1330.
 [7] Needleman B, Wunsch D: A general method applicable to the search for similarities in the amino acid sequence of two proteins. *Journal of Molecular Biology* 48 (1970), 443–53.
 [8] Cristianini N, Hahn W: *Introduction to Computational Genomics: A Case Studies Approach*. Cambridge University Press (2007).

CHARACTERIZATION OF ELECTROCHEMICAL DNA BIOSENSORS WITH PROTECTIVE MEMBRANES IN SOLUTIONS CONTAINING SURFACE ACTIVE COMPOUNDS

Lenka HLAVATA, Anton AMBROZY, Jan LABUDA*

Institute of Analytical Chemistry, Faculty of Chemical and Food Technology, Slovak University of Technology in Bratislava, Radlinského 9, 812 37 Bratislava, Slovakia
*jan.labuda@stuba.sk

ABSTRACT

Bare and DNA modified screen printed carbon electrodes were tested against fouling in solutions containing surface active compounds like polyethylene glycol (PEG), Triton X100, and sodium dodecylsulphate (SDS) using cyclic voltammetry with the $[\text{Fe}(\text{CN})_6]^{3-/4-}$ redox indicator and electrochemical impedance spectroscopy. Polymer protective membranes were introduced on the surface of electrodes and the sensors were applied to tests of tea and beer.

INTRODUCTION

On the topic of DNA based biosensors there is a large research activity as they represent effective tools for tests of DNA association interactions with low molecular weight compounds like drugs and chemicals as well as tests of effects of various chemical and physical agents on DNA structure and its integrity [1, 2]. Disposable electrochemical biosensors are of particular interest as rather simple sensors used mostly at screening and warning tests [3]. Such sensors were also applied to tests of food samples and waste water [4]. Together with building stability of the biosensors, interferences by surface active compounds represent the biggest problems at the application of in systems containing surface active compounds. Here, we report on effect of standard surface active compounds PEG, Triton X100 and SDS as well as tea extract and beer on the commercial screen printed carbon electrode (SPCE) and DNA/SPCE biosensors and on effect of some protective polymer films placed on the SPCE and DNA/SPCE electrodes.

2. MATERIAL AND METHODS

Reagents

Salmon sperm dsDNA with low molecular weight (product No. 31149) was obtained from Sigma-Aldrich, Germany. Its stock solution (0.5 mg ml^{-1}) was prepared in 0.1 mol l^{-1} phosphate buffer solution (PBS) of pH 7.0 and stored at -4°C . Chitosan (from shrimp shells) of low viscosity (CHIT) was obtained from Fluka, Germany (product No. 50494). Its 0.5% (w/w) solution was prepared in 1% (v/v) acetic acid (99.8%, Lachema, Czech Republic) and filtered through a simple paper strip. The final CHIT solution

was of pH 5.0 [24]. Nafion preparative was diluted to 1% by PBS. Polyethylene glycol, Triton X100 and sodium dodecylsulphate were used in concentration of 1 mg l^{-1} . Tea extracts were prepared using commercial black tea bags and recommended 5 min extraction with hot water (98°C). Then, the extracts were cooled to ambient temperature. Commercial beer was used as received after 10 min staying at open air.

Apparatus and measurements

Voltammetric measurements were performed using the potentiostat Autolab PGSTAT-100 and the software GPES version 4.9.005 (Eco Chemie, Netherlands). EIS measurements were carried out on the Autolab using impedance module FRA2 driven by software FRA version 4.9.006 (Eco Chemie, Netherlands). Screen-printed carbon electrode assembly (SPCE) consisting of a carbon working electrode (25 mm^2 geometric surface area), a silver/silver chloride reference electrode (Ag/AgCl/SPCE) (potential of 0.284 V vs conventional Ag/AgCl/saturated KCl electrode) and the same counter electrode was obtained from Food Research Institute, Bio-center, Modra, Slovakia.

The SPCE surface was pretreated first by applying a potential of $+1600 \text{ mV}$ for 120 s and $+1800 \text{ mV}$ for 60 s in 10 ml of acetate buffer solution (0.25 mol l^{-1} containing 10 mmol l^{-1} KCl, pH 4.75), under stirring. During this procedure contaminants present on the carbon surface are oxidized and the surface is activated for DNA immobilization. Then, $5 \mu\text{l}$ of dsDNA stock solution were deposited and let to evaporate to dryness. Protective membranes have been prepared by application of $5 \mu\text{l}$ of the polymer solu-

tion and evaporation to dryness.

The cyclic voltammograms of a 1:1 mixture of $1 \times 10^{-3} \text{ mol l}^{-1} [\text{Fe}(\text{CN})_6]^{3-/4-}$ in 0.1 mol l^{-1} PBS of pH 7.0 were recorded from -800 mV to 750 mV using the scan rate 50 mV s^{-1} , the step potential 5 mV and evaluated against the CV record obtained in blank PBS. EIS measurements were carried out in the presence of $1 \times 10^{-3} \text{ mol l}^{-1} [\text{Fe}(\text{CN})_6]^{3-/4-}$ in 0.1 mol l^{-1} PBS of pH 7.0 at the potential 0.1 V , within the frequency range $0.1\text{--}5000 \text{ Hz}$ and using the potential amplitude 10 mV [5].

RESULTS AND DISCUSSION

Three types of electrodes, i.e. bare SPCE, simple DNA/SPCE biosensors, polymer covered SPCE (Nafion/SPCE and CHIT/SPCE) and DNA/SPCE (Nafion/DNA/SPCE and CHIT/DNA/SPCE) have been prepared and investigated regarding the CV anodic peak current (I_{pa}) and peak to peak potential separation (ΔE_p) of $1 \times 10^{-3} \text{ mol l}^{-1} [\text{Fe}(\text{CN})_6]^{3-/4-}$ in 0.1 mol l^{-1} PBS of pH 7.0. In addition, electrochemical impedimetric spectra have been obtained and the charge transfer resistance (R_{ct}) as described in Experimental.

Then, bare SPCE and simple DNA/SPCE have been incubated in solutions of selected surface active compounds such as polyethylene glycol (PEG), Triton X100, and sodium dodecylsulphate (SDS) for 2, 5, and 15 min under stirring and, after medium exchange, the CV and EIS experiments have been performed. The I_{pa} , ΔE_p and R_{ct} responses have been evaluated which exhibit some shift with time of the electrode incubation indicating effect of individual surface active compounds on the sensor behavior. Generally, an increase in I_{pc} and decrease in R_{ct} responses as well as decrease in ΔE_p have been found which may indicate change of the electrode composition due to some loss of pasting liquid under action of surfactants, particularly Triton X100.

Moreover, black tea extracts and beer have been tested regarding their effect on the I_{pa} , ΔE_p and R_{ct} values for the electrodes without and with polymer protective membranes. Rather strong SPCE and DNA/SPCE fouling indicated by decrease in I_{pa} and increase in ΔE_p and R_{ct} was observed with some dependence on incubation time, the last one particularly for beer. While the Nafion membrane has helped significantly to protect the sensors against surfactant of tea, the chitosan film has been more effective barrier in the case of beer.

CONCLUSION

Surface active compounds in tested solution exhibit an influence on the bare and DNA modified carbon electrodes voltammetric and electrical responses depending on type of the compound and time of incubation. Polymer membranes deposited on the electrodes have been shown to avoid

to some degree electrode fouling and diminish response changes with incubation time.

ACKNOWLEDGEMENT

This work was supported by the Scientific Grant Agency VEGA of the Slovak Republic (Project No. 1/0182/11), the Slovak Research and Development Agency (Project SK-RO-0028-10) and the European Fund for Regional Development (ITMS project code 26240220072).

REFERENCES

- [1] Labuda J, Brett AMO, Evtugyn G, Fojta M, et al.: *Pure Appl. Chem.* 82 (2010), 1161–1187
- [2] Fojta M, In: *Electrochemistry of Nucleic Acids and Proteins – Towards Electrochemical Sensors for Genomics and Proteomics*, Eds. Palecek E, Scheller F, Wang J, Elsevier, Amsterdam, 2005
- [3] Labuda J, Vyskocil V, In: *Encyclopedia of Applied Electrochemistry, DNA/ Electrode Interface*, Eds. R.F. Savinell, K. Ota, G. Kreysa, Springer, Berlin, 2011. <http://www.springerreference.com/index/chapterdoi/10.1007/303710>
- [4] Labuda J, In: *Nucleic Acid Biosensors for Environmental Pollution Monitoring*, Eds. M. Mascini and I. Palchetti, 121-140, ISBN: 978-1-84973-269-7, Royal Society of Chemistry, Cambridge, 2011
- [5] Ziyatdinova G, Labuda J, *Anal. Methods*, 3 (2011), 2777 – 2782

STRUCTURE AND EPR SPECTROSCOPY OF COPPER(II) COMPLEXES WITH PHENANTROLINE AND DERIVATIVES OF SALICYCLIC ACID

Michael LAWSON^{1*}, Marián VALKO¹, Jan MONCOL²,
Klaudia JOMOVA³, Andrea CONGRADYOVA³

¹Department of Physical Chemistry, Faculty of Chemical and Food Technology, Slovak University of Technology, Radlinského 9, 812 37 Bratislava, Slovakia

²Department of Inorganic Chemistry, Faculty of Chemical and Food Technology, Slovak University of Technology, Radlinského 9, 812 37 Bratislava, Slovakia

³Department of Chemistry, Faculty of Natural Sciences, Constantine The Philosopher University, Tr. A. Hlinku 1, 949 74 Nitra, Slovakia

*Michael.lawson@stuba.sk

ABSTRACT

Copper(II) complexes with 1,10-phenantroline and derivatives of salicylic acid with potential biological activity were prepared and characterised using X-ray and EPR spectroscopy. It has been shown that copper forms monomeric and dimeric complexes with penta- or hexa-coordination around the copper atom. The EPR spectra show typical characteristics of solid state copper(II) complexes. A weak exchange interaction between copper centres was observed.

INTRODUCTION

Copper ions are important in a broad range of intracellular processes under both normal and pathological conditions [1]. In particular copper functions as a cofactor in the mechanism of tumour angiogenesis. It has been reported that the copper complex with 1,10-phenantroline is able to induce formation of free radicals which in turn degradate DNA under in vitro conditions [2]. The mechanism of action of this complex is derived from the potential intercalation of planar phenantroline into DNA and the *in situ* generation of free radicals, predominantly hydroxyl radicals mediated by the presence of Cu(II) [3]. A necessity for the biological activity of the copper(II)-phenantroline complex is the presence of reducing ligands - agents such as glutathione, ascorbate, salicylate or organic thiols, all of which can mediate the formation of free radicals through the redox cycling process between cupric and cuprous ions [4].

These results have directed our attention on the preparation and physical characterization of potentially bioactive copper(II) phenantroline complexes with anions of derivatives of salicylic acid. Mono-deprotonated salicylic acid in the presence of metal ions leads to complexes containing the $\text{OHC}_6\text{H}_4\text{COO}^-$ anion. Further deprotonation leads to the formation of the $\text{OC}_6\text{H}_4\text{COO}^{2-}$ anion.

2. MATERIAL AND METHODS

Experimental part

Synthesis

The copper complexes were prepared similarly to methods described elsewhere [5]. The

following copper complexes were prepared and studied:

$[\text{Cu}(\text{phen})(3,5\text{-Cl}_2\text{sal})(3,5\text{-Cl}_2\text{salH}_2)]_2$, $[\text{Cu}(\text{phen})(5\text{-Cl}_2\text{sal})(5\text{-Cl}_2\text{salH}_2)]_2$, $[\text{Cu}(\text{phen})(4\text{-Cl}_2\text{sal})]_2$, $[\text{Cu}(\text{phen})(5\text{-Br}_2\text{sal})(\text{EtOH})]$.

Apparatus and equipment

Data collection and cell refinement of presented complexes were carried out using a Gemini R CCD (Oxford Diffraction) diffractometer. Intensity data were corrected for Lorenz and polarization factors. The structure was solved by the direct methods with SHELXS-97 [6] or SIR-97 [7], and subsequent Fourier synthesis using SHELXL-97 [6]. Geometrical analysis was performed using the SHELXL-97 and the structure was drawn using XP in SHELXTL program [6].

EPR spectra were measured in solid polycrystalline state at room temperature (290 K) using a Bruker EMX spectrometer (operating at X-band, with 100-kHz field modulation). The g-factors were quoted with an uncertainty of ± 0.001 using an internal reference standard marker containing 1,1-diphenyl-2-picrylhydrazyl (DPPH) built into the EPR spectrometer.

RESULTS AND DISCUSSION

The structure of $[\text{Cu}(\text{phen})(3,5\text{-Cl}_2\text{sal})(3,5\text{-Cl}_2\text{salH}_2)]_2$ (1) is shown in Figure 1 and exhibits dinuclear molecular structure. Each copper atom is hexa-coordinated by two oxygen atoms (fenolic group O1, and carboxylic group O3), two nitrogens of pyridine rings of phenantroline ligands (N1, N2), and two oxygen atoms of the fenolic group (3a) and the carboxylic group of coordinated molecules of 3,5-dichlorosalicylic acid (O4) in apical positions.

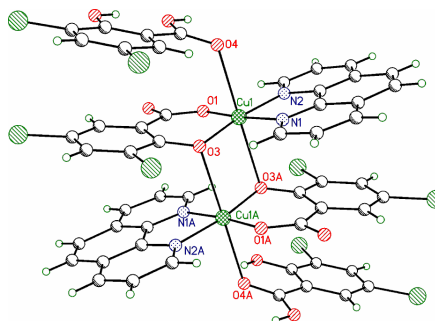


Figure 1. Structure of complex $[\text{Cu}(\text{phen})(3,5\text{-Cl}_2\text{sal})(3,5\text{-Cl}_2\text{salH}_2)]_2$ of 1

The complex $[\text{Cu}(\text{phen})(5\text{-ClSal})(5\text{-ClSalH}_2)]_2$ (2) is shown in Figure 2. It also has a dimeric structure with hexa coordinated Cu atoms but with some longer and presumably weaker bonds indicated by the dotted lines.

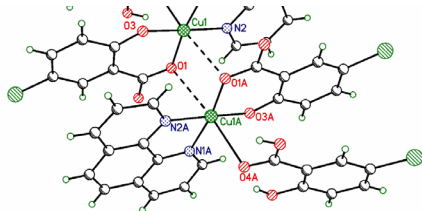


Figure 2. Structure of complex $[\text{Cu}(\text{phen})(5\text{-ClSal})(5\text{-ClSalH}_2)]_2$ of 2

The structure of $[\text{Cu}(\text{phen})(4\text{-ClSal})_2]$ is shown in Figure 3. It is also dinuclear, but each copper atom is only five coordinated by two phenanthroline nitrogen atoms (N1, N2) and the axial position is occupied by phenolic oxygen atom (O1A) of bridging 4-chlorosalicylate(2-) anions.

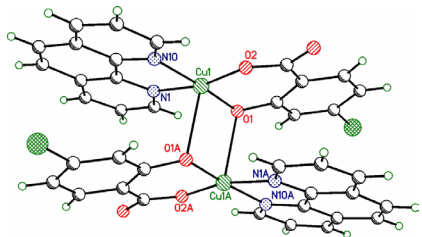


Figure 3. Structure of complex $[\text{Cu}(\text{phen})(4\text{-ClSal})_2]$ of 3

The complex $[\text{Cu}(\text{phen})(5\text{-Brsal})(\text{EtOH})]$ shown in Figure 4 has only a mononuclear molecular structure, and the copper atom is attached to two phenanthroline nitrogen atoms (N1, N2), with two oxygen atoms of 5-bromosalicylate(2-) anions (O1, O3) and the axial position is occupied by the oxygen atom (O4) of coordinated ethanol molecule.

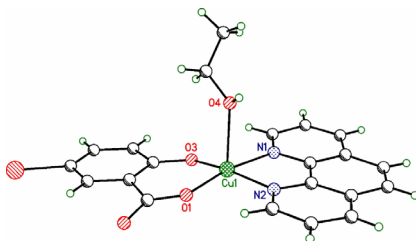


Figure 4 Structure of complex $[\text{Cu}(\text{phen})(5\text{-Brsal})(\text{EtOH})]$ of 4

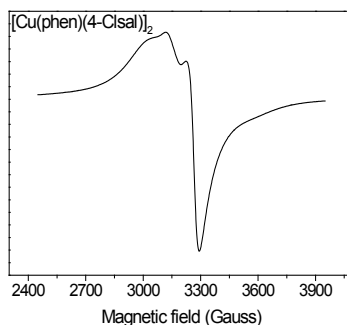


Figure 5 The EPR spectrum of $[\text{Cu}(\text{phen})(4\text{-ClSal})_2]$ of 3 measured in solid state at room temperature. The g-factors: $g_{\perp} = 2.041$, $g_{\parallel} = 2.222$.

The EPR spectra of the complexes were investigated in the solid state and therefore exhibit typical features of solid state-like EPR spectra [8].

The EPR spectrum of $[\text{Cu}(\text{phen})(4\text{-ClSal})_2]$ is shown in Figure 5. The spectrum shows axial symmetry with features of weak exchange inte-

reaction between copper ions.

The EPR spectrum of [Cu(phen)(5-Brsal)(EtOH)] is given in Figure 6 and shows a singlet line most probably due to the exchange broadening as a result of copper-copper interaction.

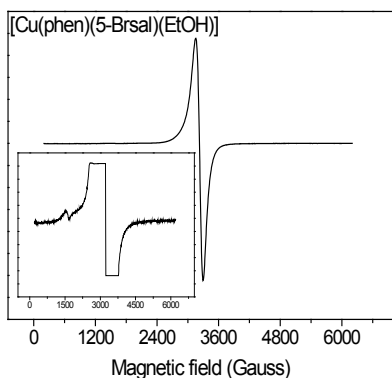


Figure 6 The EPR spectrum of [Cu(phen)(5-Brsal)(EtOH)] of 4 measured in the solid state at room temperature. Inset shows half-field transition observed at 1500 Gauss recorded at increased gain. The g-factors: $g_{\text{iso}} = 2.098$.

CONCLUSION

The X-ray study of copper(II)-phenantroline complexes with derivatives of salicylic acid revealed monomeric and dimeric complexes with penta- or hexa-coordination around the copper atom. The solid state EPR spectra are in agreement with the X-ray conclusions.

ACKNOWLEDGEMENT

The work has been supported by the Slovak Ministry of Education (VEGA project 1/0856/11) and APVV (project number 0202-10) and APVV-VVCE (0004-07).

REFERENCES

- [1] D.C. Weatherburn, in Handbook on Metalloproteins (I. Bertini, A. Sigel, and H. Sigel, Eds.), Marcel Dekker, Inc., New York, NY, 2001
- [2] D.S. Sigman, D.R. Graham, V. D'Aurora and A.M. Stern, J. Biol. Chem., 254 (1979) 12269
- [3] D.S. Sigman, Acc.Chem.Res., 1 (1986) 180
- [4] K. Jomova and M. Valko, Toxicology, 283 (2011) 65
- [5] J. Moncol, J. Maroszova, M. Koman, M. Melnik, M. Valko, M. Mazur and T. Lis, J. Coord. Chem., 61 (2008) 3740.

- [6] G.M. Sheldrick, Acta Crystallogr. A64 (2008) 112
- [7] A. Altomare, M.C. Burla, M. Camalli, G.L. Cascarano, C. Giacovazzo, A. Guagliardi, A.G.G. Moliterni, G. Polidori and R. Spagna, J. Appl. Crystallogr., 32 (1999) 115
- [8] L. Martiška, L. Husáriková, Z. Repická, D. Valigura, M. Valko and M. Mazúr, Appl. Magn. Reson., 39 (2010) 423.

NAD(P)H:QUINONE OXIDOREDUCTASE EXPRESSION IN TRANSGENIC MOUSE MODELS AND ITS INFLUENCING BY CARCINOGENIC ARISTOLOCHIC ACID I

Katerina LEVOVA¹, Michaela MOSEROVA¹, Daniel H. NEBERT², Colin J. HENDERSON³, C. Roland WOLF³, David H. PHILLIPS⁴, Eva FREI⁵, Heinz H. SCHMEISER⁶, Volker M. ARLT⁴, Marie STIBOROVA^{1*}

¹ Department of Biochemistry, Faculty of Science, Charles University, Prague, Albertov 2030, 128 40 Prague 2, Czech Republic

² Department of Environmental Health, University of Cincinnati Medical Center, Cincinnati, OH 45267-0056, USA

³ Cancer Research UK Molecular Pharmacology Unit, Biomedical Research Institute, Ninewells Hospital and Medical School, Dundee, United Kingdom

⁴ Analytical and Environmental Sciences Division, MRC-HPA Centre for Environment and Health, King's College London, London, United Kingdom

⁵ Division of Preventive Oncology, National Center for Tumor Diseases, German Cancer Research Center (DKFZ), Im Neuenheimer Feld 280, 69 120 Heidelberg, Germany,

⁶ Research Group Genetic Alterations in Carcinogenesis, German Cancer Research Center (DKFZ), Im Neuenheimer Feld 280, 69120 Heidelberg, Germany

*stiborov@natur.cuni.cz

ABSTRACT

Aristolochic acid (AA) causes aristolochic acid nephropathy, Balkan endemic nephropathy and their urothelial malignancies. Using Western blotting, an electrochemical method suitable to determine expression of proteins in tissues of most organisms including humans, we investigated expression of NAD(P)H:quinone oxidoreductase (NQO1), the most efficient enzyme catalyzing reductive activation of AAI in several transgenic mouse models. Employing this method, we found that expression of mouse NQO1 is increased in the liver of a mouse model absenting NADPH:cytochrome P450 (Cyp) reductase in the liver, whereas no differences in expression of this enzyme were detected in the transgenic *Cyp1a1* and *Cyp1a2* knock-out, *CYP1A*-humanized and wild-type mouse lines. The results found also demonstrate that expression of NQO1 protein is induced by treating mice with AAI, which resulted in an increase in reductive activation of this carcinogen. Hence, by inducing of NQO1, AAI increases its own activation metabolism leading to reactive species forming DNA adducts, thereby modulating its own genotoxic potential.

INTRODUCTION

The herbal drug aristolochic acid (AA) derived from *Aristolochia* species has been shown to be the cause of so-called Chinese herbs nephropathy (CHN), now termed aristolochic acid nephropathy (AAN) [1,2]. The plant extract AA is a mixture of structurally related nitrophenanthrene carboxylic acids, the major components being aristolochic acid I (AAI) and aristolochic acid II (AAII). AAN is a rapidly progressive renal fibrosis that was observed initially in a group of Belgian women who had ingested weight loss pills containing *Aristolochia fangchi* [3,4]. Within a few years of taking the pills, AAN patients also showed a high risk of upper urothelial tract carcinoma (about 50%) and, subsequently, bladder urothelial carcinoma. In the meantime, similar cases have been reported elsewhere in Europe and Asia [2]. More recently, exposure to AA has been linked to Balkan endemic nephropathy (BEN) and its

associated urothelial cancer [5,6]. This nephropathy is endemic in certain rural areas of Serbia, Bosnia, Croatia, Bulgaria and Romania. Exposure to AA was demonstrated by the identification of specific AA-DNA adducts in urothelial tissue of AAN and BEN patients [2,5-7]. The most abundant DNA adduct detected in patients is 7-(deoxyadenosin-*N*⁶-yl)-aristolactam I (da-AAI), which leads to characteristic AT → TA transversions. Such AT → TA mutations have been observed in codon 139 (Lys→Stop) of exon 5 of the *TP53* tumor suppressor gene in tumors from AAN and BEN patients [5,6], indicating a probable molecular mechanism associated with AA-induced carcinogenesis. AA has recently been classified as carcinogenic to humans (Group I) by the IARC [9].

The activation pathway for AA is nitroreduction catalyzed by both cytosolic and microsomal enzymes; in this process NAD(P)H:quinone oxidoreductase (NQO1) is the most efficient cytosolic enzyme [10-12]. In contrast to NQO1, conjugation enzymes such as human sulfotrans-

ferases (SULTs, e.g. SULT1A1, 1A2, 1A3, 1E or 2A1) or *N,O*-acetyltransferases (NATs, e.g. NAT1 or NAT2) were without capacity to activate AA [13,14]. In human hepatic microsomes AAI is activated by cytochrome P450 (CYP) 1A2 and to a lesser extent by CYP1A1; P450 oxidoreductase (POR) also plays a minor role [15,16]. Whereas the enzymes catalyzing the reductive activation of AAI leading to covalent DNA adducts have been widely investigated, those participating in its detoxication have been studied to a much lower extent. Several preliminary studies have indicated that induction of CYP1A protects mice from AAI-induced acute renal injury [17]. One detoxication metabolite identified is 8-hydroxyaristolochic acid I (aristolochic acid Ia, AAIa), which is formed by AAI demethylation, and which leads, in turn, to glucuronide or sulfate esters [18,19]. To identify enzymes involved in the metabolism of AAI we have recently used HRN [Hepatic Cytochrome P450 (Cyp) Reductase Null] mice, in which NADPH:Cyp oxidoreductase (Por) is deleted in hepatocytes [20] and the *Cyp1a1(-/-)* and *Cyp1a2(-/-)* single-knockout and *Cyp1a1/1a2(-/-)* double-knockout mouse lines [21]. Human and rodent CYP1A1 and 1A2 can oxidize AAI to AAIa *in vitro* [18,21,22] and CYP1A1 and 1A2 in mice appear to mediate this reaction *in vivo* [20,22]. CYP1A1 and 1A2 also reductively activate AAI in human and rodent livers [11,12,15,16,20,23]. In addition, the higher AAI-DNA adduct levels in HRN than WT mice were not only the result of the lack of hepatic AAI demethylation, but also by a higher activity of mouse cytosolic NQO1, which activates AAI [20].

Recently, we have also evaluated the oxidative detoxication and the reductive activation of AAI mediated by human CYP1A1 and 1A2 expressed in other transgenic mouse models. We have employed two humanized mouse lines, both carrying functional human *CYP1A1* and *CYP1A2* genes in place of the orthologous mouse genes; one line carries the high-affinity aryl hydrocarbon receptor (AHR) [*hCYP1A1_1A2_Cyp1a1/1a2(-/-)_Ahr^{hi}*], whereas the other line carries the poor-affinity AHR [*hCYP1A1_1A2_Cyp1a1/1a2(-/-)_Ahr^{pd}*] [24]. The latter line is believed to be more relevant to human risk assessment vis-à-vis human CYP1A1 and CYP1A2 substrates, because poor-affinity, rather than high-affinity, AHR is known to exist in human populations. Human and mouse hepatic microsomes, and human recombinant CYPs were also studied. DNA adduct formation *in vivo* and *in vitro* was investigated by the ³²P-postlabeling method. Urinary AAIa and the CYP-mediated formation of AAIa *in vitro* in hepatic microsomes and by human recombinant CYPs were measured by HPLC [24].

Human CYP1A1 and 1A2 were found to be principally responsible for reductive activation of AAI to form AAI-DNA adducts, and for oxidative detoxication to 8-hydroxyaristolochic acid AAIa, both in the intact mouse and in microsomes. Overall, AAI-DNA adduct levels were higher in *CYP1A*-humanized mice relative to wild-type mice, indicating that expression of human CYP1A1 and 1A2 in mice leads to higher AAI bioactivation than in mice containing the mouse CYP1A1 and 1A2 orthologs [24]. Furthermore, an exclusive role of human CYP1A1 and 1A2 in AAI oxidation to AAIa was observed in human liver microsomes under the aerobic (*i.e.* oxidative) conditions. The results suggest that, in addition to CYP1A1 and 1A2 expression levels, *in vivo* oxygen concentration in specific tissues might affect the balance between AAI nitroreduction and demethylation, which in turn would influence tissue-specific toxicity or carcinogenicity. Nevertheless, the contribution of either the major enzyme to reductive activation of AAI, NQO1, or CYP1A1/2, might be also dictated by expression of NQO1 in transgenic mouse models employed in our former study [20,21,24]. Therefore, expression of NQO1 in these mouse models and influencing of this expression by treating them with AAI remains to be investigated. The Western-blotting-electrochemical method was used in this work to evaluate these features.

MATERIAL AND METHODS

Animal Experiments

HRN (*Por^{lox/lox} + Cre^{ALB}*) mice on a C57BL/6 background (CXR Bioscience Ltd, Dundee, UK) used in this study were derived as described previously [25]. Mice homozygous for loxP sites at the *Por* locus (*Por^{lox/lox}*) were used as wild-type (WT). Groups of male HRN and WT mice (3 months old; 25-30 g; *n* = 3/group) were treated orally with a single dose of 10 or 50 mg/kg body weight (bw) of AAI as described previously [20]. All procedures with these mouse models were carried out under the Animal (Scientific Procedures) Act (1986) in accordance with UK law, and following local ethical review. Generation of *Cyp1a1(-/-)* [26], *Cyp1a2(-/-)* [27], and *Cyp1a1/1a2(-/-)* [28] knockout mouse lines (on a >99.8% C57BL/6J background) have previously been described. Age matched 57BL/6J *Cyp1(+/+)* wild-type (WT) mice were purchased from The Jackson Laboratory (Bar Harbor, ME, USA). The *CYP1A*-humanized mice, namely the *hCYP1A1_1A2_Cyp1a1/1a2(-/-)_Ahr^{hi}* and *hCYP1A1_1A2_Cyp1a1/1a2(-/-)_Ahr^{pd}* lines, both on a >99.8% C57BL/6J background, were generated as reported [28,29]. Age-matched C57BL/6J mice WT mice were purchased from The Jackson Laboratory (Bar Harbor, ME,

USA). Groups of female mice (3 months old; 25-30 g; $n = 4$ /group) were treated with a single dose of 50 mg/kg body weight AAI by oral gavage as described [21,24]. All experiments with these mouse models were approved by, and conducted in accordance with, the National Institute of Health standards for the care and use of experimental animals and the University of Cincinnati Medical Center Institutional Animal Care and Use Committee. Cytosols from all mouse models used in this study were isolated from the livers, kidneys and lungs of rats either untreated (control) and AAI-treated mice as described [10,20,21,24]. Furthermore, hepatic and renal cytosols from HRN and WT mice pre-treated (i.p.) with 125 mg/kg bw benzo[*a*]pyrene (BaP) daily for 5 days were obtained from a previous study [30]. Pooled cytosolic fractions isolated from liver, kidney and lung of all mouse models were used for further analysis.

Determination of NQO1 activity and protein levels by electrochemical determination (Western blotting)

NQO1 antibodies were prepared as described previously [31]. Immunoquantitation of cytosolic NQO1 was carried out by sodium dodecyl sulfate (SDS)-polyacrylamide gel electrophoresis [31]. Human recombinant NQO1 (Sigma) was used to identify the band NQO1 in murine cytosols. NQO1 activity was measured essentially as described by Ernster [32], but the method was improved by addition of cytochrome *c* [33]. Antibody against glyceraldehyde phosphate dehydrogenase (GAPDH) (1:750, Millipore, MA, USA) was used as loading control.

DNA adduct analysis by ³²P-postlabeling

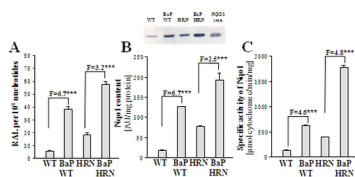
DNA from mouse tissues was isolated by standard phenol/chloroform extraction. ³²P-Postlabelling analysis using the nuclease P1 enrichment version, and thin layer chromatography (TLC) and HPLC were performed as described [8,10]. TLC sheets were scanned using a Packard Instant Imager (Dowers Grove, USA) and DNA adduct levels (RAL, relative adduct labeling) were calculated as described [8,10]. Results were expressed as DNA adducts/10⁸ nucleotides.

RESULTS AND DISCUSSION

Using electrochemical determination (Western blot analysis with antibodies raised against human NQO1), mouse NQO1 protein expression in WT and HRN hepatic cytosols was analyzed [20]. Mouse NQO1 is expressed in cytosols of both animal models (Fig. 1). Interestingly, expression of NQO1 protein in hepatic cytosolic samples of HRN mice was more than 3-fold higher than that in cytosols of WT mice (Fig. 1). This was paralleled by an increase in NQO1 enzyme activity and AAI-DNA adduct formation in these cytosolic samples (Fig. 1). These results suggest that deletion of gene for Por and ab-

sence of this enzyme in the mouse liver is partially compensated by an increase in expression of the cytosolic reductase NQO1. We also tested whether pretreatment of WT and HRN mice with BaP, a NQO1 inducer [34], influences expression of this enzyme in hepatic cytosols of these mouse models. More than 2.5- and 6-fold higher NQO1 protein expression in hepatic cytosols of HRN-BaP and WT-BaP mice than untreated mice were determined, respectively (Fig. 1). This was paralleled by an increase in NQO1 enzyme activity and levels of AAI-DNA adducts in these samples (Fig. 1).

Figure 1: DNA adduct formation by AAI activated with hepatic cytosols isolated from livers of HRN and WT mice, control mice (untreated) or mice pretreated (i.p.) with 125 mg/kg bw BaP daily for 5 days [xx] as determined by TLC ³²P-postlabeling (A). RAL, relative adduct labeling. NQO1 protein expression in hepatic cytosols as determined by Western blotting (see insert) (B). NQO1 enzymatic activity in hepatic cytosols (C). Human recombinant NQO1 (Sigma; NQO1 stan, see insert B) was used to identify the mouse NQO1 band in murine cytosols. All values are given as means \pm SD ($n = 3$). Values significantly different from control (untreated) mice: *** $p < 0.001$ (Student's *t*-test), (data taken and adapted from [20])



Using Western blotting employing antibodies raised against NQO1, mouse NQO1 protein expression was also analyzed in other transgenic mouse models, the *Cyp1a1*^{-/-} and *Cyp1a2*^{-/-} single-knockout and *Cyp1a1/1a2*^{-/-} double-knockout mouse lines and the *CYP1A1*-humanized mouse lines, namely *hCYP1A1 IA2*, *Cyp1a1/1a2*^{-/-} *Ahr^{pl}* and *hCYP1A1 IA2* *Cyp1a1/1a2*^{-/-} *Ahr^{pl}* mice and compared with that in WT mice. In addition, the effect of treatment of all mouse lines with AAI was also examined. Liver, kidney and lung cytosolic samples were used for the analyses. No statistically significant

changes in expression of NQO1 protein in either transgenic mice or in a WT mouse line. Likewise, no differences in AAI-DNA adduct formation were found when AAI was incubated with liver and kidney cytosolic samples isolated from these organs of either mouse lines. However, up to a 3-fold increase in levels of NQO1 protein was detected in most of mouse lines treated with AAI than in untreated (control) mice. This finding indicates that AAI might induce NQO1 in used mouse models and is consistent with the results of previous studies. NQO1 activity was found to be increased in rats treated with AAI [35] and the NQO1 protein expression is induced by AAI in mice [36]. Hence, this enzyme might also be induced in AAN and BEN patients, which might lead to an increased risk for urothelial cancer.

CONCLUSION


Utilizing the Western-blotting-electrochemical method, expression of NQO1 protein in several transgenic mouse models, where genes for *Cyp1a1*, *Cyp1a2* or *Por* enzymes were deleted, or in mice humanized with human *CYP1A1* and *IA2* genes, was analyzed. Whereas deletion of *Por* in the mouse liver resulted in compensation of this reductase by higher expression of cytosolic NQO1, no differences in levels of NQO1 were found in transgenic mice absenting *Cyp1a1* and/or *Cyp1a2* or in the *CYP1A1*-humanized mouse lines. The results also indicate a potential of AAI to induce this cytosolic enzyme in mice. Therefore, further study investigating the mechanisms of such an NQO1 induction by AAI is planned to be performed in our laboratory in future.

ACKNOWLEDGEMENT

The work has been supported by Grant Agency of the Czech Republic (grants 303/09/0472 and 305/09/H008) and Charles University in Prague (grant UNCE #42).

REFERENCES

- [1] Debelle F.D., Vanherweghem J.L., Nortier J.L.: *Kidney International*, 74 (2008), 158-169.
- [2] Schmeiser H.H., Stiborova M., Arlt V.M. *Current Opinion in Drug Discovery and Development*, 12 (2009), 141-148.
- [3] Vanherweghem J. L., Depierreux M., Tielemans C., et al.: *Lancet*, 341 (1993), 387-391.
- [4] Nortier J.L., Martinez M.C., Schmeiser, H.H., et al.: *New England Journal of Medicine*, 342 (2000), 1686-1692.
- [5] Arlt V.M., Stiborova M., vom Brocke J., Simoes, et al.: *Carcinogenesis* 28 (2007), 2253-2261.
- [6] Grollman A.P., Shibusani S., Moriya M., et al.: *Proceedings of American Chemical Society U.S.A.*, 104 (2007), 12129-12134.
- [7] Arlt V.M., Ferluga D., Stiborova M., et al.: *International Journal of Cancer*, 101 (2002), 500-502.
- [8] Schmeiser H.H., Bieler C.A., Wiessler M., et al.: *Cancer Research*, 56 (1996), 2025-2028.
- [9] Grosse Y., Baan R., Straif K., et al.: *Lancet Oncology*, 10 (2009), 13-14.
- [10] Stiborova M., Frei E., Sopko B., et al.: *Carcinogenesis* 24 (2003), 1695-1703.
- [11] Stiborova, M., Frei, E. Arlt, V. M., et al.: *Mutation Research*, 658 (2008), 55-67.
- [12] Stiborová M., Frei E., Schmeiser H. H.: *Kidney International* 73 (2008), 1209-1211.
- [13] Stiborova M., Mares J., Frei E., et al.: *Environmental and Molecular Mutagenesis*, 52 (2011), 448-459.
- [14] Martínek V., Kubickova B., Arlt V.M., et al.: *Neuro Endocrinology Letters*, 32 (Suppl 1) (2011), 57-70.
- [15] Stiborova M., Frei E., Wiessler M., et al.: *Chemical Research in Toxicology*, 14 (2001), 1128-1137.
- [16] Stiborova M., Frei E., Hodek P., et al.: *International Journal of Cancer*, 113 (2005), 189-197.
- [17] Xue X., Xiao Y., Zhu H., et al.: *Nephrology dialysis transplantation*. 23 (2008), 3074-3081.
- [18] Šístková J., Hudeček J., Hodek P., et al.: *Neuro Endocrinology Letters*, 29 (2008), 733-737.
- [19] Shibusani S., Bonala R.R., Rosenquist T., et al.: *International Journal of Cancer*, 27 (2010), 1021-1027.
- [20] Levova K., Moserova M., Kotrbova V., et al.: *Toxicological Sciences*, 121 (2011), 43-56.
- [21] Arlt V.M., Levová K., Bárta F., et al.: *Chemical Research in Toxicology*, 24 (2011), 1710-1719.
- [22] Rosenquist T.A., Einolf H.J., Dickman K.G., et al.: *Drug Metabolism and Disposition*, 38 (2010), 761-768.
- [23] Stiborova M., Sopko B., Hodek P., et al.: *Cancer Letters*, 229 (2005), 193-204.
- [24] Stiborová M., Levová K., Bárta F., et al.: *Toxicological Sciences*, 125 (2012), 345-358.
- [25] Henderson C.J., Otto D.M., Carrie D., et al.: *Journal of Biological Chemistry*, 278 (2003), 13480-13486.
- [26] Dalton T.P., Dieter M.Z., Matlib R.S., et al.: *Biochemical and Biophysical Research Communications*, 267 (2000), 184-189.
- [27] Liang H.C., Li H., McKinnon R.A., et al.: *Proceedings of American Chemical*

- 
- Society U.S.A., 93 (1996), 1671-1676.
- [28] Dragin N., Uno S., Wang B., et al.:
Biochemical and Biophysical Research
Communications, 359 (2007), 635-642.
- [29] Shi Z., Chen Y., Dong H., et al.: Biochemical
and Biophysical Research Communications,
376 (2008), 775-780.
- [30] Arlt V.M., Stiborova M., Henderson C.J., et al.:
Carcinogenesis 29 (2008), 656-665
- [31] Stiborová M., Dračínská H., Hájková J., et al.:
Drug Metabolism and Disposition., 34 (2006),
1398-1405
- [32] Ernster L.: Methods in enzymology, 10 (1967),
309-317.
- [33] Mizerovská J., Dračínská H., Frei E., et al.:
Mutation Research, 720 (2011), 34-41.
- [34] Hockley S.L., Arlt V.M., Brewer D., et al.:
Chemical Research in Toxicology, 20 (2007),
1797-810.
- [35] Stiborová M, Hájek M, Vošmiková H, et
al.: Collection of Czechoslovak Chemical
Communication, 66 (2001), 959-972.
- [36] Arlt V.M., Zuo J., Trenz K., et al.: International
Journal of Cancer, 128 (2011), 21-32.

THE GROW OF MICROORGANISMS DURING THE RIPENING OF SEMI-HARD CHEESE

Iva BLAZKOVA¹, Libor KALHOTKA¹, Kvetoslava SUSTOVA²

¹Department of Agrochemistry, Soil Science Microbiology and Plant Nutrition, Faculty of Agronomy, Mendel University in Brno, Zemedelska 1, 613 00 Brno, Czech Republic

²Department of Food Technology, Faculty of Agronomy, Mendel University in Brno, Zemedelska 1, 613 00 Brno, Czech Republic

ABSTRACT

The aim of this paper is monitoring of the growth of microorganisms during the ripening of semi-hard cheese. Bacteria of the species *Escherichia coli*, *Bacillus cereus* and *Enterococcus faecalis* were inoculated into the milk used for cheese production. The counts of microorganisms were analyzed after one and four weeks of ripening. There were total bacterial counts (TBC), lactic acid bacteria (LAB), enterococci, coliform bacteria, psychrotrophic bacteria, yeasts and molds determined in cheeses. They were stored at 6°C and 22°C.

INTRODUCTION

Microorganisms play important roles in cheese. They can be divided into two main groups: starters and secondary flora [1]. The starter lactic acid bacteria are primarily responsible for acid production during manufacturing. The secondary microflora is important for the ripening process. Microorganisms gain entry into the cheese not only by deliberate addition, but also from the environment [2]. Some microorganisms can also survive pasteurization and can grow in cheeses; they can be pathogenic or produce biogenic amines [3]. That's the reason to concern the growth of microorganisms in cheese.

MATERIAL AND METHODS

The pasteurized cow's milk (72°C, 30 seconds) was supplemented with CaCl₂ and inoculated with the starter culture (*Lactococcus lactis* and *Leuconostoc mesenteroides*) and one of the bacterial culture (cheeses without culture - standard: *Escherichia coli* (CCM 3988), *Bacillus cereus* (CCM 2010) or *Enterococcus faecalis* (CCM 4224) and matured for 40 minutes at 35°C. Then the rennet (Naturen®Premium) was added. After incubation for 40 minutes the curd was cut, stirred, heated to 40°C and transferred into cheese forms. Next day the cheeses were brined, they ripened four weeks at 6°C and 22°C.

The determination of microorganisms in cheese samples was carried out as follows:

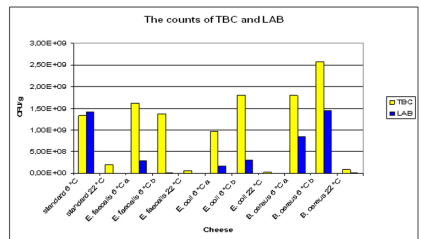
10 g of the cheese core part was homogenized in Saline solution. The homogenate was serially diluted. Parallel plate counts were performed on these agars: Plate Count Agar with skimmed milk - Biokar Diagnostics, France (TBC; 30°C, 72 h), PCA_M (psychrotrophic; 6.5°C, 10 days), MRS (LAB; 30°C, 72 h), Compass Ente-

rococcus Agar (enterococci; 45°C, 24 h), VRBL (coliform; 37°C, 24 h), YGC_M (yeast and mold; 25°C, 3 - 5 days).

RESULTS AND DISCUSSION

The microbiological quality of handmade cheeses was done. The counts of TBC correlated with LAB after one week of storage (Fig. 1). The counts of LAB decreased during ripening, it corresponds to literature [4]. There were much more TBC and LAB in cheeses stored at 6°C. The LAB are mesophilic microorganisms, so they should grow better at 22°C. The reason, why they grew better at 6°C, could be higher moisture content, because the cheeses at higher temperature released more whey. Another factor is, that there was not so much salt in these cheeses. Or the LAB grew very quickly at 22°C, so they dropped before they were analyzed.

Figure 1.: Dependence of inoculated bacteria into the cheese and the count of TBC and LAB



The counts of moulds and yeasts were higher in cheeses stored at 22°C. They might produced toxins, which inhibited the growth of LAB. The highest amount reached moulds (especially *Penicillium*) and yeast in standard cheese. The lowest counts were in cheese with inoculated *Escherichia coli*. The first week they were not almost present in cheeses at 6°C, and they rose

after three weeks, but they were still lower than the counts in cheeses stored at 22°C.

Enterococcus faecalis was contained only in cheese, where it was inoculated. Contrary to the literature their counts decreased [5 - 7]. The presence of enterococci usually indicates poor bacteriological quality and poor hygiene during manufacture [8]. The coliform microorganisms were not almost present. Used *Escherichia coli* culture grew slowly and inadequately.

The psychrotrophic bacteria grew over the whole ripening period much better at 22°C. That's because of the *Bacillus cereus* is mesophilic microorganism growing at temperatures between 10 - 48°C, optimally 28 - 35°C [9]. Cheese with *Bacillus cereus* stored at 6°C had comparable levels of these microorganisms with other cheeses. But in this cheese, stored at 22°C, the counts of psychrotrophic bacteria have risen rapidly.

CONCLUSION

The comparison of amount of microorganisms in cheese is presented in this paper. The total count of microorganisms depends on the presence of different species of microorganisms and storage conditions. The microbiological quality of these cheeses was very varying.

Used bacterial cultures are common cheese contaminants and they have potential to produce biogenic amines. Thus we are going to do other analyses and determine the amount of biogenic amines in cheeses.

REFERENCES

- [1] Beresford T. P, Fitzsimons N. A, Brennan N. L, et al.: International Dairy Journal, 11 (2001), 259-274
- [2] Fox P. F: Cheese: chemistry, physics, and microbiology, (2004) 617
- [3] Coton M, Delbes-Paus C, Irlinger F, et al.: Food Microbiology, 29 (2012), 1, 88-98
- [4] Bunkova L, Bunka F, Mantlova G, et al.: Sbornik prispevku z odborného seminare Mleko a syry, 1 (2010), 104-110
- [5] Leuchner R. GK, Kurihara R, Hammes W. P: Journal of the Science of Food and Agriculture. 79 (1999) 1141-1144
- [6] Marino M, Maifreni I, Bartolomeoli I, et al.: Journal of Applied Microbiology, 105 (2008), 2, 540-549
- [7] Schneller R, Good P, Jenny M, Zeitschrift für Lebensmittel Untersuchung und Forschung, 204 (1997), 4, 265-272
- [8] Burdychova R.: Acta Universitatis Agriculturae et Silviculturae Mendelianae Brunensis, 57 (2009), 5, 49-56
- [9] Gorner F. -- Valik L. Aplikovana mikrobiologia pozivatin, (2004) 528

ELECTROCHEMICAL GROWTH OF POLYPYRROLE ON BORON DOPED DIAMONDS

Egor UKRAINTSEV¹, Alexander KROMKA¹, Ken HAENEN², Bohuslav REZEK¹

¹ *Institute of Physics ASCR, Prague, Czech Republic*

² *University Hasselt, Diepenbeek, Belgium*

*ukraints@fzu.cz

ABSTRACT

To find out the mechanism of the electrochemical attachment of polypyrrole (PPy) to diamond we grow PPy layers on hydrogen and oxygen terminated boron doped diamond surfaces (BDD) using constant current applied between the BDD and the platinum wire. Boron doping of diamond ensures conductivity on both types of surfaces. The obtained layers have thickness > 5 nm on O-BDD and > 40 nm on H-BDD. Surface morphology was evaluated by atomic force microscopy (AFM). To resolve type of PPy-diamond bonding, PPy layer was removed using the AFM tip. Scanning electron microscopy (SEM) was then used to compare the secondary electron emission from untreated BDD regions and regions where PPy layers were grown and removed. SEM data show that on the oxygen terminated diamond surface these regions have similar intensity of secondary electrons. Intensity on hydrogen terminated diamond surface below the PPy layer is reduced. This is a preliminary indication of different type of PPy bonding on H- and O-terminated BDD.

INTRODUCTION

Diamond electrodes are well-known due to their very high overpotential for both oxygen and hydrogen evolution [1]. B-doping makes diamond p-type semiconductor [2]. The type of surface conductivity may play a crucial role in many experiments. The O-BDD is conductive due to presence of boron atoms and hopping conductivity. At low boron doping level the H-BDD is conductive mainly due to presence of thin adsorbate layer on top on hydrogen terminated surface, so called surface transfer doping [3].

Polypyrrole, a well-studied conjugated polymer, is widely used in optoelectronics [4] and field-effect transistor (FET) devices [5]. PPy growth on H-MCD was studied earlier in details [4, 6]. The boron doping allows us to switch the surface atoms from hydrogen to oxygen without loss of conductivity. The type of grafting between chemically grown material and substrate is important for many applications. Here we report SEM data which show the possibility of different grafting of PPy to hydrogen and oxygen terminated BDD.

MATERIAL AND METHODS

Hydrogen and oxygen termination of boron diamond. Sample preparation.

Boron doped diamond was grown on diamond substrate by plasma enhanced chemical vapor deposition (PECVD) in a home made NIRIM type reactor. Diamond layer is grown in a mixture of 1% of methane (6 N) diluted in hydrogen (6 N) at a total pressure of 110 mbar, a microwave power of 500 W and a substrate temperature

of 1100°C. Boron doping is achieved using 2.4 ppm trimethylboron (TMB) diluted in hydrogen (200 ppm) [7]. **Boron doped diamond was hydrogen and oxygen terminated using plasma processes according to the protocol [8].**

Gold contacts were thermally evaporated (50nm of Au) on the sample through the mask prepared by photolithography. Ma-P15 resist was used. For better contact Pelco Colloidal Silver Liquid was applied on top of gold contact.

Polypyrrole growth

PPy was grown using Metrohm Autolab Potentiostats / Galvanostats setup. Constant currents 1 μ A and 5 μ A were applied for 150 s. The droplet volume was 0.1-0.3 μ L. Pyrrole solution (240 mM Py and 100 mM NaCl in de-ionized water) was used. Distance between H/O-BDD (working electrode) and Pt wire (counter electrode and reference electrode) was about 100 μ m.

Atomic force microscopy

AFM study was performed using Mutli75Al-G and Mutli75Al-E cantilevers on Ntegra AFM in tapping, contact and KFM modes. The thickness of PPy layer was measured using contact mode nanoshaving [9, 10]. In case of thick layer it was removed using wood stick.

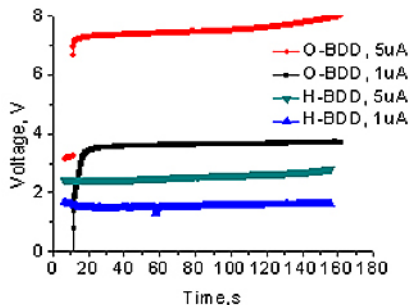
Scanning electron microscopy

PPy layers were characterized by scanning electron microscopy (MIRA3 FEG SEM, TESCAN) using 5kV acceleration voltage and In-Beam detector.

RESULTS AND DISCUSSION

The resistance of O-BDD sample before PPy growth was $R_0 \sim 2.4$ MOhm, distance between contacts is ~ 3 mm. The resistance of H-BDD sample was $R_H \sim 70$ kOhm. Fig. 1 illustrates the PPy growth curves on H/O-BDD. The tendencies are clear, higher currents require higher voltages. The induced voltages are higher on O-BDD compared to H-BDD due to higher electrical resistance.

Figure 1.: Polypyrrole growth curves under $1\mu\text{A}$ and $5\mu\text{A}$ on H- and O-terminated BDD surfaces.



In all cases PPy layer was synthesized. The minimal measured thickness is $\sim 1\text{-}5\text{nm}$ on $1\mu\text{A}$ spot on O-BDD, up to ~ 80 nm on $5\mu\text{A}$ spot on O-BDD, the spots on H-BDD has inhomogeneous thickness $\sim 40\text{nm}$ near the spot border and much thicker in the middle. The thicknesses vary on the same spot because of microscopic setup where electric field and current is not distributed homogeneously.

The morphology of PPy layers on O- and H-BDD is presented on Fig. 2. The observed RMS roughness increased from 1 nm on 5 nm thin PPy layer on O-BDD to 5-15 nm on H-BDD. The PPy clusters with RMS $\sim 100\text{-}200$ nm were observed on the thickest part of PPy layer. Morphology appears similar on both types of surfaces at comparable thickness. PPy layer with higher thickness has not only higher roughness compare to thin layer, but also larger PPy aggregates (fig. 2c). This result illustrates higher degree of cross-linking between the pyrrole molecules on thicker layers compared to thin layers.

Figure 2.: a) The image was obtained on thin (5nm) PPy layer on O-BDD. b) The image was obtained on thin PPy layer on H-BDD. c) The image was obtained on thick (40nm) PPy layer on H-BDD. The size of images is $1 \times 1 \mu\text{m}^2$. The Z-scale is 10 nm.

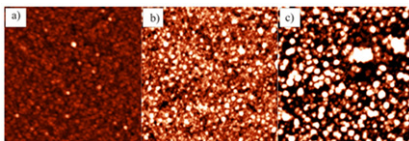
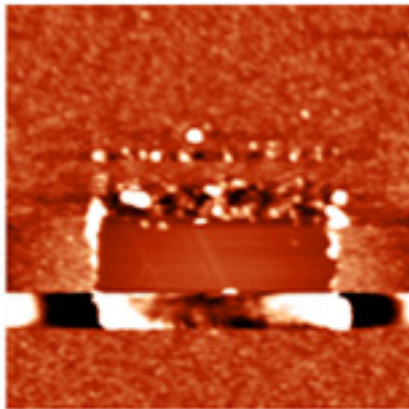


Figure 3.: The image was obtained on thin (5nm) PPy layer on O-BDD. The image size is $2 \times 2 \mu\text{m}^2$. The Z-scale is 20 nm

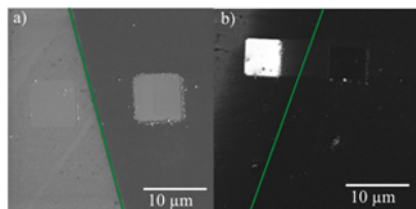


Multi75Al-G AFM tip is able to remove only thin PPy layers (thickness $\sim 5\text{-}20$ nm) as shown on Fig. 3. The threshold for layer removal is 180 nN in this case. Thicker layer can be removed with wood stick. Higher PPy removal forces than typically found on H-MCD [6] and other covalently grafted molecules [11] indicate cross-linking of PPy on O-BDD.

Contact mode nanoshaving was performed near the PPy/diamond border, i.e. on i) PPy on diamond and ii) on adsorbate on diamond surface. Scanning electron microscope measurements, performed on the same spots, reveal that in case of O-BDD, the intensity of secondary electrons from diamond surface below adsorbate layer and below PPy layer is the same, as shown on Fig. 4. In case of H-BDD, the intensity of secondary electrons from diamond surface below adsorbate layer is higher than from diamond surface below PPy layer. Note that the border between diamond and PPy layers, visible in AFM/KFM and SEM in case of H-BDD (Fig. 4b) are situated in different places. This effect will be clarified in future experiments with more doped BDD sample.

Figure 4.: a) The SEM image was obtained on thin (5nm) PPy layer on O-BDD. The intensity of secondary electrons from diamond surface below adsorbate layer (left) and below PPy layer (right) is the same. The green line indicates diamond/PPy border visible in AFM/KFM. b)

The SEM image was obtained on PPy layer on H-BDD. The intensity of secondary electrons from diamond surface below adsorbate layer (left) is higher than intensity from diamond surface below PPy layer (right).



Different intensity of secondary electrons in SEM on same diamond with different surface terminations reflects the change of surface atoms (hydrogen vs. oxygen or carbon) because they provide different (opposite) electron affinity [12]. This conclusion is corroborated also by other studies where SEM was used to study grafting of alkenes to diamond. It was shown that the molecular contrast between surfaces with different terminations is consistent with the expected trends in molecular electron affinity [13].

CONCLUSION

Presented results illustrate that low boron doping makes BDD enough conductive for PPy growth. SEM measurement show that some changes occur on H-BDD surface after PPy growth. This is in agreement with covalent grafting of PPy to H-terminated intrinsic diamond [14]. No such changes in SEM contrast were observed on O-BDD, thus probably no chemical bond between PPy and diamond was formed in this case.

ACKNOWLEDGEMENT

Technical support of Jitka Libertínová, Oleg Babchenko, Ondřej Rezek and Zdeňka Poláčková is gratefully appreciated. This research was financially supported by the project P108/12/G108 (GACR).

REFERENCES

- [1] Swain M, Anderson A.B and Angus J.C: MRS Bulletin, (1998) 56
- [2] Haenni W, Rychen P, Fryda M, et al.: Thin-Film Diamond Part B, Ch. Nebel, Editor, Academic Press, Semiconductors and Semimetals series, Elsevier, (2004), p. 149
- [3] Ristein J, Appl. Phys. A, 82 (2006) 377
- [4] Rezek B, Čermák J, Kromka A, et al.: Diam. Relat. Mater., 18 (2009) 249-252
- [5] Shirale D.J, Bangar M.A, Chen W, et al.: J Phys Chem C Nanomater Interfaces, 114 (2010), 31, 13375–13380
- [6] Čermák J, Kromka A, Ledinský M, et al.: Diam. Relat. Mater., 18 (2009) 800-803
- [7] Mortet V, Daenen M, Teraji T, et al.: Diam. Relat. Mater., 17 (2008) 1330–1334

- [8] Rezek B, Michalíková L, Ukraintsev E, et al.: Sensors 9, (2009) 3549–3562
- [9] Rezek B, Shin D, Nebel C.E: Langmuir 23, (2007) 7626-7633
- [10] Ukraintsev E, Rezek B, Kromka A, et al.: phys. stat. sol. (b), 246 (2009) 2832-2835
- [11] Rezek B, Shin D, Uetsuka H, et al.: phys. stat. sol. (a), 204 (2007) 2888-2897
- [12] Rezek B, Sauerer C, Nebel C.E, et al.: Appl. Phys. Lett., 82 (2003) 2266-2268
- [13] Wang X, Colavita P.E, Metz K. M, et al.: Langmuir, 23, (2007), 23, 11623-11630
- [14] Čermák J, Rezek B, Kromka A, et al.: Diam. Relat. Mater., 18 (2009) 1098–1101

AUTOMATED IMMUNOSEPARATION OF Zn-PROTEINS FROM *STAPHYLOCOCCUS AUREUS* BY MAGNETIC NANOPARTICLES FOLLOWED BY THEIR ELECTROPHORETIC

Eva JILKOVA^{1*}, Sona KRIZKOVA^{1,2}, David HYNEK^{1,2}, Ludmila KREJCOVA¹, Jiri SOCHOR^{1,2}, Vojtech ADAM^{1,2}, Petr HODEK³, Libuse TRNKOVA^{2,4}, Marie STIBOROVA³, Jaromir HUBALEK^{2,5}, Rene KIZEK^{1,2}

¹ Department of Chemistry and Biochemistry, Faculty of Agronomy, Mendel University in Brno, Zemedelska 1, 613 00 Brno, Czech Republic

² Central European Institute of Technology, Brno University of Technology, Technicka 3058/10, 616 00 Brno, Czech Republic

³ Department of Biochemistry, Faculty of Science, Charles University, Albertov 2030, CZ128 40 Prague 2, Czech Republic, European Union

⁴ Department of Chemistry, Masaryk University, Kotlarska 2, 611 37 Brno, Czech Republic

⁵ Department of Microelectronics, Faculty of Electrical Engineering and Communication, Brno University of Technology, Technicka 3058/10, 616 00 Brno, Czech Republic

*kizek@sci.muni.cz

ABSTRACT

Automated immunoseparation of Zn-proteins from *Staphylococcus aureus* by magnetic nanoparticles followed by their electrophoretic is the aim of this paper. For isolation of cells *S. aureus* was used magnetic nanoparticles with specific antibodies. For electrophoretic detection of zinc binding proteins SDS-PAGE was used. For electrochemical determination measuring system Metrohm (Autosampler 813 Compact and measuring unit VA Computrace 797) was employed.

INTRODUCTION

Magnetic nanoparticles (MPs) are used in a sphere of biomedical and biotechnological fields. MPs are often used to detect biomolecules such as nucleic acids or proteins. They are highly active due to very large surface and have very good physical properties. Their selectivity is better compared to other commonly used detection methods. Other specific use of the MPs consists in the detection of microorganisms and their bio-components [1, 2].

Staphylococcus aureus Rosenbach is bacterial species naturally present on the skin and mucous membranes of warm-blooded animals and humans [3]. It causes infections of skin and soft tissues as well as a life threatening sepsis, toxic shock syndrome and necrotizing pneumonia [4]. The main problem consists in its resistance to antibiotics [5]. In 1947, only four years after beginning of the mass production of penicillin, first *S. aureus* penicillin resistant strains have been identified [6]. In 1959, a new antibiotic compound against penicillin-resistant staphylococci called methicillin was found. The great plasticity of this bacteria resulted in the discovery of the first methicillin-resistant strain of *S. aureus* (MRSA) in 1961. Nowadays, approximately 65 % of staphylococcal strains have MRSA phenotype [5]. From this reason, new compounds alternative to antibiotics, especially heavy metals and their complexes, heavy metal nanomaterials and nanoparticles, are searched [7].

In 2010, the first work confirming the connection between staphylococcal resistance to methicillin and zinc was published [8]. The gene *czrC* associated with the resistance of *S. aureus* was then discovered. There are zinc binding proteins that are probably closely connected with multiple bacterial antibiotic resistances in the cells of *S. aureus* [9]. Antibiotic resistance factor HmrA (extracellular protease) from MRSA is a zinc-dependent endopeptidase. An antibiotic resistance is caused by a widespread factor HmrA and next proteins, for example superantigen [10, 11], lysostafin [12] and other extracellular proteases [13], enterotoxins [14], adhesion factors [15], biofilm formation [16], transcription factors and DNA-binding proteins [17]. Due to these facts, the rapid method for the isolation of bacterial cells and detection of the zinc binding protein(s) is needed to be found, which the main of our study was.

MATERIAL AND METHODS

Bacterial growth in the presence of Zn^(II)

For all experiments, *Staphylococcus aureus* (NCTC 8511, Czech Collection of Microorganisms, Brno, Czech Republic) stored on agar slants (meat-peptone agar No. 1, MPA 1) was used. Cultivation was performed in liquid broth (meat peptone 5 g/l, NaCl 5 g/l, beef extract 1.5 g/l, yeast extract 1.5 g/l, pH = 7.4 ± 0.2 HIMEDIA, India). Bacteria were cultivated for 6 hours at 37 °C while shaking under 600 rpm

using Incubator Hood TH 15 (Edmund Buhler GmbH, Germany), until the optical density of the culture reached value of 0.1 at 600 nm (Specord 210, AnalytikJena, United Kingdom). The culture in exponential phase of growth determined using the optical density parameter was used for the experiments. For immunoseparation of staphylococci and Zn-proteins, 100 μM ZnCl_2 was added to 25 ml of bacterial culture and cultivated for another 6 hours.

Modification of magnetic particles

Immunoglobulin (Ig) G from human serum was purchased from Sigma-Aldrich (USA). Chicken antibodies were prepared according to the manufacturer's instructions (Henna, Czech Republic). For covalent immobilization of antibodies, paramagnetic particles (Dynabeads®MyOne™ Tosylactivated, Invitrogen, Norway) were used. 1000 μg of antibodies were used for preparation of 25 mg of paramagnetic particles. Before establishment, sodium azide was removed and antibodies were acidified to the final pH = 2.5 by HCl adjustment (0.1 M). After 15 minutes, antibodies were placed in phosphate buffer (PBS, pH=7.4). Amicon Ultra 0.5 with 50 K (Millipore, USA) filters were used for each filtration. Covalent immobilization was performed in a total volume of 625 ml in 0.1 borate buffer (pH 9.5) with 0.1 M $(\text{NH}_4)_2\text{SO}_4$ for 24 hours under slow rotation. Free surface on the particles was blocked by 0.5 % BSA (bovine serum albumin) in PBS (w/v) with 0.05 % Tween-20 (v/v) for 10 hours. After blocking, the particles were washed three times in 1 ml 0.1 % BSA in PBS (w/v) with 0.05 % Tween-20 (v/v). Subsequently, they were resuspended in 625 ml of storage buffer (washing buffer with 0.02 % NaN_3 (w/v)). The functionality of MPs with anti-Zn IgE was verified by the conjugation of rabbit's antibodies to the hen's Ig with HRP (*horseradish peroxidase*). For the isolation of cells, automatic pipetting station epMotion 5075 (Eppendorf, Germany) was used.

Detection of zinc ions

Differential pulse voltammetry using Brdiczka reaction was used for the determination of zinc(II) ions. As a measurement system, 813 Compact Autosampler (Metrohm, Switzerland) 797 VA+ Computrace (Metrohm, Switzerland) with three electrode system consisting of a hanging mercury drop electrode as working electrode with an area of 0.4 mm^2 , argento-chloride (Ag/AgCl/3 M KCl) as referent electrode and carbon instrumental electrode was used. Acetate buffer (0.2 M $\text{CH}_3\text{COONa}+\text{CH}_3\text{COOH}$, pH=5) was used as a supporting electrolyte. Differential pulse voltammetry parameters were as follows: argon bubbling 90 s, initial potential -1.5 V, final potential -0.75 V, modulation time 0.3 s, the time

interval 0.04 s, potential step 5.04 mV, modulation amplitude 250 mV, temperature 37 °C. The volume of dosed sample was 100 ml and a volume of electrolyte was 1900 μl .

Sodium dodecyl sulphate polyacrylamide gel electrophoresis (SDS-PAGE) Isolated proteins were detected by SDS – PAGE electrophoresis. Electrophoresis was performed on a Mini Protean Tetra apparatus with a gel of the size of 8.3 x 7.3 cm (BioRad, USA). Separation buffer concentration was 15 % (w/v) and concentration of the focusing gel was 5 % (w/v). Gels were prepared from 30 % (w/v) acrylamide stock solution of 1% (w/v) bisakrylamid. Gel polymerization was performed at room temperature for 45 minutes (separation gel) or 30 minutes (focusing gel). Before analysis, samples were mixed 2:1 with application buffer and incubated at 93°C for 3 minutes. To determine the molecular weight, standard «Precision Plus Protein standards» (Biorad, USA) was used. Electrophoresis was proceeded at 150 V for one hour at 23 °C (Power Basic Biorad, USA) in Tris (2-amino-2-hydroxymethyl-propane-1,3-diol buffer) glycine separation buffer (0.025 M Trizma-base, 0.19 M glycine and 3.5 mM SDS, pH = 8.3). Then the gels were stained with Coomassie blue dye and subsequently by silver with the omission the fixation step (1.1% (v/v), acetic acid 6.4% (v/v), methanol and 0.37% (v/v) formaldehyde). Further, two washing steps follow (50% (v/v) methanol).

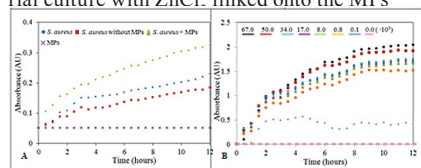
RESULTS AND DISCUSSION

Magnetic separation of bacterial cells

For immunoelectroextraction bacterial cells *S. aureus* from broth, MPs with human IgG were used. Immunoelectroextraction was performed on a programmable rotary disc (Biosan, Lithuania) in 2 ml tubes for 1 hour at 23 °C. After the separation, MPs were washed with 250 μl of nutrient media and pipetted into the 250 μl of nutrient media to the first well of microplate (Nunc, Germany). 250 μl of bacterial culture *S. aureus* was pipetted to the second pit and 250 μl *S. aureus* with 100 μM ZnCl_2 to the third after separation of MPs. The microplate was inserted into the spectrophotometer at 37 °C and 600 rpm. The absorbance was measured in 30 minute intervals for 12 hours (Fig. 1A). For the isolation, 5 mg/ml MPs per 500 μl of bacterial culture was used. It was possible to detect 104 cells with an experimental error of 10 % using this procedure. The suggested manual procedure was subsequently adapted to the automated robotic system. MPs IgG (10 μl) were pipetted to the plate and twice washed with the nutrient broth (300 μl). The culture of *S. aureus* (500 μl) cultivated with ZnCl_2 was pipetted into the micro-

plate wells. Afterwards the microplate was transferred to the thermostatic position and incubated at 37 °C for 60 minutes. Samples were washed four times with the nutrient broth (750 µl). The supernatant was removed and 500 µl of the nutrient broth was added. The cultivation (on the thermostatic position in the epMotion) of the samples proceeded for 3 hours at 37 °C. After this step, turbidity of media was measured (Fig. 1B). A very good reproducibility of the experiment with a maximum error of 5.5 % was determined. Using the robotic system, the errors caused by another service were significantly reduced and it was possible to detect less than 100 cells with an experimental error of 4.3 % (n=5). The scheme of culture growing is shown in Fig. 2A.

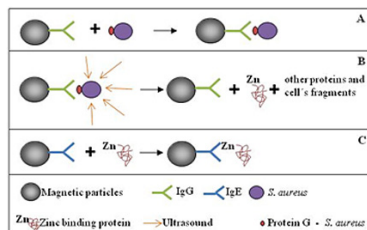
Fig. 1 Detection of Zn^(II) and zinc-binding proteins from *S. aureus* bacterial culture: A) experimental verification of the functionality of MPs with IgG, B) growth curves of dilution series of *S. aureus* bacterial culture with ZnCl₂ linked onto the MPs



Magnetic separation of bacterial cells cultured in the presence of zinc(II) ions

Our aim was to propose an experimental methodology for the isolation of zinc-binding proteins. Applied concentration of zinc ions caused reduction of growth for about 20 % compared to the control variant. The zinc-binding proteins were captured by the hen antibodies on the MPs. Applied modifications allowed the detection of sub-nanomolar concentrations of zinc-containing albumin with the error of 5 %. The methodology was used for immunoseparation of zinc-binding proteins from the bacterial cells: 0, 0.1, 0.8, 8.0, 17.0, 34.0, 50.0 a 67.0 · 10³. During the automatic analysis the microplate was removed from the automatic pipetting station. The cells of *S. aureus* linked to MPs have been broken by ultrasonic needle (2 minutes, 450 Hz) (Fig. 2B). Bacterial lysate was pipetted in the epMotion to the clean position on the DPW plate. After it, MPs with anti-ZnIgE (10 µl) were transported to the DPW plate and washed three times by PBS buffer (pH=4.5, 300 µl). **Bacterial lysate** of *S. aureus* was added (90 µl) and the samples were incubated at 25 °C for 30 minutes. The samples were then washed by PBS buffer (pH=7.4, 700 µl) and three times by the citrate (0.1 M, pH=2.5, 50 µl). The citrate released the zinc-binding proteins. After it, samples were used for the determination of zinc ions and zinc proteins using the SDS-PAGE (Fig. 2C).

Fig. 2 The process of isolation of cells from *S. aureus* bacterial culture: A) establishment of *S. aureus* cells to MPs, B) *S. aureus* cells were broken by ultrasound, C) isolation of zinc-binding proteins from the lysate using MPs



Zinc-containing proteins were studied by SDS-PAGE electrophoresis. Protein concentration depended on the dilution of bacterial culture (0, 0.1, 0.8, 8.0, 17.0, 34.0, 50.0 and 67.0 · 10³). The proteins with molecular weights of approximately 70, 60, 45, 30, 25 and less than 10 kDa (Fig. 3A) were present in samples. Molecular weight of the main bands (70, 45 and 25 kDa) corresponds to the molecular weight of immunoglobulin subunits (large subunit, Fab fragment and a small subunit), which are released into the extract in the process of ultrasonic homogenization. Proteins of 25 kDa represent a group of proteins, which specifically bind ions of heavy metals (metallothionein). Presence of metallothionein (MT) was confirmed in the lysate and the quantity of MT was compared to control variant (increase for about 250 % compared to control).

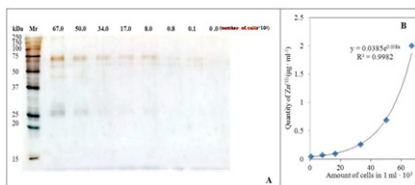
The quantity of the zinc ions in the isolated proteins was confirmed by the electrochemical technique of differential pulse voltammetry (Tab. 1). We found that the amount of zinc increased with increasing number of cells and that reflected that the proteins contained zinc (Fig. 3B).

Tab. 1

The quantity of the zinc ions in the isolated proteins from the *S. aureus* bacterial culture using MPs.

Amount of microorganisms (10^9)	67.0	50.0	34.0	17.0	8.0	0.8	0.1	0
Concentration of Zn in bacterial culture ($\mu\text{g}\cdot\text{ml}^{-1}$)	2.22	1.21	0.51	0.19	0.13	0.08	0.02	0

Fig. 3 Detection of $\text{Zn}^{(II)}$ and zinc-binding proteins from *S. aureus* bacterial culture: A) SDS-PAGE of zinc binding proteins, B) dependence of the quantity of zinc-binding proteins on the applied zinc concentration.



CONCLUSION

We proposed and verified a rapid and automated method for the isolation of bacteria with subsequent isolation of zinc-containing proteins from *S. aureus* cells. Isolation of bacterial cells and zinc-binding proteins from bacterial culture of *S. aureus* by an automatic pipetting station took about 8 hours. We are able to detect 96 samples within one analysis. We were able to isolate *S. aureus* in quantities lower than 100 cells per 1 ml of the sample using the paramagnetic micro-particles and the results of our analyses verified that it is possible to determine the amount of bound zinc in the organism at a concentration of $0.02 \text{ mg}\cdot\text{ml}^{-1}$ in the number of cells.

ACKNOWLEDGEMENT

Financial support from the following projects is highly acknowledged: CEITEC CZ.1.05/1.1.00/02.0068 funded by the Operational Program Research & Development for innovation, CYTORES GA CR P301/10/0356 and NANOSEMED GA AV KAN208130801 funded by the Grant Agency of the Academy of Sciences of the Czech Republic.

REFERENCES

[1] Khlyntseva, A.E., et al., Design of a Test System Based on Magnetic Particles with Immobilized Monoclonal Antibodies for Selective Bacillus anthracis Spore Concentration. *Applied Biochemistry and Microbiology*, 2011. 47(7): p. 700-706.

[2] Baldrich, E. and F.X. Munoz, Enzyme shadowing: using antibody-enzyme dually-labeled magnetic particles for fast peacock detection. *Analyst*, 2008. 133(8): p. 1009-1012.

[3] Peacock, S.J., I. de Silva, and F.D. Lowy, What determines nasal carriage of *Staphylococcus aureus*? *Trends in*

Microbiology, 2001. 9(12): p. 605-610.

[4] Fitzgerald, J.R., et al., Evolutionary genomics of *Staphylococcus aureus*: Insights into the origin of methicillin-resistant strains and the toxic shock syndrome epidemic. *Proceedings of the National Academy of Sciences of the United States of America*, 2001. 98(15): p. 8821-8826.

[5] Murray P. R., R.L., Ken S., Pfaller, Michael A. , *Medical microbiology*. 2005.

[6] Dumitrescu, O., et al., *Staphylococcus aureus* resistance to antibiotics: key points in 2010. *M S-Medecine Sciences*, 2010. 26(11): p. 943-949.

[7] Taylor, E. and T.J. Webster, Reducing infections through nanotechnology and nanoparticles. *International Journal of Nanomedicine*, 2011. 6: p. 1463-1473.

[8] Aarestrup, F.M., L. Cavaco, and H. Hasman, Decreased susceptibility to zinc chloride is associated with methicillin resistant *Staphylococcus aureus* CC398 in Danish swine. *Veterinary Microbiology*, 2010. 142(3-4): p. 455-457.

[9] Botelho, T.O., et al., Structural and Functional Analyses Reveal That *Staphylococcus aureus* Antibiotic Resistance Factor HmrA Is a Zinc-dependent Endopeptidase. *Journal of Biological Chemistry*, 2011. 286(29): p. 25697-25709.

[10] Papageorgiou, A.C., et al., CRYSTAL-STRUCTURE OF THE SUPERANTIGEN ENTEROTOXIN C2 FROM *STAPHYLOCOCCUS-AUREUS* REVEALS A ZINC-BINDING SITE. *Structure*, 1995. 3(8): p. 769-779.

[11] Langley, R., et al., *Staphylococcal Superantigen Super-Domains in Immune Evasion*. *Critical Reviews in Immunology*, 2010. 30(2): p. 149-165.

[12] Park, P.W., et al., BINDING AND DEGRADATION OF ELASTIN BY THE STAPHYLOLYTIC ENZYME LYSOSTAPHIN. *International Journal of Biochemistry & Cell Biology*, 1995. 27(2): p. 139-146.

[13] Hase, C.C. and R.A. Finkelstein, Bacterial extracellular zinc-containing metalloproteases. *Microbiol. Rev.*, 1993. 57(4): p. 823-837.

[14] Hui, J., et al., *Staphylococcus aureus* enterotoxin C2 mutants: biological activity assay in vitro. *Journal of Industrial Microbiology & Biotechnology*, 2008. 35(9): p. 975-980.

[15] Conrady, D.G., et al., A zinc-dependent adhesion module is responsible for intercellular adhesion in staphylococcal biofilms. *Proceedings of the National Academy of Sciences of the United States of America*, 2008. 105(49): p. 19456-19461.

[16] Quoc, P.H.T., et al., Isolation and characterization of biofilm formation-defective mutants of *Staphylococcus aureus*. *Infection and Immunity*, 2007. 75(3): p. 1079-1088.

[17] Pennella, M.A. and D.P. Giedroc, Structural determinants of metal selectivity in prokaryotic metal-responsive transcriptional regulators. *Biomaterials*, 2005. 18(4): p. 413-428.

SELECTIVE FOCUSING AND ANALYSIS OF Na⁺, Ca²⁺, Mg²⁺, Mn²⁺, Cd²⁺, Zn²⁺, Ni²⁺, Pb²⁺, Cu²⁺ USING LIGAND STEP GRADIENT FOCUSING IN COMBINATION WITH ITP (LSGF-ITP)

Eliska GLOVINOVA, Jan POSPICHAL

¹Department of Chemistry and Biochemistry, Faculty of Agronomy, Mendel University, Zemědělská 1, 61300 Brno, Czech Republic

*eliska@mendelu.cz

ABSTRACT

The capillary electrophoretic method for the pre-concentration of metals based on selective focusing of metal chelates with subsequent on-line ITP analysis was developed and verified. The selected ions of nine metals (Na⁺, Ca²⁺, Mg²⁺, Mn²⁺, Cd²⁺, Zn²⁺, Ni²⁺, Pb²⁺, Cu²⁺) were subjected to pre-concentration from the mixture and analyzed. Focusing of metals was carried out in ligand step gradient, which was created by an addition of a convenient ligand agent to the regular stationary and/or steady state pH step gradient.

The metal ions were continuously dosed into the column, where they were selectively trapped (with exception of Na) on the ligand step gradient in the form of zones of citrate complexes with effective charge dependent on step gradient velocity. After accumulation of detectable amount of analyte, the dosing was stopped and accumulated zones were mobilized to the analytical column, where they were analyzed by ITP method with conductivity or photometric detection. The reached increase in cLOD is ca. two orders of magnitude using acceptable dosing time 25min.

INTRODUCTION

To reach higher sensitivity in metal analysis we developed convenient sample pre-concentration method which was on-line combined with common analytical ITP.

Developed pre-concentration method is based on the principle of stationary neutralization reaction boundary-NRB and its combination with ligand - chelating agents. A stationary ligand step gradient – LSG [1] boundary is created in the column with two adjacent electrolytes branches of different chelating power and pH. In acid phase, metal and metal complexes are positively charged and forced migrate to the LSG boundary, in the alkaline phase, the complexes are negatively charged and again migrate towards LSG-boundary. A steady state zone of concentrated metal complexes is created. Focused zones are then mobilized and analyzed by ITP. Presence of sample metal ions in one electrolyte /dosing electrolyte-DE/ during the focusing causes a time dependent accumulation of the metals.

MATERIAL AND METHODS

Apparatus

The commercially available isotachophoretic apparatus (CS Isotachophoretic Analyzer, Villa Labeco, Slovak Republic) in the column-coupling configuration equipped with conductivity detection in the pre-separation and analytical column was used.

ELECTROLYTES

Alkaline primary (focusing) electrolyte: LE/PE: 0.01M NH₄Ac + 0.01M NH₄OH + 0.002M ammonium citrate + 1% polyethyleneglycole, pH=9.24

Acidic dosing (focusing) electrolyte: DE: 0.01M HAc + 0.001M NH₄Ac + 0.1% Tritone X100+sample metals.

ITP analytical electrolyte: LE: 0.02M NH₄Ac + 0.1M HAc + 0.002M ammonium citrate, 0.1% Tritone X100, pH=4.00, TE: 0.03M HAc

PROCEDURE

The column is filled with proper electrolytes. The anodic terminating chamber is filled with the acidic dosing electrolyte /DE/, the separation column and the proper (cathodic) electrolyte chamber is filled with primary alkaline electrolyte /PE/, the analytical capillary and the corresponding (cathodic) electrolyte chamber is filled with the leading electrolyte /LE/.

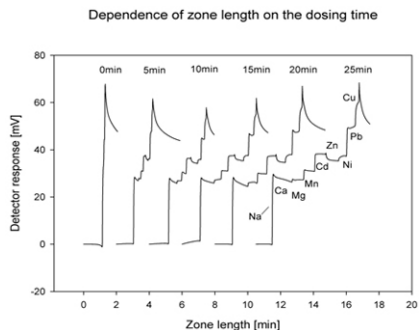
By switching on the driving current, a sharp LSG boundary is created in the column in between dosing and primary electrolyte and continuous dosing procedure starts. Metal cations and positively charged metal citrate complexes are driven from the acidic dosing electrolyte to the LSG boundary, where are focused. After accumulation of sufficient amount of metals for the analysis, a dosing electrolyte in the terminating electrolyte /TE/ chamber is changed for the terminating which causes mobilization. The focused zones of non charged metal citrate complexes are acidified; they gain a positive charge

or break down, releasing free metal cations, and migrate to the second analytical column. Here are analyzed by ITP in the leading electrolyte, and detected.

RESULTS AND DISCUSSION

For experimental verification, an equimolar mixture of nine metals Na^+ , Ca^{2+} , Mg^{2+} , Mn^{2+} , Cd^{2+} , Zn^{2+} , Ni^{2+} , Pb^{2+} , Cu^{2+} ($2 \times 10^{-6} \text{M}$ each – 20% of cLOD) was focused. A time dependence of the zone length of each metal as a function of time was plotted - Fig.1. The dependence is fairly linear for all metals, Ca b[0]4,9 b[1]4,56 r2 0,9989; Mg b[0] 0,8 b[1] 2,82 r2 0,9999; Mn b[0] 1,1 b[1] 2,74 r2 0,9989; Cd b[0] 1 b[1]2,82 r20,9931; Zn b[0] 0,7 b[1] 2,8 r2 0,9894; Ni b[0]1,7 b[1] 1,94 r2 0,9958; Pb b[0]1,4 b[1] 2,1 r2 0,9993; Cu b[0] 0,6 b[1] 0,78 r2 0,9825, with except of sodium, which is not focused on the LSG boundary.

Figure 1.



CONCLUSION

Metal complexes were pre-concentrated, focused and analyzed using the combination of ligand step gradient focusing method with subsequent mobilization and on-line ITP analysis. A continuous dosing technique was used for the lowering the detection limit ca. two orders of magnitude, with acceptable dosing time of 25 min. Using citrate as a complexing agent yields in selective removing of alkali metals /e.g. Na/ from the sample mixture.

ACKNOWLEDGEMENTS

This work was supported by the Grant Agency of the Czech Republic, Grant No. 206/10/1219.

REFERENCES

- [1] E. Sisperova, E.Glovinova, J.Budilova and J.Pospichal, J. Chromatogr.A. 1281 (2011) p. 3105.

PRACTICAL DIFFICULTIES OCCURRING DURING SOLID PHASE PEPTIDE SYNTHESIS

Libor JANU^{1,2}, Marketa RYVOLOVA^{1,3}, Ondrej ZITKA¹, Vojtech ADAM^{1,3},
Rene KIZEK^{1,3*}

¹ Department of Chemistry and Biochemistry, Faculty of Agronomy, Mendel University in Brno, Zemedelska 1, 613 00 Brno, Czech Republic

² Clonestar peptide services, Brno, Czech republic

³ Central European Institute of Technology, Brno University of Technology, Technicka 3058/10, CZ-616 00 Brno, Czech Republic

*kizek@sci.muni.cz

ABSTRACT

Fmoc solid phase peptide synthesis is the most powerful and the most popular method for preparing synthetic peptides today. It is possible to prepare up to 60mer or make numerous peptide modifications using this technique. Possible side reactions are well documented and can be prevented. Despite the power of the method, some peptide sequences must be considered with special attention before synthesis, because of their tendency to form by-products in significant amounts. Here we report a results and comparison of two difficult peptide syntheses.

INTRODUCTION

The solid phase peptide synthesis is based on construction of a peptide chain on the solid (insoluble) support. To achieve a highest purity of the product, each coupling step should be performed with maximal efficiency. Fmoc solid phase synthesis (Fmoc SPPS) is the most popular method today. The excess reagents can be employed to drive reactions to completion, and physical losses can be minimized as the peptide remains attached to the support throughout the synthesis [1]. Using appropriate activating agents, Fmoc SPPS allows to couple up to 60 amino acids, by step-by-step approach. Despite above mentioned advantages, many sequences require special attention, because of their tendency to form a by-product during synthesis or postsynthetic manipulations, which can lead to significant decrease of crude product quality [1,3,7,8]. Today, most of side reactions are well documented and can be generally avoided by careful planning of the synthesis and by appropriate selection of protecting groups and resin linkers [1]. **In this paper, we report practical example of two difficult peptide sequences.**

MATERIAL AND METHODS

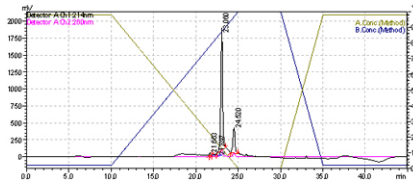
Peptides were synthesized on Prelude peptide synthesizer (Protein technologies, USA). Amino acids were purchased from Sigma Aldrich (USA), Merck (Germany). We used PEG-PS resins from Applied Biosystems. Solvents for peptide synthesis were purchased from Biosolve (Netherlands) and Sigma Aldrich (USA). Solvents for HPLC analysis were purchased from BDL (Czech Republic) and Sigma Aldrich (USA).

RESULTS AND DISCUSSION

Not only long sequences, but also sequences with higher number of neutral and/or hydrophobic amino acids, represent a challenge for peptide synthesis. It is due to the poor solvation of peptide chain during synthesis. In a fully solvated system, the reactive peptide amino termini are well separated and readily accessible for incoming amino acid residue [1]. In the case of hydrophobic sequence, the amino terminus is poorly solvated, resulting in significant N-terminus collapse and inability to react with incoming amino acid [1, 2]. This usually leads to incomplete or truncated sequences. Significant improvement can be achieved when prolines or pseudoprolines are presented or incorporated to the synthesized sequence. Proline/pseudoproline side chain poses a unique structure with natural propensity to disrupt the secondary structure of peptide and thereby to avoid the collapse of the peptide chain during chain assembly in length up to 6 residues.

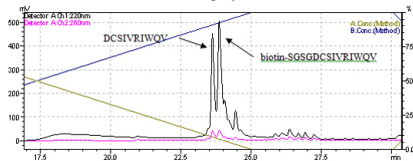
In this study, we report a comparison of crude abaecin (34mer) YVPLPNVQPGRPPFTF-PGQGFNPKIKWPQGY and biotinylated 14mer biotin-SGSGDCSIVRIWQV. Abaecin is major antibacterial response peptide in the honeybee [1, 2]. Despite the 34mer abaecin is much longer than biotinylated peptide, it represents an easier synthesis due to high occurrence of proline residues and their relatively regular distribution within the sequence. Purity of crude 34mer abaecin was about 79% (Fig.1).

Figure 1: HPLC result of crude abaecin (34mer)



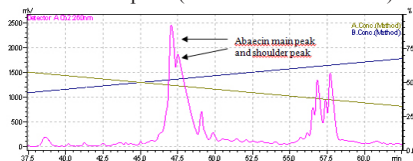
In contrast to this, purity of crude peptide biotin-SGSGDCSIVRIWQV is only 37% (Fig. 2). MALDI-MS revealed the impurity of significant amount (35%) comprising a truncated sequence DCSIVRIWQV. Incorporation of GS pseudoproline dipeptide did not increase the final peptide purity indicating the collapse of peptide on D5 position.

Figure 2: Detailed HPLC result of crude biotin-SGSGDCSIVRIWQV. There are two major peaks. Left one is peptide lacking biotin-SGSG and right one is peptide with correct mass (biotin-SGSGDCSIVRIWQV)



However, in the case of 34mer abaecin, the secondary structure of final peptide must be also considered. In more detailed analysis of main fraction, shoulder peak was found (Fig. 3). It could be a peptide with same mass but with different secondary structure of peptide chain. This phenomenon is usually associated with synthesis of longer or proline rich peptides [1].

Figure 3: Detailed chromatogram of abaecin purification. Main peak (retention time 47.0 min.) with shoulder peak (retention time 47.5 min.)



CONCLUSION

We report results of two difficult peptides prepared by Fmoc solid phase synthesis. 34 amino acids long peptide was challenging for their outstanding length, while much shorter biotinylated 14 mer leads to truncated sequence with final purity about 37%. Low purity of short peptide

is probably due to collapse of the N-terminus during synthesis. Comparison of these two practical examples demonstrates the fact, that not only length, but also amino acid composition of the peptide is crucial from point of view of peptide synthesis.

ACKNOWLEDGEMENT

The financial support NANOSEMED GA AV KAN208130801 and IGA IP10/2012 is highly acknowledged.

REFERENCES

- [1] Chantell C A, Onaiyekan M A, Menakuru M, J. Pept. Sci., 18 (2012), 88-91.
- [2] Hammer R P, Albericio F, Gera L, *et al.*, Int. J. Pept. Protein Res., 36 (1990), 31-45.

STUDY OF ANTIOXIDANT PROFILE OF CATTLE

Jiri SOCHOR^{1,2,3}, Branislav RUTTKAY-NEDECKY^{2,3}, Marie BALABANOVA⁴, Petr MARES⁴, Ladislav ZEMAN⁴, Vojtech ADAM^{1,2,3}, Rene KIZEK^{1,2,3}

¹Department of Chemistry and Biochemistry, Faculty of Agronomy, Mendel University in Brno, Zemedelska 1, CZ-613 00 Brno, Czech Republic

²Central European Institute of Technology, Brno University of Technology, Technicka 3058/10, CZ-616 00 Brno, Czech Republic

³Department of Microelectronics, Faculty of Electrical Engineering and Communication, Brno University of Technology, Technicka 10, CZ-616 00 Brno, Czech Republic

⁴Department of Animal Nutrition and Forage Production, Faculty of Agronomy, Mendel University in Brno, Zemedelska 1, 613 00 Brno, Czech Republic

ABSTRACT

The aim of this study is to monitor an oxidant stress elicited by gravidity and birth of high productive cows. Twelve pregnant Holštýn heifers were observed. We focused on the oxidant stress monitored by antioxidant enzymes; superoxide dismutase, catalase, glutathione peroxidase, glutathione reductase. The parameters were monitored in blood plasma in the time of ten and five days before birth, in the day of birth, five and ten days after birth. Increase of the antioxidant enzyme activity during gravidity was caused by higher oxygen intake, which was formed superoxide, scavenged by antioxidant enzymes.

INTRODUCTION

It is known that, in the time of gravidity, increased production of free oxygen radicals occurs, which is caused by higher oxygen intake during this period [1]. This fact is confirmed by many papers dealing with the increased levels of markers of oxidative stress [2-5]. Production of reactive forms of oxygen is impeded by oxidant system formed from low-molecular-weight antioxidants, which are present in organism, and mainly by enzymes interacting with reactive forms of oxygen, such as peroxides, catalases and superoxide dismutase [6-10]. Unfortunately, monitoring of antioxidant enzymes during gravidity is not sufficient. However, it is generally stated that activity of antioxidant enzymes is increasing due to the increased oxidative stress caused by higher oxygen intake and higher energetic demands during gravidity. This statement has been confirmed by Garrel et al. a Hung et al. [11, 12] in their studies of levels of antioxidant enzymes SOD, CAT, GSHPx, GR. According to their results, even amount of selenium, significant trace element, was increasing during gravidity. This correlation was caused by desirable effect on function of antioxidant enzymes to reduce superoxide and hydrogen [10].

Our paper is pilot study of oxidative stress monitoring during birth of heifers. The aim of study is to determine the impact of birth to chosen antioxidant enzymes. According to our findings, the following experiment will be based on administering an addition to heifers to improve their health state during gravidity and the level of oxidant stress will be examined.

MATERIAL AND METHODS

Twelve pregnant Holštýn heifers stalled in group were involved in the experiment. Heifers were monitored in five periods - ten days before birth, five days before birth, in the day of birth, five days after birth and ten days after birth.

Blood samples collecting

Samplings of blood were collected from a tail vein of each heifer ten days before birth, five days before birth, in the day of birth, five days after birth and ten days after birth. Samplings of blood were taken to test tube containing heparin.

Collected samples of blood were cooled to 4 °C, and then centrifuged (temperature 4 °C, 2000 rpm for 10 min, Eppendorf 5402, USA). Separated plasma was pipetted to micro test tubes of 1.5 ml volume. Prepared supernatant was used for analysis on automated spectrophotometer BS-400 (Mindray, China).

Determination of superoxide dismutase

8167 times diluted with buffer). It was incubated for 72 s (1min, 12 s) and than absorbance was measured at $\lambda = 450$ nm. Kinetic reaction was measured for 108 s (3 min) and absorbance was read every 9 s.

Determination of Catalase (CAT)

Kit of company Sigma Aldrich, USA was used for assay of catalase activity. A plastic cuvette and a BS 400 automated spectrophotometer (Mindray, China) was used for measurement. Agent A (phosphate buffer) was used for dilution of peroxide, preparation of standards and dilution of samples. Final concentrations of che-

micals in agent A were: 50 mM dihydrogen monopotassium phosphate a 0.5 mM EDTA in ACS water. The pH of agent was changed to the level 7 using 1 M KOH. Agent B was solution of hydrogen peroxide of concentration 10 mM (0.045 %) prepared with diluting of 30 % water solution of hydrogen peroxide in the agent A. A 950 μ l volume of agent B (10 mM H₂O₂ in 50 mM phosphate buffer and 0.5 mM EDTA) was pipetted into a plastic cuvette, agent was warmed to 37 °C and than a 50 μ l volume of sample was pipetted, content of cuvette was mixed and the absorbance immediately measured at $\lambda = 240$ nm. Kinetic reaction was measured for 60 s in 5-second intervals.

Determination of Glutathione peroxidase (GSHPx)

Glutathione Peroxidase Cellular Activity Assay Kit (CGPI, Sigma Aldrich, USA) was used for GPx assay, determination was done in erythrocytes. For determination of glutathione peroxidase activity, a BS 400 automated spectrophotometer (Mindray, China) was used. A 260 μ l volume of reagent R1 (0.3 mM NADPH in GPx buffer) was pipetted into a plastic cuvette with subsequent addition of 10 μ l of sample and after mixing, a 30 μ l volume of reagent R2 (3 mM tert-butyl hydroperoxide) is added to the cuvette which starts the reaction. The decrease in absorbance is measured at 340 nm using kinetic program for 2 minutes and 6 seconds. The spectrophotometer calculates GPx activity according to a calibration curve.

Determination of Glutathione Reductase

A Glutathione Reductase Assay Kit (Sigma Aldrich, USA) was used for glutathione reductase (GR) activity, determination, determination was done in erythrocytes. For determination of glutathione reductase activity, a BS 400 automated spectrophotometer (Mindray, China) was used. Reagents R1 and R2 were prepared by dissolving in an assay buffer (100 mM potassium phosphate buffer, pH 7.5, with 1 mM EDTA). A 260 μ l volume of the reagent R1 (1.15 mM oxidized glutathione in the assay buffer) is poured with 10 μ l of sample and 30 μ l volume of reagent R2 (1 mM NADPH in GR assay buffer) into a plastic cuvette. The decrease in absorbance is measured at 340 nm using kinetic program for 126 s. The same device and conditions were used for GR as in the case of total protein assay.

RESULTS AND DISCUSSION

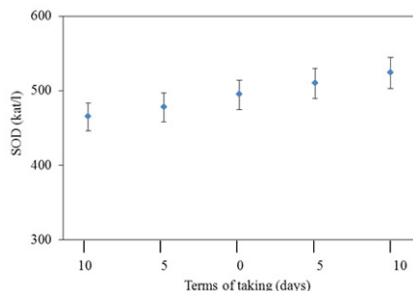
Antioxidant effect of enzymes provides cells and their structures with protection against undesirable impacts of radicals. Level of reactive forms of oxygen is, due to its effect in organism, kept in particular limits of protection. Oxidative

stress appears towards oxidation in the case of disturbed balance of oxygen forms. In our study, activity of important antioxidant enzymes capable of eliminating free radicals, such as SOD, CAT, GSHPx, and GR, was monitored. Values of individual enzyme activity were averaged.

Determination of superoxide dismutase activity

Superoxide dismutase is enzyme transforming superoxide radical into hydroxide peroxide, which does not represent such a risk for organism [6]. Results of determination of this enzyme are shown in Fig. 1. Average value of SOD from the day of birth was increased by 6 % in comparison with value of SOD of ten days before birth. Value of SOD of ten days after birth was increased by 13 % in comparison with value of SOD of ten days before birth. In the period of gravidity, there are increased demands on oxygen and therefore the level of oxidant stress increases. After birth, oxidative stress should be decreased due to lower demands on oxygen. Therefore, the hypothesis of decreasing SOD values after birth was created, according to Genz et al [5]. However, average values of SOD were increasing (Fig. 1). This result can be explained by short term of evaluating, which was not sufficient for an organism to restore to common state [2].

Fig. 1: Average values of enzyme activity SOD of all heifers ten days before birth, five days before birth, in the day of birth, five days after birth and ten days after birth

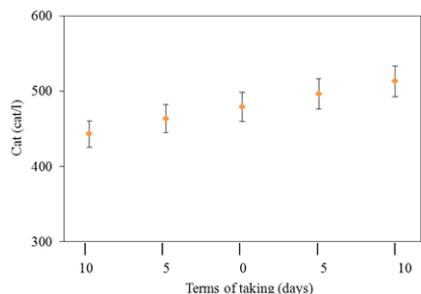


Determination of catalase activity

Catalase is enzyme linked with the product of superoxide dismutase, dissociating hydrogen peroxide into water and oxygen [9, 13]. This enzyme is highly effective in the case of high levels of oxidative stress and provides protection against peroxide [14]. Final results from our experiment are shown in Fig. 2. Average value of CAT from the day of birth was increased by

8 % in comparison with value of CAT of ten days before birth. Value of CAT of ten days after birth was increased by 16 % in comparison with value of CAT from the time of ten days before birth. High correlation ($r=0.986$) between CAT and SOD was found and is caused by the fact that CAT dissimilate the product of SOD (hydrogen peroxide) [15].

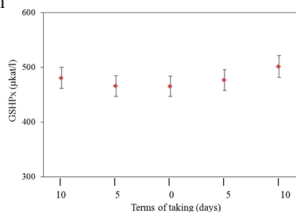
Fig. 2: Average values of enzyme activity CAT of all heifers ten days before birth, five days before birth, in the day of birth, five days after birth and ten days after birth



Determination of Glutathione peroxidase

Glutathione peroxidase is enzyme dissociating product of superoxide dismutase, hydrogen peroxide, into water and simultaneously oxidising glutathione [7]. Values of GSHPx are shown in Fig. 3. Average value of GSHPx from the day of birth was decreased by 3 % in comparison with value of GSHPx from the time of ten days before birth. Value of GSHPx of ten days after birth was increased by 5 % in comparison with value of GSHPx from the time of ten days before birth. GSHPx, as well as CAT, dissociates hydrogen peroxide, unlike CAT, GSHPx is not capable of dissociating hydrogen peroxide in the case of its increased concentration in organism and thus the dissociation is not so intensive. Fig. 3 shows decrease of GSHPx activity in the time of birth, which is probably caused by the increased amount of produced peroxide, as described in paper by Preziosi et al [16] a Flohe et al [17].

Fig. 3: Average values of enzyme activity GSHPx ten days before birth, five days before birth, in the day of birth, five days after birth and ten days after birth



Determination of Glutathione reductase

Glutathione reductase is enzyme closely linked to glutathione peroxidase, as oxidant glutathione is restored to reduced form using coenzyme NADPH, which is oxidised into NADP+ [8]. Our results, shown in Fig. 4, correspond with this fact. Average value of GR from the day of birth was decreased by 4 % in comparison with value of GR of ten days before birth. Value of GR of ten days after birth was increased by 4 % in comparison with value of GR of ten days before birth. Activity of glutathione reductase provides the balanced level between glutathione reductase and peroxidase which assists the activity of glutathione reductase enzyme to dissociate hydrogen peroxide to water [18]. Our results point out the connection between these two enzymes (GR and GPx), the trend of their levels was decreasing to the day of birth and equilibrating after the birth, which was confirmed by high correlation coefficient ($r=0.973$).

Fig. 4: Average values of enzyme activity GR of all heifers ten days before birth, five days before birth, in the day of birth, five days after birth and ten days after birth

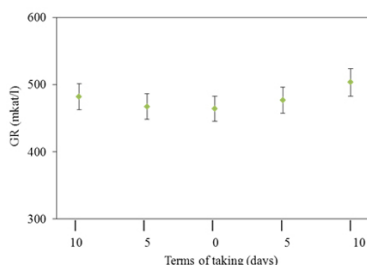


Table 1 summarizes correlation coefficients of antioxidant enzymes. High correlations were observed between enzymes SOD and KAT ($r=0.986$), GR and GSHPx ($r^2=0.973$).

Tab. 1 Values of correlation coefficients between antioxidant enzymes.

	KAT	GSHPx	GR
SOD	0.986	0.497	0.501
KAT		0.415	0.439
GSHPx			0.973

CONCLUSION

Values of enzyme SOD evinced the increasing trend during the whole period of monitoring. The hypothesis of presumed decreased values of enzyme SOD due to increased oxidative stress after birth was not confirmed. This result can be caused by short period of monitoring after birth.

Values of CAT enzyme were increasing, too. The high correlation ($r=0.986$) was found between SOD and KAT, probably due to the fact that CAT dissociates a final product of SOD and thus follows processes of SOD. The level of GSHPx and GR enzyme activity was decreasing before birth and equilibrating after birth. The high correlation ($r=0.973$) between these two enzymes was observed.

ACKNOWLEDGEMENTS

The work was supported by the Research centre CZ.1.05/2.1.00/03.0072 and grants TP 2/2011 and TP 3/2012.

REFERENCES

- [1] Moretti M, Phillips M, Abouzeid A, et al., *American Journal of Obstetrics and Gynecology*, 190 (2004), 1184-1190.
- [2] Toescu V, Nuttall S L, Martin U, et al., *Clin. Endocrinol.*, 57 (2002), 609-613.
- [3] Makedou K, Kourtis A, Gkiomisi A, et al., *Gynecol. Endocrinol.*, 27 (2011), 1070-1073.
- [4] Behne D, Wolters W, *Journal of Clinical Chemistry and Clinical Biochemistry*, 17 (1979), 133-135.
- [5] Genc H, Uzun H, Benian A, et al., *Arch. Gynecol. Obstet.*, 284 (2011), 1367-1373.
- [6] Kharrazi H, Vaisi-Raygani A, Rahimi Z, et al., *Clinical Biochemistry*, 41 (2008), 932-936.
- [7] Imai H, Nakagawa Y, *Free Radical Biology and Medicine*, 34 (2003), 145-169.
- [8] Kocsy G, Tóth B, Berzy T, et al., *Plant Science*, 160 (2001), 943-950.
- [9] Luo D, Rando T A, *Biochemical and Biophysical Research Communications*, 303 (2003), 609-618.
- [10] Mistry H D, Broughton Pipkin F, Redman C W G, et al., *American Journal of Obstetrics and Gynecology*, 206 (2012), 21-30.
- [11] Garrel C, Fowler P A, Al-Gubory K H, *Journal of Endocrinology*, 205 (2010), 107-116.
- [12] Hung T H, Lo L M, Chiu T H, et al., *Reproductive Sciences*, 17 (2010), 401-409.
- [13] Nicholls P, *Archives of Biochemistry and Biophysics*.
- [14] Muhsan M S, Ahmed A, Khurshid S, *Asian J. Chem.*, 24 (2012), 451-454.
- [15] Chelikani P, Fita I, Loewen P C, *Cell. Mol. Life Sci.*, 61 (2004), 192-208.
- [16] Preziosi P, Arnaud J, Richard M J, et al., *Relationship between serum selenium and red cell and plasma glutathione peroxidase levels - Effect of supplementation with nutritional doses of antioxidants in elderly and adult subjects*, Kluwer Academic/ Plenum Publ, New York 2000.
- [17] Flohe L, Schaich E, Voelter W, et al., *Hoppe-Seylers Zeitschrift Fur Physiologische Chemie*, 352 (1971), 170-&.
- [18] Zablocka A, Janusz M, *Postep. Hig. Med. Dosw.*, 62 (2008), 118-124.

INTERACTION OF CADMIUM WITH GLUTATHIONE

Renata KENSOVA^{1,2}, David HYNEK^{1,2}, Josef ZEHNALÉK¹, Jaromir HUBALEK^{2,3}, Libuse TRNKOVA^{2,4}, Vojtech ADAM^{1,2}, Rene KIZEK^{*1,2}

¹ Department of Chemistry and Biochemistry, Faculty of Agronomy, Mendel University in Brno, Zemedelska 1, 613 00 Brno, Czech Republic

² Central European Institute of Technology, Brno University of Technology, Technicka 3058/10, 616 00 Brno, Czech Republic

³ Department of Microelectronics, Faculty of Electrical Engineering and Communication, Brno University of Technology, Technicka 10, CZ-616 00 Brno, Czech Republic

⁴ Department of Chemistry, Masaryk University, Kotlarska 2, 611 37 Brno, Czech Republic

*kizek@sci.muni.cz

ABSTRACT

The aim of study was electrochemical monitoring of the interaction cadmium(II) ions with glutathione. Attention was focused on the study of basic electrochemical behaviour of cadmium(II) ions and low molecular mass glutathione. For electrochemical determination measuring system Metrohm (746 VA Trace Analyzer and 695 Autosampler) was employed.

INTRODUCTION

Heavy metals are currently threat to humans but also animals, plants and microorganisms. The largest source of unwanted pollutants in the environment is from human activity (mining and heavy industry, traffic, agriculture) [1-4]. Among the most toxic metals includes cadmium, which is widely used in the production of Ni-Cd batteries, and today is used in electronics too. Organisms strongly protect themselves against exposed to high levels of metal ions creating a range of organic compounds (e.g. glutathione). Glutathione (GSH) is tripeptide, composed of amino acids (glutamic acid, cysteine and glycine), located in the cells of animals, plants and bacteria and protects the body against oxidative stress. Cysteine, which contains a thiol group (-SH), is the reason of GSH redox properties. Free oxygen radicals that can be produced by the cell itself can be detoxified by GSH [5]. A dimer called oxidized glutathione (GSSG) is product of GSH oxidation [6]. There is GSSG reduced again to GSH in the glutathione cycle. GSH is almost found in its reduced form.

MATERIALS AND METHODS

Determination of cadmium by differential pulse voltammetry were performed with 746 VA Stand instrument connected to 695 Autosampler (Metrohm, Switzerland), using a standard cell with three electrodes. For data processing VA Database 2.2 by Metrohm CH was employed. The parameters of the measurement were as follows: initial potential of -0.8 V, end potential 0.15 V, adsorption potential -0.8 V, deposition 240 s, deoxygenating with argon 90 s, time pulse 0.04 s, step potential 4 mV, modulation amplitude 25 mV, volume of injected sample: 100 μ l, volume of measurement cell 2 ml (100 μ l of sample + 1900 μ l acetate buffer).

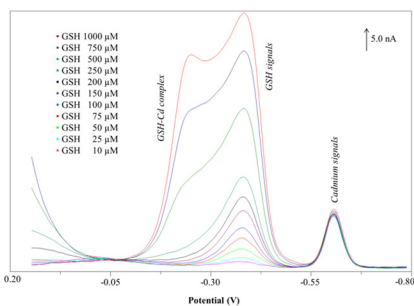
Fully automated pipetting was carried out on automated pipetting system epMotion 5075 (Eppendorf, Germany). Measured concentrations of glutathione were $0, 0.5, 1, 2.5, 5, 10, 25, 50, 75, 100, 150, 200, 250, 500, 750$ and 1000 μ M, and cadmium(II) ions $250, 500, 750$ and 1000 nM. Well developed peaks of cadmium(II) ions at -0.6 V, GSH at -0.35 V and GSH-Cd complex at -0.2 V were detected. After that we characterized the obtained differential pulse voltammograms, we followed with the studying of their mutual interactions. Each from the above mentioned thiols concentrations were mixed $250, 500, 750$ or 1000 nM cadmium(II) ions and incubated ($0, 5, 10$ and 15 h). Based on the affinity of $-SH$ moiety to metal ion, cadmium-thionein complexes were formed.

RESULTS AND DISCUSSION

Recently, we investigated electrochemically interaction of heavy metals with glutathione using differential pulse voltammetry [7]. The observed signal probably relates with forming of thiol-heavy metal ion complex adsorbed on the surface of the working electrode [7]. The observed affinity of glutathione to metal ions can be also related to the fact that level of these compounds can be considered as a marker of metal ion environmental pollution [8-10].

In this study, cadmium(II) ions was accumulated at -0.9 V onto surface of hanging mercury drop electrode for 240 s. Formed Cd(Hg) was then electrochemical stripped and typical peak appeared (Fig. 1).

Figure 1: DP voltammograms of cadmium glutathione interactions; concentration cadmium(II) ions ($10, 25, 50, 75, 100, 150, 200, 250, 500, 750$ and 1000 μ M), time of incubation 15 h.



By interaction Cd+GSH concentration of cadmium(II) ions was constant. Greatest cadmium(II) ions signal was observed after incubation 10 h. Glutathione signal continuously grow with increasing glutathione concentration (Fig. 2). The highest values of the glutathione signal were again incubated for 10h (Fig. 2). The measured signals of GSH-Cd complex are shown in Figure 3. The resulting complex was detected only to concentration of 500 μM . At lower concentration of glutathione was no signal recorded. With increasing incubation time decreased signal of GSH-Cd complex.

Figure 2.: Glutathione signal as a function of glutathione concentration for concentration of cadmium(II) ions 750 nM. Various times of in-teraction are presented (-♦- 0h; -■- 5h; -●- 10h; -▲- 15h)

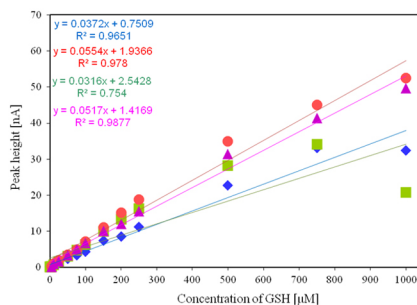
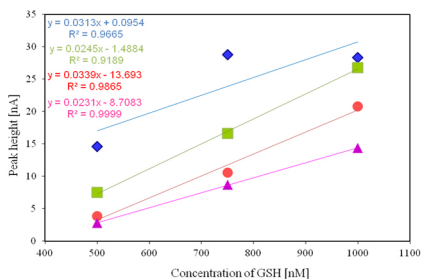


Figure 3.: GSH-Cd complex signal as a function of glutathione concentration for concentration of cadmium(II) ions 750 nM. Various times of in-teraction are presented (-♦- 0h; -■- 5h; -●- 10h; -▲- 15h)



CONCLUSION

Study of cadmium and glutathione interaction is presented in this paper. Electrochemical methods represent analytical instruments with good reproducibility, effortless service and relatively rapid determination. Studying interaction can be used for construction a simple sensor for determination of Cd(II) based on the modification of the hanging mercury drop electrode surface by thiols. Based on the obtained results we assume that the suggested technique offers detection of heavy metals in the environment and can be also used for studying of biomolecules.

ACKNOWLEDGEMENT

The work has been supported by NANO-SEMED GA AV KAN208130801, CEITEC CZ.1.05/1.1.00/02.0068 and UNEP Lead and Cadmium Activities.

REFERENCES

- [1] Huska D, Zitka O, Krystofova O, *et al.*, *Int. J. Electrochem. Sci.*, 5 (2010), 1535-1549.
- [2] Kleckerova A, Sobrova P, Krystofova O, *et al.*, *Int. J. Electrochem. Sci.*, 6 (2011), 6011-6031.
- [3] Majzlik P, Strasky A, Adam V, *et al.*, *Int. J. Electrochem. Sci.*, 6 (2011), 2171-2191.
- [4] Villiers F, Ducruix C, Hugouvieux V, *et al.*, *Proteomics*, 11 (2011), 1650-1663.
- [5] Mittler R, *Trends Plant Sci.*, 7 (2002), 405-410.
- [6] Noctor G, Arisi A C M, Jouanin L, *et al.*, *J. Exp. Bot.*, 49 (1998), 623-647.
- [7] Baloun J, Adam V, Trmkova L, *et al.*, *Environ. Toxicol. Chem.*, 29 (2010), 497-500.
- [8] Babula P, Ryant P, Adam V, *et al.*, *Environ. Chem. Lett.*, 7 (2009), 353-361.
- [9] Kovarova J, Kizek R, Adam V, *et al.*, *Sensors*, 9 (2009), 4789-4803.
- [10] Potesil D, Petrlova J, Adam V, *et al.*, *J. Chromatogr. A*, 1084 (2005), 134-144.

INFLUENCE OF MYCORRHIZA ON PRODUCTION OF THIOL COMPOUNDS IN MAIZE EXPOSED TO COPPER

Marketa KOMINKOVA¹, Ondrej ZITKA¹, Miguel-Angel MERLOS²,
Nuria FERROL², Vojtech ADAM^{1,3}, Rene KIZEK^{1,3*}

¹ Department of Chemistry and Biochemistry, Faculty of Agronomy, Mendel University in Brno, Zemedelska 1, 613 00 Brno, Czech Republic

² Departamento de Microbiología del Suelo y Sistemas Simbióticos, Estación Experimental del Zaidín, CSIC, Profesor Albareda 1, Granada 18008, Spain

³ Central European Institute of Technology, Brno University of Technology, Technická 3058/10, 616 00 Brno, Czech Republic

*kizek@sci.muni.cz

ABSTRACT

In this work we studied the influence of mycorrhiza on the thiol content in maize, which was treated with concentrations of copper 0, 100 a 250 mg Cu/kg of soil. We determined total accumulated copper by plant by electrochemical method of differential pulse voltammetry in mineralized sample. The thiol content was determined in sample which was homogenized in phosphate buffer using HPLC method with electrochemical detection. We finally subtracted the concentration both of total copper and thiol contents of mycorrhizal variant from control one (nonmycorrhizal). Data for two species of Maize Oropesa and Orense were thus interpreted.

INTRODUCTION

Many of anthropogenic affects are more visible in less developed countries but consequences are touching rest of the global world. One of many cases is high concentrations of heavy metals, which are occurring in soil or water due to mining, industry, traffic or bad handling with dangerous waste. One of these is electronic integrated components where copper is widely occurring. On the other way copper is an essential element for normal growth of plants [1], but in higher concentrations it might be toxic for them [2]. There are many papers which are oriented on the study of influence of trace metals on vital or tolerant mechanisms of plants published every year [3, 4]. Possibilities of absorption of free copper and dissolved copper as ions in solution [5] and possibilities in pharmacy [6] has been reported as well. It was found that concentration of thiol compounds in plants [7], which were exposed to heavy metals is elevation up to critical level, which is differing dependently on the each organism, physically-chemical conditions and factors from the environment [8, 9]. The copper toxicity was previously studied [10]. This work was pointed to study of influence of micorrhiza on synthesis of thiol compounds (CYS, GSH, N-acetylcystein, GSSG, Des-Gly-PC, PC2, PC3, PC4, PC5) in two species of maize exposed to various concentrations of copper ions (0, 100, 250 mg/kg of soil).

2. MATERIAL AND METHODS

HPLC-ED thiol determination

HPLC-ED system consists of two chromatographic pumps Model 582 ESA (ESA Inc., Chelmsford, MA) (working range 0.001-9.999

ml min⁻¹) and chromatographic column with reverse phase Zorbax eclipse AAA C18 (150 × 4.6; 3,5 μm particles, Agilent Technologies, USA) and twelve-channel CoulArray electrochemical detector (Model 5600A, ESA, USA). Detector consists of three flow analytical chambers (Model 6210, ESA, USA). Each chamber contains four analytical cells. One analytical cell contains two referent (hydrogen-palladium), and two counters and one porous graphite working electrode. Electrochemical detector is situated in control module which is thermostated. Sample (20 μl) was injected by autosampler (Model 542, ESA, USA), which has thermostated space for column. Column was thermostated at 35°C. Flow rate of mobile phase was 1 ml min⁻¹. Mobile phase consists of A: trifluoroacetic acid (80 mM) a B: 100% Met-OH. Compounds were eluted by following linear increasing gradient: 0 - 7 min (3 %B), 8 - 15 min (15 %B), 25 min (30 %B), 28 - 33 min (98 %B). Detection was carried out at applied potential 900mV. Time of one analysis was 45 minutes.

Electrochemical determination of copper

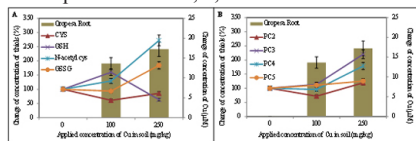
For electrochemical determination the sample (10 mg) was resuspended in 700 μl HNO₃ and 300 μl H₂O₂ (30 %). Sample was mineralized using MW Anton Paar, rotor MG-65. Further, we added 900 μl of acetic buffer 0.2 M in pH 5 to the 100 μl of the sample for subsequent determination. Concentration of copper was determined by differential pulse voltammetric with classical three electrode connection. We used hanging mercury electrode (HMDE) as working, platinum wire (Pt) as auxiliary electrode and Ag/AgCl/3 M KCl as referent electrode. Analysis

was carried out on 813 Compact Autosampler + 797 VA Computrace (Metrohm, CH). Amount of sample (500 µl) was refilled by 1500 µl acetic buffer pH 5 (0.2 M CH₃COOH + 0.2 M CH₃COONa). Overall volume of measuring cell was 2 ml. Parameters of electrochemical determination was as follows: potential scale from -1.3 V to +0.2 V, potential step 0,005 V, time of accumulation 120 s; accumulation potential -1.15, degassing of sample by argon was 90 s and time of equilibration was 5 s.

RESULTS AND DISCUSSION

For our experiment two species of maize (Orense sp. and Oropesa sp.) were used. These were grown in soil, which contained 0, 100 a 250 mg of copper per 1 kg of soil. Both species were also grown in mycorrhizal and nonmycorrhizal (control) variants. For determination of the thiol compounds and total copper the plants were divided into shoot and root part. For thiols determination 0.1g of fresh weight was homogenised with 1 ml of phosphate buffer in pH 7.5 (20 mM). Homogenate was centrifuged (20 minutes, 25000 rpm a 4°C). Supernatant was analysed by HPLC-ED. After obtaining the thiol data using peak areas of identified peaks in chromatograms we made subtraction of mycorrhizal variants from controls. Then we correlated obtained data with copper contents, which were analysed by differential pulse voltammetry after mineralization of the samples. Mycorrhizal variants by both studies species contained lower levels of copper than control. This dependence was observable very well in root but in shoots it was almost same. The thiol content was also well observable in roots of both Orense and Oropesa. But only in Oropesa we determined progressive accumulation of copper(II) ions into the plants, which is visible in Fig. 1. From these results it clearly follows that Oropesa species is well answering on the stress induced by copper ions than Orense.

Figure 1: (A) Comparison of percentage amount of thiols (left side) to the copper (right side) in roots of Oropesa for Cys, GSH, GSSG and N-acetyl-cys. (B) Comparison of percentage amount of thiols (left side) to the copper (right side) in roots of Oropesa for PC - 2, 3, 4 and 5.



CONCLUSION

From results obtained we can assume that mycorrhizal fungus can have relatively high influence on thiol biosynthesis in the plant. It was

observed that mycorrhizal variants had lower concentrations of total copper, which was slowed by mycorrhiza because transport of copper. In addition we were able to monitor the development of the important thiol concentration levels in dependence of total copper concentration thanks to two electrochemical methods, which were used for this study. Finally we found that two tested species of maize reacted very differentially on the mycorrhizal symbiosis during copper treatment, which was observable especially under the highest applied concentration of copper 250 mg/kg.

ACKNOWLEDGEMENT

The work has been supported by GAČR NANIMEL 102/08/1546 and CEITEC CZ.1.05/1.1.00/02.0068.

REFERENCES

- [1] Kopittke P M, Menzies N W, Plant and Soil, 279 (2006), 287-296.
- [2] Kopittke P M, Blamey F P C, Asher C J, et al., Journal of Experimental Botany, 61 (2010), 945-954.
- [3] Clemens S, Biochimie, 88 (2006), 1707-1719.
- [4] Babula P, Adam V, Opatrilova R, et al., Environmental Chemistry Letters, 6 (2008), 189-213.
- [5] Romkens P, Bouwman L A, Boon G T, Environmental Pollution, 106 (1999), 315-321.
- [6] Soudek P, Petrova S, Benesova D, et al., Chemicke Listy, 102 (2008), 346-352.
- [7] Grill E, Winnacker E L, Zenk M H, Method Enzymol., 205 (1991), 333-347.
- [8] Zitka O, Krystofova O, Sobrova P, et al., J. Hazard. Mater., 192 (2011), 794-800.
- [9] Xu H, Song P, Gu W B, et al., Ecotox. Environ. Safe., 74 (2011), 1685-1692.
- [10] Zitka O, Merlos M A, Adam V, et al., J. Hazard. Mater., 203 (2012), 257-263.

PREPARATION OF APOFERRITIN SILVER PHOSPHATE NANOPARTICLES

Pavel KOPEL^{1,2}, Dana DOSPIVOVA¹, David HYNEK^{1,2}, Jaromir HUBALEK^{2,3}, Libuse TRNKOVA^{2,4}, Marie STIBOROVA⁵, Tomas ECKSCHLAGER⁶, Vojtech ADAM^{1,2} and Rene KIZEK^{*1,2}

¹ Department of Chemistry and Biochemistry, Faculty of Agronomy, Mendel University in Brno, Zemedelska 1, 613 00 Brno, Czech Republic

² Central European Institute of Technology, Brno University of Technology, Technicka 3058/10, 616 00 Brno, Czech Republic

³ Department of Microelectronics, Faculty of Electrical Engineering and Communication, Brno University of Technology, Technicka 10, CZ-616 00 Brno, Czech Republic

⁴ Department of Chemistry, Masaryk University, Kotlarska 2, 611 37 Brno, Czech Republic

⁵ Department of Biochemistry, Faculty of Science, Charles University, Albertov 2030, CZ-128 40 Prague 2, Czech Republic

⁶ Department of Paediatric Haematology and Oncology, 2nd Faculty of Medicine, Charles University, V Uvalu 84, CZ-150 06 Prague 5, Czech Republic

*kizek@sci.muni.cz

ABSTRACT

Methicillin-resistant *Staphylococcus aureus* (MRSA) is responsible for several difficult-to-treat infections in humans. Therefore, it is not surprising that other ways how to treat these bacteria are looked for. Silver(I) ions and silver nanoparticles exhibited the highest antimicrobial activity against MRSA but their transporting to the place of needs and *in situ* determination is an issue. We studied the encapsulation of silver(I) ions into apoferritin as a possible way for transportation of these ions. Primarily we optimized the encapsulation conditions to prepare the most stable complex, which was subsequently utilized for treatment of *S. aureus*. Based on the results obtained it can be concluded that silver(I) ions remain enclosed in the apoferritin structure until decomposition of apoferritin by bacterial enzymatic apparatus occurs.

INTRODUCTION

Drug delivery systems have been designed for a number of drug-carrier platforms including synthetic (silica, polymers, gels) and natural (lipids, proteins, oligosaccharides) to solve the problems with drug transportation and to improve their pharmacological properties. Much attention is focused upon the protein nanomedicine. Naturally self-assembled protein subunits of the same protein or a combination of proteins make up a complete system that due to their biocompatibility and biodegradability shows low toxicity. A variety of proteins have been used and characterized including apoferritin, viruses, albumin, casein, soy protein, collagen and gelatin. [1]

The apoferritin is naturally occurring protein used to store iron and to keep it from building to toxic levels in cells. When the iron atoms are removed from ferritin, apoferritin is obtained. It is composed of 24 subunits, which assemble into hollow cages of 12 nm diameter with 8 nm cavity in the interior. In the cavity can be placed up to 4500 iron ions. Apoferritin contains 14

channels for transport of ions into and outside the interior. Due to its biological role of storing iron ions, the protein cage has been successfully modified to contain a variety of inorganic cores for therapeutic and imaging purposes. Moreover, apoferritins disassembly at low pH and reassembly again at higher pH. It also allows loading of insoluble and soluble compounds or drugs for delivery.

For example, drug delivery of cisplatin, carboplatin, oxaliplatin or daunomycin was studied by Xing [2] and Ma-Ham [3] and complexes of Gd [4, 5] and Eu [6] in apoferritin cage were tested as MRI contrast agents. Semiconductor nanoparticles CdS [7, 8] and PbS [9, 10], can be utilized for electrochemical biosensing, bioassays and product identification and phosphate nanoparticles prepared in apoferritin cavity as tags for bioanalytical or product identification were reported by Liu et al. [11-14] In this work we present our results on preparation of apoferritin nanoparticles, detection of loaded silver ions by differential pulse voltammetry on carbon paste electrode and its biological activity study.

MATERIALS AND METHODS

Preparation of apoferritin nanoparticles

Apoferritin solution (0.25 mg/ml, equine spleen, Sigma-Aldrich) was filtered through Microcon YM-30 to remove aggregates. Filtrate was diluted with ACS water and centrifuged on a centrifugal filter device Amicon Ultra 3k (Millipore) (centrifugation at 10000 rpm Centrifuge 5417R (Eppendorf, Germany), 10 °C). Apoferritin was washed several times with ACS water on the same filter. 500 μ l of 10 mM AgNO_3 was slowly added. The mixture was shaken (Vortex Genie2 (Scientific Industries, USA) for 1h to let the silver ions to diffuse into the cavity of the apoferritin. Silver phosphate inside the apoferritin was prepared by slow addition of 0.2 M phosphate buffer (pH = 7.0).

Electrochemical determination

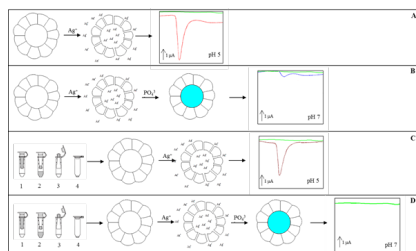
Measuring system CH Instruments (Austin, USA) was employed for the determination of silver. The working electrode was the carbon paste electrode (CPE), reference electrode was $\text{Ag}/\text{AgCl}/3\text{M KCl}$ and as an auxiliary electrode the platinum electrode was used. Samples were measured in 2 ml of acetate buffer (pH 5). Differential pulse voltammetry was used for the measurement with these parameters: range of potential from -0.2V to 0.5V, pulse amplitude 0.05V, pulse time 0.05s, unit step 0.001V.

RESULTS AND DISCUSSION

Purification and detection of apoferritin is given in Fig. 1. The supernatant was used for voltammetric measurements. Samples (Fig 1A) and (Fig 1B) were prepared with apoferritin without purification. Variant "A" represents mixture of apoferritin with silver(I) ions, when opening of apoferritin structure with subsequent release of silver ions occurs after addition of acetate buffer (pH = 5); released silver(I) ions were detected electrochemically. Variant "B" represents the same mixture, but with addition of phosphate, when higher pH (pH = 7) causes enclosure of apoferritin structure; this fact may clarify only minimal detected signal of silver(I) ions.

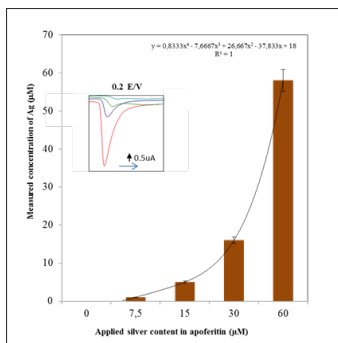
Fig. 1: Scheme of the preparation of silver phosphate nanoparticles: A) apoferritin with AgNO_3 (10 mM), silver ions diffused into the apoferritin cavity, electrochemical measurement of silver ions; B) apoferritin with AgNO_3 (10 mM) and phosphate buffer, formation of silver phosphate, electrochemical measurement of remaining silver ions; C) and D) the same procedure as in the part A) and B) but with the purification of apoferritin before addition of silver(I) ions. Purification of apoferritin: 1) apoferritin diluted with ACS water filled in filter device, 2) centrifugation at

10.000 rpm (10 °C), 3) recovery of purified apoferritin, 4) collected sample of apoferritin



Silver(I) ions surplus have to be removed to take advantage of apoferritin carrier as a mark based on heavy metal. Changes in silver(I) ions signals were caused by the binding-enclosure of silver(I) ions in apoferritin structure. Purification was based on the membrane permeability of metal ions. Final purified apoferritin provided no electrochemical signals. pH decrease leads to the opening of apoferritin structure and entering the silver(I) ions. pH increasing causes closure of apoferritin structure without release of metal ions from the structure. Subsequent change in pH enables repeated opening of the apoferritin structure under encapsulates ions release. Our experiment demonstrated that addition of acetate buffer (pH 5.0) leads to the release of silver(I) ions and their concentration is then electrochemically detected. Four concentrations of silver(I) ions (0, 7.5, 15, 30 and 60 μ M) were designed for examination of preparation procedure and electrochemical detection.

Fig. 2: Influence of dose Ag concentration to detected silver concentration after encapsulation in apoferritin structures. A – Dependence of dose concentration to detected silver concentration (as a percent of dose concentration); B – measured concentration of Ag relates to dose amount of silver ions. Measuring method was DPV with these parameters: Initial potential -0.2V, end potential -0.5V, amplitude 0.05V, pulse width 0.005s, pulse period 0.05s, sensitivity 1.10-5 A/V. Supporting electrolyte was acetate buffer pH 5.



[14] Wu H, Engelhard M H, Wang J, *et al.*, *J. Mater. Chem.*, 18 (2008), 1779-1783.

CONCLUSION

Biotechnological applications based on nanotechnology approaches are modern tools for the targeted transport of active compounds/drugs with only minimal risk and possible damage to the non-targeted cells and tissues. Proposed apoferritin-based silver ion carrier will be further applied in therapeutic targeting of bacterial cells.

ACKNOWLEDGEMENTS

The financial support from the following project CYTORES GA ČR P301/10/0356, NANOSEMED GA AV KAN208130801, Nano Ceva TA ČR TA01010088 and CEITEC CZ.1.05/1.1.00/02.0068 is highly acknowledged.

REFERENCES

- [1] MaHam A, Tang Z W, Wu H, *et al.*, *Small*, 5 (2009), 1706-1721.
- [2] Xing R M, Wang X Y, Zhang C L, *et al.*, *J. Inorg. Biochem.*, 103 (2009), 1039-1044.
- [3] Ma-Ham A H, Wu H, Wang J, *et al.*, *J. Mater. Chem.*, 21 (2011), 8700-8708.
- [4] Sanchez P, Valero E, Galvez N, *et al.*, *Dalton Trans.*, (2009), 800-804.
- [5] Makino A, Harada H, Okada T, *et al.*, *Nanomed.-Nanotechnol. Biol. Med.*, 7 (2011), 638-646.
- [6] Liu X Y, Ye Z Q, Wei W, *et al.*, *Chem. Commun.*, 47 (2011), 8139-8141.
- [7] Iwahori K, Yamashita I, *Nanotechnology*, 19 (2008).
- [8] Naito M, Iwahori K, Miura A, *et al.*, *Angew. Chem.-Int. Edit.*, 49 (2010), 7006-7009.
- [9] Turyanska L, Bradshaw T D, Sharpe J, *et al.*, *Small*, 5 (2009), 1738-1741.
- [10] Turyanska L, Bradshaw T D, Li M, *et al.*, *J. Mater. Chem.*, 22 (2012), 660-665.
- [11] Liu G D, Wu H, Wang J, *et al.*, *Small*, 2 (2006), 1139-1143.
- [12] Liu G D, Wu H, Dohnalkova A, *et al.*, *Anal. Chem.*, 79 (2007), 5614-5619.
- [13] Wu H, Wang J, Wang Z M, *et al.*, *J. Nanosci. Nanotechnol.*, 8 (2008), 2316-2322.

PREPARATION OF METALLOTHIONEIN OLIGONUCLEOTIDE QUANTUM DOTS COMPLEXES

Pavel KOPEL^{1,2}, Ludmila KREJCOVA^{1,2}, David HYNEK^{1,2}, Vojtech ADAM^{1,2}, Jaromir HUBALEK^{2,3}, Libuse TRNKOVA^{3,4}, Rene KIZEK^{*1,2}

¹Department of Chemistry and Biochemistry, Faculty of Agronomy, Mendel University in Brno, Zemedelska 1, 613 00 Brno, Czech Republic

²Central European Institute of Technology, Brno University of Technology, Technicka 3058/10, 616 00 Brno, Czech Republic

³Department of Microelectronics, Faculty of Electrical Engineering and Communication, Brno University of Technology, Technicka 10, CZ-616 00 Brno, Czech Republic

⁴Department of Chemistry, Masaryk University, Kotlarska 2, 611 37 Brno, Czech Republic

*kizek@sci.muni.cz

ABSTRACT

Nanotechnology opens new possibilities for the application of nanoparticles in biosensors and bioassays. The aim of this work was based on electrochemical determination of silver(I) ions using various types of modified carbon paste electrodes with different content of carbon nanoparticles. The most suitable procedure was used for determination of free silver(I) ions capped in the apoferritin structure.

INTRODUCTION

Nanotechnology opens new possibilities for the application of nanoparticles in biosensors and bioassays. Especially electrochemical biosensors and bioassays have received considerable interest due to high performance, miniaturization and low cost. [1] Semiconductor nanoparticles also called quantum dots (QD) are of particular interest because of their special properties i.e. size-tuneable fluorescence [2, 3]. They can be applied not only for electrochemical detection but also for optical biodetection. From the electrochemical point of view, their redox properties are especially sensitive for stripping analysis and thus low detection limits can be achieved. CdS nanoparticles functionalized with thiolated oligonucleotides were used for binding to target DNA. Their photocurrents generated by the DNA-cross-linked array were used for the quantitative detection of DNA. [4/

Wang et al. developed electrochemical coding technology based on several semiconductor nanoparticle labels. They employed CdS, PbS and ZnS QD for multiple DNA detection. [5, 6] The three encoding nanoparticles were used to differentiate the signals of three DNA targets in connection with a sandwich hybridization assay and stripping voltammetry of the corresponding heavy metals. The new multi-target sandwich hybridization assay involves a dual hybridization event, with probes linked to the QD marker. The targets can be detected simultaneously. [6] Liu et al. [7] reported an electrochemical im-

munoassay protocol for the simultaneous measurements of multiple protein targets based on the use of CdS, ZnS and PbS QDs. QDs can be also delivered to a target by a small molecules – viruses or proteins like apoferritin. CdS QDs in apoferritin cavity were reported by Wong [8] and Iwahori [9] and PbS QDs with application for imaging in biology and medicine were reported by Turyanska et. al. [10-12]. The aim of this work was based on electrochemical determination of silver(I) ions using various types of modified carbon paste electrodes with different content of carbon nanoparticles. The most suitable procedure was used for determination of free silver(I) ions capped in the apoferritin structure.

MATERIALS AND METHODS

Synthesis of QD and complexes

Preparation of CdS quantum dots (QDs)

All chemicals were purchased from Sigma-Aldrich and used without further purification. CdS quantum dots (QDs) were prepared with a slightly modified method published in [1]. Cadmium nitrate tetrahydrate $\text{Cd}(\text{NO}_3)_2 \cdot 4\text{H}_2\text{O}$ (0.0308 g, 0.1 mM) was dissolved in ACS water (25 ml). 3-mercaptopropionic acid (35 μl , 0.4 mM) was slowly added to stirred solution. Afterwards, pH was adjusted to 9.11 with 1M NH_3 (1.5 ml). Sodium sulphide nanohydrate $\text{Na}_2\text{S} \cdot 9\text{H}_2\text{O}$ (0.024 g, 0.1 mM) in 23 ml of ACS water was poured into the first solution with vigorous stirring. Obtained yellow solution was stirred for 1 h. CdS QDs were stored in dark at 4 °C.

Oligonucleotide-SH (ODN-SH) labelling with CdS QD

ODN-SH (100 μ l, 100 μ g/ml) was mixed with a solution of CdS QD (100 μ l). This mixture was shaken for 24 h at room temperature (Vortex Genie2 (Scientific Industries, USA)). Subsequently, solution was dialyzed against 2000 ml of miliQ water (24 h, 4 $^{\circ}$ C) on Millipore membrane filter 0.025 μ m VSWP. During dialysis the sample was diluted to 800 μ l. Diluted sample was concentrated to 500 μ l final volume on a centrifugal filter device Amicon Ultra 3k (Millipore). Centrifuge 5417R (Eppendorf, Germany) was utilized with following parameters 15 min, 4500 rpm, 15 $^{\circ}$ C.

Electrochemical determination

Measuring system 663 VA Stand, 800 Dosino, 846 Dosing Interface, Autolab was employed. To evaluate the results the GPES software was used. A standard cell with three electrodes was used for the measurement. A hanging mercury drop electrode (HMDE) with a drop area of 0.4 mm² was employed as the working electrode. An Ag/AgCl/3M KCl electrode served as the reference electrode. Pt electrode was used as the auxiliary electrode. Differential pulse voltammetry was used for the measurement with these parameters: a) Detection of CA peak (Cd-SH-ODN) initial potential 0 V; end potential -1.85 V; frequency 10 Hz; potential step 0.005 V; amplitude 0.025 V; b) Detection of Cd peak (Cd-SH-ODN) initial potential of -0.9 V; end potential -0.45 V; deposition potential -0.9 V; duration 240 s; equilibration time 5 s; modulation time 0.06; time interval 0.2 s; potential step 0.002 V; modulation amplitude 0.025 V

RESULTS AND DISCUSSION

In this work we present our results on preparation of cadmium sulphide nanoparticles and their further use as a marker of oligonucleotides. Synthesis is based on a reaction of cadmium ions with sulphides in the presence of mercaptopropionic acid, which prevents nanoparticles to form aggregates and to keep the nanoparticles water soluble. High pH also prevents aggregate formation. Thus prepared CdS QDs were utilized to form a complex with thiolated oligonucleotide. Complex was formed during shaking of QDs with SH-ODN at room temperature. Dialysis was used for purification of reaction product from unreacted species and centrifugal filter device served for volume reduction.

SH-ODN and SH-ODN QDs complexes were studied by electrochemical methods. Time of accumulation was studied first followed by concentration dependence on height of CA and Cd peaks. Results are given in Figures 1 and 2, respectively. In Figure 1, there are two curves obtained for SH-ODN and complex with CdS QDs

in concentration range of 0.0019 – 2 μ g/ml. We can observe that height of peaks of simple SH-ODN is higher to that of the complex. The data correlate well with calculated amount of molecules. Calibration curve, for cadmium in SH-ODN QDs complex obtained in 0.35 – 67.8 μ g/ml range, shows linear dependence. It was proved by voltammetric measurements that CdS QDs were successfully bounded with thiolated oligonucleotide.

Fig. 1: Dependence of height of CA peak on SH-ODN concentration and number of molecules. Red squares relates to unmodified SH-ODN, whereas blue squares are experimental data for CdS SH-ODN complex. Differential pulse voltammetry – HMDE working electrode, Ag/AgCl/3M KCl, Pt auxiliary electrode.

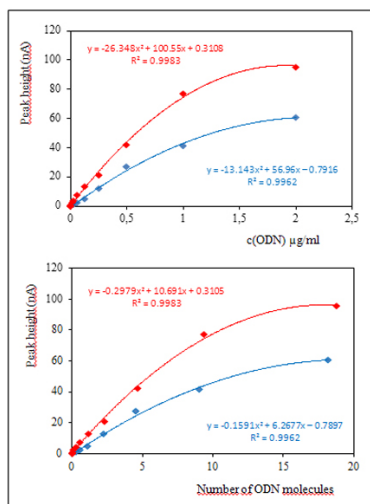
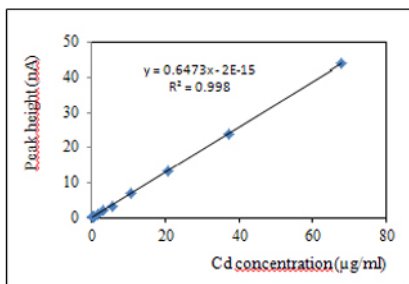


Fig. 2: Calibration curve of cadmium in CdS SH-ODN complex. Differential pulse voltammetry – HMDE working electrode, Ag/AgCl/3M KCl, Pt auxiliary electrode, initial potential of -0.9 V; end potential -0.45 V; deposition potential -0.9 V; accumulation time 240 s



CONCLUSION

Cadmium sulphide nanoparticles with mercaptopropionic acid were successfully prepared and used for labelling of thiolated oligonucleotides. For characterization of CdS SH-ODN electrochemical methods were used. These labels will be further tested and used for hybridization with biological samples and finally applied in diagnosis.

ACKNOWLEDGEMENTS

The work has been supported by NANIMEL GA CR 102/08/1546, CEITEC CZ.1.05/1.1.00/02.0068, Nano Ceva TA ČR TA01010088 and NANOSEMED GA AV KAN208130801

REFERENCES

- [1] Liu G D, Wang J, Wu H, *et al.*, *Electroanalysis*, 19 (2007), 777-785.
- [2] Drbohlavova J, Chomoucka J, Hrdy R, *et al.*, *Int. J. Electrochem. Sci.*, 7 (2012), 1424-1432.
- [3] Drbohlavova J, Vorozhtsova M, Hrdy R, *et al.*, *Nanoscale Res. Lett.*, 7 (2012).
- [4] Willner I, Patolsky F, Wasserman J, *Angew. Chem.-Int. Edit.*, 40 (2001), 1861-1864.
- [5] Wang J, Liu G D, Polsky R, *et al.*, *Electrochem. Commun.*, 4 (2002), 722-726.
- [6] Wang J, Liu G D, Merkoci A, *J. Am. Chem. Soc.*, 125 (2003), 3214-3215.
- [7] Liu G D, Wang J, Kim J, *et al.*, *Anal. Chem.*, 76 (2004), 7126-7130.
- [8] Wong K K W, Mann S, *Adv. Mater.*, 8 (1996), 928-&.
- [9] Iwahori K, Yamashita I, *Nanotechnology*, 19 (2008).
- [10] Hennequin B, Turyanska L, Ben T, *et al.*, *Adv. Mater.*, 20 (2008), 3592-+.
- [11] Turyanska L, Bradshaw T D, Sharpe J, *et al.*, *Small*, 5 (2009), 1738-1741.
- [12] Turyanska L, Bradshaw T D, Li M, *et al.*, *J. Mater. Chem.*, 22 (2012), 660-665.

ISOLATION AND DETECTION OF NUCLEIC ACID INFLUENZA VIRUSES

Ludmila KREJCOVA¹, David HYNEK^{1,2}, Jana DRBOHLAVOVA^{2,3}, Pavel KOPEL^{1,2}, Libuse TRNKOVA^{2,4}, Jaromir HUBALEK^{2,3}, Vojtech ADAM^{1,2} and Rene KIZEK^{*1,2}

¹ Department of Chemistry and Biochemistry, Faculty of Agronomy, Mendel University in Brno, Zemedelska 1, 613 00 Brno, Czech Republic

² Central European Institute of Technology, Brno University of Technology, Technicka 3058/10, 616 00 Brno, Czech Republic

³ Department of Microelectronics, Faculty of Electrical Engineering and Communication, Brno University of Technology, Technicka 10, CZ-616 00 Brno, Czech Republic

⁴ Department of Chemistry, Masaryk University, Kotlarska 2, 611 37 Brno, Czech Republic

*kizek@sci.muni.cz

ABSTRACT

There is the design of isolation and detection of influenza viruses ODN in this study. Usage of conjugated MPs and QDs-based hybridization target molecule and their application for the detection of the avian influenza virus (H5N1) is presented. For analysis of oligonucleotide labelled with Cd QDs two electrochemical methods were applied. For cadmium (Cd peak) differential pulse voltammetry was used, for oligonucleotide (CA peak) square wave voltammetry (SWV) was applied.

INTRODUCTION

Influenza is an infectious disease caused by RNA viruses of the family *Orthomyxoviridae*. It spreads by droplet infection in seasonal epidemics. These epidemics occur regularly during the winter months with a six-month gap between the northern and southern hemispheres. The most important measure against infection is prevention in the form of vaccination. Influenza vaccine exists, but does not protect for whole life, is only effective for one year. This is due to mutational changes in the structure of the virus changes so that the reuse of the same vaccine the following year, this would be against a mutated virus did not protect [1]. Despite prevention, the flu epidemic results in 250 000 to 500 000 deaths annually. The greatest influenza pandemic was called Spanish flu, which took place in late 1918 and 1919, which is described as the worst pandemic (20 to 50 million victims) in human history at all [2].

The aim of this study was isolation and detection of CdS quantum dots labelled influenza oligonucleotide-SH (ODN-SH) H5N1. Isolation of QDs labelling influenza oligonucleotide (ODN-SH-Cd) was performed with using of nanoparticles and dual hybridization. The combination of nanoparticles and QDs for detection of influenza virus is a good tool [3]. Paramagnetic (MPs) or superparamagnetic particles are able to respond to external magnetic field, which is used for efficient separation of analytes from liquid samples [4, 5]. Depending on the size these objects are divided into micro- and nanoparticles. The advantage of magnetic separation is the possibility of modifying the surface of

MPs, and thus the elimination of unwanted interfering adsorption of biomolecules [6-8]. Isolation of biomolecules using paramagnetic particles followed by electrochemical detection, is a way of detection, which is less time-consuming and laboratory equipment and is highly sensitive to even small quantities of sample [9, 10].

For the detection of isolated Cd labelling oligonucleotides was chose electrochemical analysis. For analysis of Cd oligonucleotide two electrochemical methods was used. Differential pulse voltammetry was used for detection of cadmium (Cd peak), Square wave voltammetry was used for detection of oligonucleotide (peak CA). Electrochemical methods are generally characterized by the dependence on the current flowing through the electrode potential - polarization curve. Differential pulse voltammetry is one of the most widely used electroanalytical method. In this method, the potential grows linearly in time and is interspersed with voltage pulse amplitude from 10 to 100 mV. The voltage pulse is applied at the end of life mercury drops. Records the difference currents measured before entering the pulse and at the end. In contrast, square-wave voltammetry (SWV) using positively and negatively oriented towards Potential Directive. SWV allows unlike DPV work in the high rate of change of potential and is particularly suitable for sensitive detection of reversible electrochemical systems [9].

MATERIAL AND METHODS

First step was preparation of CdS quantum dots (Cd QDs). Further step was preparation of influenza oligonucleotide-SH (ODN-SH) and labelling by CdS QDs. The last step was isolati-

on and detection of ODN-SH-Cd.

Preparation of CdS quantum dots (Cd QDs)

All chemicals were purchased from Sigma-Aldrich and used without further purification. CdS quantum dots (QDs) were prepared with a slightly modified method published in [11]. Cadmium nitrate tetrahydrate Cd (NO₃)₂·4H₂O (0.03085 g, 0.1 mM) was dissolved in ACS water (25 ml). 3-mercaptopropionic acid (35 µl, 0.4 mM) was slowly added to stirred solution. Afterwards, pH was adjusted to 9.11 with 1M NH₃ (1.5 ml). Sodium sulphide nanohydrate Na₂S·9H₂O (0.02402 g, 0.1 mM) in 23 ml of ACS water was poured into the first solution with vigorous stirring. Obtained yellow solution was stirred for 1 h. CdS QDs were stored in dark at 4 °C.

Preparation of CdS QDs labeled influenza oligonucleotide

ODN-SH H5N1 (100 µl, 100 µg/ml) was mixed with a solution of CdS QDs (100 µl). This mixture was shaken for 24 h at room temperature (Vortex Genie2 (Scientific Industries, USA)). Subsequently, solution was dialysed against 2000 ml of MilliQ water (24 h, 4 °C) on Millipore membrane filter 0.025 µm VSWP. During dialysis the sample was diluted to 800 µl. Diluted sample was concentrated to 500 µl final volume on a centrifugal filter device Amicon Ultra 3k (Millipore). Centrifuge 5417R (Eppendorf, Germany) was utilized with following parameters 15 min, 4500 rpm, 15 °C.

Isolation of Cd labelling influenza oligonucleotide (ODN-SH-Cd)

All chemicals and oligonucleotides were purchased from Sigma-Aldrich and used without further purification. For oligonucleotide isolation automatic pipetting station EP motion 5075 (Eppendorf, Germany) with original devices was used.

The buffers used in this part of experiments were as follows – phosphate buffer I: 0.1 M NaCl + 0.05 M Na₂HPO₄ + 0.05 M NaH₂PO₄; phosphate buffer II: 0.2 M NaCl + 0.1 M Na₂HPO₄ + 0.1 M NaH₂PO₄; hybridization solution: 100 mM Na₂HPO₄ + 100 mM NaH₂PO₄; 0.5 M NaCl, 0.6 M Guanidium thiocyanate, 0.15 M Trizma base adjusted by HCl on pH of 7.5.

In each well in the plate (PCR 96, Eppendorf, Germany) 10 µl of Dynabeads Oligo dT₂₅ (Invitrogen, Oslo) was dispensing, plate was subsequently transfer to the magnet and stored solution from nanoparticles was aspirate to waste, beads were further washed 3 times by 20 µl of phosphate buffer I. The next step was first hybridization. In each wells 10 µl of poly A labelling anti sense H5N1 oligonucleotide and 10 µl of hybridization buffer (0.1 M phosphate buffer, 0.6 M guanidine

thiokynate, 0.15 M Tris) was added and the plate was incubated (15 min, 25 °C, pipetting), followed by washing by 20 µl phosphate buffer I

The next step was second hybridization. In each wells was added 10 µl of Cd labelled H5N1 oligonucleotide and 10 µl of hybridization buffer (0.1 M phosphate buffer, 0.6 M guanidine thiocyanate, 0.15M Tris) and the plate was incubated (15 min, 25 °C, pipetting), followed by washing by 20 µl phosphate buffer I. Further, 30 µl of elution solution (phosphate buffer II) was dispensed followed incubation (5 min, 85 °C, pipetting). After elution was plate transfer to the magnet, and product from each well was transferred to separate well. Isolation of H5N1 oligonucleotide was followed by electrochemical detection.

Detection of Cd labelling influenza oligonucleotide (ODN-SH-Cd)

For the detection of Cd labelled influenza oligonucleotide (ODN-SH-Cd) was selected electrochemical analysis. For electrochemical detection two voltammetric methods were used. Differential pulse voltammetry was used for detection of cadmium (Cd peak), for detection of oligonucleotide (CA peak) square wave voltammetry was selected. Both methods were optimized. Limit of detection for Cd and CA peak was established.

Method for detection of CA peak (Cd-SH-ODN)

For detection of CA peak we used square wave voltammetry (adsorptive transfer technology). Measurements were carried out in an electrochemical cell in the classic three-electrode system, where the mercury electrode (HMDE) was a working electrode, reference electrode was an argentochloride (Ag / Ag Cl/3M KCl) electrode and auxiliary electrode was a carbon electrode. All measurements were performed in acetate buffer 0.2 M CH₃COOH + 0.2 M CH₃COONa (pH 5.0) at temperature 25°C. Samples were deoxygenated by argon (99.99%, 120s). Equipment: 663 VA Stand, 800 Dosino, 846 Dosing Interface, Autolab. To evaluate the results the GPES software was used. *Parameters*: initial potential 0 V; end potential - 1.85 V; frequency 10 Hz; potential step 0.005 V; amplitude 0.025 V.

Method for detection of Cd peak (Cd-SH-ODN)

For electrochemical detection of Cd peak we used the differential pulse voltammetry. Measurements were performed in an electrochemical cell in the classic three electrode, where the mercury electrode (SMDE) was a working electrode, reference electrode was

an argentochloride (Ag / Ag Cl/3M KCl) electrode and auxiliary electrode was a carbon electrode. All measurements were performed in acetate buffer (pH 5.0) at temperature 25°C. Samples were deoxygenated by argon (99.99%, 120s). Equipment: 663 VA Stand, 800 Dosino, 846 Dosing Interface. Autolab. To evaluate the results the GPES software was used. *Parameters:* initial potential of -0.9 V; end potential -0.45 V; deposition potential -0.9 V; duration 240 s; equilibration time 5 s; modulation time 0.06; time interval 0.2 s; potential step 0.002 V; modulation amplitude 0.025

RESULTS AND DISCUSSION

In this study, we described the design of conjugated MPs and QDs-based hybridization target molecule and their application for the detection of the avian influenza virus (H5N1). The hybridization complex contains four items: (i) MPs modified oligo probes (oligo anti-sense) (ii) Cd QDs labelling of target oligonucleotide, (iii) capturing of target QDs labelled oligonucleotide derived from a influenza sequence, and (iv) electrochemical detection of metal from QDs marker and electrochemical detection of influenza derived oligonucleotide.

QDs labelling of target oligonucleotide in their combination with isolation by MPs are sensitive diagnostics tool for detection of influenza virus. In order to examine the usage of MPs and QDs as tools in nucleic acid hybridization assays, we designed a MP and QD-based hybridization assay for the detection of avian influenza H5N1 respectively H5N1 derived oligonucleotide. Figure 1 shows a schematic view of the hybridization procedure for the MP and QD-based probes with the target. Figure 2 shows the influence of temperature on amount of isolated nucleic acids. The temperature optimum of second hybridization was 25°C.

Figure 1: Scheme of H5N1(ODN-SH-CdS) electrochemical detection. A – AntiH5N1 binding to magnetic particle, B – addition of ODN-SH-Cd, C – binding of ODN-SH-Cd to magnetic particle with AntiH5N1, D – electrochemical detection of ODN and Cd.

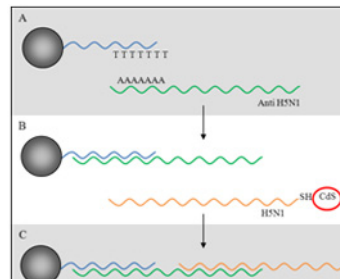
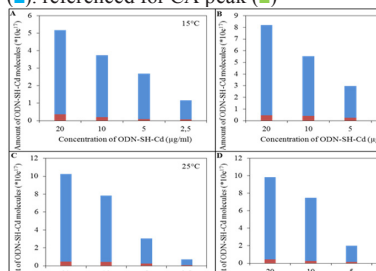
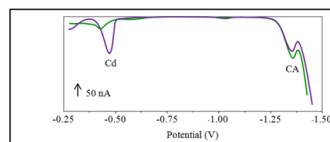


Figure 2: Influence of temperature of second hybridization **A** (15°C); **B** (20°C); **C** (25°C); **D** (30°C); referenced for Cd peak (■), referenced for CA peak (■)



Electrochemical characterization ODN and ODN-SH-Cd (Fig. 3) shows considerable differences in voltammograms. ODN-SH voltammogram shows only one peak (peak CA) at the potential -1.35 V. Oligonucleotide ODN-SH-Cd shows two peaks. The first one corresponding to cadmium (Cd peak, potential -0.58 V) and the second one corresponds to the nucleic acid (CA peak, potential -1.36 V). There are also significant differences between CA peaks of Cd labelled and non labelled oligonucleotides. Non labelled ODN reported higher and closer CA peak then Cd labelled ODN. Also peak position is divergent (labelled: -1.362V, non labelled: -1.348V)

Figure 3: Comparison of real voltammograms of ODN-SH (-) and ODN-SH-Cd (-)



The measured parameters were CA and Cd peak height. With increasing temperature amount of hybridized target (ODN-SH-Cd) and thus CA and Cd peak height increased. We have demonstrated the influence of hybridization temperature on the height of the CA and Cd peak.

CONCLUSION

It was suggested and optimized method for isolation of Cd labelling influenza oligonucleotide using automated pipetting station. It was observed the effect of hybridization temperature (second hybridiza-

tion) on CA and Cd peak height. More sensitive response provides cadmium from QDs oligonucleotide marker, than influenza derived target oligonucleotide. With increasing hybridization temperature amount of hybridized ODN-SH-Cd and thus CA and Cd peak height increased. The temperature optimum of second hybridization was 25°C.

ACKNOWLEDGEMENT

The financial support from the following project NANOLABSYS CZ.1.07/2.3/00/20.148, GA ČR 102/10/P618, NANIMEL GA ČR 102/08/1546 and CEITEC CZ.1.05/1.1.00/02.0068 is highly acknowledged.

REFERENCES

- [1] Feng Z L, Towers S, Yang Y D, Aaps J., 13 (2011), 427-437.
- [2] Ghendon Y, Eur. J. Epidemiol., 10 (1994), 451-453.
- [3] Bakalova R, Zhelev Z, Ohba H, *et al.*, J. Am. Chem. Soc., 127 (2005), 11328-11335.
- [4] Agrawal A, Sathe T, Nie S M, J. Agric. Food Chem., 55 (2007), 3778-3782.
- [5] Spiro A, Lowe M, Brown D, Appl. Environ. Microbiol., 66 (2000), 4258-4265.
- [6] Hsing I M, Xu Y, Zhao W T, Electroanalysis, 19 (2007), 755-768.
- [7] Katz E, Willner I, Angew. Chem.-Int. Edit., 43 (2004), 6042-6108.
- [8] Chomoucka J, Drbohlavova J, Masarik M, *et al.*, Int. J. Nanotechnol., in press (2012).
- [9] Adam V, Huska D, Hubalek J, *et al.*, Microfluid. Nanofluid., 8 (2010), 329-339.
- [10] Halfpenny K C, Wright D W, Wiley Interdiscip. Rev.-Nanomed. Nanobiotechnol., 2 (2010), 277-290.
- [11] Li H, Shih W Y, Shih W H, Ind. Eng. Chem. Res., 46 (2007), 2013-2019.

ELECTROCHEMICAL DETECTION OF IRON IN BLOOD SAMPLES OF MINIPIGS WITH MELANOMA

Ludmila KREJCOVA¹, Monika KREMPLOVA¹, David HYNEK^{1,2}, Vratislav HORAK³, Jiri SOCHOR^{1,2}, Natalia CERNEJ¹, Libuse TRNKOVA^{2,5}, Jaromir HUBALEK^{2,4}, Vojtech ADAM^{1,2} and Rene KIZEK^{*1,2}

¹ Department of Chemistry and Biochemistry, Faculty of Agronomy, Mendel University in Brno, Zemedelska 1, 613 00 Brno, Czech Republic

² Central European Institute of Technology, Brno University of Technology, Technicka 3058/10, 616 00 Brno, Czech Republic

³ Laboratory of Tumour Biology, Department of Animal Embryology, Cell and Tissue Differentiation, Institute of Animal Physiology and Genetics, Academy of Sciences of the Czech Republic, v.v.i., CZ-277 21 Libechov, Czech Republic

⁴ Department of Microelectronics, Faculty of Electrical Engineering and Communication, Brno University of Technology, Technicka 10, CZ-616 00 Brno, Czech Republic

Department of Chemistry, Masaryk University, Kotlarska 2, 611 37 Brno, Czech Republic
*kizek@sci.muni.cz

ABSTRACT

The aim of this study was the determination of iron in erythrocytes at Me-Lim pigs. Influence of melanoma stadium to amount of iron (erythrocytes) in blood from Me-Lim pigs was studied. There was employed a new electrochemical automation system for iron determination.

INTRODUCTION

Electrochemical methods allow us to detect peptides, proteins, nucleic acids, drugs and metals [1-3]. In case of metal determination voltammetric analysis is most commonly used [4-6]. Nanomolar concentrations of metal is possible to detect and limits of detection are lower than 10^{-10} M [7]. This fact shows that combination of catalytic and adsorptive processes can lead to detection limit in pM range [8].

One of most important metals, which is contained in biological samples, is iron. Iron is an important element in environmental and in many biological systems [9]. Iron has beneficial or deleterious effects on the properties of many substances, biological systems and organisms. Its presence is in haemoglobin synthesis and oxidative processes of living tissues, provides a fundamental structure of myoglobin, and many co-factors involved in enzymes activities [9]. For iron detection there are commonly used methods as voltammetry [10], chromatography, spectrophotometric methods, capillary electrophoresis, controlled potential coulometry and potentiometry [11]. Measuring of iron in various samples (clinical, environmental, industrial, and pharmaceutical) is very common. We focused our attention to automated electrochemical measuring system and perform program for this instrument. To test of this system we decided to detect iron in erythrocytes from blood samples of mini pigs.

MATERIALS AND METHODS

Preparation of samples

Blood samples were centrifuged (2000 rpm, 10 min). Followed by aspirate away plasma, we used for analysis only erythrocytes. For the first it was weighed 0.1 g of erythrocytes into Eppendorf tubes. After that the sample was frozen with liquid nitrogen for 5 min to disrupt the cells. Then we added 500 μ l mM HCl and sample was ultrasounded for 2 minutes at 40 W using needle (Bandelin, Germany). Homogenates were then vortexed for 10 minutes at 400 rpm (Genie, USA) and then centrifuged for 30 minutes at 16,000 rpm (Eppendorf, Germany) prior to analysis. The obtained supernatant (100 μ l) was pipetted into Eppendorf tubes with 100 μ l TFA solution (20% trifluoroacetic acid). Diluted sample was then centrifuged for 10 minutes at 16,000 rpm (Eppendorf, Germany) and supernatant (10 μ l) was used for electrochemical determination. For this determination it is necessary to used mixture of sample (20 μ l) and triethanolamine buffer (2380 μ l).

Determination of iron

Determination of Fe ions were performed with 797 VA Stand instrument connected to 889 IC Sample Center (Metrohm, Switzerland). The analyser (797 VA Computrace from Metrohm, Switzerland) employs a classical three-electrode system with a hanging mercury drop electrode (HMDE) working electrode: 0.4 mm², Ag/AgCl/3MKCl as reference electrode, and a platinum auxiliary electrode. The following setup assembled of automated voltammetric analysis

is supplied by Metrohm (Switzerland). A sample changer (Metrohm 889 IC Sample Center) performs the sequential analysis of 96 samples in plastic test tubes. For the addition of standard solutions and reagents, automatic dispenser (Metrohm 800 Dosimat) is used, while peristaltic pump station (Metrohm 843 Pump Station) is employed for transferring the rinsing solution in the cell and for removing solutions from the voltammetric cell. Automatic dispenser and peristaltic pump station are controlled by central unit (Metrohm 846 Dosing Interface). Differential pulse voltammetric measurements were carried out under the following parameters: deoxygenating with argon 120 s; start potential -0.6 V; end potential -1.3 V; deposition potential 0V; accumulation time 0 s; pulse amplitude 0.05 V; pulse time 0.06 s; step potential 5.951 mV; time of step potential 0.1 s; volume of injected sample 20 μ l; cell was filled with 2400 ml of electrolyte (0.1M KBrO_3 ; 0.3M NaOH; 0.01M triethanolamin (TEA)).

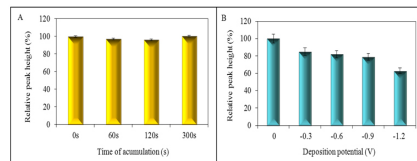
RESULTS AND DISCUSSION

Influence of melanoma to amount of iron (erythrocytes) in blood from Me-Lim pigs was studied. Group one was control group of health pigs, group two were pigs with melanoma progress. We demonstrate dependence of iron concentration in erythrocytes on melanoma stadium at MeLiM pigs. There was used differential pulse voltammetry for iron determination. After optimization of measuring method the whole measuring procedure was automated. Our system consists from four basic parts (electrochemical measuring stand (797 VA Computrace, Metrohm), autosampler (889 IC Sample Centre), dosage unit (800 Dosino Unit, 846 Dosing Interface, both Metrohm) and pumps (843 Pump Station, Metrohm)). Electrochemical analysis of biological samples is very often connected with one special need, and it is cooling of samples. This system is in connection of cooling sample area in autosampler and possibility of samples injection of units of μ l. The second need, as important as first, is automation of measurement process.

First step of our experiment was suggesting method for electrochemical determination of iron in erythrocytes, followed by optimization two basic parameters. Optimized parameters were time of accumulation (0; 60; 120; 300 s, Fig. 1A) and deposition potential (0; -0.3; -0.6; -0.9; -1.2 V, Fig. 1B). Selected parameters were 0 s for time of accumulation and 0 V for deposition potential. Samples were measured in solutions consisted from 20 μ l of samples and 2400 μ l of electrolyte (KBrO_3 + NaOH + TEA). As a measure method differential pulse voltammetry was applied. As a supporting electrolyte mixture of 0.1M KBrO_3 ;

0.3M NaOH and 0.01M triethanolamin was used. Calibration curve is shown in Fig. 2.

Figure 1: Optimization of method for iron determination, triethanolamine buffer (KBrO_3 0.1M, NaOH 0.3M, TEA 0.01M) was use as a supporting electrolyte. Influence of accumulation time on iron signal intensity (A). Dependence of signal intensity on deposition potential (B).



For measuring of real samples on automatic electrochemical system samples of MeLiM pigs blood were applied. Measured samples were compared with calibration curve of Fe, which was measured by the same method as electrolyte. The control group with healthy pigs had concentration of iron in erythrocytes three times higher than group with melanoma progress. Successful application of new electrochemical system to iron determination in real biological samples was proved.

Figure 2: Calibration curve of Fe measured in automatic system. Voltammograms for various iron concentrations (inset). Differential pulse voltammetry as measure method was applied. As a supporting electrolyte mixture of KBrO_3 + NaOH + TEA was used.

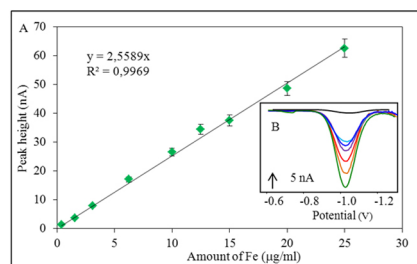
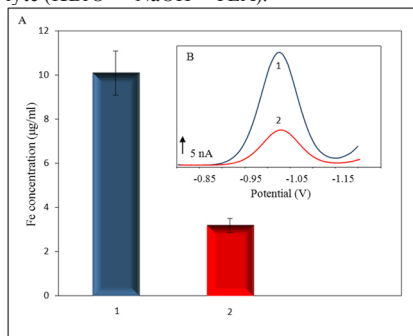


Figure 3: Influence of melanoma stadium to amount of erythrocytes in blood from MeLiM pigs. Group one was control group of health pigs, group two were pigs with melanoma progress. Part A shows dependence of iron concentration in erythrocytes on melanoma stadium at MeLiM pigs. There was differential pulse voltammetry for iron determination used. Part B represents measured voltammograms. Parameters of electrochemical determination were as follows: start potential -0.6 V; end po-

tential -1.3 V; deposition potential 0 V; accumulation time 0 s; equilibration time 10 s; purge time 120 s; pulse amplitude 0.05005 V; pulse time 0.06 s; voltage step 0.005951 V; voltage step time 0.5 s; sweep rate 0.0119 V/s. Samples were measured in solutions consist from 20 μl of sample and 2400 μl of electrolyte (KBrO + NaOH + TEA).



CONCLUSION

The full automated electrochemical method for iron determination in biological samples was developed and optimized. Differential pulse voltammetry as an electrochemical method was applied. Series of real samples (blood from MeLiM pigs) as a testing set was used. Testing group was divided in two groups – first group was control (samples from healthy pigs), second group was from pigs with progressive melanoma. Control group had iron concentration three times higher than group with melanoma progress.

ACKNOWLEDGEMENT

The financial support from the following project NANIMEL GA ČR 102/08/1546, NANOSEMED GA AV KAN208130801 and CEITEC CZ.1.05/1.1.00/02.0068 is highly acknowledged.

REFERENCES

- [1] Adam V, Huska D, Hubalek J, *et al.*, *Microfluidics and Nanofluidics*, 8 (2010), 329-339.
- [2] Chen D J, Lu Y H, Wang A J, *et al.*, *J. Solid State Electrochem.*, 16 (2012), 1313-1321.
- [3] Lee G, Park I, Kwon K, *et al.*, *Biomed. Microdevices*, 14 (2012), 375-384.
- [4] Cousino M A, Jarbawi T B, Halsall H B, *et al.*, *Analytical Chemistry*, 69 (1997), A544-A549.
- [5] Bersier P M, Howell J, Bruntlett C, *Analyst*, 119 (1994), 219-232.
- [6] Majzlik P, Prasek J, Trnkova L, *et al.*, *Listy Cukrov. Reparske*, 126 (2010), 413-414.
- [7] Feria J J, Marrugo J L, Gonzalez H, *Rev. Fac. Ing.-Univ. Antioquia*, (2010), 35-44.

- [8] Wang J, Zadei J, Lin M S, *Journal of Electroanalytical Chemistry*, 237 (1987), 281-287.
- [9] R. C, *Wiley Interscience England*, (2001).
- [10] Croot P L, Johansson M, *Electroanalysis*, 12 (2000), 565-576.
- [11] Gholivand M B, Geravandi B, Parvin M H, *Electroanalysis*, 23 (2011), 1345-1351.

ELECTROCHEMICAL DETERMINATION OF PLATINUM IN BIOLOGICAL SAMPLES

Monika KREMPLOVA², David HYNEK^{1,2}, Miroslava BEKLOVA³, Ondrej ZITKA¹, Vojtech ADAM^{1,2} and Rene Kizek^{*1,2}

¹ Department of Chemistry and Biochemistry, Faculty of Agronomy, Mendel University in Brno, Zemedelska 1, 613 00 Brno, Czech Republic

² Central European Institute of Technology, Brno University of Technology, Technicka 3058/10, 616 00 Brno, Czech Republic

³ Department of Veterinary Ecology and Environmental Protection, Faculty of Veterinary Hygiene and Ecology, University of Veterinary and Pharmaceutical Sciences, Palackeho 1-3, CZ-612 42 Brno, Czech Republic

*kizek@sci.muni.cz

ABSTRACT

Electrochemical determination of platinum in biological samples is the aim of this paper. There were used samples of maize and pea after their exposure to PtCl₄ and mineralization. The concentration of platinum was determined by using differential pulse voltammetry.

INTRODUCTION

Platinum group elements are formed by metals such as platinum, palladium, rhodium, ruthenium, iridium and osmium. These elements are found in the environment (e.g. soil, road dust, water, sediments, or biota) in very low concentrations. [1, 2] These metals play an important role in the motor vehicles exhaust systems and some household devices to reduce emissions of poisonous gases such as carbon monoxide, nitrogen oxides and hydrocarbons. [3-10] The majority of platinum group-containing compounds are highly toxic at very small concentrations and in most cases cause severe allergic reactions. In connection with the increasing concentrations of platinum in the environment there are changing modes on the availability of these metals. [11] It seems necessary to monitor emissions of platinum metals in the environment and create a new concept that would protect the future health of mankind and the entire ecosystem. [1] Determination of platinum metals in environmental samples requires very sensitive analytical methods considering their very low concentrations in the environment. [12] The aim of this study was to determine the concentration of platinum in samples of peas and maize. Due to the high sensitivity differential pulse voltammetry was selected.

MATERIAL AND METHODS

Preparation of samples

The aim of this work was to optimize the electrochemical detection of platinum, as well as to determine the effect of platinum metals (Pt, Rh, Pd) on germination and plant growth considering the length of exposure to that metal. Seeds of pea (*Pisum sativum* L.) and maize (*Zea mays*

L.) was used to determine the inhibitory effects of platinum metals on germination and plant growth in the early stages of development. In the experiment, seeds of plants were exposed to PtCl₄ in concentrations of 0, 5, 10, 25, 50 and 100 μM. Each concentration was used for 100 seeds (5 bowls, 20 seeds) distributed to plates coated with cellulose. Plates were placed on the edge of the container of 500 ml. To every container 300 ml of metal solution with appropriate concentration was applied due to be wetted by the end of the cellulose in the solution and causing its rise to the seeds. Distilled water was used as the dilution water. Samples were cultivated for 8 and 12 days in the dark at 25 °C and humidity of 60 %. Sampling was carried out on the 8th day - 3 bowls = 60 plants and 12th day - 2 bowls of 40 plants. At each sampling time there were 6 samples of fresh green plant parts, 6 samples of fresh root parts, 6 samples of dry green plant parts and 6 samples of dry root parts. After processing the samples were frozen to a temperature of -80 °C.

Mineralization of samples

For the digestion 0.01 g plant (dry weight) + 700 μl HNO₃ + 300 μl H₂O₂ was used. Samples were digested using an apparatus Multiwave 3000 (Anton-PaarGmbH, Austria) and a program SUP6 (50W-10 min, 100W-30 min, 0W (cooling)-10 min, IR-140°C).

Electrochemical determination of platinum

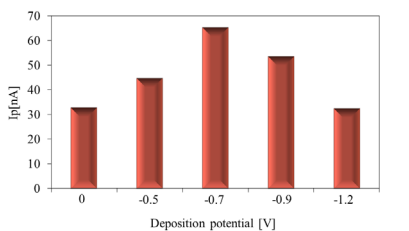
Platinum concentration was determined by differential pulse voltammetry. At first, the analysed samples were deprived of oxygen by purging argon (99.999%) for 200 s. Platinum detection was performed using mercury drop electrode (HMDE). Experimental parameters were chosen

as follows: modulation time 0.057 s, time interval 0.2 s, potential step of 1.95 mV, scan rate 10 mV/s, modulation amplitude 49.95 mV, deposition potential of -0.7 V, deposition time of 0 s. Platinum was measured by adsorptive stripping voltammetry in 1.98 ml of ACS reagent containing 17.8 mol/l sulphuric acid (Sigma Aldrich), 0.24 ml of 0.015 mol/l hydrazine (Sigma Aldrich) and 0.01 ml of 2 mol/l formaldehyde (Sigma Aldrich). Pt-formazan complex were formed in measuring container during the 2 min purging time and was accumulated for 15 second on the HMDE. The scan was from -0.5 to -1.2 V with scan rate 10 mV/s. Characteristic peak for platinum was recorded at potential -0.9 V. Sample volume was 20 μ l, total volume in the measuring vessel was 2 ml (20 ml sample and 1980 μ l electrolyte).

RESULTS AND DISCUSSION

Electrochemical detection of platinum in samples of peas and maize were determined by differential pulse voltammetry in 3-electrodes arrangement. The hydrazine-formaldehyde buffer containing 0.356 mol/l H_2SO_4 , 0.15 mmol/l hydrazine and 0.02 mol/l HCHO was chosen for detection. The deposition potential and accumulation of time of analyte on hanging mercury drop electrode was optimized. Deposition potential of -0.7 V was selected as the most suitable (Fig. 1). This potential gave the highest signal in our chosen concentration of platinum (6.25 ng/ml).

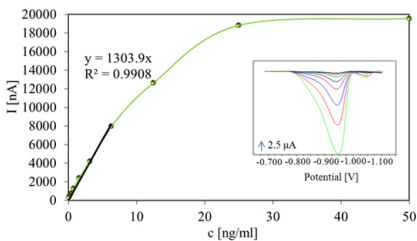
Figure 1.: The influence of deposition potential (0; -0.5; -0.7; -0.9; -1.2 V), measuring method was DPV, supporting electrolyte was 0,356 M sulphuric acid (Sigma Aldrich), 0.15 mM hydrazine with 0,02 M formaldehyde



In the deposition potential of -0.7 V there was studied the influence of the accumulation time. With increasing accumulation time the signal didn't change thus the accumulation time was set to 0 s. After optimization there was measured the calibration curve using platinum standard solution within concentration range from 0.098 to 50 ng/ml. Linear dependence of the platinum concentration in catalytic signal was set to a concentration of 6.25 ng/ml ($y = 1303.9 x$, $R^2 = 0.9908$,

Fig. 2). Limit of detection LOD = 0.01 ng/ml and limit of quantification LOQ = 0.04 ng/ml was estimated using data from the linear part of the calibration curve.

Figure 2.: The calibration curve of platinum. Range of concentration was 0.098 – 50 ng/ml, the linear dependence for platinum concentration was to 6.25 ng/ml



Subsequently, the concentration of platinum in mineralized samples of maize and peas was determined. The results were plotted in graphs and calculated using regression equation the concentrations of platinum in real samples. The maize-graph shows that the platinum concentration was higher in the root parts in both fresh and dried samples (Fig. 3). At the green parts there were very low concentrations of platinum, sometimes not detectable. On the contrary for samples of peas a higher concentration of platinum was found in green plant parts (both fresh and dry), in the root parts higher concentrations were measured only in dry samples (Fig. 4). Fresh samples provided very low signal.

Figure 3.: Platinum levels in maize. Measuring method was DPV. E24-E19: root part, dry samples; E18-E13: green part, dry samples; F12-F7: root part, fresh samples; F6-F1: green part, fresh samples

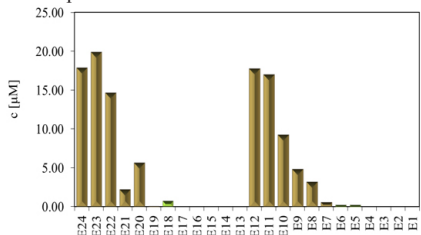
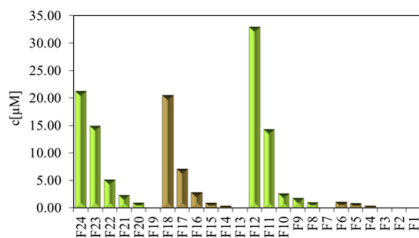


Figure 4.: Platinum levels in pea. Measuring method was DPV. F24-F19: green part, dry samples; F18-F13: root part, dry samples; F12-F7: green part, fresh samples; F6-F1: root part, fresh samples



CONCLUSION

The results of this study confirm that the differential pulse voltammetry is a very effective method for the determination of trace concentrations of platinum in plant samples. The biggest advantage in addition to high sensitivity is the absence of any interference from other elements or metal ions present in the studied matrices. After optimizing the parameters of the method we were able to achieve the desired detection limit and thus analyse real samples.

ACKNOWLEDGEMENT

The financial support from the following project NANIMEL GA ČR 102/08/1546 and NANOSEMED GA AV KAN20813080, CEITEC CZ.1.05/1.1.00/02.0068 is highly acknowledged.

REFERENCES

- [1] Dubiella-Jackowska A, Polkowska Z, Namiesnik J, Polish Journal of Environmental Studies, 16 (2007), 329-345.
- [2] Soukupova I, Beklova M, Zitka O, *et al.*, Toxicology Letters, 205 (2011), S77-S77.
- [3] Dubiella-Jackowska A, Polkowska Z, Namiennik J, in: Whitacre, D M (Ed.), *Reviews of Environmental Contamination and Toxicology; Vol 199* (2009), pp. 111-135.
- [4] Fornalczyk A, Saternus M, Metalurgija, 48 (2009), 133-136.
- [5] Kolodziej M, Baranowska I, Matyja A, Electroanalysis, 19 (2007), 1585-1589.
- [6] Orecchio S, Amorello D, Microchemical Journal, 99, 283-288.
- [7] Yang Y, Li X, Li Y L, *et al.*, Global Nest Journal, 10 (2008), 169-173.
- [8] Zimmermann S, Menzel C M, Berner Z, *et al.*, Analytica Chimica Acta, 439 (2001), 203-209.
- [9] Zimmermann S, Messerschmidt J, von Bohlen A, *et al.*, Analytica Chimica Acta, 498 (2003), 93-104.
- [10] Soukupova I, Krystofova O, Sobrova P, *et al.*, Listy Cukrovarnicke a Reparske, 126 (2010), 415-415.
- [11] Lustig S, Zang S, Michalke B, *et al.*, Fresenius Journal of Analytical Chemistry, 357 (1997), 1157-1163.
- [12] Paraskevas M, Tsopelas F, Ochsenkuhn-Petropoulou M, Microchimica Acta, 176, 235-242.

ELECTROCHEMICAL DETERMINATION OF RHODIUM IN BIOLOGICAL SAMPLES

Monika KREMPLOVA¹, David HYNEK^{1,2}, Miroslava BEKLOVA⁴,
Ondrej ZITKA¹, Jaromir HUBALEK^{2,3}, Vojtech ADAM^{1,2} and Rene Kizek^{*1,2}

¹ Department of Chemistry and Biochemistry, Faculty of Agronomy, Mendel University in Brno, Zemedelska 1, 613 00 Brno, Czech Republic

² Central European Institute of Technology, Brno University of Technology, Technicka 3058/10, 616 00 Brno, Czech Republic

³ Department of Microelectronics, Faculty of Electrical Engineering and Communication, Brno University of Technology, Technicka 10, CZ-616 00 Brno, Czech Republic

⁴ Department of Veterinary Ecology and Environmental Protection, Faculty of Veterinary Hygiene and Ecology, University of Veterinary and Pharmaceutical Sciences, Palackeho 1-3, CZ-612 42 Brno, Czech Republic

*kizek@sci.muni.cz

ABSTRACT

Electrochemical determination of rhodium in biological samples is the aim of this paper. There were used samples of maize and pea after their exposure to RhCl_3 and mineralization. The concentration of rhodium was determined by using differential pulse voltammetry.

INTRODUCTION

Platinum group elements are formed by metals such as platinum, palladium, rhodium, ruthenium, iridium and osmium. These elements are found in the environment (e.g. soil, road dust, water, sediments, or biota) in very low concentrations [1, 2]. Rhodium due to its unique physico-chemical properties is the necessary component for the development of many fields of industry: from fine organic synthesis and precise instrument engineering to large-tonnage manufacturing [3]. It plays an important role in the motor vehicles exhaust systems and some household devices, to reduce emissions of poisonous gases such as carbon monoxide, nitrogen oxides and hydrocarbons. The majority of platinum group-containing compounds are highly toxic at very small concentrations and in most cases cause severe allergic reactions [4-10]. It seems necessary to monitor emissions of platinum metals in the environment and create a new concept that would protect the future health of mankind and the entire ecosystem [1]. Determination of rhodium in environmental samples requires very sensitive analytical methods considering its very low concentrations in the environment. The aim of this study was to determine the concentration of rhodium in samples of peas and maize. Due to the high sensitivity as a measuring method the differential pulse voltammetry was chosen [11, 12].

MATERIAL AND METHODS

Preparation of samples

Seeds of pea (*Pisum sativum* L.) and maize (*Zea mays* L.) was used to determine the inhibitory effects of rhodium on germination and

plant growth in the early stages of development. In the experiment, seeds of plants were exposed to RhCl_3 in concentrations of 0, 5, 10, 25, 50 and 100 μM . Each concentration was used for 100 seeds (5 bowls, 20 seeds) distributed to plates coated with cellulose. Plates were placed on the edge of the container of 500 ml. To every container was applied 300 ml of metal solution with appropriate concentration due to be wetted by the end of the cellulose in the solution and causing its rise to the seeds. Distilled water was used as the dilution water. Samples were cultivated for 8 and 12 days in the dark at 25 °C and humidity of 60%. Sampling was carried out on the 8th day - 3 bowls = 60 plants and 12th day - 2 bowls of 40 plants. At each sampling time there were 6 samples of fresh green plant parts, 6 samples of fresh root parts, 6 samples of dry green plant parts and 6 samples of dry root parts. After processing the samples were frozen to a temperature of -80 °C.

Digestion of samples

For the digestion 0.01 g plant (dry weight) + 700 μl HNO_3 + 300 μl H_2O_2 was used. Samples were digested using an apparatus Multiwave 3000 (Anton-Paar GmbH, Austria) and a program (50W - 10 min, 100W - 30 min, 0W (cooling) - 10 min, IR-140 °C).

Electrochemical determination of Rhodium

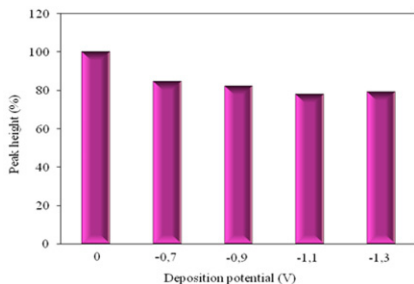
Rhodium concentration was determined by differential pulse voltammetry. At first, the analyzed samples were deprived of oxygen by purging argon (99.999%) for 200 s. Rhodium detection was performed using mercury drop electrode (HMDE). Method parameters were

chosen as follows: modulation time 0.057 s, time interval 0.2 s, potential step of 1.95 mV, scan rate 10 mV/s, modulation amplitude 49.95 mV, deposition potential of 0 V, deposition time of 0 s. Rhodium was measured by adsorptive stripping voltammetry in 3.8 ml of electrolyte containing 0.16 mol/l hydrochloric acid (Sigma Aldrich), and 3 mmol/l formaldehyde (Sigma Aldrich). The scan was from -0.7 to -1.3 V with scan rate 10 mV/s. Characteristic peak for rhodium was recorded at potential -1.175 V. Sample volume was 40 μ l, total volume in the measuring vessel was 3.84 ml (40 μ l of sample and 3800 μ l of electrolyte).

RESULTS AND DISCUSSION

The aim of this work was to optimize the electrochemical detection of rhodium, as well as to determine the effect on germination and plant growth considering the length of exposure to that metal. Electrochemical detection of rhodium in samples of peas and maize were determined by differential pulse voltammetry in 3-electrodes arrangement. The electrolyte buffer with 0.16 mol/l HCl and 3 mmol/l HCHO was chosen for detection. The influence of the deposition potential and accumulation time of analyte on HMDE was studied. Deposition potential of 0 V was selected as the most suitable (Fig. 1). This potential gave the highest signal in our chosen concentration of platinum (6.25 ng/ml).

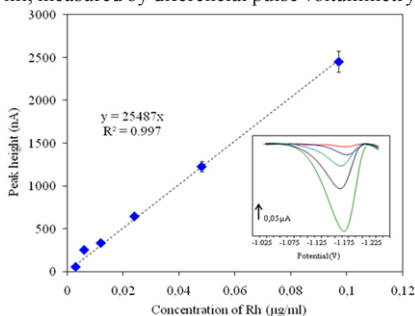
Figure 1: The influence of deposition potential (0; -0.7; -1.1; -1.3 V), measuring method was DPV, supporting electrolyte was 0.16 M hydrochloric acid (Sigma Aldrich) with 3 mM formaldehyde (Sigma Aldrich)



There was studied the influence of the accumulation time in the deposition potential of 0 V. With increasing accumulation time the signal didn't change thus the deposition time was set to 0 s. After optimization there was measured the calibration curve using rhodium standard solution within concentration range from 0.003 to 0.098 μ g/ml prepared. Linear dependence of the rhodium concentration in catalytic signal was set to a concentration of 0.098 μ g/ml ($y = 25487x$,

$R^2 = 0.997$, Fig. 2). Limit of detection LOD = 0.700 ng/ml was observed using data from the calibration curve.

Figure 2: The calibration curve of rhodium. Range of concentration was 0.003 – 0.098 μ g/ml, measured by differential pulse voltammetry



Subsequently, the concentration of rhodium in digested samples of maize and peas was determined. The results were plotted in graphs and using regression equation the concentrations of rhodium in real samples were calculated. The maize-graph shows that the rhodium concentration was higher in the root parts in both, the fresh and dried samples (Fig. 3). At the green parts there were very low concentrations of rhodium, in most cases immeasurable. On the contrary for samples of peas a higher concentration of rhodium is found in green plant parts (both fresh and dry), in the root parts the higher concentrations were measured only in dry samples (Fig. 4). Fresh samples provided very low signal.

Figure 3: Rhodium levels in maize (*Zea mays* L.). Measuring method was DPV. Samples D24-D19: root part, dry samples; D18-D13: green part, dry samples; D12-D7: root part, fresh samples; D6-D1: green part, fresh samples

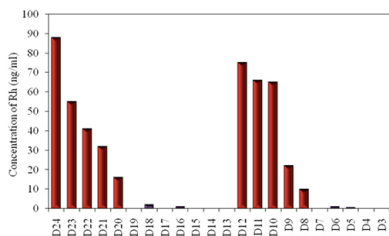
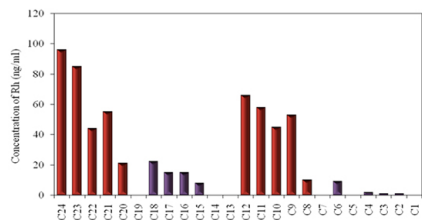


Figure 4: Rhodium levels in pea. Measuring method was DPV. Samples C24-C19: green part, dry samples; C18-C13: root part, dry sam-

ples; C12-C7: green part, fresh samples; C6-C1: root part, fresh samples



CONCLUSION

The results of this study confirm that the differential pulse voltammetry is a very effective method for the determination of trace concentrations of rhodium in plant samples. The biggest advantage in addition to high sensitivity is the absence of any interference from other elements or metal ions present in the studied matrices. After optimizing the parameters of the method we were able to achieve the desired detection limit and thus complete and representative results.

AKNOWLEDGEMENT

The financial support from the following project NANIMEL GA ČR 102/08/1546 and NANOSEMED GA AV KAN208130801 is highly acknowledged.

REFERENCES

- [1] Dubiella-Jackowska A, Polkowska Z, Namiesnik J, Polish Journal of Environmental Studies, 16 (2007), 329-345.
- [2] Soukupova I, Beklova M, Zitka O, *et al.*, Toxicology Letters, 205 (2011), S77-S77.
- [3] Orecchio S, Amorello D, Journal of Hazardous Materials, 174 (2010), 720-727.
- [4] Ek K H, Morrison G M, Rauch S, Science of the Total Environment, 334 (2004), 21-38.
- [5] Hooda P S, Miller A, Edwards A C, Science of the Total Environment, 384 (2007), 384-392.
- [6] Melucci D, Locatelli C, Annali Di Chimica, 97 (2007), 373-384.
- [7] Wichmann H, Anquandah G A K, Schmidt C, *et al.*, Science of the Total Environment, 388 (2007), 121-127.
- [8] Zereini F, Wiseman C, Puttmann W, Environmental Science & Technology, 41 (2007), 451-456.
- [9] Zimmermann S, Messerschmidt J, von Bohlen A, *et al.*, Analytica Chimica Acta, 498 (2003), 93-104.
- [10] Soukupova I, Krystofova O, Sobrova P, *et al.*, Listy Cukrovarnicke a Reparske, 126 (2010), 415-415.
- [11] Leon C, Emons H, Ostapczuk P, *et al.*, Analytica Chimica Acta, 356 (1997), 99-104.
- [12] Wang J, Taha Z, Talanta, 38 (1991), 489-492.

CHIP CAPILLARY ELECTROPHORETIC STUDIES OF PSA

Sona KRIZKOVA^{1,2}, Marketa RYVOLOVA^{1,2}, Michal MASARIK^{2,3}, Rene KIZEK^{1,2*}

¹ Department of Chemistry and Biochemistry, Faculty of Agronomy, Mendel University in Brno, Zemedelska 1, 613 00 Brno, Czech Republic

² Central European Institute of Technology, Brno University of Technology, Technicka 3058/10, 616 00 Brno, Czech Republic

³ Department of Pathological Physiology, Faculty of Medicine, Masaryk University, Kamenice 5, CZ-625 00 Brno, Czech Republic

*kizek@sci.muni.cz

ABSTRACT

Capillary electrophoresis (CE) is a powerful separation technique, which is suitable for miniaturization. Therefore microfluidic chip-based CE analysis is attracting great attention. Especially in the field of proteomics, rapid and effective analytical tools are required due to the high biological importance of numerous proteins for diagnostic purposes. In this work, chip-based CE method has been used for analysis of prostatic-specific antigen, which is so far the most commonly used marker for prostate cancer diagnosis.

INTRODUCTION

Prostatic-specific antigen (short name PSA and alternative name: gamma-seminoprotein, kallikrein-3, P-30 antigen and semenoglyase) is a serine protease (EC 3.4.21.77) secreted by both normal prostate glandular cells and prostate cancer cells [1]. PSA occurs in two forms as bound to α -1-antichymotrypsin and free often abbreviated with f-PSA. The total amount of bound PSA and f-PSA is known as total PSA (t-PSA). An increasing of t-PSA level at more than 4 ng/ml represents strong indicators of the possibility of prostate cancer, which is the most common cancer in men and is the second leading cause of cancer death in men worldwide [2]. Commonly used methods like immunobased ones have good sensitivity and specificity, but they are time-consuming and demand on laboratory equipment. Based on this, sensors and biosensors are of great interest for determination of PSA [3]. Microfluidic and chip techniques coupled with nanoparticles based isolation and electrochemical detection can be also used in multiplex immunosensors for PSA detection and have good potential to be miniaturized [4-8]. The aim of this study was to use chip based capillary electrophoresis for determination of PSA.

MATERIAL AND METHODS

Capillary electrophoresis

Analyses on an automated microfluidic Experion electrophoresis system (Bio-Rad, USA) were carried out according to the manufacturer's instructions with supplied chemicals (Experion Pro260 analysis kit, Bio-Rad). A sample (4 μ l) was mixed either with 2 μ l of non-reducing sample buffer or 2 μ l of reducing sample

buffer (30 μ l of nonreducing sample buffer and 1 μ l β -mercaptoethanol, and after 4 min boiling, 84 μ l of water was added. After the priming of the chip with the gel and gel-staining solution in the diluted priming station sample, the mixture (6 μ l) was loaded into the sample wells. The Pro260 Ladder included in the kit was used as a standard. For operation and standard data analysis Experion software version 3.10 (Bio-Rad, USA) was used.

Sodium dodecyl sulphate polyacrylamide gel electrophoresis (SDS-PAGE)

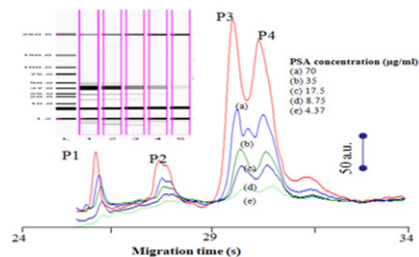
The electrophoresis was performed according to Laemmli [9] using a Mini Protean Tetra apparatus (Bio-Rad, USA). First 12.5 % (*m/V*) running, then 5 % (*m/V*) stacking gel was poured. The polymerization of the running or stacking gels was carried out at room temperature for 45 min. Prior to analysis, the samples were mixed with reducing (3% β -mercaptoethanol) or non-reducing sample buffer in a 2:1 ratio. The samples were boiled for 2 min, and then 4 μ l of the sample was loaded onto a gel. The electrophoresis was run at 150 V for 1 h (Power Basic, Biorad USA) in tris-glycine buffer (0.025 M Trizma-base, 0.19 M glycine and 3.5 mM SDS, pH = 8.3). Silver staining of the gels was performed according to Oakley et al. [10].

RESULTS AND DISCUSSION

Analysis of PSA using SDS-PAGE showed that protein structure with molecular mass app. 35 kDa was formed under reducing conditions and protein with molecular mass app. 25 kDa under non-reducing conditions. Higher molecular structure detected under reducing conditions can be related to the fact that PSA sub-units could form higher molecular mass complexes

due to reduced -SH moieties. Moreover, PSA as glycoprotein behave atypically in electrophoresis and can form other types of complexes [11]. From the point of view of sensitivity, we were able to detect 8.7 ng of PSA under reducing conditions, but PSA of 17.5 ng was not detected under non-reducing ones.

Figure 1.: Capillary chip electrophoresis of PSA (4.37, 8.75, 17.5, 35 and 70 ng); in inset: virtual gel based on the chip analysis shown below.



To our knowledge, this system has not been previously used for PSA analysis. Therefore, unique results of chip capillary electrophoretic analysis of PSA are shown Fig. 1. We found that the most intensive band on the virtual gel shown in inset in Fig. 1 was determined at 37 kDa under reducing conditions and at 26 kDa under non-reducing. Band at 37 kDa corresponds to a reduced, and at 26 kDa to non-reduced PSA. Band of molecular mass of 15 kDa can be considered as a product of PSA auto-proteolytic reaction. Glycosylation of PSA is the most likely explanation for atypical migration of this protein. It was shown previously that places, in which PSA is glycosylated, or other interactions with proteins and other biomolecules significantly affect the mobility of PSA [1, 11].

During PSA analysis, there were identified four electrophoretic peaks marked as P1 (migration time “MT” = 26 s), P2 (MT = 27.5 s), P3 (MT = 31 s) and P4 (MT 32 s). Majority P3 and P4 signals correspond to the predominant protein structure PSA. Moreover, we found that all identified electrophoretic signals depend on the concentration of PSA (analysis performed in the concentration range of 4.37 µg/ml to 70 µg/ml. Peak P1 was strictly linear as showing the calibration dependence with the following equation $y = 0.868x - 2.2752$, $R^2 = 0.9979$, Peaks P2 and P4 linearly enhanced with the increasing concentration of PSA according to the following equations $y = 0.9939x + 2.5554$, $R^2 = 0.9865$, and $y = 4.9747x + 4.6162$, $R^2 = 0.9810$. Dependence of Peak P3 height on concentration of PSA was expressed as $y = 4.013x + 8.6233$ with the lowest $R^2 = 0.9524$.

CONCLUSION

Label-free detection techniques for protein analysis and/or microarrays are required because of their simple interpretation, less demanding sample preparation and thus also reduce the time and material consumption [12]. This study shows the good possibility to use such technique for determination of PSA, which could be of interest for some easy-to-use and well portable analyzers.

ACKNOWLEDGEMENT

The work has been supported by NANOSEMED GA AV KAN208130801 and NanoBioTECell GA ČR P102/11/1068.

REFERENCES

- [1] Denmeade S R, Lou W, Lovgren J, *et al.*, *Cancer Research*, 57 (1997), 4924-4930.
- [2] Reynolds M A, Kastury K, Groskopf J, *et al.*, *Cancer Letters*, 249 (2007), 5-13.
- [3] Healy D A, Hayes C J, Leonard P, *et al.*, *Trends in Biotechnology*, 25 (2007), 125-131.
- [4] Chikkaveeraiah B V, Mani V, Patel V, *et al.*, *Biosensors & Bioelectronics*, 26 (2011), 4477-4483.
- [5] Henares T G, Mizutani F, Hisamoto H, *Analytica Chimica Acta*, 611 (2008), 17-30.
- [6] Ko Y J, Maeng J H, Ahn Y, *et al.*, *Electrophoresis*, 29 (2008), 3466-3476.
- [7] Panini N V, Messina G A, Salinas E, *et al.*, *Biosensors & Bioelectronics*, 23 (2008), 1145-1151.
- [8] Zani A, Laschi S, Mascini M, *et al.*, *Electroanalysis*, 23 (2011), 91-99.
- [9] Laemmli U K, *Nature*, 227 (1970), 680-&.
- [10] Oakley B R, Kirsch D R, Morris N R, *Analytical Biochemistry*, 105 (1980), 361-363.
- [11] Kurkela R, Herrala A, Henttu P, *et al.*, *Bio-Technology*, 13 (1995), 1230-1234.
- [12] Ray S, Mehta G, Srivastava S, *Proteomics*, 10 (2010), 731-748.

SPECTROMETRIC STUDY OF TAURINE

Lukas NEJDL¹, Jiri SOCHOR^{1,2}, Ondrej ZITKA^{1,2}, Branislav RUTTKAY-NEDECKY^{1,2}, Vojtech ADAM^{1,2}, Rene KIZEK^{1,2*}

¹Department of Chemistry and Biochemistry, Faculty of Agronomy, Mendel University in Brno, Zemedelska 1, 613 00 Brno, Czech Republic

²Central European Institute of Technology, Brno University of Technology, Technicka 3058/10, 616 00 Brno, Czech Republic

*kizek@sci.muni.cz

ABSTRACT

This study aims at analysing of complex-forming reactions with respect to use them for easy-to-use and sensitive determination of taurine in biological samples including tissues extracts and body fluids. Particularly, we focused on studying of taurine complexes with phenol and sodium hypochlorite, and/or of taurine with sodium hypobromite. The formed complexes were studied under various temperatures (10 °C, 20 °C, 30 °C, 40 °C, 50 °C and 60 °C) and in various time intervals (0, 5, 10, 15, 20, 25 and 30 min.).

INTRODUCTION

Taurine (2-aminoethanesulfonic acid) is contained in low concentrations in most tissues of the human body [1], occurs naturally in foods, particularly seafood and meat [2]. It acts and anti-inflammatory agent and antioxidant on the human body [3], participates in physiological processes such as stabilization of cell membranes, inhibition of oxidative burning of neutrophils and macrophages [4], regulation of adipose tissue [5], regulation of a constant level of calcium in the blood [6]. In addition, it is necessary for cardiovascular function [7], development and function of skeletal muscle, the retina and the central nervous system [7, 8].

High performance liquid chromatography (HPLC) [9, 10] and capillary electrophoresis (CE) [11] belongs to the most commonly used methods for analysis of taurine. It is also possible to use spectrometry due to the ability of taurine to form complexes with ninhydrin [12], o-phthalaldehyde [13] and 1-fluoro-2,4-dinitrobenzen [14].

The aim of our study was to optimize methods for determination of taurine based on complex formation of the analyte with phenol and sodium hypochlorite, and/or with sodium hypobromite.

MATERIAL AND METHODS

Chemicals

All chemicals of ACS purity used were purchased from Sigma Aldrich Chemical Corp. (USA), unless noted otherwise. The following stock solutions of the chemicals were prepared 800 mM taurine, 680 mM phenol, 300 mM NaClO and 100 mM NaBrO.

Preparation of taurine

To study taurine complexes, taurine of the following concentrations were prepared: a) 100, b)

50, c) 25, d) 12.5, e) 6.25 and f) 3.13 mM. To study the influence of time and temperature on the measured absorbance, taurine of the following concentrations were prepared: a) 4, b) 2, c) 1, d) 0.5, e) 0.25 and f) 0.125 mM. Milli Q water was used for solutions preparation.

Preparation of complex of taurine with phenol and sodium hypochlorite

To micro-test tubes, the following chemicals were pipetted: 100 µl taurine, 100 µl phsopshtae buffer (pH 10.35), 100 µl phenol and 100 µl sodium hypochlorite.

Preparation of complex of taurine with sodium hypobromite

To micro-test tubes, the following chemicals were pipetted: 200 µl taurine and 200 µl sodium hypobromite.

Measurements

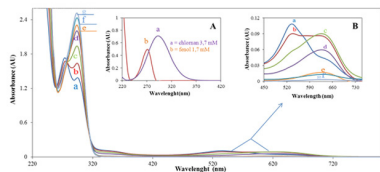
Spectra were measured within the range from 220 to 800 nm using SPECORD 210 (Analytik Jena, Germany) in quartz cuvettes with 1 cm diameter (Hellma, UK). Monitoring resulting complexes was carried out at times 0, 5, 10, 15, 20, 25 and 30 minutes. Cell area was heated by thermostat Julabo (USA) at temperatures 10 °C, 20 °C, 30 °C, 40 °C, 50 °C and 60 °C.

RESULTS AND DISCUSSION

Our experiment was aimed at comparison of two complex-forming methods. Primarily, we measured spectra of the complex forming chemicals without taurine (phenol and sodium hypochlorite Fig. 1A, and/or with sodium hypobromite Fig. 2A). Further, we analysed taurine itself (Fig. 2A), which was not detectable by spectrometry. Change of absorbance of phenol (at 270 nm) and sodium hypochlorite (at 290 nm) was determined at reaction of taurine with these chemicals. The presence of coloured complexes was detected at 530 and 630 nm (Fig. 1B). Determined change at 290 nm was proportional to

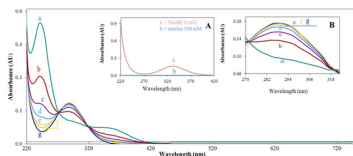
concentration of taurine ($R^2=0.971$). This wavelength is suitable for determination of taurine

Fig. 1: Spectrum of taurine with phenol and sodium hypochlorite. Measured after 30 min. long interactions at 60 °C. (A) Spectrum record of sodium hypochlorite (a) and phenol (b). (B) Complex formed at 530 nm (a, b) and 630 nm (c - g)



Three coloured complexes were detected at 230, 288 a 370 nm after reaction of taurine with sodium hypobromite (Fig. 2). Tuerine complex with this chemical was detected at 288 nm.

Fig. 2: Spectrum of taurine with sodium hypobromite. Measured after 30 min. long interactions at 60 °C. (A) Spectrum record of sodium hypobromite and taurine. (B) Complex formed at 288 nm



Interaction of taurine with phenol and hypochlorite (Fig. 3) and taurine with sodium hypobromite (Fig. 4) was monitored under changing temperature and time of interaction as the change in absorbance. The concentration of taurine as 4 mM, 2 mM, 1 mM, 0.5 mM, 0.25 mM and 0.125 mM were used.

Fig. 3: Dependences of absorbance of taurine with phenol and hypochlorite (4, 2, 1, 0.5, 0.25 and 0.125 mM of taurine) after 0, 5, 10, 15, 20, 25 and 30 min. long interactions and temperatures 10 °C, 20 °C, 30 °C, 40 °C, 50 °C and 60 °C. The reaction was recorded at 290 nm.

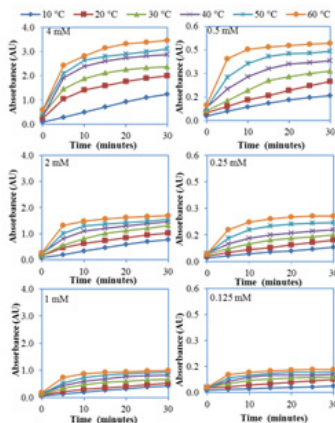
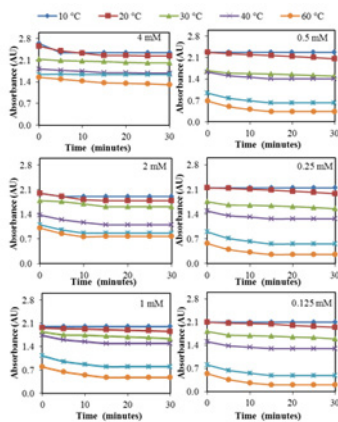


Fig. 4: Dependences of absorbance of taurine with sodium hypobromite (4, 2, 1, 0.5, 0.25 and 0.125 mM of taurine) after 0, 5, 10, 15, 20, 25 and 30 min. long interactions and temperatures 10 °C, 20 °C, 30 °C, 40 °C, 50 °C and 60 °C. The reaction was recorded at 288 nm.



CONCLUSION

For both complexes studied, taurine and phenol with hypochlorite and taurine with sodium hypobromite, significant dependence on the concentration of taurine, reaction temperature

and time of reaction was observed. For taurine complex with phenol and hypochlorite, the increase in temperature from 10 °C to 60 °C caused the increase in absorbance at different concentrations on average by 274 %. The resulting taurine complex with phenol and hypochlorite at 290 nm appears to be suitable for determining the concentration of taurine.

ACKNOWLEDGEMENT

The work has been supported by NANIMEL GA CR 102/08/1546 and NANOSEMED GA AV KAN 208130801 and CEITEC CZ.1.05/1.1.00/02.0068.

REFERENCES

- [1] Bouckenooghe T, Remacle C, Reusens B, Curr. Opin. Clin. Nutr. Metab. Care, 9 (2006), 728-733.
- [2] Lau O W, Luk S F, Chiu T P Y, Analyst, 115 (1990), 653-655.
- [3] Marcinkiewicz J, J. Biomed. Sci., 17 (2010).
- [4] Condron C, Casey R G, Kehoe S, et al., Urol. Res., 38 (2010), 215-222.
- [5] Ueki I, Stipanuk M H, J. Nutr., 139 (2009), 207-214.
- [6] Ribeiro R A, Vanzela E C, Oliveira C A M, et al., Br. J. Nutr., 104 (2010), 1148-1155.
- [7] Warskulat U, Flogel U, Jacoby C, et al., Faseb J., 18 (2004), 577-+.
- [8] Ito T, Oishi S, Takai M, et al., J. Biomed. Sci., 17 (2010).
- [9] Chen Z, Chen B, Yao S Z, Anal. Chim. Acta, 569 (2006), 169-175.
- [10] Wang X F, Chi D F, Su G M, et al., Biomed. Environ. Sci., 24 (2011), 537-542.
- [11] Kelly M T, Fabre H, Perrett D, Electrophoresis, 21 (2000), 699-705.
- [12] Seracu D, Rev. Chim., 39 (1988), 54-58.
- [13] Gaitonde M K, Short R A, Analyst, 96 (1971), 274-&.
- [14] Chen L, Chen Q, Zhang Z Z, et al., J. Food Compos. Anal., 22 (2009), 137-141.

STUDY OF OXIDATIVE STRESS IN *STAPHYLOCOCCUS AUREUS* BACTERIAL CULTURE TREATED WITH SILVER(I) IONS

Andrea BEZDEKOVA¹, Jiri SOCHOR^{1,2,3}, Branislav RUTTKAY-NEDECKY^{1,2},
Petr BABULA^{1,2}, Vojtech ADAM^{1,2,3}, Ivo PROVAZNIK⁴, Rene KIZEK^{1,2,3}

¹ Department of Chemistry and Biochemistry, Faculty of Agronomy, Mendel University in Brno, Zemedelska 1, CZ-613 00 Brno, Czech Republic

² Central European Institute of Technology, Brno University of Technology, Technicka 3058/10, CZ-616 00 Brno, Czech Republic

³ Department of Microelectronics, Faculty of Electrical Engineering and Communication, Brno University of Technology, Technicka 10, CZ-616 00 Brno, Czech Republic

⁴ Department of Biomedical Engineering, Faculty of Electrical Engineering and Communication, Brno University of Technology, Kolejni 4, CZ-612 00 Brno, Czech Republic

ABSTRACT

We focused on the study of the antibacterial effect of silver(I) ions on microorganisms (model *Staphylococcus aureus* bacterial culture) in this study. The effect of eight concentrations of AgNO₃ (0, 1.25, 2.5, 5, 10, 15, 25 and 50 µg·ml⁻¹) was studied. We aimed at the studying of oxidative stress as the resulting effect of silver(I) ions. Five principally different methods (namely ABTS, DPPH, DMPD, FRAP and Free Radicals method) were used to determine the oxidative stress. Obtained results were mathematically evaluated. Correlation between individual analytical techniques was found. The increased antioxidant activity was well evident with the increasing concentration of applied silver(I) ions. Our results indicate the possibility of the application of above-mentioned analytical techniques in microbiology for determination of oxidative stress in bacterial cultures.

INTRODUCTION

Oxidative stress is one of the markers, which enables monitoring of toxic effects of heavy metals including silver(I) ions on microorganisms [1]. This toxic effect is based on the binding of silver(I) ions to the bacterial cell wall and membranes, which leads to inhibition of the respiratory process [2]. Due to ability of silver(I) ions to induce excessive production of reactive oxygen species (ROS) that affect almost all biomolecules. Moreover, they are also able to cause metabolic toxicity. Organisms have the protective mechanisms that can effectively eliminate formed free radicals and thus eliminate their toxic effects [3]. On the other hand, these protective mechanisms have limited capabilities based on the proteosynthetic and generally biosynthetic abilities. On the other hand, excess of ROS enables the monitoring of oxidative stress based on determination of antioxidant capacity [4].

Numerous methods for determination of antioxidant activity have been developed in the field of chemical analysis and biological evaluation of antioxidant characteristics in recent years [5]. Their diversity is given by the fact that low molecular mass antioxidants may act by different mechanisms, most often by the direct reaction with free radicals (quenching, trapping). A more precise definition of the chemical mechanism of their effect is often an

issue. Therefore, the procedures evaluating the antioxidant activity are based on chemically different principles [6].

Spectrophotometric methods are the most used methods in the determination of antioxidant activity/capacity. We studied antioxidant capacity of *Staphylococcus aureus* treated with silver(I) ions within the concentration range from 0 to 50 µg·ml⁻¹. In our study, we took advantage of five principally different methods for antioxidant capacity determination - ABTS, DPPH, DMPD, FRAP and Free Radicals.

MATERIAL AND METHODS

Cultivation of *Staphylococcus aureus*

Staphylococcus aureus (NCTC 8511) was obtained from the Collection of Microorganisms, Brno, Czech Republic. The culture was removed under sterile conditions from the slant agar and incubated for 24 hours in an incubator Hood TH 15 (Edmund Buhler GmbH, Germany) at 37 °C at 600 rpm. Bacterial culture cultivated under these conditions was diluted to was grown for another experiment the culture medium diluted to OD₆₀₀ = 0.1 by cultivation medium and used for next experiments. The composition of cultivation medium was as follows: meat peptone 5 g·l⁻¹, NaCl 5 g·l⁻¹, beef extract powder 1.5 g·l⁻¹, yeast extract 1.5 g·l⁻¹ (HIMEDIA, Mumbai, India), sterile distilled water MilliQ 18 MQ. pH of cultivation medium was adjusted prior the sterilization to pH = 7.4. Sterilization of media was

carried out in an autoclave (Tuttnauer 2450EL, Israel) at 121 °C for 30 min. The prepared cultivation medium was subsequently aseptically pipetted into 25 ml Erlenmeyer flasks. In the next step, cultivation media were supplemented with silver(I) ions (0; 1.25; 2.5; 5; 10; 15; 25 and 50 µg·ml⁻¹). After inoculation, bacterial cultures were cultivated on a shaker for 24 hours at 600 rpm and 37 °C. Samples were collected after 24 h of cultivation by centrifugation (5000 rpm, 15 min.). Bacterial cells were three times washed by phosphate buffer (pH = 7). Finally, cells were resuspended in phosphate buffer (pH = 7, volume 1.5 ml) and sonicated using the ultrasound needle (Hielscher, Germany) for 2 minutes. Homogenates were vortexed (5 min, BioSan, Riga, Latvia) and centrifuged (1600 rpm, 30 min.). Obtained supernatant was used for the determination of antioxidant capacity.

All spectrophotometric analyses were performed on automated analyzer BS-400 (Mindray, China). Reaction solutions and samples were placed in the cooled disk (4 °C) and automatically pipetted into plastic cuvettes with optical path of 5 mm. The mixture was then stirred. Incubation took place in the cuvette compartment thermostated to 37 °C. Washing of dispensing needles with distilled water was carried out between pipetting. The instrument was controlled by a software BS-200 (Mindray, China).

Determination of antioxidant capacity using the DPPH method

150 µl of R1 reagent (0.095 mM 2,2-diphenyl-1-picrylhydrazyl - DPPH) was pipetted into plastic cuvette. Subsequently, volume of 15 µl of sample was added. This method is based on the ability of stable free radical of 2,2-diphenyl-1-picrylhydrazyl to react with donors of hydrogen. DPPH[•] has strong absorption in UV-VIS spectrum, absorbance was measured for 12 min at λ = 505 nm.

Determination of antioxidant capacity using the ABTS method

150 µl of R1 reagent (7 mM ABTS^{•+} (2,2-azino-bis(3-ethylbenzothiazolin-6-sulphonic acid and 4.95 mM potassium peroxydisulphate) was pipetted into plastic cuvette. Subsequently, volume of 3 µl of sample was added. Absorbance was measured for 12 min at λ = 660 nm.

Determination of antioxidant capacity using the FRAP method

150 µl of reagent (Solution 1: 10 mmol.L⁻¹ solution of TPTZ in 40 mmol.L⁻¹ of hydrochloric acid. Solution 2: 20 mmol.L⁻¹ solution of ferric chloride hexahydrate in ACS water. Solution 3: 20 mmol.L⁻¹ acetate buffer, pH 3.6, these three solutions are mixed in a 1:1:10 ratio) was pipetted into plastic cuvette and subsequently 3 µl of sample was added. Absorbance was measured for 12 min at λ = 605 nm.

Determination of antioxidant capacity using the DMPD method

160 µl of reagent R1 (200 mM N,N-dimethyl-*p*-phenylenediamine - DMPD; 0.05 M FeCl₃, 0.1 M acetate buffer - pH = 5.25) was pipetted into plastic cuvette with subsequent addition of 4 µl of measured sample. Absorbance was measured for 12 min at λ = 505 nm.

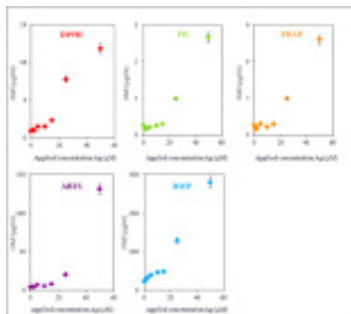
Determination of antioxidant capacity using the Free radicals method

150 µl of R1 reagent (0.1 M HCl, chlorophyllin extract, reaction buffer, catalyser) was pipetted into plastic cuvette. Subsequently, volume of 6 µl of sample was added. Absorbance was measured for 12 min at λ = 450 nm.

RESULTS AND DISCUSSION

The aim of our experiment was to study oxidative stress in *Staphylococcus aureus* culture influenced by silver(I) ions. Oxidation stress was monitored by the determination of antioxidant capacity using five different principle methods: DPPH (2,2-difenyl-1-picrylhydrazyl), ABTS (2,2'-azinobis(3-ethylbenzothiazolin-6-sulfonátu)), DMPD (N,N-dimethyl-1,4-diaminobenzen), FRAP (Ferric Reducing Antioxidant Power) and FR (Free Radicals). These methods are based on the reaction of monitored molecule with free radicals under measurement of absorbance of nascent complex. Finally, results are recalculated to gallic acid equivalent (GAE). In conclusion, high value of antioxidant capacity and thus GAE means lower rate of oxidative stress.

Figure 1. Spectrophotometric analysis of *Staphylococcus aureus* antioxidant capacity. Dependence of antioxidant capacity on applied silver(I) ions concentration (0, 1.25, 2.5, 5, 10, 15, 25 and 50 µg·ml⁻¹). Obtained results were recalculated to gallic acid equivalents and subsequently to cell number after 24 h cultivation.



We can presume from the obtained results that the increasing concentration of silver(I) ions leads to the increasing of antioxidant capacity. The increase of antioxidant capacity was up to

the concentration of 15 μM . However, two highest used silver(I) ions concentrations (25 and 50 μM) led to the increase of antioxidant capacity for more than 200 % compared to control. In the case of DPPH method, concentration of 25 μM increased capacity for 800 % compared to control untreated culture. Under the highest concentration of silver ions (50 μM), this value exceeded 1300 %. In the case of free radicals method, concentration of 25 μM demonstrated increase for 380 % compared to control, under the 50 μM for 1000 % in comparison with control. Similar results were obtained using FRAP method: increase for 380 % under 25 μM and for 1000 % under 50 μM . ABTS methods also proved similar results as the increase for 550 % under the concentration of 25 μM , under the concentration of 50 μM even for 3500 %. In the case of DMPD method, the results were as follows: 25 μM – increase for 550 %, 50 μM – increase for 1200 %. The most visible increase in antioxidant capacity compared to control was determined using the ABTS method under the highest applied concentration of silver(I) ions, which was 3500 %. Obtained values indicate the increase of protective antioxidant compounds biosynthesis. This mechanism is responsible for maintenance of homeostasis and reduction of effects of heavy metals. This fact is closely connected with the increased biosynthesis of protective enzymes, such as superoxide dismutase [7], glutathione reductase [8] and glutathione peroxidase [9], under stress caused by heavy metals.

Moreover, we determined correlation between individual used methods. They were proved by Pearson's correlation coefficient (Tab. 1). The highest correlation rates were detected between FR and FRAP ($r^2=0.999$), FR and DMPD ($r^2=0.994$) and FRAP and DMPD ($r^2=0.994$) methods. These three methods are based on the reaction between free radicals and iron ions [10, 11]. This fact may be responsible for detected correlation coefficients.

Table 1. Values of correlation coefficients between individual methods by the use of Pearson's correlation coefficient.

Methods	ABTS	DPPH	DMPD	FRAP	FR
ABTS	x	0.888	0.965	0.978	0.980
DPPH	0.888	x	0.976	0.959	0.958
DMPD	0.965	0.976	x	0.994	0.994
FRAP	0.978	0.959	0.994	x	0.999
FR	0.980	0.958	0.994	0.999	x

CONCLUSION

In recent decades, amount of knowledge about the role of free radicals in oxidative stress in living organisms have significantly increased. The obtained results enabled determination of the role of silver(I) ions in oxidative stress in bacterial culture of *Staphylococcus aureus*. For this purpose, determination of antioxidant capacity was used. The increased concentration of applied silver(I) ions led to the increase

in antioxidant capacity. These values indicate the involvement of protective mechanisms in the protection against the effect of silver(I) ions. On the other hand, we can deduce the ability of silver(I) ions to induce free radicals and thus oxidative stress in *Staphylococcus aureus* bacterial culture.

ACKNOWLEDGEMENT

The work has been supported by Research centrum SIX, CZ.1.05/2.1.00/03.0072 and NanoCeva TA CR TA01010088.

REFERENCES

- [1] Nel A, Xia T, Madler L, *et al.*, Science, 311 (2006), 622-627.
- [2] Klasen H J, Burns, 26 (2000), 117-130.
- [3] Hussain S M, Hess K L, Gearhart J M, *et al.*, Toxicol. Vitro, 19 (2005), 975-983.
- [4] Sochor J, Ryvolova M, Krystofova O, *et al.*, Molecules, 15 (2010), 8618-8640.
- [5] Sochor J, Salas P, Zehnalek J, *et al.*, Lis. Cukrov. Repar., 126 (2010), 416-417.
- [6] Hana Paulová H B a E T, Chemické listy, 98 (2004), 174-179.
- [7] Sevcu A, El-Temsah Y S, Joner E J, *et al.*, Microbes Environ., 26 (2011), 271-281.
- [8] Lushchak V I, Biochem.-Moscow, 66 (2001), 476-489.
- [9] Forman H J, Torres M, Am. J. Respir. Crit. Care Med., 166 (2002), S4-S8.
- [10] Šulc M. L J, Hamouz K., Orsák M., Dvořák P., Horáčková V., Chemické listy, 101 (2007).
- [11] Yuan X Y, Gao M Z, Xiao H B, *et al.*, Food Chem., 133 (2012), 10-14.

VOLTAMMETRY OF LAWSONE-COPPER(II)-DNA COMPLEXES

Petr BABULA^{1,2}, Jan VANCO³, Ludmila KREJCOVA⁴, David HYNEK^{2,4}, Jiri SOCHOR^{2,4}, Vojtech ADAM^{2,4}, Libuse TRNKOVA^{2,5}, Jaromir HUBALEK^{2,6}, Rene KIZEK^{2,4*}

¹Department of Natural Drugs, Faculty of Pharmacy, University of Veterinary and Pharmaceutical Sciences Brno, Palackeho 1-3, CZ-612 42, Czech Republic

²Central European Institute of Technology, Brno University of Technology, Technicka 3058/10, CZ-616 00 Brno, Czech Republic

³Department of Chemical Drugs, Faculty of Pharmacy, University of Veterinary and Pharmaceutical Sciences Brno, Palackeho 1-3, CZ-612 42, Czech Republic

⁴Department of Chemistry and Biochemistry, Faculty of Agronomy, Mendel University in Brno, Zemedelska 1, CZ-613 00 Brno, Czech Republic

⁵Department of Chemistry, Faculty of Science, Masaryk University, Kotlarska 2, CZ-611 37 Brno, Czech Republic

⁶Department of Microelectronics, Faculty of Electrical Engineering and Communication, Brno University of Technology, Technicka 3058/10, CZ-616 00 Brno, Czech Republic

*kizek@sci.muni.cz

ABSTRACT

Metal complexes of fungal and plant secondary metabolites are in the centre of interest, especially due to their biological properties including cytotoxicity. In our work, we were focused on electrochemical behaviour of seven newly prepared complexes of lawsone with the second ligand represented by derivatives of pyridine, aminopyridine and pyrazole with copper(II) ions using methods of cyclic voltammetry and differential pulse voltammetry. In addition, we tested ability of these complexes to interact with DNA. Our results indicate that the most simple complex of lawsone - Cu(lawsone)₂(H₂O)₂·0.5H₂O proved significant prooxidant properties, which may contribute to its cytotoxicity that has been demonstrated in recent literature.

INTRODUCTION

Electrochemistry represents suitable tool for detection and quantification of different compounds from metal ions to high molecular mass organic compounds [1-7]. However, the number of papers focused on electrochemistry of naphthoquinones is relatively limited compared to other compounds and applications. Electrochemistry was used for characterization of 1,4-naphthoquinone complexes [8], rhodium(III) 1,2-naphthoquinone-1-oxime complexes [9] or palladium-1,4-naphthoquinone complexes containing bis(pyrazol-1-yl)methane ligands [10]. Babula et al. demonstrates using electrochemical techniques for detection and quantification of naphthoquinones lawsone, juglone and plumbagin in plant tissues [11]. Besides possibility to quantify naphthoquinones, electrochemistry is suitable for studying of interactions between drugs and their possible targets, most of all, with DNA due to outstanding sensitivity [12-18]. DNA biosensor technologies are in the focus of interest of many scientists due to their application in recognition of mechanism of interaction of compounds with DNA [19-26]. In this study, we aimed at studying of interactions of newly prepared complexes of lawsone (2-hydroxy-1,4-naphthoquinone) with

copper(II) ions with DNA. Possible mechanisms of DNA-lawsone complexes were suggested.

MATERIAL AND METHODS

Lawson complexes

Lawsone (Law, 2-hydroxy-1,4-naphthoquinone), monohydrate of copper(II) acetate ((CH₃COO)₂Cu·H₂O), and other chemicals of p.a. purity, which were used for synthesis of complexes, were purchased from Sigma-Aldrich (Sigma-Aldrich, St. Louis, USA). Lawson complexes were prepared in cooperation with Department of Chemical Drugs, Faculty of Pharmacy, University of Veterinary and Pharmaceutical Sciences Brno. Structure of complexes has been evaluated by elemental analysis and purity by spectrophotometric methods.

Differential pulse voltammetry for studying the interactions of lawsone complexes with dsDNA

Carbon paste electrode prepared according to the protocol mentioned above and modified with dsDNA (stock solution 1,000 µg/ml, applied volume 10 µl, time of accumulation 2, 4, 6, 10 and 20 min.) was used for the studying the interactions between dsDNA and lawsone complexes. Prior dsDNA carbon paste electrode incubation, solution of lawsone complex (stock solution 1,000 µg/ml, applied volume 10 µl, time

of interaction 2 min.) was applied for electrode modification. Then, the modified electrode was carefully washed with miliQ water to remove excess complex. In the next step, the electrode was incubated with dsDNA (stock solution 1,000 µg/ml, applied volume 10 µl, time of accumulation 2, 4, 6, 10 and 20 min.). Further, the electrode surface was washed with MiliQ water. Measurements were carried out in the presence of 0.2 M acetate buffer (pH = 5.0, volume = 2.000 µl). All measurements were carried out in triplicates. The conditions of measurement were as follows: time of accumulation 60 s, modulation time 0.057 s, interval time 0.2 s, initial potential 0.3 V, end potential -1.2 V, step potential 10 mV, modulation amplitude 25 mV.

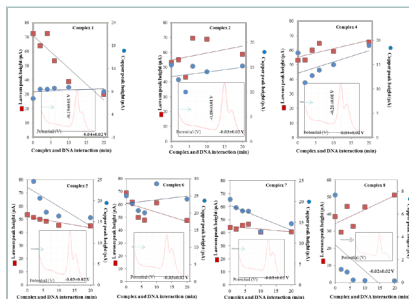
RESULTS AND DISCUSSION

dsDNA-modified carbon paste electrode was used for determination of dsDNA-lawsonone complexes interactions. DNA immobilized on the surface of carbon paste electrode brings interesting possibilities in the determination of interactions between this DNA and studied compounds. These techniques elucidated mechanism of interactions between important pharmaceuticals, such as antibiotics like levofloxacin [27] and rifampicin [28], compounds with DNA intercalating potential, such as acridine orange [29], anticancer agent daunomycin [30] and mitomycin [31] or compounds, which are commonly used as stains or eventually as DNA stains [32-34]. In this study, we focused on the decrease of signal 1 (copper(II) ions) and signal 2 (lawsonone) after accumulation on dsDNA modified carbon paste electrode. Briefly, carbon paste electrode was modified by studied complex (see Experimental part). In this step, we obtained first voltammogram for comparison with further voltammograms; after removing the excess of complex with miliQ water, electrode was incubated with 10 µl of dsDNA stock solution (1.000 µg/ml) for strictly defined time intervals as 2, 4, 6, 10 and 20 min. For each time of accumulation, independent voltammogram was obtained. Finally, we evaluated changes of heights of both signal 1 and signal 2, which inform us about possible interactions with dsDNA (Fig. 1).

The highest value of signal 1 (copper(II) ions) was detected for complex 6 followed by complexes 5, 4, 7, 2, 1 and 8. In the case of signal 2 (lawsonone), its highest value was determined for the most simple complex as complex 1 followed by complexes 2, 4, 6, 5, 7 and 8. Based on these results, we compared also individual signals. In this case, all values were recalculated to the value determined for complex 6 with the highest signal (= 100 %). The subsequent values for signal 1 in individual complexes were as it follows: 86.15 % (complex 5), 66.84 % (complex 4), 64.78 % (com-

plex 7), 53.31 % (complex 2), 46.94 % (complex 1) and 4.10 % (complex 8). Also in the case of comparison of heights of signal 2, the highest obtained value (complex 1) was taken as 100 % and values detected for remaining complexes were recalculated to this value. The values for other complexes were as it follows: 95.58 % (complex 2), 90.60 % (complex 4), 85.55 % (complex 6), (77.69 % (complex 5), and 64.23 % (complex 7). The lowest value of signal 2 height was determined for complex 8 (61.11 %).

Figure 1: Dependences of heights of copper(II) ions and naphthoquinone lawsonone signals of individual studied complexes on the time of dsDNA interaction within the range from 0 to 20 min. Voltammograms for individual complexes with marked potentials are introduced in insets.



CONCLUSION

Experimental work brings new knowledge not about oxidation/reduction properties of newly prepared copper(II)-lawsonone based complexes, but also knowledge about possibility of these complexes to interact with DNA. This knowledge can be used in further experiments focused on determination of mechanisms of cytotoxicity of studied complexes.

ACKNOWLEDGEMENT

Financial support from NANI-MEL GA CR 102/08/1546 and CEITEC CZ.1.05/1.1.00/02.0068 is highly acknowledged. The authors wish to express their thanks to Michal Doupovec for excellent technical assistance.

REFERENCES

- [1] Masarik M, Stobiecka A, Kizek R, et al., *Electroanalysis*, 16 (2004), 1172-1181.
- [2] Hodek P, Hanustiak P, Krizkova J, et al., *Neuroendocrinol. Lett.*, 27 (2006), 14-17.
- [3] Krizkova S, Adam V, Petrolova J, et al., *Electroanalysis*, 19 (2007), 331-338.

- [4] Masarik M, Cahova K, Kizek R, et al., *Analytical and Bioanalytical Chemistry*, 388 (2007), 259-270.
- [5] Petrlova J, Masarik M, Potesil D, et al., *Electroanalysis*, 19 (2007), 1177-1182.
- [6] Masarik M, Kynclova H, Huska D, et al., *Int. J. Mol. Med.*, 26 (2010), S46-S46.
- [7] Sochor J, Zitka O, Hynek D, et al., *Sensors*, 11 (2011), 10638-10663.
- [8] Singh W M, Baruah J B, J. Chem. Crystallogr., 41 (2011), 952-958.
- [9] Liu Y N, Liang W Z, Sang X G, et al., *Inorg. Chim. Acta*, 363 (2010), 949-956.
- [10] Scheuermann S, Sarkar B, Bolte M, et al., *Inorg. Chem.*, 48 (2009), 9385-9392.
- [11] Babula P, Huska D, Hanustiak P, et al., *Sensors*, 6 (2006), 1466-1482.
- [12] Petrlova J, Potesil D, Zehnalek J, et al., *Electrochim. Acta*, 51 (2006), 5169-5173.
- [13] Huska D, Fabrik I, Baloun J, et al., *Sensors*, 9 (2009), 1355-1369.
- [14] Huska D, Adam V, Babula P, et al., *Electroanalysis*, 21 (2009), 487-494.
- [15] Hynek D, Krejcová L, Zitka O, et al., *Int. J. Electrochem. Sci.*, 7 (2012), 34-49.
- [16] Hynek D, Krejcová L, Zitka O, et al., *Int. J. Electrochem. Sci.*, 7 (2012), 13-33.
- [17] Huska D, Adam V, Hubalek J, et al., *Chim. Oggi-Chem. Today*, 28 (2010), 18-20.
- [18] Huska D, Adam V, Krizkova S, et al., *Chim. Oggi-Chem. Today*, 28 (2010), 15-17.
- [19] Homola J, *Analytical and Bioanalytical Chemistry*, 377 (2003), 528-539.
- [20] Wang J, *Anal. Chim. Acta*, 469 (2002), 63-71.
- [21] Wang J, *Electroanalysis*, 17 (2005), 7-14.
- [22] Fojta M, Havran L, Kizek R, et al., *Talanta*, 56 (2002), 867-874.
- [23] Kizek R, Havran L, Fojta M, et al., *Bioelectrochemistry*, 55 (2002), 119-121.
- [24] Kizek R, Havran L, Kubicarova T, et al., *Talanta*, 56 (2002), 915-918.
- [25] Palecek E, Billova S, Havran L, et al., *Talanta*, 56 (2002), 919-930.
- [26] Palecek E, Kizek R, Havran L, et al., *Anal. Chim. Acta*, 469 (2002), 73-83.
- [27] Radi A, El Ries M A, Kandil S, *Anal. Chim. Acta*, 495 (2003), 61-67.
- [28] Girousi S T, Gherghi I C, Karava M K, J. Pharm. Biomed. Anal., 36 (2004), 851-858.
- [29] Gherghi I C, Girousi S T, Voulgaropoulos A N, et al., *Chem. Anal.*, 49 (2004), 467-480.
- [30] Wang J, Ozsoz M, Cai X H, et al., *Bioelectrochem. Bioenerg.*, 45 (1998), 33-40.
- [31] Ozkan D, Karadeniz H, Erdem A, et al., *J. Pharm. Biomed. Anal.*, 35 (2004), 905-912.
- [32] Kara P, Kerman K, Ozkan D, et al., *Electrochem. Commun.*, 4 (2002), 705-709.
- [33] Yang W R, Ozsoz M, Hibbert D B, et al., *Electroanalysis*, 14 (2002), 1299-1302.
- [34] Yang Z S, Zhang D P, Long H Y, et al., *Electroanalysis*, 19 (2007), 2577-2582.

EFFECT OF PLATINUM, PALLADIUM AND RHODIUM ON DUCKWEED (*LEMNA MINOR*)

Ivana BEDNAROVA¹, Hana MIKULASKOVA¹, Barbora NEMCOVA¹, Lenka STRAKOVA¹, Miroslava BEKLOVA¹, Jiri SOCHOR^{2,3}, Olga KRYSSTOFOVA², David HYNEK^{2,3}, Vojtech ADAM^{2,3}, Rene KIZEK^{2,3*}

¹ Department of Ecology and Environmental Protection, Faculty of Hygiene and Ecology, University of Veterinary and Pharmaceutical Sciences, Palackeho 1/3, 612 42 Brno, Czech Republic

² Department of Chemistry and Biochemistry, Faculty of Agronomy, Mendel University in Brno, Zemedelska 1, 613 00 Brno, Czech Republic

³ Central European Institute of Technology, Brno University of Technology, Technicka 3058/10, CZ-616 00 Brno, Czech Republic

*kizek@sci.muni.cz

ABSTRACT

The significant source of platinum group elements (PGE; Pt, Pd and Rh) is road traffic and the residues of widely used platinum based cytostatics. We can surmise that these metals can migrate into sewages and thus pollute aquatic ecosystem. The aim of our study was to analyze the effects of PtCl₄, PdCl₂ and RhCl₃ on morphology and vegetative growth of colonies of aquatic plant duckweed (*Lemna minor*) and then compare their inhibitory effects. In the case of PtCl₄ we focused on the antioxidant activity of this plant employing photometric analysis using biochemical analyzer BS-400 (Mindray, China).

INTRODUCTION

Trace concentrations of the platinum group elements (PGE; Pt, Pd and Rh) are nowadays an irreplaceable part of the environmental analysis and assessment. Their importance is based on their growing use as active compartments in automobile exhaust catalysts and also on their use in anti-cancer therapy in medicine [1-3]. Due to their harmful (allergenic and cytotoxic) potential, it is necessary to monitor their content and behaviour in different samples like water, soil, grass, urine or blood. The introduction of catalytic converters in cars since the mid 1970s (USA-1975, EU-1993) eliminated the necessity to add lead to fuel thus diminishing its release to the environment. However, a new environmental problem seems to appear since catalysts emit several other elements, some of which are among the least distributed in nature [4]. Vascular plant duckweed (*Lemna minor*) belongs to the group of bioindicators of ecotoxicological changes, mainly in aquatic system. A number of studies based on the ability of duckweed to accumulate metals have been done, because this property makes them suitable for water quality monitoring [5-7].

2. MATERIAL AND METHODS

Tested concentration row for each PGM (PtCl₄, PdCl₂ and RhCl₃) was 0, 1, 5, 10, 25, 50, 100 µM. We used samples of 100 ml volume (conventional test: 150 ml beaker), the initial number of fronds was 10. The vessels were in-

cubated during seven days under a continuous warm fluorescent lightning and with the temperature of 24±2°C. The toxic influence of PGE was evaluated on a basis of growth inhibition expressed as number of fronds and comparison of growth rates. Control groups of *Lemna minor* were cultivated under the recommended conditions in SIS (Swedish standard) medium. For the photometric determination we choose concentrations: 1, 10 and 100 µM. The test groups of duckweed were cultivated by 1, 10 and 100 µM and the samples were collected 2nd, 4th and 6th day of the experiment.

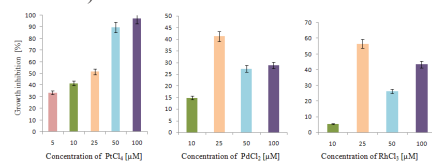
To determine the antioxidant activity, we used a biochemical analyzer BS – 400 (Mindray, China) and choose two methods: FRAP (Ferric Reducing Antioxidant Power) and ABTS radical method. The ABTS radical method is one of the most used assays for the determination of the concentration of free radicals. It is based on the neutralization of a radical-cation arising from the one-electron oxidation of the synthetic chromophore. The FRAP method (Ferric Reducing Antioxidant Power) is based on the reduction of complexes of 2,4,6-tripyridyl-s-triazine (TPTZ) with ferric chloride hexahydrate [8,9].

RESULTS AND DISCUSSION

Increasing concentrations of PGE negatively affected the growth of *Lemna minor*. During the experiment, we observed the growth slowdown and changing the appearance of fronds. Plants started to turn yellow (chlorosis), and at the end of the experiment, we observed leaves

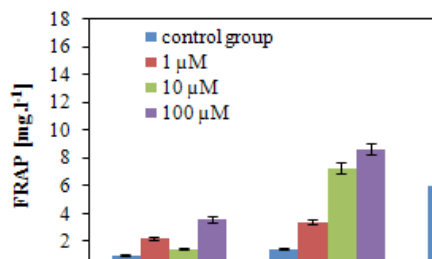
with white or colourless areas (necrosis). It can be concluded that in the case of $PtCl_4$, with the increasing concentration of metal the plant growth is considerably inhibited. $168hEC_{50}$ (effective concentration) $PtCl_4$ was estimated on $11.8 \mu M$. In the case of $PdCl_2$ and $RhCl_3$ the results were difficult to estimate. The lower concentrations ($5 \mu M$) caused slight growth stimulation and the higher inhibition effect was found under the $25 \mu M$ (Fig. 1 A - C). Due to poor solubility of both metals ($PdCl_2$ and $RhCl_3$) in concentrations 50 and $100 \mu M$ the growth inhibition declines, despite of pH adjustment. In addition, we observed insoluble precipitates at the bottom of tested vessels. We could not verify the expected trend of toxicity $Rh(III) \ll Pt(IV) < Pd(II)$ [10].

Figure 1.: The growth inhibition effect of a) $PtCl_4$, b) $PdCl_2$ and c) $RhCl_3$ on duckweed (*Lemna minor*).



We recalculated our results of the antioxidant activity on a basis of the total protein (reaction with red pyrogallol). Fig. 2 showed increasing antioxidant activities from 2nd day. The highest increase occurred at the end of the experiment. The increase in the antioxidant activity well corresponds with the increasing concentration of solution $PtCl_4$.

Figure 2.: The influence of $PtCl_4$ on the antioxidant activity of duckweed (*Lemna minor*).



CONCLUSION

$168hEC_{50}$ $PtCl_4$ was estimated on $11.8 \mu M$. The higher inhibition effect of $PdCl_2$, $RhCl_3$ was found under the concentration $25 \mu M$. The influence of $PtCl_4$ on *Lemna minor* was observed as a change of plant antioxidant activity. There is an evident dependence between duration of the experiment and increasing concentrations of me-

tals. The experiment showed a good correlation with the increase of the antioxidant activity: the last sampling day leads to a very high increase of the antioxidant activity.

ACKNOWLEDGEMENT

The work has been supported by MSMT 6215712402, IGA 82/2011/FVHE and Nano-BioMetal Net CZ.1.07/2.4.00/31.0023.

REFERENCES

- [1] Hees, T., Wencławiak, B., Lustig, S., Schramel, P., Schwarzer, M., Schuster, M., Verstraete, D., Dams, R., Helmers, E.: Environmental Science and Pollution Research, 5 (1998), 2, 105 – 111.
- [2] Dubiella-Jackowska, A., Kudlak, B., Polkowska, Z., Namiesnik, J.: Critical Reviews in Analytical Chemistry, 39 (2009), 4, 251-271.
- [3] Ravindra, K., Bencs, L., Van Grieken, R. Science of the Total Environment, 318 (2004), 1-43.
- [4] Djingova, R, Kovacheva, P, Wagner, G, Markert, B.: The Science of the Total Environment, 308 (2003), 1-3, 235–246.
- [5] Supalkova, V., Beklova, M., Baloun, J, Singer, CH., Sures, B., Adam, V., Huska, D., Pikula, J., Rauscherova, L., Havel, L., Zehnalek, J., Kizek, R.: Bioelectrochemistry, 72 (2008), 59-65.
- [6] Korner, S., Vermaat, J., E., Veenstra, S.: Journal of environmental quality, 32 (2003), 5, 1583-1590.
- [7] Vermaat, J., E., Hanif, M., K. Water research, 32 (1998), 9, 2569-2576.
- [8] Sochor, J., Ryvolova, M., Krystofova, O., Salas, P., Hubalek, J., Adam, V., Trnkova, L., Havel, L., Beklova, M., Zehnalek, J., Provaznik, I., Kizek, R.: Molecules. 15 (2010), 8618-8640.
- [9] Ou, B., X., Huang, D., J., Hampsch-Woodill, M., Flanagan, J., A., Deemer, E., K. Journal of Agricultural and Food Chemistry, 50(2002), 11, 3122-3128.
- [10] Farago, M.E., Parsons, P. J.: Chemical Speciation and Bioavailability, 6(1994), 1, 1-12.

COULOMETRIC DETERMINATION OF SARCOSINE

Natalia CERNEJ¹, Marketa KOMINKOVA¹, Ondrej ZITKA¹, Michal MASARIK^{2,4}, Jaromir HUBALEK^{2,3}, Tomas ECKSCHLAGER³, Libuse TRNKOVA^{2,6}, Vojtech ADAM^{1,2}, Rene KIZEK^{1,2*}

¹ Department of Chemistry and Biochemistry, Faculty of Agronomy, Mendel University in Brno, Zemedelska 1, 613 00 Brno, Czech Republic

² Central European Institute of Technology, Brno University of Technology, Technicka 3058/10, 616 00 Brno, Czech Republic

³ Department of Microelectronics, Faculty of Electrical Engineering and Communication, Brno University of Technology, Technicka 10, CZ-616 00 Brno, Czech Republic

⁴ Department of Pathological Physiology, Faculty of Medicine, Masaryk University, Kamenice 5, CZ-625 00 Brno, Czech Republic

⁵ Department of Paediatric Haematology and Oncology, 2nd Faculty of Medicine Charles

⁶ Department of Chemistry, Masaryk University, Kotlarska 2, 611 37 Brno, Czech Republic

*kizek@sci.muni.cz

ABSTRACT

Sarcosine, N-methylglycine, is a natural water soluble amino acid, which is a side product during the synthesis and degradation of glycine. Recently the hypothesis has been formulated that sarcosine can serve as a marker of prostate cancer and it is suitable for distinguishing of benign, localized and metastatic tumours. The aim of this work is to optimize the electrochemical coulometric detection coupled to flow injected analysis (FIA-ED). Limit of detection obtained by this method was 110 nM, which is sufficient for determination of sarcosine in various matrices including urine or blood of patients.

INTRODUCTION

The prostate cancer is still a major threat for men because it is the second most often diagnosed type of cancer. Moreover it is the third most often cause of death among cancer diseases [1]. Therefore the early diagnosis is so important. Current diagnostic procedure includes analysis of prostate specific antigen (PSA) in the blood, digital rectoscopy and biopsy [2, 3]. Even though PSA is commonly used marker, it still has some weak point regarding to accuracy and sensitivity of determination [4]. Due to this new markers suitable for fast and easy determination are still searched for. In 2009, sarcosine was highlighted as a potential cancer marker able to distinguish benign, localized and metastatic tumours from the urine or blood sample by simple and non-invasive diagnosis [5]. The opinions on sarcosine application in this area are inconsistent and publications refuting its applicability as a tumour disease marker have appeared. [6-10]. In this work, we developed the electrochemical method for sarcosine determination because electrochemistry is beneficial due to the short analysis times, low cost and high potential of miniaturization with high sensitivity [11, 12].

2. MATERIAL AND METHODS

Flow injection analysis with electrochemical detection (FIA-ED) system consists of two chromatographic pumps Model 582 ESA (ESA Inc., Chelmsford, MA) (working range 0.001-9.999

ml/min) and CoulArray electrochemical detector (Model 5600A, ESA, USA). Detector consists of flow analytical chamber (Model 6210, ESA, USA). Chamber contains four analytical cells. One analytical cell contains two referent (hydrogen-palladium), and two counter electrodes and one porous graphite working electrode. Electrochemical detector is situated in control module, which is thermostated. Sample (5 µl) was injected by manual valve (Rheodyne, USA). Flow rate of mobile phase was 1 ml/min.

RESULTS AND DISCUSSION

FIA-ED method was optimized for determination of sarcosine. In all optimization steps, standard solution of sarcosine was used. 10 µl of this solution was injected and free buffers - Britton-Robinson, borate buffer and phosphate buffer, all at pH of 7, 7.5, 8, 8.5, 9 a 9.5 (except phosphate buffer, which does not reach pH 9.5) were used.

For each buffer option the hydrodynamic voltammogram (HDV) was measured with tested potentials 500-1000 mV with potential step of 100 mV. The optimal flow rate 1 ml.min⁻¹ was determined. Plots shown in Fig. 1 were constructed from obtained values. It follows from the results that the highest signal was obtained using phosphate buffer pH 9. Moreover from Fig. 1A it follows that the optimal potential value in the electrochemical cell was 1000 mV. Calibration curve is shown in Fig. 2 and it can be concluded that sarcosine in the range 0.024-

50 $\mu\text{g}\cdot\text{ml}^{-1}$ can be determined. The limit of detection of 110 nM calculated, which is sufficient for determination of the sarcosine as a marker of prostate cancer because its amount in the urine is approximately 1.5 μM [13].

Figure. 1: The influence of (A) phosphate buffer, (B) borate buffer, (C) buffer Britton-Robinson on HDV of sarcosine (100 $\mu\text{g}/\text{ml}$).

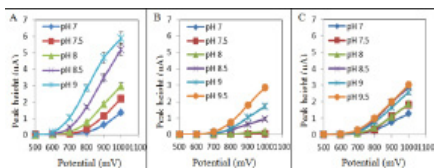
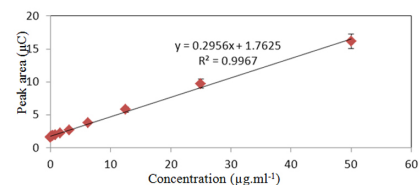


Figure. 2: Calibration curve of sarcosine in the range 50 – 0.024 $\mu\text{g}\cdot\text{ml}^{-1}$



CONCLUSION

It was proved that FIA-ED could be potentially suitable for determination of sarcosine in real samples such as urine. These methods can be potentially used for screening and contribute to the early diagnosis of cancer.

ACKNOWLEDGEMENT

This work has been supported by NANIMEL GA ČR 102/08/1546 and CEITEC CZ.1.05/1.1.00/02.0068.

REFERENCES

- [1] Boyle, P. and J. Ferlay, Cancer incidence and mortality in Europe, 2004. *Ann. Oncol.*, 2005. 16(3): p. 481-488.
- [2] Ellis, W.J., et al., Diagnosis of prostatic carcinoma - The yield of serum prostate specific antigen, digital rectal examination and transrectal ultrasonography. *J. Urol.*, 1994. 152(5): p. 1520-1525.
- [3] Gerber, G.S. and G.W. Chodak, Routine screening for cancer of the prostate. *J. Natl. Cancer Inst.*, 1991. 83(5): p. 329-335.
- [4] Jiang, Y.Q., et al., Quantitative Determination of Sarcosine and Related Compounds in Urinary Samples by Liquid Chromatography with Tandem Mass

- Spectrometry. *Anal. Chem.*, 2010. 82(21): p. 9022-9027.
- [5] Sreekumar, A., et al., Metabolomic profiles delineate potential role for sarcosine in prostate cancer progression. *Nature*, 2009. 457(7231): p. 910-914.
- [6] Meyer, T.E., et al., A Reproducible and High-Throughput HPLC/MS Method To Separate Sarcosine from alpha- and beta-Alanine and To Quantify Sarcosine in Human Serum and Urine. *Analytical Chemistry*, 2011. 83(14): p. 5735-5740.
- [7] Struys, E.A., et al., Serum sarcosine is not a marker for prostate cancer. *Annals of Clinical Biochemistry*, 2010. 47: p. 282-282.
- [8] Cao, D.L., et al., Efforts to resolve the contradictions in early diagnosis of prostate cancer: a comparison of different algorithms of sarcosine in urine. *Prostate Cancer and Prostatic Diseases*, 2011. 14(2): p. 166-172.
- [9] Jentzmk, F., et al., Sarcosine in Urine after Digital Rectal Examination Fails as a Marker in Prostate Cancer Detection and Identification of Aggressive Tumours. *European Urology*, 2010. 58(1): p. 12-18.
- [10] Schalken, J.A., Is Urinary Sarcosine Useful to Identify Patients With Significant Prostate Cancer? The Trials and Tribulations of Biomarker Development. *European Urology*, 2010. 58(1): p. 19-20.
- [11] Kalanur, S.S., et al., Electrochemical behavior of an anti-cancer drug at glassy carbon electrode and its determination in pharmaceutical formulations. *Int. J. Electrochem. Sci.*, 2008. 3(7): p. 756-767.
- [12] Gazdik, Z., et al., Determination of Vitamin C (Ascorbic Acid) Using High Performance Liquid Chromatography Coupled with Electrochemical Detection. *Sensors*, 2008. 8(11): p. 7097-7112.
- [13] Bellon, G., et al., Fluorometric evaluation of sarcosine in urine and serum. *J. Chromatogr.*, 1984. 311(2): p. 405-410.

HILIC SEPARATION OF SARCOSINE HYPHENATED TO COULOMETRIC DETECTION

Natalia CERNEJ¹, Marketa KOMINKOVA¹, Ondrej ZITKA¹, Jaromir GUMULEC⁴, Michal MASARIK^{2,4}, Vojtech ADAM^{1,2}, Jaromir HUBALEK^{2,3}, Libuse TRNKOVA⁵, Marie STIBOROVA⁶, Tomas ECKSCHLAGER⁷, Rene KIZEK^{1,2*}

¹ Department of Chemistry and Biochemistry, Faculty of Agronomy, Mendel University in Brno, Zemedelska 1, 613 00 Brno, Czech Republic

² Central European Institute of Technology, Brno University of Technology, Technicka 3058/10, 616 00 Brno, Czech Republic

³ Department of Microelectronics, Faculty of Electrical Engineering and Communication, Brno University of Technology, Technicka 10, CZ-616 00 Brno, Czech Republic

⁴ Department of Pathological Physiology, Faculty of Medicine, Masaryk University, Kamenice 5, CZ-625 00 Brno, Czech Republic

⁵ Department of Chemistry, Faculty of Science, Masaryk University, Kamenice 5, CZ-625 00 Brno, Czech Republic

⁶ Department of Biochemistry, Faculty of Science, Charles University, Albertov 2030, CZ-128 40 Prague 2, Czech Republic

⁷ Department of Paediatric Haematology and Oncology, and 2Department of Clinical Biochemistry and Pathobiochemistry, 2nd Faculty of Medicine, Charles University, V Uvalu 84, CZ-150 06 Prague 5, Czech Republic

*kizek@sci.muni.cz

ABSTRACT

Recently, sarcosine has been identified as a potential prostate cancer marker. To provide early determination of this compound, number of methods is still developed. Sarcosine is relatively small molecule, which is polar enough to enable separation by chromatography with reverse phase. For this reason we optimized method for separation by Hydrophilic interaction chromatography (HILIC). The aim of this work was to suggest the method for HILIC separation and determination of sarcosine with electrochemical detection. This aim was reached as shown by the limit of detection (350 nM), which was determined from calibration curve.

INTRODUCTION

The prostate cancer is still a major threat for men because it is the second most often diagnosed type of cancer. Moreover it is the third most often cause of death among cancer diseases [1]. **Therefore the early diagnosis is so important.** Current diagnostic procedure includes analysis of prostate specific antigen (PSA) in the blood, digital rectoscopy and biopsy [2, 3]. Even though PSA is commonly used marker, it still has some weak point regarding to accuracy and sensitivity of determination [4]. Due to these facts new markers suitable for fast and easy determination are still searched for. In 2009, sarcosine was highlighted as a potential cancer marker able to discriminate benign, localized and metastatic tumors from the urine or blood sample by simple and noninvasive diagnosis [5]. The opinions on sarcosine application in this area are inconsistent and publications refuting its applicability as a tumor disease marker have

appeared [6-10]. **To verify either of the hypotheses new methods for sarcosine determination have to be searched.**

Hydrophilic interaction chromatography (HILIC) has been suggested in 1990 [11], however it is based on "normal phase" chromatography, which started at the beginning of 20th century and it is complementary to commonly use reverse phase chromatography. HILIC is suitable for hydrophilic and polar compounds both macromolecular (such as histons and membrane proteins) as well as low molecular mass ones (such as phosphorylated amino acids and peptides). Due to the wide range of applicable buffers and ionic strengths the possibilities for method development are broad [12]. The aim of this work was to suggest the method for HILIC separation and determination of sarcosine with electrochemical detection.

MATERIAL AND METHODS

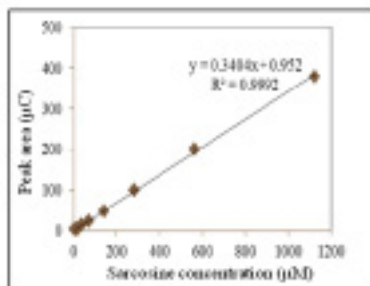
For determination of sarcosine high performance liquid chromatography with electrochemical detection system consists of three chromatographic pumps Model 582 ESA (ESA Inc., Chelmsford, MA) (working range 0.001-9.999 ml min⁻¹) was used. Two pumps was used for separation mobile phase A and B to the column and third pump was connected behind the column just before the detector for post column addition of mobile phase C (phosphate buffer) for effective electrochemical detection. HILIC chromatographic column Luna HILIC 200A (150 × 4.6; 3.5 μm particles, Phenomenex, USA) was used. Column was thermostated at ambient temperature. As electrochemical detector four-channel CoulArray electrochemical detector

(Model 5600A, ESA, USA). Detector consists of one flow analytical chambers (Model 6210, ESA, USA) which contain four analytical cells. One analytical cell contains two referent (hydrogen-paladium), and two counters and one porous graphite working electrode. Electrochemical detector is situated in control module which is thermostated. Sample (5 μ l) was injected manually by injection valve (Rheodyne, USA) and injection needle (Hamilton, USA).

RESULTS AND DISCUSSION

The method for determination of sarcosine by HILIC with electrochemical detection was optimized. Standard solution of sarcosine (100 μ g/ml, 10 μ l) was injected and following optimal conditions were determined: mobile phase A – acetonitrile, mobile phase B – water in ratio A:B 70:30, post column addition of mobile phase C (200 mM phosphate buffer pH 9). Optimal mixing ratio was A+B:C 1:1 with the flow rate 0.8 ml/min. Electrochemical potential was 1 000 mV. Under these optimal conditions calibration curve was constructed (Fig. 1) and the limit of detection of 350 nM was calculated.

Fig. 1.: Calibration curve of sarcosine obtained by HPLC(HILIC) with coulometric detection



CONCLUSION

The method for sarcosine determination using high performance liquid chromatography with HILIC stationary phase and electrochemical detection was developed. This method is suitable for determination of sarcosine in real samples such as urine.

ACKNOWLEDGEMENT

This work has been supported by NANIMEL GA ČR 102/08/1546, CYTORES GA CR P301/10/0356 and CEITEC CZ.1.05/1.1.00/02.0068.

REFERENCES

[1] Boyle, P. and J. Ferlay, *Cancer incidence and mortality in Europe, 2004*. Ann. Oncol., 2005. **16**(3): p. 481-488.

[2] Ellis, W.J., et al., *Diagnosis of prostatic carcinoma - The yield of serum prostate specific antigen, digital rectal examination and transrectal ultrasonography*. J. Urol., 1994. **152**(5): p. 1520-1525.

[3] Gerber, G.S. and G.W. Chodak, *Routine screening for cancer of the prostate*. J. Natl. Cancer Inst., 1991. **83**(5): p. 329-335.

[4] Jiang, Y.Q., et al., *Quantitative Determination of Sarcosine and Related Compounds in Urinary Samples by Liquid Chromatography with Tandem Mass Spectrometry*. Anal. Chem., 2010. **82**(21): p. 9022-9027.

[5] Sreekumar, A., et al., *Metabolomic profiles delineate potential role for sarcosine in prostate cancer progression*. Nature, 2009. **457**(7231): p. 910-914.

[6] Meyer, T.E., et al., *A Reproducible and High-Throughput HPLC/MS Method To Separate Sarcosine from alpha- and beta-Alanine and To Quantify Sarcosine in Human Serum and Urine*. Analytical Chemistry, 2011. **83**(14): p. 5735-5740.

[7] Struys, E.A., et al., *Serum sarcosine is not a marker for prostate cancer*. Annals of Clinical Biochemistry, 2010. **47**: p. 282-282.

[8] Cao, D.L., et al., *Efforts to resolve the contradictions in early diagnosis of prostate cancer: a comparison of different algorithms of sarcosine in urine*. Prostate Cancer and Prostatic Diseases, 2011. **14**(2): p. 166-172.

[9] Jentzmik, F., et al., *Sarcosine in Urine after Digital Rectal Examination Fails as a Marker in Prostate Cancer Detection and Identification of Aggressive Tumours*. European Urology, 2010. **58**(1): p. 12-18.

[10] Schalken, J.A., *Is Urinary Sarcosine Useful to Identify Patients With Significant Prostate Cancer? The Trials and Tribulations of Biomarker Development*. European Urology, 2010. **58**(1): p. 19-20.

[11] Alpert, A.J., *HYDROPHILIC-INTERACTION CHROMATOGRAPHY FOR THE SEPARATION OF PEPTIDES, NUCLEIC-ACIDS AND OTHER POLAR COMPOUNDS*. Journal of Chromatography, 1990. **499**: p. 177-196.

[12] Guo, H., et al., *A novel click lysine zwitterionic stationary phase for hydrophilic interaction liquid chromatography*. Journal of Chromatography A, 2012. **1223**(0): p. 47-52.

ELECTROCHEMICAL DETECTION OF SILVER IONS USING CARBON PASTE ELECTRODE

Dana DOSPIVOVA¹, David HYNEK^{1,2}, Jaromir HUBALEK^{2,3},
Libuse TRNKOVA^{2,4}, Vojtech ADAM^{1,2}, Rene KIZEK^{*1,2}

¹ Department of Chemistry and Biochemistry, Faculty of Agronomy, Mendel University in Brno, Zemedelska 1, 613 00 Brno, Czech Republic

² Central European Institute of Technology, Brno University of Technology, Technicka 3058/10, 616 00 Brno, Czech Republic

³ Department of Microelectronics, Faculty of Electrical Engineering and Communication, Brno University of Technology, Technicka 10, CZ-616 00 Brno, Czech Republic

⁴ Department of Chemistry, Masaryk University, Kotlarska 2, 611 37 Brno, Czech Republic
*kizek@sci.muni.cz

ABSTRACT

Electrochemical determination of silver ions using carbon paste electrode is the aim of this paper. There were prepared 4 types of carbon paste. The concentration of silver was determined by electrochemical methods of differential pulse voltammetry. As the measuring system the Electrochemical Workstation, CH Instruments (*Austin*, USA) with 3-electrode involvement was chosen.

INTRODUCTION

Among some of the major environmental contaminants include silver ions and silver colloidal particles. Silver is found in mine waters from the processing of ores and also in waste waters, in the photographic industry and silver cyanide technology. Another source of waste is in the glass industry, electro industry and medicine. [1] All forms are highly toxic to aquatic environment in particular and the entire aquatic ecosystem. [2] To study the acute toxicity is important to determine the concentration of free silver ions. This allows quantification of electrochemical methods using solid electrodes. [3]

Solid electrodes are usually used for routine analysis. The most often used electrode is a carbon paste electrode (CPE). It consists of a mixture of graphite powder (85%) and mineral oil (15%). The advantage is polarizability of electrode into the positive potential (up over +1 V), the recoverability of the surface and also the possibility of modifying the carbon paste. [4] The low and high molecular substances can be used to modifying these electrodes. This procedures have two basic reasons, first is modification of kinetic condition on the surface of electrode, second is increasing concentration of analyte on the surface due to better interactions. [3, 5] The modification improves the properties of the electrode, increases sensitivity and above all avoids adverse reactions and interferences that arises imperfections analyte. [6, 7] Is normally achieved LOD in the unmodified CPE 1.10^{-6} – 1.10^{-7} to mol.l^{-1} direct determination of the accumulation analyte leads to the even lower concentrations. [8, 9]

In our study, we examined the determination of silver ions using electrochemical methods of differential pulse voltammetry using carbon

paste electrode.[10]

MATERIAL AND METHODS

The first step of the experiment was preparation of 100 μM silver nitrate stock solution, AgNO_3 (Sigma Aldrich). The calibration curves of silver ions were measured in the concentration range from 63.5 to 0.03 μM . Comparison of four types of carbon powder was studied next. Carbon paste electrode (CPE) was used as the working electrode. Four concentration dependences were measured with the carbon paste prepared from four different types of carbon powder (a) Glassy Carbon, 2-12 micron spherical powder, 99.99% (Sigma Aldrich), (b) Glassy carbon spherical powder 10-40 microns, 99% (Sigma Aldrich), (c) Carbon multi-walled nanotube, 6-13 nm > 99% (Sigma Aldrich), (d) Expanded carbon. All carbon pastes consisted of a mixture of the carbon powder and mineral oil (Sigma Aldrich) in different ratios.

For carbons (a) and (c) were selected composition of 1.0 g carbon powder and 300 μl of mineral oil, (b) consisted from 1.0 g of carbon powder and 500 μl of mineral oil. For expanded carbon was weighed 0.1 g carbon powder and 300 μl of oil. Carbon powder was rubbed with mineral oil in an agate mortar for 25 minutes. To determine the calibration curves basic electrochemical method of differential pulse voltammetry (DPV) was selected. The measurement instrumentation was used as follows: Electrochemical Workstation, CH Instruments (*Austin*, USA) with 3-electrode involvement. The working electrode was the carbon paste electrode (CPE) prepared in our laboratory and reference electrode was $\text{Ag/AgCl}/3\text{M KCl}$ and as an auxiliary electrode the platinum electrode was used. Samples were measured in volume of 2 ml acetate buffer pH5

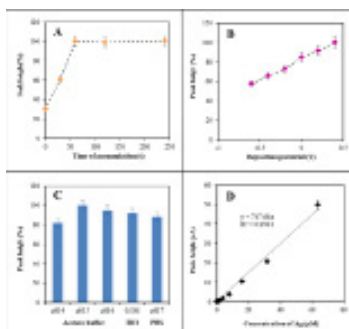
electrolyte. The potential range was from -0.2 to +0.5 V, the pulse period 0.05 s. The characteristic signal of silver was observed at 0.2 V. Other parameters of the method were: Incr. E 0.001 V, 0.005 with Pulse Width, Sample Width 0.0025 s, 0.05 s pulse period, 0.05 s Quit Time, Sensitivity (A / V) 1×10^{-5} , the amplitude of 50 mV. The comparison of signal intensity for used electrodes was made for silver concentration $3.9 \mu\text{M}$.

RESULTS AND DISCUSSION

In our work we focused on the detection of silver ions using an electrochemical method of differential pulse voltammetry on solid carbon paste electrode.

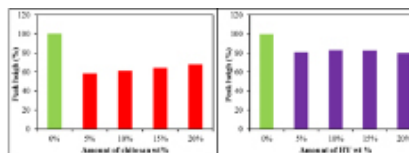
We have prepared four types of carbon pastes (a), (b), (c), (d) and calibration dependences were determined for concentrations from 63.5 to $0.03 \mu\text{M}$, for the expanded carbon we achieved even 10 times lower concentration. Calibration points were smoothed and were obtained a regression equation for each of the carbon paste. The best result was obtained for the paste prepared from expanded carbon, where we set a linear dependence to $0.003 \mu\text{M}$ ($y=550.35x$, $R^2=0.994$), and therefore this paste was used in other experiments. The method of DPV was optimized in several parameters: the influence of deposition, accumulation time and influence of the used buffer. All these parameters were compared with our chosen silver concentration $3.9 \mu\text{M}$. The influence of deposition has been investigated for potentials of -0.6; -0.4, -0.2, 0, 0.2 and 0.4 V. The intensity of signal growth with deposition potential linearly, therefore we chose the highest possible deposition at 0.5 V. Time of accumulation were investigated at these values 0, 30, 60, 120 and 240 s. Intensity of signal growth to time of 60 s, then the signal remained at constant value. Then has been investigated the influence of composition of the electrolyte, acetate buffer pH 4, 5, 6, PBS pH 7 and 0.1 M HCl were used. The highest signal was achieved with acetate buffer pH 5. When PBS and HCl were used, the signal maximum was moved from 0.2 V to the potential 0.03 – 0.04 V.

Figure 1: Optimization of measuring conditions: A – time of accumulation, B – deposition potential, C – various electrolytes, D – calibration curve measured with optimal condition (time of accumulation 60s, deposition potential 0.5V, acetate buffer



The last optimization was the modification of carbon paste. The carbon powder was mixed with chitosan and hyaluronic acid (5, 10, 15 and 20 wt%). In both cases the modifications caused a reduction of signal. The chitosan was reduced on average by 37%, in case of hyaluronic acid it was in average 18.5%. Modification of electrode led probably to the reduction of silver electroactivity.

Figure 2: Optimization of measuring conditions: A – modification by chitosan B – modification by hyaluronic acid (HY)



At the conclusion of the whole work there was the silver calibration curve ($y = 637.9x$, $R^2 = 0.9929$) in optimized condition measured (DPV, accumulation 60s, deposition 0.5 V, acetate buffer pH5).

CONCLUSION

Differential pulse voltammetry in connection with carbon paste electrode of expanded carbon was a suitable method for the electrochemical detection of silver ions in solution. The method was optimized and due to appropriate parameters we obtain a representative, reproducible and accurate results.

ACKNOWLEDGEMENTS

The financial support from the following project NANIMEL GA ČR 102/08/1546 and NANOSEMED GA AV KAN208130801 and TACR TA01010088 is highly acknowledged.

REFERENCES

- [1] Li T, Albee B, Alemayehu M, et al., *Anal. Bioanal. Chem.*, 398 (2010), 689-700.
- [2] Bianchini A, Wood C M, *Environ. Toxicol. Chem.*, 22 (2003), 1361-1367.
- [3] Vytras K, Svancara I, Metelka R, *J. Serb. Chem. Soc.*, 74 (2009), 1021-1033.
- [4] Radulescu M C, Chira A, Radulescu M, et al., *Sensors*, 10 (2010), 11340-11351.
- [5] Tashkhourian J, Javadi S, Ana F N, *Microchim. Acta*, 173 (2011), 79-84.
- [6] Ye X Z, Yang Q H, Wang Y, et al., *Talanta*, 47 (1998), 1099-1106.
- [7] Trnkova L, Krizkova S, Adam V, et al., *Biosens. Bioelectron.*, 26 (2011), 2201-2207.
- [8] Vicentini F C, Figueiredo L C S, Janegitz B C, et al., *Quim. Nova*, 34 (2011), 825-830.
- [9] Prasek J, Drbohlavova J, Chomoucka J, et al., *J. Mater. Chem.*, 21 (2011), 15872-15884.
- [10] Krizkova S, Krystofova O, Trnkova L, et al., *Sensors*, 9 (2009), 6934-6950.

MICROFLUIDIC DETECTION OF QUANTUM DOTS

Dana DOSPIVOVA¹, Pavel KOPEL^{1,2}, David HYNEK^{1,2}, Jana DRBOHLAVOVA^{2,3}, Libuse TRNKOVA^{2,4}, Libor JANU^{1,5}, Jaromir HUBALEK^{2,3}, Vojtech ADAM^{1,2}, Rene KIZEK^{*1,2}

¹ Department of Chemistry and Biochemistry, Faculty of Agronomy, Mendel University in Brno, Zemedelska 1, 613 00 Brno, Czech Republic

² Central European Institute of Technology, Brno University of Technology, Technicka 3058/10, 616 00 Brno, Czech Republic

³ Department of Microelectronics, Faculty of Electrical Engineering and Communication, Brno University of Technology, Technicka 10, CZ-616 00 Brno, Czech Republic

⁴ Department of Chemistry, Masaryk University, Kotlarska 2, 611 37 Brno, Czech Republic

⁵ Clonestar peptide services, Brno, Czech Republic

*kizek@sci.muni.cz

ABSTRACT

Microfluidic detection of quantum dots (QDs) is the aim of this paper. In our laboratory there were prepared QDs Cd. For the determination of Cd the fully automated microfluidic system was designed. Flow injection analysis of QDs was preceded by optimization methods for Cd(NO₃)₂ • 4H₂O. The concentration of Cd was determined by electrochemical methods of differential pulse voltammetry.

INTRODUCTION

Nanotechnology is one of the most discussed current technologies. Nanotechnology is generally referred to science research and development, which deals with the targeted creation of material structures at a scale of several nanometers. Nanotechnology and nanomaterials are very extensive in the sectors of physics, chemistry and biology. [1-3]

These materials include fluorescent semiconductor nanocrystals, commonly known as quantum dots (QDs, "quantum dots"). Quantum dot is bounded conductive region of very small dimensions with large band gap energy. [4-7] One of the most important features is the ability of optical dots stain. This ability is linked to the size of quantum dots. Big dots emit in the red spectrum and little dots emit in the blue spectrum. This ability is again associated with the distribution of energetic layers in the dot and its ability to absorb not only electrons but also photons. [8, 9]

MATERIAL AND METHODS

The first step of the experiment was preparation of quantum dots (QDs). All chemicals were purchased from Sigma-Aldrich and used without further purification. CdS quantum dots were prepared with a slightly modified method published in [10] Cadmium nitrate tetrahydrate Cd(NO₃)₂•4H₂O (0.03085 g, 0.1 mM) was dissolved in ACS water (25 ml). 3-mercaptopropionic acid (35 µl, 0.4 mM) was slowly added to stirred solution. Afterwards, pH was adjusted to 9.11 with 1M NH₃ (1.5 ml). Sodium sulphide nanohydrate Na₂S•9H₂O (0.02402 g, 0.1 mM) in 23 ml of ACS water was poured into the first

solution with vigorous stirring. Prepared CdS-quantum dots were stored in dark at 4 °C. The fluorescence spectrum is shown in Fig. 5. The next step was a flow injection analysis. Microfluidic system for fully automated electrochemical detection was suggested (SFIA-ED). The system consists from solvent delivery automated analytical syringe operating in the working volume range of 1–50 µl under variable speed from 1.66 to 50 µl/s (Model eVol, SGE Analytical Science, Australia), 3-way 2-position selector valve (made from 6-way valve) (Valco, Instruments, USA), and dosing capillary that is directly entering to the electrochemical flow cell (CH Instruments, USA). To prepare a fully automated system, switching valve enabling switching between the off (waste) and sample flow positions was placed into the system. The sample (10 µl) was injected by automated syringe (SGE Analytical Science, Australia) through flow cell in speed of 1.66 µl/s. The flow cell was cleaned by rinsing of 200 µl ethanol in water (75% v/v), then 200 µl of 100% methanol and stabilized by 200 µl of supporting electrolyte. Cleaning was applied after 50 measurements. The electrochemical flow cell includes one low volume (1.5 µl) flow-through analytical cell (CH Instruments), which consisted of doubled glassy carbon (GC) working electrode, Ag/AgCl electrode as the reference electrode and output steel tubing as an auxiliary electrode. Electrochemical flow cell was connected to miniaturized potentiostat 910 PSTAT mini (Metrohm, Switzerland) as a control module. The differential pulse voltammetry (DPV) as measuring method was used and parameters were as follows: initial potential -1.2 V, end potential -0.2 V, modulation amplitude

0.05 V, step potential 0.001 V. All experiments were carried out at laboratory temperature. Acetate buffer (0.2 M, pH 5) was used as the supporting electrolyte. Every measuring sample consists from 15 μl of sample solution which was diluted in acetate buffer. The data obtained were processed by the PSTAT software 1.0 (Metrohm, Switzerland). The experiments were carried out at 20 $^{\circ}\text{C}$.

Flow injection analysis of QDs was preceded by optimization methods for $\text{Cd}(\text{NO}_3)_2 \cdot 4\text{H}_2\text{O}$ (200 μM). The calibration curves of cadmium ions were measured in the concentration range from 0.098 μM - 1.5625 μM . Optimized parameters were: time of accumulation (30, 60, 120, 180, 240, 360, 420 sec.) and deposition potential (-1.2, -1.1, 1.0; -0.9, -0.8 and -0.7 V). Parameters and measurement system was the same as the system for the detection of QDs.

RESULTS AND DISCUSSION

In our work we focused on the detection of QDs using an electrochemical method of differential pulse voltammetry in microfluidic injection system. At the beginning of experiment the method was optimized for the preparation of QDs. These QDs were subsequently detected by the concentrations of Cd using differential pulse voltammetry. This method was optimized for the standard solution of $\text{Cd}(\text{NO}_3)_2 \cdot 4\text{H}_2\text{O}$ in the concentration range from 0.098 to 1.5625 μM . Optimized parameters were: time of accumulation and deposition potential. For our setting accumulation time 360 s was chosen. This dependence is shown in Fig.1. Deposition potential of -1.2 V was selected based on the results showed in Fig. 2. Limit of detection was determined 0.17 nM. The calibration curve is shown in Fig. 3. Voltammogram of QDs is shown in Fig. 4. Peak height of Cd in quantum dots was 21.788 nA, which corresponds to a concentration of 1.28 μM of Cd. Emission spectrum of QD Cd (Excitation Wavelength 350 nm) is shown in Fig. 5.

Figure 1: Optimization of measuring conditions: time of accumulation (0, 30, 60, 120, 180, 240, 360, 420 s)

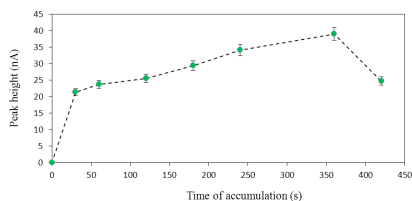


Figure 2: Optimization of measuring conditions: deposition potential (-1.2; -1.1; -1.0; -0.9; -0.8; -0.7 V)

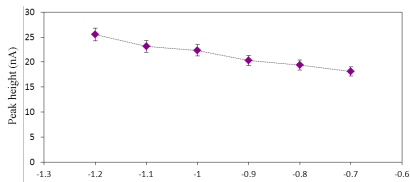


Figure 3: Calibration curve of Cd (measurement parameters: time of accumulation 360 s, deposition potential -1.2 V, dispensed volume 10 μl), DPV method was applied.

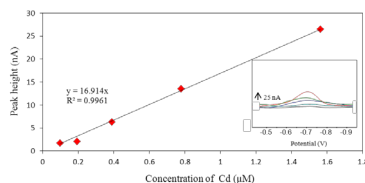


Figure 4: Voltammograms of quantum dots, characteristic peak of QD Cd in -0.6 V

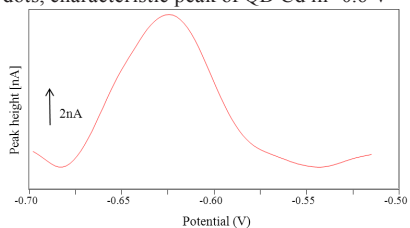
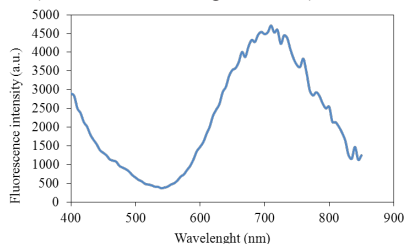


Figure 5: Emission spectrum of QD Cd (Excitation Wavelength 350 nm)



CONCLUSION

Differential pulse voltammetry in connection with microfluidic injection system was a suitable method for the electrochemical detection of Cd in quantum dots. Specified concentration of Cd in quantum dots was 1.28 μM . The method was optimized and due to appropriate parameters we obtain repeatable results.

ACKNOWLEDGEMENT

The financial support from the following project NANOLABSYS CZ.1.07/2.3/00/20.0148, GA ČR 102/10/P618, CEITEC CZ.1.025/1.1.00/02.0068 and IGA IP10/2012 is highly acknowledged.

REFERENCES

- [1] Tews M, *Ann. Phys.-Berlin*, 13 (2004), 249-304.
- [2] Schuster R, Barth M, Gruber A, *et al.*, *Chem. Phys. Lett.*, 413 (2005), 280-283.
- [3] Mackowski S, *Thin Solid Films*, 412 (2002), 96-106.
- [4] Henini M, *Nanoscale Res. Lett.*, 1 (2006), 32-45.
- [5] Warren C, *et al.*, *Curr Opin Biotech*, 13 (2002), 40-46.
- [6] Medintz I, Mattoussi H, *Nat Mat*, 4 (2005), 435-446.
- [7] Alivisatos P, *Nat. Biotech.*, 2 (2004), 47-52.
- [8] Gao X, Nie S, *Curr Opin Biotech*, 16 (2005), 63-72.
- [9] Murphy C, *Anal Chem*, 74 (2002), 520-526.
- [10] Li H, Shih W Y, Shih W H, *Ind. Eng. Chem. Res.*, 46 (2007), 2013-2019.

ELEKTROCHEMICAL STUDY OF HYALURONIC ACID-SILVER IONS COMPLEX

Matej SKLENAR¹, Andrea BEZDEKOVA¹, Dana DOSPIVOVA¹, Jiri SOCHOR^{1,2,3,4}, Petr BABULA^{2,3}, Libuse TRNKOVA^{2,5}, Jaroslav HUBALEK^{2,4}, Vojtech ADAM^{1,2,4}, Rene KIZEK^{1,2,4}

¹ Department of Chemistry and Biochemistry, Faculty of Agronomy, Mendel University in Brno, Zemedelska 1, CZ-613 00 Brno, Czech Republic

² Central European Institute of Technology, Brno University of Technology, Technicka 3058/10, CZ-616 00 Brno, Czech Republic

³ Department of Natural Drugs, Faculty of Pharmacy, University of Veterinary and Pharmaceutical Sciences Brno, Palackeho 1-3, CZ-612 42, Czech Republic

⁴ Department of Microelectronics, Faculty of Electrical Engineering and Communication, Brno University of Technology, Technicka 10, CZ-616 00 Brno, Czech Republic

⁵ Department of Chemistry, Masaryk University, Kotlarska 2, 611 37 Brno, Czech Republic

ABSTRAKT

Hyaluronic acid, nosulphated glycosaminoglycan, is widely used in pharmacy, especially in reepitelization of wound and in cosmetic applications. Silver ions are used for their antimicrobial properties. We studied formation of complex between these two compounds in this work, especially with the respect of its possible usage in development of vessel substitutions, where antibacterial properties of material together with its biocompatibility are highly demanded. Complex was studied electrochemically using the differential pulse voltammetry method.

INTRODUCTION

Hyaluronic acid (HA) is a polymer of disaccharides (D-glucuronic acid and D-N-acetylglucosamine monomers), respectively an anionic nosulphated glycosaminoglycan with wide distribution within the human body in connective, epithelial and neural tissues. For its non-toxic, biocompatible and biodegradable properties is suitable for biomedicine applications with the focus on above-mentioned tissues [1-3]. Its antimicrobial properties are widely discussed too [4, 5]. HA releases cytokines and chemokines during inflammation, so it has significant moderating role in the processes of inflammation. This effect contributes to its usage in reepitelization and wound healing [6, 7]. Even for longer periods, HA content in fetal wounds is still higher than that in adult wounds, which suggests that HA may, at least in part, reduce collagen deposition and therefore lead to reduced scarring [8].

The aim of our project consists in the determination of the stable complex with significant antibacterial properties, which will serve for development of vessel substitution (based on polypropylene and polyester material) coating (biocompatible surface). Combination of HA with "healing" properties and silver ions with significant antibacterial effect seems to be one of the most advantageous combinations. However, it is quite necessary to determine the possibility of cross-reaction between HA and silver ions under formation of a complex in the first experimental

step. Our work was focused on the possibilities of the study of HA electrochemical properties and possibility of complexation – interaction of HA with silver ions.

MATERIAL AND METHODS

Hyaluronic acid 261006-2 (100 µM, ContiPro Group, Czech Republic), which was dissolved in miliQ water, was used in our experiment. Solution of HA was mixed with 50 µM AgNO₃ (Sigma-Aldrich, USA). This mixture was subsequently incubated at 37 °C and 150 rpm for 24 h in the Incubator Hood TH 15 (Edmund Buhler GmbH, Hechingen, Germany). Like this prepared sample was electrochemically studied.

Preparation of carbon paste electrode

Carbon paste working electrode was made from expanded carbon powder and mineral oil (Sigma-Aldrich, USA). For the expanded carbon preparation, 0.1 g of carbon powder and 300 µl of oil were weighed. Carbon powder was rubbed with mineral oil in an achat mortar for 25 minutes.

Electrochemical analysis

Electrochemical measurements were performed using a CH Instruments Electrochemical Workstation (CH Instruments, USA), using glass cell with three electrodes. As working electrode carbon paste electrode was used. Reference electrode was Ag/AgCl/3M KCl (Metrohm, Switzerland) and counter electrode was platinum

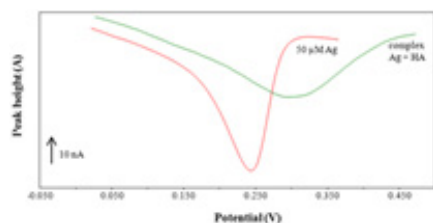
(Metrohm, Switzerland). The differential pulse voltammetry (DPV) as measuring method was used and the parameters were as follows: initial potential -0.2 V, end potential 0.5 V, modulation amplitude 0.05 V, step potential 0.001 V. All experiments were carried out at laboratory temperature. Acetate buffer (0.2 M, pH 5) was used as the supporting electrolyte. Every measuring solution consisted of 100 μ l of sample and 1900 μ l of acetate buffer (0.2 M, pH 5). For results evaluation software CHI 440A was used.

RESULTS AND DISCUSSION

Determination of silver ions in the biological matrix is usually very difficult, so, they are most frequently determined using the atomic absorption spectroscopy (AAS) technique [9]. On the other hand, electrochemical techniques represent suitable alternative analytical techniques for silver ions and especially their complexes determination [10-12]. Works focused on the electrochemical study of HA take and advantage of direct electrochemistry [13, 14] cyclic voltammetry [15], or amperometry [16].

We used differential pulse voltammetry (DPV) in the three-electrode arrangement for the HA, silver ions and their interaction determination. Carbon paste electrode based on expanded carbon was used in our work due to its quite unique properties. These electrodes are recently used due to their characteristic property – to change surface properties - which is suitable for analytical purposes [17-19]. They provide higher signals (more intensive signals) of measured compounds, they are of low costs. In addition, surface of these electrodes may be easily renewed and they are stable in almost all solvents [20-22].

Figure 1: Electrochemical detection of silver ions and hyaluronic acid



Maximum of signal of silver ions (standard) was recorded at the potential of 0.245 V, maximum of hyaluronic acid signal at the potential of 0.300 V. Signal of nascent hyaluronic acid-silver ions complex was determined at the potential of 0.290 V. Disappear of signal of silver ions and shift of the HA signal to the lower potential was observed during this interaction. In addition, interaction was characterized by the formation of

complex, which was well evident in the change of the signal height and its shift into lower potential.

CONCLUSION


Electrochemical study of hyaluronic acid, silver ions and complex of these two components is presented in this work. In addition, methods for their determination have been optimized for further study.

ACKNOWLEDGEMENT

The work has been supported by CEITEC, CZ.1.05/1.1.00/02.0068 and Nano Ceva TA ČR TA01010088.

REFERENCES

- [1] Xu F, Nacker J C, Crone W C, et al., *Biomaterials*, 29 (2008), 150-160.
- [2] Li K, Kim B J, Huh C H, et al., *J. Am. Acad. Dermatol.*, 66 (2012), AB208-AB208.
- [3] Kondo S, Kuroyanagi Y, *J. Biomater. Sci.-Polym. Ed.*, 23 (2012), 629-643.
- [4] Ardizzoni A, Neglia R G, Baschieri M C, et al., *J. Mater. Sci.-Mater. Med.*, 22 (2011), 2329-2338.
- [5] Esslinger J, Seilem R S, Herrmann G, et al., *Rev. Med. Vet.*, 145 (1994), 49-53.
- [6] Adas G, Karatepe O, Arykan S, et al., *Bratisl. Med. J.*, 110 (2009), 210-214.
- [7] Kubo K, Kuroyanagi Y, *Artif. Organs*, 29 (2005), 845-849.
- [8] Longaker M T, Chiu E S, Adzick N S, et al., *Ann. Surg.*, 213 (1991), 292-296.
- [9] Saeki S, Kubota M, Asami T, *Int. J. Environ. Anal. Chem.*, 64 (1996), 179-183.
- [10] Mikelova R, Baloun J, Petlova J, et al., *Bioelectrochemistry*, 70 (2007), 508-518.
- [11] Huska D, Krizkova S, Hubalek J, et al., *Toxicol. Lett.*, 180 (2008), S236-S237.
- [12] Krizkova S, Krystofova O, Trnkova L, et al., *Sensors*, 9 (2009), 6934-6950.
- [13] Gao R F, Shangguan X D, Qiao G J, et al., *Electroanalysis*, 20 (2008), 2537-2542.
- [14] Zhu Z H, Li X, Wang Y, et al., *Anal. Chim. Acta*, 670 (2010), 51-56.
- [15] Lu H Y, Hu N F, *J. Phys. Chem. B*, 110 (2006), 23710-23718.
- [16] Huang H, Zhou J, Huang Y, et al., *Development of a multi-channel immunosensor for determination of serum hepatic fibrosis markers*, Ieee, New York 2006.
- [17] Zhang X Z, Cui Y, Lv Z L, et al., *Int. J.*

- 
- Electrochem. Sci., 6 (2011), 6063-6073.
- [18] Sobrova P, Ryzolova M, Huska D, *et al.*, Int. J. Electrochem. Sci., 7 (2012), 1-12.
- [19] Masarik M, Kynclova H, Huska D, *et al.*, Int. J. Mol. Med., 26 (2010), S46-S46.
- [20] Raoof J B, Ojani R, Alinezhad A, *et al.*, Mon. Chem., 141 (2010), 279-284.
- [21] Kong Y, Chen X H, Ni J H, *et al.*, Appl. Clay Sci., 49 (2010), 64-68.
- [22] Adam V, Petrlova J, Wang J, *et al.*, PLoS One, 5 (2010).

DETERMINATION OF PLATINUM IN PEA PLANTS (*PISUM SATIVUM* L.) AND MAIZE (*ZEA MAYS* L.) USING DIFFERENTIAL PULSE VOLTAMMETRY

Hana MIKULASKOVA¹, Ivana BEDNAROVA¹, Barbora NEMCOVA¹, Olga KRYSOFOVA², Sona KRIZKOVA², David HYNEK², Jiri SOCHOR^{2,3}, Vojtech ADAM^{2,3}, Miroslava BEKLOVA¹, Rene KIZEK^{2,3*}

¹ Department of Veterinary Ecology and Environmental Protection, University of Veterinary and Pharmaceutical Sciences, Palackeho 1-3, CZ-612 42 Brno, Czech Republic

² Department of Chemistry and Biochemistry, Mendel University in Brno, Zemedelska 1, CZ-613 00 Brno, Czech Republic

³ Central European Institute of Technology, Brno University of Technology, Technicka 3058/10, CZ-616 00 Brno, Czech Republic

*kizek@sci.muni.cz

ABSTRACT

The platinum group metals are considered as a one of the often discussed environmental pollutants. They are mainly originated from automobile catalysts and to some extent from the hospital and industrial waste. The significant increase of platinum group metals concentrations in the environment raised questions regarding the adverse effects on human health through possibility of the food chain contamination. The aim of presented study was to evaluate the ability of penetration degree of platinum (Pt) in the form PtCl₄ in different parts of plants in connection to the length of exposure of given metal (8 and 12 days). Seeds of field pea (*Pisum sativum* L.) and corn (*Zea mays* L.) were selected for the experiment due to their important role in livestock feed and human food.

INTRODUCTION

Growing anthropogenic activities cause a gradual increase in amount of heavy metals in the environment [1]. The main source is vehicular traffic, which has negative impact on the fundamental components of the ecosystem, such as water, soil and air. Principal cause of this pollution is emission from combustion of hydrocarbon fuels, which arise due to incomplete combustion of pollutants and are emitted to the atmosphere as exhaust gases. In order to reduce the production of gaseous pollutants the automotive catalysts are introduced, with a mixture of platinum metals, especially Pt, Pd, Rh as a catalytically active substance. The combination of oxidation-reduction reactions and high temperatures inside the catalysts release these metals into the environment [2-6]. Due to growing traffic volume and the enhancement of the pollutants emitted to the environment, platinum group metals have become a global problem. The increase in concentrations of these metals in the environment raises concerns about the possible intrusion into the food chain and potential health risks in relation to the population [7-9]. The aim of presented study was to evaluate the ability of penetration degree of platinum (Pt) in the form PtCl₄ in different parts of plants in connection to the length of exposure of given metal (8 and 12 days).

MATERIAL AND METHODS

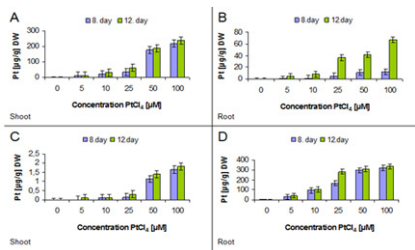
For the experimental evaluation of platinum penetration into plants seeds of pea (*Pisum sativum* L.) and maize (*Zea mays* L.), which were exposed to PtCl₄ in concentration row: 0; 5; 10; 25; 50 and 100 μM, were used. For each concentration and control 100 seeds were selected and placed on plates coated with cellulose. Plates for germination were placed in 500 ml containers. To each container 300 ml of the metal concentration was applied, and the ends of the cellulose were soaking the solution and causing its rise to the seeds. The distilled water was used as a cultivation medium. Subsequently the seeds were germinated and cultivated for 8 and 12 days in the dark at 25 °C and with humidity of 60%. Platinum concentration was determined using differential pulse voltammetry on the device Autolab (EcoChemie, Netherlands) with VA-Stand 663 (Metrohm, Switzerland). Three-electrode system consisted of hanging mercury drop electrode (HMDE). The potential was scanned from -0.5 to -1.2 V at a sweep rate of 10mV/s, and the catalytic hydrogen wave at -0.9 V was measured.

RESULTS AND DISCUSSION

In the present study we observed the ability of bioaccumulation of platinum group metals (Pt), applied as PtCl₄ in various parts of the plants of pea (*Pisum sativum* L.) and maize (*Zea mays* L.).

From Figs. 1A, B, C and D it can be concluded that with the increasing concentration of applied metal, penetration of metal into various parts of plants is also growing. Based on Fig. 1A it is evident the increase of content of platinum in aboveground parts of pea plants up to 200 times compared to control, especially at concentrations of 50 and 100 μM . In the root parts, there was a significant increase in platinum content in concentrations 25; 50 and 100 μM , mainly in the 12th day of the experiment (Fig. 1B). Based on Fig. 1C it can be concluded that in the root parts of the maize plants the content of platinum was 300 times higher than in aboveground parts. The highest platinum content in both plants sections was found in concentrations 25; 50 and 100 μM .

Figure. 1: Platinum content in the aboveground parts and roots of pea (A, B) and maize (C, D).



CONCLUSION

In our experiment we compared two types of plants, peas as a representative of dicotyledonous plant and maize as a representative of monocotyledonous plants. The observed differences in uptake of heavy metal between peas and corn can be explained by different sorption abilities of roots, which is higher in dicotyledonous plants against monocotyledonous plants and is type and age dependent [10-12]. On the basis of this information it can be concluded that the pea plants shows higher bioaccumulation ability of platinum in the aboveground parts of plants with the increasing concentration of the applied metal. In contrast the maize plants have higher platinum bioaccumulation ability in the root sections.

ACKNOWLEDGEMENT

The work has been supported by IGA 83/2011/FVHE, MSMT 6215712402, IGA 25/2012/FVHE and NanoBioMetalNet CZ.1.07/2.4.00/31.0023.

REFERENCES

- [1] Locatelli, C., D. Melucci, G. Torsi.: Analytical and bioanalytical chemistry 382 (2005), 1567 - 1573.
- [2] Sikorova, L., R. Liebinsky, and V. Adamec.:

- [3] Chemicke Listy 105 (2011), 361-366.
- [4] Konig, R., A. Schindler, and T. Herrmannsdorfer.: Physical Review Letters 82 (1999), 4528-4531.
- [5] Palacios, M., et al.: Science of the Total Environment 257 (2000), 1-15.
- [6] Wichmann, H., et al.: Science of the Total Environment 388 (2007), 121-127.
- [7] Ravindra, K., L. Bencs, R. Van Grieken.: Science of the Total Environment 318 (2004), 1-43.
- [8] Labra, M., et al.: Chemosphere 62 (2006), 1234 - 1244.
- [9] Appenroth, K. J.: Acta Physiologiae Plantarum 32 (2010) 615-619.
- [10] Kouba, A., M. Buric, and P. Kozak.: Water Air and Soil Pollution 211 (2010) 5-16.
- [11] Macek, T., et al.: Acta Biotechnol 22 (2002), 101-106.
- [12] Krystofova O, Zitka O, Krizkova S, et al., Int. J. Electrochem. Sci., 7 (2012), 886-907.
- [13] Kleckerova A, Sobrova P, Krystofova O, et al., Int. J. Electrochem. Sci., 6 (2011), 6011-6031.

DEVICE FOR AUTOMATIC CHARACTERIZATION OF SEMICONDUCTOR GAS SENSORS

Zdenek PYTLICEK¹, Imrich GABLECH¹, Jan PRASEK^{1,2*}, Jaromir HUBALEK^{1,2}

¹ Dept. of Microelectronics, Faculty of Electrical Engineering and Communication, Brno University of Technology, Technická 10, 616 00 Brno, Czech Republic

² Central European Institute of Technology, Brno University of Technology, Technická 10, 616 00 Brno, Czech Republic

*prasek@feec.vutbr.cz

ABSTRACT

This paper solves the problematic of devices for testing and evaluation of semiconductor gas sensors used for environment monitoring. The aim was to design automatic system for gas sensors characterization. The workplace was designed and implemented for simple use with LabView (National Instrument) and standard laboratory multimeters connected through GPIB interface. The demonstration measurement was done using two different sensors with SnO₂ active layer. We were able to test sensor for detect methane concentration up to 1 ppm.

INTRODUCTION

The detection and monitoring of toxic gas emissions in environment and industry processes is very important for environmental protection and human and animal safety. Gas sensors based on semiconductor active layers appear as a good solution for gas trace monitoring. The advantages of these sensors are their robustness, small size, low weight, simple design and low cost. There were described many works about gas sensors using different technology used for their fabrication in the last few years. Generally the thick film technology (TFT) is one of reported technologies used for gas sensors fabrication [1-4] due to its accessibility, non vacuum and easy fabrication process. The thin film technology or semiconductor technology is the second technology used for gas sensors fabrication as it was reported in [5-7] e.g.. The main difference between the developed gas sensors is in the semiconducting materials used for the active layers and methods for their preparation or deposition. Usually the SnO₂ [1, 2], WO₃ [8] or TiO₂ [4, 9] nanopowders are used as main sensing material, which can be covered with catalytic filters or modified by doping.

The main problem of gas sensors development is the verification of their sensing properties. Universal equipment for the verification does not exist. All researchers usually use their own setup using a little gas chamber for the sensor, the pressure tanks with detected gasses and one pressure tank with an inert gas for chamber cleaning. The problem is in the appropriate equipment for the selection of desired gas concentration. One solution is to use the pressure tanks with the desired premixed gas concentrations. The second more sophisticated solution is to use the inert gas which is mixed with the detected gas to the predefined concentration using mass flow controllers. The aim of this work was to

design and implement the appropriate sophisticated workplace for simple characterization of the gas sensors.

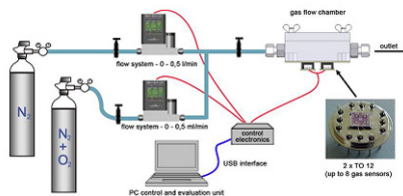
WORKPLACE CONSTRUCTION

Workplace was designed to be suitable for the gas sensors characterization. The workplace design and its implementation are shown in the next subsections.

Workplace

The designed workplace is consisted of gas flow chamber with five closing valves, two mass flow controllers for desired gas concentration setup, two pressure tanks with tested gas and air, control electronics, power source with multimeter for each sensor and personal computer with software for experiment setup and the sensors' response evaluation. The simplified designed workplace setup is shown in the figure 1.

Figure 1.: Workplace for the gas sensors characterization setup

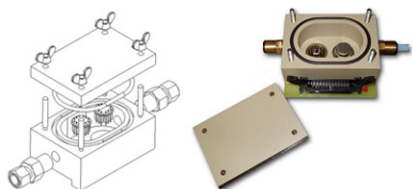


Gas flow chamber

First of all, the testing gas flow chamber was designed to be suitable for two TO-12 packages. The chamber has an exchangeable output connector, which could be used as exchangeable reducer for differently connected sensors in the TO-12 package. The maximum of the sensors

in one package is four. The gas chamber was designed to be hermetically closeable with one inlet and one outlet. The inner volume was designed to be as smallest as possible. The gas chamber design is shown in the figure 2 left. The designed gas flow chamber was fabricated from plastic material Ketron® Peek 1000. This material has good mechanical properties and is sufficiently chemically resistant. The sample of the fabricated gas chamber is shown in the figure 2 right.

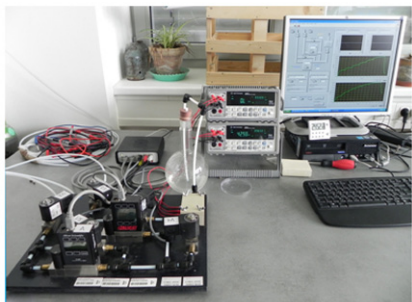
Figure 2.: Design (left) and fabricated (right) gas flow chamber for two TO-12 packages



The workplace assembling

The main part of the workplace was assembled onto one plastic board. The main part consists of the control electronics, gas flow chamber, five closing valves and two mass flow controllers for desired gas concentration setup. The mass flow controllers were selected in order to be able to assure desired concentration of the testing and inert gas to mixture them in concentrations from 4000 ppm to 10 ppb. For this purpose, the Alicat Scientific mass flow controllers for volumes 500 sccm for measured gas and 2000 sccm for synthetic air were purchased. The assembled workplace is shown in the figure 3.

Figure 3.: Assembled workplace



Control electronics

The control electronics was designed as two different parts due to its possible easy upgrade in the future. The control and communication part was designed to control desired concentration by mass flow controllers and valves and to assure the communication between the PC and electronics blocks. The analog measuring part was de-

signed for direct gas sensors measurement. It includes the sensor temperature regulation and the conductivity measurement of the sensor's active layer. Common power sources with multimeters U3606A from Agilent with the GPIB interface were used for powering heater and conductivity measurement.

Control and evaluation software

The control and evaluation software was designed and programmed in the LabView environment (National Instrument, USA). The control software part is designed for experiment setup such as time schedule of measurement, mass flow rate, valves opening, heater parameters, etc. The measurement and evaluation part is designed for online sensors response measurement and operations with measured data. The program screenshot is shown in the figure 4.

Figure 4.: Preview of the program written in LabView G-language.



MEASUREMENT DEMONSTRATION TEST

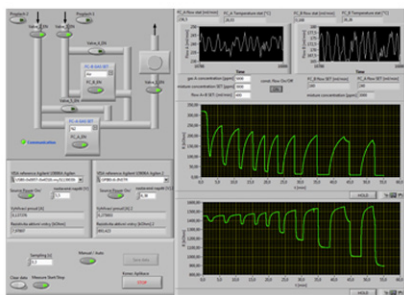
Measurement demonstration test was done using our thick-film gas sensor with SnO₂ gas sensing active layer. The TFT gas sensor is fabricated using standard thick-film techniques. The structure of the TFT gas sensor consists of platinum heater element covered by insulating layer, gold electrodes and the gas sensing layer. The heater is also used as a temperature sensor. The screen-printed sensing layer is made of 5 μm thick SnO₂ film. Each sensor is bonded on the TO-12 package through a ceramic support (due to high operating temperatures > 800 °C) as is shown in the figure 5a. Commercial sensor TGS822 (Figaro Engineering Inc., Japan) was used as a reference sensor – figure 5b.

The tested gas was methane mixed into synthetic air. The results obtained during the measurement at 250 °C operating temperature were exported to the MS Excel. The time dependence of the sensor resistance on the methane concentration change is shown in the figure 6.

Figure 5.: Our gas sensor with SnO₂ sensing layer (left) and commercial SnO₂ based gas sensor TGS822 (right)



Figure 6.: Screenshot of the measurement and setup window with resistivity dependence of our TFT (up) gas sensor and Figaro TGS822 (down) on the change of methane concentration



CONCLUSION

New workplace for the gas sensors characterization was designed and implemented. It is designed in order to be suitable for characterization of new gas sensors developed at the Department of Microelectronic, Brno University of technology. The design and construction of workplace is briefly mentioned in this paper. The designed experimental workplace is consisted of gas flow chamber with five closing valves, two mass flow controllers for desired gas concentration setup, two pressure tanks with tested and carrier gas, control electronics and personal computer with software for experiment setup and the sensors' response evaluation. All parts were designed and implemented to be easily controlled and easily exchanged. Finally the workplace was tested on the Methane detection for demonstration. We were able to detect 1 ppm of measured gas.

ACKNOWLEDGEMENT

The research has been supported by project IGA FEKT-S-11-16, project GA102/09/1601 (IMINAS) and project CZ.1.05/1.1.00/02.0068 (CEITEC).

REFERENCES

- [1] Lee S.Ch., Choi H.Y., et al.; Novel SnO₂-based gas sensors promoted with metal oxides for the detection of dichloromethane. *Sensors and Actuators B: Chemical*, Volume 138, Issue 2, 2009, pp. 446-452.
- [2] Berger F., et al.; Detection of DEMP vapors

- using SnO₂-based gas sensors: understanding of the chemical reactional mechanism. *Thin Solid Films* 436 2003, pp. 1–8.
- [3] Shoi N.J., Kwak J.H., et al.; Classification of chemical warfare agents using thick film gas sensor array. *Sens. Actuators B: Chem.* 108 (1–2) 2005, pp. 298–304.
- [4] Sotter E., Vilanova X., et al.; Thick film titania sensors for detecting traces of oxygen. *Sensors and Actuators B: Chemical*, 127 (2) 2007, pp 567-579.
- [5] Sengupta P.P., et al.; Influence of dopant in the synthesis, characteristics and ammonia sensing behavior of processable polyaniline. *Thin Solid Films*, 517 (13) 2009.
- [6] Ivanov P., Llobet E., et al.; Towards a micro-system for monitoring ethylene in warehouses. *Sensors and Actuators B: Chemical*, Volume 111, 2005, pp 63-70.
- [7] Ivanov P., et al.; SOI-CMOS compatible low-power gas sensor using sputtered and drop-coated metal-oxide active layers. *Microsystem Technologies-Micro- and Nanosystems-Information Storage and Processing Systems*, 12 (1-2) 2005, pp 160-168.
- [8] Ke M.T., Lee M.T., Ch. C.Y., Lee Y., Fu L.M.; A MEMS-based Benzene Gas Sensor with a Self-heating WO₃ Sensing Layer. *Sensors* 9 (4) 2009, pp. 2895-2906.
- [9] Kim J.C., Jun H.K., Huh J.S., Lee D.D.; Tin oxide-based methane gas sensor promoted by alumina-supported Pd catalyst. *Sensors and Actuators B: Chemical* 45, 1997, pp. 271–277.

EPR-UV/VIS/NIR SPECTROELECTROCHEMISTRY OF METAL(II) COMPLEXES CONTAINING TETRADENTATE LIGANDS

Peter MACHATA*, Peter RAPTA

Department of Physical Chemistry, Slovak University of Technology, Radlinského 9, SK-812 37 Bratislava, Slovak Republic

*peter.machata@stuba.sk

ABSTRACT

New ligands with N_2O_2 donor set containing a single phenolate moiety, protected by bulky tert-butyl substituents in the ortho and para positions of the parent phenol, enable the ligand to form a relatively stable phenoxyl radicals. The effect of tetradentate ligand substitution as well as the metal ion identity on stabilisation of phenoxyl radicals generated electrochemically was studied in detail. The electrochemically generated phenoxyl radicals were investigated by cyclic voltammetry and EPR-UV/Vis/NIR spectroelectrochemistry for series of newly prepared metal(II) complexes containing variously substituted tetradentate ligands.

INTRODUCTION

The tetradentate ligands with N_2O_2 donor were proved to be suitable for the synthesis of metal complexes as models for mimicking the electronic structure and reproducing some spectroscopic features of galactose oxidase (GAO) and glyoxal oxidase (GLO) [1,2]. Recently, the template synthesis of a new ligand with a N_2O_2 donor set with a single phenolic moiety, suitably protected by bulky tert-butyl groups in the 3,5-positions of the parent phenol able to generate a phenoxyl radical, and which contains a thiomethyl group attached to the extended pi-conjugated ligand backbone, was reported [3]. In this work the redox properties of metalo-complexes containing copper(II) or Ni(II) central atom and variously substituted tetradentate ligand (S-methyl group or S-phenyl group) are studied by cyclic voltammetry and EPR-UV/Vis/NIR spectroelectrochemistry in order to get insights into the electron transfer mechanism and the stability of the formed charged states within the investigated metalo-complexes containing pi-conjugated ligand backbone.

MATERIAL AND METHODS

A standard three electrode arrangement of a platinum wire as working electrode, a platinum wire as counter electrode, and silver wire pseudoreference electrode was used in cyclic voltammetric experiments with a PAR Potentiostat-Galvanostat Model 273A in glove box. Decamethylferrocene (DmFc) was used as internal potential standard. Sample solutions with approximate concentration of 0.5 mM, prepared with 0.2 M TBAPF₆ supporting electrolyte in CH_2Cl_2 . Spectroelectrochemical experiments were carried out in flat spectroelectrochemical cell (Pt mesh working electrode) in the optical

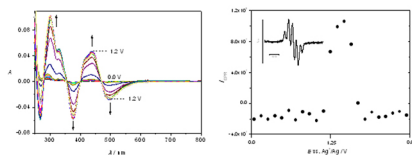
EPR cavity (ER4104OR, Bruker, Germany). The EPR spectra were recorded on an X-band EMX EPR spectrometer (Bruker, Germany). For *in situ* EPR-UV/Vis/NIR spectroelectrochemical studies, diode-array UV/Vis/NIR spectrometer system TIDAS (J&M, Aalen Germany) or Avantes UV/Vis/NIR spectrometer and potentiostat Heka PG 284 (HEKA Elektronik, Germany) were used. The investigated metalo-complexes **A** (empirical formula $C_{22}H_{29}NiN_3O_4S_2$), **A'** ($C_{25}H_{27}NiN_3O_4S_2$), **B** ($C_{22.5}H_{29}CuN_3O_4S_2$) and **B'** ($C_{25}H_{27}NiN_3O_4S_2$) were synthesized by research group of Prof. Vladimir Arion from Institute of Inorganic chemistry at University of Vienna (Austria). Spectroelectrochemical studies were performed by Prof. L. Dunsch group in the Centre of Spectroelectrochemistry at IFW Dresden (Germany).

RESULTS AND DISCUSSION

Cyclic voltammetry at scan rate of 100 mV s⁻¹ of investigated complexes proved a substantially higher reversibility of the corresponding first oxidation voltammetric peak for complexes containing pi-conjugated tetradentate ligand backbone with S-phenyl group (**A'**, **B'**) in comparison to the complexes **A**, **B** with the S-methyl substitution (not shown). During *in situ* EPR spectroelectrochemistry of studied Cu(II) complex **B'** in the region of the first oxidation peak a decrease of characteristic Cu(II) EPR signal was observed with the simultaneous increase of new absorption bands in the region from 500 to 2000 nm characteristic of ligand based phenoxyl radicals [3]. Oxidation process was reversible in the region of the first voltammetric peak even at low scan rate of 5 mV s⁻¹ for complexes **A'** and **B'**. In contrast to these observations, less reversible spectroelectrochemical response and no optical

band in NIR region was observed upon anodic oxidation of metalocomplexes **A** and **B** having S-methyl substitution of the ligand as illustrated for complex **A** in Fig. 1a. Low stable cation radical was observed in the region of the first quasi-reversible oxidation peak by EPR spectroscopy with hyperfine structure (quintet) coming probably from two nearly equivalent nitrogen atoms from N_2O_2 ligand moiety (see Fig. 1b).

Figure 1: Spectroelectrochemistry of metalocomplex **A** in 0.2 M TBAPF₆ - CH₂Cl₂ solution. Potential dependence of UV/Vis spectra (left) and potential dependence of EPR integral intensity with the corresponding EPR spectrum in inset (right)



CONCLUSION

Simultaneous in situ electrochemical, UV/Vis/NIR and EPR measurements provide insights into the stability of the monocharged investigated metalocomplexes and the extent of electron delocalisation as well as spin density distribution within the charged complex. The EPR activity of the formed species in the region of the first anodic peak was proved by in situ EPR spectroelectrochemistry.

ACKNOWLEDGEMENT

The financial support of the Science and Technology Assistance Agency (the contract No. VEGA APVV-0202-10) and Slovak Grant Agency VEGA (contract No. 1/0679/11) is gratefully acknowledged.

REFERENCES

- [1] Ito, N., V. Phillips, S. E., Yadav, K. D. S et al.: *J. Mol. Biol.* 238 (1994), 794-814.
- [2] Whittaker, M. M., Kersten, P. J., Nakamura, N., et al.: *J. Biol. Chem.*, 271 (1996), 681–687.
- [3] Arion, V. B., Rapta, P., Telser et al.: *Inorg. Chem.* 50 (2011), 2918–2931.

ELECTROCHEMICAL SENSOR WITH PERFORATED SURFACE FOR DETERMINATION OF HEAVY METALS IN WATER

Marian MARIK^{1*}, Vojtech SVATOS², Jan PEKAREK^{1,2},
Jana CHOMOUCKA^{1,2}, Jaromir HUBALEK²

¹ LabSensNano, Department of Microelectronics, Faculty of Electrical Engineering and Communication, Brno University of Technology, Technicka 3058/10, 616 00 Brno, Czech Republic

² Central European Institute of Technology, Brno University of Technology, Technicka 3058/10,616 00 Brno, Czech Republic
*hubalek@feec.vutbr.cz

ABSTRACT

The aim of this contribution is the design and preparation of electrochemical sensor with perforated surface for detecting heavy metals in water using standard electrochemical methods. The expectation is to achieve more accurate sensing than planar electrodes. Finally, the structures of fabricated electrodes are shown and discussed.

INTRODUCTION

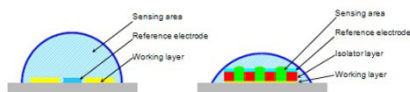
Detection of heavy metals in water using electrochemical method is widespread and very simple. Heavy metals in water represent a huge problem because of their toxicity which may cause variety of serious diseases. Nowadays the most common heavy metal detectors in use are the planar sensors. Planar sensors have relatively a large sensing surface, and for this reason these are appropriate for sensing in a larger amount of water. The expectation is to create a perforated sensor with better detecting limit. During the detection the hemispheric area is smaller and it is possible to use it with a small volume of compound.

DESIGN AND TECHNOLOGICAL PROCEDURE OF IMPLEMENTATION

A few requirements about the operation of the sensor were taken into account during the design. The expectations were about a sensor with two electrodes with a small hemispheric area during the measurement. Gold working electrode was necessary for heavy metal, for reference electrode material was selected a silver one.

The planar electrodes have a large hemispheric area during the determination and wire sensors too. Reduction of hemispheric area to zero is very difficult, but with a perforated system it is possible to create a zone, where the detection is executed only in smaller sections and not in total volume of compound. **Figure 1** This detecting method is more accurate than planar systems.

Figure 1 Hemispherical area at planar system (right) and hemispherical area at perforated system (left)



The detector was realized on the silicon wafer with 1 μm thick silicon oxide layer. Deposition of metal layers was realized with evaporation. Because the gold has poor adhesion and large surface tension, the lift off technic is not recommended for the implementation of working electrodes. Gold working electrodes were realized with etching technics.

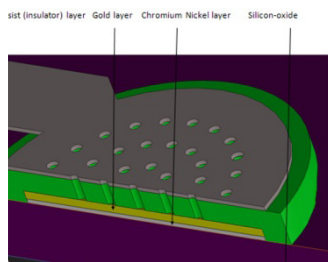
A thin adhesion layer made of chromium nickel (15 nm) and 100 nm of gold were deposited on the silicon wafer. Positive photoresist was used for creating an etching motive and expose was made by UV light. After developing, the gold and the chromium-nickel layer was etched with gold etchant standard (Sigma/Aldrich). Photoresist stripping is necessary after etching because annealing of electrodes is possible only with clean surface.

Working and reference electrodes must be electrically separated, this was resolved by a polymer layer between the two electrodes.

The reference electrode was created by lift off technique. As shown in **Figure 2** for the first time coating of insulator layer is needed and photoresist is coated on that layer for lift off technique. The insulator layer is a negative photoresist (Sigma-Aldrich) and the layer above is a positive photoresist (S1813). The upper and the bottom layers are exposed at the same time. During developing only the upper resist was needed to develop, because of the evaporation. The evaporated layer was a thin silver layer (20nm). After the evaporation the substrate was immersed in the acetone in ultrasound bath and after 60

seconds the rest of the upper layer was removed. With the rest of photoresist layer the unnecessary amount of evaporated silver layer was removed too and finally the electrode was ready to the opening of sensing holes above the gold layer. That is a very simply process, because only the developer for the bottom resist is needed. When the sensing holes are open, the electrochemical thickening occurs (from 20 nm to 1 μm). The last step was the isolation of the whole surface with polymer, except the sensing circle and the end of the electrode contacts for measuring instrument.

Figure 2. Engraving of the 3D structure



RESULTS AND DISCUSSION

The completed electrode was checked by optical and electron beam microscope. Macro details on sensing circle form and the laser coverage were checked by the optical microscope. The layer thickness and the wall structure of sensing holes were checked by the electron microscope.

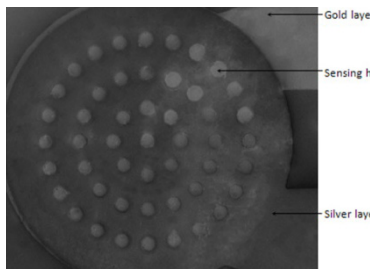
In the pictures from optical microscope not accurate covering of layers is visible. **Figure 3.** That was caused by the fact that the mask at the second lithography process was not matched perfectly with working electrodes. The form of sensing circle and sensing holes did not have perfect circle form what is probably caused by the lift off process.

The wall and layer quality control by electron microscope showed how the layers lie on each other. The pictures do not show bridges or other mistakes in the structure. **Figure 4.**

Figure 3 Part of the sensor under optical microscope.



Figure 4. Sensor controlled in electron microscope SEM.



CONCLUSION

Detection of heavy metals in water is very useful and important because of health and environment. This sensor was created for an accurate detection taking advantage of better hemispherical abilities. The sensor testing will begin in near future with better expectations on detection.

ACKNOWLEDGEMENT

The financial support from the grant GAČR 102/08/1546, project CZ.1.05/1.1.00/02.0068 (CEITEC) and CZ.1.07/2.3.00/20.0027 (NA-NOE) is highly acknowledged.

REFERENCES

- [1] Gregory T.A. Kovacs, Christopher W. Stormont, Samuel P. Kounaves, Microfabricated heavy metal ion sensor, *Sensors and Actuators B: Chemical*, Volume 23, Issue 1, January 1995, Pages 41-47, ISSN 0925-4005, 10.1016/0925-4005(94)01523-K.
- [2] Honeychurch, Kevin C. Screen-printed Electrochemical Sensors and Biosensors for Monitoring Metal Pollutants. *Insciences Journal*. 2012-03-23, č. 1, s. 1-51. ISSN 1664171x. DOI: 10.5640/insc.020101. Dostupné z: <http://journal.insciences.org/164-171x-2-1-1/>

PREPARATION AND ELECTROANALYTICAL PROPERTIES OF POROUS FILM ELECTRODES

Radovan METELKA*, Nikola VOLAKOVA, Pavlina VLASAKOVA, Ivan ŠVANCARA

Department of Analytical Chemistry, Faculty of Chemical Technology, University of Pardubice, Studentská 573, 532 10 Pardubice, Czech Republic

*radovan.metelka@upce.cz

ABSTRACT

The colloidal crystal templating technique was used to prepare porous layers of various metals at the surface of screen-printed carbon electrodes. Polystyrene spheres were left to form a colloidal crystal on selected substrate by sedimentation of particles and evaporation of solvent. In next step, a metal was electrodeposited from suitable plating solution after infiltration of liquid phase to the hollow space within the structure. Finally, the polystyrene particles were dissolved in toluene and deposit with defined size of pores was subsequently revealed. Using such approach, electrodes with porous films of antimony, bismuth, and copper were prepared and their electroanalytical properties were tested in anodic stripping voltammetry of heavy metals and amperometry of selected saccharides.

INTRODUCTION

Modification of working electrode surface is one of the ways to improve the analytical parameters of an electrochemical sensor. There are already procedures enabling to enlarge the electroactive surface of electrode comparing to its geometric area. From the available techniques, the formation of porous layers, achieved by different methods, is very often used [1]. Colloidal crystal templating represents a technique, which is easy, feasible, and widely controllable [2]. During the process, the monodisperse spheres are packed together into colloidal crystal by capillary forces during their settlement on the substrate and evaporation of solvent. The liquid precursor capable of solidifying is then infiltrated into the hollow space between particles. After conversion to solid state by suitable treatment, the template is removed by higher temperature or dissolution and porous material with defined pore size is exposed.

To convert liquid precursor, an electrodeposition is preferable from the other procedures due to easy control of amount to be deposited, its speed, and bulkiness, so the template is not mechanically stressed. It is also possible to prepare layers from metals and their alloys, metal oxides, semiconductors, and conducting polymers [3]. The use of colloidal crystal templating for preparation of porous metal electrodes via electrodeposition was presented in few papers only. Namely, the biosensors based on modified gold electrodes [4-6] and the porous antimony [7] and bismuth [8] electrodes made on gold substrate for detection of heavy metals were introduced. This article deals with the preparation of porous metal layers on the surface of screen-

-printed carbon electrodes and the evaluation of their electroanalytical properties. The porous antimony and bismuth electrodes were used in anodic stripping analysis of selected heavy metals and porous copper film electrodes were employed for enhanced amperometric detection of saccharides.

MATERIAL AND METHODS

Preparation of porous metal screen-printed carbon electrodes

Carbon printing ink (C10903P14, Gwent Electronics Materials, United Kingdom) was printed on ceramic substrate (CLS 641000396R, Coors Ceramics, USA) using semi-automatic screen-printer UL 1505 A (Tesla, Czech Republic). Printed layer was then hardened at 60 °C in oven for 30 min. To prepare a porous layer, a circular form with area of 0.1 cm² was fixed on the surface of screen-printed carbon electrode. 30 μl of aqueous suspension of monodisperse polystyrene spheres (Sigma-Aldrich, Germany) was pipetted into the form and left to evaporate the solvent. After formation of colloidal crystal by self-assembling of spheres, the electrode was carefully dipped in 0.1 M plating solution of corresponding metal and left a certain time for sufficient infiltration into the hollow space between spheres. The metals were then galvanostatically deposited using constant current of -1.2 mA for Sb, -1.5 mA for Cu, and -2.5 mA for Bi from acidified 0.1 M solutions of metal ions. Various deposition times were applied. Finally, the polystyrene spheres were dissolved in toluene and the electrode was washed with distilled water. The working electrode area was defined by isolation with nail polish. Morphologies of porous deposits were observed using scanning electron microscope JSM-5500LV (JEOL, Ja-

pan) in secondary electron imaging mode.

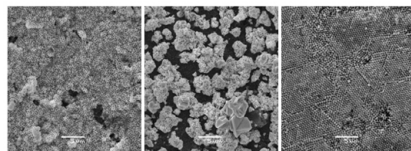
Electrochemical analysis of heavy metals and saccharides

Electrochemical analyser BAS 100B/W (BASi, USA) and square-wave anodic stripping voltammetry was used for the electroanalysis of lead and cadmium in model samples containing 0.1 M acetic buffer as supporting electrolyte. Platinum wire auxiliary and Ag/AgCl/3 M KCl reference electrodes (all BASi, USA) complement the three-electrode arrangement. The accumulation of analytes was performed at -1200 mV vs. Ag/AgCl for 120 s with subsequent stripping up to -500 mV. In cyclic voltammetry of saccharides, the potential was varied from 0 mV to 800 mV with a scan rate 50 mV s⁻¹. During hydrodynamic voltammetry measurements, the solution was stirred with Teflon® bar at 600 rpm and the current was recorded at potential +600 mV vs. Ag/AgCl. Model solutions of 1 mM glucose, sucrose (both Lachema, Czech Republic), galactose, and fructose (both Sigma-Aldrich, Germany) were prepared in basic electrolyte 0.1 M NaOH and added to measured solution after stabilizing of baseline. Current values were then noted 50 s after the addition of saccharide.

RESULTS AND DISCUSSION

Morphology of resulting porous layers on heterogeneous carbon substrate is depending on the diameter of polystyrene spheres, their concentration in suspension, and passed charge during the electrodeposition of metals. Fig. 1 shows the porous metal structures obtained by the colloidal crystal templating. Antimony film was prepared using 1 % suspension of polystyrene spheres and deposition time 112 s, bismuth from 1 % suspension and time 96 s, and copper from 0.5 % suspension and electrodeposition of 60 s. The substrate can be completely covered by porous metal film only in case of antimony and copper. In case of bismuth, the porous crystallites were observed only. For the diameter of particles 500 nm, the final structures are not ordered in whole, there are randomly placed pores mostly. Areas with ordered pores can be observed only in case of copper films. Such behavior is closely related to high roughness of heterogeneous carbon substrate, when the formation of ordered colloidal crystal is hindered. Also, the electrodeposition starts preferably on the edges of graphitic particles. More planar substrates, i. e. gold sputtered on glass [7], could be plated completely with the possibility to control the thickness of deposited film.

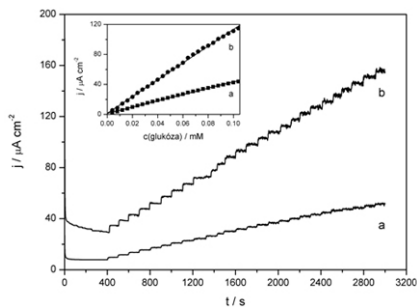
Figure 1.: Porous films of antimony (left), bismuth (middle), and copper (right).



Enhanced stripping currents of heavy metals were reported in the use of antimony or bismuth porous film electrodes prepared by the colloidal crystal templating on gold substrate [7, 8]. However, such effect was observed only in some extent at screen-printed carbon electrodes with porous film of antimony or bismuth and higher concentrations of metals.

Copper film electrodes were characterized by the cyclic voltammetry of selected saccharides in alkaline media. During their electrochemical oxidation, an interaction with oxide/hydroxide layer formed on the electrode is presumed; the adsorption takes place and oxidation follows [9]. In case of macroporous electrodes, the current increase might be as high as two orders of magnitude for abovementioned type of electrochemical reaction, where the analyte is firstly adsorbed at the electrode [2]. Recorded current densities were substantially larger at porous electrode than at *ex situ* (non-porous) copper film electrode. Fig. 2 shows hydrodynamic voltammograms of glucose oxidation at both types of copper film electrodes. The sensitivity at porous electrode was nearly three times higher comparing to that of *ex situ* copper film electrode. Similar ratio in slopes of calibrations was observed also for sucrose and galactose. The current enhancement was not so pronounced in oxidation of fructose.

Figure 2.: Amperometric detection of glucose at a) *ex situ* and b) porous copper film electrode together with corresponding calibration curves (inset).



CONCLUSION

Porous layers prepared by the colloidal crystal templating enable further improvement in sensitivity of electrochemical sensors by enlarging the surface area.

ging the available electroactive area. The procedure is neither experimentally demanding nor costly; the only need is a careful manipulation with a sensor after solvent evaporation to prevent mechanical damage to the colloidal crystal and collapse of the structure. Obtained results at copper porous electrodes are promising e.g. for non-enzymatic glucose detection in clinical samples.

ACKNOWLEDGEMENT

The work has been supported by the Ministry of Education, Youth, and Sports of the Czech Republic (project KONTAKT MEB091139) and by the Internal Grant Agency of the University of Pardubice (project SGFChT06/2012).

REFERENCES

- [1] Walcarius A: Analytical and Bioanalytical Chemistry, 396 (2010), 1, 261-272
- [2] Walcarius A, Kuhn A: Trends in Analytical Chemistry, 27 (2008), 7, 593-603
- [3] Bartlett P N, Baumberg J J, et al.: Chemistry of Materials, 14 (2002), 5, 2199-2208
- [4] Szamocki R, Reculosa S, et al.: Angewandte Chemie International Edition, 45 (2006), 8, 1317-1321
- [5] Szamocki R, Velichko A, et al.: Analytical Chemistry, 79 (2007), 2, 533-539
- [6] Ben-Ali S, Cook A D, et al.: Electrochemistry Communications, 5 (2003), 9, 747-751
- [7] Urbanová V, Vytřas K, et al.: Electrochemistry Communications, 12 (2010), 1, 114-117
- [8] Urbanová V, Bartoš M, et al.: Electroanalysis, 22 (2010), 13, 1524-1530
- [9] Sun F, Li L, et al.: Electroanalysis, 23 (2011), 2, 395-401.

ELECTROANALYSIS OF METHYLXANTHINES ON A GRAPHITE ELECTRODE

Rudolf NAVRATIL¹, Frantisek JELEN², Libuse TRNKOVA^{1,3*}

¹ Department of Chemistry, Faculty of Science, Masaryk University, Kotlarska 2, CZ-611 37 Brno, Czech Republic

² Institute of Biophysics, v.v.i., Academy of Sciences of the Czech Republic, Kralovopolska 135, CZ-612 65 Brno, Czech Republic

³ Central European Institute of Technology – CEITEC, Brno University of Technology, Technicka 3058/10, CZ-616 00 Brno, Czech Republic
*libuse@chemi.muni.cz

ABSTRACT

Electroanalysis of xanthine (Xan) and its three methylated derivatives (1-, 3-, and 7-mXan) on a pencil graphite electrode (PeGE) in the presence of copper ions is presented. For a sensitive detection of their oxidation signals represented not only by copper complexes but also by the corresponding methyl-substituted Xan the combination of adsorptive stripping and elimination techniques was used. It was found that the position of methyl group on the xanthine ring is responsible for both the potential and peak height of all methylxanthines.

INTRODUCTION

The electroactivity of Xan and its methylated derivatives has already been known for more than sixty decades. Early studies were based on investigations in connection with the mercury electrode but their electrochemical activity was largely suppressed or was not satisfactory for the interest of analytical bioelectrochemistry. The oxidation signal of Xan and methyl-substituted xanthines was studied later on carbon electrodes, and the results were summarized in review by Dryhurst [1]. The oxidation of the purine derivatives mentioned involves electron exchange between the electrode and the purine skeleton at higher oxidation potentials [2-6]. The number of papers concerning the oxidation of Xan and its derivatives in the presence of copper ions is much smaller [7-9]. It was proved that the mechanism of the overall oxidation reaction at different carbon electrodes (glassy, pyrolytic, etc.) is similar. It was stated that the copper metal deposited onto the electrodes is oxidized to Cu(I) at low negative potentials (vs. Ag/AgCl/KCl electrode) and the generated Cu(I) reacts with purine derivatives to accumulate the product on the electrode as an insoluble compound; then it was redissolved electrochemically by the oxidation of Cu(I) to Cu(II) at positive potentials [9]. The aim of the work is to test oxidation signals of xanthine and its methyl derivatives on a pencil graphite electrode (PeGE) in the presence of Cu(II) ions and to determine the optimal experimental conditions for their sensitive detection.

MATERIAL AND METHODS

The measurements were performed on the AUTOLAB analyzer (Electrochemical Analy-

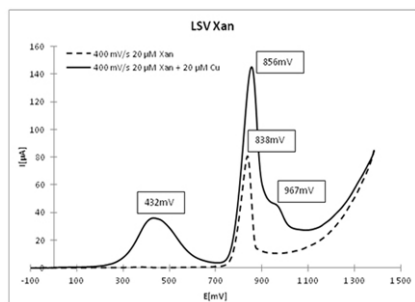
zer EcoChemie company, Utrecht, Netherlands) in connection with a VA-Stand 663 (Metrohm, Zurich, Switzerland). The voltammetric cell included a three-electrode arrangement including a working electrode PeGE (Pencil Graphite Electrode – 0.5 HB Tombow, Japan), a reference electrode (Ag/AgCl/3M KCl), and an auxiliary electrode (platinum wire). The voltammetric curves measured were processed by AUTOLAB, GPES 4.9 software, the data obtained were exported and processed in Microsoft Excel. To activate the electrodes, we used the DPV method (differential pulse voltammetry). For the measurements we used the LSV method (linear sweep voltammetry). For the processing of the data obtained during the measurement and as a control device we used the GPES 4.9 program. The smoothing of voltammetric curves was mediated by a Savitzky-Golay filter (level 2) embedded in the GPES program. Microsoft Excel was used for data evaluation. Electrochemical measurements were performed in acetate buffer pH 5.1, measurement at three different scan rates (200 mV/s, 400 mV/s, 800 mV/s) due to EVLS evaluation.

RESULTS AND DISCUSSION

LSV measurements were performed for Xan oxidation on the PeGE electrode in 0.1 M sodium acetate, pH 5.1 with scan rate of 400 mV/s in the absence of Cu(II) ions. The concentration of Xan was 20 μ M. Under these conditions Xan exhibited a well-defined and reproducible peak at 826 mV, as represented in Fig. 1 (dashed curve). When Cu(II) ions in equimolar concentration with Xan were added, the voltammogram substantially changed. A new peak at a potential of 432 mV was recorded and the original peak was enhanced and became wider due to the appearance

range of an additional small peak at a slightly positive potential (~967 mV) (Fig. 1 – full line). With reference to the earlier published results [9, 10], the new more negative signal resulted from the oxidation of the Cu(I)-Xan complex generated on the electrode surface at the initial potential. The dissolution of the complex is connected with easy oxidation of Cu(I) to Cu(II).

Figure 1: Linear sweep voltammograms of Xan in the absence (dashed line) and presence (full line) of Cu(II) ions. Scan rate 400 mV/s, initial potential -0.1 V, deposition time 120 s. The measurement was performed in 0.1 M sodium acetate, pH 5.1.



CONCLUSION

To compare the oxidation signals of xanthine and its three methylated derivatives on PeGE in the absence or presence of copper ions we can state that copper ions greatly increase the intensity of the oxidative signal of all methylxanthines. We observed the highest peaks in the case of Xan and 1-mXan. The Cu(I)-Xan or Cu(I)-mXan complexes were reflected by oxidation signals approximately at a potential of 400 mV while 1-mXan and 3-mXan are more willing to form a copper complex than are Xan or 7-mXan.

ACKNOWLEDGMENT

This research was supported by the following projects: (a) P205/10/2378 and P206/12/G151 of the Czech Science Foundation, (b) CEITEC – Central European Institute of Technology Project CZ.1.05/1.1.00/02.0068, and (c) OPVK Project (NanoBioMetalNet) CZ.1.07/2.4.00/31.0023.

REFERENCES

- [1] Dryhurst G.: *Electrochemistry of Biological Molecules*, Academic Press, New York, (1977).
- [2] Yao T., Wasa T., Musha S.: *Bull. Chem. Soc. Japan*, *50* (1977) 2917.
- [3] Yao T., Musha S.: *Bull. Chem. Soc. Japan*, *52* (1979) 2307.
- [4] Palanti S., Marrazza G., Mascini M.: *Anal.*

- Letts.*, *29* (1996) 2309.
- [5] Brett A.M.O., Matysik F.M.: *J. Electroanal. Chem.*, *429* (1997) 95.
- [6] Zhao G., Zang S., Liu K., Lin S., Liang J., Guo X., Zhang Z.: *Anal. Letts.*, *35* (2002) 2233.
- [7] Shengshui H., Dafu C., Mascini M.: *Wuhan Univ. J. Natur. Sci.*, *4* (1999) 99.
- [8] Shiraishi H., Takahashi R.: *Bioelectrochem. Bioenerg.*, *31* (1993) 203.
- [9] Ibrahim M.S., Temerk Y.M., Kamal M.M., Ahmed G.A.W., Ibrahim H.S.M.: *Microchim. Acta*, *144* (2004) 249.
- [10] Aladag N., Trnkova L., Kourilova A., Ozsoz M., Jelen F.: *Electroanalysis*, *22* (2010) 1675.

OPTIMALIZATION OF ORDERED SILVER NANOSTRUCTURES PREPARATION

Zuzana NOVAKOVA¹, Renata Orinakova², Radim HRDY³, Jaromir Hubalek³

¹ Department of Physical and Theoretical Chemistry, Faculty of Science, Comenius University, Mlynska Dolina, 842 15 Bratislava 4, Slovak Republic

² Department of Physical Chemistry, Faculty of Science, P.J. Safarik University, Moyzesova 11, 04154 Kosice, Slovak Republic

³ Department of Microelectronics, Faculty of Electrical Engineering and Communication, Brno University of Technology, Technicka 3058/10, 31600 Brno, Czech Republic

ABSTRACT

Silver ordered nanostructures were prepared by means of electrochemical deposition of silver into the pores of anodic alumina oxide template. The silver deposition was carried out using two-electrode system, in which evaporated gold layer on anodic alumina oxide membrane was used as cathode and platinum electrode as anode. SEM was used for characterization for prepared silver nanostructures. The diameter of prepared silver nanorods was affected by the template pore diameter and by the time of electrochemical deposition. The height of nanorods was influenced by the time of electrochemical deposition.

INTRODUCTION

Nanostructured materials have been extensively fabricated using many methods. They modified properties, and application ranges from fundamental science to industrial technology

[1]. Metal nanoparticles are well known for their optical, electrical, and magnetic properties [2]. One-dimensional metallic nanostructures, nanorods and nanotubes, have some advantages associated with their anisotropic ordering and allow to be used as nanometer-scaled electronic devices and optoelectronic devices [3, 4]. The conventional methods of preparing one-dimensional metallic nanostructures are nanolithography and electrochemical deposition [5]. The electrochemical method is more attractive because of low cost, operation simplicity, and capability to deposit metallic materials into nanopores such as anodic aluminum oxide membranes and polycarbonate membranes. Anodic aluminum oxide membranes have been easily and extensively employed not only as templates to fabricate one-dimensional nanostructures of wires and tubes, but also as masters to prepare ordered arrays of regularly structured nanotextures [6]. The aim of this paper was to optimize the preparation conditions of regularly ordered nanorods by electrochemical deposition into the anodic alumina oxide membrane.

MATERIAL AND METHODS

Preparation of alumina oxide membranes

The alumina membranes were prepared by using system consists from a flow-system controlled by membrane pump, power source, thermostat and personal computer providing automatic driving of all process. The alumina

membranes were prepared by anodic oxidation of aluminium thin film in 0,1 M oxalic acid solution at potential 20 V for 24 hours. Thereafter it was etched in solution containing 5g CuCl₂ and 100 ml of 1 M HCl, washed by distilled water and dried. Finally it was etched in aqueous solution containing 5 ml of 1 M H₃PO₄ and 3 g CrO₃ for 6 seconds at temperature 45°C to opening pores of membrane from both sides. The thin Au layer was deposited on the one side of final membrane by evaporation to produce the conductive junction.

Preparation of silver nanostructures

Silver nanostructures were prepared by means of electrochemical deposition from 0,1 or 0,05 M AgNO₃ electrolyte at constant current 0,5 or 22 mA for 1; 2,25; 5 and 10 seconds. The standard two electrode setup was used for the deposition of ordered silver nanostructured layers. The gold thin layer prepared by evaporation on anodic alumina oxide membrane was used as cathode and the gold sheet was used as anode. The alumina template was dissolved in 1 M NaOH for 1 hour after filling the membrane pores by the deposited silver.

Characterization of silver nanostructures

Prepared silver nanostructures were characterized using a scanning electron microscope MIRA3 FEG SEM (Czech Republic).

RESULTS AND DISCUSSION

Pore diameter of prepared anodic alumina oxide membrane was 20 nm. Resulting silver nanostructures prepared by electrochemical deposition into pores of alumina membrane were

nanotubes and nanorods with different diameter and height. Produced nanorods have formed pyramidal structures. At studied experimental conditions were whole pores filed by the deposited silver due to the long deposition time and moreover, the formed nanorods overlapped the membrane were connected together. The pyramidal surface appearance arises after the dissolution of alumina membrane (Figure 1). The effect of electrolyte concentration and applied current intensity on the diameter and height of prepared nanostructures was evaluated. Obtained results are summarised in Tab. 1.

Figure 1. SEM of prepared silver nanorods and pyramidal structure of the nanostructured layer surface

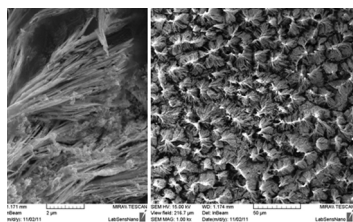
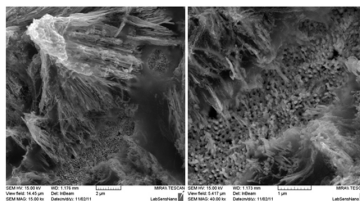


Table 1: Conditions of silver electrodeposition and template pore diameter together with the corresponding height and diameter of prepared silver nanorods-

α	Concentration of AgNO ₃ [M]	Time of deposition [s]	Diameter of pore [nm]	Height of nanostructure [μm]	Diameter of nanostructure bundle [nm]	Diameter of nanorod [- nm]
	0,05	1	25	3,3	36	28
	0,05	2,5	25	5,5	52,6	33
	0,05	5	25	28	57,14	38
	0,1	2,5	50	4	80	28
	0,1	5	50	5,5	100	55
	0,1	10	50	7	142	27
	0,1	2,5	50	4	100	90
	0,1	5	50	7,8	193	92
	0,1	10	50	11,4	285	95
	0,2	1	200	2	216	160
	0,2	10	200	4,32	216	175

The height of nanorods increased with the prolonged time of deposition as well as with the increase in current intensity. Diameter of produced silver nanorods resulted from diameter of pores of alumina membrane. The diameter of nanorods was greater or equal to pore diameter. The diameter of nanorods increased with the time of deposition. The height of membrane was ~ 1 μm. As the deposited nanorods were longer than the height of template, they merge together to form the pyramidal bundles. It is illustrated on the Figure 2.

Figure 2. Pyramidal structure of nanorod bundle



CONCLUSION

The effect of deposition conditions on the height and diameter of electrodeposited silver nanostructures was investigated in this work. From obtained results it could be concluded, that the time and current intensity during electrodeposition significantly affected length of prepared silver nanorods. The conditions of electrodeposition should be further optimised to prepare ordered nanostructured silver layers formed by nanorod arrays.

ACKNOWLEDGEMENT

This work was supported by the Grant VEGA 1/0211/12 of the Slovak Scientific Grant Agency and the Project APVV SK-CZ-0113-11 of the Slovak Research and Development Agency.

REFERENCES

- [1] Tlapin D V, Lee J S, Kovalenko M V, Shevchenko E V: Chemical Reviews, 110 (2010), 1, 289-458
- [2] Tian Y, Liu H, Zhao G, Tatsuma T: Journal of Physical Chemistry B, 110 (2006), 46, 23478-23481
- [3] Nicewarner-Pena S R, Freeman R G, Reiss B D, et al.: Science, 294 (2001), 5540, 137-141
- [4] Liu Y J, Zhang Z Y, Zhao Q, Dluhy R A, Zhao Y P: Journal of Physical Chemistry C, 113 (2009), 22, 9664-9669
- [5] Vlad A, Mátéfi-Tempfli M, Antohe V A, et al.: Small, 4 (2008), 5, 557-560
- [6] Pang Y T, Meng G W, Shan W J, et al.: Applied Physics A, 77 (2003), 5, 717-720

ANALYTICAL APPLICATIONS OF NANOSTRUCTURED SILVER LAYERS

Renata ORINAKOVA^{1*}, Lenka SKANTAROVA², Jakub DEMKO¹, Andrej ORINAK¹

¹ Department of Physical Chemistry, Faculty of Science, P.J. Šafárik University, Moyzesova 11, SK-04154 Košice, Slovak Republic

² Department of Analytical Chemistry, Faculty of Science, Comenius University, Mlynská Dolina, SK-842 15 Bratislava 4, Slovak Republic

*Renata.Orinakova@upjs.sk

ABSTRACT

In this work, electrochemical multiple CV scan method was used to prepare surface-enhanced Raman scattering (SERS)-active silver island films to investigate the effect of potential scan rate on improved SERS performance. The results indicate that the SERS enhancement capability is particle size and distribution dependent with the optimum potential scan rate of 100 mV/s. The enhancement factor for Rhodamine 6G (R6G) adsorbed on the SERS-active substrate was estimated to be 6.3×10^2 .

INTRODUCTION

Surface-enhanced Raman scattering (SERS) occurring on nanostructured metallic surfaces provides a powerful means of obtaining vibrational information on adsorbate-surface interactions in view of its unique sensitivity and excellent frequency resolution from the large increase in scattering [1 - 6]. SERS is widely applied to study the structure and orientation of the molecules at Cu, Ag and Au surfaces [7, 8]. The surface enhancement is highly surface selective so the technique is sensitive to molecules adsorbed at, or very close to the substrate surface. Moreover, the Raman cross section for water is low so that SERS can be easily used to study substrates in aqueous solution [7].

An average value for the SERS enhancement is around 10^6 , but the localized enhancement may reach peaks of 10^{10} at certain highly efficient sub-wavelength regions of the surface [4]. The generation and intensity of Raman signals are determined by the surface morphologies and structures of the substrates [4, 5, 7, 9]. Thus, considerable efforts have been directed toward the optimization of SERS enhancement via the size- and shape-controlled physical and chemical properties of the SERS active substrates [9].

In this work, the silver island films were produced using electrodeposition onto stainless steel substrates by cyclic voltammetry (CV). Morphology of substrates was changed with tuning the scan rate of the applied potential. The Raman scattering enhancement efficiency of the prepared surfaces was investigated by SERS measurements of Rhodamine 6G (R6G) as a reference molecule. The surface morphology and particle size of the Ag nanoparticle substrate were correlated with the corresponding enhancement factor.

MATERIAL AND METHODS

Electrochemical deposition of Ag island films

Silver island films were electrochemically synthesized by multiple scan CV using an electrolyte containing 0.1 M KNO_3 , 0.1 M KCN and 0.01 M AgNO_3 using a conventional three-electrode cell controlled by an Autolab PGSTAT302N (Eco Chemie). A sheet of stainless steel, a platinum sheet, and an Ag/AgCl/3 M KCl electrode were employed as the working, counter and reference electrodes, respectively. The working electrode was typically cycled for 30 cycles between -700 and -1550 mV, beginning at -700 mV, with scan rate 50 - 250 mV/s.

The SERS analyses of Ag island films

Raman spectra were obtained using an i-Raman® instrument (B&W Tek). Excitation was provided by a 532.1-nm Nd:YAG laser. The laser power at the sample was approximately 9 mW. The acquisition time for each accumulation was 5 s.

For SERS measurement, the prepared SERS-active Ag substrates were tested using R6G dye. For each test, 1 μl of the 5.10^{-4} M aqueous R6G solution was dropped onto the SERS substrate and dried naturally.

Surface morphology of Ag island films characterization

Morphology of the samples was characterized using a scanning electron microscope JEOL JSM-7000F (Japan).

RESULTS AND DISCUSSION

Silver island films were electrochemically synthesized by multiple scan CV using an electrolyte containing 0.1 M KNO_3 , 0.1 M KCN and 0.01 M AgNO_3 on a stainless steel substrate. Figs. 1(a) - (e) show SEM images of the Ag island films deposited at potential scan rate 50, 100, 150, 200 and 250 mV/s respectively. With

an increase in potential scan rate, the spherical nanoparticles and clusters become smaller and less aggregative. With a rise in scan rate the time of deposition shortens. Moreover, the lower coverage of working electrode with Ag nanostructures was observed when scan rate was increased. Formation of Ag nanoparticles and aggregates involves two competitive processes, formation and growth. At lower potential scan rate, the rate of the growth is slightly higher than that of formation. With elevating potential scan rate, the rate of formation increases while the rate of growth decreases. As the potential scan rate extends, the particle and cluster formation dominates. Thereby, the amount of small particles (90 – 270 nm in diameter) increased, diameter of aggregates decreased (ca. from 900 nm to 500 nm in diameter) and the size distribution becomes broader as the scan rate increase from 50 to 250 mV/s.

Figure 1.: SEM images of different Ag island films deposited on stainless steel substrates by multiple scan CV at different potential scan rate: a) 50 mV/s; b) 100 mV/s; c) 150 mV/s; d) 200 mV/s; e) 250 mV/s.

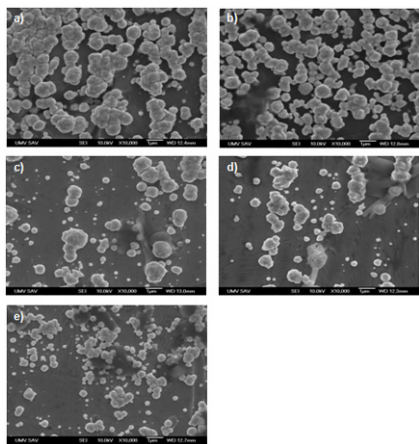
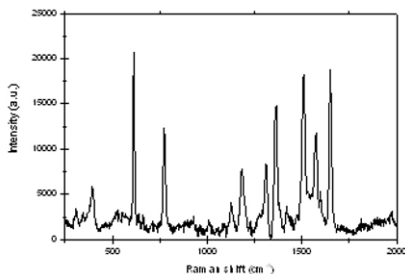


Fig. 2 demonstrates the SERS spectrum of 5×10^{-3} M R6G adsorbed on Ag film prepared by multiple scan CV at potential scan rate 100 mV/s. The peaks are characteristics of R6G in a Raman spectrum [2, 3]. The peak at ca. 612 cm^{-1} is assigned to the C–C–C ring in-plane vibration mode. The peak at ca. 775 cm^{-1} is assigned to the C–H out-of-plane bend mode. The peaks at ca. 1126 and 1185 cm^{-1} are assigned to the C–H in-plane bend mode. The peaks at ca. 1313 and 1577 cm^{-1} are assigned to the N–H in-plane bend modes. The peaks at ca. 1362 , 1508 and 1650 cm^{-1} are assigned to the C–C stretching modes.

Figure 2.: SERS spectrum of 5×10^{-3} M R6G adsorbed on Ag film prepared by multiple scan CV at potential scan rate 100 mV/s.



Values of intensity of the Raman peak of R6G adsorbed on the Ag island film at two most intensive peaks (612 and 1650 cm^{-1}) are summarized in Table 1 as a function of potential scan rate. As comparing intensities, it was found the marked increase in value of Raman intensity for first increment of potential scan rate from 50 to 100 mV/s. However, a gradual decrease in the intensity of the signal was observed with further increase of potential scan rate. Therefore, the optimum potential scan rate for obtaining the strongest SERS effect is 100 mV/s. From the SEM images of the Ag nanoparticle films prepared at elevated potential scan rate (Fig. 1) it can be seen clearly that the highest intensity of Raman peak correspond with the highest density of Ag island films, best dispersion and most uniform size of Ag particles was registered for Ag film deposited at 100 mV/s.

To estimate the enhancement ability of the Ag island film, the analytical enhancement factor (AEF) was calculated. According to the method developed by Le Ru et al. [10], AEF is defined as following:

$$AEF = \frac{I_{SERS} C_{RS}}{C_{SERS} I_{RS}}$$

where I_{SERS} denote the Raman intensity obtained for the Ag island SERS substrate under a certain concentration of C_{SERS} , and I_{RS} represents the Raman intensity obtained under non-SERS conditions at the R6G concentration of $C_{SERS} = 1 \times 10^{-3}$ M. RS stands for “reference sample”. In the present study I_{SERS} and I_{RS} were calculated using 612 and 1650 cm^{-1} as a reference peaks. The intensities as high as 598.75 and 1696.14 of Raman peak of R6G for reference sample were obtained at 612 cm^{-1} and 1650 cm^{-1} , respectively.

Table 1: Values of intensity of the Raman peak of R6G adsorbed on the Ag island film at 612 and at 1650 cm^{-1} together with values of determined AEF as a function of potential scan rate.

Potential scan rate (mV/s)	Intensity (a.u.)		AEF	
	612 cm^{-1}	1650 cm^{-1}	612 cm^{-1}	1650 cm^{-1}
50	2801.29	3887.13	9.4	4.6
100	20636.75	18772.54	68.9	22.1
150	13460.69	13436.94	45.0	15.8
200	6486.82	7772.30	21.7	9.2
250	8727.47	9096.69	29.2	10.7

From presented results it can be concluded that the highest intensity as well as signal enhancement for Ag film prepared at 100 mV/s can be related to uniformly distribute open network of aggregates (ca. between 500 - 900 nm in diameter) illustrated in Fig. 1(b).

Fig. 3 shows the SERS spectra of R6G adsorbed on the Ag film prepared at potential scan rate 100 mV/s as a function of the R6G concentration. The gradual increase in the signal intensity was observed with increasing concentration. The minimum detectable concentration was 5×10^{-16} M. Corresponding intensities together with values of determined AEF are summarized in Table 2.

Figure 3.: SERS spectra of R6G adsorbed on Ag island films prepared by multiple scan CV at potential scan rate 100 mV/s with different R6G concentrations: a) 5×10^{-4} ; b) 5×10^{-7} ; c) 5×10^{-10} ; d) 5×10^{-13} ; e) 5×10^{-16} M.

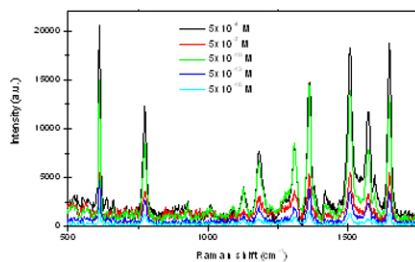


Table 2: Values of intensity of the Raman peak of R6G adsorbed on the Ag island film prepared at potential scan rate 100 mV/s at 612 and at 1650 cm^{-1} together with values of determined AEF as a function of R6G concentration.

R6G concentration (M)	Intensity (a.u.)		AEF	
	612 cm^{-1}	1650 cm^{-1}	612 cm^{-1}	1650
5×10^{-4}	20636.75	18772.54	68.9	2
5×10^{-7}	14941.24	13357.23	5.0×10^4	1.6
5×10^{-10}	5477.81	5540.93	1.8×10^7	6.5
5×10^{-13}	4650.81	3602.80	1.6×10^{10}	4.3
5×10^{-16}	1898.80	1307.15	6.3×10^{12}	1.5

The prepared SERS-active substrate based on the optimum preparation conditions demonstrates a large AEF of 6.3×10^{12} (resp. 1.5×10^{12}) which significantly reduces the practical limit of detection of R6G to 5×10^{-16} M.

CONCLUSION

The silver island films were electrodeposited on stainless steel surface by controlling the scan rate of applied potential. The produced surfaces show promising reproducible results for their use in molecule detection at ultra low concentrations.

ACKNOWLEDGEMENT

This work was supported by the Grant VEGA 1/0211/12 of the Slovak Scientific Grant Agency and the Project APVV SK-CZ-0113-11 of the Slovak Research and Development Agency.

REFERENCES

- [1] Upender G, Satyavathi R, Raju B, et al.: Chemical Physics Letters 511 (2011), 4, 309–314
- [2] Yang KH, Liu YC, Yu CC: Electrochimica Acta, 54 (2009), 17, 4202–4207
- [3] Chang CC, Yang KH, Liu YC, et al.: Analytica Chimica Acta, 709 (2012), 1, 91–97
- [4] Fan M, Andrade GFS, Brolo AG: Analytica Chimica Acta, 693 (2011), 1-2, 7–25
- [5] Sun B, Jiang X, Dai S, et al.: Materials Letters, 63 (2009), 29, 2570–2573
- [6] Jing C, Fang Y: Journal of Colloid and Interface Science, 314 (2007), 2, 46–51
- [7] Abdelsalam ME, Bartlett PN, Baumberg JJ, et al.: Electrochemistry Communications, 7 (2005), 7, 740–744
- [8] Sanci R, Volkan M: Sensors and Actuators B, 139 (2009), 1, 150–155
- [9] Huang Y, Sun L, Xie K, et al.: Journal of Raman Spectroscopy, 42 (2011), 5, 986–991
- [10] Le Ru EC, Blackie E, Meyer M, et al.: Journal of Physical Chemistry C, 111 (2007), 37, 13794–13803.

EXPERIMENTAL STUDY OF GLASS FRIT BONDING

Jan PEKAREK^{1,2*}, Radimir VRBA^{1,2}, Jan PRASEK^{1,2}, Jana CHOMOUCKA^{1,2}

¹ Department of Microelectronics, Faculty of Electrical Engineering and Communication, Brno University of Technology, Technicka 3058/10, 616 00 Brno, Czech Republic

² Central European Institute of Technology, Brno University of Technology, Technicka 3058/10, 616 00 Brno, Czech Republic

*pekarek@feec.vutbr.cz

ABSTRACT

Glass frit bonding technology provides a wide range of possibilities for the bonding of wafers at process temperatures below 450 °C. The process consists of three main steps: screen-printing of the glass paste, thermal conditioning and thermo-compressive bonding. The structured bonding layer protects moveable structures from parasitic bonding. Almost all surface layers commonly used in silicon micromachining can be bonded using glass frits. The main advantages of glass frit bonding are hermetic sealing, high process yield, low mechanical stress at the bonding interface, high bonding strength, and good reliability.

INTRODUCTION

Glass frit bonding is widely used in industrial microsystems applications where fully processed silicon wafers have to be bonded. This end-of-process-line bonding must fulfill some very specific requirements, such as: process temperature limited to 450 °C to prevent any temperature-related damage to wafers, no aggressive cleaning to avoid metal corrosion, high process yield since wafer processing to this stage is expensive, bonding of wafers with certain surface roughness or even surface steps resulting from metal lines electrically running at the bonding interface to enable electrical connections into the cavity sealed by the bonding, as well as a mechanically strong, hermetically sealed, reliable bond [1,2]. All of these requirements are fulfilled by the glass frit bonding process, which additionally can be very universally applied since it can be used to bond almost all surfaces common in microelectronics and microsystem technologies.

THEORY

For glass frit bonding, a low melting point glass is used to join two or more wafers. This kind of glass is commercially available (e.g. from Ferro Corporation, AGC Electronics) as a paste consisting of glass powder, organic binders and solvents. In case of the used glass Paste FX 11-036, the active melting glass compound is a lead-silicate glass with wetting temperature of 425 to 450 °C. This glass is non-crystallising and contains zinc oxide as a wetting agent. These two facts are advantageous for a good bonding. By adding high melting barium-silicate filler particles, the thermal expansion behaviour of the glass frit is adapted to silicon to reduce thermo-mechanical stress in the bond

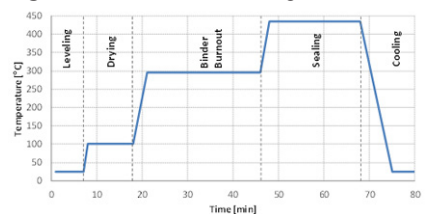
interface [2-3].

The glass frit bonding process consists of three main steps: screen printing, thermal conditioning of the glass paste and the thermo-compressive bonding itself.

EXPERIMENTAL

The paste was deposited and structured in one step using screen printing technology. The mesh openings were defined by the maximum paste particle size of 15 µm. The mesh thickness relates to the height of the printed structure, 30 µm are recommended by the material manufacturer. [4]

Figure 1.: Thermal conditioning



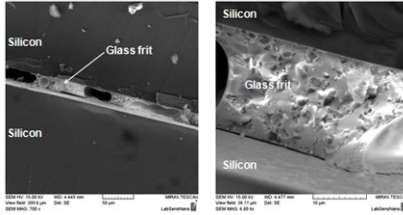
The initial step was comprised drying for 10 minutes at 100 °C in order to diffuse solvents out of the interface. This has started the polymerization of the organic binder. The organic binder of the glass paste had to be burned with heating up to a specific temperature (295 °C) where the glass is not fully melted for 25 minutes. This so called glazing ensures the outgassing of the organic additives. Further, a pre-melting or sealing step was heating the material to the process temperature between 430 °C and 440 °C for 20 minutes. The material was fully melted and formed a compact glass without any inclusions. The inorganic fillers were melted down and the properties of the bond glass were fixed. The

melting of the glass was started at the silicon-glass interface directed to the glass surface. During the melting process the porosity of the glass eliminates and based on the compression of the intermediate layer the thickness of the glass decreases significantly [4].

RESULTS AND DISCUSSION

In Figure 2 the result of glass frit bonding is shown.

Figure 2.: Cross section of glass frit bonding



The thermal conditioning is necessary in order to transform the paste into a real glass. During this pre-conditioning, the solvent is burned out and the glass is pre-melted. The process step is very important to prevent voids inside the bonded glass which lowers its strength and reliability. Bonding temperature is a critical bonding parameter because it has to be high enough to guarantee a good wetting of the bond surface with the glass as the initial process for the bond formation. The cooling of the bonded wafer pair is only critical at the higher temperatures where the bond is formed finally.

CONCLUSION

Glass frit bonding technology provides a wide range of possibilities for the bonding of wafers at process temperatures below 450 °C. The process consists of three main steps: screen-printing of the glass paste, thermal conditioning and thermo-compressive bonding. The structured bonding layer protects moveable structures from parasitic bonding. Almost all surface layers commonly used in silicon micromachining can be bonded using glass frits. The main advantages of glass frit bonding are hermetic sealing, high process yield, low mechanical stress at the bonding interface, high bonding strength, and good reliability.

ACKNOWLEDGEMENT

This research was supported by the Czech Science Foundation under 102/09/1601 and 205/10/1374 project, by project Prospective applications of new sensor technologies and circuits for processing of sensor signals, No. FEKT-S-11-16.

REFERENCES

- [1] Knechtel R, Wiemer M, Frömel J: J. Microsyst. Technol. 12 (2006) 468–472
- [2] Dresbach C, Krombholz A, Ebert M, Bagdahn J: J. Microsyst. Technol. 12 (2006) 473–480
- [3] Boettge B, Dresbach C, Graff A, Petzold M: Electrochem. Soc. Trans. 16 (2008) 441–448
- [4] Knechtel, R. (2012) Glass Frit Wafer Bonding, in Handbook of Wafer Bonding (eds P. Ramm, J. J.-Q. Lu and M. M. V. Taklo), Wiley-VCH Verlag GmbH & Co. KGaA, Weinheim, Germany. doi: 10.1002/9783527644223.ch1

SPECTROSCOPIC CHARACTERIZATION OF GOLD NANOPARTICLES

Iveta PILAROVA^{1,2}, Gabriela M. CASTILLO³, Libuse TRNKOVA^{1,4*}

¹Department of Chemistry, Faculty of Science, Masaryk University, Kotlarska 2, CZ-611 37 Brno, Czech Republic

²Central European Institute of Technology - CEITEC, Masaryk University, Zerotinovo namesti 617/9, CZ-601 77 Brno, Czech Republic

³Department of Nuclear Physics and Biophysics, FMFI UK, Mlynska Dolina F1, SK-842 48 Bratislava, Slovakia

⁴Central European Institute of Technology – CEITEC, Brno University of Technology, Technicka 3058/10, CZ-616 00 Brno, Czech Republic

*libuse@chemi.muni.cz

ABSTRACT

Gold nanoparticles (GNPs) are the object of interest in the field of nanotechnology due to their unique electronic, structural, optical, magnetic, thermal, and catalytic properties. They are extensively applied in the construction of electrochemical sensors and biosensors. The aim of this contribution is to characterize GNPs of both sizes (diameters of 5 nm and 10 nm) in buffered and non-buffered aqueous solutions with the change of ionic strength by spectroscopic methods (UV/Vis, photon correlation spectroscopy), and to investigate the GNP–aptamer–thrombin system as an application of GNPs in a sensitive aptasensor. For the immobilization the thrombin-binding aptamer (TBA) with the sequence GGT TGG TGT GGT TGG on the GNP surface was modified by a sulfhydryl group. The study showed that the spectral characterization of GNPs depends strongly not only on the aptamer–thrombin conjugate but also on the GNP size and solution composition (buffer, ions and their concentrations).

INTRODUCTION

Gold nanoparticles (GNPs) are the object of interest in the field of nanotechnology, especially due to their unique electronic, optical, magnetic, thermal, and catalytic properties. They are employed in many scientific fields such as chemistry, biology, physics, material chemistry and physics, pharmacy, and medicine. GNPs are applied for the construction of new electrochemical sensors and biosensors with immobilized DNA, oligonucleotide, or protein on the gold surface [1-4].

To analyze different proteins and their interactions with DNA fragment biosensors, in which the transducer is an electrode with anchored gold nanoparticles, sensors modified by aptamer (a short sequence of DNA specifically binding biologically important compounds such as enzymes, peptides, proteins, drugs) have been used [5]. Moreover, these sensors are presented as a potential tool for therapeutic purposes. The extensively studied aptamer is DNA 15–mer with the sequence GGT TGG TGT GGT TGG, known as the thrombin-binding aptamer (TBA). It binds specifically thrombin and thus inhibits the activity of thrombin in the cascade of reactions resulting in hemocoagulation [6].

The aim of our research was primarily the basic characterization of GNPs with sizes of 5 nm and 10 nm by means of spectroscopic methods. For the spectral behavior of GNPs in buffered and non-buffered aqueous solutions with different ionic strength and for the exact size de-

termination together with the distribution, UV/Vis absorption spectroscopy and the photon correlation spectroscopy (PCS) were chosen respectively.

To specify the dependence of the GNPs–TBA conjugate on GNPs sizes (5 nm and 10 nm) we modified GNPs by an SH–labeled TBA aptamer with the sequence GGT TGG TGT GGT TGG forming a self-assembled monolayer (SAM). In the next step, thrombin (200 nM) was specifically bound to these prepared GNPs–TBA conjugates. The created aptasensor system was characterized by UV/Vis spectroscopy.

2. MATERIAL AND METHODS

UV/Vis spectroscopy

UV/VIS spectroscopy enables both (a) to monitor the spectral behavior of 5 nm and 10 nm GNPs ($c_{5\text{ nm GNPs}} \sim 9 \cdot 10^{-8} \text{ mol} \cdot \text{l}^{-1}$; $c_{10\text{ nm GNPs}} \sim 1 \cdot 10^{-8} \text{ mol} \cdot \text{l}^{-1}$; Sigma Aldrich) in buffered and non-buffered solutions, depending on ionic strength adjusted by NaCl (Sigma Aldrich) and PBS buffer - phosphate buffer saline, pH 7.4, prepared from the following components: NaCl, Na_2HPO_4 , and NaH_2PO_4 (Sigma Aldrich) in a wavelength range of 300 to 800 nm in a 1 cm quartz cuvette, but also (b) to characterize the aptasensor system. The absorption spectra of GNPs–TBA ($c = 1.44 \cdot 10^{-5} \text{ M}$) conjugates and GNPs–TBA–thrombin (200 nM) complexes in the 1 cm quartz cuvette in a wavelength range from 220 to 800 nm were measured. In both cases a UV/Vis spectrophotometer UNICAM UV 4 was used.

Photon correlation spectroscopy (PCS)

To determine the exact size of the commercially delivered gold colloids (Sigma Aldrich) with the declared size of 5 nm (distribution from 3.0 to 5.5 nm) and 10 nm (distribution from 8.5 to 12.0 nm), the photon correlation spectroscopy (PCS), based on the Brownian motion of dispersed, non-sedimenting and randomly moving particles in a liquid solution, influenced by particle size, density, temperature and viscosity of the medium, was applied.

The PC spectra were measured using the instrument ZETASIZER MALVERN 3000 HSA, a combined instrument for measuring particle size in the range from 2 nm to 3 μm at an angle of 12° and 90° and for measuring the ZETA potential of the particles with a size from 5 nm to 30 μm . This measurement is based on sensing the charge of the particles moving between two palladium electrodes.

RESULTS AND DISCUSSION

The behavior of GNPs in buffered aqueous solutions with different ionic strengths

UV/Vis spectroscopy

The UV/Vis absorption spectra of GNPs with both sizes (diameters of 5 and 10 nm) were measured in a wavelength range from 300 to 800 nm. After the addition of NaCl or PBS, a change of the absorption spectrum accompanied by a color change of the GNPs solution was observed. It was found that the increase of ionic strength causes not only a decrease of the absorption maxima (hypochromic effect), but also their bathochromic shift (a shift to a longer wavelength). Both of these changes depend on the size of the nanoparticles studied, which was documented by the following results:

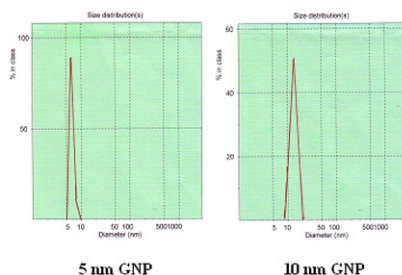
In the case of 5 nm GNP we obtained the characteristic absorption spectrum in the whole range of ionic strength (0.1 - 1 M) after the addition of 0.1 M PBS or 1.5 M NaCl. The ionic strength increase leads to a bathochromic shift of the absorption maxima, the absorbance is decreasing, and the spectral profile is wider. It is interesting that in the case of 5 nm GNPs, no color changes of the solutions due to the first addition of NaCl or buffer were observed. By contrast, in the case of 10 nm GNPs in the 0.1 M PBS medium at an ionic strength $I = 0.027$ M there occurs not only an intensive change of the shape of the spectrum, but also a substantial absorbance decrease, accompanied by a color change of the GNPs solution. Thus, the characteristic red color of the colloidal solution becomes a blue one. If the absorption spectra of 10 nm GNPs are measured in a 1.5 M NaCl medium, the changes of the shape of the spectrum and the color of the colloidal solutions are more remarkable compared to PBS medium. The change of the spectrum shape, accompanied by a considerable

hypochromic shift, was observed at an ionic strength $I = 0.0089$ M. Based on this fact it can be generalized that NaCl medium influenced the aggregation of nanoparticles more than did PBS components. It means that 10 nm GNPs are more stable in buffered solutions than in the NaCl medium. Simultaneously, a color change of GNPs solutions was observed and the typical red color changed to a blue one. Based on the spectral character and the color of the nanoparticle solutions we can conclude that nanoparticles with a size of 5 nm are more resistant to the change of ionic strength than are particles with larger diameters in both media.

Photon correlation spectroscopy (PCS)

It was found that the size of nanoparticles with a declared size of 5 nm (distribution from the Sigma-Aldrich company yields from 3.0 to 5.5 nm) is 5.6 nm (average), and the exact size of particles with a declared size of 10 nm (distribution from the Sigma-Aldrich company yields from 8.5 to 12.0 nm) is 12.3 nm (average). A comparison of both the declared and PCS average sizes indicates that a partial aggregation (about 25%) is present.

Figure 1: Hydrodynamic diameter of 5 nm and 10 nm GNPs



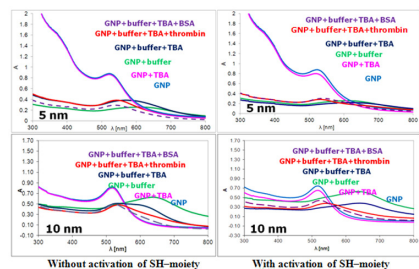
b) Characterization of the created aptasensor system

UV/Vis spectroscopy

UV/Vis spectra of (5 nm and 10 nm) GNPs-TBA conjugates, and (5 nm and 10 nm) GNPs-TBA-thrombin complexes in a wavelength range from 220 to 800 nm were recorded. The GNPs modification was conducted by means of two approaches: (1) TBA was attached on the Au surface without previous SH-moiety activation; (2) the SH-moiety of TBA was, still before the binding of the aptamer on the Au surface, activated using "Illustra microspin G-25 columns" (Amersham Biosciences). The activation consists in the desalting of the SH-moiety of TBA by column in order to ensure its attachment to gold surfaces. There was monitored not only the ability of the aptamer to bind to the gold surface, but also the GNP-

TBA–thrombin complex formation. It follows from the spectra presented that the visible hypochromic effect, achieving the binding of TBA on the gold surface, occurs only if the SH–moiety of the aptamer is activated by the G–25 column. The aptamer, without previous activation of SH–moiety, is bound only slightly, which influences the interaction between TBA aptamer and thrombin. If we add the TRIS buffer to the created GNP–TBA conjugate, a substantial bathochromic shift of the absorption maxima, caused by the changing ionic strength of the buffered solution, is observed in both cases (1 and 2). In the next step, due to the addition of thrombin or BSA (as a control sample of the specificity of TBA to thrombin) to the buffered GNP–TBA solution, a visible hypochromic shift (a shift to a shorter wavelength) is monitored in both cases (1 and 2). It can be assumed that the binding of thrombin reduces the influence of the ionic strength of the buffer. The interaction between aptamer and thrombin is generally reflected by the hypochromic effect. The absorption spectra show that an effective interaction occurs when the SH–moiety of the aptamer is activated. It means that in this case, the absorption maximum is lower than in the case of the non-activated aptamer SH–moiety. Moreover, the specificity of the TBA aptamer to thrombin can be verified only in the case of the activated SH–moiety of the aptamer when the absorption spectrum of BSA is the highest, thus indicating that the BSA does not bind to thrombin.

Figure 2: GNPs–TBA–thrombin conjugates



CONCLUSION

Using UV/Vis spectroscopy we presented not only (i) the general characterization of nanoparticles in buffered and non-buffered solutions with different ionic strengths (NaCl, PBS, pH 7.4), but also (ii) the characterization of the aptasensor system.

i) The behavior of the gold nanoparticles in buffered aqueous solutions with different ionic strengths

Based on the UV/Vis spectra we can state that the 5 nm GNPs provide characteristic absorption spectra in the whole range of ionic strengths, both in the PBS buffer and in the NaCl medium. The increasing ionic strength leads to the hypochromic effect and the bathochromic shift. Simultaneously, a photodocumentation of the color changes of GNPs solutions

was taken and it was found that with increasing ionic strength no color change was observed in this case. By contrast, in the case of 10 nm in PBS buffer and NaCl medium, the addition of buffer or salt caused an intense decrease of absorbance coupled with an intense change of the character of the absorption spectra. While in the PBS medium this effect occurs at an ionic strength $I = 0.027$ M, in the NaCl medium this change was visible at an ionic strength $I = 0.0089$ M. This phenomenon can be explained as an aggregation of nanoparticles, confirmed by the color change of the solution. The typical red color was changed to blue. Because of the aggregation of nanoparticles we can conclude that 10 nm GNPs are more stable in buffered solutions than in NaCl medium.

ii) Characterization of the created aptasensor system

The characterization of the aptasensor system was performed using UV/Vis spectroscopy. The UV/Vis spectroscopic method enabled to monitor the effect of activation of the SH–moiety of the TBA aptamer on the creation of GNP–TBA conjugates and the subsequent interaction between TBA and thrombin.

It follows from the presented UV/Vis spectra that the visible hypochromic effect, proving the binding of the TBA aptamer on the 5 nm and 10 nm GNPs surface and creation of the GNPs–TBA conjugate, is visible only in the case of the activated SH–moiety of TBA by column. The addition of the TRIS buffer to the created GNPs–TBA conjugate led, due to the changes of ionic strength, to a substantial bathochromic shift in both cases (with and without activation). It is surprising that with the addition of thrombin or the BSA solution to the buffered GNPs–TBA conjugate, a considerable hypochromic shift is observed. It can be assumed that the binding of protein decreases the influence of ionic strength. The specificity of the TBA aptamer to thrombin was verified only when the SH–moiety of the aptamer was activated. In this case the absorption spectrum of BSA was the highest, thus indicating that the BSA did not bind to thrombin.

ACKNOWLEDGMENT

This research was supported by the following Projects: (a) 106/09/H035 of the GA CR, (b) CEITEC – Central European Institute of Technology Project

CZ.1.05/1.1.00/02.0068, and (c) OPVK project
(NanoBioMetalNet) CZ.1.07/2.4.00/31.0023.

REFERENCES

- [1] Daniel M.-C., Astruc D.: *Chem.Rev.* *104* (2004), 293-346.
- [2] Pumera M, Sanchez S, Ichinose I, Tang J.: *Sensors and Actuators B-Chemical*, *123* (2007), 1195-1205.
- [3] Guo S J, Wang E K.: *Analytica Chim. Acta*, *598* (2007), 181-192.
- [4] Rezanka P, Zaruba K, Kral V.: *Chem. Listy*, *101* (2007), 881-885.
- [5] Li X. X., Shen L. H., Zhang D. D., et al.: *Biosensors & Bioelectronics*, *23* (2008), 1624-1630.
- [6] Fialova M, Kypr J, Vorlickova M.: *Biochem. Biophys. Res. Commun.*, *344* (2006), 50-54.

EFFECT OF FREQUENCY ON THE C-E CURVES AND TENSAMMETRIC PEAKS OF POLYADENYLIC ACID, OLIGODEOXYNUCLEOTIDES AND CYTOSINE DERIVATIVES

Vladimír VETTERL*, Stanislav HASON, Lukas FOJT,

Institute of Biophysics AS CR, v.v.i., Královopolská 135, 61265 Brno, Czech Republic

*vetterl@ibp.cz

ABSTRACT

The C-E curves of single stranded polynucleotides and homopurine oligodeoxynucleotides exhibit two tensammetric peaks. The more positive peak corresponds to the adsorption-desorption of sugar-phosphate backbone, the more negative is caused by the desorption of bases. The frequency dependence was analyzed by two equivalent circuits, one of them describing the Debye relaxation.

INTRODUCTION

Since 1961 when Miller [1] has published his work on differential capacitance of the mercury electrode double layer in the solutions of nucleic acids, the measurement of the impedance of electrified interfaces started to be widely used for investigation of the interactions of nucleic acids and their components with electrode surface [2–11]. Differential capacitance C of the electrode double layer is a sensitive indicator of adsorption. Usually, the dependence of C on electrode potential E (C–E curves) or the dependence of the electrode double layer impedance Z on frequency (electrochemical impedance spectroscopy, EIS) is measured. On the C–E curves of DNA and synthetic polynucleotides, adsorption–desorption (tensammetric) peaks are observed [7–9]. The native double helical DNA (double stranded, dsDNA) usually yields just only one tensammetric peak at about -1.1 V corresponding to the desorption of the sugar/phosphate backbone and denoted as peak 1 [9]. The denatured DNA (single stranded, ssDNA) yields besides peak 1 another tensammetric peak (peak 3) at about -1.4 to -1.6 V corresponding to the desorption of bases. If dsDNA contains some distorted regions in which hydrophobic bases can come into contact with the electrode, another tensammetric peak (peak 2) appears between peaks 1 and 3 [7–10].

2. MATERIAL AND METHODS

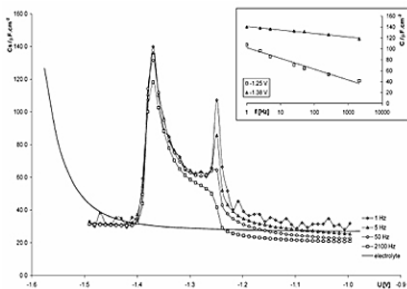
All electrochemical measurements were performed with a three-electrode system, employing a platinum wire counter electrode, an Ag/AgCl/3M KCl reference electrode, and a hanging drop mercury (HMDE; surface area 0.5mm²; VA-Stand 663, Metrohm, Switzerland) working electrode. The capacitance measurements were performed with the AUTOLAB electrochemical system (Ecochemie, Utrecht, Netherlands) at a frequency of 250 Hz and ac voltage amplitude

of 5mV. Oligodeoxynucleotides, 30-mers dA₃₀, dG₃₀, dT₃₀, dC₃₀ were purchased from Herma Electron (Ulm, Germany).

RESULTS AND DISCUSSION

Polyadenylic acid (poly A) may have (depending on pH and ionic strength) either ss or ds form [12,13]. We have found that at the frequency of 22 Hz the peak observed on C–E curves around -1.4 V of the ss poly A (pH 8, 0.1 M NaCl) is higher and more asymmetric than the peak of the ds poly A (pH 5, 0.1 M NaCl). With increasing frequency the height of the tensammetric peaks decreases. The decrease is more pronounced with the ss poly A than with the double stranded conformations [14]. At low frequencies the tensammetric peak of ss poly A splits in two peaks, the more positive one around -1.25 V corresponding to the adsorption-desorption of sugar-phosphate backbone decreases with increasing frequency faster than the more negative peak around -1.38 V corresponding to the adsorption-desorption of adenine bases. It means that the adsorption – desorption of sugar-phosphate backbone is slower than the adsorption-desorption of bases, Fig.1 [15].

Fig. 1 C–U curves of 180 Ag/ml poly A in 0.3 M NaCl + 0.05 M Na₂HPO₄, pH 8.5. Temperature 20^o C. Waiting time $t = 30$ s at -0.6 V. Potential scan from -1.0 to -1.5 V with a potential step 0.1 V every 2 s (corresponding to the potential scan rate 50 mV s⁻¹). Insert shows the dependence of peaks at -1.25 V. and -1.38 V on frequency [15].



Similar dependence of the tensammetric peaks we have observed with the homopurine oligodeoxynucleotide (dA_{30}) contrary to homopyrimidine (dT_{30}) and dC_{30} [16], where only the frequency dependence of the tensammetric peak of the sugar-phosphate backbone can be observed, Fig.2. At potentials more negative than this peak a 2D condensed layer is formed and the desorption peak of bases is depressed and is independent on frequency in the range 5 – 1000 Hz.

Fig. 2 $C-E$ curves of dT_{30} (blue), dA_{30} (red open box), dC_{30} (green open diamond), and dG_{30} (yellow) measured at the HMDE in the ex situ (transfer) mode. The $C-E$ curves were measured by potential scan from $-0.1V$ to more negative values [16].

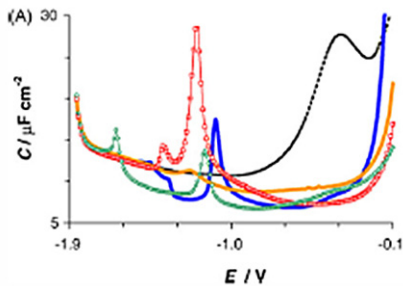
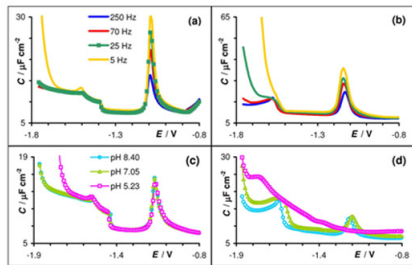


Fig 3 Frequency dependence of the capacitance – potential ($C - E$) curves of (a) $1 \mu M d(T_{30})$, and (b) $1 \mu M d(C_{30})$. Potential was scanned from $-0.8 V$ to more negative potentials. pH dependence of the $C - E$ curves of (c) $1 \mu M d(T_{30})$, and (d) $1 \mu M d(C_{30})$. The values of frequency and pH are detected in figures. The temperature of measurement was $5^\circ C$ [16] -supporting information.



The frequency dependence of the tensammetric peaks we have analyzed by 2 equivalent circuits, one of them describing the Debye relaxation [17-20]. In biopolymers the frequency effect depended upon the rate of migration of adsorbed trains from the surface phase to the loops extending to the solution and vice versa. Such segment migration could occur only in combination with rearrangement of the whole biopolymer molecule, EIS thus appeared to be capable to provide information about the kinetic of the adsorption-desorption process of the nucleic acids.

Anomalous frequency dependence of the $C-E$ curves of halogen derivatives of cytosine was observed.

CONCLUSION

The more positive tensammetric peak of single stranded DNA and poly A corresponding to the adsorption-desorption of sugar-phosphate backbone decreases with increasing frequency faster than the more negative peak corresponding to the adsorption-desorption of bases. It means that the adsorption – desorption of sugar-phosphate backbone is slower than the adsorption-desorption of bases. Similar behavior was observed with the tensammetric peaks of the homopurine oligodeoxynucleotide (dA_{30}) contrary to homopyrimidine (dT_{30}) and dC_{30}) [15], where only the frequency dependence of the tensammetric peak of the sugar-phosphate backbone can be observed. At potentials more negative than this peak a 2D condensed layer is formed.

ACKNOWLEDGEMENT

This work was supported by the Grant Agency of the Czech Republic, grant P205/10/2378 P206/11/1638 and P206/12/G151

REFERENCES

- [1] Miller I R, J. Mol. Biol. 3 (1961) 229–240
- [2] Vetterl V, Experientia 21 (1965) 9–11
- [3] Vetterl V, Czech. Chem. Commun. 31

- (1966) 2105–2126
- [4] Vetterl V, J. Electroanal. Chem. 19 (1968) 169–173
- [5] de Levie R, Chem. Rev. 88 (1988) 599–609
- [6] Vetterl V, de Levie R, J. Electroanal. Chem. 310 (1991) 305–315
- [7] Brabec V, Vetterl V, Vrána O, Experimental Techniques in Bioelectrochemistry, vol. 3., Brabec V, Walz D, Milazzo G (Eds.), Birghauser Verlag, Basel, 1996, Chap. 5, pp. 287–359
- [8] Paleček E, Vetterl V, Biopolymers 6 (1968) 917–928
- [9] Brabec V, Paleček E, Biopolymers 11 (1972) 2577–2589
- [10] Berg H, Flemming J, Paleček E, Vetterl V, Stud. Biophys. 33 (1972) 81–92
- [11] Dražan V, Vetterl V, Collect. Czech. Chem. Commun. 63 (1998) 1977–1993
- [12] Guschlbauer W, Vetterl V, FEBS Lett. 4 (1969) 57–60
- [13] Vetterl V, Guschlbauer W, Arch. Biochem. Biophys. 148 (1972) 130–140
- [14] Hanák L, Vetterl V, Bioelectrochem. Bioenerg. 46 (1998) 7–13
- [15] Strašák L, Dvořák J, Hasoň S, Vetterl V, Bioelectrochemistry 56 (2002) 37–41
- [16] Hasoň S, Vetterl V, Fojta M, Electrochimica Acta 53 (2008) 2818–2824
- [17] Pospíšil L, Experimental Techniques in Bioelectrochemistry, vol. 3, Brabec V, Walz D, Milazzo G (Eds.), Birkhauser Verlag, Basel, 1996, pp. 1–39
- [18] Ross Macdonald J, Impedance Spectroscopy, Wiley, New York, 1987
- [19] Hason S, Dvořák J, Jelen F, Vetterl V, Crit. Rev. Anal. Chem. 32 (2002) 167–169
- [20] Hasoň S, Dvořák J, Jelen F, Vetterl V, Talanta 56 (2002) 905–913

THE INFLUENCE OF PLATINUM

ON TOBACCO BY-2 CELLS (*NICOTIANA TABACUM*)

Olga KRYSTOFOVA¹, Jiri SOCHOR^{1,2,3}, Branislav RUTTKAY-NEDECKY^{1,2},
Andrea BEZDEKOVA¹, Ondrej ZITKA^{1,4}, Monika KREMPLOVA¹, Petr
BABULA⁵, Vojtech ADAM^{1,2,3}, Miroslava BEKLOVA^{2,4}, Rene KIZEK^{1,2,3*}

¹Department of Chemistry and Biochemistry, Faculty of Agronomy, Mendel University in Brno, Zemedelska 1, 613 00 Brno, Czech Republic

²Central European Institute of Technology, Brno University of Technology, Technicka 3058/10, 616 00 Brno, Czech Republic

³Department of Microelectronics, Faculty of Electrical Engineering and Communication, Brno University of Technology, Technicka 10, CZ-616 00 Brno, Czech Republic

⁴Department of Ecology and Environmental Protection, Faculty of Hygiene and Ecology, University of Veterinary and Pharmaceutical Sciences, Palackeho 1/3, 612 42 Brno, Czech Republic

⁵Department of Natural Drugs, Faculty of Pharmacy, University of Veterinary and Pharmaceutical Sciences Brno, Palackeho 1-3, CZ-612 42, Czech Republic

*kizek@sci.muni.cz

ABSTRACT

Platinum group elements (PGE; platinum, palladium, rhodium and ruthenium, less frequently iridium) in catalysts contribute to the reduction of pollutants in exhaust gases, however, their concentrations in environment have been increasing. As a results, we attempted to study the effects of platinum(IV) on BY-2 tobacco cells. The cells were treated with 0, 5, 10, 25, 50, 100, 250 and 500 μM PtCl_4 for 24 hours. After that, content of platinum, reduced and oxidised glutathione, phytochelatins and activities of phytochelatin synthase, superoxide dismutase and catalase were determined.

INTRODUCTION

Increasing anthropogenic activities result in the burden on human health and the environment due to the emissions of toxic compounds. Road traffic is one of the fundamental anthropogenic activities that affect the landscape [1-3]. Platinum group elements (PGE; platinum, palladium, rhodium and ruthenium, less frequently iridium) in catalysts contribute to the reduction of pollutants in exhaust gases. The disadvantage of using catalysts containing PGE is that there is considerable leakage of these elements into the environment. It is not surprising that the concentration of platinum metals in environmental samples such as soil, dust on roads, surface water, sediments and plants has significantly increased in the last decade [4-9].

Plants are the first link of the food chain. Study of the ability of plants to receive PGE from the soil is very important in the protection of human health [10-12]. The intake of heavy metals in the soil is mainly due to the presence of complexing agents (organic acids), which the plant is able to secrete into the soil. Available literature data suggest that PGE (mainly palladium) are received from the soil through the roots, and then PGE binds to the biologically active substances rich in sulphur as glutathione and phytochelatins [13-17]. PGE accumulation process takes place mainly in the vegetative parts of plants and decreases in the following order: root > stem >

leaves. Based on available information, we can assume that phytotoxicity of PGE depends on the following conditions: the concentration of metals in the soil, time of exposure, chemical form of metal, the chemical composition of exposed soil and plant species, however, further research on this topic is needed.

Therefore, we aimed at investigation of the influence of platinum(IV) of the following concentrations (0, 5, 10, 25, 50, 100, 250 and 500 μM) on BY-2 tobacco cells. Our attention was mainly paid to determination of low molecular mass thiols as phytochelatins. Further, studied the effects of platinum(IV) on cell morphology and activity of some detoxification enzymes.

MATERIAL AND METHODS

Plant Material and Analytical Methods

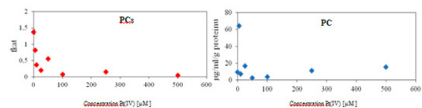
The suspension culture of *Nicotiana tabacum* BY 2 line was grown in liquid Murashige and Skoog medium supplemented with sucrose (30 $\text{g}\cdot\text{l}^{-1}$), KH_2PO_4 (0.2 $\text{g}\cdot\text{l}^{-1}$), thiamine (1 $\text{mg}\cdot\text{l}^{-1}$) and 2,4-dichlorophenoxyacetic acid (0.2 $\text{mg}\cdot\text{l}^{-1}$). The suspension cultures (20 ml) were grown in 50 ml Erlenmeyer flasks at 27°C with shaking at 135 rpm (ES-20, Biosan, Latvia). Passage was performed after 3 or 4 days by transferring 2 or 1 ml, respectively, of suspension culture into a fresh medium (total volume 20 ml). To suspension, 0, 5, 10, 25, 50, 100, 250 and/or 500 μM of

PtCl₄ diluted in HNO₃ was added. After 24 hours long treatment, the cells were harvested and analysed. Morphological changes were detected using microscopy. Activities of superoxide dismutase (SOD) and catalase (CAT) were detected using spectrometry. High performance liquid chromatography with electrochemical detection was used for determination of reduced and oxidized glutathione, phytochelatins (PC) and activity of phytochelatin synthase activity (PCs). Content of platinum was determined using differential pulse voltammetry.

RESULTS AND DISCUSSION

Based on the analyses it was found that the morphology of cells did not show any significant changes at lower concentrations of platinum. At higher concentrations of platinum, the vacuolation of cells and formation of apoptotic glands were observed. This resulted in determination of viability, where the increasing concentration of platinum reduced viability of the treated cells. It was also found the increased activity of antioxidant enzymes (SOD and CAT) in the highest concentrations of platinum (50, 100, 250 and 500 µM), indicating an active protection of cells against oxidative stress. We assume that content of GSH and GSSG may be related to inhibition and metabolic pathways associated with their formation or transformation. This told that there is confirmed by results obtained by determination of phytochelatin synthase activity and content of phytochelatin. We found that phytochelatin synthase showed reduced activity, and this was reflected in low concentrations of phytochelatin under the highest platinum doses (Fig. 1). Finally, we were also wondered how many Pt (IV) could be uptaken by a cell, depending on the applied concentration. The analysis revealed that most platinum contained cells were exposed to the highest concentrations of platinum (IV) in the medium.

Figure 1.: Determination of phytochelatin synthase activity (PCs) and the content of phytochelatin (PC) in BY-2 tobacco cells treated with platinum(IV)



CONCLUSION

The results obtained suggest that platinum in the cell acts as a potential toxic metal accumulation in the food chain. Its effects on living organisms in the formation of active oxygen species that cause oxidative stress and inhibition of me-

tabolic pathways required for metal detoxification. It is therefore important to monitor the content of platinum and platinum metals in the environment.

ACKNOWLEDGEMENT

The work has been supported by SIX CZ.1.05/2.1.00/03.0072 and NANIMEL GA ČR 102/08/1546. Many thanks to Barbora Nečasová for technical assistance.

REFERENCES

- [1] Ward J M, Young D M, Fauvie K A, *et al.*, Cancer Treatment Rep., 60 (1976), 1675-1678.
- [2] Gebel T, Lantzsch H, Plessow K, *et al.*, Mutat. Res. Genet. Toxicol. Environ. Mutagen., 389 (1997), 183-190.
- [3] Bunger J, Gebel T, Dunkelberg H, *et al.*, Naunyn-Schmiedebergs Arch. Pharmacol., 355 (1997), 629-629.
- [4] Bocca B, Petrucci F, Alimonti A, *et al.*, J. Environ. Monit., 5 (2003), 563-568.
- [5] Schafer J, Puchelt H, J. Geochem. Explor., 64 (1998), 307-314.
- [6] Gomez B, Palacios M A, Gomez M, *et al.*, Sci. Total Environ., 299 (2002), 1-19.
- [7] Moldovan M, Gomez M M, Palacios M A, Anal. Chim. Acta, 478 (2003), 209-217.
- [8] Morton O, Puchelt H, Hernandez E, *et al.*, J. Geochem. Explor., 72 (2001), 223-227.
- [9] Barbante C, Veyseyre A, Ferrari C, *et al.*, Environ. Sci. Technol., 35 (2001), 835-839.
- [10] Diopan V, Ryant P, Adam V, *et al.*, Lis. Cukrov. Repar., 125 (2009), 227-228.
- [11] Macek T, Rezek J, Vrchotova B, *et al.*, Lis. Cukrov. Repar., 123 (2007), 312-314.
- [12] Babula P, Supalkova V, Adam V, *et al.*, Plant Soil Environ., 53 (2007), 350-354.
- [13] Rojas F S, Ojeda C B, Pavon J M C, Talanta, 70 (2006), 979-983.
- [14] Hees T, Wenclawiak B, Lustig S, *et al.*, Environ. Sci. Pollut. Res., 5 (1998), 105-111.
- [15] Stejskal K, Diopan V, Adam V, *et al.*, Lis. Cukrov. Repar., 123 (2007), 328-329.
- [16] Babula P, Adam V, Opatrilova R, *et al.*, Environ. Chem. Lett., 6 (2008), 189-213.
- [17] Supalkova V, Huska D, Diopan V, *et al.*, Sensors, 7 (2007), 932-959.

EFFECT OF ORGANIC AND INORGANIC FORM OF SELENIUM ON ANTIOXIDANT STATUS OF BREEDING BOARS EJACULATE

Pavel HORKY^{1*}, Petra JANCÍKOVÁ¹, Jiri SOCHOR^{2,3,4}, Branislav RUTTKAY-NEDECKÝ^{1,2}, Sona KRIZKOVA^{2,3}, Petr MAREŠ¹, Ladislav ZEMAN¹, Vojtech ADAM^{2,3,4}, Rene KIZEK^{2,3,4}

¹ Department of Animal Nutrition and Forage Production, Faculty of Agronomy, Mendel University in Brno, Zemedelska 1, 613 00 Brno, Czech Republic

² Department of Chemistry and Biochemistry, Faculty of Agronomy, Mendel University in Brno, Zemedelska 1, 613 00 Brno, Czech Republic

³ Central European Institute of Technology, Brno University of Technology, Technicka 3058/10, CZ-616 00 Brno, Czech Republic

⁴ Department of Microelectronics, Faculty of Electrical Engineering and Communication, Brno University of Technology, Technicka 10, CZ-616 00 Brno, Czech Republic

*pavel.horky@mendelu.cz

ABSTRACT

This work deals with the influence of organic and inorganic form of selenium on selected parameters in ejaculate of breeding boars. The main aim of the present study was to determine the effects of selenium on antioxidant status of Duroc boars. In this experiment, twenty-eight Duroc boars were allocated to four experimental groups, seven boars in each group. Each group was fed in the addition of organic form in 0.3 and 0.6 mg Selenium/kg and inorganic 0.3 and 0.6 mg selenium/kg in the feed mixture. The duration of the experiment was 18 weeks. All the boars were intensively collected at a regular frequency for four times over six weeks. The activity of important enzyme glutathione peroxidase was studied photometrically using the method of Free Radicals measured antioxidant activity. Selenium content was detected by atomic absorption spectrometry. The dietary supplementation of organic form of selenium at a dose 0.6 mg/kg of feed mixture increased significantly by 6.3 % ($P < 0.001$) activity of glutathione peroxidase in the ejaculate. Selenium concentration in this group of boars in ejaculate increased by 71.9 % ($P < 0.05$). Dietary supplementation of inorganic form of selenium at a dose 0.3 mg/kg of feed mixture showed an increase of free radicals by 91.4 % ($P < 0.01$). The results of the present study indicate that dietary supplements of 0.6 mg Se/kg of feed mixture improved antioxidant potential of breeding boars ejaculate. A lower oxidative stress and higher fertility can be therefore assumed.

INTRODUCTION

Selenium is an essential element for reproduction of boars. Selenium has been considered for many years as a substance causing toxicity in livestock. The necessity of selenium was discovered in 1957. Selenium plays an important role in the correct sequence of physiological functions especially in farm animals [11]. Selenium is found in all cells and body tissues. The amount of selenium at a feeding dose changes its content in body [5]. Selenium is a component of the enzyme glutathione peroxidase, which is one of the most important antioxidants in animals [8]. Imbalance between reactive oxygen and total antioxidant capacity can cause male infertility. The recommended dose of selenium was 0.3 mg/kg in feed mixture for modern genotypes of breeding boars [3]. Currently there are organic and inorganic forms of selenium to choose from. The main aim of the experiment was to compare different levels and forms of selenium and its effect on antioxidant status of breeding boars ejaculate.

MATERIALS AND METHODS

The actual experiment was conducted at the insemination station boars (ISK) in Velké Meziříčí, Czech Republic. Twenty-eight Duroc boars were selected for this study and they were divided into four balanced groups (according to their age). The age interval of boars ranged from 1 to 3 years. The experimental animals were housed individually and had free access to water. The feed mixture (FM), containing 0.02 mg Se/kg of FM, was 3.3 kg per boar (Tab. 1) for the whole experimental period. The boars were allocated to four experimental groups. The first group (G1) boars ($n = 7$) was fed 0.3 mg Se/kg of FM in organic form. The second group (G2) boars ($n = 7$) was fed 0.3 mg Se/kg of FM in inorganic form. The third group (G3) boars ($n = 7$) was fed 0.6 mg Se/kg of FM in organic form. The last one (G4) boars ($n = 7$) was fed 0.6 mg Se/kg of FM in inorganic form. As a source of inorganic selenium sodium selenite was used. Selenium-enriched yeasts were used to supplement selenium in organic form (Sel-Plex - Alltech's).

Table I: Composition of feed mixture for boars

Component	% representation
Barley grain	36.00
Wheat grain	20.36
Oat grain	20.00
Soybean extracted scrap	14.50
EKPO T	3.00
Bergafat	2.10
Calcium carbonate	1.50
Monocalciumphosphate	1.20
Mineral vitamin premix	0.50
Sodium chloride	0.40
Magnesium oxide	0.15
L-Lysine HCl	0.14
L - Threonine	0.09
Methionine DL	0.06

The duration of the experiment was 18 weeks. All boars were trained for semen collection (every third sampling) during this period. Semen was collected at a regular frequency every six weeks. The first control sampling was performed before the experiment was begun. Native seed has been frozen immediately after the collection. Collection of semen was performed manually using the phantom. The experimental period was started in mid-April 2011 and ended in mid-August 2011. The results were processed by a statistical program using student's paired t-test.

Bergafat – palm oil; EKPO T – biskvit meal

Sample preparation

Firstly, 0.5 ml volume of native thawed semen was pipetted with subsequent addition of 2 ml liquid nitrogen and 0.5 ml phosphate buffer. Subsequently, the sample was homogenized in ULTRA-TURRAX T8 homogenizer (IKA, Königswinter, Germany) at 3000 rpm for 2 minutes. After homogenization 1 ml of phosphate buffer was added. This modified sample was homogenized in vortex Vortex-2 Genie (Scientific Industries, New York, NY, USA) at 2000 rpm for 15 minutes. Subsequently, the sample was centrifuged at Universal 32 R centrifuge (Hettich-Zentrifugen GmbH, Tuttlingen, Germany) at 16000 rpm at 4 °C for 20 minutes. It was then pipetted 1.5 ml of supernatant, which was analysed.

Determination of antioxidant activity by the Free Radicals Method

This method is based on the ability of chlorophyllin (the sodium-copper salt of chlorophyll) to accept and

donate electrons with a stable change of maximum absorption. This effect is conditioned by an alkaline environment and the addition of catalyst. Methodology was adapted from the publication [9]. The antioxidant activity was determined using automated spectrophotometer BS – 400 (Mindray, China). It was pipetted 150 µL volume of reagent R1 (0.1 M HCl, extract chlorophyllin, reaction buffer, catalyzer) into a plastic cuvette with subsequent addition of 6 µL sample. Absorbance was measured at $\lambda = 450$ nm for 12 minutes. The calibration curve of absorbance was converted into equivalent content of trolox (mmol/l).

Determination of Glutathione peroxidase (GSH-Px)

Glutathione peroxidase was determined using indirect method for determination of GSH-Px activity. IT IS based on the oxidation of reduced glutathione GSH to oxidized glutathione GSSG catalysed GPx. This reaction is associated with glutathione recycling reaction, in which GSSG is reduced to GSH by NADPH and glutathione reductase (GR). To determine the activity of glutathione peroxidase Kit CGPI was used (Sigma Aldrich, USA). The measurements were done in a plastic tube to BS 400 automatic analyzer (Mindray, China). It was pipetted 260 µL reagent R1 (0.3 mM NADPH in GPx buffer) into a plastic cuvette. The agent was incubated at 37 °C for 108 s. After pipetting the 10 ml sample the reaction was started by adding 30 ml of response R2 (3 mM tert-butyl hydroperoxid) in 378 s. The sample was incubated with 18 s, then the absorbance was measured at $\lambda = 340$ nm and measured the reaction kinetics for 126 s. The device calculates the average decrease in absorbance per minute (ΔA) and the calibration equation GSH-Px activity measured in samples.

Determination of selenium concentration in the ejaculate

The method of atomic absorption spectrometry (AAS) with the generation of hybrids after sample digestion in nitric acid and microwave decomposition system was used for the determination of selenium concentration in boar semen. Wavelength used was as follows: 196.026 nm.

RESULTS

During the experiment the addition of different levels and forms of selenium (or-

ganic and inorganic) were evaluated on the antioxidant status of breeding boars ejaculate. The observed values of free radicals (FR) did not prove significant difference between samples in the group of boars G1 (organic form of selenium - 0.3 mg Se/kg of FM). The same group of boars G1 in the second sampling had the lowest activity of FR. The decrease amounted to 26.7%. After that the occurrence of FR has almost increased in the same level as the control collection. In the second experimental group of boars G2 (inorganic form of selenium - 0.3 mg Se/kg of FM) increased the FR in the second sampling by 57.5%. The third measurement enabled to increase FR by 82.2 % (P <0.05). The last measurement showed an increase in FR even by 91.4 % (P <0.01). The results of the group boars G3 (organic form of selenium - 0.6 mg Se/kg of FM) on the contrary show a gradual reduction in FR, where the greatest decrease was measured at the fourth sampling. At the beginning of the experiment the total decrease FR has been in this group of boars G3 by 15.9 %. In the last group of boars G4 (inorganic form of selenium - 0.6 mg Se/kg of FM) no significant changes in the values of FR were observed. At the end of the experimental observations in this group of boars G4 FR value was 11.5 % higher than at the beginning. An integral part of the antioxidant system, with a direct link to the metabolism of selenium, is glutathione peroxidase enzyme (GSH-Px). Its assessment was subject of interest to our observation. No significant differences in the activity of GSH-Px in the group of boars G1 were observed. At the end of the experiment there was a slight increase by 2.3 %. Also, a second experimental group of animals G2 did not record any significant changes. During the fourth sampling was GSH-Px activity by only 1.6 % higher than before the experimental observation. Glutathione peroxidase in boar semen group G3 during the second and third measurements increased only slightly (by 2.4 %). However, taking fourth sampling in the analysis of ejaculate, this increase was already by 6.3 % (P <0.001). The last group of animals G4 showed a gradual increase in the concentration of GSH-Px (by 2.6 % at the end of the experiment), but without statistical evidence. In evaluating the concentration of selenium in ejaculate of group of boars G1 no significant change was observed in the second period. The third and fourth samplings decreased the content of selenium, up by 37.6 %. For the second group of animals G2 selenium concentration made no significant difference. In the second period it was increased by 23.7 % and then the values of the third and fourth sampling were at the same level as at the beginning of the experimental observation. In the group of boars G3 the content of selenium in the ejaculate taking was higher by 61.0 % in the second sampling. The

increase has amounted to 69.7 % (P <0.05) at the third sampling. The same trend continued during the fourth seed analysis, in which level of selenium compared to the first collection amounted to 71.9 % (P <0.05). The last group of experimental animals did not record any significant changes in the concentration of selenium. There was a non significant increase of 25.4 % at the end of the experiment. The results of all monitored parameters are presented in table II.

Table II: Illustration of changes in the antioxidant capacity of boar semen

Experimental group	Sampling	Free Radicals (nmol/l)	GSH-Px (nmol/l)	Selenium content (µg/l)
G1	I.	277.0 ± 144.0	9.6 ± 0.2	60.4 ± 38.5
	II.	203.1 ± 99.2	9.4 ± 0.1	64.3 ± 52.1
	III.	213.8 ± 147.2	9.6 ± 0.1	39.3 ± 21.6
	IV.	281.9 ± 195.2	9.8 ± 0.4	37.7 ± 26.9
G2	I.	163.2 ± 114.9	9.5 ± 0.2	41.0 ± 31.9
	II.	257.0 ± 200.3	9.5 ± 0.2	50.7 ± 37.8
	III.	297.4 ± 224.0*	9.7 ± 0.4	39.7 ± 41.8
	IV.	312.5 ± 157.0**	9.8 ± 0.6	41.9 ± 48.0
G3	I.	187.9 ± 152.2	9.5 ± 0.2	66.1 ± 24.9
	II.	175.8 ± 138.9	9.4 ± 0.2	106.4 ± 55.3
	III.	178.4 ± 171.3	9.8 ± 0.3	112.0 ± 34.8*
	IV.	157.5 ± 106.4	10.2 ± 0.2***	113.4 ± 40.0*
G4	I.	277.9 ± 140.4	9.7 ± 0.3	52.9 ± 42.1
	II.	286.7 ± 165.0	9.7 ± 0.2	61.9 ± 39.3
	III.	353.6 ± 249.2	9.7 ± 0.4	47.1 ± 23.1
	IV.	309.8 ± 200.4	9.8 ± 0.6	66.8 ± 51.1

* - symbol representing statistically significant changes (by comparison with I period - beginning of the experiment); P < 0.05 **, P < 0.01 ***, P < 0.001 ****

DISCUSSION

Marin-Guzman et al. [7] added to the diet experimental group of boars 0.5 mg Se/kg of FM in organic form. Selenium was not increased in the control group of animals in their diet. This team of authors found similar results as in our experimental observation. In the case of boars of the experimental group GSH-Px activity in semen increased by 114.0 % (P <0.01), the seminal plasma of 306.5 % (P <0.01) and sperm showed a 68.7 % higher activity compared with the control group of boars. These authors also observed a similar trend in concentration of selenium. The concentration of selenium in the total ejaculate was more than four times higher (P <0.01) in experimental animals. During evaluation they measured more than twice higher the concentration of selenium (P <0.01) in seminal plasma and sperm than boars without the addition of this element in the diet. According these results, the amount of GSH-Px of boars in seminal plasma increases with age of animals. We shared similar results with these authors. In our experiment, the group without income of trace element was missing, the amount of GSH-Px was not increased as significant in comparison with previous authors. The highest GSH-Px activity and selenium concentration were found in boars, which were supplemented with selenium in organic form at a dose of 0.6 mg/kg of FM. Similar experimental monito-

ring was done Fernandez et al. [2], who in the diet of three groups of boars, adding 0, 0.3 and 0.5 mg Se/kg of FM in organic form. During the evaluation the activity of GSH-Px they found linear growth depending on the amount of selenium supplied in the diet. When evaluating the presence of free radicals by the MDA no significant difference between the groups has been found. Ebeit [1] also argues that the addition of organic selenium to tapers feed doses of 0.3 mg/kg of FM reduced the number of free radicals and decreased lipid peroxidation. We were able to prove the highest increase of free radicals ($P < 0.01$) in the group, which was given dose of 0.3 mg/kg of FM in the inorganic form of selenium. On the contrary, a decrease of reactive forms of oxygen in a group of boars, who were supplemented by organic selenium at a dose of 0.6 mg/kg of FM. Jelezarsky et al. [4] found in the measurement of GSH-Px activity in ejaculate of boars that the highest level of this enzyme is located in the seminal plasma is more than three times higher compared to spermatozoa. This finding is confirmed by Lasota et al. [6] who also found approximately one and a half times higher GSH-Px activity in seminal plasma than in spermatozoa. Svoboda et al. [10] compared three different sources of selenium in growing pigs (bacteria *E. faecium* enriched with selenium, selenium-enriched yeast and sodium selenite) at a dose of 0.3 mg/kg of FM. Concentration of selenium in the muscle of pigs that were fed selenium-enriched bacteria *E. faecium* was comparable with sodium selenite, but were lower ($P < 0.05$) in contrast to selenium enriched yeast. Concentration of selenium and GSH-Px activity in blood serum of individual groups of pigs were similar.

CONCLUSION

Dietary supplementation of inorganic form of selenium at a dose 0.3 mg/kg of feed mixture showed an increase of free radicals by 91.4 % ($P < 0.01$). The results of the present study indicate that dietary supplements of 0.6 mg Se/kg of feed mixture improved antioxidant potential of breeding boars ejaculate. A lower oxidative stress and higher fertility can be therefore assumed.

ACKNOWLEDGMENTS

This study was supported by the Research plan TP IGA AF MENDELU v Brně 2/2011, TP IGA AF MENDELU v Brně 3/2012, IGA TP6/2012 and SIX CZ.1.05/2.1.00/03.0072. The authors would like to express their thanks to Martina Stankova for technical assistance.

REFERENCES

- [1] Ebeit TA: *British Poultry Science* 50 (2009) 641-647.
- [2] Fernandez LD, Medrano A, Arenas E, et al.: *Theriogenology*, 50 (2008) 1386.
- [3] Hending BN, Koletis PN, Sharma RK, et al.: *Journal of Urology*, 161 (1999)1831-1834.

- [4] Jelezarsky L, Vaiseberg CH, Chausveg T, et al.: *Theriogenology*, 69 (2008) 139-145.
- [5] Kim YY, Mahan DC: *Journal of Animal Science*, 79 (2001) 956-966.
- [6] Lasota B, Blaczik B, Seremak B, et al.: *Reproduction Domestic Animal*, 39 (2004) 309- 314.
- [7] Marin-Guyman J, Mahan DC, Chung YK, et al. *Journal of Animal Science*, 75 (1997) 2994-3003.
- [8] Pavlata L, Chomat M, Pechová A, et al.: *Veterinaria Med*, 2 (2011) 63-73.
- [9] Sochor J, Ryvolova M, Krystofova O, et al.: *Molecules*, 15 (2010) 8618-8640.
- [10] Svoboda M, Fajt Z, Baňoch T, et al.: *Acta Veterinaria* 79 (2010) 511-517.
- [11] Underwood EJ, Suttle NF: *The Mineral Nutrition of Livestock*. CABI Publishing, London: (1999) 614 p.
- [12] Kizek R, Dastych M, Koutnik V, et al., *Vnitřní lékařství*, 44 (1998), 135-141.
- [13] Sochor J, Pohanka M, Ruttkay-Nedecky B, et al., *Cent. Eur. J. Chem.*, in press (2012).

TREATMENT OF DIFFERENTIAL PULSE VOLTAMMOGRAMS OF TISSUE HOMOGENATES FROM RATS

Pavlina SOBROVA¹, Lenka VYSLOUZILOVA², Olga STEPANKOVA²,
Libuse TRNKOVA^{3,4}, Marketa RYVOLOVA^{1,4},
Vojtech ADAM^{1,4}, Jaromir HUBALEK^{4,5}, Rene KIZEK^{1,4,*}

¹Department of Chemistry and Biochemistry, Faculty of Agronomy, Mendel University in Brno, Zemedelska 1, 613 00 Brno, Czech Republic

²Department of Cybernetics, Czech Technical University, Technicka 2, 166 27 Prague, Czech Republic

³Department of Chemistry, Masaryk University, Kotlarska 2, 611 37 Brno, Czech Republic

⁴Central European Institute of Technology, Brno University of Technology, Technicka 3058/10, 616 00 Brno, Czech Republic

⁵Department of Microelectronics, Brno University of Technology, Technicka 2, 616 00 Brno, Czech Republic

*kizek@sci.muni.cz

ABSTRACT

In this study, a mathematical approach how to evaluate and classify datasets obtained by electrochemical analysis of metallothionein in rat 9 tissues (brain, heart, kidney, eye, spleen, gonad, blood and muscle) was suggested. Classification models have been designed using separately two groups of attributes, namely the attributes describing local extremes and the derived attributes resulting from level = 5 wavelet transformation. Based on the results obtained, we were able to construct a decision tree that makes it possible to distinguish among electrochemical analysis data resulting from measurements of all the considered tissues.

INTRODUCTION

Metallothioneins (MTs), which were discovered by Margoshes and Valec in 1957 as newly identified proteins isolated from a horse renal cortex tissue [1], belong to the group of molecules defending a cell against reactive oxygen species (ROS). Mammalian MTs are low molecular mass (app. 6 kDa) proteins with unique abundance of cysteine residues (more than 30 % from all aminoacids) occurring in conserved sequences cys-x-cys, cys-x-y-cys or cys-cys where x and y represent other amino acid. Four mammalian MT isoforms (MT-1 – MT-4) are known and 13 MT-like human proteins were identified [2]. MT-1 or MT-2 are present almost in all types of soft tissues [3], MT-3 is expressed mostly in brain tissue but also in heart, kidneys and reproductive organs [4] and MT-4 gene was detected in epithelial cells. The main function of MTs is a metal ion transport, maintenance of the oxidative-reducing conditions and regulation of gene expression in an organism.

Detection and quantification of MT is not simple due to the high content of cysteine and relatively low molecular mass. Analytical methods are usually based on a) detection of bonded metal ion, b) detection of free thiol moieties, c) protein mobility in an electric field and d) interaction with different types of sorbent or e) Enzyme-Linked Immuno Sorbent Assay (ELISA). However, Brdicka reaction in connection with

differential pulse voltammetry (catalytic reaction) is the only direct method able to quantify these proteins in both blood and tissue extract samples. Differential pulse voltammetry Brdicka reaction is one of the sensitive and common tools used for determination of metallothioneins – it generates for each studied sample from tens to hundreds values related to the sample composition. All over it there has not been offered any theoretical explanation yet, that could provide a complete model for the behaviour observed during Brdicka reaction and influence or role of MT.

We have focused our attention on observing shape of curves corresponding to different organs obtained from male *Wistar albino* laboratory rats of 56 days of age using Brdicka reaction. Obtained experimental data were analysed using our own software tool that was designed and implemented with intention to help in determining the type of tissue, from which the extract was prepared.

MATERIAL AND METHODS

Chemicals

Rabbit liver MT (MW 7143 g/mol), containing 5.9% Cd and 0.5% Zn, was purchased from Sigma Aldrich (St. Louis, USA). $\text{Co}(\text{NH}_3)_6\text{Cl}_3$ and other chemicals used were purchased from Sigma Aldrich (Sigma-Aldrich, USA) unless noted

otherwise. Stock standard solution of MT ($10 \mu\text{g mL}^{-1}$) was prepared with ACS water (Sigma-Aldrich, USA) and stored in the dark at -20°C . Working standard solutions were prepared daily by dilution of the stock solutions with ACS water. The pH value was measured using a WTW inoLab pH meter (Weilheim, Germany).

Animals

Selected male *Wistar albino* laboratory rats of 28 days of age were used without any treatment in our experiments. There were used 8 experimental animals that were kept in a vivarium with controlled air temperature ($23 \pm 1^\circ\text{C}$) and photoperiod (12 hours day: 12 hours night with maximal intensity 10,800 LUX). Tempered feed mixtures of natural barley and drinking water were accessible ad libitum for four weeks. In the end of the experiment, the animals were put to death and tissues and blood were sampled.

Preparation of biological sample

The rats' tissues (liver, kidney, spleen, heart, brain, eye, gonads and femoral muscle) and blood were used for the analysis. The animal tissues were mixed with extraction buffer (100 mM sodium phosphate, pH 6.8) and subsequently homogenized using semi-automatic homogeniser (Schuett homgen, Schuett-Biotec, Germany). The homogenates as well as samples of blood were centrifuged at 10,000 g for 15 min at 4°C (Eppendorf 5402, USA). Further, the samples were heat treated at 99°C in a thermomixer (Eppendorf Thermomixer Comfort, USA) for 15 min. with occasional stirring, and then cooled to 4°C . The denatured homogenates were centrifuged at 4°C , 15,000 g for 30 min. (Eppendorf 5402, USA). Heat treatment effectively denatures and removes high molecular weight proteins out from samples (13-15). The obtained supernatants were $100 \times$ diluted with extraction buffer (100 mM potassium phosphate, pH 6.8) prior to electrochemical measurements.

Electrochemical determination of metallothionein

Electrochemical measurements were performed with a 747 VA Stand instrument connected to 746 VA Trace Analyzer and 695 Autosampler (Metrohm, Switzerland), using a standard cell with three electrodes and cooled sample holder (4°C). A hanging mercury drop electrode (HMDE) with a drop area of 0.4 mm^2 was the working electrode. An Ag/AgCl/3M KCl electrode was the reference and glassy carbon electrode was auxiliary electrode. GPES 4.9 supplied by EcoChemie was employed. The Brdicka supporting electrolyte containing 1 mM $\text{Co}(\text{NH}_3)_6\text{Cl}_3$ and 1 M ammonia buffer ($\text{NH}_3(\text{aq}) + \text{NH}_4\text{Cl}$, pH = 9.6) was used and changed per

one analysis. DPV parameters were as follows: initial potential of -0.7 V , end potential of -1.75 V , modulation time 0.057 s, time interval 0.2 s, step potential 2 mV, modulation amplitude -250 mV , $E_{\text{ads}} = 0 \text{ V}$. All experiments were carried out at a temperature of 4°C (Julabo F12 cooler, Germany).

RESULTS AND DISCUSSION

Brdicka reaction

Brdicka reaction is frequently employed electrochemical method for MT determination in biological samples. Experimental conditions of MT detection by Brdicka method were several times modified with the aim to study the effect of concentration of some substances in Brdicka solution, which commonly consists from cobalt(II) complex and ammonia buffer. Raspor et al. [5] used 2 M $\text{NH}_4\text{Cl} + \text{NH}_4\text{OH}$, with 1.2 mM $[\text{Co}(\text{NH}_3)_6]\text{Cl}_3$ and carried out the measurements within the potential range from -0.9 to -1.9 V . Olafson and Sim suggested to use 1 M $\text{NH}_4\text{Cl} + \text{NH}_4\text{OH}$, with 0.6 mM $[\text{Co}(\text{NH}_3)_6]\text{Cl}_3$ [6, 7]. The most frequently employed method for MT detection using Brdicka procedures is differential pulse voltammetry. Brdicka reaction was used for the study of physiological concentrations of MT in many animal species [8]. Brdicka reaction finds wide range of use in MT determination in freshwater and sea fish [7, 9].

Voltammograms description

The mechanism of the reaction is based on the catalytic evolution of hydrogen on mercury electrodes from solutions of protein containing $-\text{SH}$ group in ammonia buffer and hexammincobalt chloride complex ($\text{Co}(\text{NH}_3)_6\text{Cl}_3$) called Brdicka solution [10]. The mechanisms of the reaction is not elucidated in detail, but it is expected that the cobalt (II) complex with protein, peptide or basic nitro compounds play important role in catalytic process. Interaction between cobalt(II) ion and protein causes decrease of the cobalt peak and occurrence of two new voltammetric peaks at potential area from -1.2 to -1.5 V . The reduction of complex $\text{R}(\text{SH})_2$ and $\text{Co}(\text{II})$ at potential app. -1.35 V corresponds to the first catalytic signal (RS_2Co). Other two signals Cat1 and Cat2 correspond to the reduction of hydrogen at the mercury electrode and can be used for quantification because their height is proportional to concentration of MT. In addition, the signal called Co1 could occasionally result from reduction of $[\text{Co}(\text{H}_2\text{O})_6]^{2+}$ [5]. Under our conditions we observed formation of catalytic signals in potential from 1.0 to 1.1 V for first catalytic signal (RS_2Co) and 1.2 and 1.5 for Cat1 and Cat2, respectively. The signal Co1 of varied strength was observed in

potential 0.8.

Determination of metallothionein content in rat tissues

Using electrochemical detection of metallothionein we monitored its content in the blood and rat body tissues as liver, kidney, spleen, heart, brain, eye, gonads, blood and femoral muscle (number of various considered tissues $p = 9$). To quantify metallothionein in the catalytic peak Cat2 was used. Comparison of the average MT levels in single tissues shows their variability. The highest content was found in kidney ($67.0 \pm 1.1 \mu\text{g/g}$) and liver ($48.7 \pm 0.9 \mu\text{g/g}$) as in organs responsible for the xenobiotics detoxification. The content was two times higher compared to other organs. Higher level was also determined in the brain ($50.5 \pm 1.5 \mu\text{g/g}$) and in the spleen ($41.5 \pm 1.4 \mu\text{g/g}$). The concentration in the brain corresponds only to the content of isoform MT-3 [11]. MT level in the heart (without blood) is nearby MT level in the muscle what can be explained by similar physiological function of both tissues. Moreover, we statistically evaluated differences in MT content determined in the organs. We found that MT content in the heart was not statistically different compared to the gonad and to the eye. Also the MT content in the gonad was not statistically different compared to the eye. All other mutual differences were significantly different ($p < 0.05$). Besides height of peak Cat2, heights of RS₂Co and Cat1 were determined. However, no dependence on concentration or other parameters including type of tissue was observed.

In addition, we focused our attention on the shape of curves corresponding to the different organs. We found out that each tissue gave a voltammogram of characteristic shape. The curves differed not only in their height and potential of the peaks, but also in their shape. Some voltammograms contained RS₂Co, Cat1 and Cat2 only, however, in some curves, peak Co1 was detected at -0.7 V. Voltammograms with three peaks (without Co1) were obtained by measuring of spleen, gonad and muscle homogenates. Analyses of kidney, liver, brain, eye and heart homogenates gave four peaks. In spite of the fact that apparent differences among measured voltammograms were visually observed, we were not able to distinguish between voltammograms of certain tissues using standard tools for data treatment.

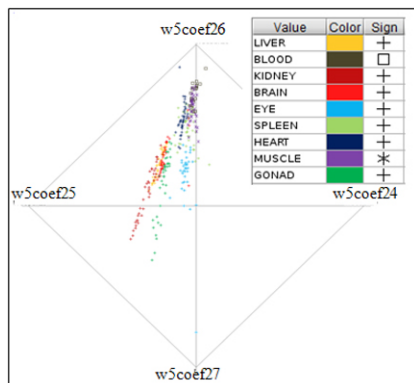
Haar's Simple Wavelet transformation

Each curve from our data set is described by 518 points obtained from equidistant measurements in the interval (-1.8 V, -0.7 V) – the domain experts confirmed that it is safe to take the line connecting all these points as a reasonable approximation of a continuous line. One of the well known approaches how to handle such type of data is to apply Haar's Simple Wavelet (HSW) transformation [12-15], which ensures a significant compression of the input data by approximating the continuous line by a step-

wise function with 2k steps (columns) of the same width, where the parameter k is referred as HSW level. To ensure this plan HSW transformation sets strict requirement on the number p of points used for representation of the curve - this number has to be a power of 2. In such a case log p is the upper limit for the HSW level parameter denoted as levelmax. The nearest power of 2 to the number 518 of our points is $512 = 2^9$. In order to use HSW for our data from Brdicka curves, we have set levelmax = 9 and we were forced to abandon six points only. We have decided to select for that purpose the 6 points with the value on the horizontal axis close to (-0.7 V), because their measured values were the same for most of the curves.

The Haar's Simple Wavelet transformation has a single parameter referred to as level which cannot exceed levelmax and which specifies the number of iterations of the process described below as well as the number of coefficients to be used for description of the curve. More precisely, the number of coefficients is equal to 2level. The initial wavelet coefficient c0 represents the mean of the whole curve. In the next steps the following process is repeated: the domain is divided into two equal parts and each part is analyzed separately (the mean of this part is considered) and compared to its 'parent part' to obtain further wavelet parameters. The interpretation of the resulting wavelet coefficients is not very transparent. That is why we have applied inverse wavelet transformation that results in the same number of novel derived attributes (denoted as coef0, ..., coef15 in the case the level is set to 4) computed by aggregation of the original wavelet coefficients. These new attributes offer more natural description of the original curve because they represent its approximation by stepwise function with 2level steps of equal width which roughly copies the shape of the original data: each new attribute coef0, ..., coef15 corresponds to the average of the original curve in the considered interval (step).

Figure 1.: RadViz image for the w5coef24 ... w5coef27 projection of the selected wavelet coefficients.



CLASSIFICATION

Classification models have been designed using separately two groups of attributes - the attributes describing local extremes (see section 3.1.3) and the derived attributes resulting from level = 5 wavelet transformation. From the number of different available classification models [15], we have selected decision trees because they highlight possible dependencies among the considered attributes and thus they offer clear insight into the considered task due to the algorithm used for decision tree construction. This algorithm applies iteratively a routine for identification of the most informed attribute to the considered dataset. This attribute is then used for partitioning the dataset - further on significantly smaller dataset is processed and complexity of the considered task is reduced in this way step by step. Those attributes that appear in the names of the upper nodes of the decision tree (close to its root) seem to be of special importance - the decision tree can be understood as a feature selection algorithm, too.

The software tool Rapid Miner and its module Decision Tree has been applied [12]. The parameter named minimal leaf size corresponding to the minimal number of instances per leaf has been set to 10 to prevent over-specialization when the leaves of the decision tree could be characterized by values of attributes of a single rat (one rat = 5 curves). This setting helped in finding more general decision tree. In both experiments described in the following two paragraphs that used two different groups of attributes selected for an abstract representation of the Brdicka curve there was applied the same approach how to estimate quality of the designed model, namely 10 fold cross validation. The available data S corresponding to different Brdicka curves were divided into 10 disjunctive sets S_1, \dots, S_{10} each of which maintained the same percentage of the considered body tissues as the original set

(stratified samples). For $i=1$ to 10 the following experiments have been ensured: the decision tree model has been created from the training data set ($S - S_i$) and tested on the remaining data, namely on S_i . The overall results of the 10 experiments were summarized using a confusion matrix with columns denoted by the body part, from which the considered sample has been taken, and with rows denoted by the classification suggested by the constructed decision trees. Consequently, the resulting table depicts all the correctly classified examples on the diagonal of the matrix while all the other points represent errors. Moreover, this presentation of the obtained results makes it possible to identify easily the most frequent mistakes or confusions appearing in our data, namely the names of body tissues the mis-classified examples came from and the predicted class, which does not seem to be fully reliable

CONCLUSION


We believe that advance in proteomics will be made possible not only by construction of new devices but also by gaining profound understanding to mechanisms of electrochemical reactions of the studied substances which can lead to more efficient utilization of numerous data already available. One of the first steps towards this goal is to find proper way how to describe various curves produced by complex electrochemical processes. The resulting representation has to be both abstract so that data compression is achieved and detailed enough to highlight the important properties of the studied curves. We have applied Haar's simple wavelet transformation to Brdicka curves to prove feasibility of suggested approach.

ACKNOWLEDGEMENT

The financial support from the following projects NanoBioTECell GA CR P102/11/1068, CEITEC CZ.1.05/1.1.00/02.0068 and MSM 6840770038 is greatly acknowledged. The authors wish to express their thanks to Anna Vasatkova for excellent work with rat breeding. The author P.S. is „Holder of Brno PhD Talent Financial Aid“.

REFERENCES

- [1] Margoshes M, Vallee B L, J. Am. Chem. Soc., 79 (1957), 4813-4814.
- [2] Simpkins C O, Cell. Mol. Biol., 46 (2000), 465-488.
- [3] Masters B A, Quaipe C J, Erickson J C, *et al.*, J. Neurosci., 14 (1994), 5844-5857.
- [4] Moffatt P, Seguin C, DNA Cell Biol., 17 (1998), 501-510.
- [5] Raspor B, Paic M, Erk M, Talanta, 55 (2001), 109-115.

- 
- [6] Olafson R W, Sim R G, *Anal. Biochem.*, 100 (1979), 343-351.
 - [7] Olafson R W, Olsson P E, *Meth. Enzymol.*, 205 (1991), 205-283.
 - [8] Bebianno M J, Machado L M, *Marine Poll. Bull.*, 34 (1997), 666-671.
 - [9] Olafson R W, *Bioelectrochem. Bioenerg.*, 19 (1988), 111-125.
 - [10] Heyrovsky M, *Electroanalysis*, 12 (2000), 935-939.
 - [11] Vasatkova A, Krizova S, Krystofova O, *et al.*, *Neuroendocrinol. Lett.*, 30 (2009), 163-168.
 - [12] Mierswa I, Wurst M, Klinkenberg R, *et al.*, *12th ACM SIGKDD International Conference on Knowledge Discovery and Data Mining (KDD-06) 2006*.
 - [13] Nievergelt Y, *Wavelets made easy*, Birkhäuser, Boston 2001.
 - [14] Chui C K, *An Introduction to Wavelets*, Academic Press, San Diego 1992.
 - [15] Witten I H, Frank E, Hall M A, *Data Mining: Practical Machine Learning Tools and Techniques*, Morgan Kaufmann 2011.

INFLUENCE OF HEAT DENATURATION OF β -SHEET BREAKER PRION PROTEIN ON ELECTROCHEMICAL RESPONSE

Pavlina SOBROVA¹, Marketa RYVOLOVA^{1,2}, David HYNEK^{1,2}, Vojtech ADAM^{1,2}, Jaromir HUBALEK^{2,3}, Libuse TRNKOVA^{2,4}, Rene KIZEK^{1,2*}

¹Department of Chemistry and Biochemistry, Faculty of Agronomy, Mendel University in Brno, Zemedelska 1, 613 00 Brno, Czech Republic

²Central European Institute of Technology, Brno University of Technology, Technicka 3058/10, 616 00 Brno, Czech Republic

³Department of Microelectronics, Faculty of Electrical Engineering and Communication, Brno University of Technology, Technicka 3058/10, 616 00 Brno, Czech Republic

⁴Department of Chemistry, Masaryk University, Kotlarska 2, 611 37 Brno, Czech Republic

*kizek@sci.muni.cz

ABSTRACT

Electrochemical study of β -sheet breaker prion protein is the main aim of this study. For this purpose, cyclic voltammetry (CV), differential pulse voltammetry, differential pulse voltammetry Brdicka reaction and chronopotentiometric stripping analysis were used. Under the optimal conditions (phosphate buffer, pH 7.38 and time of accumulation 100 s), detected by DPV prion was characterized using different techniques and their limits of detection were found. Adsorptive transfer stripping technique coupled with the abovementioned methods offers very lower detection limits. The lowest limits of detection were determined by CPSA AdTS i.e. 25 pmol in volume of 5 μ l. CPSA is therefore a very sensitive tool for the studying of prion behaviour. Moreover, the influence of heat denaturation was observed. It clearly follows from the results obtained that signals of prion decreased linearly depending on the duration of the heat treatment at 99°C for various time intervals: 0, 15, 30, 45, and 60 min. The correlation coefficients of the measured dependencies as 0.9929, 0.9973, 0.9965 and 0.9957 were determined by CV, DPV, DPV Brdicka reaction and the most sensitive CPSA, respectively.

INTRODUCTION

Transmissible spongiform encephalopathies (TSEs) are a group of fatal neurodegenerative diseases with long incubation time, which includes Creutzfeldt-Jakob disease (CJD), kuru, scrapie, chronic wasting disease (CWD), and bovine spongiform encephalopathy (BSE). The agent that causes these diseases is an abnormal prion protein (PrP^{Sc}) that is a conformational isoform of the normal prion protein (PrP^C). The conformation change, from the α -helix in the natural protein form (PrP^C) to the β -sheet of the modified protein form (PrP^{Sc}), significantly influence the protein function. The mutated form (PrP^{Sc}) is extremely resistant to the cell degradation processes and may bind other PrP^C molecules inducing the conformation change to the PrP^{Sc}.

Detection and quantification of prion is not simple due to the low amounts in biological samples especially during the early stages of disease. For this purpose, the method Protein-misfolding cyclic amplification (PMCA) for providing sensitivity improvement has been used [1]. Method is based on addition of normal prion protein to the sample containing infectious prion and its subsequent conversion to infectious form. PMCA involves repeated cycles

on incubation and sonication. These repeated cycles can amplify the amount of prion protein present in the sample from four to 40 times in two weeks [2, 3]. Analytical methods, which are used for prion detection are usually based on: (I) conformation dependent immunoassays, which are currently the most used assays for routine screening in plasma [4]. (II) Western blot assays [5] (III) CE – based methodology [6] and (IV) Spectroscopic method [7].

The main objective of our work was to explore the electrochemical behaviour of prion protein PrP^{Sc} on hanging mercury drop electrode. For these purposes fundamental electrochemical techniques such as cyclic voltammetry, differential pulse voltammetry, differential pulse voltammetry with Brdicka reaction and chronopotentiometric stripping analysis were used. To reach very low limits of detection adsorptive transfer stripping technique was used. Moreover, we focused our attention on monitoring the signal change of native and denatured form of prion.

MATERIAL AND METHODS

Chemicals

Prion protein β – sheet breaker peptide fragment (Asp-Ala-Pro-Ala-Ala-Pro-Ala-Gly-Pro-

-Ala-Val-Pro-Val; FW = 1597.9) was purchased from Sigma Aldrich (St. Louis, USA) and dissolved by 8.77 M trifluoroacetic acid bought from the same supplier. Sodium phosphate and other used chemicals were purchased from Sigma Aldrich. Working standard solutions were prepared daily by dilution of the stock solutions. The pH value was measured using WTW inoLab Level 3 with terminal Level 3 (Weilheim, Germany), controlled by personal computer program (MultiLab Pilot; Weilheim, Germany). The pH-electrode (SenTix- H, pH 0–14/3M KCl) was regularly calibrated by set of WTW buffers (Weilheim, Germany).

Electrochemical measurements

Electrochemical measurements were performed with AUTOLAB Analyser (EcoChemie, Netherlands) connected to VA-Stand 663 (Metrohm, Switzerland), using a standard cell with three electrodes. The working electrode was a hanging mercury drop electrode (HMDE) with a drop area of 0.4 mm². The reference electrode was an Ag/AgCl/3M KCl electrode and the auxiliary electrode was a graphite electrode. The supporting electrolyte was acetate buffer (pH = 5). For smoothing and baseline correction the software GPES 4.4 supplied by EcoChemie was employed.

Adsorptive transfer stripping technique

Principle of the AdTS is based on the strong adsorption of the studied analyte on the electrode surface in an open electrode circuit. The excess of analyte is rinsed from the surface of the working electrode with the buffer. The adsorbed analyte is finally detected in the presence of indifferent electrolyte. Volume of studied sample was 5 µl in all methods. Time of adsorption was tested in range from 10 to 120 s.

Cyclic voltammetry (CV) and PrP^{Sc}

Prion protein was studied using cyclic voltammetry. Amount of adsorbed sample was 5 µl. Time of accumulation pH and electrolyte type was optimized. Volume of supporting electrolyte was 5 ml in the electrochemical cell. CV parameters were as follows: an initial potential of 1.0 V, an end potential of -1.9 V, step potential of 2.44 mV, scan rate from 20 to 640 mV/s. All experiments were carried out at room temperature (22–24 °C).

Differential pulse voltammetry (DPV) and PrP^{Sc}

The amount of prion PrP^{Sc} was measured using AdTS DPV. Following supporting electrolytes were tested: 0.5 M sodium phosphate in pH range from 5.6 to 8.0, borate in pH range from 7.1 to 9.1 and acetate in pH range from 3.8 to 5.6. DPV

parameters were follows: an initial potential of -0.2 V, an end potential of -0.8 V, a modulation time 0.057 s, time interval 0.2 s, step potential 1.05 mV/s, a modulation amplitude of 250 mV, $E_{ads} = 0$ V. All experiments were carried out at room temperature (22–24 °C). The DPV samples analysed were deoxygenated prior to measurements by purging with argon (99.999%) saturated with water for 120 s.

Differential pulse voltammetry - Brdicka reaction and PrP^{Sc}

Differential pulse voltammetric Brdicka's reaction was also used for prion determination. The Brdicka supporting electrolyte containing 1 mM Co(NH₃)₆Cl₃ and 1 M ammonia buffer (NH₃(aq) + NH₄Cl, pH = 9.6) was used and changed per each analysis. DPV parameters were as follows: initial potential of -0.7 V, end potential of -1.75 V, modulation time 0.057 s, time interval 0.2 s, step potential 2 mV, modulation amplitude -250 mV, $E_{ads} = 0$ V. All experiments were carried out at a temperature of 4 °C (Julabo F12 cooler, Germany).

Peak H and PrP^{Sc}

Constant current chronopotentiometric stripping analysis (CPSA) was used for the determination of prion by recording the inverted time derivation of potential (dE/dt)⁻¹ as a function of potential E. CPSA parameters were as follows: potential limit of -1.9 V, I_{str} of -1 µA, max. time of measurement 600 s, temperature 20 °C, supporting electrolyte phosphate buffer (pH 7.38).

Descriptive statistics and estimation of detection limit

Data were processed using MICROSOFT EXCEL® (USA). Results are expressed as mean ± standard deviation (S.D.) unless noted otherwise (EXCEL®). The detection limits (3 signal/noise, S/N) were calculated according to Long and Winefordner [8], whereas N was expressed as standard deviation of noise determined in the signal domain unless stated otherwise.

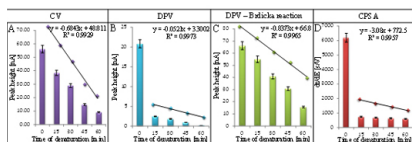
RESULTS AND DISCUSSION

Protein denaturation is a complex process [9, 10] and its complete understanding requires taking into consideration numerous aspects such as net charge, protein structure, environmental conditions (e.g. electrolyte pH and concentration) as well as equilibrium of folded and unfolded protein form. Elevated temperature is one of the most commonly used approaches for protein denaturation [11–14]. It is well known that at elevated temperatures α-PrP converted rapidly and irreversibly to the thermodynamically

cally more stable β -sheet form [15, 16]. Electrochemistry seems to be powerful tool for studying of protein denaturation and renaturation [12, 13, 17-21].

In the present study, the behaviour of native and denatured form of prion was studied using all above-mentioned methods. It clearly follows from the obtained results that signals of prion decreased linearly depending on the duration of the heat treatment at 99°C for various time intervals as 0, 15, 30, 45, and 60 min. The correlation coefficients of the measured dependencies as 0.9929, 0.9973, 0.9965 and 0.9957 were determined by CV (Fig. 1A), DPV (Fig. 1B), DPV Brdicka reaction (Fig. 1C) and the most sensitive CPSA (Fig. 1D), respectively. Electrochemical signals decreased with the increasing time of thermal treatment in all applied methods. The aggregation rate is more sensitive in case of DPV and CPSA where the prion amount decreased more than six times against native prion (0 min. of denaturation). This phenomenon suggests that the thermal treatment causes significant changes in the protein structure. Thermal denaturation is responsible for an irreversible precipitation leading to the aggregation of the denatured prion molecules and creating an undefined polymeric structure.

Figure 1.: Dependence of peak height on time of heat denaturation at 99 °C for 0, 15, 30, 45 and 60 min. measured by A) cyclic voltammetry, B) Differential pulse voltammetry, C) Differential pulse voltammetry Brdicka reaction and D) Chronopotentiometric stripping analysis. With longer influence of higher temperatures the signal significantly decreased.



CONCLUSION

Great attention on analytical determination of prion protein is paid. Electrochemical methods represent an excellent tool for such studies. As we report in the paper, adsorptive transfer stripping technique coupled with various methods represents powerful tool to detect very low concentration of specific protein. Moreover, the results of denaturation undergo to creation of more complex structures in prion molecule during heat treatment.

ACKNOWLEDGEMENT

The financial support from IGA IP 5/2012, FRVŠ 2805/G4 and CEITEC CZ.1.05/1.1.00/02.0068 is highly acknowledged. The author P.S. is „Holder of Brno PhD Talent Financial Aid“.

REFERENCES

- [1] Saborio G P, Permanne B, Soto C, Nature, 411 (2001), 810-813.
- [2] Soto C, Saborio G P, Anderes L, Trends Neurosci., 25 (2002), 390-394.
- [3] Soto C, Anderes L, Suardi S, *et al.*, FEBS Lett., 579 (2005), 638-642.
- [4] Volkel D, Zimmermann K, Zerr I, *et al.*, Transfusion, 41 (2001), 441-448.
- [5] Hartwell R C, Nelson M S, Kislan M M, *et al.*, J. Virol. Methods, 125 (2005), 187-193.
- [6] Nunnally B K, Trac-Trends Anal. Chem., 21 (2002), 82-89.
- [7] Carmona P, Monleon E, Monzon M, *et al.*, Chem. Biol., 11 (2004), 759-764.
- [8] Long G L, Winefordner J D, Anal. Chem., 55 (1983), A712-A724.
- [9] Piaggio M V, Peirotti M B, Deiber J A, Electrophoresis, 28 (2007), 2223-2234.
- [10] Kim J Y, Ahn S H, Kang S T, *et al.*, J. Colloid Interface Sci., 299 (2006), 486-492.
- [11] Myers J K, Pace C N, Scholtz J M, Protein Sci., 4 (1995), 2138-2148.
- [12] Ostatna V, Cernocka H, Palecek E, J. Am. Chem. Soc., 132 (2010), 9408-9413.
- [13] Ostatna V, Palecek E, Electrochim. Acta, 53 (2008), 4014-4021.
- [14] Teijeiro C, Nejedly K, Palecek E, J. Biomol. Struct. Dyn., 11 (1993), 313-331.
- [15] Zhang H, Stockel J, Mehlhorn I, *et al.*, Biochemistry, 36 (1997), 3543-3553.
- [16] Sokolowski F, Naumann D, Vib. Spectrosc., 38 (2005), 39-44.
- [17] Masarik M, Stobiecka A, Kizek R, *et al.*, Electroanalysis, 16 (2004), 1172-1181.
- [18] Potesil D, Mikelova R, Adam V, *et al.*, Protein J., 25 (2006), 23-32.
- [19] Ostatna V, Kuralay F, Trnkova L, *et al.*, Electroanalysis, 20 (2008), 1406-1413.
- [20] Palecek E, Ostatna V, Analyst, 134 (2009), 2076-2080.
- [21] Palecek E, Ostatna V, Masarik M, *et al.*, Analyst, 133 (2008), 76-84.

QUANTUM DOTS AND THEIR INTERACTIONS WITH BIOMOLECULES

Pavlina SOBROVA¹, Marketa RYVOLOVA^{1,2}, Libor JANU¹,
Vojtech ADAM^{1,2}, Libuse TRNKOVA^{2,3}, Jaromir HUBALEK^{2,4}, Rene KIZEK^{1,2}

¹Department of Chemistry and Biochemistry, Faculty of Agronomy, Mendel University in Brno, Zemedelska 1, 613 00 Brno, Czech Republic

²Central European Institute of Technology, Brno University of Technology, Technicka 3058/10, 616 00 Brno, Czech Republic

³Department of Chemistry, Masaryk University, Kotlarska 2, 611 37 Brno, Czech Republic

⁴Department of Microelectronics, Brno University of Technology, Technicka 2, 616 00 Brno, Czech Republic

*kizek@sci.muni.cz

Abstract

Semiconductor quantum dots (QDs) coated with thioalkyl acid ligands are often used as probes and reporters for nucleic acid sensing, or protein sensing using aptamers, and are also potential vectors for gene delivery. In such applications, the interactions that potentially lead to the adsorption of oligonucleotides onto the surface of colloidal QDs are an important consideration. The interaction between β -sheet breaker prion protein and CdTe quantum dots (QDs) was studied by differential pulse voltammetry connected with adsorptive transfer stripping technique. Results showed that the electrochemical signals of prion protein were strongly quenched by CdTe QDs. This phenomenon can be considered as a first step of suggesting of a biosensor for determination of prions in real samples without a sample pre-treatment.

INTRODUCTION

Excellent optical properties of QDs (namely high quantum yield, broad absorption spectra and narrow, symmetric fluorescence spectra from UV to NIR, large effective excitation and emission Stokes shifts), long life-time (high resistance to photobleaching) compared to ordinary fluorophores and stability (resistance to photo- and chemical degradation) predestinate them in usage for imaging and as optical probes for detection of peptides, proteins, nucleic acids and other biomolecules [1-5]. Even the systems with colloidal QDs are more frequently used for biosensing application, the systems with QDs grown on various solid substrates is no less attractive but markedly less studied. Nowadays, new approaches in biosensing with QDs consist in usage of QDs fixed on some solid substrate. However, this is generally provided by colloidal QDs incorporation in some polymer matrix or formation of colloidal QDs thin films via self-assembly [6-8]. Moreover, most of these QDs are toxic hence some biocompatible layer should cover the QDs core [9].

QDs coated with thioalkyl acid ligands are often used as probes and reporters for nucleic acid sensing, or protein sensing using aptamers, and are also potential vectors for gene delivery. In such applications, the interactions that potentially lead to the adsorption of oligonucleotides onto the surface of colloidal QDs are an important consideration. The interaction between β -sheet breaker prion protein and CdTe quantum

dots (QDs) was studied by differential pulse voltammetry connected with adsorptive transfer stripping technique.

MATERIAL AND METHODS

Quantum dots preparation

QD were prepared according to Duan et al. [10]. In a typical synthesis, 4 ml of cadmium chloride solution (CdCl_2 , 0.04 mol/l) was diluted to 42 ml with ultrapure water, and then trisodium citrate dihydrate (100 mg), Na_2TeO_3 (0.01 mol/l, 4 mL), MPA (119 mg), and NaBH_4 (50 mg) were added successively under magnetic stirring. The molar ratio of Cd^{2+} /MPA/Te was 1:7:0.25. 10 ml of the resulting CdTe precursor was put into a Teflon vessel. A CdTe QDs were prepared at 95°C and times 30 min. under microwave irradiation (400 W). After microwave irradiation, the mixture was allowed to cool to lower than 50 °C and the CdTe QDs sample was removed. Working standard solutions were prepared daily by diluting the stock solutions.

Electrochemical determination

Electrochemical measurements were performed with AUTOLAB Analyser (EcoChemie, Netherlands) connected to VA-Stand 663 (Metrohm, Switzerland), using a standard cell with three electrodes. The working electrode was a hanging mercury drop electrode (HMDE) with a drop area of 0.4 mm². The reference electrode was an Ag/AgCl/3M KCl electrode and the auxiliary electrode was a graphite electrode. The supporting electrolyte was acetate buffer (pH

= 5). For smoothing and baseline correction the software GPES 4.4 supplied by EcoChemie was employed.

Differential pulse voltammetry

The amount of QDs was measured using DPV. Differential pulse voltammetric measurements were carried out under the following parameters: deoxygenating with argon 60 s; start potential -1.5 V; end potential 0 V; a modulation time 0.057 s, a time interval 0.2 s, a step potential of 1.05 mV/s, a modulation amplitude of 250 mV, $E_{ads} = 0$ V. All experiments were carried out at room temperature (22–24 °C). The DPV samples analysed were deoxygenated prior to measurements by purging with argon (99.999%) saturated with water for 120 s.

Adsorptive transfer stripping technique

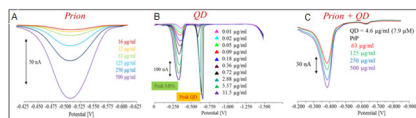
Principle of the AdTS is based on the strong adsorption of the studied analyte on the electrode surface in an open electrode circuit. The excess of analyte is rinsed from the surface of the working electrode with the buffer. The adsorbed analyte is finally detected in the presence of indifferent electrolyte. Volume of studied sample was 5 µl in all methods. Time of adsorption was tested in range from 10 to 120 s.

RESULTS AND DISCUSSION

In this study adsorptive transfer stripping technique in connection with differential pulse voltammetry (AdTS DPV) was employed for prions electrochemical characterization as sensitive electrochemical method. Primarily, the method was optimized to achieve the best condition for prion detection. Particularly, we tested the following conditions as time of accumulation, buffer composition and pH of the supporting electrolyte. Determining dependence of peak height on time of accumulation showed that current response enhanced with increasing time of accumulation (Fig. 1A). The highest peak was determined under 100 s long accumulation. Longer time of accumulation provided also sufficient responses but due to formation of polylayers the signal slightly decreased.

Moreover, electrochemical behaviour of QDs was studied. Primarily, the method was optimized to achieve the best condition for QDs detection. Two peaks at potential -0.3 V (Peak MPA) and -0.7 V (Peak QD) were observed. The very well developed signals are shown in Fig. 1B. The interaction of QDs and prion protein is shown in figure 1C. Results showed that the electrochemical signals of prion protein were strongly quenched by CdTe QDs. This phenomenon can be considered as a first step of suggesting of a biosensor for determination of prions in real samples without a sample pre-treatment.

Figure 1: Electrochemical signal of A) Prion protein B) quantum dots C) interaction of quantum dots and prion protein



CONCLUSION

The interaction Results showed that the electrochemical signals of prion protein were strongly quenched by CdTe QDs. This phenomenon can be considered as a first step of suggesting of a biosensor for determination of prions in real samples without a sample pre-treatment.

ACKNOWLEDGEMENT

The financial support from IGA IP 5/2012 and CEITEC CZ.1.05/1.1.00/02.0068 is highly acknowledged. The author P.S. is „Holder of Brno PhD Talent Financial Aid“.

REFERENCES

- [1] Bakalova R, Zhelev Z, Aoki I, *et al.*, *Nat. Photonics*, 1 (2007), 487-489.
- [2] Chomoucka J, Drbohlovava J, Adam V, *et al.*, *Synthesis of Glutathione-coated Quantum Dots*, Ieee, New York 2009.
- [3] Chomoucka J, Drbohlovava J, Babula P, *et al.*, in: Jakobý, B, Vellekoop, M J (Eds.), *Eurosensor Xxiv Conference*, Elsevier Science Bv, Amsterdam (2010), pp. 922-925.
- [4] Ryvolova M, Chomoucka J, Janu L, *et al.*, *Electrophoresis*, 32 (2011), 1619-1622.
- [5] Wang X Y, Ren X F, Kahen K, *et al.*, *Nature*, 459 (2009), 686-689.
- [6] Algar W R, Krull U J, *J. Colloid Interface Sci.*, 359 (2011), 148-154.
- [7] Algar W R, Krull U J, *Sensors*, 11 (2011), 6214-6236.
- [8] Chen L, Algar W R, Tavares A J, *et al.*, *Anal. Bioanal. Chem.*, 399 (2011), 133-141.
- [9] Chomoucka J, Drbohlovava J, Hubalek J, *et al.*, *Lis. Cukrov. Repar.*, 126 (2010), 400-401.
- [10] Duan J L, Song L X, Zhan J H, *Nano Res.*, 2 (2009), 61-68.

ELECTROCHEMISTRY OF QUANTUM DOTS

Pavlina SOBROVA¹, Marketa RYVOLOVA^{1,2}, Vojtech ADAM^{1,2},
Libor JANU¹, Libuse TRNKOVA^{2,3}, Jaromir HUBALEK^{2,4}, Rene KIZEK^{1,2}

¹Department of Chemistry and Biochemistry, Faculty of Agronomy, Mendel University in Brno, Zemedelska 1, 613 00 Brno, Czech Republic

²Central European Institute of Technology, Brno University of Technology, Technicka 3058/10, 616 00 Brno, Czech Republic

³Department of Chemistry, Masaryk University, Kotlarska 2, 611 37 Brno, Czech Republic

⁴Department of Microelectronics, Brno University of Technology, Technicka 2, 616 00 Brno, Czech Republic

*kizek@sci.muni.cz

ABSTRACT

Quantum dots (QDs), semiconductor nanocrystals small enough to exhibit size-dependent properties, have generated tremendous interest due to their unique optical properties, including broad excitation spectra, narrow, tuneable and symmetric emission spectra covering the wide range of spectra from visible to infrared, excellent photostability and large quantum yield. In this study, electrochemical behaviour of quantum dots was studied using differential pulse voltammetry and cyclic voltammetry. Based on the results obtained, we suggested novel and easy-to-use method how to quantify quantum dots and how to evaluate the ratio of their degradation, which is very important for further using of these particles.

INTRODUCTION

Quantum dots (QDs), semiconductor nanocrystals small enough to exhibit size-dependent properties, have generated tremendous interest due to their unique optical properties [1-5], including broad excitation spectra [6], narrow, tuneable [7] and symmetric emission spectra covering the wide range of spectra from visible to infrared, excellent photostability and large quantum yield [8-12]. Furthermore their surface is well suitable for modification to incorporate required functionality, and good biocompatibility [5, 13, 14] and they are also highly efficient multi-photon absorbers that can be potentially useful for three dimensional multi-photon microscopy and imaging [15] - rapidly developing area for both biological and medical applications. These features make QDs one of the most promising nanomaterials for biological staining, detection of bio-macromolecules, and immunohistochemistry [14, 16, 17]. The most popular types of QDs include CdTe, CdSe, ZnSe and ZnS; however, other semiconductor metals such as In, Ga and many others also can be used [18, 19]. Despite the interesting properties hosted by these QDs, the potential leakage of metal ions by chemical dissolution under biological conditions, the latter in the case of core-shell or alloy QDs, may generate oxidative stress in living cells. Accordingly, the passivation of the surface of the QDs in order to make them biologically inert without affecting their optical properties becomes indispensable. Silicates, thiols, organic acids, peptides, proteins and nucleic acids, forming bioconjugates have been used to cover the surface of QDs and, consequently, to reduce

the possible leaking of free cadmium ions under physiological environments [14, 20, 21].

Electrochemical detection as a sensitive detection technique in combination with QDs has already been used for numerous applications such as immobilized substrate for glassy carbon electrodes [22, 23] and/or modification of the surface of gold electrode [24, 25]. This powerful combination has also given rise to many electrochemical sensors for glucose [24], prostate specific antigen [26], thrombin [23], tumour cells [27] and/or allergens [28].

MATERIAL AND METHODS

Quantum dots preparation

QD were prepared according to Duan et al. [29]. In a typical synthesis, 4 ml of cadmium chloride solution (CdCl_2 , 0.04 mol/l) was diluted to 42 ml with ultrapure water, and then trisodium citrate dihydrate (100 mg), Na_2TeO_3 (0.01 mol/l, 4 mL), MPA (119 mg), and NaBH_4 (50 mg) were added successively under magnetic stirring. The molar ratio of Cd^{2+} /MPA/Te was 1:7:0.25. 10 ml of the resulting CdTe precursor was put into a Teflon vessel. A CdTe QDs were prepared at 95°C and times 30 min. under microwave irradiation (400 W). After microwave irradiation, the mixture was allowed to cool to lower than 50 °C and the CdTe QDs sample was removed. Working standard solutions were prepared daily by diluting the stock solutions.

Electrochemical determination

Electrochemical measurements were performed with AUTOLAB Analyser (EcoChemie, Netherlands) connected to VA-Stand 663 (Metrohm, Switzerland), using a standard cell with

three electrodes. The working electrode was a hanging mercury drop electrode (HMDE) with a drop area of 0.4 mm². The reference electrode was an Ag/AgCl/3M KCl electrode and the auxiliary electrode was a graphite electrode. The supporting electrolyte was acetate buffer (pH = 5). For smoothing and baseline correction the software GPES 4.4 supplied by EcoChemie was employed.

Cyclic voltammetry (CV) and PrP^{Sc}

QDs were studied using cyclic voltammetry. Amount of measured sample was 2 ml in in electrochemical cell. CV parameters were as follows: an initial potential 0 V, an end potential -1.9 V, vertex potential -1.5 mV, scan rate from 160 mV/s. All experiment were carried out at room temperature (22-24 °C)

Differential pulse

voltammetry - Brdicka reaction and PrP^{Sc}

The amount of QDs was measured using DPV. Differential pulse voltammetric measurements were carried out under the following parameters: deoxygenating with argon 60 s; start potential -1.5 V; end potential 0 V; a modulation time 0.057 s, a time interval 0.2 s, a step potential of 1.05 mV/s, a modulation amplitude of 250 mV, Eads = 0 V. All experiments were carried out at room temperature (22–24 °C). The DPV samples analysed were deoxygenated prior to measurements by purging with argon (99.999%) saturated with water for 120 s.

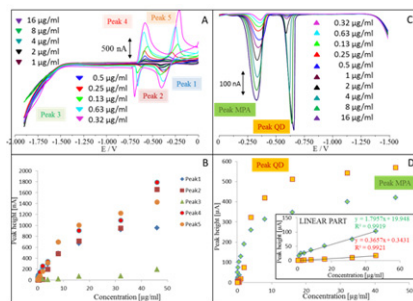
RESULTS AND DISCUSSION

Cyclic voltammetry (CV) is the most widely used electrochemical technique, and is frequently used for the characterization of a redox system and is often the first experiment performed in an electroanalytical study. It can provide rapid information about the number of redox states of the electroactive species, as well as qualitative information about the stability of these oxidation states and the electron transfer kinetics [30, 31]. For this purpose we decided to use CV for basic electrochemical characterization of QDs. It was observed using CV that QD provide three oxidation signals and two reduction signals. In oxidation part of cyclic voltammograms, three peaks at potential -0.3 V (peak 1), -0.7 V (peak 2) and -1.8 V (peak 3) were detected. In reduction part two signals at potential -0.5 V (peak 4) and -0.2 V (peak 5) were detected (Fig. 1A). Moreover, the dependence of peak on QD concentration was measured in all signals. With increasing concentration the growing of all peaks was observed (Fig. 1B).

Differential pulse voltammetry (DPV) is an extremely useful technique for measuring trace levels of organic and inorganic species. In differen-

tial pulse voltammetry, fixed-magnitude pulses – superimposed on a linear potential ramp – are applied to the working electrode at a time just before the end of the drop. The current is sampled twice, just before the pulse application and again late in the pulse life. The first current is instrumentally subtracted from the second, and this current difference is plotted versus the applied potential. In addition to improvements in sensitivity and resolution, the technique can provide information about the chemical form in which the analyte appears [30]. In this study DPV was employed for prions electrochemical characterization as electrochemical method more sensitive compared to cyclic voltammetry. Primarily, the method was optimized to achieve the best condition for QDs detection. Two peaks at potential -0.3 V (Peak MPA) and -0.7 V (Peak QD) were observed. The very well developed signals are shown in Fig. 1C. The calibration curve was measured with equation $y = 1.7957x + 19.948$ and regression coefficient R^2 higher than 0.99 for peak MPA and $y = 0.3657x + 0.3431$ and regression coefficient R^2 higher than 0.99 for peak QD. This shows very good linearity of the electrochemical response on concentration of QD. Considering the fact that QD are still of interest of numerous scientists, DPV fulfils demand on the detection of this protein in real samples after pre-treatment. The detection limit as 80 ng/ml was estimated (3 S/N) (Fig. 1D).

Figure 1: Electrochemical signal of different concentration of QD



CONCLUSION

Electrochemical behaviour of quantum dots using differential pulse voltammetry and cyclic voltammetry was presented in this paper. Based on the results obtained, we suggested novel and easy-to-use method how to quantify quantum dots and how to evaluate the ratio of their degradation, which is very important for further using of these particles.

ACKNOWLEDGEMENT

The financial support from IGA IP 5/2012 is highly acknowledged. The author P.S. is „Holder of Brno PhD Talent Financial Aid“, CEITEC CZ.1.05/1.1.00/02.0068.

REFERENCES

- [1] Bierman M J, Lau Y K A, Jin S, *Nano Lett.*, 7 (2007), 2907-2912.
- [2] Burda C, Chen X B, Narayanan R, *et al.*, *Chem. Rev.*, 105 (2005), 1025-1102.
- [3] Alivisatos A P, *Science*, 271 (1996), 933-937.
- [4] Yong K T, Sahoo Y, Choudhury K R, *et al.*, *Chem. Mat.*, 18 (2006), 5965-5972.
- [5] Drbohlavova J, Adam V, Kizek R, *et al.*, *Int. J. Mol. Sci.*, 10 (2009), 656-673.
- [6] Li Y S, Yannouleas C, Landman U, *Phys. Rev. B*, 81 (2010).
- [7] Tracy L A, Nordberg E P, Young R W, *et al.*, *Appl. Phys. Lett.*, 97 (2010).
- [8] Aldeek F, Mustin C, Balan L, *et al.*, *Eur. J. Inorg. Chem.*, (2011), 794-801.
- [9] Emin S, Loukanov A, Wakasa M, *et al.*, *Chem. Lett.*, 39 (2010), 654-656.
- [10] Ma Q F, Chen J Y, Wu X, *et al.*, *J. Lumines.*, 131 (2011), 2267-2272.
- [11] Samadpour M, Zad A I, Taghavinia N, *et al.*, *J. Phys. D-Appl. Phys.*, 44 (2011).
- [12] Zhao J J, Chen J, Wang Z P, *et al.*, *Mol. Med. Rep.*, 4 (2011), 425-429.
- [13] Huang F H, Chen G N, *Spectroc. Acta Pt. A-Molec. Biomolec. Spectr.*, 70 (2008), 318-323.
- [14] Juzenas P, Chen W, Sun Y P, *et al.*, *Adv. Drug Deliv. Rev.*, 60 (2008), 1600-1614.
- [15] Jamieson T, Bakhshi R, Petrova D, *et al.*, *Biomaterials*, 28 (2007), 4717-4732.
- [16] Jin S, Hu Y X, Gu Z J, *et al.*, *J. Nanomater.*, (2011).
- [17] Rosenthal S J, Chang J C, Kovtun O, *et al.*, *Chem. Biol.*, 18 (2011), 10-24.
- [18] Green M, O'Brien P, *Chem. Commun.*, (1998), 2459-2460.
- [19] Ryvolova M, Chomoucka J, Janu L, *et al.*, *Electrophoresis*, 32 (2011), 1619-1622.
- [20] Weng J F, Song X T, Li L A, *et al.*, *Talanta*, 70 (2006), 397-402.
- [21] Chomoucka J, Drbohlavova J, Babula P, *et al.*, in: Jakoby, B, Vellekoop, M J (Eds.), *Euroensors Xxiv Conference*, Elsevier Science Bv, Amsterdam (2010), pp. 922-925.
- [22] Hua M, Li P, Li L, *et al.*, *J. Electroanal. Chem.*, 662 (2011), 306-311.
- [23] Li Y F, Han M, Bai H Y, *et al.*, *Electrochim. Acta*, 56 (2011), 7058-7063.
- [24] Gu Z G, Yang S P, Li Z J, *et al.*, *Electrochim. Acta*, 56 (2011), 9162-9167.
- [25] Khene S, Moeno S, Nyokong T, *Polyhedron*, 30 (2011), 2162-2170.
- [26] Yang M H, Javadi A, Gong S Q, *Sens. Actuator B-Chem.*, 155 (2011), 357-360.
- [27] Li J J, Xu M, Huang H P, *et al.*, *Talanta*, 85 (2011), 2113-2120.
- [28] Yang C, Cu B X, Xu C X, *et al.*, *J. Electroanal. Chem.*, 660 (2011), 97-100.
- [29] Duan J L, Song L X, Zhan J H, *Nano Res.*, 2 (2009), 61-68.
- [30] Wang J, *Analytical Electrochemistry*, Wiley-VCH, New York 2000.
- [31] Bard A J, Faulkner L R, *Electrochemical methods - Fundamentals and applications*, Wiley-VCH, New York 2001.

ACETYLCHOLINESTERASE BASED ELECTROCHEMICAL BIOSENSOR USING INDOXYLACTATE AS A SUBSTRATE FOR A FAST ASSAY OF NERUOTOXIC COMPOUNDS

Miroslav POHANKA^{1,4*}, Alzbeta KRACMAROVA¹, Lucie DRTINOVA¹, David HYNEK^{2,3,4}, Vojtech ADAM^{2,3,4}, Jaromir HUBALEK^{2,3,4}, Rene KIZEK^{2,3,4}

¹Faculty of Military Health Sciences, University of Defence, Trebesska 1575, CZ-500 01 Hradec Kralove, Czech Republic

²Department of Chemistry and Biochemistry, Faculty of Agronomy, Mendel University in Brno, Zemedelska 1, CZ-613 00 Brno, Czech Republic, European Union

³Central European Institute of Technology, Brno University of Technology, Technicka 3058/10, CZ-616 00 Brno, Czech Republic, European Union

⁴Department of Microelectronics, Faculty of Electrical Engineering and Communication, Brno University of Technology, Technicka 3058/10, CZ-616 00 Brno, Czech Republic, European Union

*miroslav.pohanka@gmail.com

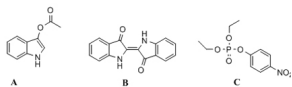
ABSTRACT

Acetylcholinesterase (AChE) is an enzyme terminating neurotransmission in cholinergic nervous system. It is targeted by several drugs and toxins. From a toxicological point of view, pesticides and nerve agents are probably the most toxic compounds inhibiting AChE activity. On the account of the enzyme inhibition, AChE is suitable for an in vitro assay of inhibitors and analytical devices such as biosensors are known to work on principle of recording of AChE residual activity. Here reported experiment is based on previously performed colorimetric dipsticks.

INTRODUCTION

Cholinergic nervous system is a target of many compounds being important due to their pharmacological or toxicological significance. In the cholinergic nervous system, enzyme acetylcholinesterase (AChE; EC 3.1.1.7) plays a prominent role as it participate in termination of acetylcholine based signal transmission through neurotransynaptic cleft or neuromuscular junction [1].

Figure 1. Chemical structure of indoxylacetatate (A), indigo (B) and paraoxon ethyl (C).



The present investigation is based on investigation of indoxylacetate as a substrate for electrochemical determination of AChE inhibitors (Fig. 2). The indoxylacetate undergo splitting of acetyl moiety and spontaneous oxidation up to blue indigo. In a biochemical point of view, the substrate suitability for AChE based assay was reported in our previous work [2].

MATERIAL AND METHODS

Electrochemical determination

Screen printed sensors (BVT, Brno, Czech Republic) were sized 25.4×7.3×0.6 mm and

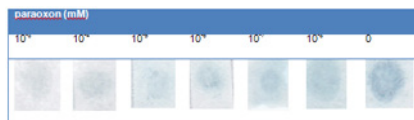
contained dot shaped platinum working electrode with diameter 1 mm, circle shaped platinum auxiliary, and circle shaped argent chloride reference electrode. The assay was done using an electrochemical device PalmSens (PalmSens BV, Houten, Netherlands) connected with a computer, and processed by PSLite 1.8 (PalmSens BV) software. AChE from electric eel (*Electrophorus electricus*) was achieved from Sigma-Aldrich (Saint Louis, Missouri, USA). The enzyme had specific activity 16.7 μ kat/mg protein. It was dissolved in phosphate buffered saline shortly before experiment and activity was adjusted up 5 U (83.4 nkat) in 20 μ l for substrate acetylthiocholine chloride and standard Ellman's protocol. AChE solution was mixed with gelatin up to final level 2% (w/w) and 20 μ l of the reagents was added on one edge of cellulose filter paper (Whatman, Kent, UK) cut into bands 50×5 mm. The wet bands were dried in a silica gel filled desiccator. The second edge of the band was imbued by 20 μ l of 100 mM indoxylacetate in ethanol and let to dry in laboratory conditions. Paraoxon ethyl (Sigma-Aldrich) was used throughout for dipstick performance. It was solved in a calibration scale 10-3, 10-4, 10-5, 10-6, 10-7, 10-8 and 10-9 mol/l. Each paraoxon solution or blank contained 5% isopropanol in deionized water. The assay was done by application of sample in a volume 40 μ l to AChE containing edge of dipstick and incu-

bated for 15 minutes. After that, the dipstick was folded in the middle and the opposite edges were pressed one to each other for 30 minutes. Finally, the edge containing immobilized AChE was pressed with electrochemical sensor and SWV was recorded.

RESULTS AND DISCUSSION

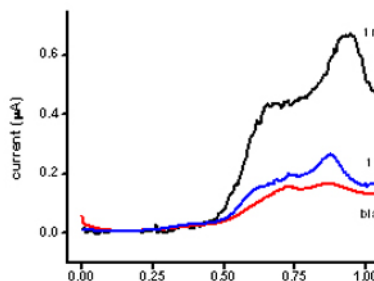
The dipstick processing provided contrast blue color when AChE remained intact by paraoxon. Coloration for the control dipstick and dipstick covered with 10 nM paraoxon was very intensive (see table 1). Compared to it, higher level of paraoxon caused decrease of coloration. Estimated limit of detection was approximately 1 μM for paraoxon when coloration evaluated by a naked eye.

Table 1. Calibration for paraoxon using colorimetric dipsticks.



When indoxylacetate based dipsticks performed by SWV, typical peaks were formed as clearly demonstrated in Fig. 2. The peaks are increasing when AChE in the dipsticks become inhibited by paraoxon. We judge that electrochemistry act as a competing process for substrate reaction. When AChE fully active, the substrate undergo into oxidation process and indoxylacetate level for electrochemical oxidation is decreased. In the opposite phenomenon, inhibited AChE cannot split indoxylacetate so the electrochemically assayed reaction has maximal response. The proportionality between peak height (area) and inhibitor level is advantageous for simple understanding and better option for pertinent commercialization of device. We were encouraged by the preliminary experimental data described previously and decide to examine dipsticks for paraoxon assay. Semi-log calibration plot (negative logarithm of paraoxon concentration versus area of peak in μAV) was made. The calibration was fitted by Boltzman equation (OriginPro 8, Origin Lab Corp, Northampton, MA, USA) and limit of detection was calculated as a point on the curve responding to triplicate of blank assay standard deviation (signal to noise equal to 3). The median inhibitory concentration for paraoxon was calculated to be 5.93 μM and limit of detection 29.1 nM for a sample sized 40 μl . The coefficient of determination R^2 for the calibration plot was 0.981.

Figure 2. SWV for colored dipsticks with bound AChE. Black and blue curves: assay of 1 mM and 1 μM paraoxon, red curve: assay of 5% isopropanol only (blank).



CONCLUSION

Previously developed colorimetric dipsticks were successfully adopted for electrochemical assay. The dipsticks are convenient for dual performance based on evaluation of coloration by a naked eye and by electrochemical assay by performance of screen printed electrodes. The principle of assay is quite intriguing as performance of electrochemical device is not compulsory but optional in the assay protocol. The dipsticks seem to be well approachable for field assay of neurotoxic pesticides as proved on the paraoxon.

REFERENCES

- [1] Ballard CD, Greig NH, Guillozet-Bongaarts AL, Darvesh S: Current Alzheimer Research, 2 (2005), 3, 307-318.
- [2] Pohanka M, Hrabanova M, Kuca K, Simonato JP: International Journal of Molecular Science 12 (2011), 4, 2631-2640.

ELECTROCHEMICAL DETERMINATION OF ENZYMES METABOLIZING ELLIPTICINE AS A TOOL TO EXPLAIN THE MECHANISMS OF ELLIPTICINE TOXICITY TO THYROID CANCER CELLS

Jitka POLJAČOVÁ¹, Tomas ECKSCHLAGER², Rene KIZEK^{3,4}, Eva FREI⁵, Marie STIBOROVA^{1*}

¹Department of Biochemistry, Faculty of Science, Charles University, Prague, Albertov 2030, 128 40 Prague 2, Czech Republic

²Department of Paediatric, Haematology and Oncology, 2nd Medical School, Charles University and University Hospital Motol, V Uvalu 84, CZ-150 06 Prague 5, Czech Republic

³Department of Chemistry and Biochemistry, Faculty of Agronomy, Mendel University in Brno, Zemedelska 1, 613 00 Brno, Czech Republic

⁴Central European Institute of Technology, Brno University of Technology, Technicka 3058/10, 616 00 Brno, Czech Republic

⁵ Division of Preventive Oncology, National Center for Tumor Diseases, German Cancer Research Center (DKFZ), In Neuenheimer Feld 280, 69 120 Heidelberg, Germany,

*stiborov@natur.cuni.cz

ABSTRACT

Ellipticine, an anticancer agent damaging DNA acting as DNA intercalator, inhibitor of topoisomerase II and the compound generating covalent DNA adducts after being activated with cytochrome P450 (CYP) and peroxidases, is cytotoxic to human BHT-101, B-CPAP and 8505-C thyroid cancer cell lines and this toxicity corresponds to ellipticine-derived DNA adduct levels formed in these cells. Cultivation of thyroid cancer cell lines under the hypoxic conditions (1% oxygen) leads to a decrease in toxicity of ellipticine to these cells. Such a lower sensitivity of the thyroid cancer cells to ellipticine correlates with a decrease in the formation of ellipticine-derived DNA adducts in these cells. Here, the effects of treatment of the cells with ellipticine on expression of CYP1A1, 1B1, 3A4 and peroxidases thyroid peroxidase (TPO) and cyclooxygenase (COX-1), the enzymes that catalyze ellipticine metabolism, and those on levels of cytochrome b_5 determined electrochemically (Western blotting) in tested thyroid cancer cells were also investigated. The highest expression of cytochrome b_5 together with CYP1A1 and 3A4 determine the highest cytotoxicity of and DNA adduct formation by ellipticine in a B-CPAP cell line. The results of this study demonstrate that formation of covalent DNA adducts by ellipticine is the predominant mechanism responsible for its cytotoxicity to studied thyroid cancer cells.

INTRODUCTION

Ellipticine (5,11-dimethyl-6H-pyrido[4,3-b]carbazole) is an anticancer agent damaging DNA, acting as DNA intercalator, inhibitor of topoisomerase II and the compound generating covalent DNA adducts after being activated with cytochrome P450 (CYP) and peroxidases (for a summary see [1-7]). Two major DNA adducts generated from 13-hydroxy- and 12-hydroxyellipticine formed by CYP- and peroxidase-mediated metabolism are formed *in vitro* and *in vivo* in DNA of healthy organs of rats and mice treated with this anticancer drug [1,3,7,8]. Of the CYP enzymes investigated, human CYP3A4 and rat CYP3A1 are the most active enzymes oxidizing ellipticine to these reactive metabolites that dissociate to ellipticine-13-ylidium and ellipticine-12-ylidium which bind to DNA [3,7,8,10], while the CYP1A enzymes preferentially form the other ellipticine

metabolites, 9-hydroxy- and 7-hydroxyellipticine, which are the detoxication products. Recently we have found that cytochrome b_5 alters the ratio of ellipticine metabolites formed by CYP1A1, 1A2 and 3A4. While the amounts of the detoxication metabolites (7-hydroxy- and 9-hydroxyellipticine) were either decreased or not changed with added cytochrome b_5 , 12-hydroxy-, 13-hydroxyellipticine and ellipticine *N*²-oxide increased considerably. The change in amounts of metabolites resulted in an increased formation of covalent ellipticine-DNA adducts, one of the DNA-damaging mechanisms of ellipticine antitumor action [10,11].

The same DNA adducts found *in vitro* were also detected in several human cancer cells such as breast adenocarcinoma MCF-7, the leukaemias HL-60 and CCRF-CEM, neuroblastoma and glioblastoma cells, and in rat mammary adenocarcinoma *in vivo* (for a summary see [1-4]).

Here, we investigated the cytotoxicity of ellipticine to another type of cancer cells, thyroid cancer cells such as BHT-101, B-CPAP and 8505-C cell lines. We also evaluated which of the mechanisms of ellipticine action is responsible for its cytotoxicity. Because cytotoxicity of ellipticine *in vitro* and *in vivo* depends on amounts and activities of enzymes that activate or detoxicate this drug, their expression levels were determined electrochemically (SDS-PAGE electrophoresis with their detection by specific antibodies raised against such enzymes) in thyroid cancer cells. In addition, DNA adduct formation by ellipticine was investigated by the ^{32}P -postlabeling method [1-3, 7,10].

MATERIAL AND METHODS

MTT assay

The cytotoxicity of ellipticine to thyroid cancer cells in exponential growth was determined in a 96-well plate under the normoxic (aerobic) and hypoxic conditions (1% oxygen). For a dose-response curve, cells in exponential growth were seeded in 100 μl of medium with 10^4 cells per well. Solution of ellipticine in dimethyl sulfoxide (DMSO) (1 μl) in final concentrations of 0.02 - 50 μM was added. Control cells and medium controls without cells received 1 μl of DMSO without drug. Tumor cell viability was evaluated by MTT test as previously described [12,13]. Each value is the mean of 8 wells with standard deviations. The IC_{50} values were calculated from at least 3 independent experiments using the linear regression of the dose-log response curves by SOFTmaxPro.

Cell cycle analysis

To determine cell cycle distribution analysis, 5×10^5 cells were plated in 60 mm dishes and treated with ellipticine (0, 1 and 10 μM) for 48 h. After treatment, the cells were collected by trypsinization, fixed in 70% ethanol, washed in PBS, resuspended in 1 ml of PBS containing 1 $\mu\text{g}/\text{ml}$ RNase and 50 mg/ml propidium iodide, incubated in the dark for 30 min at room temperature, and analyzed by flow cytometry on a FACSCalibur cytometer (BD, San Jose, CA, USA). The data were analyzed using ModFit LT software (Verity Software House, Topsham, ME, USA).

Electrochemical estimation of contents of CYPs, peroxidases and cytochrome b_5 in thyroid cancer cells

To determine the expression of cytochrome b_5 , CYP1A1, 1B1 and 3A4, thyroid peroxidase (TPO) and cyclooxygenase (COX)-1 proteins, cells were homogenized in 25 mM Tris-HCl buffer pH 7.6 containing 150 mM NaCl, 1% detergent NP-40 (Sigma, St. Louis, MO, USA), 1% sodium deoxycholate, 0.1 % SDS and with solution of COMPLETE (protease inhibitor

cocktail tablet, Roche, Basel, Switzerland) at concentration described by provider. The homogenates were centrifuged for 20 min at 14, 000 g and supernatant was used for additional analysis. Protein concentrations were assessed using the DC protein assay (Bio-Rad, Hercules, CA, USA) with bovine serum albumin as a standard, and 10-45 μg of extracted proteins were subjected to SDS-PAGE electrophoresis on a 11% gel for analysis of CYP1A1, 1B1 and 3A4, TPO and COX-1 protein expression, and a 17% gel for analysis of cytochrome b_5 protein expression [13-16]. After migration, proteins were transferred to a nitrocellulose membrane and incubated with 5% non-fat milk to block non-specific binding. The membranes were then exposed to specific rabbit polyclonal antibodies that are specific in our former study [13].

DNA isolation and ^{32}P -postlabeling of DNA adducts

DNA from thyroid cancer cells was isolated by the phenol-chloroform extraction as described [13,14]. The ^{32}P -postlabeling of nucleotides using nuclease P1 enrichment procedure, found previously to be appropriate to detect and quantify ellipticine-derived DNA adducts formed *in vitro* and *in vivo* [1-4,8-11,13,14].

RESULTS AND DISCUSSION

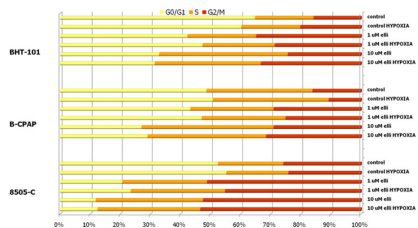
Ellipticine is cytotoxic to human BHT-101, B-CPAP and 8505-C thyroid cancer cell lines with IC_{50} values of 4.8, 2.8 and 3.2 mM, respectively. This toxicity corresponds to ellipticine-derived DNA adduct levels formed in these cells. Levels of DNA adducts expressed as relative adduct labeling (RAL) were up to 7.8 adducts per 10^7 normal (unmodified) nucleotides.

Cultivation of thyroid cancer cell lines under the hypoxic conditions (1% oxygen) leads to a decrease in toxicity of ellipticine to these cells. This decrease in toxicity of ellipticine to the thyroid cancer cells to ellipticine correlates with a decrease in the formation of ellipticine-derived DNA adducts in these cells. Nevertheless, the thyroid cancer cells treated with 1 μM ellipticine under lack of oxygen were the exception; higher levels of DNA adducts were found in these cells than in these cells treated under the standard conditions.

We also investigated the ellipticine effect on the cell cycle distribution of thyroid cancer cells cultivated under standard and hypoxic conditions. As shown in Figure 1, cell cycle arrest is produced by ellipticine

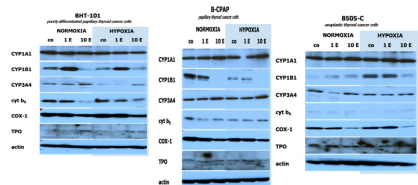
depending on the cultivation conditions.

Figure 1: Ellipticine effect on cell cycle distribution in human thyroid cancer cell lines cultivated under standard or hypoxic conditions



Since cytotoxicity of ellipticine depends on expression levels and activities of enzyme that activate or detoxicate this drug, their expression levels were determined electrochemically (SDS-PAGE electrophoresis with their detection by specific antibodies raised against such enzymes) in tested thyroid cancer cells. As shown in Figure 2, both under normoxic and hypoxic conditions CYP1A1, 1B1 and 3A4 as well as peroxidases TPO and COX-1 are expressed in studied thyroid cancer cells.

Figure 2: Western blots of enzymes involved in metabolism of ellipticine expressed in thyroid cancer cells lines and those of actin (a loading control) in these cells



Whereas amounts of CYP1A1 is either not influenced or increased by treatment of cells with ellipticine, expressing levels of CYP1B1 are affected by treating the cells with this drug. Interestingly, higher levels of CYP3A4 were expressed in a B-CPAP cell line both under aerobic and hypoxic conditions and increased by treatment of this line to ellipticine, but expression of this CYP enzyme is repressed by ellipticine in BHT-101 and 8505-C cells. The highest cytotoxicity and ellipticine-derived DNA adduct levels found in B-CPAP cells seem to follow from the highest ellipticine activation in this cell line. The highest levels of cytochrome b_5 together with high amounts of expressed CYP3A4 and 1A1, whose combination produce the highest production of 13-hydroxy- and 12-hydroxyellipticine

metabolites generating two major ellipticine-derived DNA adducts [3,7,8,10,11], were detected in a B-CPAP cell line.

CONCLUSION


This study show for the first time that ellipticine is toxic to BHT-101, B-CPAP and 8505-C thyroid cancer cell lines and that this toxic effect corresponds to ellipticine-derived DNA adduct formation in these cells. Expression of cytochrome b_5 and CYP1A1 and 3A4 dictates the cytotoxicity in the studied cell lines. Therefore, monitoring of expression levels of enzymes metabolizing (activating and detoxicating) anticancer drug ellipticine by the Western-blotting-electrochemical method, together with the ^{32}P -postlabeling technique utilized for detection and quantitation of DNA adducts are appropriate tools for evaluation of mechanism of toxicity of ellipticine in thyroid cancer cells.

ACKNOWLEDGEMENT

The work has been supported by Grant Agency of the Czech Republic (grant P301/10/0356) and Charles University in Prague (grant UNCE #42).

REFERENCES

- [1] Stiborová M., Bieler C.A., Wiessler M., et al.: *Biochemical Pharmacology*, 62 (2001), 1675-1684.
- [2] Stiborová M., Rupertová M., Schmeiser H.H., et al.: Molecular mechanism of antineoplastic action of an anticancer drug ellipticine. *Biomedical Papers*, 150 (2006), 13-23.
- [3] Stiborová M., Rupertová M., Frei E.: *Biochimica et Biophysica Acta*, 1814 (2011), 175-185.
- [4] Kizek R., Adam V., Hrabeta J., et al.: *Pharmacology & Therapeutics*, 133 (2012), 26-39.
- [5] Auclair C.: *Archives of Biochemistry and Biophysics*, 259 (1987), 1-14.
- [6] Garbett N.C., Graves D.E.: *Current Medicinal Chemistry. Anti-Cancer Agents*, 4 (2004), 149-172.
- [7] Stiborová M., Sejbal J. Bořek-Dohalská L., et al.: *Cancer Research*, 64 (2004), 8374-8380.
- [8] Stiborová M., Poljaková J., Ryšlavá H., et al.: *International Journal of Cancer*, 120 (2007), 243-251.
- [9] Stiborová M., Rupertová M., Aimová D., et al: *Toxicology*, 236 (2007), 50-60.
- [10] Stiborová M., Indra R., Moserová M., et al.: *Chemical Research in Toxicology*,

- 
- (2012), DOI: 10.1021/tx3000335.
- [11] Kotrbová V, Mrázová B, Moserová M., et al.: *Biochemical Pharmacology*, 82 (2011), 669-680.
 - [12] Cinatl J. Jr, Cinatl J., Driever P.H., et al.: Sodium valproate inhibits *in vivo* growth of human neuroblastoma cells. *Anti-Cancer Drugs*, 8 (1997), 958-963.
 - [13] Poljaková J., Eckschlager T., Hraběta J., et al.: *Biochemical Pharmacology*, 77 (2009), 1466-1479.
 - [14] Poljaková J., Hrebacková J., Dvoraková M., et al.: *Neuro Endocrinology Letters*, 32 (Suppl 1) (2011), 101-116.
 - [15] Stiborová M., Martínek V., Rýdlová H., et al.: *Cancer Research*, 62 (2002), 5678-5684.
 - [16] Stiborová M., Martínek V., Rýdlová H., et al.: *Cancer Letters*, 220 (2005), 145-154.

DOUBLE-PULSE LASER-INDUCED BREAKDOWN SPECTROSCOPY ON LIQUID JETS FOR DETERMINATION OF NUTRIENT ELEMENTS IN ALGAE

David PROCHAZKA^{1*}, Veronika KONECNA¹, Jan KOURIL⁴, Pavel PORIZKA¹, Jan NOVOTNY¹, Zdenek PILAT², Ota SAMEK², Radomir MALINA¹, Karel NOVOTNY³, Jozef KAISER¹

¹ X-ray micro CT and nano CT research group, CEITEC - Central European Institute of Technology, Brno University of Technology, Technická 2, 616 69 Brno, Czech Republic

² Institute of Scientific Instruments of the ASCR v.v.i., Academy of Sciences of the Czech Republic, Královopolská 147, Brno 61669, Czech Republic

³ Department of Chemistry, Faculty of Sciences, Masaryk University, Kotlářská 2, Brno 611 37, Czech Republic

⁴ Institute of Physical Engineering, Faculty of Mechanical Engineering, Brno University of Technology, Technická 2, 616 69 Brno, Czech Republic

*prochazka.d@fme.vutbr.cz

ABSTRACT

We report on the optimization of double-pulse laser-induced breakdown spectroscopy (DP LIBS) for determination of nutrient elements in algae. The measurements were performed with nozzle specially designed for algal solution and the optimal measurements parameters have been determined. The calibration curves and limits of detection have been established.

INTRODUCTION

In order to utilize algae for efficient biofuel, food industry, and bioremediation applications [1, 5] the optimal cultivation parameters have to be determined for each purpose which leads to a high production of oil in the selected cell line, increased production of carotenoids/3-omega oils and potential absorption of heavy-metals in the selected cell line, respectively. This can be accomplished using small-scale photobioreactors that allow precise monitoring and control of the culture irradiance, temperature, pH, and gas composition in the medium. However, the ability to monitor the elemental distribution in cells and consequently cell response to external stimuli on-line (ratios/distribution of elements within algae cells might be significantly changed) is not provided [4].

LIBS seems to be one of the most promising methods for on-line qualitative/quantitative analysis of algae directly inside of photobioreactors.

A number of investigations that describe LIBS measurements of liquid samples in the form of static surfaces, jets, and aerosols have been reported [2, 4, 6, 7]. But in all these cases the medium was homogeneous. Algae however are particles (with diameter ~20 μm) floating in medium so it must be ensured that they are deployed equally all the time of experiment in the whole volume. Other problem is blocking of the liquid-jet nozzle because of algae clumping.

EXPERIMENTAL

Liquid measurements were performed in laboratory-made glass vessel (Fig. 1).

Continuous and relatively steady thin flow of liquid sample has to be achieved for liquid LIBS measurements. We use peristaltic pump (PCD 81, Kouřil, CZ) working at 100 ml/min. Liquid sample was led to the lab-made flat spray nozzle via silicone tubes and a thin water wall was created. The nozzle was mounted to the XY movement (ThorLabs, US) for precise positioning of the thin water wall.

The liquid DP LIBS experimental setup is in collinear arrangement – the first pulse 532 nm (LQ529a, SOLAR, BY) and second pulse 1064 nm (Brilliant B, QUANTEL, FR) are led by mirrors (ThorLabs, US / Newport, UK) and harmonic separator (Eksma Optics, LT) with reflectance for 1064 nm and transmittance for 532 nm and focused by lens with 75 mm focal length.

Fig. 1 LIBS system employing laminar water jet setup



The LIBS plasma radiation was collected with UV-NIR achromatic collimating mirror system (CC52, ANDOR, UK) and transported by a fiber optic system (25 μm in diameter) onto the entrance of the spectrometer in echelle configuration (ME5000, Mechelle, ANDOR, UK). As a

detector an ICCD camera (iStar 734, ANDOR, UK) was employed. The time-resolved studies were performed by controlling the gate width t_W (time during which the spectra are integrated), the gate delay time t_d (delay time of detection after laser pulse) and the interpulse delay Δt . Both lasers and ICCD camera were triggered by Delay generator (DG535, Stanford Research System, US) and specially developed electronic switch and controlled via computer equipped with lab-made software. t_W , t_d and Δt were optimized to obtain the best signal to noise ratio.

RESULTS AND DISCUSSION

Depth of focusing and effective volume

It is well known that the depth of focusing of the laser beam onto a surface in LIBS is a critical parameter in determining the emission intensity of the observed spectral lines. It has been shown in the case of liquid jets that the emission intensity is maximized if the laser beam is focused a few mm beneath the front surface of the jet and that this optimum focusing condition is also laser energy-dependent [8]. This phenomenon cannot be explained on the basis of electron density and plasma temperature effects alone. The maximum observed emission intensity as a function of laser defocusing correlates very well with the maximum of the “effective volume” function, this being the volume of sample located in the region where the laser power exceeds the breakdown threshold. The moving breakdown model can be very successfully applied for our case. It makes a number of key assumptions to simplify the optical breakdown process there were describe elsewhere [8], so here we describe only the main principles.

The effective volume for given irradiance I and at the axial position z is a sum of thin discs i.e.

$$V(I, z) \approx \sum_z \pi r_{ef}^2(z) \Delta z$$

where r_{ef} and Δz are an effective radius and a thickness of each elementary disc, respectively. The effective radius as a function of axial position is given by

$$r_{ef} = \sqrt{-w_z^2 \ln \frac{I_{th}}{I_z}}$$

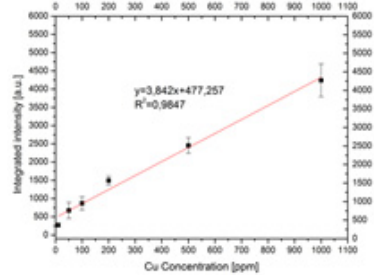
where w_z is the size of beam waist at the axial position z , I_{th} is a threshold irradiance and I_z is a local laser irradiance. From the equations described above we can plot effective volume

functions, allowing us to predict the amount of defocusing required at a given energy to optimize signal in water flow.

Calibration curve

To determine quantities of selected elements on the base of DP LIBS analysis, calibration curves must be constructed. In Fig. 2 the typical Cu calibration curve measured in thin liquid flow is shown. The measurements were performed in $\text{CuSO}_4 \cdot 5\text{H}_2\text{O}$ solution with concentration from 10 ppm to 1000 ppm.

Fig. 2 Calibration curve of Cu in $\text{CuSO}_4 \cdot 5\text{H}_2\text{O}$ solution.



The detection limit was calculated from equation

$$\text{LOD} = \frac{3s_0}{b}$$

where s_0 is a standard deviation of background and b is intercept of calibration curve [3].

CONCLUSION


The optimal experimental parameters for measure algal solutions such as laser energy, effective volume, interpulse delay, gate width and gate delay were determined theoretically and experimentally. The calibration curve was constructed for some elements of interests and detection limits were calculated.

ACKNOWLEDGEMENT

We acknowledge the Ministry of Education, Youth and Sports of the Czech Republic for bestowing the research projects ME10061 and the support of Brno University of Technology on the frame of grant FSI-S-11-22 (Application of advanced optical methods). This work was also supported by the project “CEITEC - Central European Institute of Technology” (CZ.1.05/1.1.00/02.0068) from European Regional Development Fund.

REFERENCES

- [1] KHOZIN-GOLDBERG, I. et al. LC-PUFA from photosynthetic microalgae: occurrence, biosynthesis, and prospects in

- 
- biotechnology. In *Applied Microbiology and Biotechnology*. 2011. Vol. 91, no. 4, s. 905-915.
- [2] KUMAR, A. et al. Double-pulse laser-induced breakdown spectroscopy with liquid jets of different thicknesses. In *Applied optics*. 2003. Vol. 42, no. 30, s. 6047-6051. .
- [3] LONG, G.L. - WINEFORDNER, J.D. Limit of detection. A closer look at the IUPAC definition. In *Analytical Chemistry*. 1983. Vol. 55, no. 7, s. 712A-724A. .
- [4] POŘÍZKA, P. et al. Application of Laser-Induced Breakdown Spectroscopy to remote and in situ analysis of algal biomass utilisation for industrial biotechnology. In *Spe*. 2012. .
- [5] SAMEK, O. et al. Application of laser-induced breakdown spectroscopy to in situ analysis of liquid samples. In *Optical*. 2000. .
- [6] VOL, L. et al. A review of heavy metal adsorption by marine algae. In *Chinese Journal of Oceanology and Limnology*. 2000. Vol. 18, no. 3, s. 260-264. .
- [7] YAROSHCHYK, P. et al. Quantitative determination of wear metals in engine oils using laser-induced breakdown spectroscopy: A comparison between liquid jets and static liquids. In *Spectrochimica Acta Part B: Atomic Spectroscopy*. 2005. Vol. 60, no. 7-8, s. 986-992. .
- [8] YAROSHCHYK, P. et al. Theoretical modeling of optimal focusing conditions using laser-induced breakdown spectroscopy in liquid jets. In *APPLIED SPECTROSCOPY*. 2004. Vol. 58, no. 11, s. 1353-1359. .

LEAD DETECTION ON DIRECT GROWN CNTS BASED WORKING MIKROELECTRODE

Jan PRASEK^{1,2*}, Jan PEKAREK^{1,2}, Ondrej JASEK³, Petra BUSINOVA^{1,2}, Jana DRBOHLAVOVA^{1,2}, Jana CHOMOUCKA^{1,2}, Radim HRDY^{1,2}, Jaromir HUBALEK^{1,2}

¹ Department of Microelectronics, Faculty Electrical Engineering and Communication, Brno University of Technology, Technicka 10, 616 00 Brno, Czech Republic

² Central European Institute of Technology, Brno University of Technology, Technicka 10, 616 00 Brno, Czech Republic

³ Department of Physical Electronics, Faculty of Science, Masaryk University, Kotlarska 2, 611 37 Brno, Czech Republic

*prasek@feec.vutbr.cz

ABSTRACT

The aim of this paper is to show the possibilities of heavy metals electrochemical detection on direct grown multiwalled carbon nanotubes (MWNTs) based microelectrode. The electrode substrate was fabricated using standard lithography and thin film technology on silicon substrate. The working electrode (WE) deposition in a form of vertically aligned MWNTs was done on the electrode substrate using CVD. Fabricated electrodes were tested optically using scanning electron microscopy with good result and electrochemically using electrochemical detection of lead ions in acetate buffer solution. The electrochemical measurement confirmed the suitability of fabricated electrode for lead with the detection limit of $3 \mu\text{mol/L}^{-1}$. Finally the comparison of fabricated WE with the WE from commercial electrochemical based on carbon nanotubes (CNTs) have been done resulting in almost two times better sensitivity of our electrode.

INTRODUCTION

Accurate and fast detection of species in environment is one of the most discussed problems in these days. In general the samples need to be collected and then analyzed in laboratories using big laboratory equipment. Recently many research works in the field of measurement systems that could be used for fast on-field analysis were reported. Such system usually use electrochemical methods for detection of species dissolved in water solutions which could be miniaturized easily using sensor systems [1, 2].

The main problem of electrode systems miniaturization is reduction of geometrical size of the electrodes in comparison to standard electrodes resulting in lower current response. This problem could be solved by creation of some 3D structure on the geometricaly reduced electrode which could increase the active size of the electrode several times. 3D structure could be fabricated using several methods. The easiest way is to prepare high porous structure on the electrode surface as a mixture of active electrode material with some, usually polymer binder, that could be screen-printed, drop-coated, dip-coated, etc. on the electrode substrate [3, 4]. Next possibility is to grow nanostructures in a form of nanotubes, nanowires, nanopillars, quantum dots, etc. directly on the electrode substrate using process of anodization [5, 6] or grown vertically aligned CNTs directly on the electrode substrate using CVD techniques [7, 8]. Electrode systems with

nanostructured electrodes could be also used as a base for intelligent sensors [9].

In this work we fabricated thin-film MWCNTs based WE and compared with commercial CNTs based electrochemical sensor.

EXPERIMENTAL

Electrode design and fabrication

Electrode was designed to be used as a working electrode of a three-electrode system for electrochemical analysis of species dissolved in aqueous solutions. The diameter of the electrode is 3 mm and the silicon substrate size is 25×5 mm. Working electrode design is shown in the figure 1a. Electrode was fabricated on silicon wafer. Thermal CVD was used for direct grown MWCNTs based electrode. Fabricated electrode is shown in the figure 1b.

Successfully fabricated electrodes with deposited MWCNTs were analyzed optically using SEM (TESCAN, Czech Republic) as is shown in the figure 2. Uniform homogenous layer of MWCNTs was obtained after fabrication process optimization

Figure 1.: Working electrode design (a) and fabricated electrode (b)

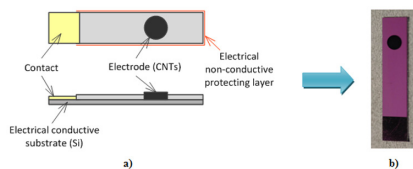
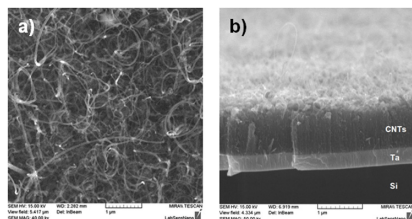


Figure 2.: SEM microimage of direct grown MWCNTs based electrode top view a), cross-section b)



Chemicals and experimental method

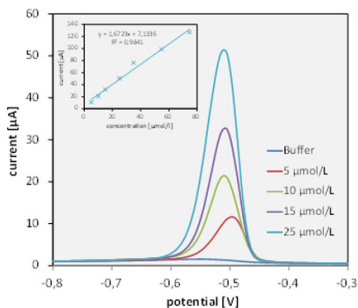
Acetate buffer solution (pH 5.4) was prepared by mixing 0.2 M CH_3COOH and 0.2 M CH_3COONa . A stock solution of $\text{Pb}(\text{C}_2\text{H}_3\text{O}_2)_2 \cdot 3\text{H}_2\text{O}$ with an initial concentration of 10 mmol/L was prepared using acetate buffer solution mentioned above.

All measurements were done employing differential pulse voltammetry (DPV) in range of the potential from -1 to 0 V with scan rate of 25 mV/sec using PalmSens handheld potentiostat/galvanostat (Palm Instruments BV, Netherlands). Electrochemical experiments were carried out in a 8 mL voltammetric cell at room temperature (25°C), using a three-electrode configuration electrochemical system with the standard Ag/AgCl reference electrode type 6.0726.100 and platinum auxiliary electrode type 6.0343.000 (both from Metrohm, Switzerland).

RESULTS AND DISCUSSION

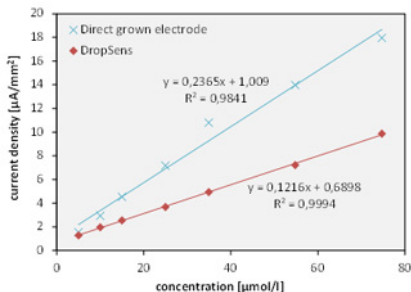
As is shown in the figure 1 MWCNTs based electrode was fabricated successfully. Then the electrodes were characterized electrochemically. Electrochemical characterization was carried out in acetate buffer solution employing differential pulse voltammetry. The detected matters were lead ions. Sample of DPV response of fabricated electrode in a three electrode system against standard electrodes is shown in the figure 3.

Figure 3.: DPV response of fabricated Si electrode to lead ions (inset: calibration curve)



From the figure 3 is clear that the current response to lead ions addition is good and the electrode could be used for lead ions detection with relative good linearity as is shown in the inset in the figure 3.

Figure 4.: Calibration curves of fabricated MWCNTs based electrode and MWCNTs based working electrode from DropSens DS 110CNT type commercial sensor comparison on the lead ions detection



Fabricated MWCNTs based WE was compared with working electrode from commercial sensor DS 110CNT (DropSens, Spain). The calibration curves comparison for lead ions detection of both electrodes is shown in the figure 4. Figure 4 shows that with considering of the results recounted to the current density, the sensitivity of fabricated electrode with direct grown MWCNTs to lead ions is on higher concentrations almost two times higher than the sensitivity of working electrode from commercial DS 110CNT type MWCNTs based sensor. The linearity of our electrode is little bit worse than the one from the commercial sensor. The detection limit was successfully tested up to 3 µmol/L of lead ions on both electrodes.

CONCLUSION

In this work we fabricated MWCNTs based

working microelectrodes for electrochemical sensors on thin-film silicon substrate. Direct-grown multiwalled carbon nanotubes as an active electrode material were successfully synthesized on the silicon substrate using thermal CVD. Fabricated electrodes were examined optically using scanning electron microscopy resulting in relative good and homogenous layer of MWCNTs and compared with MWCNTs based WE from DS 210CNT commercial sensor on electrochemical detection of lead ions in a three-electrode system using differential pulse voltammetry.

Obtained results shown in chapter 3 confirmed the suitability of fabricated electrode for electrochemical analysis. Considering of the results recounted to current density, the sensitivity of fabricated electrode with direct grown MWCNTs to lead ions was on higher concentrations almost two times higher than the sensitivity of WE from commercial DS 110CNT type MWCNTs based sensor. The linearity of our electrode is little bit worse than the one from the commercial sensor. , the detection limit was successfully tested up to 3 $\mu\text{mol/L}$ of lead ions.

ACKNOWLEDGEMENT

Funding for this work was provided by the Grant agency of the Czech Republic under the contracts GACR P205/10/1374, GACR 102/08/1546 (NANIMEL), and project CZ.1.05/1.1.00/02.0068 (CEITEC).

REFERENCES

- [1] Li Z, Zeng G M, Tang L, et al.: *Biochemical Engineering Journal*, 55 (2011), 3, 185-192
- [2] Mulazimoglu I E: *Energy Education Science and Technology Part a-Energy Science and Research*, 28 (2011), 1, 393-400
- [3] Krejci J, Prasek J, Fujcik L, et al.: *Microelectronics International*, 21 (2004), 3, 20-24
- [4] Souza L P, Calegari F, Zarbin A J G, et al.: *Journal of Agricultural and Food Chemistry*, 59 (2011), 14, 7620-7625
- [5] Calavia R, Mozalev A, Vilanova X, et al.: *Proceedings of the 2009 Spanish Conference on Electron Devices*, (2009), 327-329
- [6] Mozalev A, Smith A J, Borodin S, et al.: *Electrochimica Acta*, 54 (2009), 3, 935-945
- [7] Pekarek J, Ficek R, Vrba R, et al.: *32nd International Spring Seminar on Electronics Technology*, (2009), 629-633
- [8] Prasek J, Hubalek J, Adamek M, et al.: *IEEE Sensors*, (2006), 1253-1256
- [9] Fajcik L, Prokop R, Prasek J, et al.: *Microelectronics International*, 27 (2010), 1, 3-10

SYNTHESIS, STRUCTURE, AND OPTO-ELECTRONIC PROPERTIES OF ORGANIC DYES ON DIAMOND

Bohuslav REZEK, Jan CERMAK, Egor UKRAINTSEV, Pavel HUBIK, Jiri J. MARES, Martin LEDINSKY, Antonin FEJFAR, Jan KOCKA, Alexander KROMKA

Institute of Physics ASCR, Cukrovarnicka 10, 16200 Prague 6, Czech Republic

*rezek@fzu.cz

ABSTRACT

We prepare a thin-film heterojunction of polypyrrole (PPy) on hydrogen-terminated diamond by electro-polymerization from solution. We combine advanced scanning probe techniques (AFM, KFM, micro-Raman) to characterize microscopic structural, chemical, and opto-electronic properties of such system. These data are further correlated with electronic transport measurements. We identify covalent bonding of PPy to diamond. This heterojunction also facilitates efficient dissociation of excitons in PPy and transfer of free charge carriers from polypyrrole to diamond.

INTRODUCTION

Electronic and opto-electronic devices are mostly based on inorganic semiconductors (e.g., silicon or germanium) nowadays. This is related with relatively higher cost of materials and industrial processes (high-purity source materials, high-vacuum technology, clean rooms, etc.). A possible way to reduce costs is the use of organic materials with semiconducting or metallic properties. Although the first report on the conductivity of doped polypyrrole (PPy) was published in 1963, the breakthrough is attributed to the studies on doped polyacetylene since 1977 by Heeger, Shirakawa, and MacDiarmid, for which they were awarded the Nobel prize in 2000. Since then we have seen emerging practical applications in energy conversion (organic photovoltaics) as well as in display (OLED, AMOLED) technologies. However, broad application of organic materials is still limited due to unresolved technological and scientific challenges. For instance, photovoltaic effect in organic materials proceeds via generation of strongly bound excitons, unlike in inorganic materials. Due to high dissociation energy (1 eV) and short diffusion length (10 nm) of the excitons, much research effort has been put into optimizing organic-based opto-electronic systems for efficient generation of free charge carriers.

A typical example of promising organic-inorganic (hybrid) systems is the dye-sensitized photovoltaic cell. In this so-called Grätzel cell, a photo-excited organic dye provides electrons to the electrode via porous inorganic TiO_2 . Another, more novel example of an organic-inorganic system being extensively studied is a combination of organic molecules with diamond. Such systems are highly promising not only for opto-electronic [1,2] but also for bio-electronic [3] applications. Inherently, interplay of microscopic structural, chemical, and electronic properties plays crucial role in such systems.

In our studies, we employ and combine advanced scanning probe techniques as well as macroscopic electronic transport characteristics to elucidate these properties and their correlation [4]. We demonstrate benefits of such multi-dimensional characterizations on thin-film hetero-junction of PPy electro-polymerized on hydrogen-terminated diamond, indicating covalent bonding and enhanced exciton dissociation in such systems [2,5-7]. We have chosen PPy as a model of a chemically and optically sensitive organic dye with wide applicability. PPy is a well known material yet it is still a subject of intensive research for diverse applications such as chemical sensors, biosensors, fuel cells, corrosion protection, or rechargeable batteries [8].

2. MATERIAL AND METHODS

We synthesized and grafted the PPy on diamond electrochemically from pyrrole (240 mM) and NaCl (100 mM) aqueous solution. We applied constant current (current density in the order of 0.1 mA/cm²) on a hydrogen-terminated monocrystalline diamond (synthetic IIa CVD diamond) as a working electrode [5]. For electronic transport measurements [7], we defined H-terminated “mesa” structure on a monocrystalline diamond surface by selective oxygen plasma treatment through a photolithographic mask. PPy was then locally electrochemically synthesized on the structure as shown in Fig.1a.

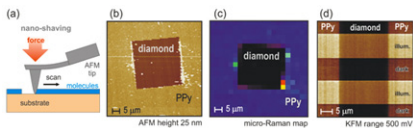
Figure 1.: (a) Diamond device for PPy synthesis and electronic transport measurements (b) Schematic cross-sectional view of PPy-diamond interface and effect of illumination.



RESULTS AND DISCUSSION

To study optoelectronic properties at the PPy-diamond interface we first removed PPy from a small area ($10 \times 10 \mu\text{m}$) using the AFM nanoshaving. We applied contact-mode AFM with increasing contact force. Micro-Raman spectroscopy (excitation wavelength 780 nm, mapping of the intensity at 1600 cm^{-1}) confirmed the removal of PPy. The results are shown in Fig.2. At certain threshold contact force, the sharp tip starts to penetrate and remove the organic film [9]. The threshold force was about 40 nN. This also provided thickness of the PPy layer of about 25 nm. Surface potential measured by KFM on the place where the PPy film had been deposited and removed is significantly lower (by about 0.1 V) than the potential on pristine H-terminated diamond surface. The nanoshaved area and its surroundings were then studied by Kelvin force microscopy (KFM) in the dark and under the white light illumination. Under illumination, the observed positive shifts of surface potentials correspond to a decrease of work function in both PPy and diamond. Such effects were not observed when PPy was deposited on gold. These shifts of surface potentials are attributed to the photovoltage effects that indicate dissociation of excitons at PPy-diamond junction as shown schematically in Fig.1b. This has been supported also by current-voltage and Hall effect measurements [7].

Figure 2.: (a) Scheme of AFM nanoshaving experiment. (b) AFM topography of the nanoshaved area. (c) Micro-Raman map of the nanoshaved area. (d) Local photovoltage effects across the nanoshaved area measured by KFM



The AFM nanoshaving and KFM data are similar to reports on DNA-diamond interfaces [9] and lead to conclusion that PPy molecules are linked to diamond surface covalently via removal of hydrogens on the surface. Studies on B-doped diamond indicate that PPy grows also on oxidized diamond surfaces, yet hydrogen termination is needed for PPy covalent grafting (reported on this conference by Ukraintsev et al.).

CONCLUSION

By correlating AFM nanoshaving, KFM surface potentials, as well as $I(V)$ characteristics, we proved that during the electrochemical synthesis

a covalent bond between diamond and PPy is formed. Such conclusion is difficult to make based on commonly applied techniques such as X-ray photoelectron spectroscopy because here we have all-carbon systems (polymer-diamond). Furthermore, based on microscopic KFM and SPV measurements, the model of charge transfer from PPy to diamond under illumination was proposed. The model was supported by in-plane $I(V)$ and Hall effect measurements.

ACKNOWLEDGEMENT

The work has been supported by GAČR projects P108/12/G108, P108/12/0996, and KAN400100701 (AVČR). The authors appreciate technical assistance of Z. Poláčková, J. Potměšil, V. Jurka, K. Jurek, and J. Zemek.

REFERENCES

- [1] Ouyang T, Loh K, Qi D, et al.: Chem. Phys. Chem. 9 (2008) 1286-1293
- [2] Rezek B, Čermák J, Kromka A, et al.: Diam. Relat. Mater. 18 (2009) 249-252
- [3] Rezek B, Krátká M, Kromka A, et al.: Biosens. Bioelectron. 26 (2010) 1307-1312
- [4] Rezek B, Čermák J, Kromka A, et al.: Nanoscale Res. Lett. 6 (2011) 238
- [5] Čermák J, Rezek B, Kromka A, et al.: Diam. Relat. Mater. 18 (2009) 1098-1101
- [6] Čermák J, Kromka A, Ledinský M, B. Rezek: Diam. Relat. Mater. 18 (2009) 800-803
- [7] Čermák J, Rezek B, Hubík P, et al.: Diam. Relat. Mater. 19 (2010) 174-177
- [8] Mihranyan A, Nyholm L, Bennet A, et al.: J. Phys. Chem. B 112 (2008) 12249-12255
- [9] Rezek B, Shin D, Nakamura T, et al.: J. Am. Chem. Soc. 128 (2006) 3884-3885

CATALYTIC CO-CRACKING OF USED FRYING OILS, MUNICIPAL AND BIO-WASTE

Eduard BUZETZKI¹, Jan RIMARCIK^{1*}, Zuzana CVENGROSOVA¹,
Andrea KLEINOVA¹, Imre SARKOZY², Jan CVENGROS¹

¹ Institute of Physical Chemistry and Chemical Physics, Faculty of Chemical and Food Technology, Slovak University of Technology in Bratislava, Radlinského 9, SK-812 37 Bratislava, Slovakia

² WTS, Győr, Hungary

*jan.rimarcik@stuba.sk

ABSTRACT

Nowadays, treatment of waste is important issue from economical, as well as environmental point of view. Production of liquid fuels based on waste treatment is required. In our work, we have studied catalytic cracking of various wastes (used frying oils – UFO, municipal waste, bio-waste from agriculture) with traditional catalysts (zeolites) and new discovered lignocellulositic bio-catalysts.

INTRODUCTION

With increasing living standard of the population, the amount of waste is increasing both, in the consumer and the manufacturing, sector. Composition of wastes threatens the quality of water, soil and air, as well as public health. The European Union pays great attention to the problem of wastes. Since municipal waste is a blend of various materials, their processing is quite difficult. Specific waste management methods are various chemical and biotechnological processes. At present, the waste as a secondary raw material begins to have increasing importance (production of biomass fuel, ethanol, etc.). Recycling appears to be the most important form of waste utilization. It results in the material recovery. This is an important step not only in environmental point of view, but also in economical one. There is the recovery of raw materials, which do not necessarily originate in renewable sources [1–6].

MATERIAL AND METHODS

Municipal wastes for the testing of catalytic cracking procedure include plastics, paper, wood, textiles, metals, glass, biological waste and water (as the moisture of used material). Agricultural waste for the testing of catalytic cracking includes: corn combs, shrub cuttings, straw, hay, sawdust and reed. They also contain certain amount of water. We have studied used vegetable frying oil, too. Waste samples were collected from local sources. Particle size was adjusted to 5 mm. As the catalyst, natural zeolite or lignocellulosic material with various particle size were used.

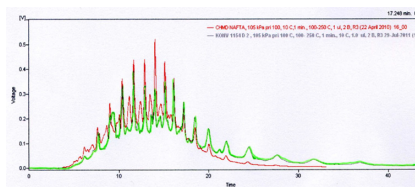
For analytical evaluation of gained cracking liquid products, GLC chromatography using the apparatus Chrompack CP 9000 equipped with packed glass column with 10 % SE 30 on Chro-

matone NAW-DMCS (1.8 m × 3 mm) and with FID, or the apparatus HP 5890 Serie II with FID and a capillary column HP-1 (5 m × 0.53 mm × 2.65 μm) were employed.

RESULTS AND DISCUSSION

Our measurements show that during the catalytic cracking of wastes we have obtained a liquid condensate with a relatively high yield of input material. With an increasing portion of the catalyst, the share of the gas phase and the yield of liquid condensate increased. Simultaneously, the amount of the cracking residue was reduced. In the case of municipal waste, the share of liquid condensate is mainly dependent on the proportion of plastics in the input stream. Obtained liquid condensate was distilled and its fractions were analyzed by GLC chromatography.

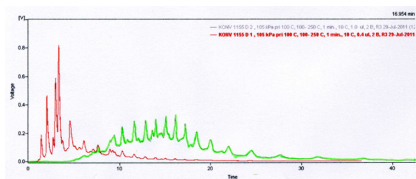
Figure 1.: GLC of diesel fraction gained by cracking with 5% wt. of catalyst (green) compared with fossil diesel (red).



In Fig. 1 chromatogram of diesel fraction (recycled diesel) is confronted with the chromatogram of fossil diesel. General shape of GLC of gained diesel fraction is in agreement with the shape for fossil diesel, recycled diesel fraction contains also heavier fractions. Figure 2 shows comparison of GLC chromatograms for diesel and gasoline fractions obtained from cracking

experiments.

Figure 2.: GLC of diesel (green) and gasoline [6]
(red) fractions gained by cracking with 5% wt.
amount of catalyst.



The by-products from the cracking, cracking residue and gaseous products, can serve as the energy sources, too. Our further study will be focused on the problem of chlorine and aromatic compounds content. Hydrogenation treatment of distilled condensate would solve its acidity and density.

CONCLUSION

Cracking of waste running at temperature range from 390 to 550 °C provided a liquid condensate with a relative high yield of the starting material. The yield depended mainly on the type of used waste. In the condensate, after its distillation we have gained a fuels with typical gasoline and diesel GLC profile, but with higher density in comparison to the fossil diesel.

ACKNOWLEDGEMENT

This program was supported by ESPAN Burgenland Austria; European Union. European Regional Development Fund

REFERENCES

- [1] Buzetzkí E., Sidorová K., Cvengrošová Z., Cvengroš J.: Effect of oil type no products obtained by crackings of oils and fats. *Fuel Proc. Technol.* 92 (2011) 314-323
- [2] Buzetzkí E., Sidorová K., Cvengrošová Z., Cvengroš J.: Catalytic role of municipal waste in fuel production. *Journal of analytical and Applied Pyrolysis* 92 (2011) 314-323
- [3] Buekens A.G., Huang H.: Catalytic plastic cracking for recovery of gasoline-range hydrocarbons from municipal plastic wastes, *Resources, Conservation and Recycling* 23 (1998) 163-181
- [4] Miskolczi N., Bartha L., Deák G., Jóver B.: Thermal degradation of municipal plastic wastes for production of fuel-like hydrocarbons, *Polymer Degradation and Stability* 86 (2004) 357-366
- [5] Buzetzkí E., Sidorová K., Cvengrošová Z., Kaszonyi I., Cvengroš J.: The influence of zeolite catalyst on the products of rapeseed oil cracking. *Fuel Proc. Technol.* 92 (2011)

1623-1631

Scheirs J., Kaminski W.
(Editors): Feedstock recycling and
pyrolysis of wastes plastics. J.
Wiley&Sons, Chichester, UK, 2006

GEOMETRY-BASED DESCRIPTORS OF SUBSTITUENT EFFECT ON BOND DISSOCIATION ENTHALPIES OF ANILINES, PHENOLS AND THIOPHENOLS

Jan RIMARCIK*, Lenka ROTTMANNOVA, Adam VAGANEK, Vladimir LUKES, Erik KLEIN

Institute of Physical Chemistry and Chemical Physics, Faculty of Chemical and Food Technology, Slovak University of Technology, Radlinského 9, SK-812 37 Bratislava, Slovak Republic

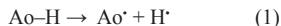
*jan.rimarcik@stuba.sk

ABSTRACT

For mono-substituted anilines, phenols, and thiophenols, it has been found that corresponding N–H, O–H and S–H bond dissociation enthalpies (BDE) depend on Hammett constants approximately linearly. However, for substituents placed in *meta* position, linearity of found dependences is often considerably worse in comparison to *para*-substituted molecules. Therefore, we have found geometry-based descriptor of substituent effect on BDEs.

INTRODUCTION

Anilines, phenols and thiophenols are small aromatic molecules widely used in organic syntheses. They also represent model structures of various primary antioxidants present in living organisms or employed in stabilization of synthetic polymers. Radicals formed after abstraction of hydrogen atom from NH₂, OH and SH groups also represent important intermediates in many biological and industrial applications [1–3]. The first step of the reactive radical termination by a primary antioxidant is hydrogen atom transfer (HAT) from the antioxidant molecule to the reactive radical. This process is governed by corresponding bond dissociation enthalpy (BDE). This thermodynamic quantity contributes to the understanding of antioxidant (AoH) action, which can be expressed using this equation



The study of substituent effect on BDE is important for the comparison of reactions differing only in the substitution. The Hammett equation (and its extended forms) is widely applied in the study and interpretation of various organic reactions. Hammett constants σ_m (for a substituent in *meta* position) and σ_p (for a substituent in *para* position) obtained from ionization of organic acids in solutions can successfully predict equilibrium and rate constants for a variety of families of reactions [4, 5]. Usually, Hammett constants correlate with the changes in N–H, O–H and S–H BDEs for *para*-substituted anilines, phenols or thiophenols well [6–8]. For *meta*-substituted anilines, phenols and thiophenols the linearity of such dependences is worse, correlation coefficients are in 0.85–0.92 range. Besides, published values of Hammett constant

for a substituent may vary in a wide range. In our previous work [6], the linear dependences of O–H BDE on the phenolic C–O bond length, $R(\text{C–O})$, and its shortening after hydrogen atom abstraction, $\Delta R(\text{C–O}) = R(\text{C–O, molecule}) - R(\text{C–O, radical})$ were found. Recently, we have shown that this approach can also be applied for thiophenols [9]. Thus, we have also tried to ascertain the applicability of these simple geometry-based descriptors of substituent effect for *para*- and *meta*-substituted anilines.

COMPUTATIONAL DETAILS

All calculations were performed using the Gaussian 03 program package [10]. The geometry of each compound and corresponding radical was optimized using DFT method with the B3LYP [11] functional without any constraints during geometry optimization (energy cut-off of 10⁻⁵ kJ mol⁻¹, final RMS energy gradient under 0.01 kJ mol⁻¹ Å⁻¹). For the species having more conformers, all conformers were investigated. Calculations were performed in 6-311++G** basis set [12]. The optimized structures were confirmed to be real minima by frequency analysis (no imaginary frequency).

RESULTS AND DISCUSSION

In this work we have used B3LYP/6-311++G** data for 21 *para*- and *meta*-substituted anilines [13]. N–H BDEs were approximated from total electronic energies. Relative BDE values, denoted as DBDE, were obtained as the difference in BDEs of substituted (X–ArNH₂) and non-substituted aniline (ArNH₂)

$$\text{DBDE} = \text{BDE}(X\text{-ArNH}_2) - \text{BDE}(\text{ArNH}_2) \quad (2)$$

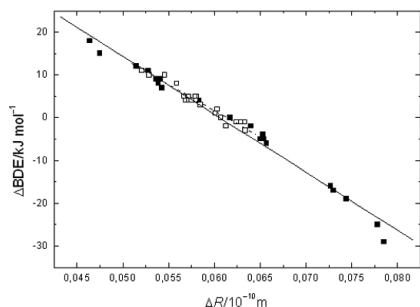
For C–N bond length, $R(\text{C–N})$, in studied anilines, the linearity of found $\Delta\text{BDE} = f(R(\text{C–N}))$ dependences can be considered very good, co-

relation coefficients reached -0.956 and -0.961 for *para*- and *meta*-substituted molecules. Found dependences enable fast prediction of N–H bond dissociation enthalpy from $R(\text{C–N})$. For shortening of C–N bond after $\text{H}\cdot$ atom abstraction

$$\Delta R(\text{C–N}) = R(\text{C–N, molecule}) - R(\text{C–N, radical}) \quad (3)$$

the linearity of found dependences for B3LYP results is even better. Correlation coefficients reached values of 0.991 (*para*) and 0.970 (*meta*), Fig. 1.

Figure 1.: Dependence of ΔBDE values on $\Delta R(\text{C–N})$ for substituents in *para* position (solid squares, solid line) and *meta* position (open squares, dashed line) [13]



Standard deviations of regression parameters confirm that there is no significant difference in the intercepts and line slopes in obtained dependences. For all 42 substituted anilines, following dependence was obtained

$$\Delta\text{BDE}/\text{kJ mol}^{-1} = 82 - 1350 \times \Delta R(\text{C–N})/\text{\AA} \quad (4)$$

with correlation coefficient value of 0.989 . Analogously, for thiophenols, single $\Delta\text{BDE} = f(\Delta R(\text{C–S}))$ dependence is able to describe the effect of substituents in *para* and *meta* positions [9]. On the other hand, *para*- and *meta*-substituted phenols have to be treated separately [6].

CONCLUSION

C–N, C–O and C–S bond lengths or their shortening after hydrogen atom abstraction linearly correlate with N–H, O–H and S–H BDEs in *para*- and *meta*-substituted anilines, phenols and thiophenols, respectively. In the case of *meta*-substituted anilines and thiophenols, the two geometry parameters correlate with BDEs significantly better than Hammett σ_m constants. This fact can be useful also for antioxidants action study, because the three families of aromatic compounds represent the model compounds of primary antioxidants.

ACKNOWLEDGEMENT

This work has been supported by the Slovak Grant Agency VEGA (Projects Nos. 1/0137/09 and 1/1072/11).

REFERENCES

- [1] Halliwell B, Gutteridge J C M: Free Radicals in Biology and Medicine, Oxford University Press, Oxford, 1989.
- [2] Gugumus F: Oxidation Inhibition in Organic Materials, CRC Press, Boca Raton, 1990.
- [3] Zhu Q, Zhang X M, Fry A J: Polym. Degrad. Stab., 57 (1997), 43-50
- [4] Hansch C, Leo A, Taft R W: Chem. Rev., 91 (1991) 165-195
- [5] Krygowski T M, Stępień B T: Chem. Rev., (2005), 105, 3482-3512
- [6] Klein E, Lukeš V: J. Mol. Struct. (Theochem), 767 (2006), 43-50
- [7] Klein E, Lukeš V, Cibulková Z, Polovková J: J. Mol. Struct. (Theochem), 758 (2006), 149-159
- [8] Rimarčík J, Lukeš V, Klein E, Rottmannová J: Comput. Theor. Chem. 967 (2011), 273-283
- [9] Rottmannová L, Vagánek A, Rimarčík J, Lukeš V, Klein E: Acta Chimica Slovaca 5 (2012), 33-37
- [10] Frisch M J, Trucks G W, Schlegel H B et al (2003) GAUSSIAN 03, Revision A.1, Gaussian, Inc., Pittsburgh, PA.
- [11] Becke A D: J. Chem. Phys. 98 (1993), 5648-5652
- [12] Binkley J S, Pople J A, Hehre W J: J. Am. Chem. Soc. 102 (1980), 939-947
- [13] Vagánek A, Rimarčík J, Lukeš V, Klein E: (2012) to be published

STEROLS OXIDATION: C–H AND O–H BOND DISSOCIATION ENTHALPIES

Peter SKORNA, Jan RIMARCIK*, Vladimir LUKES, Erik KLEIN

Institute of Physical Chemistry and Chemical Physics, Slovak University of Technology in Bratislava, Radlinského 9, SK-812 37 Bratislava, Slovakia

*jan.rimarcik@stuba.sk

ABSTRACT

Phytosterols, as components of human diet, received much attention because of their cholesterol-lowering and antioxidant properties. We have theoretically studied three sterols oxidation in terms of C–H and O–H bond dissociation enthalpies (BDE).

INTRODUCTION

Phytosterols (plant sterols) are triterpenes representing important structural components of plant membranes. Free phytosterols stabilize phospholipid bilayers in plant cell membranes. Their structure and function is analogous to cholesterol in animal cell membranes. Most phytosterols contain 28 or 29 carbon atoms and one or two C=C bonds, typically one in sterol nucleus and the second one may be present in the alkyl side chain [1]. Sterols having double bond between C5 and C6 atoms (Fig. 1) in sterol nucleus are called Δ^5 -sterols; Δ^7 -sterols have double bond between C7 and C8 carbons [1]. In our previous work [2], we have theoretically studied BDEs for C–H and O–H bonds splitting-off for the relevant oxidation sites in 15 Δ^5 -phytosterols or Δ^7 -phytosterols and two cholesterol (animal sterols). In this work, we decided to study ergosterol, dehydroergosterol and vernosterol (Fig. 2), which have more than one C=C double bond in the nucleus. Actually, the susceptibility of sterols to oxidation is caused by the presence of C=C double bonds which easily undergo free radical attack followed by hydrogen abstraction on the carbon atoms in α -positions to the double bonds [3, 4].

2. COMPUTATIONAL DETAILS

Calculations were performed using Gaussian 03 program package [5]. The geometries of compounds and corresponding radicals were optimized using DFT method with B3LYP functional [6] without any constraints (energy cut-off of 10^{-5} kJ mol⁻¹, final RMS energy gradient under 0.01 kJ mol⁻¹ Å⁻¹). The calculations were performed in 6-31G* basis set [7]. The optimized structures were confirmed to be real minima by frequency analysis.

Figure 1.: Atom numbering in sterols according to IUPAC.

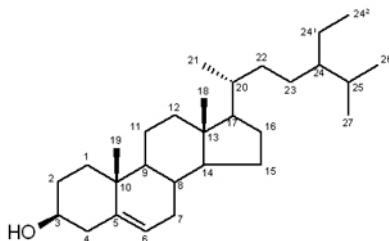
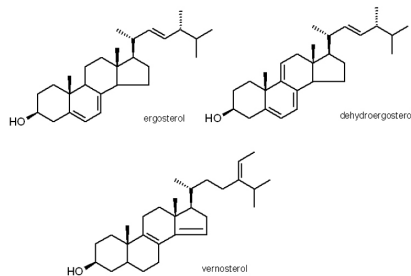


Figure 2.: Studied sterols.



RESULTS AND DISCUSSION

Bond dissociation enthalpy, BDE, is defined as

$$\text{BDE} = H(R\cdot) + H(H\cdot) - H(R-H)$$

where $H(R\cdot)$ is the total enthalpy of the radical, $H(H\cdot)$ is the total enthalpy of the abstracted hydrogen atom, and $H(R-H)$ is the total enthalpy of the molecule at 298.15 K. In our previous work [2] we have shown that chosen computational approach is able to provide reliable C–H BDE values. These are also in agreement to values obtained using larger 6-311++G** basis set – differences do not exceed 2 kJ mol⁻¹ [2]. Used 6-31G* basis set, however, gives lower O–H BDEs than 6-311++G** by ca 20 kJ mol⁻¹ [2].

In three studied sterols, lowest C–H BDEs were found for C–H bonds in α -positions to a C=C bond (Table 1). In ergosterol and dehydro-

roergosterol, hydrogen atom splitting-off from C6 and C7 carbons participating in C5=C6 and C7=C8 double bonds requires considerably higher energy than homolytic dissociation of other C–H bonds. Just for the illustration, in [2] we have calculated several C–H BDEs for methyl groups present in saturated side chains of Δ^5 -cholesterol and Δ^5 -sitosterol. These BDEs reached 406–413 kJ mol⁻¹. In Δ^5 -cholesterol, for selected –CH₂– groups in side chain, BDEs also reached high values (391 and 398 kJ mol⁻¹).

Lowest C–H BDEs reached 276 kJ mol⁻¹ in ergosterol, 296 kJ mol⁻¹ in dehydroergosterol and 317 kJ mol⁻¹ in vernosterol. All these BDEs are related to C–H bonds in nuclei. Lowest values obtained for nuclei of Δ^5 - and Δ^7 -sterols were in the range from 312 to 329 kJ mol⁻¹ [2]. O–H BDEs reached values practically identical with BDEs of Δ^5 -phytosterols and Δ^7 -phytosterols [2].

Table 1: Calculated C–H and O–H bond dissociation enthalpies in kJ mol⁻¹. The lowest value for a molecule is set in bold

Ergosterol		Dehydroergosterol		Vernosterol	
C4–H	292	C4–H	313	C7–H	339
C6–H	453	C6–H	456	C11–H	317
C7–H	455	C7–H	459	C16–H	322
C9–H	300	C12–H	305	C23–H	337
C14–H	276	C14–H	296	C24 ^a –H	346
C20–H	328	C20–H	340	C25–H	343
C24–H	325	C24–H	328		
O–H	394	O–H	395	O–H	398

CONCLUSION

In this work, we have theoretically studied O–H and C–H bond dissociation enthalpies for oxidation attack sites chosen on the basis of experimental reports on the oxidation products of most common sterols. Homolytic dissociation of hydroxyl O–H bond requires considerably larger energy in comparison to studied C–H bonds.

ACKNOWLEDGEMENT

This work has been supported by the Slovak Grant Agency VEGA (Project No. 1/0137/09) and the Science and Technology Assistance Agency (Project LPP-0230-09).

REFERENCES

- [1] Moreau R A, Whitaker B D, Hicks K B: Progress in Lipid Research, 41 (2002), 457-500
- [2] Lengyel J, Rimarčík J, Vagánek A, Fedor J, Lukeš V, Klein E: Food Chemistry, 133 (2012), 1435-1440
- [3] Gugumus F: In Oxidation inhibition in organic materials. (vol. 1), Boca Raton: CRC Press, 1990
- [4] Choe E, Min D B: Comprehensive Reviews in Food Science and Food Safety, 8 (2009),

- [5] Pople J A, et al.: GAUSSIAN 03, Revision A.1, Gaussian, Inc., Pittsburgh, PA, 2003
- [6] Becke A D: Journal of Chemical Physics, 98 (1993), 5648-5652
- [7] Rassolov V A, Ratner M A, Pople J A, Redfern P C, Curtiss L A: Journal of Computational Chemistry, 22 (2001), 976-984

EFFECT OF METALS ON METALLOTHIONEIN CONTENT IN FISH FROM SKALKA AND ŽELIVKA RESERVOIR

Marie SEVČIKOVÁ^{1*}, Helena MODRA¹, Kamila KRUIKOVÁ¹, Zdenka SVOBODOVÁ¹, Olga CELECHOVSKÁ², Rene KIZEK³

¹ Department of Veterinary Public Health and Toxicology, Faculty of Veterinary Hygiene and Ecology, University of Veterinary and Pharmaceutical Sciences, Palackého 1-3, 612 42, Brno, Czech Republic

² Department of Biochemistry, Chemistry and Biophysics, Faculty of Veterinary Hygiene and Ecology, University of Veterinary and Pharmaceutical Sciences, Brno, Palackého 1-3, 612 42, Czech Republic

³ Department of Chemistry and Biochemistry, Faculty of Agronomy, Mendel University in Brno, Zemedelska 1, 613 00 Brno, Czech Republic
*H10374@vfu.cz

ABSTRACT

The aim of this study was to assess the metal content (Hg, Cd, Cu, Ni, Pb, Zn and As) in fish tissues in Skalka and Želivka reservoirs and the ability of metals to induce synthesis of metallothioneins under field conditions. Muscle and liver were used for metal determination. Metallothionein content was measured in muscle, liver and gills of fish. The content of total mercury was significantly higher ($p < 0.05$) in muscle and liver samples from Skalka reservoir than in samples from Želivka reservoir. Methylmercury content was presented as a majority of total mercury in muscle in all samples. Significant differences ($p < 0.05$) between tested sites were observed in copper, lead and arsenic content. Metallothionein liver content was negatively correlated ($p < 0.05$) with total mercury in liver at both reservoirs. The results showed that metallothionein content do not response to high metal contamination, therefore the suitability of metallothioneins in fish as a marker of chronic metal exposure is uncertain under field conditions.

INTRODUCTION

Metal contamination of aquatic environment is a long-term issue, because metals accumulate in aquatic organisms, including fish, and persist in water and sediments [1]. Metallothioneins, low molecular weight proteins rich in cysteine residues, are involved in the regulation of the essential metals and in the detoxification of the non-essential metals [2]. Metallothioneins seem to be a suitable biomarker of metal exposure in fish [3]. The aim of the present study was to assess the effect of metals on metallothionein levels in fish tissues under natural conditions.

MATERIAL AND METHODS

Animals and sampling

The study was carried out at Skalka and Želivka reservoirs. Skalka reservoir had been contaminated by sewage water containing mercury from a chemical factory in Marktredwitz (Germany) since 1974 [4]. Želivka reservoir is considered to be mercury uncontaminated and it is a control locality in this study [5]. Sampling was performed in April 2011 by electro-fishing. A total of 53 fish (8 species) was caught from the Skalka reservoir and 50 fish (11 species) from the Želivka reservoir. Fish were weight and measured, and scales were collected for age determination. Samples of liver, gills and muscle were

taken. The samples were kept at -18°C until the analyses were carried out.

Metal determination

Total mercury content in muscle and liver was determined by the direct method of cold vapours using an AMA 254 (Altec Ltd.) analyser. Methylmercury was determined in muscle in the form of methylmercury chloride by gas chromatography with an electron captured detector GC 2010A. Samples of muscle and liver for determination of Cd, Cu, Ni, Pb, Zn and As, were mineralized in laboratory autoclaves with microwave heating, using nitric acid and hydrogen peroxide. Arsenic was determined by means of AAS hydride technique, determination of Pb, Cd, Cu and Ni was performed by means of AAS electrothermic technique, Zn was determined by means of AAS flame technique.

Metallothionein determination

Levels of MT in liver, gills and kidney were determined by the differential pulse voltammetry Brdicka reaction. Differential pulse voltammetric measurements were performed with 747 VA Stand instrument connected to 693 VA Processor and 695 Autosampler (Metrohm, Switzerland), using a standard cell with three electrodes and cooled sample holder and measurement cell to 4°C (Julabo F25, JulaboDE). A hanging mercury drop electrode (HMDE) with a

drop area of 0.4mm² was the working electrode. An Ag/AgCl/3M KCl electrode was the reference and platinum electrode was auxiliary. For data processing VA Database 2.2 by Metrohm CH was employed. The analyzed samples were deoxygenated prior to measurements by purging with argon (99.999 %) saturated with water for 120 s. Brdicka supporting electrolyte containing 1mM Co(NH₃)₆Cl₃ and 1M ammonia buffer (NH₃(aq) + NH₄Cl, pH = 9.6) was used. The supporting electrolyte was exchanged after each analysis. The parameters of the measurement were as follows: initial potential of -0.7 V, end potential of -1.75 V, modulation time 0.057 s, time interval 0.2 s, step potential 2 mV, modulation amplitude -250 mV, Eads = 0 V, volume of injected sample: 10 µl, volume of measurement cell 2 ml (10 µl of sample + 1990 µl Brdicka solution).

RESULTS AND DISCUSSION

In evaluating differences among the localities, age normalization was used to eliminate differences in sampled fish. In line with expectations, total mercury content and methylmercury content in muscle (Table 1) and liver was significantly higher in various species from Skalka reservoir compared to Želivka reservoir. The results confirm continuing high mercury contamination of the locality.

Table 1: Content of total mercury (THg) and methylmercury (MeHg) in muscle (mean ± SD). Data are adjusted for age. *Significant differences (p < 0.05) are indicated by asterisk.

Species	Skalka reservoir		Želivka reservoir	
	n	THg (mg/kg)	n	MeHg (mg/kg)
asp (<i>Aspinus aspinus</i>)	5	0.395 ± 0.229 *	9	0.391 ± 0.229 *
perch (<i>Perca fluviatilis</i>)	5	0.431 ± 0.070 *	7	0.408 ± 0.072 *
pike (<i>Esox lucius</i>)	5	0.271 ± 0.087 *	7	0.264 ± 0.067 *
pikeperch (<i>Sander lucioperca</i>)	5	0.725 ± 0.793 *	4	0.697 ± 0.671 *
bream (<i>Abramis brama</i>)	5	0.209 ± 0.136 *	9	0.160 ± 0.070 *
chub (<i>Leuciscus cephalus</i>)	5	0.078 ± 0.033	6	0.055 ± 0.022
roach (<i>Rutilus rutilus</i>)	5	0.132 ± 0.024 *	6	0.104 ± 0.051 *

Statistically significant differences (p < 0.05) were found in copper, lead and arsenic content among the sites. Higher copper content (0.061 ± 0.034 mg/kg; mean ± SD) was in muscle of pikeperch from Skalka reservoir. Higher copper content was observed also in liver of pike and bream from Skalka reservoir (0.054 ± 0.024; 0.023 ± 0.008 mg/kg respectively). Possible source of copper can be application of algicide containing copper sulphate widely used in 1970s on the lo-

cality. Lead content in muscle of chub (0.020 ± 0.012 mg/kg) was higher in samples from Želivka reservoir. Although currently an unleaded gasoline is used in Czech Republic, near location of frequent motorway can be a cause of lead pollution [6]. Higher arsenic levels in muscle of perch, roach and chub (0.041 ± 0.019, 0.041 ± 0.031 and 0.019 ± 0.017 mg/kg respectively) and in liver of perch, roach and bream (0.317 ± 0.270, 0.080 ± 0.050 and 0.052 ± 0.020 mg/kg respectively) were measured in samples from Želivka reservoir. Arsenic levels in fish from Želivka reservoir are higher compared to Skalka reservoir. However, the arsenic content in fish tissue is comparable with levels from arsenic-uncontaminated localities [7].

No significant differences were found in metallothionein levels among the localities. Metallothionein concentration in liver was negatively correlated with total mercury content in liver (p < 0.05) in both sites. Negative correlation (p < 0.05) of metallothionein kidney content was observed with cadmium and copper liver content in samples from Želivka reservoir and with total mercury content in muscle and liver in samples from Skalka reservoir.

CONCLUSION

The results showed that metallothionein content does not response to high metal contamination, therefore the suitability of metallothioneins in fish as a marker of chronic metal exposure remain uncertain under field conditions and more well designed studies need to be performed.

ACKNOWLEDGEMENT

The work has been supported by IGA VFU Brno 88/2011/FVHE.

REFERENCES

- [1] Fleeger JW, Carman KR, Nisbet JM: The Science of the Total Environment, 317 (2003), 207–233
- [2] Roesijadi G: Comparative Biochemistry and Physiology, C 113 (1996), 117–123
- [3] Amiard JC, Amiard-Triquet C, Barka S, et al.: (2006): Aquatic Toxicology 76 (2006), 160–202
- [4] Maršálek P, Svobodová Z, Randák T, et al.: Acta Veterinaria Brno, 74 (2005), 427–434
- [5] Kružíková K, Dušek L, Jarkovský J, et al.: International Journal of Electrochemical Science, 6 (2011), 5956–5967
- [6] Legret M, Pagotto C: The Science of the Total Environment, 234 (1999), 1–3, 143–150
- [7] Harkabusová V, Macharáčková B, Čelechovská O, et al.: Czech Journal of Food Science, 27 (2009), S404–406

DEVELOPMENT OF NEW FLUORENSOR FOR SELECTIVE AND SENSITIVE DETERMINATION OF LN(III) IONS

Romana SEVCIKOVA¹, Jakub VANEK^{1,2}, Premysl LUBAL^{1,2*}

¹ Department of Chemistry, Faculty of Science, Masaryk University, Kotlářská 2, 611 37 Brno, Czech Republic

² Central European Institute of Technology, Masaryk University, Kamenice 5, 625 00 Brno, Czech Republic

*lubal@chemi.muni.cz

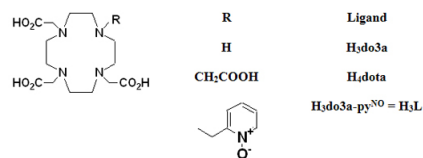
ABSTRACT

The new macrocyclic ligand, H₃do3a-py^{NO}, forms thermodynamically stable and kinetically inert Ln(III) complexes. Its Eu(III) and Tb(III) complexes exhibit a strong long-lived fluorescence as a result of the antenna effect of the pyridine-*N*-oxide fluorophore pendant arm. Using an excitation wavelength of 286 nm, this ligand can be employed as a fluorogenic reagent for the determination of Eu(III) and Tb(III) at pH 6.5 and $c_L = 1$ mM detected luminescence at 615 nm for Eu(III) complex and at 547 nm for Tb(III) complex. Detection limits are at concentrations around 1.0 μ M and linearity of the method spans over 2 orders of magnitude. The method was applied to artificial and real samples (spiked mineral waters, extracts from luminophore CRT dust) with satisfactory results. The method is simple and rapid without interfering other metal ions.

INTRODUCTION

Ln(III) complexes of macrocyclic ligands are utilized in medicine and preclinical research as MRI (Gd), optical (Eu/Tb or Yb/Nd) luminescence in VIS or NIR region) or nuclear probes for diagnostics and/or for cancer treatment (e.g. metal radioisotopes ⁹⁰Y, ¹⁵³Sm, ¹⁶⁶Ho, ¹⁷⁷Lu in nuclear medicine [1]). For biomedical applications, such complexes should exhibit a high thermodynamic stability as well as kinetic inertness under physiological conditions and their knowledge of thermodynamic/kinetic properties (e.g. dissociation rate constants for an estimation of kinetic inertness) is important to evaluate their possible *in vivo* applications. In this work, the kinetic and thermodynamic study of Ln(III) complexes of macrocyclic ligand having the pyridine-*N*-oxide pendant arm (H₃do3a-pyNO, Scheme 1) was carried out and the application of this ligand for determination of chosen Ln(III) ions by molecular fluorescence spectroscopy was proposed.

Scheme 1 The formulas of macrocyclic ligands discussed in the text



MATERIAL AND METHODS

All measurements were carried out on a HP-8453A diode array (Hewlett-Packard, USA), a

Unicam UV2 (ATI Unicam, UK) spectrophotometers and Aminco-Bowman AB2 (Aminco-Bowman, USA) spectrofluorimeter. The studied ligand was synthesized according to procedure described elsewhere [2-4]. Stock solutions of the individual metal cations were prepared by dissolving LnCl₃ compounds (99.9 %; Strem/Alfa) and their Ln(III) content was determined by chelatometric titration.

Formation kinetics of the LnL complexes (Ln = Ce, Eu, Gd, Yb) was followed under ligand excess over metal ion in the pH range 4.0–5.5, at constant ionic strength ($I = 0.1$ M) and temperature 25 °C. Dissociation kinetics of LnL complexes (Ln = Ce, Eu, Gd, Yb) were measured in the range of proton concentration 0.01–3.00 M and ionic strength ($I = 3.0$ M). The experimental data were processed by PRO-K II software.

The real samples for analysis were obtained from industrial extraction process of cathode ray tubes (CRT) and they were analyzed by analytical method mentioned in this contribution. The proposed analytical procedure for determination of Eu(III) ion concentration was tested in presence of other Ln(III) or transition metal ions (Cu(II), Mn(II), Co(II), Fe(II), Ni(II)) in 50-times higher excess) under optimal experimental conditions. The results of chemical analysis were verified by capillary isotachopheresis (CITP) with EA 101 equipment (Villa Labeco, Slovakia) and inductively-coupled plasma atomic emission spectrometry (ICP-AES) with JobinYvon 170 Ultratrace equipment (Horiba, Japan).

RESULTS AND DISCUSSION

The organic reagents employed in analytical chemistry for determination of metal ions should form thermodynamically and kinetically stable complexes therefore the experimental conditions (e.g. concentration of organic reagent, pH, reaction time, etc.) have to be optimized in order to reach a quantitative formation of the metal complexes exhibiting the desired physico-chemical properties. The stability constants of Ln(III) complexes are varied within region 19.8–22.7 which confirm the suitability of the complexes for a quantitative analytical determination of Ln(III) ions [5].

Dissociation kinetics

The studied Ln(III) complexes are kinetically inert and therefore their dissociation study has to be carried out in acidic medium in order to ensure the complete complex decomposition. The dissociation reaction for Ln(III) complexes was studied by molecular absorption spectroscopy due to presence of pyridine-*N*-oxide moiety as chromophoric group having absorption band of the complex about 250 nm which is changed in the course of complex. The characteristic isosbestic points (about 230 and 260 nm) show presence of Ln(III) complex and free ligand in solution. The time-absorbance traces were used for calculation of pseudo-first order rate constants for various experimental conditions and following times for 99% Ln(III) complex dissociation in 3 M acid and temperature 25 °C were found: 0.47 h (Ce), 3.95 (Eu), 5.49 (Gd), 5.24 (Yb). Thus, the manipulation with Ln(III) complexes in a slightly acidic solution does not lead to any dissociation as it is common for the Ln(III) complexes of the open-chain aminopolycarboxylates, e.g. for the Ln(III)-H₃edta complexes.

Formation reaction

The formation of Ln(III) complexes with macrocyclic ligands having pendant arms is usually described by two-step reaction mechanism while the rapid formation of an reaction intermediate (LnL)^{*} in which the Ln(III) ion is bound incompletely by pendant functional groups is followed by slow step where the species are transformed into final product (LnL) [1, 5]. The formation of Ln(III) complexes was studied in pH region 4.5–6.0. It is interesting that Ln(III) ions with HL²⁻ species follow the rate of formation of Ln(III) complex according ionic radius while H₃L⁻ species is reacting 10⁴–10⁵ slower than with HL²⁻ species. The formation of Ln(III) complex is complete within several minutes ($c_L = 10 \times c_{L_0} = 0.1$ mM) as a consequence of a high preorganization and a higher basicity of the macrocyclic ligands.

Application of H₃do3a-pyNO as a fluorosensor

The pyridine-*N*-oxide as strong chromophore ($\approx 10^4$ M⁻¹ cm⁻¹) serves as an antenna for central Eu(III) ion transferring the excitation energy from excited states of organic group to the central ion which lost by radiation emitted from the ion after some time delay. In addition, the hydrophobic pyridine-*N*-oxide pendant arm is somewhat shielding Eu(III) ion from surrounding water molecules which are able to quench fluorescence. In aqueous solution, the complexes contain one coordinated water molecule ($q = 1$). The decrease of number (q) of coordinated water molecules in comparison with [Eu(do3a)] complex ($q = \sim 2$) leads to a longer fluorescence decay from 0.372 ms (H₃do3a complex) to 0.680 ms (H₃L complex). The quantum yield is increased 60-times (1.37×10^{-2} and 2.40×10^{-4} for [Eu(do3a)] and [Eu(L)] complexes, respectively) for the H₃L complex due to a lower extent of non-radiative (vibrational) quenching processes caused by the coordinated water molecules [5].

The physico-chemical and photophysical studies of Eu(III) and Tb(III) complexes show that H₃L is a suitable ligand for fluorimetric determination of both metal ions. Using excitation wavelength 286 nm, the highest selectivity and sensitivity can be achieved by a choice of the suitable wavelength of fluorescence (Eu(III) 615.2 nm and Tb(III) 546.6 nm) while the high slopes of calibration plots (Eu: $(6.71 \pm 0.03) \times 10^6$ M⁻¹, Tb: $(5.73 \pm 0.03) \times 10^6$ M⁻¹) enable a sensitive determination of both Ln(III) ions. Advantage of the method are operating under favourable experimental conditions or the application of one excitation wavelength (286 nm) for both complexes simultaneously in order to improve the sensitivity and limit of detection of fluorimetric determination of both ions in time-resolved mode (it has been tested in our labs but it is more time-consuming procedure). An interference of other Ln(III) ions was also examined where the calibration plot was constructed in presence of 50-times higher concentration of Ce(III), Dy(III), Sm(III), Nd(III), Gd(III), Ho(III) and Yb(III) ions over Eu(III) ion. The sensitivity of fluorimetric Eu(III) determination was slightly decreased and the limit of detection was slightly increased to 3 μM; therefore, the standard addition technique is recommended for an analysis of the real samples containing some other Ln(III) ions.

The described method was also applied for analysis of Eu in real samples obtained from solid CRT waste obtained after treatment of old PC monitors/TV sets. Since the precise content of Eu(III) ion in sample concerning of high excess of Y(III) ions is not known, the samples

were analyzed by ICP-OES and CITP methods. The results mostly agree, therefore this procedure can be employed for control of purity of obtained chemical substances in industrial process. Also the determination of Eu(III) or Tb(III) ions in natural mineral water ("Vincentka") which contains some possible interfering ions in relatively high concentrations (e.g. alkali metal and alkali earth metal ions, transition metal ions - Fe²⁺ and Mn²⁺, halides, hydrogen-carbonate, sulphate, *etc.*) was tested and the results are not loaded by any systematic error.

CONCLUSION

The title ligand, H₂DO3A-py^{NO}, is suitable as analytical reagent for fluorimetric determination of Eu(III)/Tb(III) ions under optimized experimental conditions. Once the formed complex is thermodynamically stable and kinetically inert and thus this property enables us to work with complexes in a relatively acidic medium to make separation from other interfering ions. Introduction of coordinating fluorophor

ACKNOWLEDGEMENT

The work has been supported by Ministry of Education of the Czech Republic (ME09065, CEITEC CZ.1.05/1.1.0/02.0068).

REFERENCES

- [1] Sastri VR, Perumareddi JR, Ramachandra Rao V., Rayudu GVS., Bünzli JC, *Modern Aspects of Rare Earths and their Complexes*, Elsevier, Amsterdam 2003
- [2] Polášek M, Rudovský J, Hermann P, Lukeš I, Elst LV, Muller RN, *Chem. Comm.* (2004) 2602–2603
- [3] Polášek M, Šedinová M, Kotek J, Elst LV, Muller RN, Hermann P, Lukeš I, *Inorg. Chem.* 48 (2009), 455–465
- [4] Polášek M, Kotek J, Hermann P, Císařová I, Binnemans K, Lukeš I, *Inorg. Chem.* 48 (2009), 466–475
- [5] Vaněk J, Lubal P, Ševčíková R., Polášek M, Hermann P, *J. Luminiscence* 132 (2012), 2030–2035

COMPARISON OF CHROMATOGRAPHIC AND IMMUNO DETERMINATION OF LACTOFERRIN

Sylvie SKALICKOVA¹, Ondrej ZITKA¹, Sona KRIZKOVA^{1,2},
Marcela VLKOVA³, Vojtech ADAM^{1,2}, Rene KIZEK^{1,2*}

¹ Department of Chemistry and Biochemistry, Faculty of Agronomy, Mendel University in Brno, Zemedelska 1, 613 00 Brno, Czech Republic

² Central European Institute of Technology, Brno University of Technology, Technicka 3058/10, 616 00 Brno, Czech Republic

³ Department of Clinical Immunology and Allergology, University Hospital, Pekarska 53, CZ-656 91 Brno, Czech Republic

*kizek@sci.muni.cz

ABSTRACT

Lactoferrin is glycoprotein, which is classified to nonspecific immune system of organism. Increased concentration in saliva and other body fluids indicates progressing inflammatory illnesses. The aim of this study was to compare ion exchange chromatography using monolithic column UV-VIS detector with enzyme-linked immunosorbent assay.

INTRODUCTION

Lactoferrin is 80 kDa glycoprotein [1], which has antimicrobial, anti-carcinogenic and anti-inflammatory effects on organism because of its capability to binding and transferring metal ions (Fe, Cu, Zn, Mn) [2]. Enzyme-linked immunosorbent assay (ELISA), high performance liquid chromatographies (HPLC) or various electrochemical assays are mostly used to its quantification but even other methods have been used [3, 4]. Limit of detection by these methods varies within the range from 4.5 to 100 µg/ml [5], [6]. We optimized the method for determination of lactoferrin from human saliva using ion-exchange liquid chromatography (IELC) with monolithic column and off-line photometric detection as a reference method to common ELISA in our experiment. This type of monolithic column is quite different from usual filled chromatographic columns. They are constituted of one piece of porous polymer material which is modified by $-SO_3$ functional groups [7]. The big size of pores (~50 µm) allows separating the protein without their damage or back pressures formation. Detection of isolated fraction was carried out of photometry using Bradford's method.

MATERIALS AND METHODS

Chemicals

Lactoferrin and other chemicals (Trizma base, HCl, NaCl, Ethanol, H_3PO_4 , ACS water, Coomassie brilliant blue) were purchased by Sigma-Aldrich (St. Louis, USA). ELISA kit were purchased from AssayPro (St. Charles, USA) Distilled water was prepared using AquaOsmotic 02 (AquaOsmotic, Tišnov, Czech republic) and subsequently purified by Millipore RG

(MilliporeCorp., USA, 18 MΩ) to deionized (MiliQ) water.

Preparation of samples

For experiment 6 health subjects in age 23 – 28 years were chosen. Saliva was taken using Salivette tubes (Sarstedt, Germany) and centrifuged by 3000 rpm, 5 min (Universal 320, Hettich Zentrifugen, Germany). Supernatant was diluted by Tris-HCl buffer (pH = 7) in ratio 1:1 and subsequently filtered through micro filter (microStar 0.45µm CA, Costar Cambridge).

Ion exchange chromatography with monolithic column and UV detection

Biologic DuoFlow (Biorad, USA) system consists of two chromatographic pumps, monolithic column with CIM disc modified by $-SO_3$ function groups, injection valve, UV-VIS detector and automatic fraction collector. Flow rate of mobile phase was 4 ml/min. The used mobile phase A (MFA) was 25 mM Tris-HCl buffer (pH=7) and mobile phase B 2 M NaCl in MFA (MFB). Fraction containing lactoferrin was collected in elution volume 10.62 – 11.62 ml in acquired volume of the fraction 1 ml. Offline photometric detection was carried out using automatic spectrophotometer BS-200 (Mindray, China) using Bradford's assay.

Enzyme linked immuno-assay (ELISA)

Assay was carried out using commercial ELISA kit (AssayMax Human Lactoferrin ELISA kit, AssayPro, USA). Standard or diluted sample (1000) were adsorbed on polystyrene 96 wells microplate and incubated for 2 hours at 25 °C. After five-times repeated washing of wells with

wash buffer, biotinylated lactoferrin antibody was added to each well and incubated for one hour. After washing the microplate, the 50 μl of streptavidin-peroxidase conjugate per a well was added and incubated for 30 min. Subsequently, the third washing was applied. For detection 50 μl of chromogen substrate was used per a well and incubated for 15 minutes. Finally, 50 μl of stop solution was added. Absorbance was determined on a microplate reader at a wavelength of 450 nm immediately.

RESULTS AND DISCUSSION

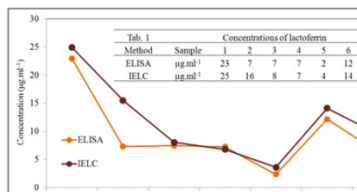
Lactoferrin determination using IELC with off-line photometric detection

Samples were analysed by optimized IELC with monolithic column and off-line photometric detection using Bradford's method [8]. This method is sensitive, with limit of detection 0.1 $\mu\text{g}\cdot\text{ml}^{-1}$. It allows to detect low concentrations of lactoferrin in saliva which numerous papers demonstrates as 0.16 $\mu\text{g}\cdot\text{ml}^{-1}$ [9], 5.16 $\mu\text{g}\cdot\text{ml}^{-1}$ [10], 5.42 $\mu\text{g}\cdot\text{ml}^{-1}$ [11] - 37 $\mu\text{g}\cdot\text{ml}^{-1}$ [12]. Determined concentrations of lactoferrin were $35.52 \pm 7 \mu\text{g}\cdot\text{ml}^{-1}$ with the lowest value $10.89 \pm 3 \mu\text{g}\cdot\text{ml}^{-1}$ and the highest value $74 \pm 5 \mu\text{g}\cdot\text{ml}^{-1}$.

Correlation between IELC with off-line photometric detection and ELISA assay for lactoferrin determination

The commercial AssayMax Human Lactoferrin kit was used for lactoferrin determination by ELISA. Method was carried out according to kit protocol. Calibration was prepared within concentration range from 0.0705 to 1.019 $\mu\text{g}\cdot\text{ml}^{-1}$ with linearity $R^2 = 0.998$. Limit of detection was 0.1 $\mu\text{g}\cdot\text{ml}^{-1}$. Saliva was taken using Salivette test tubes and loaded into wells on microplate on polystyrene table. Coefficient of correlation $R^2 = 0.7576$ was determined by the last squares method. The relation between ELISA and IELC results can be expressed by following equation: $\text{ELISA} = 2.675x \text{ IELC} - 12.168$. Resulting concentration of lactoferrin determined by ELISA was 4.6 $\mu\text{g}\cdot\text{ml}^{-1}$ lower than results from IELC (Fig. 1).

Figure. 1: Correlation between IELC method and ELISA assay. The table 1 shows determined concentration in saliva samples.



CONCLUSION

Determination of lactoferrin using IELC with monolithic column and off-line photometric detection is correlated with ELISA method with correlation dependence $R^2 = 0.907$. IELC determination could be used as a reference method for clinical applied ELISA of lactoferrin determination from saliva samples or other biological fluids.

ACKNOWLEDGEMENT

The work has been supported by Liga proti rakovině Praha 2011, IGA TP6/2012 and CEITEC CZ.1.05/1.1.00/02.0068.

REFERENCES

- [1] Levay P F, Viljoen M, *Haematologica*, 80 (1995), 252-267.
- [2] Arslan S Y, Leung K P, Wu C D, *Oral Microbiol. Immunol.*, 24 (2009), 411-416.
- [3] Zitka O, Horna A, Stejskal K, et al., *Acta Chim. Slov.*, 54 (2007), 68-73.
- [4] Zitka O, Krizkova S, Adam V, et al., *Chem. Listy*, 104 (2010), 197-201.
- [5] Drackova M, Borkovcova I, Janstova B, et al., *Czech. J. Food Sci.*, 27 (2009), S102-S104.
- [6] Campanella L, Martini E, Pintore M, et al., *Sensors*, 9 (2009), 2202-2221.
- [7] Barut M, Podgornik A, Urbas L, et al., *J. Sep. Sci.*, 31 (2008), 1867-1880.
- [8] Seevaratnam R, Patel B P, Hamadeh M J, *Journal of Biochemistry*, 145 (2009), 791-797.
- [9] Lin J C, Borregaard N, Liebman H A, et al., *American Journal of Medical Genetics*, 100 (2001), 145-151.
- [10] Sikorska M H J, Mielnik-Blaszczyk M, Kapec E, *Oral Microbiol. Immunol.*, 17 (2002), 272-276.
- [11] Mukherjee S, Crawford J M, McClear N, et al., *Biological Trace Element Research*, 57 (1997), 1-8.
- [12] Komine K, Kuroishi T, Ozawa A, et al., *Molecular Immunology*, 44 (2007), 1498-1508.

RELATION BETWEEN THIOL

CONTENT AND TUMORS OF PROSTATE AND BRAIN

Sylvie SKALICKOVA¹, Ondrej ZITKA¹, Jarmila KRUSEOVA²,
Jaromir GUMULEC², Michal MASARIK^{2,3}, Sonja KRIZKOVA^{1,3},
Tomas ECKSCHLAGER⁴, Vojtech ADAM^{1,3}, Rene KIZEK^{1,3*}

¹Department of Chemistry and Biochemistry, Faculty of Agronomy, Mendel University in Brno, Zemedelska 1, 613 00 Brno, Czech Republic

²Department of Pathological Physiology, Faculty of Medicine, Masaryk University, Kamenice 5, CZ-625 00 Brno, Czech Republic

³Central European Institute of Technology, Brno University of Technology, Technicka 3058/10, 616 00 Brno, Czech Republic

⁴Department of Paediatric Haematology and Oncology, 2nd Faculty of Medicine Charles University, and University Hospital Motol, V Uvalu 84, CZ-150 06 Praha 5, Czech Republic

*kizek@sci.muni.cz

ABSTRACT

The ratio between oxidized (GSH) and reduced (GSSG) glutathione is considered to be a marker of oxidative damage of an organism. Values of GSH/GSSG below 10 are signal of increased oxidative stress influencing the human organism due to the progressing disease or as a reaction on applied treatment. In our experiment, the GSH/GSSG was determined in patients with brain and prostate carcinoma by high performance liquid chromatography with electrochemical detection.

INTRODUCTION

Cancer is currently one of the most feared diseases. The prevalence is increasing each year not only due to the progress in diagnostics but also due to the environmental influences and life style. One of the most serious forms of this disease is the brain cancer. Medulloblastoma is an embryonal neuroectodermal carcinoma of cerebellum often metastasizes to central neural system (CNS). Statistics states that a successful recovery occurs in 70% of moderate cases [1]. Tumor disease, which occurs 2x more in children patients, ependymoma anaplastic, the most often affects brain cavities and spinal cord. Unlike medulloblastoma in numerous cases radiation therapy is the only applicable treatment method [2]. Prostate cancer is nowadays one of the most often diagnosed diseases in men and the risk increases with age. At the beginning it is manifested in various urination difficulties, however later problems with locomotive system are recognized [3]. It has been proved in numerous experiments that variety of these diseases is caused among others also by oxidative damage of the organism [4]. An important role in biochemical processes equalizing oxidative stress plays glutathione, a tripeptide composed of cysteine, glycine and glutamic acid, which is present in cells of animals, plants and bacteria. Due to its properties it become a marker of oxidative damage [5]. We simultaneously determined glutathione reduced (GSH) and oxidized (GSSG) by high performance liquid chromatography with electrochemical detection (HPLC-ED) and thus its ratio in the blood serum of different types of cancer – ependymoma anaplastic [6], medulloblastoma [7][8][9] and prostate cancer [10].

MATERIAL AND METHODS

Chemicals and pH measurements

Reduced (GSH) and oxidized (GSSG) glutathione, and trifluoroacetic acid (TFA) were purchased from Sigma-Aldrich (St. Louis, USA). HPLC-grade methanol (>99.9%; v/v) was from Merck (Dortmund, Germany) were used. Other chemicals were purchased from Sigma-Aldrich (St. Louis, USA) unless noted otherwise. Stock standard solutions of the thiols (1 mg.ml⁻¹) were prepared with ACS water (Sigma-Aldrich, USA) and stored in dark at -20 °C. Working standard solutions were prepared daily by dilution of the stock solutions. All solutions were filtered through 0.45 µm Nylon filter discs (Millipore, Billerica, Mass., USA) prior to HPLC analysis. The pH value was measured using WTW inoLab Level 3 with terminal Level 3 (Weilheim, Germany).

HPLC-ED analysis

HPLC-ED system consists of two chromatographic pumps Model 582 ESA (ESA Inc., Chelmsford, MA) (working range 0.001-9.999 ml min⁻¹) and chromatographic column with reverse phase Zorbax eclipse AAA C18 (150 × 4.6; 3,5 µm particles, Agilent Technologies, USA) and twelve-channel CoulArray electrochemical detector (Model 5600A, ESA, USA). Detector consists of three flow analytical chambers (Model 6210, ESA, USA). Each chamber contains four analytical cells. One analytical cell contains two referent (hydrogen-palladium), two counters and one porous graphite working electrode. Electrochemical detector is situated

in control module which is thermostated. Sample (20 μ l) was injected by autosampler (Model 542, ESA, USA), which has thermostated space for column. Column was thermostated at 35°C. Flow rate of mobile phase was 1 ml min⁻¹. Mobile phase consists of A: trifluoroacetic acid (80 mM) and B: 100% Met-OH. Compounds were eluted by following linear increasing gradient: 0-1 min (3%B), 1-2 min (10%B), 2-5 min (30%B), 15-16 min (98%B). Detection was carried out at applied potential 900 mV. Time of one analysis was 20 minutes.

Sample preparation

Blood samples were obtained from 29 patients hospitalized at Department of Pediatric Hematology and Oncology of Faculty Hospital Motol with diagnosed solid tumors ependymoma anaplastic (n = 4), medulloblastoma (n = 15) and prostate cancer (n=10). The samples were stored in -80°C until assayed. Samples were diluted in ratio 1:1 by solution of TFA (5 % v/v) and vortexed within 20 seconds. Following centrifugation takes 15 minutes (16400 rpm, 4°C) (Eppendorf centrifuge 5417R). Supernatant was analyzed by HPLC-ED.

RESULTS AND DISCUSSION

Calibration parameters

After that the separation and detection parameters have been optimized, calibration curve was determined for GSH and GSSG in the concentration range 0.2-100 μ M. The dependence of electrochemical signal (peak area in μ C) on concentration was strictly linear with correlation coefficient $R^2 = 0.9997$ for GSH and $R^2 = 0.9936$ for GSSG. Limit of detection for GSH was 0.3 μ M with RSD 3.8 % and 1.2 μ M for GSSG with RSD 5.5%.

Recovery of analysis

The recovery was determined by standard addition method prior to precipitation by 5% TFA and subsequent centrifugation. The concentration of standard solution was 10 μ g/ml for both GSH and GSSG. The recovery in range between 83% and 96% was obtained.

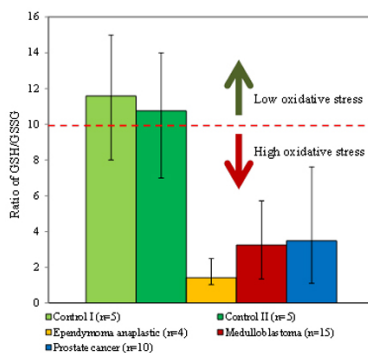
Analysis of patients

The samples of patients and controls were prepared according to the described method and analyzed by high performance liquid chromatography with electrochemical detection. Concentrations of GSH and GSSG determined from chromatograms of samples were recalculated for recovery and the GSH/GSSG ratio was determined. Values of ratios were connected to the group of patients with particular diagnosis and compared with control group.

(Fig. 1). According to the literature the GSH/GSSG ratio in healthy persons is around 10 [11],

which is in agreement with our results of control groups I and II. For control group No. I the lowest value of GSH/GSSG was 8.1 and the highest value was 15.7 with average 11.6. The lowest value of GSH/GSSG in control group II was 7.4, the highest was 13.9 and the average was 10.8. In case of Ependymoma anaplastic, the lowest ratio was 1.03, the highest ratio was 2.49 and the average GSH/GSSG ratio was 1.4, which is 8-times lower comparing to control group I. In the group of patients with medulloblastoma the lowest determined ratio was 1.3, the highest ratio 5.7 and the average value was 3.5, which is 3-times lower. Also in the group of prostate cancer patients the lowest ratio was 1.1 and highest ratio was 7.61 and the average value was 3.9. Our results confirm that long term action of the oxidative stress caused by diseases or certain drugs increases the amount of reduced glutathione and the amount of oxidized glutathione is decreased.

Figure 1: Comparison of oxidative stress between controls I, II; two brain tumors (ependymoma anaplastic, medulloblastoma) and prostate cancer. Age of subjects of control I was 6 – 12 years. Age of subjects of control II was 49 – 62 years. Low ratio of GSH/GSSG of patients shows a high oxidative stress which corresponded with incidence of cancer



CONCLUSION

Samples from three groups of patients suffering from brain cancer (Ependymoma anaplastic and medulloblastoma) and prostate cancer were analyzed using optimized method for determination of GSH and GSSG by HPLC-ED. The method recovery of 86-93% was determined and from obtained concentrations the GSH/GSSG ratio was established. The lowest ratio (average of 1.4) was determined in the group (n=4) of patients suffering from Ependymoma anaplastic. Patients (n=15) diagnosed with medulloblastoma the average ratio of 3.5

was determined. Prostate cancer patients exhibit the average ratio of 3.9. In two control groups of healthy persons, the GSH/GSSG of 11.6 and 10.8 was determined. It can be concluded from the results obtained that different tumor diseases have different impact on the redox status of patients.

ACKNOWLEDGEMENT

The work has been supported by Liga proti rakovině LPR 2011 and GACR CYTORES P301/10/0356.

REFERENCES

- [1] Rousseau A, Mokhtari K, Duyckaerts C, Current Opinion in Neurology, 21 (2008), 720-727.
- [2] Phi J H, Wang K C, Park S H, *et al.*, Journal of Neuro-Oncology, 106 (2012), 619-626.
- [3] Dhanasekaran S M, Barrette T R, Ghosh D, *et al.*, Nature, 412 (2001), 822-826.
- [4] Valko M, Rhodes C J, Moncol J, *et al.*, Chemico-Biological Interactions, 160 (2006), 1-40.
- [5] Laval J, Pathologie Biologie, 44 (1996), 14-24.
- [6] Okcu M F, Selvan M, Wang L E, *et al.*, Clin. Cancer Res., 10 (2004), 2618-2625.
- [7] Louis D N, Ohgaki H, Wiestler O D, *et al.*, Acta Neuropathologica, 114 (2007), 547-547.
- [8] Lin Y H, Chiu J H, Tseng W S, *et al.*, Cancer Chemother. Pharmacol., 57 (2006), 525-532.
- [9] Lee Y Y, Kao C L, Tsai P H, *et al.*, Childs Nerv. Syst., 24 (2008), 987-994.
- [10] Bostwick D G, Burke H B, Djakiew D, *et al.*, Cancer, 101 (2004), 2371-2490.
- [11] Navarro J, Obrador E, Carretero J, *et al.*, Free Radic. Biol. Med., 26 (1999), 410-418.

ELECTROCHEMICAL

BEAD-BASED ASSAY FOR LACTOFERRIN

Dana DOSPIVOVA^{1,2}, Sylvie SKALICKOVA¹, Sona KRIZKOVA^{1,2}, Ondrej ZITKA^{1,2}, David HYNEK^{1,2}, Marketa RYVOLOVA^{1,2}, Rene KIZEK^{1,2*}

¹Department of Chemistry and Biochemistry, Faculty of Agronomy, Mendel University in Brno, Zemedelska 1, 613 00 Brno, Czech Republic

²Central European Institute of Technology, Brno University of Technology, Technicka 3058/10, 616 00 Brno, Czech Republic

*kizek@sci.muni.cz

ABSTRACT

Lactoferrin is an iron-binding antibacterial protein. It is involved mainly in protection of the organism against bacterial infection, thus it is present in many bodily liquids, such as blood, milk, tears, sweat, saliva and urine. Its increased level is used as a marker of inflammation diseases. The aim of this work was to suggest an electrochemical bead-based immunoassay for lactoferrin.

INTRODUCTION

Lactoferrin (LF) is a 80 kDa non-haeme iron-binding protein composed from one polypeptide chain in length of 692 aminoacid residues [1],[2] with isoelectric point (pI) within the range from 8 to 8.5 [3],[4]. Its tertiary structure is composed from two domains with bound divalent heavy metals, mostly Fe²⁺ or Cu²⁺, Zn²⁺ and Mn²⁺ [3],[4]. This protein is present in bodily fluids such as milk, saliva, tears, sweat, blood, ascitic fluid, urine, semen and vaginal secretions, where it is involved in protection of the organism against bacterial infection [3]. Its increased level is used as a marker of inflammation diseases, such as periodontitis, inflammatory bowel disease, diarrhoea, sepsis, peritonitis or eye infection during wearing of contact lenses. Except of LF antibacterial effect, its role in cancer is also investigated. It was found that its antioxidant effect, which is connected with its iron content is responsible for its antitumour activity. Therefore, the increasing of level of lactoferrin in blood is connected to the inflammation processes in the body [5]. For quantitative determination there is commonly used enzyme immunosorbent assay (ELISA) [6],[7],[8], radioimmunoanalysis (RIA) [9],[10] or luminescence based immunoanalysis (LSA) [11]. Next to the prevalently used above-mentioned methods there was also published the determination using other method like electrochemical amperometric detection (LOD = 35 nM) [12] or CE (LOD = 1.3 nM) [12].

The aim of this work was to suggest a paramagnetic bead-based electrochemical immunoassay for LF determination in bodily fluids.

MATERIAL AND METHODS

Bead-based immunoassay

The magnetic beads with protein G (DB-G) (25 µl) were washed twice in the 100 µL of PBS buffer. Goat antibody against lactoferrin (10 µg in 100 µl of PBS) was added to DB-G and the Ab-DB-G complex was incubated for 30 minutes at room temperature in a multi-spin MSC-3000 centrifuge (Biosan, Latvia) to avoid beads sedimentation. After that, unbound antibody was removed and the beads were washed with PBS and were blocked with 0.1 mg/ml of non-specific human IgG. Then the beads were resuspended in 100 µl of PBS with 0.01 % Tween-20 and stored for further usage at 4 °C. Murine monoclonal anti-LF antibody was used for detection of LF captured to the beads after incubation with rabbit anti-mouse HRP-conjugated secondary antibody.

The concentration of detection antibody, incubation times and temperature were optimized.

The efficiency of antibody labelling with AP and functionality of the bead-antigen-antibodies complex was determined by reaction of HRP with a chromogenic substrate (0.9 mM 3,3',5,5'-tetramethylbenzidine (TMB) in HRP substrate buffer (10 µl of hydrogen peroxide (30%, v/v), 0.5 mL of 2 M sodium acetate adjusted to pH 5.8 with 1 M citric acid and 10mL of Milli-Q water) in volume of 100 µl. After 10 min the reaction was stopped with 50 µl of 0.5 M H₂SO₄ and the absorbance was read at wavelength of 450 nm (InfinitePro 200, TECAN, Switzerland).

Tetramethylbenzidine determination

The stock solution of 3,3',5,5'-tetramethylbenzidine (TMB) in concentration of 10 mM was prepared. As electrolyte we used substrate buffer 2.72 g of sodium acetate in 100 ml of water adjusted to pH 5.8 by H₂SO₄. Substrate buffer was 20× diluted before usage as electrolyte. Total volume of the buffer was 2 ml. Electrochemical signal of TMB was analysed using me-

thod of cyclic voltammetry with three electrode connection. Glassy carbon GC electrode was used as working, Ag/AgCl in 3 M KCl was used as referent electrode and a Pt wire was used as counter electrode. GC electrode was polished by alumina emulsion before each usage. Parameters of method were as follows: initial E 0.8 V, final potential -0.6 V, scan rate 0.05 V/s, sweep segments 2, sample Interval 0.001, sensitivity $2 \cdot 10^{-5}$. We used Electrochemical Workstation, CH Instruments (Austin, USA) for acquiring the data. Obtained records were analysed by software chi440a (Austin, USA) and GPES (Metrohm, Switzerland). Analysis of calibration curve of TMB was carried out using method of differential pulse voltammetry where parameters were as follows: initial potential E 0.8 V, final potential -0.6 V, amplitude (V) = 0.05, pulse width (s) = 0.0167, pulse period (s) = 0.2, deposition potential (V) = 0.2, deposition time (s) = 30, sensitivity (A/V) $2 \cdot 10^{-5}$.

RESULTS AND DISCUSSION

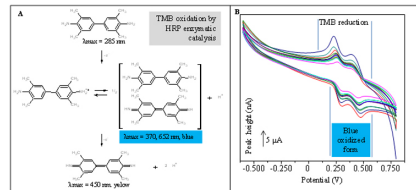
Electrochemical detection is in many cases advantageous, mainly in biosensors construction because of its low price and possibility of field use. Due to this we studied electrochemical properties of 3,3',5,5'- tetramethylbenzidine (TMB) [13], commonly used chromogenic substrate for horseradish peroxidase, a system, which is routinely used for immunodetection.

For observing of redox change of TMB we added 185 μ l of stock solution of TMB into the rest of reagents, which were as follows: 1.9 μ l of H_2O_2 , 92.5 μ l of horseradish peroxidase (HRP) with antibody (diluted 1:10) and finally 1720 μ l of substrate buffer. During the reaction we observed the colour change of the whole solution. At the start of the reaction the solution was colourless but during progress of the reaction it gained a brightly blue colour which subsequently changed to the deeper blue. The electrochemical signal was acquired within 5 minutes interval up to 60 minutes using CV method (Fig. 1). Finally the most sensitive approach was method of DPV, which was also selected for estimation of calibration curve.

In order to achieve quick and selective determination of lactoferrin we chose a bead-based antibody separation based on sandwich ELISA. Polyclonal goat anti-LF antibodies were immobilized to the surface of paramagnetic beads. After blocking with unspecific immunoglobulins the beads were incubated with a sample premixed with monoclonal mouse anti-LF antibodies. After the incubation the beads were washed and incubated with a secondary rabbit anti-mouse HRP conjugate and consequently with chromogenic substrate TMB. For its determination above-mentioned electrochemical detection was used

and the results were controlled spectrophotometrically at 450 nm.

Figure 1: (A) Scheme of the TMB conversion from reduced to oxidized form. (B) Time dependent TMB conversion in presence of H_2O_2 catalysed by HRP of TMB as overlay of CV scans



CONCLUSION

We successfully developed a bead-based immunochemical method of lactoferrin determination, which is suitable for various types of biological matrices. For detection of the end product of enzymatic reaction catalysed by HRP we developed an electrochemical detection as a field-usable alternative.

ACKNOWLEDGEMENT

The work has been supported by NANOSEMED GA AV KAN208130801, CEITEC CZ.1.05/1.1.00/02.0068 and IGA TP 6/2012.

REFERENCES

- [1] Rey, M.W., et al., *COMPLETE NUCLEOTIDE-SEQUENCE OF HUMAN MAMMARY-GLAND LACTOFERRIN*. Nucleic Acids Research, 1990. **18**(17): p. 5288-5288.
- [2] Powell, M.J. and J.E. Ogden, *NUCLEOTIDE-SEQUENCE OF HUMAN LACTOFERRIN CDNA*. Nucleic Acids Research, 1990. **18**(13): p. 4013-4013.
- [3] Levay, P.F. and M. Viljoen, *Lactoferrin - a general-review*. Haematologica, 1995. **80**(3): p. 252-267.
- [4] Lonnerdal, B. and S. Iyer, *LACTOFERRIN - MOLECULAR-STRUCTURE AND BIOLOGICAL FUNCTION*. Annual Review of Nutrition, 1995. **15**: p. 93-110.
- [5] Sukharev, A.Y., et al., *IMMUNOCHEMICAL STUDIES OF SALIVARY LACTOFERRIN*. Klinicheskaya Laboratornaya Diagnostika, 2009(4): p. 38-39.
- [6] Sato, R., et al., *Plasma lactoferrin concentration measured by ELISA in healthy and diseased cows, in International Congress Series; Lactoferrin: Structure, function and*

- applications*. 2000. p. 111-116.
- [7] Shinmoto, H., et al., *Competitive ELISA of bovine lactoferrin with bispecific monoclonal antibodies*. *Bioscience Biotechnology and Biochemistry*, 1997. **61**(6): p. 1044-1046.
- [8] Yoshise, R.E., et al., *Profiles of bovine lactoferrin in the gastrointestinal tracts of rats as observed by ELISA, Western blotting and SELDI-affinity MS*. *Milchwissenschaft-Milk Science International*, 2007. **62**(4): p. 446-450.
- [9] Sykes, J.A.C., et al., *PLASMA LACTOFERRIN LEVELS IN PREGNANCY AND CYSTIC-FIBROSIS*. *Clinica Chimica Acta*, 1982. **122**(3): p. 385-393.
- [10] Boxer, L.A., et al., *LACTOFERRIN DEFICIENCY ASSOCIATED WITH ALTERED GRANULOCYTE FUNCTION*. *New England Journal of Medicine*, 1982. **307**(7): p. 404-410.
- [11] Maacks, S., H.Z. Yuan, and W.G. Wood, *DEVELOPMENT AND EVALUATION OF LUMINESCENCE-BASED SANDWICH ASSAY FOR PLASMA LACTOFERRIN AS A MARKER FOR SEPSIS AND BACTERIAL-INFECTIONS IN PEDIATRIC MEDICINE*. *Journal of Bioluminescence and Chemiluminescence*, 1989. **3**(4): p. 221-226.
- [12] Campanella, L., et al., *Determination of Lactoferrin and Immunoglobulin G in Animal Milks by New Immunosensors*. *Sensors*, 2009. **9**(3): p. 2202-2221.
- [13] Volpe, G., et al., *3,3',5,5'-tetramethylbenzidine as electrochemical substrate for horseradish peroxidase based enzyme immunoassays. A comparative study*. *Analyst*, 1998. **123**(6): p. 1303-1307.

STUDY OF INTERACTION OF QUANTUM DOTS WITH METALLOTHIONEIN USING DIFFERENTIAL PULSE VOLTAMMETRY

Sylvie SKALICKOVA¹, Lukas NEJDL¹, Ondrej ZITKA¹, David HYNEK^{1,2}, Libor JANU¹, Jaromir HUBALEK^{2,3}, Jarmila ZIDKOVA⁵, Vojtech ADAM^{1,2}, Libuse TRNKOVA⁴, Rene KIZEK^{1,2*}

¹Department of Chemistry and Biochemistry, Faculty of Agronomy, Mendel University in Brno, Zemedelska 1, 613 00 Brno, Czech Republic

²Central European Institute of Technology, Brno University of Technology, Technicka 3058/10, 616 00 Brno, Czech Republic

³Department of Microelectronics, Faculty of Electrical Engineering and Communication, Brno University of Technology, Technicka 10, CZ-616 00 Brno, Czech Republic

⁴Department of Chemistry, Masaryk University, Kotlarska 2, 611 37 Brno, Czech Republic

⁵Department of Biochemistry and Microbiology, Institute of Chemical Technology, Prague, Technicka 3, 166 28 Prague, Czech Republic

*kizek@sci.muni.cz

ABSTRACT

Quantum dots (QDs), are emerging as a new class of fluorescent agent for biochemical, medicinal or other purposes. QDs based on cadmium or else heavy metal composition can be risky for an organism. In the organism cadmium can be neutralized by protein metallothionein (MT). MT is cysteine rich and the chelation of other metals including essential zinc is well described. For the reason of high affinity of metallothionein to cadmium ions we attempted to develop an approach for study of possible interaction with (QDs). We prepared QDs with Cd-Te core and studied the interaction with Apo-MT, which was prepared from Cd immunized rabbit. For determination of Cd ions concentration in QDs we used method of differential pulse voltammetry (DPV) and for study of complex of QDs with Apo-MT we used DPV – Brdicka's reaction.

INTRODUCTION

Interaction of inorganic based nanomolecules with biomolecules as proteins can lead to pathological states or can be used for biomedicine applications. In many technologies the cadmium usage is very frequent. Nanotechnology is an emerging field of human activity which begins to take a stronger position in industry. In nanotechnology field the quantum dots, tiny light-emitting particles on the nanometre scale are emerging as a new class of fluorescent agent for studying of in vivo imaging [1]. The quantum dots are very often consisting of ions of cadmium and ions of other metal such as Selenium, tellurium or zinc. If the nontoxic quantum dot is modified by recognition molecule such as antibody it can be used as specific identification and visualisation of necrotic lesion or tumour region [2]. The toxicity of quantum dots is predominantly caused by releasing of Cd²⁺ ions due to deterioration of the CdSe lattice [3]. Metallothionein which is an animal protein is rich in content of cysteine aminoacids [4] and therefore it is also electrochemically active and suitable for sensitive detection [5] [6]. Thanks to this fact it is able to bind number of metal ions especially essential zinc or toxic cadmium [7]. Its structure

is divided to two domains and it can bind 7 divalent or 12 monovalent metal ions [8]. For the reason of high affinity of metallothionein to cadmium ions we attempted to develop an approach for study of possible interaction with quantum dots. In this work we isolated metallothionein from rabbit liver using approach published elsewhere. Then we prepared Apo-MT which served as chelating agent for QDs. Quantum Dots with Cd-Te core were prepared according to [9]. We attempted to study the complex creation between MT and QDs. For that purpose we used spectrophotometric and electrochemical method of differential pulse voltammetry. Subsequently we used the fast protein chromatography for purification of protein-quantum dot conjugates. The intensity of fluorescence of our prepared QDs in high ionic strength was also evaluated before the experiment.

MATERIAL AND METHODS

All chemicals of ACS purity used were purchased from Sigma Aldrich Chemical Corp. (Sigma-Aldrich, USA), unless noted otherwise. Fast protein separation system Biologic Duoflow (Biorad, USA) was used for MT isolation and for separation of MT-QD complex. Gel filtration column (HiLoad 26/60, GE Healthcare,

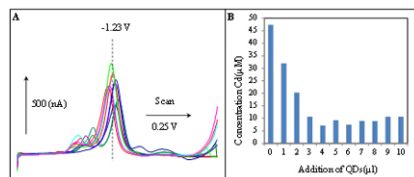
Uppsala Sweden), dosing valve with 2 ml loop, Four channel UV-VIS detector (Quadtec, Biorad, USA) and automated fraction collector (Biorad, USA) were used. As mobile phase for separation we used 150 mM NaCl in 10 mM Tris-HCl buffer (pH 8.6) Mobile phase flow rate was 4 ml.min⁻¹. As external calibrator we used a BSA 1 mg/ml. MT was obtained from rabbit liver after Cd administration. Then we extracted the MT using fast protein liquid chromatography (FPLC). Signal of MT was monitored at 254 nm according to [10]. Isolated fractions were subsequently analysed by SDS-PAGE and dot blot. After dialysis we lyophilized the fractions and obtained pure MT but containing Cd ions. For removing Cd ions from MT to obtaining Apo Mt we used procedure according to [4]. Spectrophotometric analysis of complexes was carried out with by UV-VIS spectrophotometer Specord 210 (Analytik Jena, Germany). Experimental conditions were adopted according to papers [4] and [11] and further optimized. QD's were prepared according to Duan et al. [9]. Cadmium chloride solution (CdCl₂, 0.04 M, 4 ml) was diluted to 42 ml with ultrapure water, and then trisodium citrate dihydrate (100 mg), Na₂TeO₃ (0.01 M, 4 ml), MPA (119 mg), and NaBH₄ (50 mg) were used. Synthesis was carried out in microwave reactor under 400 W (Multiwave3000, Anton-Paar GmbH, Austria). Repurification of QD's was carried out using isopropanol condensing. The QD's was mixed with isopropanol in ratio 1:2 and then centrifuged 10 minutes under 25 000 rpm (Eppendorf centrifuge 5417R). Supernatant (clear QD's) was than resuspended in initial volume of Tris-HCl Buffer pH 8.5. For electrochemical determination Differential Pulse Voltammetry [12] with μ AUTOLAB III (EcoChemie, Netherland) in connection to VA-Stand 663 (Metrohm, Switzerland) was used. Method of Differential Pulse Voltammetry-Brdicka's reaction was used according to [12]. Fluorescence spectra were acquired by multifunctional microplate reader Tecan Infinite 200 PRO (TECAN, Switzerland). 350 nm was used as an excitation wavelength and the fluorescence scan in the range from 400 to 750 nm was measured every 2 nm. The fluorescence pictures were obtained by In vivo Xtreme system by Carestream, USA.

RESULTS AND DISCUSSION

Firstly we determined the concentration of Cd ions in Cd-Te QDs, which we prepared. We found that concentration of Cd ions in stock solution of QDs was 68 μ M. Then we mixed QDs with Apo-MT in volumes 60 μ l (Apo MT) and 120 μ l of phosphate buffer (pH 7.5, 20 mM). For study of interaction we used the mixture of both components MT (0.5 μ M): QD's(0, 0.74, 1.48, 2.96, 5.92, 11.84 and 23.68 μ M). The addition of QDs was

made using one millilitre volume from stock solution. The mixtures were studied by spectrophotometry within the range from 200 to 750 nm with observable maximum in 260 and 505 nm. Same mixtures were also studied by electrochemical method of Brdicka's reaction (Fig. 1A), which supported data from spectrophotometry. Concentration of QDs based on cadmium signal is shown in Fig. 1B. Subsequently we used the fast protein chromatography for purification of protein-quantum dot conjugates. The intensity of fluorescence of our prepared QDs in high ionic strength was also evaluated before the experiment. We obtained the different chromatograms for Apo MT, QDs and MT-QD complex. MT-QD complex exhibited rather lower retention than only MT and only QDs. This is due to higher molecular mass and thus higher permeation in molecular sieve of the column. However the FPLC signal of free MT was negligible at 245 nm due to absence of Cd or aromatic amino acids in its amino acid structure. Thanks to this fact we observed only MT-QD and QDs signals in the chromatogram.

Figure 1: (A) Electrochemical analysis of QD-MT conjugates by Brdicka's reaction. (B) Change of concentration of Cd(II) after addition of QD to MT.



CONCLUSION


In this work we isolated and prepared Apo-MT, synthesized the QDs and then made interaction study documented by UV-VIS spectra, supported by electrochemical analysis and finally confirmed by FPLC separation of prepared conjugates of quantum dots with metallothionein.

ACKNOWLEDGEMENT

The work has been supported by NANO-SEMED GA AV KAN208130801, NanoBioTECell GA ČR P102/11/1068 and CEITEC CZ.1.05/1.1.00/02.0068.

REFERENCES

- [1] Gao X H, Yang L L, Petros J A, et al., *Curr. Opin. Biotechnol.*, 16 (2005), 63-72.
- [2] Chen F Q, Gerion D, *Nano Lett.*, 4 (2004), 1827-1832.
- [3] Derfus A M, Chan W C W, Bhatia S N,

- 
- Nano Lett., 4 (2004), 11-18.
- [4] Adam V, Krizkova S, Zitka O, et al.,
Electroanalysis, 19 (2007), 339-347.
- [5] Adam V, Baloun J, Fabrik I, et al., Sensors, 8
(2008), 2293-2305.
- [6] Petrova J, Potesil D, Mikelova R, et al.,
Electrochim. Acta, 51 (2006), 5112-5119.
- [7] Cosson R P, Amiardtriquet C, Amiard J C,
Water Air Soil Pollut., 57-8 (1991), 555-567.
- [8] Coyle P, Philcox J C, Carey L C, et al., Cell.
Mol. Life Sci., 59 (2002), 627-647.
- [9] Duan J L, Song L X, Zhan J H, Nano Res., 2
(2009), 61-68.
- [10] Demuyneck S, Grumiaux F, Mottier V, et
al., Comp. Biochem. Physiol. C-Toxicol.
Pharmacol., 144 (2006), 34-46.
- [11] Yue S, Zhong W Q, Zhang B L, et al., J. Inorg.
Biochem., 62 (1996), 243-251.
- [12] Diopan V, Shestivska V, Zitka O, et al.,
Electroanalysis, 22 (2010), 1248-1259.

ELECTROCHEMICAL IMMUNOSENSORS FOR DETECTION OF MICROORGANISMS IN BIOAEROSOLS

Petr SKLADAL^{1,2,*}, David KOVAR², Vit KRAJICEK¹,
Jan PRIBYL², Eva SVABENSKA²

¹ Department of Biochemistry, Faculty of Science, and ² CEITEC MU Masaryk University, Kamenice 5, 625 00 Brno, Czech Republic

*skladal@chemi.muni.cz

ABSTRACT

Electrochemical immunosensors for detection of microbial strains of *Escherichia coli* and *Bacillus atrophaeus* (cells and spores) is described. The portable detector was combined with the cyclone air sampler to detect bioagents in aerosols. The capture antibody was immobilised on gold electrodes, antibody-peroxidase conjugate served as tracer. In buffer, the immunosensor measured 10^3 to 10^8 CFU/mL in 30 min. Detection in air was realised in chambers. Automated dissemination of cells, sampling and measurement allowed testing of the cyclone / immunodetector combination, 150 CFU/L in air was indicated in 20 min.

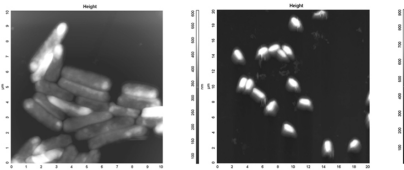
INTRODUCTION

The growing requirements on detection of bioagents originated from field military operations, however, the current interest comes mainly from civil rescue and security services, protection of public buildings and homeland security. Development of portable, rapid and simple instrumentation based on the bioanalytical detection principles is widely supported. Various types of immunochemical devices are preferred for the early response, good sensitivity and continuous monitoring capabilities. Electrochemical sensors for bioagents represent a promising alternative approach combining highly sensitive, cheap and easily miniaturised format with excellent specificity of antibodies. The prototype device ImmunoSMART was tested for detection of microbial cells in bioaerosols. The safe bioagents were adopted including the strain *Escherichia coli* DH5a and *Bacillus atrophaeus* cells and spores. For bioaerosols, a special closed chamber with physical sensors as well as particle counter for reference data was constructed.

MATERIAL AND METHODS

The screen-printed electrodes modified with specific antibodies against the target microbes were constructed. Sensors were used in a flow-through cell and linked to the detector ImmunoSMART (Smart Brno). Sampling of bioaerosols was carried out using the cyclone SASS 2300 (Research International). Cultivated cells of *E. coli* and *B. atrophaeus* were centrifuged and suspended in phosphate buffer (50 mM, pH 7.0). Spores of *B. atrophaeus* were stored in the presence of calcium ions (20 mM). The microbes were imaged using atomic force microscope Ntegra Vita (Figure 1) and after fluorescence labelling using optical microscope Olympus BX41.

Figure 1.: Atomic force images of *Bacillus atrophaeus* cells (left) and spores (right).



RESULTS AND DISCUSSION

The electrochemical immunosensors operated in the sandwich format (Figure 2); the antibody covalently linked to the electrode surface captured the microbes and after washing, the cells were labelled using the peroxidase-antibody conjugate. The signal was generated in the presence of hydrogen peroxide and iodide, the enzymatically produce iodine was measured amperometrically at -50 mV. For example, the cells of *E. coli* were successfully measured from 1000 to 10^8 CFU/ml (Figure 2). In case of *B. atrophaeus* cells and spores, the capture antibody (9 types were tested) did not formed sufficiently stable immunocomplexes with the cells and/or spores, thus limiting sensitivity of the assay. For bioaerosols tests, two versions of aerosol chambers (67 and 1 m³ internal volume) were used, the latter being constructed in our laboratory was suitable for automated and remotely controlled operation (Figure 3). The microbes spread inside the cells were captured by cyclone, transferred to the amperometric immunodetector and measured. Reference data confirming presence and amount of microbes inside the chamber included slit sampler with agar cultivation and particle counting based on light scattering.

Figure 2.: Calibration curve of the electrochemical immunosensor for *E. coli*. The empty point in brackets indicates the background signal (in the absence of cells). The schematic view of the sandwich assay realized on the gold sensing electrode is shown in the inset.

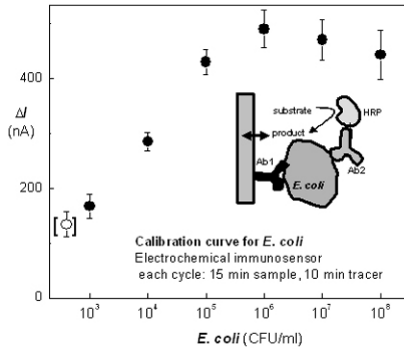
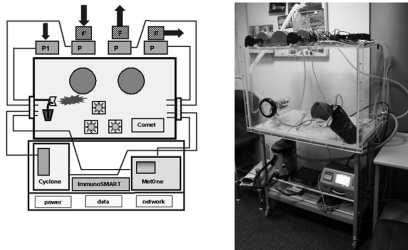


Figure 3.: Schema (left) and picture (right) of the constructed bioaerosol chamber.



CONCLUSION

The parallel monitoring of cells demonstrated the presence of 150 CFU/l in air and this level was clearly indicated by the tested cyclone / immunodetector system. This amount of microbes detected in 20 min seems promising for future field tests.

PREPROCESSING AND CLASIFICATION OF ELECTROPHORETIC GEL IMAGE USING DYNAMIC TIME WARPING

Helena SKUTKOVA^{1*}, Martin VITEK¹, Rene KIZEK², Ivo PROVAZNIK¹

¹ Department of Biomedical Engineering, Brno University of Technology, Technicka 3058/10, 616 00 Brno, Czech Republic

² Department of Chemistry and Biochemistry, Faculty of Agronomy, Mendel University in Brno, Zemedelska 1, 613 00 Brno, Czech Republic

*skutkova@feec.vutbr.cz

ABSTRACT

The automatization of a classification process of the electrophoresis gel image is a very difficult problem, because the result depends on the quality of the gel image digitalization, but also on imprecisions in an electrophoretic process. Our methodology proposes approach of removing the most of image distortions and also solves the problem of un-uniformity in an electrophoretic process.

INTRODUCTION

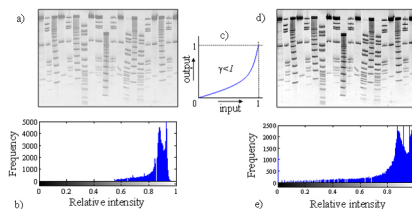
The gel electrophoresis is a known technique in molecular biology suitable for separating macromolecules according to their molecular weight. The result of the gel electrophoresis – the electrophoretogram is usually digitalized for subsequent analysis. The common requirement for analyzing of electrophoretic gel image is evaluation of similarity between samples recorded in gel.[1-2] The mutual similarity between samples of microbial organisms in combination with a cluster analysis can be interpreted as a relationship of microorganisms. In this case, the result of the similarity analysis in the form of dendrogram is phylogenetic tree.

The cluster analysis of the image record of electrophoretic gel depends on the quality of digitalization of the gel image, but also on the imprecisions in electrophoretic process such as the unequal samples application, the gel consistency, the samples contamination, uneven speed of samples migration etc. These imprecisions occurring in a gel image must be removed or compensated before the cluster analysis by image preprocessing [3]. This article presents methodology for preprocessing of electrophoretic gel images. The combination of chosen image filtering techniques for improvement of image quality increases identification of individual bands, but the greatest benefit is the application of the dynamic time warping (DTW). The individual lanes in a gel image include a lot of the same bands, but even small variances in their positions can product errors in comparison stage. These errors increase in comparison of samples from several gel records. The application of DTW before the comparative analysis adjusts the positions of similar bands in a gel record for the better similarity evaluation.

MATERIAL AND METHODS

The image quality improvement

Figure 1: The enhancement of image contrast using nonlinear monotone transformation with gamma correction of the grayscale image histogram. a) The original electrophoretic gel image. b) Grayscale histogram of the original image. c) The transformation function with γ correction for modification of intensity values range. d) Enhanced image of electrophoretic gel. e) Grayscale histogram of the enhanced image transformed by using $\gamma=0.65$.



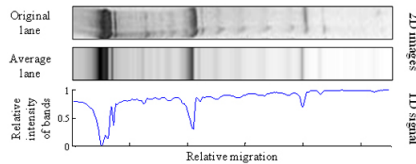
The classical problem of gel image records is a low contrast of bands and background. This problem can be solved by the transformation of the image histogram. The gel image is represented by the grayscale image.[3] The grayscale histogram represents the number of pixels (frequency) in image which have the same grayscale level. The relative intensity of the grayscale is defined on range $<0, 1>$, when 0 corresponds to black color and the white color has value of 1. The nonlinear transformation function with gamma correction can unequally distribute the number of pixels at each grayscale level. The gamma parameter lower than 1 increases contrast of dark colors and higher than 1 conversely. The operation of image contrast enhancement using

the gamma correction function with settings $\gamma =$ values 0.65 is shown in the Figure 1.

Conversion of 2D grayscale image to 1D signal representation

The individual lanes in the grayscale image of electrophoretic gel describe distribution of black bands in the lane depending relative migration speed. The transformation of the grayscale to the range of $<0, 1>$ and the relative migration speed to a timeline allows interpret the grayscale lane as 1D signal (Figure 2). The signal representation can be obtained for every lane crosscut. The average signal constructed from each crosscut signal was used to remove lane distortions. The average lane in Figure 2 was constructed from the average signal. The average lanes (signals) were used for next signal analysis.[4]

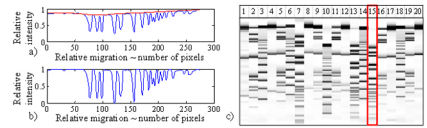
Figure 2.: The principle of conversion of 2D grayscale image of one lane in electrophoretogram to 1D signal: the relative intensity of bands is in the range of values from 1 (white) to 0 (black)



The balance of the background level

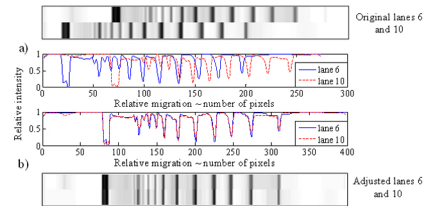
The individual lanes have often different background for example due to: samples contamination, exposure process or differences in processing of multiple gels. The comparison of lanes requires the normalization of grayscale levels and removing of the unequal background. For this purpose, we propose a special filtration technique. The first step of the filtration is the estimate of upper signal envelope which is specific for every signal (Figure 3 a). The signal envelope presents unequal gray background of the gel lane. The removal of envelopes compensates the lanes background and highlight black bands. The final step after background balance is a normalization of maximal and minimal level of gray to the same value for all lanes (Figure 3 b). The image after the background balance and the normalization of gray levels is shown in the Figure 3 c.

Figure 3.: Removing of the non-uniform background of electrophoretic lanes. a) The signal of the lane 15 (blue) with estimation of the signal envelope (red). b) The signal of the lane 15 with removed envelope and normalized range of values. c) The gel image after removal of the lanes envelope and normalization of the range of lanes



The adjustment of the mutual positions of bands using DTW

Figure 4.: The adjustment of bands positions between two lanes using DTW. a) The image of two lanes containing similar bands which are not positionally aligned (upper) and the signal representation of these two lanes (lower). b) The positional adjustment of signal peaks between two lanes (upper) and an adequate image representation of adjusted lanes (lower)



The dynamic time warping is mostly used for the speech analysis. [5] The same spoken word in the speech of different people has the same meaning (signal has the same shape), but its timing and offset is specific for each person. The dynamic time warping method can adapt the timing and offset of signals. [6] This property can be used for adjustment of bands positions between two gel lanes. The DTW adapts positions of the same bands but the specificity of each lane is maintained. The principle of adjustment using DTW is shown in the Figure 4. The Figure 4 a) shows two very similar lanes with different migration speed in image and signal representation. The classical similarity analysis evaluates only a small amount of mutual similarity in this case. The application of DTW on signal form of these two signals in Figure 4 b) modifies lengths of signals for positional adjustment. The adapted signals were again converted to the image form. The similarity between these adapted signals is very high.

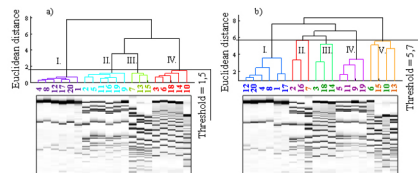
The similarity analysis of gel lanes

The similarity between lanes is represented by a dendrogram. The Ward method was used as a clustering algorithm for the dendrogram reconstruction. The mutual similarity of each

pair of lanes was determined using Euclidean distances. [1-2]

RESULTS AND DISCUSSION

Figure 5.: Classification of electrophoretic lanes by a mutual similarity. Color coded clusters in the dendrogram correspond to the results of classification techniques, color coded numbers of lanes correspond to the true values of similarity. a) The result of a cluster analysis with using DTW. b) The result of a cluster analysis without DTW



The result dendrograms were reconstructed for both cases: with using DTW (Figure 5 a) and without DTW in the Figure 5 b). The positions of lanes in gel image were reordered according to the dendrogram classification. The comparison between color codes of clusters in dendrogram and correct classification which is shown by color code of lanes numbers is perfect with using DTW. The classification by Ward method applied on mutual Euclidean distances of lanes without using DTW [1-2] gives result with many inaccuracies. The lanes with some offset to others were classified to wrong clusters for example lanes 6, 7, 10 (the original order of lanes is in Figure 3.) The similarity between clusters II and IV in the Figure 5 b) should be evaluated much earlier in the tree topology. The decision threshold in the tree with DTW is also lower than without DTW, it corresponds to the fact that the lanes with DTW have a much bigger similarity.

CONCLUSION

The combination of our proposed filter technique with DTW applied to the electrophoretic gel image allows very precise classification of individual gel lanes. A lot of image distortions and imprecisions in electrophoretic process were removed. The often problem of wrong classification of two very similar lanes with different migration speed was solved by positional adaptation of lanes using DTW.

ACKNOWLEDGEMENT

This work was supported in part by: GAČR 102/09/H083, GAČR P102/11/1068.

REFERENCES

- [1] Shadle, S.E. et all.: Nucleic acids research. 25 (1997), 4, 850-60.
- [2] Amp, F. and Miambi, E. International journal of food microbiology. 60 (2000), 1, 91-7.
- [3] Bajla, I. and Hollander, I. Measurement science

review. 1, 1 (2001), 5-10.

- [3] Zhang, T.: Biotechnology letters. 22 (2000), 399-405.
- [4] Sakoe, H. and Chiba, S.: IEEE Transactions on Acoustics, Speech, and Signal Processing. 26 (1978), 1, 43-49.
- [5] Giorgino, T.: Journal of Statistical Software. 31 (2009), 7, 1-24.

CAPILLARY ELECTROPHORESIS CHIP FOR DNA DETECTION

Jan SLAVIK¹, Vojtech SVATOS², Marian MARIK¹, Jan PEKAREK^{1,2}, Jana CHO-
MOUCKA^{1,2}, Rene KIZEK² and Jaromir HUBALEK^{1,2*}

¹ Department of Microelectronics, Faculty of Electrical Engineering and Communication, Brno
University of Technology, Technicka 3058/10, 616 00 Brno, Czech Republic

² Central European Institute of Technology, Brno University of Technology, Technicka 3058/10,
616 00 Brno, Czech Republic

*hubalek@feec.vutbr.cz

ABSTRACT

The aim of this paper is to introduce arrangement microfluidic chip for DNA detection, made of polydimethylsiloxane (PDMS) and glass. Design of this chip is based on commercially available chip from the company Agilent Technologies. The chip was fabricated in our laboratory using silicon template prepared by microfabrication using wet etching and polymerization of DMS. Second part of the chip contains electrodes on a glass substrate.

INTRODUCTION

One of the trend in analytical techniques, is their miniaturization. Research in miniaturization is driven mainly by reducing cost of analysis by reducing the amount of used reagents. Recently, microfluidic devices become an effective tool for the analysis of biological material such as DNA, proteins, etc. Different kinds of such chips are already commercially available. Due to the optical characteristics, chemical compatibility and well-development fabrications, these chips are usually made of glass. PDMS is an even more suitable material for these applications. The combination of glass substrates and PDMS layers is currently used for microfluidic chips fabrication very often. [1, 2]

MATERIAL AND METHODS

Design of capillary electrophoresis chip for DNA detection is matching DNA LabChip from the company Agilent Technologies. The commercial DNA LabChip is made from glass. Microchannels are manufactured on the glass substrate using photolithography and wet etching. Sealing of the microchannels is done by thermal bonding with top glass substrate with holes for accessing microchannels to reagents and samples. These holes create reservoirs. Capillary electrophoresis electrodes are not integrated in the DNA LabChip, but they are part of another device.

Our chip is fabricated from PDMS layer with microchannels and glass substrate with capillary electrophoresis electrodes. The patterns of desired structures, i.e., microchannels, inlet and outlet, are simultaneously transferred into this layer via standard photolithography process. Then the liquid PDMS prepolymer (Sylgard 184 silicone elastomer base and curing agent are mixed in a

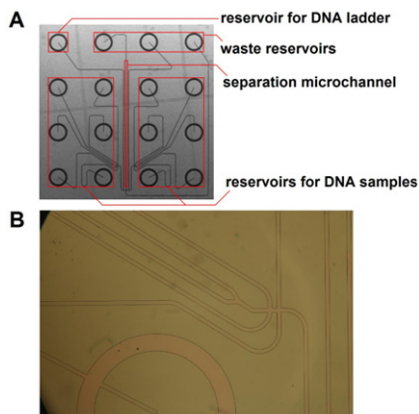
10:1 weight ratio) is poured onto positive resist mold (Microresist S1813). After complete curing at room temperature for 24hours, the PDMS layer with inverse structures has been transferred from the mold. The electrodes are manufactured by photolithography, wet etching and thermal vacuum evaporation. Reservoirs are created by mechanical pricking of PDMS layer. Optical detector is located in the end part of separation microchannel. The size of the chip is 17,8 x 17,8 mm. Reagents can be used similar to that of capillary electrophoresis.

RESULTS AND DISCUSSION

Our chip has capillary electrophoresis electrodes incorporated directly on glass substrate, and upper layer is made from PDMS. Using PDMS for microfluidic have several advantages. PDMS is a cheap, flexible and mechanically strong material, transparent from 240 nm to 1100 nm with low autofluorescence. PDMS is also permeable to gas and biocompatible [3]. **The aim is to compare** described chip with DNA LabChip from Agilent Technologies. LabChip is designed to analysis of DNA fragments to determine their size and concentration. It can perform up to 12 analysis in approximately 30 minutes.

Silicon mold and microchannels arrangement are depicted in Figure 1.

Figure 1: Photographs of (A) etched silicon mold for PDMS (B) magnified microchannels of silicon mold



CONCLUSION

This paper describes PDMS capillary electrophoresis chip based on commercial available chip - DNA LabChip. In the next step we would like to compare functions of this chip with DNA LabChip.

ACKNOWLEDGEMENT

This work has been supported by project KAN208130801 (NANOSEMED), project GACR 102/08/1546 (NANIMEL) and project NANOE CZ.1.07/2.3.00/20.0027 and CEITEC CZ.1.05/1.1.00/02.0068.

REFERENCES

- [1] McDonald J, Duffy D, Anderson J, et al.: *Electrophoresis*, 21 (2000), 1, 27-40
- [2] Yassine O, Morin P, Dispagne O, et al.: *Analytica Chimica Acta*, 609 (2008), 2, 215-222
- [3] Mata A, Fleischman A, Roy S: *Biomedical microdevices*, 7 (2005), 4, 281-293

OPTIMIZATION OF DNA ISOLATION USING MAGNETIC MICROPARTICLES

Simona DOSTALOVA¹, Kristyna SMERKOVA², Marketa RYVOLOVA^{2,3}, Jaromir HUBALEK^{3,4}, Libuse TRNKOVA⁵, Vojtech ADAM^{2,3}, Rene KIZEK^{2,3*}

¹Department of Biomedical Engineering, Faculty of Electrical Engineering and Communication, Brno University of Technology, Kolejní 4, 612 00 Brno, Czech Republic

²Department of Chemistry and Biochemistry, Faculty of Agronomy, Mendel University in Brno, Zemedelska 1, 613 00 Brno, Czech Republic

³Central European Institute of Technology, Brno University of Technology, Technicka 3058/10, 616 00 Brno, Czech Republic

⁴Department of Microelectronics, Brno University of Technology, Technicka 2, 616 00 Brno, Czech Republic

⁵Department of Chemistry, Masaryk University, Kotlarska 2, 611 37 Brno, Czech Republic

*kizek@sci.muni.cz

ABSTRACT

The aim of this work is optimization of DNA isolation by magnetic microparticles. Used microparticles have surface with silica-like chemistry. Partial steps of the isolation procedure including washing, immobilization and elution were optimized. Electrochemical analysis by square-wave voltammetry was employed for detection of the yield of DNA.

INTRODUCTION

Isolation of nucleic acid is one of the most important technique for molecular biology [1]. There are many methods for separation of DNA, like phenol-chloroform extraction [2] or adsorption on silica in the presence of a chaotropic salt [3]. But these methods can be time consuming, laborious and cross-contamination can occur. That is the reason why experiments with magnetic particles (MPs) are carried out [4, 5]. MPs are structures which have paramagnetic or superparamagnetic properties and their size is in the range from nano- to micrometers. The advantage is that MPs react to an external magnetic field and their surface can be chemically modified. According to the type of this modification specific isolation of the biomolecules, viruses or cells is ensured [6]. Except isolation, MPs have several another potential applications. Such as targeted gene delivery [7] or drug delivery, tissue repairing [8] or magnetic resonance imaging [9]. For isolation of DNA the silica-like surface of MPs is used and the magnetic separation is based on electrostatic interaction of DNA with surface. This separation is simple and very effective [10]. For these facts this work deals with isolation of DNA using magnetic particles.

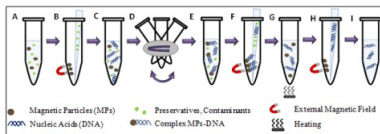
MATERIAL AND METHODS

Magnetic separation

The whole magnetic separation a total of four steps contains: washing, immobilization, washing and elution (Fig. 1).

Figure 1: Diagram of DNA isolation by magnetic particles: **A** MPs in suspension with pre-

servatives **B** Washing MPs to remove preservatives **C** Adding sample with DNA **D** Vortexing and centrifuging **E** Immobilization of DNA to MPs **F** Washing MPs with coupled DNA to remove contaminants **G** Heating MPs to elution DNA **H** Pipetted away of DNA **I** Purified DNA



Washing procedure

MPs in a storage solution with preservatives (10 μ l) were transferred to the test-tube in magnetic stand (DynaL MPC-S, Dynal, Norway). After adhesion of MPs to the test-tube wall the storage solution was pipetted out. Subsequently, 20 μ l of washing solution (phosphate buffer) was added and MPs were resuspended by. Then the washing solution was pipetted out using magnetic field. MPs were washed three times.

Immobilisation

In this step DNA is binding to MPs. 10 μ l of sample (PCR product sized 500 bp) and 10 μ l of immobilisation buffer were added to MPs. Immobilisation was carried out for 5 minutes with shaking.

Washing procedure

After immobilisation MPs were again three times washed with 5M NaCl.

Elution

30 μ l of elution buffer (Tris-EDTA) was added to MPs coupled with DNA. Elution took 15 minutes. After adhesion MPs to the test-tube wall by magnetic force the solution with purified nucleic acids was pipetted to clean test-tube.

Electrochemical detection

For determination of the DNA yield electrochemical analysis was used. Electrochemical measurements were performed with AUTOLAB PGS30 Analyzer (EcoChemie, Netherlands) connected to VA-Stand 663 (Metrohm, Switzerland) using a standard cell with three electrodes. A hanging mercury drop electrode (HMDE) with a drop area of 0.4 mm² was employed as a working electrode. An Ag/AgCl/3M KCl electrode served as the reference electrode. Pt electrode was used as the auxiliary electrode.

Adsorptive transfer technique was used for the electrochemical determination DNA. The adsorptive transfer technique is based on the sample accumulation (120 s) onto the working electrode surface and consequently on the electrode washing and square wave voltammetric (SWV) measurement. SWV measurements were carried out in the presence of acetate buffer pH 5.0. SWV parameters: potential step 5 mV, frequency 280 Hz, time of accumulation 120 s.

RESULTS AND DISCUSSION

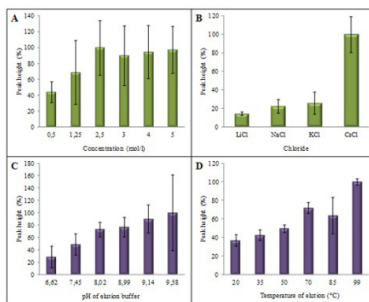
For obtaining maximal yield of PCR product during isolation using magnetic microparticles the immobilisation and elution solutions and conditions were optimised. From each experiment the peak, which had highest value, was determined as 100 %.

Optimization of immobilisation

Effect of concentration of NaCl in the immobilisation solution is illustrated in Fig. 2A. The highest yield of DNA was reached using 2.5 M NaCl in the immobilisation solution. Relative standard deviation (RSD) was 34 %. The best repeatability was obtained using 0.5 M NaCl (RSD 13.2 %) but the yield was only 44 %. With the increased concentration of NaCl and by its ionic strength the amount of isolated DNA is increasing.

The effect of ionic strength of immobilisation solution was further observed. Solutions of chlorides of different alkali metals were tested. Their concentration was 2.5 M. The highest yield of DNA was obtained using CsCl in the immobilisation solution (Fig. 2B). The amount of DNA increased with increasing relative atomic mass and ionic strength.

solutions and conditions on the yield of DNA: **A** Effect of concentration NaCl in the immobilisation solution **B** Effect of alkali metals **C** Effect of elution solution pH **D** Effect of elution temperature



Optimization of elution

The pH of elution solution (Tris-EDTA) was optimised (Fig. 2C). With the increasing pH of elution solution the yield of DNA increased. The highest amount of isolated DNA was observed with value of pH 9.6 but the RSD was high (61 %). The value of 9.1 was determined as an optimal pH, because the yield of isolation was 89.9 % and RSD was 22.7 %. Finally, the effect of elution temperature was observed (Fig. 2D). With increasing the temperature the increase of isolated amount of DNA was observed. The highest yield of DNA was reached by temperature 99 °C. The reproducibility at this temperature expressed as RSD was 3.5 %.

CONCLUSION

This work deals with the isolation of DNA using magnetic microparticles. The immobilisation and elution solutions and conditions were optimised for maximization the yield of isolated DNA. Fast and simple technique was developed. This method can be use to further study of nucleic acids.


ACKNOWLEDGEMENT

The work has been supported by NANIMEL GA ČR 102/08/1546, NANOSEMED GA AV KAN208130801, NanoBioTECell GA ČR P102/11/1068, IGA IP19/2012 and CEITEC CZ.1.05/1.1.00/02.0068.

REFERENCES

- [1] Guyot C, Stieger B, J. Hepatol., 55 (2011), 1368-1376.
- [2] Coombs N J, Gough A C, Primrose J N, Nucleic Acids Research, 27 (1999), 3.
- [3] Yang D Y, Eng B, Wayne J S, *et al.*, Am. J. Phys. Anthropol., 105 (1998), 539-543.

Figure 2: Effect of immobilisation and elution

- 
- [4] Berensmeier S, Appl. Microbiol. Biotechnol., 73 (2006), 495-504.
 - [5] Cler L, Bu D W, Lewis C, *et al.*, Mol. Cell. Probes, 20 (2006), 191-196.
 - [6] Hsing I M, Xu Y, Zhao W T, Electroanalysis, 19 (2007), 755-768.
 - [7] Scherer F, Anton M, Schillinger U, *et al.*, Gene Ther., 9 (2002), 102-109.
 - [8] Gupta A K, Gupta M, Biomaterials, 26 (2005), 3995-4021.
 - [9] Yezhelyev M V, Gao X, Xing Y, *et al.*, Lancet Oncol., 7 (2006), 657-667.
 - [10] Kang K, Choi J, Nam J H, *et al.*, J. Phys. Chem. B, 113 (2009), 536-543.

UTILIZATION OF PROTEIN-QUANTUM DOTS INTERACTION FOR VISUALIZATION OF PROTEINS AFTER SDS-PAGE ELECTROPHORESIS

Sona KRIZKOVA^{1,2}, Libor JANU¹, Natalie MATIJESCUKOVA¹, Marketa RYVOLOVA^{1,2}, Jaromir HUBALEK^{2,3}, Vojtech ADAM^{1,2}, Rene KIZEK^{1,2*}

¹Department of Chemistry and Biochemistry, Faculty of Agronomy, Mendel University in Brno, Zemedelska 1, 613 00 Brno, Czech Republic

²Central European Institute of Technology, Brno University of Technology, Technicka 3058/10, 616 00 Brno, Czech Republic

³Department of Microelectronics, Brno University of Technology, Technicka 2, 616 00 Brno, Czech Republic

*kizek@sci.muni.cz

ABSTRACT

Polyacrylamide gel electrophoresis in the presence of sodium dodecyl sulphate (SDS-PAGE) is one from the most commonly used separation technique for complicated protein samples. The aim of this study was to test the utilization of unspecific interaction of quantum dots with proteins for their staining in SDS-PAGE gel.

INTRODUCTION

Sodium dodecyl sulphate polyacrylamide gel electrophoresis (SDS-PAGE) as one of the most commonly used separation technique for proteins uses Coomassie-blue [1] or silver staining [2] for detection of protein in the gel. These methods vary in the sensitivity and time required for analysis. Compared to silver staining Coomassie-blue staining is not so laborious, it is quantitative, but it has lower sensitivity. Both staining methods are hardly reversible and incompatible with further analysis like mass spectroscopy, thus their numerous modifications have been developed [3, 4]. Except this other methods compatible with western-blotting are used like imidazole-zinc salts [5], SYPRO, amidoblack or fluorescent stains [6]. Colloidal and semicolloidal nanocrystals, referred as quantum dots or QD have attracted much attention because of potential applications in biological markers by combining the advantages of ultrasensitive photoluminescence, high photobleaching threshold, good chemical stability and tuneable spectral properties [7, 8].

Interaction of bare QD with proteins is known and it has been previously used for proteins staining in the gel. The authors used red CdTe QD for proteins detection after native electrophoresis [9]. The aim of this study was to test the utilization of unspecific interaction of red and yellow CdTe quantum dots with proteins for their staining in SDS-PAGE gel.

MATERIAL AND METHODS

SDS-PAGE

The electrophoresis was performed according

to Laemmli [10] using a Mini Protean Tetra apparatus (Bio-Rad, USA). First 12.5 % (*m/V*) running, then 5 % (*m/V*) stacking gel was poured. The polymerization of the running or stacking gels was carried out at room temperature for 45 min. Prior to analysis, the samples were mixed with reducing (3% β -mercaptoethanol) sample buffer in a 2:1 ratio. The samples were boiled for 2 min, and then 4 μ l of the sample was loaded onto a gel. The electrophoresis was run at 150 V for 1 h (Power Basic, Biorad USA) in tris-glycine buffer (0.025 M Trizma-base, 0.19 M glycine and 3.5 mM SDS, pH = 8.3). Gels were stained with rapid Coomassie-blue method according to Wong et al. [11] and then the gels were re-stained with silver [2].

QD synthesis

QDs were prepared according to [12]. Briefly, 4 ml CdCl₂ (0.04 ml/l) was diluted to 42 ml with ultrapure water, then trisodium citrate dihydrate (100 mg), 4 ml Na₂TeO₄ (0.01 mol/l), 98 μ l mercaptopropionic acid (MPA), and NaBH₄ were added under magnetic stirring. Then the samples were subjected to microwave irradiation. Parameters were as follows: Yellow QDs – 300 W, 20 min. (constant irradiation). Red QDs – 280 W, 130 °C, 35 min (constant temperature 130°C). Purification was performed by isopropanol precipitation.

QD staining

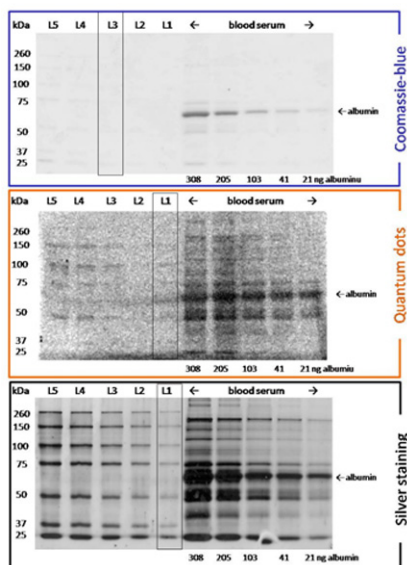
After electrophoresis the gels were washed three-times in distilled water for 5 min. Then the gels were immersed in 0.1 M NaOH with 1.25 % quantum dots (*v/v*) and 0.27 % TEMED (*v/v*) for 30 min. The bands were visualized on

UV transilluminator at wavelength of 312 nm and photographed.

RESULTS AND DISCUSSION

Two types of quantum dots, which differed in their size and therefore in emission wavelengths, were synthesized. The emission maximum of red QD was 619 nm, the emission maximum of yellow QD was 580 nm. Both types were used for proteins staining. In order to improve stability of QD in the solution and to enhance their fluorescence, TEMED in concentrations of 0, 0.5, 0.15, 0.3, 0.5 and 0.7 % (v/v) was added [13]. The best result was obtained with 0.3 % TEMED and after 30 min incubation. Yellow QD performed much better than red, possible reason is their lower size, which allows them to penetrate quickly to the gel. Comparison of yellow QD, silver and Coomassie-blue staining of protein standards and human serum is shown in Fig. 1. It is obvious that after QD staining even the lowest proteins concentration corresponding to 21 ng of albumin could be visualized. The Coomassie-blue staining allowed us to detect 10 × higher proteins concentration (205 ng of albumin) in blood serum. Compared to silver staining, QD staining has lower sensitivity, but it is considerably less time-consuming and laborious. Sensitivity of the staining with quantum dots can be further improved using more sophisticated detection system.

Figure 1.: Comparison of Coomassie-blue, QD- and silver-staining of SDS-PAGE gels.



CONCLUSION

Utilizability of red and yellow fluorescent quantum dots for proteins staining in SDS-PAGE gels was tested. For this purpose yellow QD are more suitable than red because their size.

ACKNOWLEDGEMENT

The work has been supported by IGA MENDELU TP6/2012, NANIMEL GA ČR 102/08/1546 and CEITEC CZ.1.05/1.1.00/02.0068. The authors wish to express their thanks to Natalie Matiješčuková for excellent technical assistance.

REFERENCES

- [1] Blakesley R W, Boezi J A, *Analytical Biochemistry*, 82 (1977), 580-582.
- [2] Oakley B R, Kirsch D R, Morris N R, *Analytical Biochemistry*, 105 (1980), 361-363.
- [3] Shevchenko A, Wilm M, Vorm O, *et al.*, *Analytical Chemistry*, 68 (1996), 850-858.
- [4] Gharahdaghi F, Weinberg C R, Meagher D A, *et al.*, *Electrophoresis*, 20 (1999), 601-605.
- [5] Fernandezpatron C, Castellanoserra L, Rodriguez P, *Biotechniques*, 12 (1992), 564-&.
- [6] Antharavally B S, Carter B, Bell P A, *et al.*, *Analytical Biochemistry*, 329 (2004), 276-280.
- [7] Mattoussi H, Mauro J M, Goldman E R, *et al.*, *Journal of the American Chemical Society*, 122 (2000), 12142-12150.
- [8] He H, Qian H F, Dong C Q, *et al.*, *Angew. Chem.-Int. Edit.*, 45 (2006), 7588-7591.
- [9] Na N, Liu L, Taes Y E C, *et al.*, *Small*, 6 (2010), 1589-1592.
- [10] Laemmli U K, *Nature*, 227 (1970), 680-&.
- [11] Wong C, Sridhara S, Bardwell J C A, *et al.*, *Biotechniques*, 28 (2000), 426-+.
- [12] Duan J L, Song L X, Zhan J H, *Nano Res.*, 2 (2009), 61-68.
- [13] Huang C G, Na N, Huang L Y, *et al.*, *J. Proteome Res.*, 9 (2010), 5574-5581.

INTERACTIONS OF BIOTINYLATED OLIGONUCLEOTIDES WITH STREPTAVIDIN-MODIFIED QUANTUM DOTS STUDIED BY CAPILLARY ELECTROPHORESIS WITH UV DETECTION

Maja STANISAVLJEVIC¹, Libor JANU¹, Marketa RYVOLOVA^{1,2}, Marie STIBOROVA³, Tomas ECKSCHLAGER⁴, Vojtech ADAM^{1,2}, Rene KIZEK^{1,2*}

¹Department of Chemistry and Biochemistry, Faculty of Agronomy, Mendel University in Brno, Zemedelska 1, CZ-613 00 Brno, Czech Republic

²Central European Institute of Technology, Brno University of Technology, Technicka 3058/10, CZ-616 00 Brno, Czech Republic

³Department of Biochemistry, Faculty of Science, Charles University, Albertov 2030, CZ128 40 Prague 2, Czech Republic, European Union

⁴Department of Paediatric Haematology and Oncology, 2nd Faculty of Medicine Charles University, and University Hospital Motol, V Uvalu 84, CZ-150 06 Praha 5, Czech Republic

* kizek@chemi.muni.cz

ABSTRACT

Capillary electrophoresis detection of created complex between biotinylated oligonucleotides and streptavidin modified QDs and its behaviour through the time is the aim of this paper.

For CE detection capillary electrophoresis system with absorbance detection was employed.

INTRODUCTION

Quantum dots (QDs) are 1-10 nm nanoparticles with unique size-depending optical and electronic properties [1]. They are new fluorescent materials, which can be used instead of organic dyes for biological labelling. They have better photostability, narrow emission and continuous absorption spectra than organic dyes [2]. QDs applications are wide as for early detection of cancer, for drug delivery, *in vivo* imaging and targeting and many others [3-7]. Due to the toxicity of their inorganic core, the surface of QDs has to be chemically modified [8]. After modification QDs are suitable for conjugation with biomolecules, such as proteins, fragments of DNA or RNA or others molecules [9-10]. In this work the study of interaction between streptavidin-modified QDs and biotinylated oligonucleotides by capillary electrophoresis is presented.

MATERIAL AND METHODS

All chemicals were purchased by Sigma Aldrich (Czech Republic) in ACS purity. Solutions were made using MiliQ water (Milipore, Czech Republic).

QDs synthesis

CdTe QDs were prepared by microwave synthesis (using microwave system by Anton Paar) and capped by mercaptopropionic acid (MPA) according to the following procedure: the solution of CdCl₂ (4 ml, 0.04 M) was mixed with Na₂TeO₃ (4 ml, 0.01 M), 100 mg of sodium citrate and 50 mg NaBH₄, 119 mg MPA and 42 ml

of H₂O. The mixture was heated by microwave radiation for 10 minutes (300 W).

Streptavidin modification

100 µl of MPA capped CdTe QDs were diluted to 1 ml and the pH was adjusted to 6 by MPA solution. Streptavidin solution (9.6 µl, 5 mg/ml) was added and the solution was intensively agitated for 60 minutes. Subsequently the solution was centrifuged for 80 minutes at 25000 rcf. The supernatant was disposed and the precipitated QDs were dissolved in 100 µl of water.

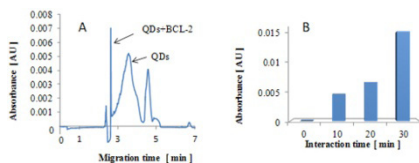
CE-UV

Electrophoretic measurement was done using capillary electrophoresis system (Beckman P/ACE 5500) with absorbance detection at 214 nm. Uncoated fused silica capillary with total capillary length of 47 cm, effective length of 40 cm and internal diameter of 75 µm was used. 20 mM borate (pH 9) was used as background electrolyte. Separation was carried out at 20 kV and the sample was injected hydrodynamically for 20 seconds using 3.4 kPa. Sample of oligonucleotide BCL-2 was mixed with quantum dots in 1:1 ratio and the final concentration of oligonucleotide was 5 µM. Biotinylated oligonucleotide specific for hepatitis B virus (VHB-biotin) was mixed with quantum dots in 1:1 ratio and the final concentration of VHB-biotin was 5 µM, subsequently an oligonucleotide with sequence complementary to VHB-biotin (VHB-CP) was added. VHB-CP had final concentration of 0.077 µM.

RESULTS AND DISCUSSION

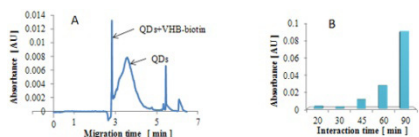
The formation of complex between quantum dots and biotinylated oligonucleotides created through the streptavidin-biotin linkage can be studied by CE. The complex is present as a sharp peak unlike the signal of QDs, which are represented by broad peak. The time dependence of formation of the complex showed that the kinetics is relatively slow. CE analysis of mixture of streptavidin coated QDs and biotinylated fragment BCL-2 is shown in Fig. 1. The sharp signal of complex is observed. The presence of other (non-labelled) peaks in Fig. 1A is caused by the presence of streptavidin excess. The signal enhanced with the increasing time of interaction (Fig. 1B).

Figure 1 A) CE of BCL-2 and QDs mixture, B) Time dependence of the signal intensity of BCL-2-QDs complex



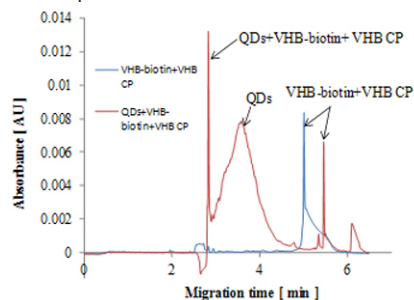
Based on results shown above, the interaction of streptavidin QDs with DNA fragment specific for hepatitis B virus (VHB-biotin) was investigated (Fig. 2A). Created complex between quantum dots and VHB-biotin through the streptavidin-biotin linkage appeared as high, sharp signal, which grows with time (Fig. 2B).

Figure 2 A) CE of VHB-biotin and QDs mixture B) Time dependence of signal intensity of VHB-biotin-QDs complex



After adding a complementary DNA sequence fragment (VHB-CP) to already created complex of quantum dots and VHB-biotin it is noticed that complex signal increased significantly (Fig. 3) indicating that two complementary DNA sequences fragment interacted. This interaction enables unlabeled VHB-CP to be detected. It follows from the result that biotinylated oligonucleotides can be labelled by QDs and subsequently used as probes for selective conjugation with complementary fragments.

Figure 3: CE of QDs, VHB-biotin and VHB CP complex with CE of VHB-biotin and VHB CP complex



CONCLUSION


Application of QDs as fluorescent labels enables sensitive fluorescence detection of non-fluorescent molecules. Capillary electrophoresis as a powerful separation technique can monitor the process of creation of QD-biomolecule complex and the use of UV absorbance detection is beneficial at the first stage of research because it enables visualization of both fluorescent as well as non-fluorescent components of the reaction. Once the process is optimized, more sensitive laser-induced fluorescence detection will be employed.

ACKNOWLEDGEMENT

The work has been supported by NanoBioTE-Cell GA ČR P102/11/1068, IGA IP10/2012 and CEITEC CZ.1.05/1.1.00/02.0068.

REFERENCES

- [1] S. Neeleshwar, C. L. Chen, C. B. Tsai, and Y. Y. Chen, *Physical Review B* 71 (2005) 201307(R)
- [2] Yu W W, Chang E, Drezek R, *et al.*, *Biochemical and Biophysical Research Communications*, 348 (2006), 781-786.
- [3] Choi Y-E, Kwak J-W, Park J W, *Sensors*, 10 (2010), 428-455.
- [4] Bharali D J, Mousa S A, *Pharmacology & Therapeutics*, 128 (2010), 324-335.
- [5] Sharma P, Brown S, Walter G, *et al.*, *Advances in Colloid and Interface Science*, 123-126 (2006), 471-485.
- [6] Mudshinge S R, Deore A B, Patil S, *et al.*, *Saudi Pharmaceutical Journal*, 19 (2011), 129-141.
- [7] Walling M A, Novak J A, Shepard J R E,

- 
- Int. J. Mol. Sci., 10 (2009), 441-491.
- [8] Sutherland A J, *Current Opinion in Solid State and Materials Science* 6 (2002) 365-370
- [9] Qiao Xu, Jian-Hao Wang, Zhan Wang, Zhao-Hui Yin, Qin Yang, Yuan-Di Zhao, *Electrochemistry Communications* 10 (2008) 1337-1339
- [10] Jamieson T, Bakhshi R, Petrova D, I Pocock R, Imani M, Seifalian AM, *Biomaterials* 28 (2007) 4717-4732

H-TERMINATED DIAMOND-CAPPED IMPEDANCE TRANSDUCER: NOVEL MOLECULAR SENSOR

Stepan Stehlik^{1*}, Tibor Izak¹, Alexander Kromka¹, Bohumil Dolensky², Martin Havlik², Bohuslav Rezek¹

¹ Institute of Physics, Academy of Sciences of the Czech Republic, v.v.i., Cukrovarnicka 10, 162 00, Prague 6, Czech Republic

² Department of analytical chemistry, Institute of Chemical Technology Prague, Technicka 5, 166 28, Prague 6, Czech Republic

* stehlik@fzu.cz, tel: +420-220 318 475

ABSTRACT

Sensitivity of an intrinsic nano-crystalline diamond (NCD) layer to naphthalene Tröger's base derivative decorated with pyrrole groups (TBPyr) was characterized by impedance spectroscopy. The transducer was made of Au interdigitated electrodes (IDE) with 50 μm spacing on alumina substrate which were capped with the NCD layer. The NCD-capped transducer with H-termination was able to electrically distinguish TBPyr molecules dispersed in methanol from the pure methanol (change of surface resistance).

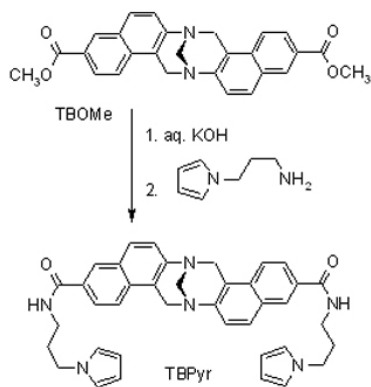
INTRODUCTION

Tröger's base (TB) attracts a lot of attention since this V-shaped molecule offers application as a unique building block for unusual molecular designs and for various molecular receptors [1]. However, electrical detection of TB properties has not been accomplished so far. In that context diamond offers great application potential as an electrically active interface to TB with possibility to tailor its structural, chemical, and electronic properties. Our group has demonstrated that interdigitated electrodes (IDE) capped with nanostructured H-NCD are highly sensitive and selective to phosgene gas that dissolves in the surface adsorbate layer and increases surface conductivity of H-terminated diamond [2, 3]. By using the impedance spectroscopy we demonstrate here that the NCD capped IDE transducer is able to electrically distinguish the naphthalene TB derivative having pyrrole moieties (TBPyr) adsorbed from methanolic suspension from the pure methanol.

MATERIAL AND METHODS

TBPyr derivative was prepared from TBOMe according to simplified Scheme 1.

Scheme 1. Preparation of TBPyr

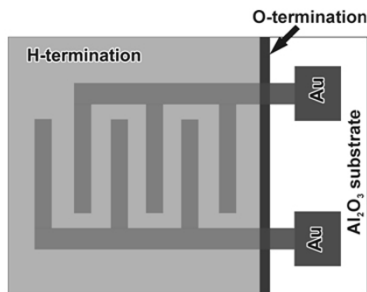


Scheme 1. Preparation of TBPyr

For the electrical transducer the Ti/Au electrodes (Ti/Au = 30/50 nm) were deposited on the polycrystalline Al_2O_3 substrates by thermal evaporation method in vacuum. The IDE structure was fabricated by means of standard UV-lithography and lift-off technique. The gap between IDE electrodes was 50 μm . The NCD layer was deposited by microwave plasma chemical vapor deposition process in Aixtron P6 reactor [4]. The thickness of the deposited NCD films was about 400 nm as determined optically from a smooth reference sample. For the impedance measurements of H-terminated surface, a stripe of oxidized surface was covered by an SU-8 photoresist at the border to the contacts (to pre-

vent shunts) and the rest of the NCD surface was H-terminated in hydrogen microwave plasma for 10 min. Finally the SU-8 photoresist was removed by acetone. Figure 1 shows the scheme of the transducer in top and cross-sectional view with an idealized visualization of TBPyr molecules adsorbed onto the surface.

Figure 1.: Schematic drawing of diamond-capped IDE transducer device.

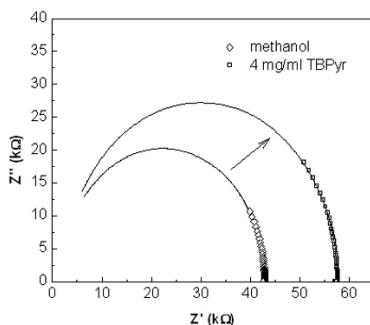


Impedance spectra were measured using a HIOKI 3532-50 LCR analyzer in frequency range 100 kHz – 10 Hz at room temperature. The amplitude of the AC voltage was 0.5V. The impedance response of the transducer to pure methanol (1 μ l) was checked prior to measurements with TBPyr suspension (4mg/ml). For testing the impedance response of the transducer 1 μ l of the suspension was applied onto the transducer using a micropipette. Methanol evaporated in few seconds and the impedance spectrum was measured after 5 min.

RESULTS AND DISCUSSION

Impedance spectra of the transducer measured at 5 min after application of the pure methanol and TBPyr suspension is shown in the Figure 2.

Figure 2.: Impedance spectra as measured after 5 min. The lines in the impedance spectra correspond to $R_1(CR_2)$ equivalent circuit fits extrapolated to the frequency of 1MHz.



The impedance spectra were fitted by $R_1(CR_2)$ equivalent circuit which produced reliable physical parameters. We have found that while the value R_1 remained relatively stable for both measurements, the resistance R_2 strongly varied depending on the conditions on the transducer surface. Taking into account these observations the particular resistances were assigned as follows: the resistance R_1 represents the transverse resistance of the NCD layer. The resistance R_2 is then attributed to the longitudinal surface resistance of H-terminated NCD layer. Functionality of the transducer may be explained by mechanism proposed by Rezek et. al [5] where the decrease of surface conductivity of H-NCD was attributed to a replacement of surface ions by adsorbed proteins which lead to decrease of the surface conductivity. However details of the sensing mechanism remain to be elucidated.

CONCLUSION


We successfully fabricated and demonstrated functionality of H-NCD capped IDE as an electrical transducer sensitive to TBPyr molecules. This demonstrates the feasibility of coating diverse sensor structures by NCD that can provide improved or completely new specific functions. Impedance spectroscopy resolved that the transducer response is given by a change in longitudinal surface conductivity while transverse resistance of NCD cap layer remains constant.

ACKNOWLEDGEMENT

The work has been supported by Grant Agency of the Czech Republic (203/08/1445 and P108/12G108).

REFERENCES

- [1] Sergejev S, Helvetica Chimica Acta 92 (2009), 415-444
- [2] Kromka A, Davydova M, Rezek B, Vanecek M, Stuchlik M, Exnar P, Kalbac M, Diamond and Related Materials 19

- 
- (2010), 196-200.
- [3] Davydova M, Kromka A, Rezek B, Babchenko O, Stuchlik M, Hruska K, Applied Surface Science 256 (2010), 5602-5605.
 - [4] Kromka A, Rezek B, Remes Z, Michalka M, Ledinsky M, Zemek J, Potmesil J, Vanecek M, Chemical Vapor Deposition 14 (2008), 181-186.
 - [5] Rezek B, Krátká M, Kromka A, Kalbacova M, Biosensors and Bioelectronics 26 (2010), 1307-1312.

EXPRESSION LEVELS OF ENZYMES METABOLIZING AN ANTICANCER DRUG ELLIPTICINE DETERMINED BY WESTERN BLOTTING DICTATE ITS CYTOTOXICITY TO NEUROBLASTOMA CELLS

Marie STIBOROVA^{1*}, Jitka POLJAKOVA¹, Tomas ECKSCHLAGER², Rene KIZEK^{3,4}, Eva FREI⁵

¹ Department of Biochemistry, Faculty of Science, Charles University, Prague, Albertov 2030, 128 40 Prague 2, Czech Republic

² Department of Paediatric, Haematology and Oncology, 2nd Medical School, Charles University and University Hospital Motol, V Uvalu 84, CZ-150 06 Prague 5, Czech Republic

³ Department of Chemistry and Biochemistry, Faculty of Agronomy, Mendel University in Brno, Zemedelska 1, 613 00 Brno, Czech Republic

⁴ Central European Institute of Technology, Brno University of Technology, Technicka 3058/10, 616 00 Brno, Czech Republic

⁵ Division of Preventive Oncology, National Center for Tumor Diseases, German Cancer Research Center (DKFZ), In Neuenheimer Feld 280, 69 120 Heidelberg, Germany,

*stiborov@natur.cuni.cz

ABSTRACT

Ellipticin anticancer action is based mainly on DNA intercalation, inhibition of topoisomerase II and formation of cytochrome P450 (CYP)- and peroxidase-mediated covalent DNA adducts. The cytotoxicity of ellipticine to UKF-NB-3 and UKF-NB-4 neuroblastoma cells was increased by pre-treating these cells with histone deacetylase inhibitors valproic acid (VPA) or trichostatin A (TSA). A higher sensitivity of cells to ellipticine corresponded to an increase in formation of covalent ellipticine-DNA adducts in these cells. The effects of ellipticine in the presence of VPA and TSA on expression of CYPs and peroxidases relevant for ellipticine metabolism and levels of cytochrome b_5 determined electrochemically (Western blotting) in neuroblastoma cells were investigated. The results found in this study demonstrate that most of the enhancing effects of VPA and TSA on ellipticine cytotoxicity due to enhancing ellipticine-DNA adduct is caused by an increase in expression levels of cytochrome b_5 , CYP3A4 and CYP1A1 proteins in neuroblastoma cells.

INTRODUCTION

Ellipticine (5,11-dimethyl-6H-pyrido[4,3-b]carbazole), an alkaloid isolated from Apocynaceae plants, exhibits significant antitumor and anti-HIV activities (for a summary see [1-4]). The major mechanisms of antitumor, mutagenic and cytotoxic activities of ellipticine were suggested to be (i) intercalation into DNA [5,6] and (ii) inhibition of DNA topoisomerase II activity [1-4]. We have demonstrated that ellipticine also covalently binds to DNA after being enzymatically activated by cytochromes P450 (CYP) or peroxidases [1-3,7-9], suggesting a third DNA-damaging mechanism of action. Two major DNA adducts generated from ellipticine-13-ylium and ellipticine-12-ylium, by CYP- and peroxidase-mediated metabolism are formed *in vitro* and *in vivo* in DNA of healthy organs of rats and mice treated with this anticancer drug [1,3,7,8]. Of the CYP enzymes investigated, human CYP3A4 and rat CYP3A1 are the most active enzymes oxidizing ellipticine to 13-hydroxy- and 12-hydroxyellipticine, the reactive metabolites that dissociate to ellipticine-13-ylium and ellipticine-12-ylium

which bind to DNA [3,7,8,10], while the CYP1A isoforms preferentially form the other ellipticine metabolites, 9-hydroxy- and 7-hydroxyellipticine, which are the detoxication products. Recently we have found that cytochrome b_5 alters the ratio of ellipticine metabolites formed by CYP1A1, 1A2 and 3A4. While the amounts of the detoxication metabolites (7-hydroxy- and 9-hydroxyellipticine) were either decreased or not changed with added cytochrome b_5 , 12-hydroxy-, 13-hydroxyellipticine and ellipticine N^2 -oxide increased considerably. The change in amounts of metabolites resulted in an increased formation of covalent ellipticine-DNA adducts, one of the DNA-damaging mechanisms of ellipticine antitumor action [10,11].

The same DNA adducts found *in vitro* were also detected in human cancer cells in culture, such as breast adenocarcinoma MCF-7, the leukaemias HL-60 and CCRF-CEM, neuroblastoma and glioblastoma cells, and in rat mammary adenocarcinoma *in vivo* (for a summary see [1-4]). Toxic effects of ellipticine in these cancer cells correlated with levels of ellipticine-derived DNA adducts and were dependent on expression of either CYP 1A1, 1B1, 3A4, lactop-

eroxidase, cyclooxygenase or myeloperoxidase in these cells [1-4]. Interestingly, cytotoxicity of ellipticine to UKF-NB-3 and UKF-NB-4 neuroblastoma cells [12] was increased by pre-treating these cells with histone deacetylase (HDAC) inhibitors valproic acid (VPA) or trichostatin A (TSA) [13]. A higher sensitivity of cells to ellipticine and these HDAC inhibitors correlated with an increase in formation of covalent ellipticine-derived DNA adducts in these cells [13]. Here, based on electrochemical determination of expression levels of some of these enzymes, we describe one of the mechanisms that might explain these phenomena.

2. MATERIAL AND METHODS

Electrochemical estimation of contents of CYPs, peroxidases and cytochrome b_5 in neuroblastoma cells

To determine the expression of cytochrome b_5 , CYP1A1, 1B1 and 3A4, lactoperoxidase (LPO) and cyclooxygenase (COX)-1 proteins, cells were homogenized in 25 mM Tris-HCl buffer pH 7.6 containing 150 mM NaCl, 1% detergent NP-40 (Sigma, St. Louis, MO, USA), 1% sodium deoxycholate, 0.1 % SDS and with solution of COMPLETE (protease inhibitor cocktail tablet, Roche, Basel, Switzerland) at concentration described by provider. The homogenates were centrifuged for 20 min at 14, 000 g and supernatant was used for additional analysis. Protein concentrations were assessed using the DC protein assay (Bio-Rad, Hercules, CA, USA) with bovine serum albumin as a standard, and 10-45 μ g of extracted proteins were subjected to SDS-PAGE electrophoresis on a 11% gel for analysis of CYP1A1, 1B1 and 3A4, LPO and COX-1 protein expression, and a 17% gel for analysis of cytochrome b_5 protein expression [13-15]. After migration, proteins were transferred to a nitrocellulose membrane and incubated with 5% non-fat milk to block non-specific binding. The membranes were then exposed to specific rabbit polyclonal anti-cytochrome b_5 (1:750, AbCam, MA, USA), anti-CYP1A1 (1:1000, Millipore, MA, USA), anti-CYP1B1 (1:500, AbCam, MA, USA), anti-CYP3A4 (1:5000, AbD Serotec, Oxford, UK), anti-LPO (2 μ g/ml, AbCam, MA, USA) and anti-COX-1 (1:1000, AbCam, MA, USA) antibodies overnight at 4 °C. Membranes were washed and exposed to peroxidase-conjugated anti-IgG secondary antibody (1:3000, Bio-Rad, Hercules, CA, USA), and the antigen-antibody complex was visualized by enhanced chemiluminescence's detection system according to the manufacturer's instructions (Immun-Star HRP Substrate, Bio-Rad, Hercules, CA, USA). X-Rays films from MEDIX XBU (Foma, Hradec Králové, Czech Republic). Antibody against glyceraldehyde phosphate dehydrogenase (GAPDH)

(1:750, Millipore, MA, USA) was used as loading control.

DNA isolation and 32 P-postlabeling of DNA adducts

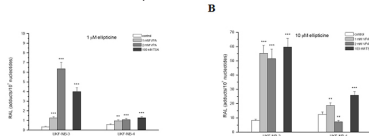
DNA from cells was isolated by the phenol-chloroform extraction as described [12,13]. The 32 P-postlabeling of nucleotides using nuclease P1 enrichment procedure, found previously to be appropriate to detect and quantify ellipticine-derived DNA adducts formed *in vitro* and *in vivo* [1-4,8-13]. From experiments performed earlier, calf thymus DNA incubated with 13-hydroxy- and 12-hydroxyellipticine [7,8,10] and DNA of breast adenocarcinoma of rats treated i.p. with 4 mg ellipticine per kilogram body weight [3] were labeled with 32 P to compare adduct spot patterns.

RESULTS AND DISCUSSION

As shown previously, ellipticine inhibits growth of several neuroblastoma cell lines [12]. Moreover, pre-treatment of UKF-NB-3 and UKF-NB-4 cells with either VPA or TSA made cells more sensitive to ellipticine. The decrease in IC_{50} values for ellipticine caused by both compounds in UKF-NB-3 and UKF-NB-4 cells was dose-dependent, being higher in UKF-NB-3 cells than in UKF-NB-4 cells [12,13].

A higher sensitivity of cells to ellipticine correlated with an increase in formation of covalent ellipticine-derived DNA adducts in these cells. Ellipticine-DNA adduct levels were ellipticine dose dependent in both neuroblastoma cell lines [13] (Fig. 1).

Figure 1: The effect of valproate and trichostatin A on DNA adduct formation by 1 μ M (A) and 10 μ M ellipticine (B) in human UKF-NB-3 and UKF-NB-4 neuroblastoma cell lines. *Columns:* Mean RAL (relative adduct labeling) \pm standard deviations shown in the figure represent total levels of DNA adducts of three 32 P-postlabeling analyses. The data were analyzed statistically by Student's *t*-test. Values significantly different from cells exposed to ellipticine alone. ** $P < 0.01$, *** $P < 0.001$.

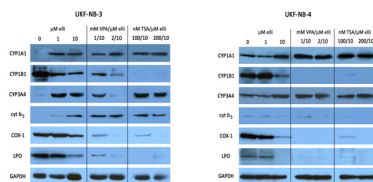


Using electrochemical determination (Western blot analysis with antibodies raised against CYP1A1, 1B1, 3A4, LPO, COX-1 and cytochrome b_5), the effects of exposure of the cells to ellipticine with and without VPA or TSA on

protein levels of these enzymes were analyzed (Fig. 2). The CYP-mediated formation of ellipticine-derived DNA adducts in analyzed neuroblastoma cells depends on expression levels of CYP1A1 and 3A4 enzymes and also on expression of another protein present in the membrane of endoplasmic reticulum, cytochrome b_5 (Fig. 2). On the contrary, the peroxidases COX-1 and LPO that are expressed in UKF-NB-3 and UKF-NB-4 cells do not participate in the increased sensitivity of these neuroblastoma cells to ellipticine in the presence of VPA and TSA. Their expression levels are even decreased in neuroblastoma cells exposed to ellipticine plus either HDAC inhibitor (Fig. 2).

The ellipticine-mediated modulations of levels of cytochrome b_5 seem to play a key role in higher formation of ellipticine-derived DNA adducts in UKF-NB-3 cells. This heme protein was found to influence oxidation of ellipticine catalyzed by CYP3A4 [7,10], the enzyme oxidizing this compound mainly to 12-hydroxy- and 13-hydroxylated metabolites that form DNA adducts, and by CYP1A1, which predominantly detoxicate ellipticine [1-4,7,10,11]. In the case of CYP3A4, stimulating effects of cytochrome b_5 on oxidation of ellipticine to 12-hydroxy- and 13-hydroxyellipticine lead to an increase in ellipticine-DNA adduct formation [7,10]. In the case of CYP1A1, cytochrome b_5 has been recently found to alter the ratio of ellipticine metabolites formed by this CYP, “switching” CYP1A1-mediated oxidation of this anticancer drug from detoxication (9-hydroxy- and 7-hydroxyellipticine) to DNA-forming metabolites (12-hydroxy- and 13-hydroxyellipticine). These changes resulted in an increase in formation of covalent DNA adducts by ellipticine [11]. We have found that ellipticine increases amounts of cytochrome b_5 in UKF-NB-3 cells, but not in UKF-NB-4 cells [13] (Fig. 2). The higher levels of cytochrome b_5 and the increase in CYP1A1 levels induced by ellipticine with VPA or TSA in UKF-NB-3 cells, therefore, promote the activation of ellipticine catalyzed by CYP1A1 in these cells. On the contrary, because of low levels of cytochrome b_5 in UKF-NB-4 cells, the elevated expression levels of CYP1A1 caused by exposure to ellipticine in the presence of VPA and TSA results in higher ellipticine detoxication in these cells. Hence, both these induction effects produce concerted regulatory effects of ellipticine, VPA and TSA on ellipticine pharmacological action.

Figure 2: Immunoblots showing the effects of exposing UKF-NB-3 cells (A) and UKF-NB-4 cells (B) to ellipticine with VPA or to ellipticine with TSA for 48 h on expression of CYP1A1, CYP1B1, CYP3A4, cytochrome b_5 , COX-1 and LPO. Cell homogenates were subjected to SDS-PAGE, proteins transferred to nitrocellulose membranes and probed with antibodies as described in Material and Methods. GAPDH was used as loading control.



CONCLUSION


Monitoring of expression levels of enzymes metabolizing (activating and detoxicating) anticancer drug ellipticine by the Western-blotting-electrochemical method, together with the ^{32}P -postlabeling technique utilized for detection and quantitation of DNA adducts are suitable tools for evaluation of mechanism of cytotoxicity of ellipticine in neuroblastomas.

ACKNOWLEDGEMENT

The work has been supported by Grant Agency of the Czech Republic (grant P301/10/0356) and Charles University in Prague (grant UNCE #42).

REFERENCES

- [1] Stiborová M., Bieler C.A., Wiessler M., et al.: *Biochemical Pharmacology*, 62 (2001), 1675-1684.
- [2] Stiborová M., Rupertová M., Schmeiser H.H., et al.: *Biomedical Papers*, 150 (2006), 13-23.
- [3] Stiborová M., Rupertová M., Frei E.: *Biochimica et Biophysica Acta*, 1814 (2011), 175-185.
- [4] Kizek R., Adam V., Hrabeta J., et al.: *Pharmacology & Therapeutics*, 133 (2012), 26-39.
- [5] Auclair C.: *Archives of Biochemistry and Biophysics*, 259 (1987), 1-14.
- [6] Garbett N.C., Graves D.E.: *Current Medicinal Chemistry. Anti-Cancer Agents*, 4 (2004), 149-172.
- [7] Stiborová M., Sejbal J., Bořek-Dohalská L., et al.: *Cancer Research*, 64 (2004), 8374-8380.
- [8] Stiborová M., Poljaková J., Ryšlavá H., et al.: *International Journal of Cancer*, 120 (2007), 243-251.
- [9] Stiborová M., Rupertová M., Aimová D., et al.: *Toxicology*, 236 (2007), 50-60.
- [10] Stiborová M., Indra R., Moserová M., et al.: *Chemical Research in Toxicology*, (2012), DOI: 10.1021/tx3000335.
- [11] Kotrbová V., Mrázová B., Moserová

- 
- M., et al.: *Biochemical Pharmacology*, 82 (2011), 669-680.
- [12] Poljaková J., Eckschlager T., Hraběta J., et al.: *Biochemical Pharmacology*, 77 (2009), 1466-1479.
- [13] Poljaková J., Hrebacková J., Dvoraková M., et al.: *Neuro Endocrinology Letters*, 32 (Suppl 1) (2011), 101-116.
- [14] Štiborová M., Martínek V., Rýdlová H., et al.: *Cancer Research*, 62 (2002), 5678-5684.
- [15] Štiborová M., Martínek V., Rýdlová H., et al.: *Cancer Letters*, 220 (2005), 145-154.

THE NEW MILLENNIUM WITH NEW CARBON PASTES

Ivan SVANCARA^{1*}, Matej STOCES¹, Tomas MIKYSEK¹,
Radovan METELKA¹, Jiri LUDVIK², and Karel VYTRAS¹

¹ Department of Analytical Chemistry, Faculty of Chemical Technology, University of Pardubice, Studentska 573, HB/C, 532 10 Pardubice, Czech Republic;

² J. Heyrovský Institute of Physical Chemistry ASCR, v.v.i., Dolejškova 3, 182 23 Prague 8, Czech Republic.

*Ivan.Svancara@upce.cz

ABSTRACT

New types of carbon paste electrodes appearing in electrochemistry and electroanalysis during the last decade are highlighted; namely, those being prepared from alternate carbon paste constituents, such as carbon nanotubes, carbon fibres, glassy-carbon spheres, acetylene and carbon black, fullerenes, graphene, or diamond powder (all having replaced traditional powdered graphites) and ionic liquids, some organic esters, or polymeric fillers (all acting as a binder instead of common mineral oils). All newly proposed configurations are discussed with respect to their basic physicochemical characterisation and the individual specifics in close relation with possibilities and limitations in modern electrochemical measurements, including numerous examples of typical electroanalytical applications. In the end, the authors' contribution to the field is also surveyed and some future prospects given.

INTRODUCTION

After more than fifty years in use, carbon paste electrodes (CPEs) already belong among classical types of electrodes [1 - 3]. Traditionally, under term "carbon paste in electro-chemistry" one usually assumes laboratory made mixtures whose two principal constituents are the spectroscopic graphite as the conductive moiety and some of mineral or silicone oil in the role of liquid binder. Such configuration had been the rule for almost four decades despite the fact that the respective mixtures often contained yet another component – a modifier changing intentionally some qualitative properties of the resultant electrode (system).

However, the commencement of the new millennium has brought a principal breakthrough in the form of the so-called "new carbon pastes", where one or even both major components are purposely replaced with an alternative. Thanks to quite a wide choice in both carbon material and pasting liquid, the area of newly coming CPEs expanded very rapidly, establishing soon two special categories of carbon paste-based electrodes, sensors, and detectors that are of particular interest in the following two sections. The third part is then devoted to some other interesting configurations that can also be classified as new / novel carbon pastes .

CARBON NANOTUBE-BASED PASTE ELECTRODES

Actually, the cylindrical allotrope of carbon in two basic modifications, single-walled and multi-walled carbon nanotubes (SW-CNTs and MW-CNTs, respectively) joined firstly the fa-

mily of CPEs in pioneering studies by Rivas' and Palleschi's research groups. Since then and up until now, CNTs in the proper paste mixtures can be found in *ca.* 150 reports published in the period of 2003-2012 (see e.g. [3] and refs. therein). These turbulent activities and dynamic progress were a logical result of repeated findings that the presence of CNTs in carbon paste mixtures brings marked improvements of electrochemical and electroanalytical parameters, giving rise to highly selective electrocatalytic properties.

Carbon nanotubes can be applied as substitute of graphite powder, giving rise to two-component mixtures of the "CNTs + liquid binder" type known as (i) **carbon nanotube paste electrodes (CNTPEs)**. The second combination is then symbolised by (ii) **carbon nanotube-modified carbon paste electrodes (CNT-CPEs)**, where CNTs themselves play the role of an additional constituent; typically, as electrocatalytic agent. In other words, these three-component systems consist of (a) traditional graphite powder, (b) CNTs added in, and (c) mineral oil. In addition, even more complex variants can be made, when originally two- or three-component arrangements are additionally combined with other constituents. Then, one can obtain: (iii) **chemically modified carbon nanotube paste electrodes (CM-CNTPEs)**; (iv) **biologically carbon nanotube paste electrodes (CNTP-biosensors)**; (v) **carbon paste electrodes modified with CNTs and other reagent(s) [X(Y)/CNT-CPEs]**; (v) **carbon paste electrodes modified with CNTs and an enzyme / mediator system (CNT-CP-biosensors)**.

Most of CNT-based electrodes have also su-

ccessfully applied in practical electroanalysis, where the individual configurations could be employed for the determination of numerous analytes. Among them, one has: (a) inorganic ions and molecules (e.g.: Hg^{2+} , Cu^{2+} , Cd^{2+} , Pb^{2+} , and $\text{Sb}^{\text{III,V}}$, SO_3^{2-} , H_2O_2 , N_2H_4); (b) organic substances (MeOH , EtOH , PhOH , quinones, CH_3NO_2 , or $\text{C}_6\text{H}_5\text{N}_2\text{H}_3$) and (c) biologically important compounds (amino acids, GLU , UA , AA and other vitamins, neurotransmitters $\frac{3}{4}$ mainly dopamin and DOPAC , enzymes and coenzymes (NADH), hormones, flavonoids, and macromolecules (DNA); (d) pharmaceuticals (e.g.: Paracetamol, Methamphetamine, Oxytetracycline, or Piroxicam); (e) environmental organopollutants (organophosphate and carbamate insecticides, triazol-based herbicide).

CARBON IONIC LIQUID ELECTRODES

Carbon paste mixtures as such offer almost ideal platform for using (room temperature) ionic liquids, (RT)ILs, when a variability in use of different liquid binders had opened a particular position for still popular ionic liquids. Thus, since the reports by Liu et al. in the mid-2000s, in which (RT)ILs were for the first time intentionally added into the carbon paste bulk, the ionic liquid-based CPEs have been the central subject of interest in *ca.* 100 scientific papers appearing up until now (again, see [3] and refs. therein).

The individual contributions have shown clearly that electrochemical measurements with CPEs may benefit from a number of specific properties of (RT)ILs; namely: (i) their excellent solvating properties, (ii) high conductivity, (iii) non-volatility, (iv) electrochemical stability with (v) wide polarizability, (vi) specific chemical activity (ion-exchanging properties and electrocatalytic effect), and (vii) typically low toxicity. To complete this characterization, ionic liquid-containing CPEs possess (viii) favorable surface microstructure with markedly smooth pattern.

Similarly as with CNT-CPEs and CNTes, one can distinguish a variety of different configurations, when the basic types are: (i) **carbon ionic liquid electrodes (CILEs)** forming *two-component (binary)* mixtures, with an (RT)IL as the alternate pasting liquid; (ii) **ionic liquid-modified carbon paste electrodes (IL-CPEs)** with three components in the paste and ionic liquid used as additional component; usually, in the form of modifier enabling some of the facilities mentioned above. Furthermore, there are other combinations: (iii) **carbon nanotubes ionic liquid electrodes (CNTILEs)** as truly new kind of CPEs, where both key constituents are replaced by alternate materials; (iv) **chemically and biologically modified IL-CPEs, CILEs, and CNT-ILEs** with other sub-variants of the following types: (a) “CM-IL-CPE”, (b) “CM-

-CILE”, (c) “CM-CNTILE”, or (d) CIL- and (e) CNTIL-biosensors. The survey can then be completed by (v) mixtures of **new carbons with ionic liquids**, offering three attractive examples: (a) “**GC-ILE**” type (made of glassy carbon microspheres), (b) “**CNF-ILE**” (with carbon nanofibers) and (c) “**GR-ILE**” (with graphene).

Practically oriented electroanalytical applications of IL-CPEs, CILEs, and CNTILEs are minimally as diverse as the individual variants and sub-variants of ionic liquid-based carbon pastes. Herein, the following analytes can be mentioned. *Inorganic ions and molecules ...* Cd^{2+} , Pb^{2+} , Cu^{2+} , Hg^{2+} , and Ce^{3+} , NO_2^- , SO_3^{2-} , ClO_3^- , H_2O_2 , O_2 , and N_2H_4 ; *Organic compounds:* PhOH , H_2Q , metol catechol, CH^3NO_2 , nitrophenols, and CCl_3COOH ; *Biologically important compounds ...* aminoacids, UA , AA , glucose, neurotransmitters (dopamine, adenosine), enzymes and coenzymes: NADH proteins and metaloproteins, anti-oxidants, and macromolecules of DNA ; *Pharmaceuticals and abuse drugs ...* Dobesilate, Paracetamol, Methamphetamine, Viagra, heroin; *Organic eco-pollutants ...* Methylparathion (herbicide) and TNT (explosive).

OTHER NEW CARBON PASTES

Both CNTPEs and CILEs, including their combination CNTILEs, exist also in special **thin-layer configurations**, where the carbon paste-based sensing site is reduced to a film attached to the “foreign” electrode substrate, which can be another CNTE, CILE, traditional CPE, and mainly polished discs of the glassy carbon electrode. The corresponding configurations have rather special applications; mostly, in more theoretical studies.

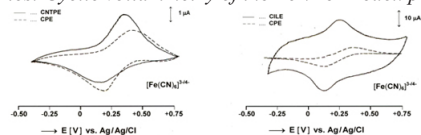
Not less interesting are **diamond paste electrodes (DPEs)** made of synthetic diamond powder of micrometer particle size and ordinary mineral oils. Reportedly (see commentary in [3]), the inevitable conductivity of otherwise totally insulating diamond is ensured by trace impurities. The bare DPE (in unmodified form) has already been recommended for numerous electroanalytical applications, involving both inorganic and organic analytes, as well as some substances of biological origin.

Last but not least, also certain types of the so-called **screen-printed carbon electrodes (SPEs)** can be quoted herein due to their close relation with classical CPEs with respect to analogical preparation, the same heterogeneous character, and similar ways of modification. However, because of great diversity and often different construction, the SPEs are typically classified extra (see a separate chapter in [2]).

CONCLUSION

The main goal of this contribution is to document and briefly comment the recent boom in the field of carbon paste-based electrodes. Indeed, there is the only period in the entire history of these electrodes or—the era of chemically and biologically modified CPEs [2]—when their popularity has achieved such a level like one can see in the present time. Regarding the authors' contribution to the turbulent 2000s, it follows their previous work on systematic characterisation of CPEs started in the early 1990s [4,5], continuing through the 2000s (see e.g. [6,7]) and now focused on specific ohmic-resistance studies with CNTPEs, CILEs, and other CP-mixtures ([8-10]; see Fig. 1 overleaf). At the end, it can be stated that the present day's activities with new carbon pastes, together with their hitherto unmentioned compatibility with newest technologies are the best warranty for further achievements in the future.

Figure 1: From the testing of two new carbon pastes: Cyclic voltammetry of the Fe^{II}/Fe^{III} redox pair



ACKNOWLEDGEMENT

A support from the Ministry of Education, Youth, and Sports of the Czech Republic (project KON-TAKT, No MEB091139) is gratefully acknowledged.

REFERENCES

- [1] Švancara I, Vytřas K, Kalcher K, et al.: *Electroanalysis*, 21 (2009), 7-28.
- [2] Kalcher K, Švancara I, Metelka R, et al.; in: *Encyclopedia of Sensors*, Volume 4 (Grimes C.A., Dickey E.C., Pishko M.V., Eds.). American Scientific Publishers, Stevenson Ranch, (2006), pp. 283-430.
- [3] Švancara I, Kalcher K, Walcarius A, Vytřas K: *Electroanalysis with Carbon Paste Electrodes*. CRC Press, Boca Raton, (2012).
- [4] Švancara I, Vytřas K: *Analytica Chimica Acta*, 273 (1993), 195-204.
- [5] Švancara I, Hvizdaldová M, Vytřas K, et al.: *Electroanalysis*, 8, (1996), 61-65.
- [6] Švancara I, Ogorevc B, Hočevar S.B, Vytřas K: *Analytical Science (Japan)*, 18, (2002), 301-305.
- [7] Švancara I, Kotzian P, Bartoš M, Vytřas K: *Electrochemistry Communications*, 7, (2005), 657-662.
- [8] Mikysek T, Švancara I, Bartoš M, et al.: *Analytical Chemistry* 81, (2009), 6327-6333.
- [9] Mikysek T, Jovanoski V, Sopha H.-I., et al.; in: *Sensing in Electroanalysis*, Volume 6 (Kalcher K, Metelka R, Švancara I, Vytřas K; Eds.), Univ. Pardubice Press, Pardubice, pp. 157-166,

(2011).

- [10] Mikysek T, Stočes M, Švancara I, Ludvík J: *RSC Advances* (London), DOI: 10.1039/c2ra20202f.

DESIGN AND FABRICATION OF MEMS LOW POWER HEATING MEMBRANE

Vojtech SVATOS¹, Marian MARIK¹, Jan PEKAREK¹, Radim HRDY¹, Jana CHOMOÜCKA¹, Jaromir HUBALEK¹,

¹ LabSensNano, Department of Microelectronics, Faculty of Electrical Engineering and Communication, Brno University of Technology, Technicka 3058/10, CZ-616 00 Brno, Czech Republic

*jaromir.hubalek@ceitec.vutbr.cz

ABSTRACT

Design and fabrication of micro-hotplates is the aim of this paper. This type of device is very often used for gas-sensing applications. The main aim of this work is to produce the structure of the heating membrane. Two types of membranes are discussed – suspended and close type of the membrane. The sample which is going to be produced will be the membrane with size of 1×1 mm, to ascertain the applicable process of the fabrication technology and the applicable design of the micro-hotplate. The micro-hotplates power consumption has to be up to 100 mW at the operating temperature 480 °C.

INTRODUCTION

Micro-hotplates have the tremendous importance in the field of high temperature gas-sensing devices since they allow the reduction of the sensor power consumption and the use of new modes of operations such as temperature cycling due their low thermal mass [1].

The fabrication process includes micromachining: deposition of thin layers, photo lithography, and etching to create close or suspended type of the membrane. The heater will be probably produced using Au as the heating electrode. Metal film hotplate offers precise temperature control, which can be also used as a thermometer; it simplifies the device structure [6]. Meander will be used as design of the heater.

DESIGN

The design has been supported using mechanical and the thermal simulation in ConvertorWare. The most important and fundamental parameters during design of micro-hotplates, are power consumption, operating temperature, robustness of the structure.

There are three main contributions to the total thermal loss: first a thermal loss due to conduction; second, a loss to the surrounding air due to the thermal convection, a size (thickness, membrane length, and active area dimension), the specific thermal conductivity of the membrane material, silicon dioxide in these experiments [6].

The size of the designed membrane was from 0.5 to 1.0 mm. The beams of the suspended membrane were 100 to 150 µm wide.

Figure 1.: Model of suspended membrane structure



FABRICATION

The standard fabrication process was as follows. The starting material was a (100) one side polished silicon wafer with thickness of 500 µm. A thermal oxide of 1.1 µm was grown both side. The first step was to create top structure of the suspended membrane then backside etching to release the membrane in the second step. The structure of the micro-hotplate was created in the layer of silicon dioxide using solution of HF and CH₃COOH. In this case the photoresist was use as the protective mask during etching. The silicon dioxide was used to create the top structure of the micro-hotplate during etching, as well as, this layer was used to the back side protection during wet chemical etching in KOH (30%, 80°C). The top structure was etched 30 µm deep in the silicon wafer.

The second step was to release the membrane by wet chemical etching using the same solution of KOH. The sample was laid down on the piece of polymer which can dismiss the vapors of KOH to etch just the back side of the wafer.

RESULTS AND DISCUSSION

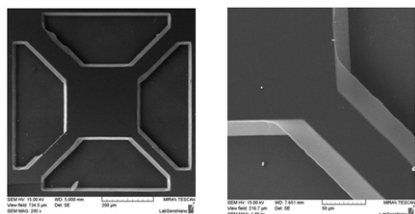
The structure of the suspended membrane was created by using wet chemical etching, but the final structure prepared for a heating electrode is not completely intimate. The structure of the micro-hotplate is damaged because of etching process, and due to the imperfect mask used during lithography. One beam of the hot plate is thinner due to previously mentioned reasons as shown in Fig. 1.

Other improvement could be reached by making the beams orthogonal to the hotplate. This step may cause a smaller rate of etching beams. Of course, the lithography process needs to be done more precisely.

The used type of beams causes to bend the structure up and down when the temperature is increasing to the operating point of a device. The orthogonal beams cause to turning of hot-plate then bending this structure up and down. This effect may help to decrease the stress of the micro-hotplate.

In the stage of the experiment is necessary to find a more optimal protective mask for the etching process (e.g. silicon nitride). When the structure of membrane is optimal (robustness, thermal losses), the heater is fabricated.

Figure 2.: SEM photograph of micro-hotplate structure (left) and the detail of the beam (right)



CONCLUSION

Design and fabrication of micro-hotplates has been described many times over the literature, but improving the design and the fabrication is still needed to reach as minimum power consumption as possible, therefore, the membrane and hotplate structure have to be investigated. This paper reports on the other techniques that are not used so much for fabrication of this kind of structures.

ACKNOWLEDGEMENT

The financial support from the grant GAČR 102/08/1546 and project SIX CZ.1.05/2.1.00/03.0072 is highly acknowledged.

REFERENCES

[1] BRIAND, D, et al. Design and fabrication of high-temperature micro-hotplates for

drop-coated gas sensors. *ScienceDirect* [online]. 2000, 68, [cit. 2011-11-14]. Dostupný z WWW: <<http://www.sciencedirect.com/science/article/pii/S0925400500004330/engineering/MCEN/micronanobio/Supplementary/microhotplate.pdf>>.

[2] HSU, Tai-Ran. *MEMS and microsystems*. second edition. New Jersey: John Wiley & Sons, 2008, 550 s. ISBN 978-0-40-08301.

[3] LALINSKÝ, T; DRŽÍK, M; JAKOVENKO, J. GaAs based micromachined thermal converter for gas sensor. *EuroSensors XX The 20th European conference on Solid-State* [online]. 2007, 142, [cit. 2011-10-23]. Dostupný z WWW: <<http://www.sciencedirect.com/science/article/pii/S0924424707003925>>.

[4] SEMANCIK, S, et al. Microhotplate platforms for chemical sensor research. *Elsevier* [online]. 2001, 77, [cit. 2011-10-18]. Dostupný z WWW: <<http://www.colorado.edu/engineering/MCEN/micronanobio/Supplementary/microhotplate.pdf>>.

[5] UDREA, F et al. Design of a silicon microsensor array device for gas analysis. *Microelectronics Journal* 22[online]. 1996. 449 – 457, [cit. 2011-12-3]. Dostupný z WWW:< <http://www.sciencedirect.com/science/article/pii/0026269295001123>>

[6] XIAN, Y, et al. Fabrication of MEMS micro-hotplate. *ScienceDirect* [online]. 2011, 276, [cit. 2011-12-3]. Dostupný z WWW: <http://iopscience.iop.org/1742-6596/276/1/012098/pdf/1742-6596_276_1_012098.pdf>

MONITORING THE VIABILITY OF CELL LINE MTF-KO DEPENDING ON THE CONCENTRATION OF Zn²⁺ USING XCELLIGENCE SYSTEM

Marketa SZTALMACHOVA^{1,2*}, Veronika TANHÄUSEROVA¹, Marian HLAVNA¹, Jaromir GUMULEC¹, Martina RAUDENSKA¹, Vojtech ADAM², Rene KIZEK², Michal MASARIK¹

¹ Department of Pathological Physiology, Faculty of Medicine, Masaryk University, Kamenice 5, 625 00 Brno, Czech Republic

² Department of Chemistry and Biochemistry, Faculty of Agronomy, Mendel University in Brno, Zemědělská 1, 613 00 Brno, Czech Republic

*marketa.sz@seznam.cz

ABSTRACT

The aim of our work was real-time monitoring of MTF-KO cell line viability using xCELLigence system after zinc ion treatments. The cell line is mouse embryonic fibroblast cell culture obtained by knock-out of metal regulatory transcription factor 1 (MTF-1). In mammals, MTF-1 is transcription factor activating transcription of Metallothionein as reaction on oxidative stress stimuli, especially caused by heavy metals.

INTRODUCTION

Metallothioneins (MTs) are low-molecular mass cysteine-rich proteins. Due to thiol bounds in its structure is metallothionein capable to bind metals and thus play a role in metal transportation, cell detoxification and oxidative stress protection [1]. Metallothionein is closely related to zinc metabolism, as zinc is essential compound of mammalian living cells [2]. MT transcription is mediated and controlled thru MTF-1 factor which is activated by metal caused oxidative stress [3-5]. It was published, that MTF-1 factor play also role during embryonal development of liver. It is obvious that MTF-1 plays role not only in detoxification and oxidative stress protection, but also in ontogenetic processes [2]. The cell line used in our study was obtained by knock-out of metal regulatory transcription factor 1 (MTF-1) in mouse embryonic fibroblast cell culture MEF-1. We focused on viability monitoring of MTF-KO cell culture viability after zinc ion treatments.

MATERIAL AND METHODS

Cell line MTF-KO was cultured in DMEM High glucose (4,5g/l) medium with 1% penicillin/streptomycin and 10% FBS in incubator (37°C and 5% CO₂). Figure 1 shows the cell line MTF-KO (400x magnification). We used MTT test for determination of optimal zinc concentration used in further experiments. MTT compound used in this standard end-point viability test is yellow colour tetrazolium dye which is turned into blue product by living cells. Viability is than determined by colorimeter. Optimal zinc concentrations where after that used in real-time cell viability experiment performed on

xCELLigence system. This method allows real-time monitoring of cell proliferation, adhesion, cell morphology and viability changes in time. Therefore provides more complex information about cytotoxicity of investigated compounds.

RESULTS AND DISCUSSION

MTF-1 is in mammalian organisms essential. We focused on monitoring of viability of cell line in which this factor was knocked-out. MTT test was performed with Zn²⁺ ion concentration as follows: 0, 25, 50, 60, 70, 80, 90, 100, 125 a 150 µM. To every column cell was transferred suspension of app. 6000 cells. After 48 hours was zinc added. After another 48 hours of incubation was test terminated and results are shown in figure 2. As you can see, IC₅₀ Zn²⁺ concentration for MTF-KO cell line was determined as 80 µM, in higher concentrations were Zn²⁺ ions toxic.

Figure 1.: The cell line MTF-KO (400x magnification)

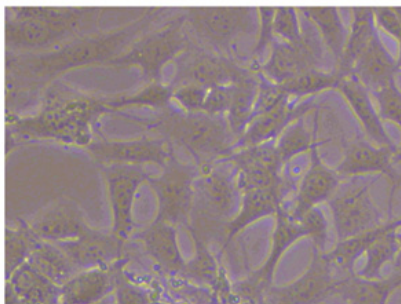
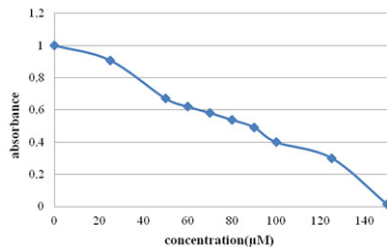
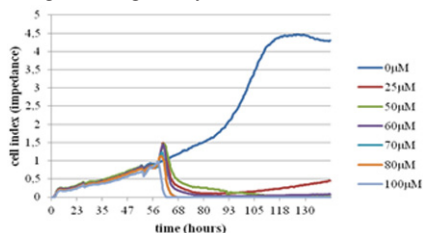


Figure 2.: MTT test



Based on MTT test results have been Zn²⁺ concentration line for real-time monitoring determined as follows:: 0, 25, 50, 60, 70, 80, a 100 µM. To xCELLigence microplate was transferred cell culture suspension with app. 3000 cells. We let cells growing until cell index reached 1.2 value, after this point we added Zn²⁺ in previous mentioned concentrations. Treatment duration was 24 hours. Results are shown in figure 3. We can see a reaction to added Zn²⁺ (after 60 hours of growth). After the addition of Zn²⁺ leads to growth inhibition at low concentration of metal due to knock-out MTF-1.

Figure 3.: Real-time monitoring using xCELLigence system.



CONCLUSION

The present study demonstrates monitoring of viability of MTF-KO cell line after zinc treatment. This cell line has knock-out metal regulatory transcription factor 1 (MTF-1). Compared to wild type form of mouse embryonic fibroblasts, the growth of MTF-KO cell line is inhibited at lower zinc concentrations.

ACKNOWLEDGEMENT

The work has been supported by NanoBioMetalNet CZ.1.07/2.4.00/31.0023

REFERENCES

- [1] Eckschlager, T., et al., *Metallothioneins and Cancer*. Current Protein & Peptide Science, 2009. **10**(4): p. 360-375.
- [2] Okumura, F., et al., *The zinc-sensing transcription factor MTF-1 mediates zinc-induced epigenetic changes in chromatin*

of the mouse metallothionein-I promoter. Biochimica Et Biophysica Acta-Gene Regulatory Mechanisms. **1809**(1): p. 56-62.

- [3] Ushakova, G.A. and O.A. Kruchinenko, *Peculiarities of the Molecular Structure and Functions of Metallothioneins in the Central Nervous System*. Neurophysiology, 2009. **41**(5): p. 355-364.
- [4] Egli, D., et al., *Knockout of 'metal-responsive transcription factor' MTF-1 in Drosophila by homologous recombination reveals its central role in heavy metal homeostasis*. Embo Journal, 2003. **22**(1): p. 100-108.
- [5] Langmade, S.J., et al., *The transcription factor MTF-1 mediates metal regulation of the mouse ZnT1 gene*. Journal of Biological Chemistry, 2000. **275**(44): p. 34803-34809.
- [6] Daniels, P.J. and G.K. Andrews, *Dynamics of the metal-dependent transcription factor complex in vivo at the mouse metallothionein-I promoter*. Nucleic Acids Research, 2003. **31**(23): p. 6710-6721.

ANALYSIS OF SELECTED REGULATORY GENES IN PROSTATE CANCER CELL LINES

Marketa SZTALMACHOVA^{1,2*}, Marian HLAVNA^{1,4}, Jaromir GUMULEC^{1,2}, Monika HOLUBOVA¹, Petr BABULA⁴, Jan BALVAN¹, Veronika TANHÄUSEROVA¹, Martina RAUDENSKA¹, Vojtech ADAM^{2,3}, Rene KIZEK^{2,3}, Michal MASARIK^{1,3}

¹ Department of Pathological Physiology, Faculty of Medicine, Masaryk University / Kamenice 5, CZ-625 00 Brno, Czech Republic

² Department of Chemistry and Biochemistry, Mendel University in Brno / Zemedelska 1, CZ-613 00 Brno, Czech Republic

³ Central European Institute of Technology, Brno University of Technology, Technicka 3058/10, CZ-616 00 Brno, Czech Republic

⁴ Department of Natural Drugs, Faculty of Pharmacy, University of Veterinary and Pharmaceutical Sciences, Palackeho 1-3, CZ-612 42 Brno, Czech Republic

*marketa.sz@seznam.cz

ABSTRACT

In this study, we aimed our attention on determining of expression of Bcl-2, c-Fos, c-Jun, Ki-67, NF- κ B and p53 genes in two prostate cell lines as 22Rv1 cell line, a model of aggressive partially androgen-sensitive prostate cancer and as PNT1A cell line, a model of healthy cell line.

INTRODUCTION

Prostate cancer is the second most frequently diagnosed cancer and the sixth leading cause of cancer death in males worldwide [1, 2]. Due to its high incidence and mortality, early diagnosis, identification of highly aggressive forms of clinically silent and understanding of disease pathogenesis with typical metabolic differences in order to develop specifically targeted therapy are needed. As a results of numerous studies on cell as well as on prostate cancer patients, there have been found several compounds connected with tumorigenesis in prostate cells including Bcl-2. This intracellular protein belongs to a large group of proteins called "Bcl-2 family" [3]. Bcl-2 acts as an inhibitor of apoptosis. It has been suggested that overexpression of the Bcl-2 oncoprotein in human cancer cells contributes to their resistance to chemotherapy- and radiotherapy-induced apoptosis and is connected with unfavourable prognosis [4]. In the fact, the majority of human prostate tumours overexpress Bcl-2, which is responsible for tumours resistance to radiotherapy and chemotherapy [5, 6]. Moreover, it has been reported that Bcl-2 expression is associated with tumour progression and unfavourable prognosis in prostate cancer patients [4, 7, 8] and is associated with the development of androgen-independent prostate cancer [9]. Possible associations with other proteins connected with tumour processes as c-Fos, c-Jun, Ki-67, NF- κ B and p53 can be assumed. Therefore, we aimed our attention on determining of expression of Bcl-2, c-Fos, c-Jun, Ki-67, NF- κ B and p53 genes in two prostate cell lines as 22Rv1 cell line, a model of aggressive par-

tially androgen-sensitive prostate cancer and as PNT1A cell line, a model of healthy cell line.

MATERIAL AND METHODS

Cell line PNT1A was cultivated in RPMI 1640 medium with 1% penicillin/streptomycin and 10% FBS. Cell line 22Rv1 was cultivated in RPMI 1640 without phenol red. Both lines were cultivated in incubator (37°C and 5% CO₂).

For RNA isolation was used High pure total RNA isolation kit (Roche, Switzerland). RNA isolation was performed according to manufacturer's instructions. Isolated RNA was used for cDNA construction. 600 ng of total RNA was transcribed using Transcriptor first strand cDNA synthesis kit (Roche, Switzerland). 20 μ l of prepared cDNA was diluted with RNase free water to 100 μ l and directly analysed by real-time polymerase chain reaction.

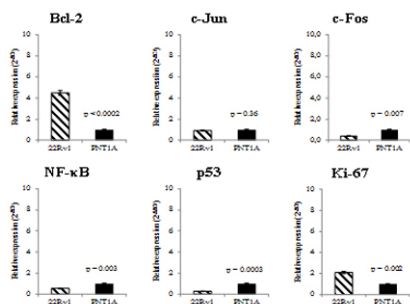
RT-PCR was performed in triplicates using the TaqMan gene expression assay system with 7500 real-time PCR system (Applied Biosystems, USA). The amplified DNA was analysed by the comparative Ct method using β -actin as an endogenous control. Real-time PCR was performed under following amplification conditions: total volume of 20 μ l, initial denaturation 95 °C/10 min, than 40 cycles 95 °C/15 sec, 60 °C/1 min.

RESULTS AND DISCUSSION

We focused on comparison the base line expression of Bcl-2, c-Fos, c-Jun, NF- κ B, Ki-67 and p53 genes on the RNA level in prostate cell lines. Fig. 1 shows that 22Rv1 cells demonstrate different expression patterns in monitored genes compared to PNT1A cells. 22Rv1 cell line has 4.5-fold higher level of Bcl-2 anti-apoptotic

gene expression (n = 5). Interestingly, we found no significant differences (p > 0.05) in c-Jun gene expression in both cell lines. c-Fos gene that together with c-Jun forms important part of AP-1 transcription factor shows 2.5-fold down regulation in 22Rv1 cells. Ki-67, a nuclear protein that is associated with cellular proliferation, is present in 22Rv1 cell line in 2-fold higher concentration compared to PNT1A. Moreover, NF- κ B is present in half concentration in 22Rv1 cells compared to PNT1A and p53, a key regulator of apoptosis, shows 3.3-fold decreased level compared with PNT1A cell line.

Figure 1.: Comparison the base line expression of c-Fos, c-Jun, Nfk-B, Ki-67 and p53 genes on the RNA level. Base line transcription level of selected genes was conducted by RT-PCR.



CONCLUSION

Our results revealed that the base line expression of anti-apoptotic gene Bcl-2 is 4.5-fold higher in 22Rv1 than in PNT1A. This result is in accordance with the previously published papers, where elevated Bcl-2 expression in prostate cancer tumours has been reported [5, 7]. Furthermore, this elevation was associated with the development of androgen-independent prostate cancer [9] and also with radiotherapy and chemotherapy resistance.

ACKNOWLEDGEMENT

The work has been supported by CYTORES P301/10/0356, CEITEC CZ.1.05/1.1.00/02.0068, LPR 2011, IGA VFU 43/2011/FaF and NanoBio-MetalNet CZ.1.07/2.4.00/31.0023.

REFERENCES

- [1] Bray, F., et al., *Prostate cancer incidence and mortality trends in 37 European countries: An overview*. Eur. J. Cancer, 2010. **46**(17): p. 3040-3052.
- [2] Ghoneum, M. and S. Gollapudi, *Susceptibility of the human LNCaP prostate cancer cells to the apoptotic effect of marina crystal minerals (MCM) in vitro*. Oncol. Rep., 2009. **22**(1): p. 155-159.

- [3] Cory, S., D.C.S. Huang, and J.M. Adams, *The Bcl-2 family: roles in cell survival and oncogenesis*. Oncogene, 2003. **22**(53): p. 8590-8607.
- [4] Anai, S., et al., *Knock-down of Bcl-2 by antisense oligodeoxynucleotides induces radiosensitization and inhibition of angiogenesis in human PC-3 prostate tumor xenografts*. Mol. Cancer Ther., 2007. **6**(1): p. 101-111.
- [5] Xu, L., et al., *(-)-gossypol enhances response to radiation therapy and results in tumor regression of human prostate cancer*. Mol. Cancer Ther., 2005. **4**(2): p. 197-205.
- [6] Nomura, T., et al., *Expression of the inhibitors of apoptosis proteins in cisplatin-resistant prostate cancer cells*. Oncol. Rep., 2005. **14**(4): p. 993-997.
- [7] Concato, J., et al., *Molecular Markers and Death From Prostate Cancer*. Ann. Intern. Med., 2009. **150**(9): p. 595-U6.
- [8] Dachille, G., et al., *Prognostic role of cell apoptotic rate in prostate cancer: Outcome of a long-time follow-up study*. Oncol. Rep., 2008. **19**(2): p. 541-545.
- [9] Catz, S.D. and J.L. Johnson, *BCL-2 in prostate cancer: A minireview*. Apoptosis, 2003. **8**(1): p. 29-37.

OPTIMIZATION OF SHEATHLESS AND ELECTRODELESS INTERFACE FOR INORGANIC ION SEPARATION

Anna TARANTOVA^{1,2}, Frantisek FORET¹

¹ Institute of Analytical Chemistry, Czech Academy of Sciences
Veveří 967/97, 602 00 Brno, Czech Republic

² Department of Chemistry, Faculty of Science, Masaryk University
Kotlářská 267/2, 61137 Brno, Czech Republic

ABSTRACT

The analysis of inorganic ions by capillary electrophoresis (CE) with contactless conductive detection is in this paper depicted. Separation in a commonly used CE instrumentation is reached due to the potential gradient created by applying voltage between the entrance and exit of the separation capillary. In our experimental design the voltage is applied only at the entrance of the capillary while the opposite capillary end is sharpened into an electrospray tip positioned in front of the grounded vacuum inlet electrode. This simple experimental design aims at optimization of on-line coupling of capillary electrophoresis to a mass spectrometer^{1,2}.

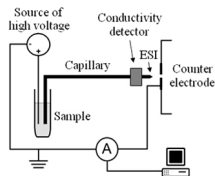
INTRODUCTION

A very sensitive analysis of complex samples is required in modern analytical chemistry. Coupling a separation method to a sensitive detector such as mass spectrometer can appear as an ideal approach. The use of a proper interface is critical for successful coupling. We have employed an interesting type of interface utilizing a thin separation capillary where the electrophoretic current is in balance with the electrospray current. This system is called a sheathless and electrodeless interface¹.

MATERIAL AND METHODS

Our experiments were carried out using a laboratory made instrumentation (Figure 1). CE was performed in silica fused capillaries of 15 cm and 25 μm I.D with the end sharpened into a tip. Nine kV voltage was applied at the capillary inlet. Approximately 1 mm in front of the electrospray tip a ground electrode was situated. For detection of analyzed ions TradeDec Contactless Conductivity Detector was positioned 13 cm from the injection entrance of the capillary. Sample was loaded from a gas pressurized chamber used also to assist the liquid flow inside the capillary during the experiments with electrospray.

Figure 1: The instrumentation employing sheathless and electrodeless interface



RESULTS AND DISCUSSION

When optimizing electrophoretic separation driven by the electrospray current the most challenging task is adjustment of suitable current conditions to reach effective separation and maintaining sufficient potential at the spray tip². Voltage is applied into sample reservoir, where the start of a separation capillary is dipped. This voltage is distributed partly along the capillary, driving the separation, and partly on the electrospray plume. The electric field strength inside the separation capillary depends mainly on its length and diameter and also on the composition of the separation buffer.

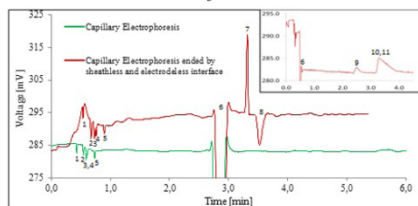
In the previous papers sharp tips were reached by pulling wide bore capillaries (i.d. 75 μm)². Unfortunately, this leads to narrowing of the separation channel resulting in a large potential drop. To avoid this phenomenon a narrow bore capillary (i.d. 25 μm) was sharpened only from the outside in our system. Although organic solvents significantly help electrospray plume formation³ we have deliberately avoided them to prevent poor reproducibility of the electrophoretic separations and low conductivity of the separation electrolyte. We have used 1% formic acid as the separation electrolyte ensuring low pH for sufficient

charging of analytes and preventing charging of capillary walls. The electrospray plume was monitored by a CCD camera.

Mixture of inorganic cations (Na^+ , K^+ , Li^+ , Ca^{2+} , Zn^{2+}) and anions (Cl^- , I^- , NO_3^- , CH_3COO^-) have been chosen as a model sample. The comparison of separation by our instrumentation and separation by usual capillary electrophoresis is in Figure 2. Whereas all five cations were detected, anions were visible only at higher flow rates, because of their negative motilities prevent reaching the detector under chosen conditions.

Figure 2.: Separation of inorganic ions by CE and CE ended by ESI at flow rate 3,4 nL/min. The inset shows separation at 16,3 nL/min. Separation voltage: +9 kV, Capillary: L = 13/15 cm, i.d 25 μm , BE: 1% HCOOH , Sample concentration: 12 $\mu\text{g/mL}$, Loading of sample: P = 0,1 Atm, t = 10 s.

1 - K^+ , 2 - Ca^{2+} , 3 - Na^+ , 4 - Zn^{2+} , 5 - Li^+ , 6 - water, 7, 8 - unknown, 9 - NO_3^- , 10 - I^- , 11 - Cl^-



CONCLUSION

We have investigated main characteristics of sheathless and electrodeless interface and we have successfully used this interface for separation of inorganic ions. In further studies we are going to replace ground electrode for a mass spectrometer and analyzed larger organic molecules.

ACKNOWLEDGEMENT

The work has been supported by GACR P20612G014, P206-11-2377, P301-11-2055 and CZ.1.07/2.3.00/20.0182.

REFERENCES

- (1) M. Mazereeuw, A. J. P. Hofte, U.R. Tjaden and J. van der Greef *Rapid Communications in Mass Spectrometry* **1997**, *11*, 981-986.
- (2) L. Goodwin, J. R. Startin, B. J. Keely, D. M. Goodall *Journal of Chromatography A* **2003**, *1004*, 107-119.
- (3) G. A. Valaskovic, J. P. Murphy, III and M. S. Lee *Journal of American Society for Mass Spectrometry* **2004**, *15*, 1201-1215.

CONSTRUCTION OF ELECTROCHEMICAL BIOSENSORS BASED ON NANOMATERIALS

Jan TKAC*, Jana SEFCOVICOVA, Jaroslav FILIP, Peter GEMEINER

Department of Glycobiotechnology, Institute of Chemistry, Slovak Academy of Sciences, Dúbravská cesta 9, 845 38 Bratislava, Slovak Republic

*Jan.Tkac@savba.sk

ABSTRACT

Construction of electrochemical biosensors with enhanced performance of detection has been carried out by an integration of carbon nanotubes into a sensing interface. Two main dispersing agents from the group of biopolymers namely chitosan and hyaluronic acid were chosen to prepare stable dispersions of carbon nanotubes in a short time with high reproducibility. Such dispersions provided a matrix compatible with enzymes and microbial cells, a feature important for construction of robust electrochemical biosensors. Implementation of other nanomaterial graphene into an electrochemical transduction scheme is shortly discussed, as well.

INTRODUCTION

Carbon nanotubes (CNTs) have been recognised as one of the most promising electrode materials in the field of electroanalysis because many electroactive species can be detected at lower overvoltage compared to ordinary electrodes resulting in increased selectivity and sensitivity of detection in a complex matrix [1]. However, unmodified CNTs are extremely hydrophobic and assemble into bundles and ropes of individual nanotubes. For applications in electrochemistry, it is often necessary to make them soluble. Different approaches to solubilise CNTs have appeared in the literature [2,3], but the use of biopolymers might be beneficial due their biocompatibility and natural occurrence. In this work application of two biopolymers chitosan and hyaluronic acid to disperse CNTs was investigated with subsequent integration of such dispersions of CNTs for construction of electrochemical biosensors.

MATERIAL AND METHODS

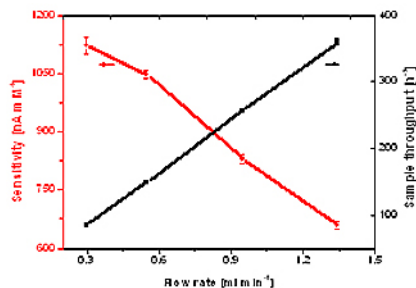
Electrochemical measurements including chronoamperometry, cyclic voltammetry and electrochemical impedance spectroscopy have been carried out as previously described [3-8] using glassy carbon electrode (GCE) as working, Pt electrode as counter and Ag/AgCl as a reference electrode. Dispersions of CNTs in various agents were prepared with the aid of sonication [3-8]. A CNT modified GCE electrode was further modified by enzymes galactose oxidase [4] and D-sorbitol dehydrogenase [5,6], or by bacterial cells *Gluconobacter oxydans* [7,8]. Biosensors were tested in their ability to detect analytes in complex samples such as blood plasma [4], fermentation samples during conversion of D-sorbitol into L-sorbose (a precursor of vitamin C) [6] or during conversion of glucose into ethanol [8]. The biosensor performance

was validated by a reference analytical method - HPLC [6,8].

RESULTS AND DISCUSSION

A wide range of dispersants including solvents, polyelectrolytes and biopolymers were tested in the ability to prepare dispersions of CNTs with high yield, dispersion stability in a short time [3]. The most efficient dispersing agent was a biopolymer chitosan able to prepare stable CNTs dispersion in just 15 min. Moreover, such chitosan dispersions of CNTs were subsequently used for preparation of a robust biosensor device for galactose detection in human sera [4]. When the biosensor was integrated into a flow injection system, a high performance of galactose detection by the biosensor was found out e.g. sensitivity of $16 \mu\text{A mM}^{-1} \text{cm}^{-2}$, a sample throughput of 150 injections *per* hour and assay precision of 1.5% [4].

Figure 1: The effect of a flow rate on the response sample throughput of the galactose biosensor



Recently our effort culminated in using another biopolymer – hyaluronic acid (HA) as a per-

spective dispersant of CNTs. It was proved HA-CNT dispersions were able to provide a highly stable interface in detecting of NADH, a cofactor of more than 500 enzymes [5]. Moreover, dispersions of CNTs in HA provided reversible electrochemistry of two redox probes (Table 1), a very stable electrochemistry towards NADH (Fig. 2) and a high selectivity of NADH detection (Fig. 3). This observation can have huge consequences for preparation of stable electrochemical biosensors and biofuel cells.

Table 1: Redox behaviour of two redox probes on GCE modified by three CNT dispersions

	[Fe(CN) ₆] ³⁻			[Ru(NH ₂) ₂] ²⁺		
	ΔE _p [mV]	I _{pc} [μA]	I _{pa} [μA]	ΔE _p [mV]	I _{pc} [μA]	I _{pa} [μA]
CNT-DMF	93	6.4	6.1	64	8.2	5.6
CNT-HA	65	8.8	8.5	63	9.0	6.7
CNT-CHI	71	7.9	8.4	68	8.6	5.0

DMF – dimethylformamide, HA – hyaluronic acid, CHI – chitosan

Figure 2: A) An operational stability of two devices towards NADH and B) a device based on CNT-HA. A response shown at time interval of 22 h (full red circles) is due to injection of a fresh NADH

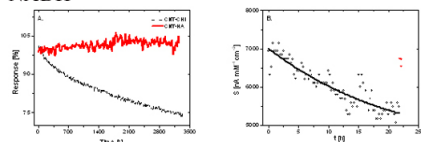
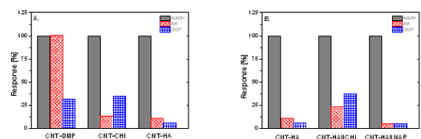
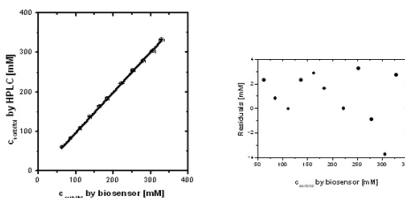


Figure 3: A) An interference study with two interfering compounds AA (ascorbic acid) and DOP (dopamine) for NADH sensor. B) The effect of an outer layer (e.g. chitosan – CHI or Nafion – NAF) on the selectivity performance of NADH device in the presence of interfering compounds



HA as a negatively charged biopolymer was subsequently used for electrostatic docking of a redox shuttle to increase an overall performance of a biosensor device for D-sorbitol [6]. The biosensor performed very well in analysis of D-sorbitol samples during its bioconversion into L-sorbose, which is a precursor in vitamin C synthesis (Fig. 4).

Figure 4: Validation of D-sorbitol analysis in fermentation samples by the biosensor with HPLC



The last approach based on CNTs was their direct mixing with bacterial cells of *G. oxydans* in order to prepare high-performance microbial 3-D bioanode for a mediated biosensor device [7]. Such ethanol biosensor offered a short response time of 18 s and a sensitivity of 162 μA cm⁻² mM⁻¹, the highest so far observed for microbial-based biosensor bioanodes for ethanol sensing and this device was successfully applied in an off-line monitoring of ethanol during fermentation (Table 2) [8]. Such bioanode is a perspective for preparing of low cost microbial biofuel cells, as well.

Table 2 Analysis of EtOH in fermentation samples by the biosensor (Bs) and by HPLC

Sample No.	EtOH – HPLC [mM]	EtOH – Bs [mM]	(Bs – HPLC)/HPLC [%]
1	1265	1208	-4.49
2	1353	1352	-0.05
3	1445	1481	2.49
4	1572	1525	-3.00
5	1710	1669	-2.43

CONCLUSIONS

CNTs showed beneficial properties for enhancement of an overall performance of electrochemical sensors and biosensors. Protocols of surface patterning by nanomaterials established so far for biosensors are utilisable in construction of bioanalytical devices based on biorecognition and for preparation of biofuel cells, as well. A substantial effort is focused on the use of graphene for surface patterning with practical applications in preparing lectin biochips, electrochemical biosensors and biofuel cells.

ACKNOWLEDGEMENT

The financial support from SAV-FMEHP-2008-04-04 and from VEGA 2/0127/10 was acknowledged. This contribution/publication was the result of the project implementation: Centre for materials, layers and systems for applications and chemical processes under extreme conditions—stage II, supported by the Research and Development Operational Program funded by the ERDF.

REFERENCES

- [1] Sassolas A, Blum LJ, Leca-Bouvier BD: *Biotechnology Advances*, 30 (2012), 489-511
- [2] Vashist SK, Zheng D, Al-Rubeaan K, et al: *Biotechnology Advances*, 29 (2011), 169-188
- [3] Tkac J, Ruzgas T: *Electrochemistry Communications*, 8 (2006), 899-903
- [4] Tkac J, Whittaker JW, Ruzgas T: *Biosensors and Bioelectronics*, 22 (2007), 1820-1824
- [5] Filip J, Šefčovičová J, Tomčík P, Gemeiner P, Tkac J: *Talanta*, 84 (2011), 355-361
- [6] Šefčovičová J, Filip J, Tomčík P, et al.: *Microchimica Acta*, 175 (2011), 21-30
- [7] Šefčovičová J, Filip J, et al.: *Electrochemistry Communications*, 13 (2011), 966-968
- [8] Šefčovičová J, Filip J, et al. *Biotechnology Letters*, DOI: 10.1007/s10529-012-0875-x

ELECTROCHEMICAL FABRICATION OF OPTICAL BIOSENSOR FOR DNA DETECTION

Jirina VALKOVICOVA¹, Radim HRDY^{2,3}, Jana DRBOHLAVOVA^{2,3*},
Jaromir HUBALEK^{2,3}

¹ Brno University of Technology, Faculty of Electrical Engineering and Communication,
Department of Biomedical Engineering, Kolejní 2906/4, 612 00 Brno, Czech Republic

² Brno University of Technology, Faculty of Electrical Engineering and Communication,
Department of Microelectronics, Technická 3058/10, 616 00 Brno, Czech Republic

³ Central European Institute of Technology, Brno University of Technology, Technická 3058/10,
616 00 Brno, Czech Republic

*drbohla@feec.vutbr.cz

ABSTRACT

The work is focused on quantum dots (QDs) array fabrication from non-toxic titanium dioxide using template based non-lithographic method, their luminescence properties study and finally their usage for DNA optical detection *in situ*. The paper describes TiO₂ QDs surface modification with gold using suitable template technique and subsequent functionalization of gold modified QDs surface via avidin-biotin molecules and further with single stranded DNA (ssDNA) or oligonucleotides. This functionalization step provides a suitable base for subsequent hybridization reaction with detected nucleic acid. The system of biosensor (TiO₂ QDs modified with gold and biomolecules) is designed for rapid optical diagnosis of viral diseases.

INTRODUCTION

Nucleic acids are found in all living cells and viruses. Their main task is to store the genetic information, which is ensured by transmission of hereditary characteristics from one generation to another. The main reasons why it is important to detect nucleic acids, are quick and early diagnosis of diseases and monitoring and improving the effects of mutations in gene therapy.

The term of biosensor is understood as a device that is able to detect the biochemical properties of macromolecules that are part of living systems, or even to monitor all living systems. For effective analysis, biosensor distinct specificity and ability to clearly detect intended target - in this case DNA – are the most significant issues to be solved [1].

For achieving specific detection, the system of titanium dioxide QDs (TiO₂ QDs)-gold (Au)-avidin-biotin-single-stranded nucleic acid (ssNA) is designed in this paper. TiO₂ QDs array fabricated through highly ordered nanoporous alumina template serves as an optical biosensor for the detection of nucleic acids *in situ* [2]. Due to the quantum confinement effect, these QDs exhibit the light emission after irradiation, so-called fluorescence. Modification of their surface with gold should increase the intensity of luminescence and simultaneously allows the strong conjugation to hydrogen containing functional groups, such as amine (NH₂) and thiol (SH) groups.

One of the possibilities how to modify the surface of QDs with gold is the electrochemi-

cal deposition. Modifying material is dispersed in the aqueous solution, which represents the electrolyte. The substrate with TiO₂ QDs represents the cathode, on which the reduction of gold ions takes place. The deposition of gold through nanoporous template fabricated directly on the substrate enables the formation of highly ordered nanostructures (e.g. nanoshells or nanowires) instead of thin compact gold layer [3]. Modified TiO₂/Au QDs array may be functionalized with avidin, which contains two cysteine molecules bearing -SH group. Further, avidin may be conjugated with biotinylated ssNA (or oligonucleotide), which is able to bind the detected nucleic acid through hybridization reaction. The detection of viral NA should be easily performed with spectrofluorimetry. The process of detection is based on the presumption of free viral NA presence in a patient blood if one is infected with viral diseases such as influenza, AIDS, or hepatitis. A drop of patient blood may be put on the biosensor surface and in the case when the patient is infected, the viral nucleic acid will hybridize with ssNA on the biosensor surface. The hybridization may result in the decrease of fluorescence intensity of QDs. If the patient is healthy, the free NA is not presented in his blood, therefore the hybridization will not occur and the fluorescence intensity remains unchanged.

MATERIAL AND METHODS

Formation of TiO₂ QDs via anodization process

TiO₂ QDs were made by template anodic oxidation of titanium layer sputtered on silicon wafer. Two thickness combinations of Ti/Al bilayers were used: 20 nm/500 nm and 150 nm/250 nm. The detailed procedure is described in paper [4]. Briefly, 3 M sulphuric acid was chosen as an electrolyte and two step anodization process of Ti/Al bilayer ran in constant potential mode at 4 V and 11 °C.

Electrochemical deposition of gold

The alumina nanoporous template was kept after the anodization of Ti/Al was finished, to ensure the galvanic deposition of gold on TiO₂ QDs surface only. 100 ml electrolyte solution was composed of 0.6 g of K[Au(CN)₂] and 0.232 g of H₃BO₃. Various deposition conditions were tested including long pulses in the range of several tens of seconds at low and high current, as well as short pulses lasting 1 second at low or high currents. The conditions are summarized in Table 1. When the process of gold deposition ended, the alumina template was removed by etching in a mixture of H₃PO₄ (50 ml L⁻¹) and CrO₃ (30 g L⁻¹) at 60 °C for 10 min.

Table 1: Conditions of galvanic deposition of gold on TiO₂ QDs surface through alumina nanoporous template

	constant current (mA)	time (s)
1.	50	30
2.	50	1
3.	0.5	30
4.	0.5	1
5.	0.5	2x1
6.	0.4	1
7.	0.2	1

TiO₂/Au QDs characterization

The physical properties including TiO₂ QDs size, homogeneity in distribution and immobilization of gold were analyzed using scanning electron microscopy (SEM) Mira II MLU (TeScan Mira, Brno, Czech Republic). The fluorescence properties of fabricated system were investigated by fluorescence spectroscopy (Horiba, Jobin-Yvon) with laser diode excitation at

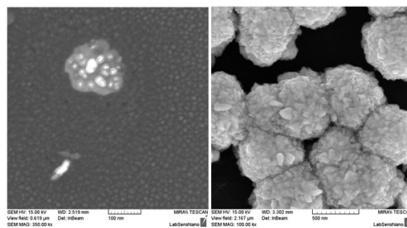
350 nm and using photomultiplier (T1 PMT) detector.

RESULTS AND DISCUSSION

To obtain the small QDs size, small pore diameter in alumina template is required. The choice of suitable anodization conditions allowed us to fabricate alumina template with pore diameter about 5 nm and subsequently TiO₂ QDs with size of 10 nm, which is necessary to reach the quantum confinement effect and thus their desired optical properties.

Concerning the QDs modification with gold, first promising results were observed when short times and low pulses were applied during galvanic deposition, because more homogeneous gold distribution was achieved compared to long times and pulses at high current (50 mA), which resulted in gold deposition over all TiO₂ QDs surface in the form of rocks (see Figure 1). However, the process was limited by small current and time range of the measuring device, hence further optimization of deposition equipment will be done to reach suitable low current values. At this moment, the best results, i.e. the most homogenous coverage according to SEM analysis, were achieved applying the pulse of 1 s under constant current of 0.2 mA. The detailed analysis of samples using energy-dispersive X-ray spectroscopy (EDX) is currently in the process to detect the deposited gold on TiO₂ QDs.


Figure 1. SEM images of gold aggregates on TiO₂ QDs deposited under 0.2 mA at 1 s (left) and large gold rocks on the surface of TiO₂ QDs deposited under 50 mA at 30 s (right).



The samples evaluation using spectrofluorimetry showed that before annealing, TiO₂ QDs did not reveal the fluorescence properties. After annealing, which is necessary for transformation of amorphous titania into anatase phase and thus for luminescence effect, the additional measurements of the samples will be done together with biomolecules functionalization.

CONCLUSION

The process of Au deposition on TiO₂ QDs



surface was strictly influenced with alumina template quality, since the defects in this layer facilitate the deposition at these places and thus results in non-homogeneous distribution in the form of aggregates instead of thin nanoshells. To solve this issue, new Al deposition approach is now tested, which should improve the morphology of template layer.

ACKNOWLEDGEMENT

The work has been supported by the grants GACR P102/10/P618, KAN 208130801 and CEITEC CZ.1.05/1.1.00/02.0068.

REFERENCES

- [1] Brown E, et al., *Analytical Biochemistry*, 383 (2008), 2, 226-235
- [2] Drbohlavova J, et al., *International Journal of Electrochemical Sciences*, 7 (2012), 1424-1432
- [3] Cao G Z and Liu D W, *Advances in Colloid and Interface Science*, 136 (2008), 2, 45-64
- [4] Drbohlavova J, et al., *Nanoscale Research Letters*, 7:123 (2012), 1-4

INSTANTANEOUS QUALITATIVE ANALYSIS OF PIGMENTS BY RAMAN SPECTROSCOPY

Lubomir VANCO*¹, Magdalena KADLECIKOVA¹

¹Faculty of Electrical Engineering and Information Technology, Slovak University of Technology, I. L. Kovicova 3, 812 19 Bratislava, Slovak Republic

*lubomir.vanco@stuba.sk

ABSTRACT

The aim of this paper is identification of pigments used in artistic paintings by Raman spectroscopy. We collected Raman spectra from a real painting by classical method as well as the surface enhanced spectrum of 1,2-dihydroxyanthraquinone. We demonstrated exceptional capability of Raman spectroscopy for rapid and comfortable identification of pigments for archeometric or forensic purposes.

INTRODUCTION

Raman spectroscopy as a complementary method to infrared spectroscopy is governed by inelastic scattering of light. Both methods yield complete information about vibrational and rotational states of a molecule. The frequencies of the vibrations depend on the elasticity constants within the molecule (internal modes) or in the crystal (external modes). Since the Raman spectrum is a fingerprint of a molecule, the method is applied commonly in chemical analysis. From the viewpoint of an analyst, Raman spectroscopy has many advantages when compared with other analytical tools. The method is non-destructive, contactless, instantaneous and appropriate for analysis of samples in any state (solid, liquid or gaseous). Furthermore, it does not require vacuum conditions and therefore it is widely used for identification of pigments [1–4], mainly in cases when it is of crucial interest to distinguish between the different pigments composed of the same elements.

MATERIAL AND METHODS

Samples coated with real oil paint (and the sample with 1,2-dihydroxyanthraquinone diluted in methyl alcohol) were examined using a JobinYvon Labram 300 Raman confocal microscope. The apparatus included a He-Ne laser providing 632.8 nm monochromatic light, a grid monochromator with 1800 grooves per mm and a CCD air cooled multichannel detector with resolution better than 1.3 cm⁻¹. During measurement, the laser power was set up either 1.7 or 17 mW. The spectrometer was calibrated on the band of single crystalline silicon (100), 520.7 cm⁻¹. The confocal hole and the slit were maintained at maximum apertures to ensure all the scattered light entering the detection system. Each spectrum was recorded via an 80× long working distance objective in backscattering geometry. The spectra were processed by the software package Labspec and by Origin.

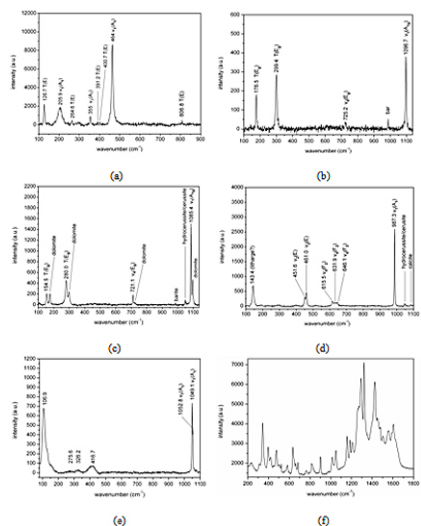
RESULTS AND DISCUSSION

The time needed to collect Raman spectra depends on chosen measurement conditions and on character of a sample. Normally, pure pigments which exhibit Raman spectrum are identified within few seconds but in some cases it is not possible to measure a spectrum due to enhanced fluorescence [5]. In general one has two main possibilities when adjusting the measurement conditions. Both are based on manipulation of the acquisition time. Either the number of accumulations or the integration time can be adjusted. In the first case measured spectrum is averaged after each acquisition within the set number of measurements. When photobleaching is exploited, then fluorescence can be partially reduced and spectrum can be visible. The higher the accumulations number the lower noise pattern. If the Raman signal is not enough strong it is possible to increase integration time which is defined as the time of detector filling. Once the integration time expired, detector is drained and accumulated signal is processed. Increased integration time does strongly affect the intensity of Raman bands and noise can be suppressed when apparatus is set up in total counts regime. Therefore the total time for collecting the spectra is given by the product of $AN \times IT \times n$, where AN is accumulation number and IT is integration time and n is the number of shifts of grating in dispersive spectrometers (in Fourier transform spectrometer n can be considered as one). Every spectroscopic method including Raman spectroscopy should be used as only qualitative (or in the very best cases as semiquantitative) method.

The very effective method of surface enhanced Raman spectroscopy (SERS) has been developing through the late 70's until now. The technique has been continuously used not only for the background suppression in Raman spectra but also for enhancing those Raman peaks

which can be measured but are of low intensity [6]. SERS needs an active substrate to work properly and analysis on active substrates requires a liquid sample. Therefore the technique is used.

Fig. 1.: Raman spectra taken from historical pigments, vibrations observed are denoted by their irreducible representation. (a) α -quartz, (b) dolomite, (c) calcite + dolomite mixture, (d) bar-ryte + unknown component, possibly litharge, (e) lead white, all spectra were accumulated with AN=500, IT=1, n=1. (f) Surface enhanced spectrum of 1,2-dihydroxyantraquinone (10^{-5} M solution in methyl alcohol) dropped on active substrate, AN=2, IT=1, n=2



rather in analysis of liquid samples than in solid state analysis [7–8]. The physical principles of enhanced Raman scattering are based on localized plasmon resonances. Proper conditions for plasmon excitation are easily met in noble metals like silver or gold in the visible region. As a consequence, substrates based on nanostructured silver or gold surface can be used as active substrates. We demonstrate herein the example of surface enhanced Raman spectrum which is typical for very short acquisition time and well developed Raman bands (Fig. 1f).

CONCLUSION

Identification of the artistic pigments by Raman spectroscopy is presented in this paper. Raman spectroscopy has exceptional competence for distinguishing such substances and occasional problems with fluorescence can be overcome

by surface enhanced technique. Analysis of pigments is crucial for purposes of restoring of art pieces and can be useful in forensic science. The method is very rapid and requires minimum of effort.

ACKNOWLEDGEMENT

This work was financially supported by grant of Scientific Grant Agency of the Ministry of Education of Slovak Republic and the Slovak Academy of Sciences No. VEGA-1/1102/11 and VEGA-1/1103/11.

REFERENCES

- [1] Bersani D, Antonioli G, Lottici P P : *Spectrochimica Acta Part A*, 59 (2003) 2409–2417
- [2] Bersani D, Lottici P P, Casoli A, et all.: *Journal of Cultural Heritage*, 9 (2008) 97–102
- [3] Smith G D, Clark R J H : *Journal of Archaeological Science*, 31 (2004) 1137–1160
- [4] Duran A, Siguenza M B, Franquelo M L, et all.: *Analitica Chimica Acta* 671 (2010) 1–8
- [5] Bell S E J, Bourguignon E S O, Dennis A : *Analyst* 123 (1998) 1729–1734
- [6] Chen S T, et all.: *Diamond and Related materials*, 24, 161–165 (2012)
- [7] Kulisch W, et all.: *Diamond and Related materials*, 20, 1076–1081 (2011)
- [8] Zhao J, Tian R, Zhi J : *Thin Solid Films*, 516, 4047–4052 (2008)

ELECTROANALYSIS OF POLYAMINO ACIDS ON MERCURY ELECTRODE

Veronika VARGOVA, Marko ZIVANOVIC, Veronika OSTATNA, Emil PALECEK

Institute of Biophysics, Acad. Sci. CR, v.v.i., Kralovopolska 135, 612 65 Brno, CR

ABSTRACT

Polyamino acids (poly(aa)) can be considered as an intermediate model system between peptides and macromolecular proteins. Here we used polyamino acids such as polylysine, polyarginine and polyhistidine to explore how different amino acid (aa) residues contribute to the catalytic hydrogen evolution reaction.

INTRODUCTION

At mercury electrodes, peptides and proteins produce chronopotentiometric peak H due to the catalytic hydrogen evolution (CHER) [1]. Peak H represents thus an analogy with the polarographic presodium wave, but in contrast to this wave, it is well developed and suitable for the analysis [2]. Peak H was displaying sensitivity to local and global changes in protein structure of proteins at submicromolar concentrations [2-4]. Recently experiments with polyAA showed that at pH 6.0 polylysine and polyarginine, Trp produced peak H but polyglutamic acid did not [5]. The height of the polylysine peak increased with the buffer capacity and decreased with increasing pH, in a good agreement with properties of the catalytic hydrogen evolution reaction (CHER). It can be concluded that close to neutral pH, amino acid residues containing labile protons, such as cysteine, lysine, and arginine, can be involved in the electrocatalysis responsible for peak H.

MATERIAL AND METHODS

Polylysine (polyLys, M.W.= 4-15 kDa pKa=10), polyarginine (polyArg, M.W.= 5-15 kDa, pKa=12.5), polyhistidin (polyHist, M.W. = 5-15 kDa, pKa = 6) were purchased from Sigma. Poly(aa)s were dissolved in triply distilled water. Concentration of investigated poly(aa)s in stock solution was 1mg/ml.

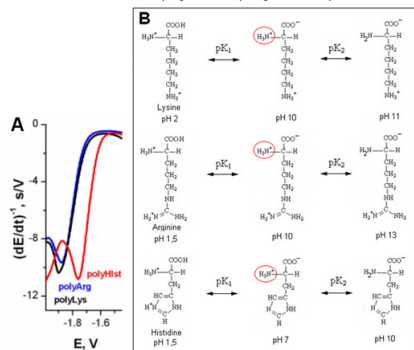
In all adsorptive stripping experiments, the analyte was adsorbed on the mercury surface from the stirred poly(aa) solution at a given accumulation potential (E_A -1.4 V), during the chosen accumulation time (100 s); after a quiescent period of 4 s, voltammograms were then recorded. A standard three electrodes system was used for the measurement. A hanging mercury drop electrode (HMDE) was employed as the working electrode. An Ag/AgCl/3M KCl electrode was used as the reference electrode and Pt electrode as the auxiliary electrode.

LSV parameters: step 2 mV, scan rate 20 mV/s, t_A 100s, E_A -1.4 V

RESULTS AND DISCUSSION

We studied ability of different polyLys, polyArg and polyHis to catalyze hydrogen evolution on at HMDE using linear sweep voltammetry (LSV).

Figure 1 A. Voltammograms of polyArg (blue), polyLys (black) and polyHist (red) in 50 mM McIlvaine at pH 6 B Scheme of dissociation of lysine, arginine and histidine, LSV: step 2 mV, scan rate 20 mV/s, t_A 100 s, E_A -1.4 V, t 26 °C



5 μ g/ml of poly(aa) was adsorbed at accumulation potential, E_A of -1.4 V, during accumulation time, t_A of 120 s, followed by linear sweep voltammograms recording. Accumulation potential -1.4 V was chosen to positively charged poly(aa) were immobilized at negatively charged HMDE surface. All of these poly(aa) produced well developed LSV peak at pH 6 (Fig 1A). We observed no significant differences in the height of LSV peaks of these poly(aa)s, but changes in their peak potentials. PolyLys yielded LSV peak at the most negative potential (E_p of -1.9 V), about 20 mV more negative than peak of polyArg and about 130 mV more negative than peak of polyHis. Our preliminary results show that po-

lyLys, polyHist and polyArg induce CHER at the Hg electrode in a wide pH range. A more detailed study of poly(aa)s is under way.

CONCLUSION

In recent years CHER of proteins measured by chronopotentiometric and voltammetric stripping at Hg and amalgam electrodes appeared as a new tool in protein analysis [1, 2] (and references therein). Study of poly(aa) contributes to elucidation of CHER by proteins. The disadvantage of poly(aa) are their poorly defined lengths and conformations. Further work is ongoing to study of peptides with well defined properties.

ACKNOWLEDGEMENT

This work was supported by GACR P301/11/2055 and AV0Z50040702.

REFERENCES

- [1] T. Doneux, V. Ostatna, E. Palecek, *Electrochim. Acta* **2011**, *56*, 9337.
- [2] E. Palecek, V. Ostatna, *Electroanalysis* **2007**, *19*, 2383.
- [3] E. Palecek, V. Ostatna, *Analyst* **2009**, *134*, 2076.
- [4] E. Palecek, V. Ostatna, M. Masarik, C. W. Bertoncini, T. M. Jovin, *Analyst* **2008**, *133*, 76.
- [5] M. Zivanovic, M. Aleksic, V. Ostatna, T. Doneux, E. Palecek, *Electroanalysis* **2010**, *22*, 2064.

MULTIMEDIA DATABASE OF THE FRUIT CROP VARIETIES

(AVAILABLE AT WWW.SUMPERACEK.WEBPARK.CZ)

Jiri VYSLOUZIL¹, Tomas NECAS²

¹Department of Food Technology, Faculty of Agronomy, Mendel University in Brno, Zemedelska 1, 613 00 Brno, Czech Republic

²Department of Fruit Growing, Faculty of Horticulture, Valticka 337, 69144 Lednice, Czech Republic

ABSTRACT

The main purpose of this work is a creation of the Multimedia database of fruit varieties, which will be accessible for everyone on the internet (<http://www.sumperacek.webpark.cz>). Each variety is provided with a picture or detail of the fruit and description. Different fruit crops are divided into 13 categories for better orientation. Most of the fruit crops contained are varieties which are suitable to grow in the Czech Republic climate. The database has the aim to upgrade regularly with new varieties from the breeding programs and also ones that recently appeared on the Czech market.

INTRODUCTION

In the Czech Republic, pomology (the science of growing, storing, and processing fruit) has a long tradition. In the past, many breeding programs were involved in development of new fruit varieties, for instance resistant apple varieties against apple scab (*Venturia inaequalis*), plum pox virus resistant plums (*Jojo*) etc. [1]. Big interest in growing fruits led specialists to write books of pomology for public readers. With large outbreak of internet use, information about pomology became available also in electronic form. This database of fruit crop varieties can be considered as one of them.

MATERIAL AND METHODS

When creating this database, Adobe software Dreamweaver CS4 was used to create a complete HTML code. ABBYY FineReader 9.0 was used to pick up a written text from pomological literature. Small corrections of pictures and resizing were performed in ACD See Pro 3.0. Most pictures of fruits were taken by the author; some photos were published with permission of co-author and correspondents, friends and other specialists in this field. Written literature about fruit varieties was the most important source of information, foreign digital publications and web documents concerning the topic were also incorporated.

RESULTS AND DISCUSSION

This database was not made from scratch. The original idea came from Mr. Tomas Necas, who in 2002 published a database on the web pages of Horticultural faculty in Lednice [2]. The continuation of his contribution was this new database, compiled for the purpose of diploma thesis introduced and defended in 2010. In contrast

with the old database, the new graphical design has been invented and supplemented by large amount of new varieties, which were newly integrated into the Czech assortment and by other important varieties. The 13 fruit categories include: Apples, Pears, Apricots, Peaches, Plums, Cherries and Sour Cherries, Strawberries, Raspberries and Blackberries, Rowans, Gooseberries, Currants, Nuts, Blueberries and Cranberries. Most of the varieties can be found in the Apple category (over 200), in Pears more than 80. The user interface is displayed in Fig. 1. The description of variety is processed into 2 frame model (Fig. 2).

Figure 1.: The main user interface



Figure 2.: The variety description

Gold Bohemia



Původ: Objevena jako náhodná plemenitá matice odrůdy 'Bohemia' na zahrádě v Písnici Josefem Tholem.

Zrání: Sklízí se ve druhé polovině října, srážce probrákos. Plody drží na stoncích vzhledem k delší stopce a spadají před sklízí. Konzumní zralost z vyřídilých políh je od ledna až do dubna.

CONCLUSION

The idea of having all fruit varieties on one place available for everyone on the internet is not new. However, it was difficult to find extensive and unaffected information on one place. This database is regularly upgraded and provides information for interested gardeners and fruit producers, as well as students of horticultural schools, where the subject of pomology is taught. Yet most important advantage of this work is obvious. The possibility to add and correct any wrong information mentioned should prevent this database to undergo aging.

ACKNOWLEDGEMENT

Authors would like to express thanks to all contributors who allowed them to use their photographs. In particular - Tomas Jan, Dusan Nestrta, Libor Dokoupil and other correspondents.

REFERENCES

- [1] Blazek J: Ovocnictví, (1998), 383 s.
- [2] Necas T, et al.: Multimedial database, (2004)

MONITORING OF RHEOLOGICAL PROPERTIES OF WINTER WHEAT FLOUR

Jiri VYSLOUZIL¹, Ludek HRIVNA¹

¹Department of Food Technology, Faculty of Agronomy, Mendel University in Brno, Zemedelska 1, 613 00 Brno, Czech Republic

ABSTRACT

The objective of this study is to collect and evaluate the parameters obtained by baking quality of 80 winter wheat cultivars, obtained from laboratories of company Penam from the crop years 2003-2010. The acquired data is applied to determine the suitability of each variety for bakery applications. The rheological characteristics of wheat dough were measured on Alveograph Chopin, particularly: deformation energy (W) and Alveograph ratio (P/L). Rheological parameters are subsequently compared with internal company quality standard and determine ability of each variety to correctly interpret the resulting quality of wheat bread.

INTRODUCTION

Wheat is one of the three major cereals dominating world agriculture today. Knowing the likely dough quality of wheat before it is purchased is of great value to millers. By knowing the dough quality, millers can avoid purchasing grain that does not meet their needs or can adjust the milling and blending process for given wheat properties [1]. Rheological characteristics, such as elasticity, viscosity, and extensibility, are important in view of the prediction of the dough processing parameters and the end products quality [2]. Chopin Alveograph is one of the most popular instruments used to measure rheological properties [3].

MATERIAL AND METHODS

Hard winter wheat samples from the crop years 2003-2010 were collected and analyzed by laboratories of company Penam and in breeding stations. List of all tested varieties and classification into quality groups in the Czech Republic shown in Table 1.

Table 1: Quality grouping of studied varieties

Quality group	Variety
Elite	Akteur, Ebr, Federer, Ludwig, Magister, Sulamit
A	Aladin, Alana, Alibaba, Bakfio, Baleška, Banquet, Barroko, Barvaton, Batis, Bill, Bodvák, Bohemia, Brilliant, Caphorn, Clever, Compost, Cubus, Darwin, Drifter, Elix, Euroflor, Globus, Grandor, Hana, Helmut, Ilias, Indum, Jinda, Karolínou, Kerubín, Manager, Megas, Mulan, Nela, Niagara, Radoza, Samantá, Sassia, Sultan
B	Apneche, Buteo, Hedvika, Herrik, Košutka, Meritto, Nikol, Orlando, Pitbull, Rbeha, RW, Nadal, Secese, Seladon, Simla, Svitava, Sárka, Vlasta
C	Bagoz, Biscay, Cibus, Corsaire, Dromos, Estico, Etela, Euroflor, Grandios, Hermann, Hertsido, Kodex, Mladá, Rapsoda, Sakura, Semper, Sitael, Versailles

Samples of grain (flour) were tested by selected baking quality parameters according to internal company standard (Table 2). Samples were analyzed for Moisture - according to DIN ISO 712, Grain mass - according to ISO 7971-2, Falling Number according to ISO 3093, Wet gluten content - PN 235/93-ICC 155, Gluten index (GI) - PN 235/93, Zeleny test - PN 252/95, pro-

tein content - PN 252/95. Rheological properties (Deformation energy W and Alveograph ratio P/L) of wheat flour were determined by a Chopin alveograph according to ISO 27971.

Table 2: Penam company standard

parameter	value	A	B	C
sampling	collective sample			
Humidity (%)	max.	14.5	14.5	15
Gluten % in dry matter	min.	28	26	23
Wet gluten % in dry matter	min.	31	29	26
Protein content (%)	min.	13.2	12.2	11.2
	min.	230	190	on agreement
Falling number (s)	max.	400	400	150-170-400
Zeleny test (ml)	min.	40	30	30
Deformation energy (W)	min.	220	190	170
Alveograph ratio (P/L)	interval	0.45-1.0	0.45-1.0	0.45-1.2
Grain mass (kg/hl)	min.	80	77	76
Grain admixtures (%)	max.	4	4	6
Impurities (%)	max.	0.3	0.5	0.5
Gluten index - GI	min.	70	55	40

RESULTS AND DISCUSSION

One-way ANOVA applied to compare means of rheological parameters in quality groups is shown in Fig. 1 and Fig. 2. The graphs show that samples of winter wheat from higher quality groups tends to show increased deformation energy. The highest average values of deformation energy W reached varieties from the group A: Barroko (305) and Caphorn (298), followed by elite variety Sulamit (284). Alveograph ratio P/L in contrast does not show linear trend and elite varieties tend to show the lowest mean values. This is confirmed by Hadnadev et al., who claims the ideal range of P/L from 0.4 to 0.8 for baking purposes. Value of 0.50 indicates either resistant and very extensible dough or moderately extensible, less resistant dough. Wheat suitable for confectionary products should exhibit P/L value lower than 0.50 [4]. The ideal Alveograph ratio combined with the best Deformation energy value (according to Penam laboratory experiences) corresponds on average with varieties: Akteur, Košutka, Iliad, Euroflor

and Ebi. The complete data set (693 samples) was also compared with the corporate standard Penam using other measured characteristics (Zeleny test, Grain mass, Falling number, Wet gluten content). 378 out of 693 samples met the criteria. Distribution of passed samples for each quality group shows Fig. 3.

Figure 1.: Mean Deformation energy in different quality groups

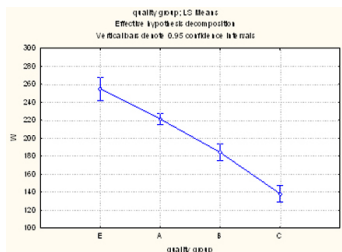


Figure 2.: Mean Alveograph ratio in different quality groups

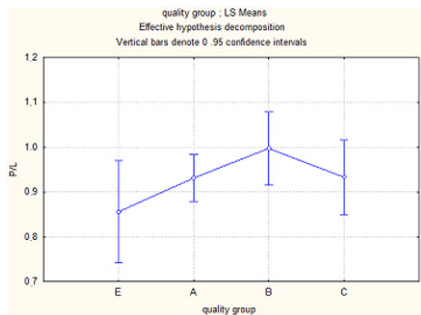
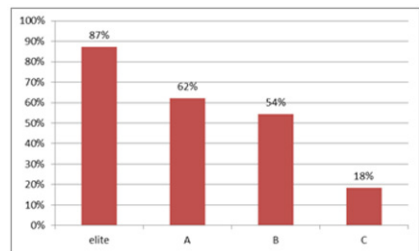


Figure 3.: Percentage of samples complying with Penam standard



CONCLUSION

Finding from this research showed that alveo-

graph measurement has a significant importance in winter wheat quality control. However, it is only one measure of flour quality. To accurately evaluate flour quality, performing basic wheat quality tests are necessary and they are still believed to be substantial in quality assessment. Varieties Akteur, Košútka, Iliad, Eurofit and Ebi seemed to be the most satisfactory when fitting the rheological parameters of company Penam. Particularly surprising is the convenience of variety Košútka, belonging to B quality group.

ACKNOWLEDGEMENT

Authors would like to express thanks to company Penam for providing with rheological values of different varieties and internal standards for evaluation of wheat samples in terms of rheology.

REFERENCES

- [1] Hruskova M, Smejda P: Czech Journal of Food Science, 21(1), (2003), 28-33
- [2] Jirsa O, Hruskova M, Svec I: Czech Journal of Food Sciences, 25, (2007), 243–248
- [3] Miralbes C: Food Chemistry, 88(4), (2004), 621-628
- [4] Hadnađev, Tamara D, Milica P, et al.: Wide Spectra of Quality Control, (2011)

ELECTROCHEMICAL DETERMINATION OF LOW CONCENTRATION POTASSIUM IONS IN UREA SOLUTIONS

Dmitry SOLOVEI, Petra BUSINOVA, Jaromir ZAK, Jiri SEDLACEK, Jaromir HUBALEK*

Department of Microelectronics, Brno University of Technology/Faculty of Electrical Engineering and Communication, Technická 3058/10, CZ-616 00, Brno, Czech Republic
*hubalek@feec.vutbr.cz

ABSTRACT

In our work electrochemical determination of low concentrations (0.4 – 16 mg/l) potassium ions in urea solutions and water has been done. Also, measurements of pH and conductivity of investigated solutions have been made. The influence of low (1, 10 %) and high (50 %) concentrated urea solution on the potassium ions measurements has been investigated. Obtained information can be used for analysis of dehydration state of human body through monitoring of potassium ions level in urea, which is a basic component of urine.

INTRODUCTION

An average human body excretes approx. 2 – 2.5 l of water daily, thereof 1 – 1.5 l of urine, approx. 600 ml of sweat and 300 – 400 ml is consumed by metabolic processes [1]. Urine osmolality is commonly used for analysis of urine concentration. It is determined by the concentration of sodium, potassium and urea. Low osmolality can point to dehydration [2]. Potassium is one of the most widespread and important elements determining human health. 98 % of potassium is inside the cells. In case of excess intake of potassium, there is a balance between the intake and release in the urine. When the balance is matching, the secretion of potassium in the urine is usually in the range of 60 – 100 mmol/24 hours, and the loss by sweating is about 10 mmol/l [3]. If the potassium intake is restricted markedly, the excretion of potassium in the urine diminishes close to zero and excretion in the stool is about 3.5 mmol per day. If there is no equilibration of mineral and liquid losses, the organism dehydrates. Dehydration becomes evident with the loss of average weight and with the potassium concentration growth or decrease in the urine [4]. We have made measurements of low potassium ions concentrations in the urea solutions and water by means of commercial potassium selective electrode. This data will be used for creation of controlling electronic system for human body dehydration state monitoring by measurements of potassium ions losses through urination in the toilet.

MATERIAL AND METHODS

Methodology of pH, conductivity and potassium ions concentration measurements

The potassium ion selective electrode was obtained from Elektrochemické detektory s.r.o. (Trutnov, Czech Republic) and conditioned before use in a 0.5 mmol/l KCl (PENTA, Czech Republic) aqueous solution for 1 h. Then the

electrode was calibrated in KCl solutions in Milli-Q water (Millipore, USA) with five different concentrations in the range of 1.10^{-1} to 1.10^{-5} mol/l. Another four sets of KCl solutions with K^+ concentration of 10, 50, 100, 200 and 400 mg/l were prepared. One set was in Milli-Q water and three others in various concentrated urea solution (PENTA, Czech Republic), namely 1 %, 10 % and 50 %. Before measurement, all samples were diluted (2 ml of sample was made up to 50 ml with Milli-Q water). By using pH meter Syberscan PC 6500 (Eutech Instruments), the pH and conductivity measurement has been done after preparation of diluted KCl and urea solutions. A 34410A Digital Multimeter (Agilent) with high input impedance (10 GOhm) was used for potential measurements.

RESULTS AND DISCUSSION

In previous work we made measurements of high concentrated (10 – 400 mg/l) potassium ions solutions [5]. But for detection of potassium ions in urine dissolved in toilet water is necessary to make measurements of low potassium concentration. In this work we focused on investigation of pH value, property of conductivity and measurements of low potassium ions concentrations (0.4 – 16 mg/l) urea solutions and water. Information about pH and conductivity of solutions depending on potassium ions concentrations are shown in Fig. 1. As can be seen from the graph, the pH value of all solutions and potassium concentrations is in the range between 6 and 7. It is a typical pH value for human urine and low potassium ions concentrations does not significantly influence on mentioned pH values. On contrary, the conductivity of urea solutions and water grow linearly in dependence on increasing potassium ions concentration.

The results of potassium ions concentration measurements are shown in Fig. 2. As can be seen from the graph for water and low (1, 10 %)

concentrated urea solutions the potential of selective electrode is within $\pm 5\%$ of deviation (see error bars on the plot), and only for high (50%) concentrated urea solution the potential deviation exceeds the $\pm 5\%$ barrier in the investigated K^+ interval. This result correlates with our previous investigation with high (10 – 400 mg/l) potassium ions concentrated urea solutions and can be explained similarly. Increasing urea concentration in water also leads to increasing concentration of ammonium ions that contributes to increase of solution ionic strength and in this case the electrode potential shows higher absolute value [5]. The dynamic range of potassium determination is from 0,4 to 16 mg/l which is acceptable for potassium output level monitoring in human urine to recognize significant increase or decrease during urination in the toilet.

Figure 1: Dependence of pH and conductivity of the urea solutions and water from low K^+ concentration

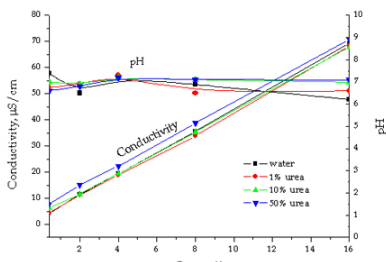
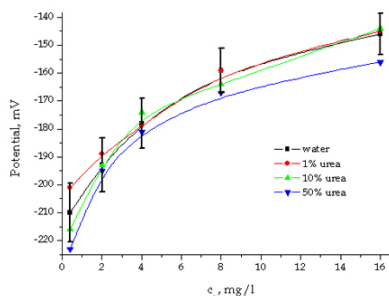


Figure 2: Dependence of selective electrode potential from low K^+ concentration in water and urea solutions



CONCLUSION

The measurements results of low K^+ concentration in urea and water solutions show that it is possible to use a commercial selective electrode for these purposes. The influence of urea concentration on electrochemical potential was investigated during measuring concentration of potassium ions. As for low urea solutions concentrations and water, the obtained results are

within $\pm 5\%$ of deviation. Regarding high concentration of urea solution the potential deviation exceeds the $\pm 5\%$ barrier of the potential, which resulted from quick increase of ionic strength of solution in comparison with low urea concentration. The level of pH does not depend on potassium ions concentrations for all solutions and are in the range of about 6 – 7. The conductivity of investigated solutions linearly increases with increasing of potassium ions concentrations. Therefore using selective potassium electrode is possible to make measurements of potassium ions concentration in human urine for monitoring the health body status and liquids level in organism.

ACKNOWLEDGEMENT

The work has been supported by project GACR 102/08/1546 (NANIMEL) and project CZ.1.05/2.1.00/03.0072 (SIX).

REFERENCES

- [1] Montain S, et al.: International Journal of Sport Nutrition and Exercise Metabolism, 17 (2007), 574-582
- [2] Armstrong L, Soto J, Hacker F, et al.: International Journal of Sport Nutrition and Exercise Metabolism, 8 (1998), 345-355
- [3] Jimenez C, Regnard J, et al.: European Journal of Applied Physiology, 108 (2010), 49-58
- [4] Baker L, Lang J, Kenney W: European Journal of Applied Physiology, 105 (2009), 959-967
- [5] Solovej D, Businova P, et al.: Proceedings of the IEEE SENSORS 2011 CONFERENCE, Limerick, Ireland (2011), 1113-1116.

INFLUENCE OF LMWOAS ON TRANSPORT OF CADMIUM AND COPPER IONS ACROSS PHOSPHOLIPID BILAYER USING CALCIUM IONOPHORE A23187

Ivana SESTAKOVA^{1*}, Martina PARISOVA¹,
Tomas NAVRATIL¹, Jana JAKLOVA DYTRTOVA²

¹ J. Heyrovský Institute of Physical Chemistry of the AS CR, v.v.i., Dolejškova 3, 182 23 Prague 8, Czech Republic

² Institute of Organic Chemistry and Biochemistry of the AS CR, v.v.i., Flemingovo náměstí 2, 166 10 Prague 6, Czech Republic

* ivana.sestakova@jh-inst.cas.cz

ABSTRACT

The influence of oxalic, citric or malic acid on transport of cadmium and copper ions in dependence on pH has been studied. Artificial phospholipid bilayer containing wide-spectrum ionophore was prepared on polycarbonate support and its formation and stability was followed with electrochemical impedance spectroscopy. The species, transported across phospholipid bilayer were determined with voltammetry. The substantial influence of complexes formed with metal ions and LMWOAs on their transport has been confirmed.

INTRODUCTION

Cadmium is a toxic element without any known physiological function, whereas copper is an essential element for plants, animals and humans, which can be toxic above a certain concentration. The main source of both elements entry into animal and human food chain is connected with plants grown on more or less contaminated soil.

Plant root plasma membrane is the first place where a metal, generally in ionic form can enter plant root cell. After the uptake, processes of transport, chelation and sequestration follow. In plants, metal chelators include phytochelatins, metallothioneins, organic acids, and amino acids [1].

Organic acids, namely oxalic, citric and malic acid are present in cytosol (concentration range 0.5 – 10 mM) and are released into the rhizosphere as root exudates, which can regulate further metal uptake [2]. In connection with our earlier studies [3-6], we performed here experiments with ionophore A23187 incorporated into artificially prepared phospholipid bilayer. This ionophore, known as important for calcium transport, can transport also wide spectrum of other divalent cations [7]. Formation and stability of PLB was followed with electrochemical impedance spectroscopy. Voltammetry was employed in determination of metal ions or complexes transported across phospholipid bilayer with ionophore from solution of cadmium or copper ions in absence or in presence of selected LMWOA.

EXPERIMENTAL

The electrochemical impedance spectroscopy measurements were realized using CHI 650C Electrochemical Analyzer/Workstation, Soft-

ware: CHI v 8.1 (IJ Cambria Scientific, UK) and Potentiostat No. 283 and FRA No. 1025, No. 5210 (Princeton Applied Research, USA). The electrochemical impedances were determined using silver/silver chloride electrodes (silver wire, diameter 1 mm, electroplated by silver chloride). Platinum wire, diameter 1 mm, served as the auxiliary electrode.

The experiments were realized with 1,2-dipalmitoyl-*sn*-glycero-3-phosphocholine (lecithin, DPPC, GPCho (16:0/16:0), CAS No. 63-89-8) (Avanti Polar Lipids, Alabaster, USA). The PLBs were formed by self-assembling in the holes of the Isopore™ Membrane Filters (Millipore, USA) polycarbonate, hydrophilic 8.0 μm, and the supporting membrane thickness amounted to 7-22 mm. Electrochemical cells for ESI measurements consisted from two parts, separated by PLB on polycarbonate support – or glued on plastic cap or inserted between two Teflon rings [8]. Electrolyte 1 was 0.1 M KCl to which metal ions and LMWOAs were applied, electrolyte 2 was again 0.1 M KCl, where species transported across the PLB were collected.

The voltammetric determinations of metal ions or its complexes were carried out by the PC-controlled voltammetric analyzer ECO-TRIBO polarograph (Polaro-Sensors, Prague, Czech Republic), equipped with POLAR.PRO software v. 5.1 and with MultiElchem v. 2.1 software (J. Heyrovský Institute of Physical Chemistry of AS CR, v.v.i., Czech Republic). Pen-type electrode – HMDE was used as the working electrode, Ag/AgCl/KCl(3 mol.L⁻¹) as a reference electrode to which all potentials are referred and platinum wire served as a counter electrode (both Elektrochemické Detektory, Turnov, Czech Republic). For the determination of metal ions, the samp-

le was acidified by addition of HNO_3 , Suprapur (Merck, Czech Republic), to pH 1. For the complexes with LMWOAs, pH of the solution was adjusted to desired value (5.8 – 7.5) with NaOH (Suprapur, Merck, Czech Republic). Differential pulse anodic stripping voltammetry (DPASV) was performed at conditions: $E_{\text{acc}} = -850$ mV, $E_{\text{in}} = -700$ mV, $E_{\text{fin}} = -200$ or 0 mV, scan rate $10 \text{ mV}\cdot\text{s}^{-1}$, pulse amplitude 50mV. Adsorption voltammetry in DP or DC mode was performed using adsorption potential $E_a = -100$ mV. A new drop was used for each record; measurement has been realized in nitrogen atmosphere.

RESULTS AND DISCUSSION

Phospholipid Membrane Preparation

The 1,2-dipalmitoyl-*sn*-glycero-3-phosphocholine monohydrate was used for preparation of PLB on porous membranes. The capacity of membranes increases with time after the bilayer formation, until a steady-state value attained some 20-30 min. later. In our experiments, there were the PLBs formed as self-assembled in the holes of the supporting membrane (Isopore™ Membrane Filters, Millipore, USA); polycarbonate, hydrophilic, 8.0 μm) by application of 10 or 20 μL of phospholipid solutions in *n*-heptane on the membrane surface. The ionophore A23187 (solution in EtOH) was added to phospholipid solution before the application on the support. Formation of PLB was monitored by ESI measurement. After steady state has been reached, changes of electrolyte 1 were realized (change of pH, addition of metal ions, LMWOA) and to them the PLB was exposed for exactly 1 hour. Subsequently, voltammetric analysis of the electrolyte 2 has been performed.

Voltammetric Analysis

Two sets of experiments were performed, differed in pH adjustment of the electrolyte 1.

In acidic region (pH 2.4 - 2.6), the presence of LMWOAs had no influence on transport of cadmium or copper ions – transported amount of ions were about the same when LMWOA was present or not. When pH of electrolyte 1 is at values of 5.8 – 6.5, copper or cadmium complexes with oxalic, citric or malic acid are formed and reduced amount of ions should be transported across the phospholipid bilayer [9]. This has been confirmed with voltammetric analysis of electrolyte 2. Subsequently, the presence or absence of transported ligand has been checked, using anodic stripping voltammetry in case of oxalic acid [10-11] and DP or DC voltammetry with adsorptive accumulation in case of citric and malic acid.

Obtained results are in agreement with models, considering the free ion as the major bioavailable species [12]. Citric or malic acid were not found in electrolyte 2, when transport was realized in

acidic or close to neutral media. On the other hand, oxalic acid was transferred in both cases, but no quantitative data are available at present.

CONCLUSION

The use of artificially prepared phospholipid bilayer with built-in ionophore A23187 has been demonstrated as a tool for the study of cadmium and copper transport, present as a free ions or complexes with oxalic, citric or malic acid. Based on changes in composition of initial solution, the fulfillment or exceptions from the free ion activity model can be discovered.

ACKNOWLEDGEMENT

The research was supported by GAAVCR (project No. IAA400400806) and by GACR (project No. P206/11/1638 and project No. P208/12/1645).

REFERENCES

- [1] Clemens S.: *Planta*, 212 (2001), 475 – 486.
- [2] Jones DL: *Plant and Soil*, 205 (1998), 25 - 44.
- [3] Navratil T, Sestakova I, Stulik K et al.: *Electroanalysis*, 22 (2010), 17-18, 2043-50.
- [4] Navratil T, Sestakova I, Jaklova Dyttrtova J et al.: *WSEAS Transactions on Environment and Development*, 6 (2010), 3, 208-219.
- [5] Navratil T, Sestakova I, Marecek V: *International Journal of Electrochemical Science* 6 (2011), 12, 6032 -6046.
- [6] Sestakova I, Jaklova Dyttrtova J, Jakl M, Navratil T.: *International Journal of Energy and Environment*, 5 (2011), 3, 347-55.
- [7] Stanish I, Monbouquette H G. : *J. Memb. Sci.*, 192 (2001), 99-113.
- [8] Navratil T, Sestakova I, Marecek V, Stulik K.: *Modern Electrochemical Methods XXX*, 2010, Jetrichevice, Czech Republic, pp.119-123.
- [9] Strobel BW: *Geoderma* , 99 (2001), 169 -198.
- [10] Jaklova Dyttrtova J, Sestakova I, Jakl M et al.: *Electroanalysis*, 21(2009), 3-5, 573 -579.
- [11] Sestakova I, Navratil T, Marecek V.: *Mathematical Models and Methods in Modern Science*, 2011, Puerto De La Cruz, Spain, pp.201 – 206.
- [12] Degryse F, Smolders E, Merckx R.: *Environ. Sci. Technol* 40 (2006), 830 -836.

ON-BODY SYSTEM FOR DEHYDRATION DETECTION

Jaromir ZAK¹*, Jiri SEDLACEK¹, Dmitry SOLOVEI¹, Vojtech ADAM¹, Rene KIZEK¹, Jaromir HUBALEK¹

¹ Department of Microelectronics, Faculty of Electrical Engineering and Communication, Brno University of Technology, Technická 10, 616 00 Brno, Czech Republic

*hubalek@feec.vutbr.cz

ABSTRACT

There are a lot of intrusive or invasive medical systems for patients biomedical monitoring. We need to make biomedical telemonitoring devices which can be taken everywhere by the patients. This project is aimed at creating a non-obtrusive system for easy and precise measurement of patient's life signs. The main part of this project is focused on developing of a dehydration detector system which will be cooperating with other various devices for real time precise dehydration state detection.

INTRODUCTION

Dehydration monitoring is important for elderly people, diabetics, sportsman, etc. Exact determination of the organism hydration state is a complicated problem. A lot of different values have to be measured to accurate determination of hydration state or limit value of the dehydration. Dehydration can be determined from long time monitoring of water metabolism which was found to be significantly presented by water intake and outtake monitoring and/or measuring of the potassium or sodium ions concentration in the urea or sweat [1]. Additional values (such as patient's weight, age or gender) must be known in all cases.

All of needed values can be measured by different sensors that belong to the certain person. These sensors can be included in a single sensor network linked to the user. In this case, we can talk about body area network (BAN) which can consist of on-body sensors strictly used by one person and of ambient sensors. Ambient sensors are connected directly to the network but each ambient sensor can be shared among other users with other BANs.

Measured data can be collected in the BAN coordinator or in the external acquisition point (computer or mobile phone e.g.). Coordinator is placed on the user's body and measured data can be temporarily saved or in it but cannot be resent to the database or third persons (hospitals, doctors, family members, etc.) through internet. There is an acquisition point used for this purpose which is connected online to the internet databases but it doesn't need to be connected directly to the on-body sensors.

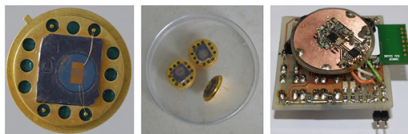
EXPERIMENTS

To detect dehydration from the actual body state a special automatic computer system was developed and fabricated (see Fig. 1). We use

two methods: water intake/outtake monitoring and urea potassium concentration measuring [1] for dehydration detection. Measurement of sodium is less significant than potassium measurement [3] and it will not used. Additional information is measured (weight) or entered (age, gender).

Water output is measured by SWEAT sensor which measures differential humidity level between close to skin sensor and ambient sensor with accurate distance. We developed a new sensor with improved high-humidity response for measurements of humidity level near the skin surface (see Fig. 1). The sensor is based on nanostructured metal oxide semiconductor titanium layer in the crystalline modification of rutile. The resistance of the sensitive layer at the surface is reduced by physical sorption of water molecules [4].

Figure 1: Humidity sensor and electrical module developed for humidity measurements



We can calculate water-loss through the skin (per square meter of the skin) due to sensor distances from equation published in [5]. We have made SWEAT sensor module using this mathematical model. This module is one of the wearable sensors and it will be attached to the arm in real conditions. Photography of the completed module prototype is shown in Fig. 2.

The second sensor for dehydration detection (urea sensor) can be used by other persons (it is an external device) and its analog circuits consist of a voltage amplifier with potassium

sensor zero value rejection only. The last sensor connected directly to WBAN is personal scales which uses four strain gauge sensors connected to the Wheatstone's bridge. The actual weight and scales position is compensated before each measurement.

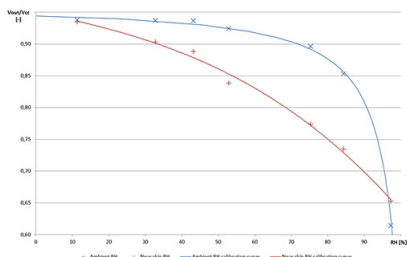
Figure 2: Prototype of the SWEAT sensor module



RESULTS AND DISCUSSION

A lot of measurement methods for relative humidity were made and published earlier [4]. Sensors connected to the electronics were calibrated after characterization in the atmosphere with defined relative humidity (near the surface of supersaturated salt solution) [6]. Accuracy after calibration was determined about 10%RH (for $RH \leq 50\%$) and 3 %RH (for $RH > 50\%$), see Fig. 3. Error drift over time (about 10 %RH) were detected during one month after calibration (only for low humidity values). Commercial sensor accuracy was determined about 4 %RH, in the most cases below 0.5 %RH (two errors near 40 %RH and 50 %RH were caused by unstable calibration salt liquids probably). Personal scales have absolute error about 0.3 kg with time drift < 0.1 kg after calibration.

Figure 3: Ambient and skin RH sensor calibration curve



The measurements in real conditions on the man's hand were made after sensors and devices calibration and the results show few facts: method for water loss determining is working, but

accuracy has to be verified. Skin RH sensor stabilization can be viewed at first minutes of measurement – sensor of the skin humidity needs a few minutes for it after power up.

CONCLUSION

A new type of relative humidity sensor was created and tested and later used in the newly developed wireless sensor system for dehydration monitor in this project. The completion of the dehydration detection system is only the first part of the project and a lot of additional devices need to be created and implemented into WBAN which has been designed too.

The next development will be focused on the increasing accuracy and stability of the new type of relative humidity nanosensor and on decreasing size of the on-body sensor.

ACKNOWLEDGEMENT

The work has been supported by the project MAS No. 120228 supported by ENIAC JU and the project SIX No. CZ.1.05/2.1.00/03.0072.

REFERENCES

- [1] Montain S, J, et al, Sweat mineral-element responses during 7 h of exercise-heat stress, *International Journal of Sport Nutrition and Exercise Metabolism*, 2007, strana 574-582.
- [2] Alemdar H, Ersoy C, *Wireless sensor networks for healthcare: A survey*, *Computer networks*, 2010, strana 2688-2710.
- [3] Solovej D, Businova P, Drbohlavova J, et. al., *Non Invasive Possibility of Body Dehydration Monitoring*, Limerick, Ireland, 2011, strana 1113-1116.
- [4] Solovej D, Hubalek J, *Synthesis of nanoscale semiconducting titanium oxide pillars array and investigation of its structural and humidity properties*, *Nanocon*, Brno, 2011, strana 310-315.
- [5] Oberg P. A, Hammarlund K, Nilsson G. E, Sedin G, *Measurement of Water Transport Through the Skin*, *Upsala Journal of Medical Science*, 1981, strana 23-26.
- [6] Zhang H, Li Z, Liu L, *Mg²⁺/Na⁺-doped rutile TiO₂ nanofibre mats for high-speed and anti-fogged humidity sensors*, *Talanta*, 2009, strana 953-958.

ELECTROCHEMICAL STUDY OF INTERACTION OF 23 FRAGMENTS OF METALLOTHIONEIN WITH CISPLATIN – HIGH THROUGHPUT METHOD

Ondrej ZITKA¹, Marketa KOMINKOVA¹, Sylvie SKALICKOVA¹, Vojtech ADAM^{1,2}, Tomas ECKSCHLAGER³, Marie STIBOROVA⁴, Libuse TRNKOVA^{2,5}, Rene KIZEK^{1,2}*

¹Department of Chemistry and Biochemistry, Faculty of Agronomy, Mendel University in Brno, Zemedelska 1, 613 00 Brno, Czech Republic

²Central European Institute of Technology, Brno University of Technology, Technicka 3058/10, 616 00 Brno, Czech Republic

³Department of Paediatric Haematology and Oncology, 2nd Faculty of Medicine Charles University, and University Hospital Motol, V Uvalu 84, CZ-150 06 Praha 5, Czech Republic

⁴Department of Biochemistry, Faculty of Science, Charles University, Albertov 2030, CZ 128 40 Prague 2, Czech Republic, European Union

⁵Department of Chemistry, Masaryk University, Kotlarska 2, 611 37 Brno, Czech Republic

*kizek@sci.muni.cz

ABSTRACT

Metallothionein is metal binding protein occurring intracellularly in animals. It can bind essential zinc ions and also toxic metals like cadmium. In cancer research the problem of resistance of cancer cells against anticancer drugs was described. Metallothionein was found to be one of cause of the resistance due to its ability to bind toxic metals. In this study we determined the influence of aminoacid sequence in metallothionein on to affinity to cisplatin using electrochemical method. For high throughput automatic analysis we designed automated flow injection analysis with electrochemical detection, which was carried out by Coulochem III as amperometric detector.

INTRODUCTION

Metallothionein low molecular mass protein (6-7 kDa) discovered in 1957 in horse kidney [1]. From these times, this protein has been explored in many other animal and even plant species [2]. Its most abundance is in the cells, blood or blood serum. Its crucial role in the organism is detoxification of toxic metals, regulation of metabolism of some important trace metals, detoxification of reactive oxygen species, repressing of chemical toxicity and carcinogenesis. [3] [4]. Structure of metallothionein is very simple but it is rich in cysteine content. It has several isoforms (MT-1, MT-2, MT-3 and MT-4) [5], where most abundant are MT-1 and MT-2 [6]. It was reported that cells are able to secrete the forms MT-1 and MT-2 [7]. Up to date it was described 250 structural forms, which differ at least in one aminoacid in its structure. Its tertiary structure is divided into domains alpha and beta which creates the cysteine clusters. Into alpha domain it can bind 4 divalent metal ions and into beta domain it can bind 3 divalent metal ions. As a total, it can bind 7 divalent or possibly 12 monovalent metal ions [8]. Due to high frequency of cysteine placement in the primary structure of metallothionein it is possible to determine a sequence, which contributes to the metal binding. For study of the interaction with metals it is suitable to choose a special sequence (peptide) of metallothionein and, then to study it by suitable

methods. Similar approaches in peptide interaction study have been applied [9]. Thanks to the absence of aromatic amino acids in its structure and for reason that because its molecular mass it is not creating any secondary structures it is badly detected by most of conventional detection methods [10].

Metallothionein was previously studied by electrochemical methods which are suitable especially due to its cysteine content. The hexapeptide of metallothionein was previously electrochemically analysed [11, 12]. There was also studied the complex of fragment of metallothionein with cadmium(II) ions using hanging mercury electrode using method of cathodic stripping voltammetry [13]. Square wave voltammetry [14] or cyclic voltammetry [15, 16] has been also applied. In this study, we attempted to use amperometric detection implemented in flow injection system for determination of structure influence of various fragments of metallothionein during interaction with cisplatin.

MATERIAL AND METHODS

Chemicals and pH measurements

Standards of fragments of metallothionein were synthesized by Clonestar (Clonestar s.r.o., Brno, Czech Republic). Other chemicals were purchased from Sigma-Aldrich, USA in ACS purity unless noted otherwise. Stock standard solutions were prepared with ACS water (Sigma-Aldrich) and stored in dark at -20 °C. The

pH value was measured using WTW inoLab Level 3 with terminal Level 3 (Weilheim, Germany), controlled by software MultiLab Pilot (Weilheim). The pH-electrode (SenTix H, pH 0..14/0..100°C/3mol.l⁻¹ KCl) was regularly calibrated by set of WTW buffers (Weilheim).

FIA-ED system

FIA-ED was consisting of one chromatographic pump Model 582 ESA, injecting valve and electrochemical detector. Sample (20 μ l) was injected by autosampler (Model 542, ESA, USA). Electrochemical detector Coulochem III (ESA, USA) was connected directly to the autosampler via 1 m long reaction coil. For electrochemical detection the electrochemical cell model 5040 (ESA, USA) was used. This cell is equipped by planar electrode from glassy carbon. Mobile phase was phosphate buffer pH 7.5 (20mM). Flow rate of mobile phase was 1 ml/min.

RESULTS AND DISCUSSION

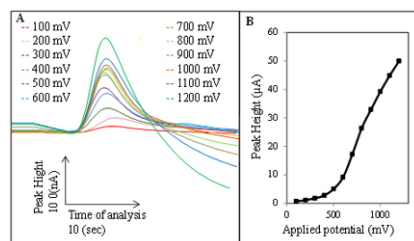
In this experiment we chose various 23 fragments (decapeptides) of metallothionein (FMT). We focused on different amino acids in surrounding relatively conservative Cysteine placement in each peptide. We tested the ability of interaction of studied peptides with cisplatin drug under various conditions using our designed automatic method FIA-ED. For study of interaction we changed options like temperature, time of interaction, and concentration ratio of both components. All these parameters were taken as most influencing of the interaction in FMT and cisplatin in the presence of phosphate buffer. Incubation of complex was done in overall volume 400 μ l and was vortexed in thermo block (400 rpm). After processing of preparing of each variant we analysed the sample using FIA-ED method. This was done by repetitive injections of one sample in different potentials for obtaining of hydrodynamic voltammogram (HDV) for each particular sample in range 100-1200 mV with 100 mV potential step. Thus 12 injections (n=3) were carried out for each sample sequentially with potential change before each injection. The potential change was driven by TIMELINE program method integrated in software in Coulochem III module which was started using external signal from autosampler, which was driven by Clarity software. This setup was designed especially for our high throughput analysis needs. After each series of the HDV measurement the electrochemical cell was cleaned by changing of potential cycles twice from -1200 to +1200 mV for 30 seconds (each cycle).

The obtained hydrodynamic voltammograms (HDVs) was displayed like a plot and the regression equation was established. From differences of slopes from obtained regression equations we

assumed on change of structure. Basically there was measured only HDV values for FMTs only in the presence phosphate buffer. From these HDVs the background information was obtained. The change of progress of the HDV obtained from interaction measurement was taken like a plus (+) or minus value (-) comparatively to the basic HDV of simple FMT. Additionally we needed to sub duct the HDV of only cisplatin as well because it also contributes to the overall HDV while mixture of complex is analysed. After these procedures we obtained the number which represents the change of structure as total constant slope. The records from one of studied FMT are shown in Fig. 1.

Firstly we studied temperatures which were 10, 15, 25, 35 and 45 °C. Samples were incubated during 1 hour in concentration ratio FMT 100 μ M and cisplatin 100 μ M and after that it was immediately analysed by automated FIA-ED. We found that the best temperature for change of the slope was 45°C for all FMTs. Then we tested the concentration of added cisplatin to FMT, which was 100 μ M. We made various addition of cisplatin in resulting concentrations 50, 100 and 200 μ M. Incubation was carried out under optimized temperature 45 °C and 1 hour duration. After analysis of each variant we found the applied concentration of 100 μ M the most valuable for testing of all FMTs. The last tested parameter was time of incubation which was set on the 1, 2, 3, 4, 5, 6, 7 and 8 hours under abovementioned best obtained conditions.

Figure 1: (A) Hydrodynamic voltammograms of FMT-21 as overlay of typical records from HDV determination by FIA-ED with Coulochem III as electrochemical detector. (B) Obtained HDV from FMT 21 analysis



For final interpretation we designed special plotting for determination of total influence of all parameters to the interaction result. Total count of slopes from all parameters (temperature, concentration and time) was laid against each of these parameters. And thus we obtained the point plots where we defined the clusters for each tested parameter by median interval.

Finally we counted values of hits inside the median interval for all tested parameters and from these we obtained final constant which height represents the intensity of interaction between FMT and cisplatin.

CONCLUSION

In our interaction study we found that studied Fragments 2, 4, 7, 8, 16, 18, 20, 21, 22 a 23 had significantly higher intensity of interaction with cisplatin. Our determined results were in good agreement with the fact that these FMTs had the most different structures according the structure cognition comparison. According obtained data our developed high throughput method is valuable tool for such kind of analysis.

ACKNOWLEDGEMENT

This work has been supported by

- IGA MENDELU IGA IP23/2012
- NANOSEMED GA AV KAN208130801
- CEITEC CZ.1.05/1.1.00/02.0068

REFERENCES

- [1] Margoshes M, Vallee B L, *J. Am. Chem. Soc.*, 79 (1957), 4813-4814.
- [2] Adam V, Fabrik I, Eckschlager T, *et al.*, *TRAC-Trends Anal. Chem.*, 29 (2010), 409-418.
- [3] Sato M, Bremner I, *Free Radic. Biol. Med.*, 14 (1993), 325-337.
- [4] Nakazato K, Nakajima K, Kusakabe T, *et al.*, *Pathol. Int.*, 58 (2008), 765-770.
- [5] Miles A T, Hawksworth G M, Beattie J H, *et al.*, *Critical Reviews in Biochemistry and Molecular Biology*, 35 (2000), 35-70.
- [6] Masters B A, Quaife C J, Erickson J C, *et al.*, *J. Neurosci.*, 14 (1994), 5844-5857.
- [7] Trayhurn P, Duncan J S, Wood A M, *et al.*, *Am. J. Physiol.-Regul. Integr. Comp. Physiol.*, 279 (2000), R2329-R2335.
- [8] Coyle P, Philcox J C, Carey L C, *et al.*, *Cell. Mol. Life Sci.*, 59 (2002), 627-647.
- [9] Kotrba P, Doleckova L, Pavlik M, *et al.*, *Biotechnol. Tech.*, 10 (1996), 773-778.
- [10] Bell S G, Vallee B L, *ChemBioChem*, 10 (2009), 55-62.
- [11] Mendieta J, Chivot J, Munoz A, *et al.*, *Electroanalysis*, 7 (1995), 663-669.
- [12] Munoz A, Rodriguez A R, *Electroanalysis*, 7 (1995), 674-680.
- [13] Sestakova I, Mader P, *Cell. Mol. Biol.*, 46 (2000), 257-267.
- [14] Nieto O, Rodriguez A R, *Bioelectrochem. Bioenerg.*, 40 (1996), 215-222.
- [15] Harlyk C, Bordin G, Nieto O, *et al.*, *Electroanalysis*, 9 (1997), 608-613.
- [16] Marshall N M, Garner D K, Wilson T D, *et al.*, *Nature*, 462 (2009), 113-U127.

COULOMETRIC AND PHOTOMETRIC DETERMINATION OF ANTIOXIDANT CAPACITY IN BIOLOGICAL SAMPLE OF HONEYSUCKLE

Ondrej ZITKA¹, Sylvie SKALICKOVA¹, Jiri SOCHOR^{1,2}, Branislav RUTTKAY-NEDECKY^{1,2}, Otakar ROP⁴, Tunde JURIKOVA⁵, Boris KRSKA⁶, Jaromir HUBALEK^{2,3}, Vojtech ADAM^{1,2}, Rene KIZEK^{1,2*}

¹Department of Chemistry and Biochemistry, Faculty of Agronomy, Mendel University in Brno, Zemedelska 1, 613 00 Brno, Czech Republic

²Central European Institute of Technology, Brno University of Technology, Technicka 3058/10, 616 00 Brno, Czech Republic

³Department of Microelectronics, Faculty of Electrical Engineering and Communication, Brno University of Technology, Technicka 10, CZ-616 00 Brno, Czech Republic

⁴Department of Food Technology and Microbiology, Faculty of Technology, Tomas Bata University in Zlin, Namesti T. G. Masaryka 275, CZ-762 72 Zlin, Czech Republic

⁵Faculty of Central European Studies, Institute of Natural and Informatics Sciences, Constantine the Philosopher University in Nitra, Nabrezie mladeze 91, SK-949 76 Nitra, Slovakia

⁶Department of Fruit Growing, Faculty of Horticulture, Mendel University in Brno, Valticka 337, CZ-691 44 Lednice, Czech Republic

*kizek@sci.muni.cz

ABSTRACT

Herein we present a complex multi-approach analysis of antioxidant activity of less common fruits (Honeysuckles) 'Altaj' LKL – 2, LKL – 21, 'Bakčarskaja'. The aim of our study was to demonstrate the suitability of HPLC – ED technique with gradient elution for determination of nine phenols as specific antioxidant capacity (Specific-AC), same technique for determination of total electrochemical signal as total area of chromatogram obtained as overall antioxidant capacity (Overall-AC) and spectrophotometric method as DPPH test for estimation of relative antioxidant capacity (relative-AC) in edible honeysuckle. We evaluated the correlation between the Specific-AC and Overall-AC with regression correlation coefficient $R^2 = 0.7194$.

INTRODUCTION

Antioxidants are wide group of compounds which have health beneficial effects because of their ability to protect cells against the effects of free radicals. Studies of these substances increase because of connection between their uptake in nutrition and reduction of occurrence of cancer or cardiovascular diseases [1]. They display antimutagenic, anticarcinogenic and antiinflammatory properties. In general, berry crop had the greatest antioxidant capacity, their high antioxidant capacity, in agreement with the literature [2], [3], [4], is likely due to the high content of phenolic acids and flavonoids such as anthocyanins [5]. The edible honeysuckle represent a lesser – known berry crop originated

from territory of Russia, rich in antioxidants, especially there was determined a high value of ascorbic acid and polyphenolic compounds – phenolic acids and flavonoids [6] [7]. Our work was focused on elaboration of specific, overall and relative antioxidant capacity of 4 selected perspective genotypes of edible honeysuckle coupled with determination of nine polyphenolic compounds (Specific-AC) and total oxidized compound by HPLC – ED method and total electrochemical signal (Overall-AC) and Relative-AC by spectrophotometric determination using DPPH test.

2. MATERIAL AND METHODS Chemicals and pH measurements

Standards of target phenolic compounds for HPLC-ED analysis (Sigma – Aldrich Fluka Co. St. Louis, MO, USA) were used. Liquid nitrogen was purchased from Messer technogas s.r.o. (Czech Rep.), methanol (>99.9%; v/v), formic acid acetic acid and 96 % ethanol for HPLC from Dr. Kulich Pharma Czech Republic. 2,2 – diphenyl – 1- picrylhydrazyl DPPH, acetonitril for HPLC (Sigma Aldrich, Chemical Corp., St. Louis, USA). HPLC-grade methanol (>99.9%; v/v) from Merck (Dortmund, Germany) was used. Reduced (GSH) and oxidized (GSSG) glutathione, and trifluoroacetic acid (TFA) were purchased from Sigma-Aldrich (St. Louis, USA). Other chemicals were purchased from Sigma-Aldrich (St. Louis, USA) unless noted otherwise.

Samples

For experiment the 4 genotypes of honeysuckles were used 'Altaj' LKL – 2, LKL – 21, 'Bakčarskaja'. All samples had the same origin, the trial plots of Mendel University of Agriculture and Forestry in Brno are situated in Žabčice. From fruits representative samples were taken and weighted 10 g. Further, they were transferred to mortar, and liquid nitrogen was added in 4 °C and samples were homogenised by 10 ml 99 % methanol. The homogenate was transferred to test tube and under the same conditions they were grinding for 30 min. The next step was sonification and centrifugation of samples (Eppendorf 5804R, Germany) for 30 min at 16 400 rpm. Supernatants were filtered through a membrane filter (0.45 µm), (Metachem, Torrance, Ca, USA). 500 µl of each filtrate was diluted by 500 µl methanol.

HPLC-ED system

The instrument for HPLC-UV analysis consisted of solvent delivery pump (Model 582 ESA Inc., Chelmsford, MA, USA), chromatographic column Phenomenex Gemini C18 (150 × 4.6; 3 µm particles, Phenomenex, USA), UV-VIS detector (Model 528, ESA, USA) and twelve-channel CoulArray electrochemical detector (Model 5600A, ESA, USA). The sample (20 µl) was injected using autosampler (Model 542, ESA, USA). The data obtained were treated by Coularray data station (ESA, USA). The experiments were carried out at room temperature. Mobile phase consists of A: citric acid (75 mM) a B: Acetonitrile with ammonium acetate (25mM). Flow rate was 1 ml min⁻¹. Chromatographic column was thermostated to 35°C. Compounds were eluted by following linear increasing gradient: 0,1 min (5% B), 0,01 → 4 min (6 %B), 4 → 20 min (25 % B), 20 → 30 min (100% B), 30 → 36 min (100% B), 36 → 38 min (5% B), 38 → 45 min (5% B). Electrochemical detection was carried out at 600 mV. Time of one analysis was 45 minutes.

Spectrometric

determination of antioxidant activity

For spectrophotometric determination of samples was used an automated VIS spectrophotometer (BS 200, Mindray, China). Reagents and samples were stored in a cooled carousel at 4 °C and automatically pipetted into plastic cuvettes (Mindray, China). Changes in absorbance were measured for 21 min at 16-second intervals from mixing of reagents at below mentioned wavelengths and optical trace 5 mm. Cuvettes were incubated at 37°C. Absorbance was measured at wavelength 734 nm.

RESULTS AND DISCUSSION

Berry fruit species displayed high level of antioxidant compounds, especially flavonoids and phenolic acids [8]. Because there exists direct relation between antioxidant activity and ability of compounds to be easily electrochemically oxidized (to give signal in electrochemical detection), selective and very sensitive electrochemical detection coupled with high performance liquid chromatography (HPLC-ED) make possible separated more analysed compounds simultaneously, thus so it is ideal analytical tool for solution of this issue [7]. Results are expressed as a percentage value of sum of determined values.

Determination of polyphenolic compounds as specific antioxidant capacity

To the determine of specific antioxidant capacity, the content of nine polyphenolic compound was detected: gallic acid, catalposide, rutin, resveratrol, quercitrin, chlorogenic acid, quercetin, diosmin and salicylic acid. On the basis of HPLC profile it is evident that in all examine samples chlorogenic acid represented the major antioxidant. Derivatives of hydroxybenzoic acid are presented in berries in form of its esters with the most different structures of gallic acid and salicylic acid. From this group of antioxidants gallic acid predominated in all analysed samples. From group of antioxidants with flavonoid skeleton was the most presented quercitrin, in genotypes 'Altaj' 'Bakčarskaja' and LKL – 21 was also measured the significant amount of Trans – resveratrol. Generally, the highest content of gallic acid, catalposide, rutine and resveratrol was measured in Klčov' s genotypes of *Lonicera kamschatica* (LKL – 2 and LKL – 21).

Determination of complex electrochemical profile as overall antioxidant capacity

The conditions during the electrochemical detection in coulometric detection by Coularray detector can simulate the effective conditions for the oxidation of active compounds very realistically. The overall antioxidant capacity which also can be called as total antioxidant capacity (TAC) determined by HPLC-ED Coularray might be thus expressed as total current represented by peak area in Coulombs (mC, µC), which is expressed as electric current per time [9]. Overall final area of individual peaks of detected phenolic acids and flavonoids were summarized, accounted area expressed the total antioxidant of active components in analysed samples. The LKL2 genotype shows the highest overall antioxidant capacity than other genotypes. Despite the fact the method of electroanalytical detection is less applied for detec-

tion of biological value of fruit, the sensitivity and selectivity of these procedures is higher in comparison with utilisation of conventional method [10], [11].

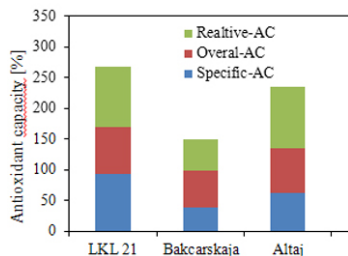
Determination of relative antioxidant activity

The relative antioxidant activity was spectrometrically measured using DPPH free radical test, which is the basis of a common antioxidant assay. This test is the most nonspecific next to these which were mentioned above. The method is based on the reaction between DPPH (2,2-diphenyl-1-picrylhydrazyl) and antioxidant molecule, which occurs in the sample. The change of absorbance can be thus monitored due to change of structure of DPPH. The yield of the reaction can be dependent on the matrix of sample which can differ rapidly. For that reason we called this approach as Relative-AC. In our test the best Relative-AC parameters were exhibited by Altaj tightly followed by LKL 2 with LKL 21 an almost 50% decreased values was monitored in Bakarskaja in comparison to Altaj.

CONCLUSION

On our work we presented that determination of antioxidant activity has many aspects and for complex determination of its parameter it is necessary to use more valuable approaches. Electrochemical detection is one of most selective and sensitive approach for this purpose and in our set up of Overall-AC and Specific-AC we were able to determine the real influence of polyphenols on the TAC. On the other hand, these methods need to be correlated to the commonly used method such as DPPH test which can serve as Relative-AC marker. We found that the highest parameters of Specific-AC+Overall-AC+Relative-AC was found as LKL-2 (300%), LKL-1 (265%), Altaj (230%) and Bakarskaja (145%) (Fig. 1). Thus we can recommend the LKL-2 as antioxidant most valuable less common Honeysuckle from rest which have been tested.

Figure 1.: Comparison of values obtained from determination of Relative-AC, Overall-AC and Specific-AC for 'L – K1 – 21', 'Bakarskaja', 'Altaj' and 'L – K1 – 2' as percentage values and as sums of these values.



ACKNOWLEDGEMENT

The work has been supported by Research centre SIX CZ.1.05/2.1.00/03.0072.

REFERENCES

- [1] La Vecchia C, Altieri A, Tavani A, Eur. J. Nutr., 40 (2001), 261-267.
- [2] Halvorsen B L, Holte K, Myhrstad M C W, *et al.*, Journal of Nutrition, 132 (2002), 461-471.
- [3] Kahkonen M P, Hopia A I, Vuorela H J, *et al.*, Journal of Agricultural and Food Chemistry, 47 (1999), 3954-3962.
- [4] Kalt W, Forney C F, Martin A, *et al.*, Journal of Agricultural and Food Chemistry, 47 (1999), 4638-4644.
- [5] Hakkinen S, Heinonen M, Karenlampi S, *et al.*, Food Research International, 32 (1999), 345-353.
- [6] Rop O, Reznicek V, Mlcek J, *et al.*, Hortic. Sci., 38 (2011), 63-70.
- [7] Gazdik Z, Reznicek V, Adam V, *et al.*, Molecules, 13 (2008), 2823-2836.
- [8] Ochmian I, Oszmianski J, Skupien K, Journal of Applied Botany and Food Quality-Angewandte Botanik, 83 (2009), 64-69.
- [9] Svendsen C N, Analyst, 118 (1993), 123-129.
- [10] Beklova M, Zitka O, Gazdik Z, *et al.*, Toxicology Letters, 180 (2008), S230-S230.
- [11] Adam V, Mikelova R, Hubalek J, *et al.*, Sensors, 7 (2007), 2402-2418.

APPLICATION OF COPPER SOLID AMALGAM ELECTRODE FOR DETERMINATION OF FUNGICIDE TEBUCONAZOLE

Katerina NOVAKOVA^{1,2*}, Tomas NAVRATIL¹, Jana JAKLOVA DYTRTOVA³, Jaromira CHYLKOVA²

¹ J. Heyrovský Institute of Physical Chemistry of the AS CR, v.v.i., Dolejškova 3, 182 23 Prague 8, Czech Republic

² University of Pardubice, Faculty of Chemical Technology, Institute of Environmental and Chemical Engineering, Studentská 573, 532 10 Pardubice, Czech Republic

³ Institute of Organic Chemistry and Biochemistry of the AS CR, v.v.i., Flemingovo náměstí 2, 166 10 Prague 6, Czech Republic

* Katerina.Novakova@jh-inst.cas.cz

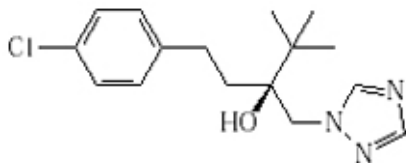
ABSTRACT

Pesticides are chemical substances which are used for preventing losses on culture plants, stocks of food, and feed. An excessive use of pesticides and other contaminants lead to an enormous burden for all components of biosphere in the final stage. Negative consequences of pesticide exposure (contamination of surface water, damage of ecosystems, and perishing of bees, and accumulation in the life systems etc.) led to an effort to reduce their use.

Tebuconazole ((RS)-1-p-chlorophenyl-4,4-dimethyl-3-(1H-1,2,4-triazol-1-ylmethyl)-pentan-3-ol; Fig. 1) is a broad-spectrum triazole fungicide used to control many plant diseases by inhibiting the biosynthesis of ergosterol to prevent fungal mycelium development. It displays an outstanding curative and protective efficacy to control numerous pathogens in various cereals, fruits, and vegetable crops [1]. Tebuconazole belongs to toxicants for the aquatic organisms as it might induce a long-term adverse effect on the aquatic environment. Some literature also showed that it can exist in the environment for a long period of time [2]. After application, tebuconazole can subsequently cause risks for soil ecosystems, groundwater and surface water [3]. Common application of this fungicide leads to its accumulation in soils. Tebuconazole may react also with essential elements in soil (by this way can cause a variation in its stability, toxicity, etc.), such as copper [4], and/or with hazardous metals such as cadmium [5]. Copper and tebuconazole together create a few different complexes at room temperature.

The voltammetric behavior of tebuconazole was studied with help the newly developed mercury meniscus-modified copper solid amalgam electrode (inner diameter 1.5 mm). Differential pulse voltammetry (DPV) and cyclic voltammetry (CV) were applied for these purposes. The reaction mechanism was investigated using CV and elimination voltammetry with linear scan (EVLS). The optimum conditions for DPV determination of tebuconazole were found in Britton-Robinson buffer/methanol (1:1, v/v) of pH 6.3, initial potential and accumulation potential $E_{acc} = +400$ mV vs. Ag/AgCl/3M KCl, scan rate 20 mV.s⁻¹. Applying the prolonged accumulation time (60 s), the limit of detection $2.10 \cdot 10^{-7}$ mol.L⁻¹ was achieved. The applicability of the developed method was verified on the analysis of the real soil solution sample.

Figure 1.: Structure of fungicide tebuconazole



ACKNOWLEDGEMENTS

The research was supported by GA AV CR (project No. IAA400400806), by GA CR (project No. P206/11/1638 and project No. P208/12/1645) and by University of Pardubice (grant No. SG-FCHT05/2012).

REFERENCES

- [1] Wang X, Wang, X, Zhang, H, et al.: *Chirality*, 24 (2012), 2, 104-11.
- [2] Shen Z, Zhu, W, Liu, D, et al.: *Chirality*, 24 (2012), 1, 67-71.
- [3] Jakl M, Jaklova Dyrtrtova, J, Cadkova, E. *Modern Electrochemical Methods XXXI*, 23.-27.5.2011 2011, Jetrichovice, pp 64-8.
- [4] Jaklova Dyrtrtova J, Jakl, M, Schroder, D, et al.: *Rapid Communications in Mass Spectrometry*, 25 (2011), 8, 1037-42.
- [5] Norkova R, Jaklova Dyrtrtova, J, Jakl, M, et al.: *Water, Air, & Soil Pollution* (2012), 10.1007/s11270-011-1055-7.

MODEL PHOSPHOLIPID MEMBRANES AND TRANSPORT OF HAZARDOUS METALS ACROSS THEM

Tomas NAVRATIL^{*}, Ivana SESTAKOVA¹, Jana JAKLOVA DYTRTOVA²

¹ J. Heyrovský Institute of Physical Chemistry of the AS CR, v.v.i., Dolejškova 3, 182 23 Prague 8, Czech Republic

² Institute of Organic Chemistry and Biochemistry of the AS CR, v.v.i., Flemingovo náměstí 2, 166 10 Prague 6, Czech Republic

^{*} Tomas.Navratil@jh-inst.cas.cz

The electrochemical methods (electrochemical impedance spectroscopy (EIS), patch clamp techniques, voltammetric techniques, etc.) belong to relatively frequently used in elucidation of transporting processes across the phospholipid membranes. The elucidation of such processes presents the first step of affecting of these processes (e.g., increasing or decreasing of the total amount of some specified ion (metal) in the cell by phytoremediation [1]). Because the real biological membranes are very complicated (integrated or partly integrated proteins, ion channels, etc.), they were replaced in our experiments by model phospholipid (PL) membranes which were composed of simple phospholipids (1,2-dipalmitoyl-*sn*-glycero-3-phosphocholine, 1,2-dipalmitoyl-*sn*-glycero-3-phosphoethanolamine, or mixture of phospholipids obtained from soybeans (commercial name Azolectin)). There are some different possibilities of formation of artificial (model) membranes for simulation of transporting processes, e.g., the form of vesicles, formation of SPLBs on the surfaces of solid materials, on the metallic substrates (mercury [2], gold, solid amalgams [3,4]). Such layers can be prepared in the form of a self-supporting membrane too (e.g., by filling a small micro-holes in a plate [5], etc.). Our team has dealt with formation and investigation of SPLBs on porous polycarbonate membranes [6-13] and on agar or agarose substrates [14].

Instead of ion channels and similar real transporters we have brought our attention to the utilization of ionophores (e.g., calcimycin, valinomycin) and low molecular weight organic acids (LMWOAs) for transport of charged as well as uncharged species (ions and their complexes) across the model biological membranes.

The compositions and the structures of these species have been investigated using electrospray ionization mass spectrometry [15]. Similar information about qualitative and first of all about quantitative composition of extracellular and intracellular solutions have been gathered using voltammetric techniques (DC voltammetry, differential pulse voltammetry (DPV), cyclic voltammetry) and ion selective electrode. The stability of tested membranes have been characterized by electrochemical impedance

spectroscopy (EIS).


We concentrated on investigation of transporting processes of heavy metal ions: cadmium, lead and copper which play very important role in environment. They form complexes with LMWOAs which are encountered mainly as important root exudates, influencing processes in the rhizosphere and influence solubility, mobilization and uptake by plant [16].

ACKNOWLEDGEMENT

The research was supported by GAAVCR (project No. IAA400400806) and by GACR (project No. P206/11/1638 and project No. P208/12/1645).

REFERENCES

- [1] Jakl M, Jaklova Dyrtrtova, J, Miholova, D, et al.: Chemical Speciation and Bioavailability, 21 (2009), 2, 111-20.
- [2] Becucci L, Moncelli, M R, Guidelli, R: Langmuir, 19 (2003), 8, 3386-92.
- [3] Yosypchuk B, Marecek, V. Modern Electrochemical Methods XXX2010, pp 197-201.
- [4] Yosypchuk B, Marecek, V: Journal of Electroanalytical Chemistry, 653 (2011), 1-2, 7-13.
- [5] Lhotsky A, Holub, K, Neuzil, P, et al.: Journal of the Chemical Society, Faraday Transactions, 92 (1996), 20, 3851-7.
- [6] Jaklova Dyrtrtova J, Sestakova, I, Jakl, M, et al.: Electroanalysis, 21 (2009), 3-5, 573-9.
- [7] Navratil T, Sestakova, I, Jaklova Dyrtrtova, J, et al. 7th WSEAS International Conference on Environment, Ecosystems and Development, Dec 14-16 2009, Puerto de la Cruz, SPAIN, pp 212-7.
- [8] Navratil T, Sestakova, I, Jaklova Dyrtrtova, J, et al.: WSEAS Transactions on Environment and Development, 6 (2010), 3, 208-19.
- [9] Navratil T, Sestakova, I, Marecek, V. Modern Electrochemical Methods XXIX, 25.-29.5.2009 2009, Jetrichevice, pp 74-6.

- 
- [10] Navratil T, Sestakova, I, Marecek, V.
Development, Energy, Environment,
Economics (DEEE '10)2010, Puerto de la
Cruz, pp 192-7.
- [11] Navratil T, Sestakova, I, Marecek, V, et al.
Modern Electrochemical Methods XXX,
24.-28.5.2010 2010, Jetrichovice, pp 119-
23.
- [12] Navratil T, Sestakova, I, Stulik, K, et al.:
Electroanalysis, 22 (2010), 17-18, 2043-50.
- [13] Sestakova I, Jaklova Dyrtrtova, J, Jakl, M,
et al. Development, Energy, Environment,
Economics (DEEE '10)2010, Puerto de la
Cruz, pp 186-91.
- [14] Navratil T, Sestakova, I, Marecek, V:
International Journal of Electrochemical
Science, 6 (2011), 12, 6032-46.
- [15] Sestakova I, Jaklova Dyrtrtova, J, Jakl, M,
et al.: International Journal of Energy and
Environment, 5 (2011), 3, 347-55.
- [16] Jakl M. In Food and Natural Resources,
Department of Agro-Environmental
Chemistry and Plant Nutrition, Faculty of
Agrobiology; Czech University of Life
Sciences: Prague, 2011, p 130.

CHARACTERIZATION OF SILVER NANOPARTICLES

Svatava ZUPKOVA^{1*}, Jiri SOPOUSEK¹, Michal SIDLO¹, Jiri BURSIK²

¹ Department of Chemistry, Faculty of Science, Masaryk University in Brno, Kamenice 753/5, 625 00 Brno, Czech Republic

² Institute of Physics of Materials, Academy of Sciences of the Czech Republic, Žižkova 22, 616 62 Brno, Czech Republic

* svatava_zup@centrum.cz

ABSTRACT

Understanding and characterization of colloidal nanoparticles is very important for their uses in the research and technology. Colloidal silver solutions have many interesting properties such as surface plasmon resonance. Plasmons are optical effects observed for silver, gold, and copper and the other nanoparticles. The value of the wavelength of this effect depends on the particle size and shape as well as on the properties of solvent or absorbent presented. As sample there were used nanoparticles of silver, which were dispersed in aqueous solution. The fluorescence, size and zeta-potential of two samples each with different date of preparation were measured. The colloidal solutions were investigated by means of fluorescence spectroscopy, dynamic light scattering, electron microscopy, and electrophoretic light scattering for zeta-potential evaluation.

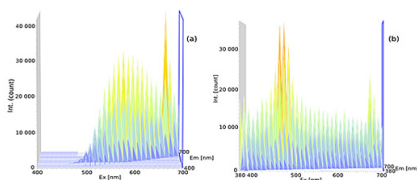
INTRODUCTION

In the last decades, nanoparticles have become very popular, especially particles of silver. Thanks to its extraordinary properties, these colloids are currently widely used. They are used as an antimicrobial agent, for catalysis or as a real-time optical sensor. The optical sensors made from silver use the surface plasmon resonance effect. Kildeby [1] writes that sensitivity of the sensor increases up to silver molar concentration 10^{-21} mol·l⁻¹. The wavelength of plasmons is directly proportional to the size, shape of the particle, solvent and absorbent [1], [2]. This contribution is focused on the characterization of nanoparticles, on their size mainly.

MATERIAL AND EXPERIMENTAL METHODS

The silver nanoparticles dispersed in aqueous solutions were studied. The colloidal solution was prepared by reduction of AgNO₃ in ammonia solution with the help of glucose [3]. Two identical solutions were obtained with different dates of preparations. The time difference was about three weeks (500hrs).

Figure 1: 3D fluorescence spectrum measured at 15/02/ 2012 where (a) is sample dated in 15/02/2012. and (b) from older sample dated 24/01/2012



The samples were investigated by fluorescence spectroscopy (measured on Thermo Scientific Lumina Fluorescence Spectrometer), dynamic light scattering (DLS), electrophoretic light scattering (both two foregoing items by instrument: Zetasizer Malvern), and transmission electron microscopy (TEM). The 3D fluorescence spectra are on Fig. 1.

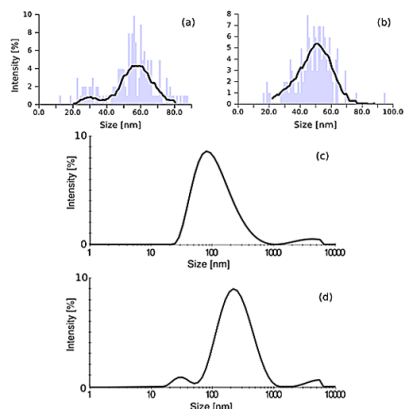
The DLS method is based on diffusion of light on particles moving by Brownian motion. This technique is used to measure the size of small particles in colloid solutions. It enables to measure a hydrodynamic diameter (Fig. 2) of the nanoparticles, which is higher than the real size [4]. The second alternative method for determining the size is TEM (Fig. 2). The zeta-potential of the nanoparticles was characterized via electrophoretic light scattering. The zeta-potential describes the surface electron potential of the particles [5]. The zeta-potential measurement is on Fig. 3.

RESULTS AND DISCUSSION

Just a simple visual comparison (by eyes) of the fresh and old samples revealed a distinct difference in colour of the samples. The difference was quantified by spectral measurement (Fig. 1). The first sample was brown with green reflection and the second one was violet with

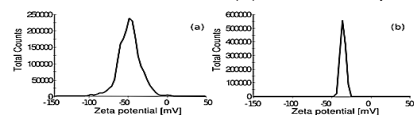
green reflection. That means that there were particles of different size in the samples.

Figure 2: Measured size distribution of silver nanoparticles. Fresh sample: (a) and (c). Old sample: (b) and (d). Real size (TEM) distribution: (a) and (b). Hydrodynamic size (DLS) distribution: (c) and (d)



The results of the fluorescence measurements, using a xenon lamp, are given on Fig. 1. There can be seen that the dispersion match to the absorption. The maximum of the fresher sample was about 660 nm, which corresponds to the absorptions of dark brown-yellow colour. The second, older sample had maximum about 480 nm. This wavelength match absorption of the blue light. There were not observed plasmons that can be due to the weak source of light.

Figure 3: Spectra of zeta potential (a) was measured from fresh and (b) from old sample.



The size was measured by two methods. The first used method was image analysis using images attained from electron microscope (TEM). The size distributions of fresh and old samples are on Fig. 2. The main nanoparticles diameter of the older sample is smaller than in younger one. This is caused by fact that some of the images were not suitable for image analysis because they show lot of big particles even in size of 200 nm. These big particles reveal visible the multiple twin effect [6]. These large particles are likely formed during ageing of the sample.

The second size method was DLS detecting the hydrodynamic radius. Results are shown in Fig 2 (c) and (d). This method is fast and sufficiently correct. The particles in younger sample were smaller and occurred primarily in the size of 80 nm. Nanoparticles in the older sample had a size of 180 nm. DLS method captured also large nanoparticles around 180 nm, so differs from the method of evaluating the TEM images.

This technique was complemented by measurements of zeta potential.

The zeta potential of particles was measured on the same instrument as the DLS. The results are shown in Fig. 3 (a) and (b). There is a noticeable shift in potential between the samples. The zeta potential does not depends on age of the nanoparticles.

CONCLUSION

The contribution presents the experimental measurements and simple characterization of the silver nanoparticles. The methods DLS, TEM, fluorescence spectroscopy and electrophoretic light scattering for zeta potential evaluation were used. The experimental study of the optical properties of the nanoparticles brings important information on the relation between size and optical properties during ageing of the samples. The difference between silver nanoparticle sizes measured by means of DLS technique and TEM image analysis showed that the thickness of the surface shell is important value, which must be studied in more details. The electrophoretic light scattering method reveals the zeta potential independence on size, which changes during ageing of the silver nanoparticles.

ACKNOWLEDGEMENT

Financial support of COST action MP0903 (LD11046) and CEITEC MU (CZ.1.05/1.1.00/02.0068) is gratefully acknowledged.

REFERENCES

- [1] Kildeby N. L., Andersen O. Z., Røge R. E., et al. Silver nanoparticles: Project p3. Aalborg University, 2005. <http://repetit.dk/>. Study material. (accessed. 13. April 2012) <http://repetit.dk/files/projects/p3.pdf>.
- [2] Yamamoto N., Ohtani S. and García de Abajo J. F. Gap and Mie Plasmons in Individual Silver Nanospheres near a Silver Surface. *Nano letters* 11, (2011) 91-95.
- [3] Vaničková M., Soukupová J., Kvítek L. Nanotechnologie ve výuce přírodních věd. *Chemické listy* 104 (2010) 945-949
- [4] Berne B. J., Pecora B. 1976 *Dynamic light scattering*. New York
- [5] Zeta Potential theory: <http://www.nbtc.cornell.edu/> (accessed 13. April 2012) <http://www.nbtc.cornell.edu/facilities/downloads/Zetasizer%20chapter%2016.pdf>
- [6] Marks L. D. Surface structure and energetics of multiply twinned particles. *Philosophical Magazine A* 49 (1984) 81-93

STUDY OF ELECTROCHEMICAL CORROSION OF A-C:N THIN FILMS

Marian MARTON*, Marian VOJS, Mario KOTLAR, Pavol MICHNIAK, Marian VESELY, Robert REDHAMMER

Institute of electronics and photonics, FEI STU, Ilkovičova 3, 84104 Bratislava, Slovakia

*marian.marton@stuba.sk

ABSTRACT

The corrosion behavior plays an important role in determining of biomedical implants feasibility. In this study nitrogen doped amorphous carbon (a-C:N) films were deposited on silicon and medical CoCrMo alloy substrates by vacuum arc discharge technique using different deposition conditions from graphite target. Potentiodynamic polarization tests and electrochemical impedance spectroscopy were employed to assess the corrosion performances of the films at room temperature in 0.89 wt. % NaCl solution. The influence of substrate bias on the electrochemical corrosion behavior was investigated.

INTRODUCTION

Nitrogen doped diamond-like carbon (a-C:N) thin films are promising candidates for coating of standard medical metal alloys (Ti6Al4V, Co-CrMo). Due to their excellent wear resistance, coefficient of friction, hardness, chemical inertness and biocompatible nature they can meet the requirements of suppressing the harmful release of ions, wear debris formation, and undesirable biological reactions with the surrounding tissue [1-4]. The properties that directly influence the corrosion behavior of DLC films are sp^3/sp^2 ratio, film structure, porosity, adhesion to substrate, surface roughness and electrical conductivity. The sp^3/sp^2 ratio is affected by the deposition conditions and varied also with used deposition method [5,6]. The application of substrate bias is frequently used to control the energy around 100 eV allowing the formation of the highest number of sp^3 bonds in the film [7, 8]. In this study, the influence of substrate bias on the electrochemical corrosion behavior and hardness was investigated.

EXPERIMENTAL

The a-C:N thin films were deposited on cylindrical CoCrMo samples in a vacuum system UVNIPA-1-001 described previously [9]. Mirror polished silicon substrates and cylindrical CoCrMo samples were used for deposition of the coatings. The substrates were cleaned for 10 min. with Ar ions prior to the deposition cycle. The sputtering frequency of the arc source pulses was 3 Hz and the total number of sputtering pulses 1.5k for Si and 3k for CoCrMo samples. Background pressure was 10^{-4} Pa and working pressure was maintained at around 1 Pa according to gas flow. Argon to nitrogen

(Ar:N) gas flow ratio was set up to 40:40 sccm. The temperature was kept below 150 °C. Negative substrate bias from 0 to -2.5 kV was applied during deposition process to change the incident ions energy. Potentiodynamic polarization tests and electrochemical impedance spectroscopy were employed to assess the corrosion performances of the films using Autolab Potenciostat Galvanostat at room temperature in 0.89 wt. % NaCl solution with Ag/AgCl reference electrode (RE). The samples were tested immediately after immersion with scan rate 80 mV/s. The structural properties of a-C:N films were studied by Raman spectroscopy with 632.8 nm He-Ne laser. The acquired Raman spectra were fitted with a Gaussian line to illustrate the D and G peak positions, G peak full width at half maximum (FWHM) and I_D/I_G ratio.

RESULTS AND DISCUSSION

Potentiodynamic polarization tests

Fig. 1a) shows the dependence of E_{corr} on substrate bias applied during deposition. It can be seen that the line is almost similar to the G peak position dependence. The highest value of E_{corr} can be observed for the sample deposited with negative bias -0.6 kV and with further increasing of U_s the corrosion potential shifts to lower values. We can see that, the highest value of E_{corr} occurs within the higher G peak position, where the lower sp^3/sp^2 ratio, higher number of graphitic rings per cluster and higher domain size can be expected.

Figure 1.: a) Dependence of Raman G peak position and E_{corr} vs. RE (Reference Electrode) of a-C:N deposited with different substrate bias, b) polarization curves of uncoated and a-C:N coated CoCrMo deposited with different substrate bias

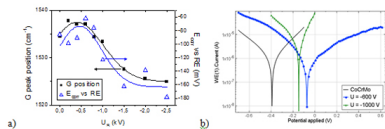
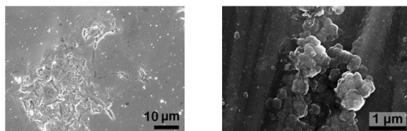


Fig. 1b) shows the polarization curves of uncoated and a-C:N coated CoCrMo substrates deposited with different substrate biases. The potential region of the a-C:N coated samples ($E_{\text{COFF}} = -47.2$ mV) was shifted towards more positive values compared to uncoated samples ($E_{\text{COFF}} = -392.4$ mV), i.e., showed more noble corrosion potentials (a shift of approximately 350 mV). Besides, it can be seen from the figures that the range of current density for protecting film formation is smaller for coated substrates than for uncoated. The samples in the corrosion behavior with lower current density and higher potential indicate better corrosion resistance evidenced by a shift of the whole polarization curve towards the region of lower current density and higher potential [10].

In the Fig. 2 we can see the SEM images of a-C:N layer deposited on CoCrMo after potentiodynamic polarization tests. After destructive corrosion tests, all of the coatings seemed to have less or more noticeable amount of surface pits. The SEM micrographs in Fig. 3 show shallow wide pits with vertical grain attack (left) and corrosion products (right). It is known that the pits initiate at defects, surface compositional heterogeneities and porosities because these imperfections degrade the cross-linking structure of the film. The increased surface roughness of CoCrMo substrates can contribute to degradation of corrosion resistance of the protection films because of a larger exposed surface area to the electrolyte during the corrosion testing.

Figure 2.: SEM images of corroded areas on a-C:N layer deposited on CoCrMo, shallow wide pits with vertical grain attack (left) and corrosion products (right)

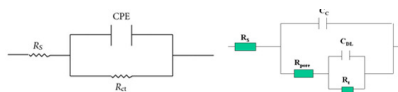


ELECTROCHEMICAL IMPEDANCE SPECTROSCOPY

The best equivalent circuits for EIS spectra of clear CoCrMo substrate is in the Fig.3 left, for the substrate covered with a-C:N layer it is the one on the right. These equivalent circuits are

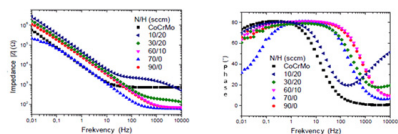
assembled of following components: resistance of used electrolyte – R_s , capacitance of a-C:N layer – C_c , porosity resistance R_p , which is contributed to the electrolyte ions flux through the thin film, double-layer capacitance – C_{dl} attributed to interface substrate/layer and polarization resistance R_{ct} .

Figure 3.: Equivalent circuits for EIS spectra of clear CoCrMo substrate (left) and for the substrate covered with a-C:N layer (right)



High value of R_{ct} causes corrosion processes slowdown and increases the corrosion resistance. Impedance and phase-frequency dependence are in Bode diagrams in Fig.4. We can see, the values of impedance by covered substrates are higher than by non-covered in the lower and middle frequencies and lower by high frequencies. Polarization resistance by non-covered substrate was $R_{ct} = 3.03$ M Ω . The value of polarization resistance for covered substrates varied from 4.4 to 20 M Ω . In Bode diagram (Fig.4 right) we can observe higher phase shift for substrates with a-C:N layers than for non-covered substrates in the range of middle and high frequencies. We can assume that, the corrosion resistance of a-C:N covered CoCrMo substrates was improved [11].

Figure 4.: Dependence of impedance Z (left) and phase shift (right) on frequency for substrates with and without a-C:N layer



CONCLUSIONS

Diamond like carbon thin films were deposited on medical grade CoCrMo alloys by arc discharge method with different substrate biasing. The corrosion potential of the a-C:N coated samples was shifted towards more positive values and the range of current density was smaller compared to uncoated samples. This indicates that the tendency towards corrosion for coated samples has become weaker. The

highest value of E_{corr} for CoCrMo substrate was measured on the coating deposited with substrate bias around -0.6 kV. The shift of E_{corr} to more positive values was approximately 350 mV. All of the coatings after polarization tests seemed to have less or more noticeable surface degradation. SEM micrographs showed a small amount of surface localized shallow wide pits with vertical grain attack and surface solid products which usually agglomerate around the defects or pores.

Using EIS, we found suitable equivalent electrical circuit for analyzed system substrate/layer. The value of polarization resistance for covered substrates varied from 4.4 to 20 M Ω . For non covered substrate it was only 3 M Ω . The increase of polarization resistance causes electrochemical corrosion speed slowdown and increases corrosion resistance.

ACKNOWLEDGEMENT

The authors would like to thank Mr. Král for technical assistance. This work was done in Center of Excellence CENAMOST (Slovak Research and Development Agency Contract No. VVCE-0049-07) and was financially supported by grants APVV-0628-06, APVV-0548-07, LPP-0149-09, and VEGA 1/1103/11, 1/1102/11, 1/0264/11.

REFERENCES

- [1] H. W. Choi et al., *Surface & Coatings Technology* 202 (2008) 2632–7
- [2] V. Řeháček et al., *Microsystem Technologies Vol. 14*, 491 (2008)
- [3] V. Řeháček et al., *Sensors and Actuators B. Chemical Vol. 127*, 193 (2007)
- [4] V. Řeháček et al., *Journal of Physics: Conference Series. Vol. 61*, 982 (2007)
- [5] C. Surdu-Bob et al., *Diamond & Related Materials* 17, 1625 (2008)
- [6] S. Muhl, J.M. Mendez, *Diamond and Related Materials* 8, 1809 (1999)
- [7] Y. Lifshitz, *Diamond and Related Materials* 8, 1659 (1999)
- [9] J. Robertson, *Material science and engineering R37*, 129 (2002)
- [10] M. Marton et al., *Vacuum* 84, 65 (2010)
- [11] J.H. Sui et al., *Nuclear Instr. and Methods in Phys. Research B* 267, 2475 (2009)
- [12] P. Papakonstantinou et al., *Diam and Rel Mat*, 11, 3-6 (2002) 1124-9

RARE „REVERSED“ EPR SPECTRA SEEN IN SOME COPPER(II) COMPLEX SYSTEMS

Lucia HUSARIKOVA*, Zuzana REPICKA, Dusan VALIGURA, Milan MAZUR

Faculty of Chemical and Food Technology, Slovak University of Technology in Bratislava, Radlinského 9, SK-812 37 Bratislava, Slovakia

*lucia.husarikova@stuba.sk

ABSTRACT

Copper(II) complex systems containing 3,5-di-, 4-, or 5-chlorosalicylic acids (X-ClsalH) with different copper(II) salts (copper acetate (Cu(ac)₂) or copper sulphate (CuSO₄)) in presence of 2,6-pyridinedimethanol (pydime) were studied by EPR spectroscopy in water/methanol solutions. The rather rare, „reversed“ Cu(II) EPR spectra were obtained and analysed.

INTRODUCTION

According to Jahn-Teller theorem [1], the copper(II) complexes can not be rigorously octahedral and the highest symmetry compatible with this theorem represents tetragonal structure. The tetragonal distortion of the octahedron (either elongation or compression) is the most simple way of the octahedral degeneracy decreasing [2]. EPR spectroscopy is a useful tool for the assignment of the stereochemistry of such complexes via analysis of the opposite g-parameter patterns arising from these two mentioned distortions [3]. Hathaway and Billing [4] attributed the following relation of g-values evaluated from the EPR spectra: i) ($g_{\perp} > g_{\parallel}$)

for elongation and ii) ($g_{\perp} < g_{\parallel}$) for compression.

MATERIAL AND METHODS

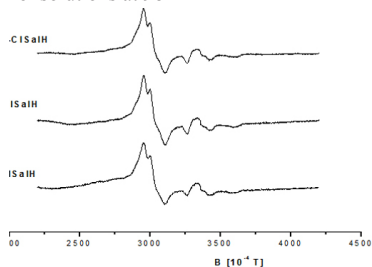
The samples for EPR experiment were prepared immediately before measurements by mixing Cu(ac)₂ or CuSO₄ with 3,5-di-, 4-, or 5-chlorosalicylic acids (X-ClsalH) and with 2,6-pyridinedimethanol (pydime) in water/methanol solvent. The resulting solution was then carefully homogenized and filled into quartz capillaries. In this case, the sets of samples for EPR measurement were obtained and the Cu(II) EPR spectra were recorded on Bruker EMX X-band EPR spectrometer at room temperature and at 98 K. Detailed information on EPR experiments, interpretations, processing (WinEPR) [5] and simulations (SimFonia) [6] of EPR spectra are summarised in Refs. [7, 8].

RESULTS AND DISCUSSION

For illustration, the experimental „reversed“ axially symmetric Cu(II) EPR spectra of systems [CuSO₄(aq) + 2 (X-ClsalH(solv)) + 4 pydime(solv)], where X = 3,5-di-, 4-, or 5-, which were measured in the frozen water/methanol solution at 98 K are shown in Figure 1. In all cases, the EPR spectra are characterised with unre-

solved perpendicular and well-resolved parallel copper hyperfine splitting of ^{63,65}Cu isotopes (I = 3/2). Neither parallel nor perpendicular superhyperfine splitting of ¹⁴N isotope (I = 1) was resolved in the Cu(II) EPR spectra.

Figure 1. Experimental first derivative „reversed“ axially symmetric Cu(II) EPR spectra of copper(II) complex systems: [Cu(ac)₂(aq) + 2 (X-ClsalH(solv)) + 4 pydime(solv)], where X = 3,5-di-, 4-, or 5-, measured in frozen water/methanol solutions at 98 K



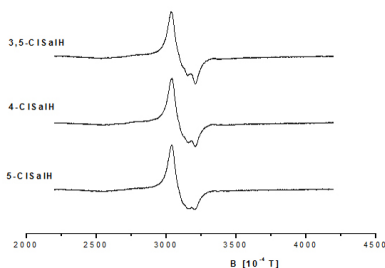
The spin Hamiltonian parameters evaluated from the experimental „reversed“ Cu(II) EPR spectra were refined by the computer simulations. The values of both g-factors ($g_{\perp} = 2.21$ and $g_{\parallel} = 2.01$) remain constant for 3,5-di-, 4-, and 5-chlorosalicylic acids. All the Cu(II) EPR spectra showed the rare, „reversed“ axial symmetry with the relations ($g_{\perp} > g_{\parallel}$) indicating the distorted compressed octahedral geometry of the copper ion [3] in these complex systems. Likewise, the parallel copper hyperfine splitting (A_{\parallel}) = 16.8 mT values remain constant for investigated X-ClsalH. The above spin Hamiltonian parameter values are in a good accordance with those published for similar „reversed“ axially symmetric Cu(II) EPR spectra of copper(II) complexes, see elsewhere [4, 9-11]. However, when ligand (pydime) was not present in the re-

action mixture, the “regular” Cu(II) EPR spectra (data not shown) with axial symmetry were observed in the frozen solutions at 98 K. In this case, the relations in g -values

($g_{\parallel} > g_{\perp}$) indicates the distorted elongated octahedral geometry of central copper atom and that the unpaired electron on copper ion is localised on the $d_{x^2-y^2}$ orbital [4].

Figure 2 illustrates the experimental Cu(II) EPR spectra of the same copper(II) complex systems, but recorded in the water/methanol solutions at room temperature. Unfortunately, the hyperfine structure of copper resonance line (quartet) due to $^{63,65}\text{Cu}$ isotopes ($I = 3/2$) was not resolved, which is probably caused by simultaneous influence of the exchange interaction and the Jahn-Teller effect [1]. Therefore, only wide, asymmetric “reversed pseudosinglet” ($g_{\text{eff}} \approx 2.15$, $\Delta B_{\text{pp}} \approx 14.5$ mT) was seen in such Cu(II) EPR spectra.

Figure 2. Experimental first derivative Cu(II) EPR spectra („reversed pseudosinglet“) of copper(II) complex systems: $[\text{Cu}(\text{ac})_2(\text{aq}) + 2(\text{X-ClsalH}(\text{solv})) + 4 \text{ pydime}(\text{solv})]$, where $\text{X} = 3,5\text{-di}, 4\text{-},$ or 5- , measured in water/methanol solutions at room temperature



Also here, when ligand (pydime) was not present in the reaction mixture the “regular pseudosinglet” was observed in the experimental Cu(II) EPR spectra (data not shown) measured in the water/methanol solutions at room temperature.

The spectral features of all the Cu(II) EPR spectra of these copper complex systems $[\text{Cu}(\text{ac})_2(\text{aq}) + 2(\text{X-ClsalH}(\text{solv})) + 4 \text{ pydime}(\text{solv})]$, where $\text{X} = 3,5\text{-di}, 4\text{-},$ or 5- , are very similar, which can indicate that for all X-ClsalHs the dominant complexes have similar structure of the first order coordination sphere around the copper atom.

In this contribution, we presented the original, preliminary results arising from the present state of the study of the above mentioned copper(II) complex systems by EPR spectroscopy. Further experiments in this topic are in the progress.

CONCLUSION

The rather rare, „reversed“ Cu(II) EPR spectra were obtained in the water/methanol solutions of the copper(II) complex systems containing 3,5-di, 4-, and 5-chlorosalicylic acids, different copper(II) salts and the ligand (2,6-pyridinedimethanol) at both temperatures. In the case of the „reversed“ axially symmetric Cu(II) EPR spectra, the unusual relation of g -values ($g_{\perp} > g_{\parallel}$) can be due to a compressed tetragonal distortion of the octahedron geometry.

5. ACKNOWLEDGEMENT

We are grateful to Prof. Vlasta Brezová for fruitful discussions. This work was supported by the Slovak Research and Development Agency under the contract Nos. (APVV-0202-10 and APVV-0339-10) and Scientific Grant Agency of the Slovak Republic (Projects VEGA 1/0856/11 and 1/0289/12).

REFERENCES

- [1] Jahn H.A. and Teller E.: Proc. Roy. Soc., 161 (1937) 220-222
- [2] Gažo J., Bersuker I.B., Garaj J., Kábešová M., Kohout J., Langfelderová H., Melník M., Senátor M., Valach F.: Coord. Chem. Rev., 19 (1976) 253-297
- [3] Hathaway B.J. and Billing B.J.: Coord. Chem. Rev., 5 (1970) 143-207
- [4] Bertini I., Gatteschi D., Scozzafava A.: Coord. Chem. Rev., 29 (1979) 67-84
- [5] Thiele H., Etstling J., Such P., Hoefler P., WIN-EPR Bruker Analytik GmbH, Bremen and Rhenstetten, Germany, (1992)
- [6] Weber R.T., WIN-EPR SimFonia, Software version 1.2, EPR Division, Bruker Instruments, Inc., Billerica, USA (1995)
- [7] Martiška L., Husáriková L., Repická Z., Valigura D., Valko M., Mazúr M.: Appl. Magn. Reson., 39 (2010) 423-435
- [8] Martiška L., Husáriková L., Repická Z., Valigura D., Valko M., Mazúr M.: Appl. Magn. Reson., 40 (2011) 405-411
- [9] Kohout J., Gažo J., Hvastijová M.: Inorg. Chim. Acta, 8 (1974) 241-245
- [10] Halcrow M.A.: Dalton Trans., (2003) 4375-4384
- [11] Kozlevčar B., Šegedin P.: Croat. Chem. Acta, 82 (2008) 369-379

CHARACTERISATION OF BORON DOPED DIAMOND FOR TRACE METAL DETECTION

Pavol MICHNIAK^{1*}, Matej JURAK¹, Marian VOJS¹, Marian VESELY¹, Andrej VINCZE², Robert REDHAMMER¹ Michael ROSSBERG³, Peter SCHAAF³

¹ Institute of Electronics and Photonics, Slovak University of Technology, Ilkovičova 3, 812 19 Bratislava, Slovak Republic

² International Laser Centre, Ilkovičova 3, 841 04 Bratislava, Slovak Republic

³ Ilmenau University of Technology, Institute of Material Science, Ilmenau 98694, Germany
*pavol.michniak@stuba.sk

ABSTRACT

In recent days the synthetically grown diamond layers are very progressive materials for various fields of technology. Thin diamond layers can be prepared using hot filament chemical vapour deposition (HF CVD) method. During the deposition and growth process in the reactor contain boron atoms are present as doping gas, boron doped diamond (BDD) can be produced. In this contribution were BDD layers analysed, which were identically grown with different concentration of boron. The resulting BDDs were analysed using Scanning Electron Microscopy (SEM) and Raman spectroscopy to determine properties of samples [1].

INTRODUCTION

The chemical vapour deposition (CVD) involves a gas phase chemical reaction occurring above a solid surface, which causes deposition onto that surface. Hot filament CVD (HF CVD) method is used for the growth of diamond thin films under low pressures, and is also the most popular method. The used hot filaments are heated up to 2 000 °C to activate the H₂ and CH₄ gases. The diamond film is then deposited onto a substrate, which is located about 10 mm under the filaments on molybdenum holder. The pressure in the chamber is up to 3 kPa and rotary pump is used for chamber evacuation. The HF CVD method is relatively cheap modification and diamond thin films can be relative easily produced. However, there is another method to produce diamond thin films, e.g., MW CVD (Microwave CVD), which uses microwaves to activate gases. It is cleaner as a HF CVD, but MW CVD reactor is more expensive [2]. Before starting the growth process, the substrate surface must be prepared for the growth. This step is described as a diamond seeding layer process or also nucleation [3]. Diamond thin films prepared with CVD are used in electrochemistry, mainly for trace metal detection. They have a high sensitivity.

EXPERIMENTAL DETAILS

The diamond thin films were prepared by Hot Filament CVD. The nucleation process was initiated using diamond powder in ultrasonic bath in demineralised water after 15 minutes. Before nucleation, samples were cleaned in ultrasonic bath in acetone and next they were rinsed in ultrasonic bath in demineralised water. Diamond thin films were prepared on SiO₂ thin layer (about 150 nm thick), which was prepared on Si substrate.

Table 1: Gas flow and B/C ratio

Sample	CH ₄ (sccm)	H ₂ (sccm)	H ₂ +TMB (sccm)	B/C (ppm)
A	6	250	50	1667
B	6	100	200	6667
C	6	50	250	8333
D	6	0	300	10000

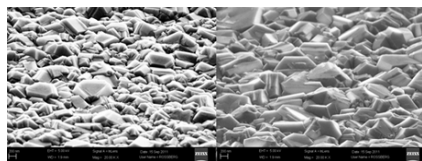
Using the hot filament CVD method the filaments in the reactor reach almost 2 000 °C and the substrate temperature is usually in the range from 600 °C to 800 °C. Samples were prepared at different gas flows of TMB (Trimethylboron), which is the source for B and B/C ratio is amount of TMB to CH₄ (ppm). In Tab. 1 gas flows during deposition are shown. All samples were prepared at 3 kPa in vacuum chamber and the time of the deposition was 120 minutes.

RESULTS AND DISCUSSION

SEM is first analytical methods, which was used to determine morphology of surfaces. SEM pictures of samples A and D shown, that surfaces are evenly covered with diamond structured. In figures is not observed significant difference between samples A and D, whose are growths with different concentration of boron. However, in sam-

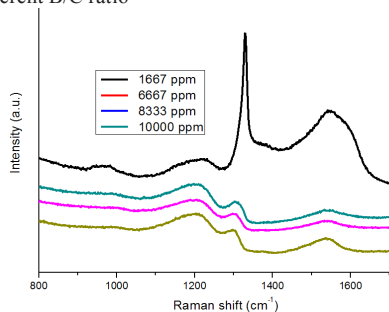
ple A, which was growth in less concentration of boron, is observed some smaller diamond crystal.

Figure 1.: SEM picture of samples A (left) and D (right)



The Fig. 2 shows the Raman spectra, which were obtained at room temperature using a He-Ne laser with wavelength of 632 nm. The diamond peak at 1333 cm^{-1} decreases with an increased B/C ratio [4]. Raman broad band centred at 1225 cm^{-1} are for boron. Peak at 925 cm^{-1} are characteristic for Si. For high boron concentration the peak at 1580 cm^{-1} characteristic for micro-graphite is less visible [5].

Figure 2.: Raman spectra of samples with different B/C ratio



CONCLUSION

In this contribution we compared a series of diamond thin film samples produced by HF CVD method prepared with different boron concentrations. Characterizations by SEM, and Raman spectroscopy methods were carried out. Boron doped diamond thin films can be produced and they will be used in other areas of science and industry, for example, now they are used in electrochemistry [1].

ACKNOWLEDGEMENT

The authors would like to thank to J. Král for technical support. This work was done with a support of Slovak Research and Development Agency project No. LPP-0094-09, APVV-0548-07, VEGA projects 1/1103/11 and 1/1102/11.

REFERENCES

- [1] Vincze, Andrej et al.: APCOM 2011. (2011), 82-85.
- [2] Paul W. May: Phil. Trans. R. Soc. Lond. A (2000) 358, 473–495
- [3] S.-Tong Lee, Zhangda Lin, Xin Jiang: Material Science and Engineering, 25 (1999) 123-154
- [4] M. Bernard et al.: Diamond and Related Materials 13(2004), 282-286
- [5] P.W.May et al.: Diamond and Related Materials 17 (2008), 105-117

ELECTROCHEMISTRY OF BIOMACROMOLECULES

Emil PALECEK, Martin BARTOSIK, Hana CERNOCKA,
Veronika OSTATNA, Mojmir TREFULKA, Veronika VARGOVA

Institute of Biophysics, Acad. Sci. CR, v.v.i., Královopolská 135, 612 65 Brno, Czech Republic
palecek@ibp.cz

ABSTRACT

Electrochemistry of nucleic acids and protein represent booming fields because of their relations to genomics and proteomics, requiring new simple and inexpensive methods for parallel analysis of nucleic acids and proteins. Recent development in these fields will be briefly reviewed. Until very recently, poly- and oligosaccharides were considered as electroinactive species and electrochemical methods were little used in their analysis. Our recent studies show that these compounds can be conveniently analyzed by electrochemical methods.

INTRODUCTION

In 1930 first paper on the ability of proteins to catalyze hydrogen evolution producing polarographic pre-sodium wave was published by Heyrovský and Babička [1]. This wave was, however, considered of little use in protein analysis because it was poorly developed and appeared too close to the background discharge. First papers on polarography of nucleic acids (NAs) were published about 30 years afterwards [2]. At present electrochemistry of NAs is a booming field because electrochemical detection appears as an interesting alternative for optical detection in sensors and detectors for DNA hybridization and DNA damage [3-5].

NUCLEIC ACIDS

Nucleic acids (NAs) are electroactive species yielding reduction and oxidation signals at mercury and oxidation signals at carbon electrodes due to redox processes involving the NA bases [5]. Electroactivity of NAs was discovered >50 years ago [2,4]. In the same time it was shown that reduction signals at Hg electrodes reflect changes in DNA structure [2,5] and that damage to DNA [6] can be detected electrochemically. In the 1980's first electroactive labels were introduced in NAs and first DNA-modified electrodes were invented [5]. The boom of NA electrochemistry started in 1990. In recent years roughly 700 papers per year have been published [4,5]. At present any nucleotide sequence as well as point mutations/single nucleotide polymorphisms can be easily electrochemically detected [5]. Mostly PCR amplified DNA is used for the analysis. Detection of specific sequences in eukaryotic DNAs in biological matrices (without PCR amplification) still represents a challenge. Based on specific engineering of the electrode surface using ternary thiol layers recently a significant progress has been made allowing detection of specific sequences in undiluted blood and urine [7].

PROTEINS

It has been shown that using the constant current chronopotentiometric stripping (CPS) and hanging mercury drop electrode (HMDE) or solid amalgam electrodes (SAEs) peptides and proteins produce well-developed electrocatalytic peaks (peak H) which, similarly to the polarographic presodium wave, are due to the catalytic hydrogen evolution reaction (CHER) [8-12]. Peak H differs from the previously studied polarographic and voltammetric signals of proteins (i) by different polarization of the mercury electrodes (ii) by its ability to detect proteins down to nanomolar and subnanomolar concentrations and (iii) by its high sensitivity to changes in protein structures [8,10,12] and redox states [9]. Using *thiol-modified Hg electrodes* changes in protein structure at the electrode surface can be well controlled [12]. Peak H was applied for recognition of changes in protein structures due to single amino acid exchange in mutated proteins such as tumor suppressor protein p53 [13]. Picomoles of the protein were sufficient for the analysis. Miniaturized solid amalgam chips were developed for parallel protein sensing [14].

CARBOHYDRATES

We have shown that sulfated polysaccharides (PS) produce electrocatalytic peak H_{ps} [15] and that electroactive labels, based on complexes of six-valent osmium with different nitrogenous ligands [Os(VI)L], can be introduced in other PSs [16] and in ribose residues at the 3'-end of RNA molecules [17], yielding different redox couples at HMDE, SAEs and carbon electrodes. Some [Os(VI)L] complexes produce at HMDE and SAEs specific peak *Cat* allowing detection of carbohydrates at picomolar level [16,18]. This peak, similarly to peak H, is due to CHER but appears at less negative potentials than peak H. It has been shown that specific glycosy-

lation patterns of proteins are associated with states of health and disease. Glycan analysis in glycoproteins is therefore increasingly applied in biomedical research, clinical practice, pharmacy, biotechnology, etc. Reliable, simple and inexpensive methodologies for the analysis of carbohydrates and particularly glycans in glycoconjugates are therefore sought. It appears that electrochemical methods will soon find use in the analysis of glycans in glycoproteins.

CONCLUSION

For several decades electrochemistry of biomacromolecules was limited to proteins. At present a large amount of literature on electrochemistry of DNA and RNA [3-5] as well as on electroactivity of non-protein components of conjugated proteins is available. We can witness growing interest in electrochemical responses of amino acid residues in proteins, not limited to a small group of conjugated proteins yielding reversible electrochemistry [8,13]. Particularly CPS responses at bare and thiol/modified Hg electrodes (**due to CHER**) attract attention because of their excellent sensitivity to changes in protein structures. Recently reported electroactivity of the adducts of Os(VI)L complexes with poly- and oligosaccharides [16-18] gives promise for wider application of electrochemistry in carbohydrate research and especially in analysis of glycoproteins and possibly in glycomics.

ACKNOWLEDGEMENT

This work was supported by GACR P301/11/2055 and AV0Z50040702.

REFERENCES

- [1] J. Heyrovsky, J. Babicka, *Collect. Czech. Chem. Commun.*, 2 (1930) 370.
- [2] E. Palecek, *Nature*, 188 (1960) 656-657.
- [3] E. Palecek, F. Jelen, in: E. Palecek, F. Scheller, J. Wang, (Eds.), *Electrochemistry of Nucleic Acids and Proteins. Towards Electrochemical Sensors for Genomics and Proteomics*, Elsevier: Amsterdam, (2005), pp. 74-174.
- [4] E. Palecek, *Electroanalysis*, 21 (2009) 239-251.
- [5] E. Palecek, M. Bartosik, *Chem. Rev.*, DOI: 10.1021/cr200303p (2012).
- [6] E. Palecek, *Collect. Czech. Chem. Commun.*, 76 (2011) 1799-1810.
- [7] S. Campuzano, F. Kuralay, M.J. Lobo-Castanon, M. Bartosik, K. Vyavahare, E. Palecek, D.A. Haake, J. Wang, *Biosens. Bioelectron.*, 26 (2011) 3577-3583.
- [8] E. Palecek, V. Ostatna, *Electroanalysis*, 19 (2007) 2383-2403.
- [9] V. Dorcak, E. Palecek, *Anal. Chem.*, 81 (2009) 1543-1548.
- [10] E. Palecek, V. Ostatna, *Chem. Commun.*, 13 (2009) 1685-1687.
- [11] T. Doneux, V. Dorcak, E. Palecek, *Langmuir*, 26 (2010) 1347-1353.
- [12] V. Ostatna, H. Cernocka, E. Palecek, *J. Am. Chem. Soc.*, 132 (2010) 9408-9413.
- [13] E. Palecek, V. Ostatna, H. Cernocka, J.A. C., A.R. Fersht, *J. Am. Chem. Soc.*, 133 (2011) 7190-7196.
- [14] P. Juskova, V. Ostatna, E. Palecek, F. Foret, *Anal. Chem.*, 82 (2010) 2690-2695.
- [15] S. Strmecki, M. Plavsic, B. Cosovic, V. Ostatna, E. Palecek, *Electrochem. Commun.*, 11 (2009) 2032 - 2035.
- [16] E. Palecek, M. Trefulka, *Analyst*, 136 (2011) 321-326.
- [17] M. Trefulka, M. Bartosik, E. Palecek, *Electrochem. Commun.*, 12 (2010) 1760-1763.
- [18] E. Palecek, M. Bartosik, V. Ostatna, M. Trefulka, *Chem. Rec.*, 12 (2012) 27-45.

ACIDITY FUNCTIONS AND THEIR CONSTRUCTIONS

Oldrich PYTELA*

¹ Department of Organic Chemistry and Technology, Faculty of Chemical Technology, University of Pardubice, Studentská 573, 532 10 Pardubice, Czech Republic

*oldrich.pytela@upce.cz

ABSTRACT

The acidity function is a thermodynamic quantitative measure of acid strength for non-aqueous and concentrated aqueous Brønsted acids. The methods of their constructions proposed by the author and some further applications are summarized in this contribution.

INTRODUCTION AND THEORY

The acidity function is a thermodynamic quantitative measure of acid strength for non-aqueous and concentrated aqueous Brønsted acids, with acid strength being defined as the extent to which the acid protonates a base of known basicity [1]. The concept of acidity function was introduced by Hammett and Deyrup [2] who denoted it H . In this concept the acidity function represents an extrapolation of pH scale to media exhibiting non-ideal behavior of components of the protonating or deprotonating medium and substrate. Definition of the acidity function is based on the equilibrium constant of the dissociation process

$$K_a = \frac{a_B a_{H^+}}{a_{BH^+}} = \frac{[B][H^+]}{[BH^+]} \cdot \frac{f_B f_{H^+}}{f_{BH^+}}$$

$$K_a = \frac{a_B a_{H^+}}{a_{BH^+}} = \frac{[B][H^+]}{[BH^+]} \times \frac{f_B f_{H^+}}{f_{BH^+}} \quad (1)$$

Taking the logarithms we obtain after modification

$$pK_a = \log \frac{[BH^+]}{[B]} - \log a_{H^+} - \log \frac{f_B}{f_{BH^+}} = \log I + H$$
$$pK_a = \log \frac{[BH^+]}{[B]} - \log a_{H^+} - \log \frac{f_B}{f_{BH^+}} = \log I + H \quad (2)$$

where the symbol I denotes the measurable concentration ratio (obviously UV-VIS spectroscopy determinate) of the protonated to the non-protonated forms, and the symbol H denotes the acidity function. Using Eq. (2) and a series of structurally similar indicators (with constant ratio f_B/f_{BH^+} at a given concentration of acid) it is possible to construct the dependence of H function on the acid concentration. A difficulty consists in that the H function depends on the type of acid, their concentration and the

indicator [3]. Several authors tried to remedy this fault by introduction of a general acidity function [4,5].

The whole measurements are only applied to acid-base equilibrium processes, but kinetic measurements are also carried out, in non-ideal media of concentrated acids and bases. In this case, it is common to plot logarithm of the observable rate constants against a suitable acidity function. Troubles are encountered, if one must work with media whose acidity functions are unknown. Therefore, several years ago, Johnson and coworkers suggested the concept of kinetic acidity function [6-8].

The electrochemical acidity function represents an interesting approach for the description of non-ideal media properties [9]. A liquid junction-free reference potential was realized at a dropping mercury electrode, using the standard potential of the metallocene redox couple. This approach is particularly suitable for determination of acidity functions that are seamlessly anchored to aqueous standard buffers.

METHODS OF CONSTRUCTION OF ACIDITY FUNCTIONS

The construction of H function [10] utilizes equation (2), while two conditions must be fulfilled. The first condition means a constant ratio of the activity coefficients f_B/f_{BH^+} . Hence, a series of structurally similar compounds are generally used as indicators. Weak bases, with pK_a differences of two consecutive indicators less than 1, are used for acid media. They are typically represented by substituted anilines (e.g. acidity function H_0), but amides (acidity function H_A) or other substances can also be used. The acidity function must follow the pH scale. Hence, the second condition is that the pK_a value of at least one indicator (usually the most basic one) must be determined within the range of pH. For the difference in pK_a of the particular acid concentrations the equation (3) is valid.

$$pK_a^{i+1} - pK_a^i = \log I^{i+1} - \log I^i \quad (3)$$

The dependence of $\log I$ on the concentrations c_{acid} for every indicator is represented by a slightly bent curve. The shape of this dependence is for all indicators and within the range of concentrations c_{acid} approximately similar. However, the curves are mutually shifted along the $\log I$ axis by the increment which corresponds to the difference in $\text{p}K_{\text{a}}$ (equation (3)).

A construction of the acidity function means shifting the curves along the $\log I$ axis to overlap as much as possible and, simultaneously, to continue the curve of the most basic indicator (“anchoring” on the pH scale). For such purposes, several numerical models have been proposed. One of them used the differences in the integral area below the curves [11], later on, another, more general and effective algorithm based on iterative smoothing was developed [12]. This method was used for the construction of acidity function H_0 of perchloric acid and was further extended by so-called “interconnected acidity function” in the same medium and two indicator types. The proposed methods of the acidity function construction were also used for the redefinition of so-called “kinetic acidity function” according to the equation (4).

$$\log k_{\text{cat}} = \log k_{\text{obs}} - H$$

(4)

The acidity function constructed in this way was further used for the study of reaction mechanisms in strong acid media [15,16].

REFERENCES

- [1] Pagni R. M.: *Found. Chem.*, 11 (2009), 43-50.
- [2] Hammett L. P., Deyrup A. I.: *J. Am. Chem. Soc.*, 54 (1932), 2721-2739.
- [3] Rochester C. H. in: *Acidity Functions in Organic Chemistry* (A. T. Blomquist, Ed.). Academic Press, New York 1970.
- [4] Marziano N. C., Cimino G. M., Passerini R. C.: *J. Chem. Soc., Perkin Trans. 2*, 1973, 1915-1922.
- [5] Cox R. A., Yates K.: *J. Am. Chem. Soc.*, 100 (1978), 3861-3867.
- [6] Greig C. C., Johnson D. C., Rose S., Taylor P. G.: *J. Org. Chem.*, 44 (1979), 745-753.
- [7] Johnson D. C., Rose S., Taylor P. G.: *J. Org. Chem.*, 44 (1979), 753-757.
- [8] Graham W. L. E., Johnson D. C.: *J. Chem. Soc., Perkin Trans. 2*, 1982, 1025-1027.
- [9] Janata J., Zuman P.: *Collect. Czech. Chem. Commun.*, 74 (2009), 11-12, 1635-1646.
- [10] Cookson R. F.: *Chem. Rev.*, 74 (1974), 5-28.
- [11] Pytela O., Vetešník P.: *Collect. Czech. Chem. Commun.*, 48 (1983), 2368-2375.
- [12] Pytela O.: *Collect. Czech. Chem. Commun.*, 62 (1997), 645-655.
- [13] Jirásková E., Kulhánek J., Nevěčná T., Pytela O.: *Collect. Czech. Chem. Commun.*, 64 (1999), 1253-1261.
- [14] Pytela O., Kulhánek J., Jirásková E., Nevěčná T.: *Collect. Czech. Chem. Commun.*, 66 (2001), 1638-1658.
- [15] Pytela O., Štumrová S., Ludwig M., Večeřa.: *Collect. Czech. Chem. Commun.*, 51 (1986), 564-572.
- [16] Pytela O., Trlída B.: *Collect. Czech. Chem. Commun.*, 72 (2007), 1025-1036.

BORON DOPED DIAMOND ELECTRODES FOR DETERMINATION OF BIOLOGICAL MOLECULES

Marian VOJS¹*, Miroslav BEHUL¹, Pavol MICHNIAK¹, Vlastimil REHACEK¹, Marian MARTON¹, Vladimír TVAROZEK¹, Marian VESELY¹

¹ Slovak University of Technology, Faculty of Electrical Engineering and Information Technology, Institute of Electronics and Photonics, Ilkovičova 3, 812 19 Bratislava, SR,

*marian.vojs@stuba.sk

ABSTRACT

Boron doped diamond (BDD) electrodes perform for electrochemical determination of biological material such as dopamine (DA) uric acid (UA) and ascorbic acid (AA). The advances of BDD electrodes are possibility surface termination including hydrogen-termination and oxygen termination. Hydrogen terminated BDD electrodes should be an effective analytical tool, especially for determining low concentrations of DA and AA. In this paper we investigated properties of BDD as a substrate for detection of biological molecules.

INTRODUCTION

Carbon substrates such as glassy carbon, carbon paste [1], carbon fiber, impregnated graphite [2], diamond-like carbon (DLC) [3], boron-doped diamond (BDD), carbon nanotubes [4], pyrolyzed photoresist [5], but also gold, platinum and others seems to be a good choice for measurement. Diamond electrodes are promising electrodes for high stability, chemical inertness, wide potential window and low background current. Combining the superior properties of BDD electrodes with the merits of biosensors, such as specificity, sensitivity, and fast response, amperometric biosensors based on BDD electrodes have attracted the interests of many researchers.

MATERIAL AND METHODS

Boron doped diamond thin film

Polycrystalline BDD films 200-280 nm thick (Fig. 1) were produced in the double bias enhanced HF CVD reactor with sheet resistivity $\sim 100 \Omega/\text{sq}$. As a substrate, highly conductive (0.008-0.024 Ωcm) N (100) type silicon substrate was used with $\sim 200\text{nm}$ wet SiO_2 oxide. Throughout the deposition, gas flows in reaction chamber were controlled to be 1 % CH_4 in H_2 and trimethylboron (TMB) in the range of 0-200 sccm (corresponding to 0-10 000 ppm of B/C), Tab 1. The total pressure in the reactor was 3 000 Pa and temperature was set to around 700 °C.

Tab. 1. Composition of process gas

Sample	CH_4	H_2	TMB	B/C
1	3	290	10	667
2	3	275	25	1 667
3	3	270	30	2 000
4	3	280	40	2 667
5	3	290	50	3 333
6	3	200	100	6 667
7	3	150	150	10 000

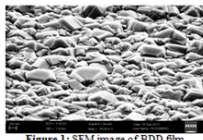


Figure 1: SEM image of BDD film

Deposition process was divided into two steps: the first step was 30 min seeding with nano-powder of diamond (Sigma Aldrich, crystals $< 10 \text{ nm}$) diluted in water in ultrasonic bath, the second step was growth of NCD thin layer for 2 hour. The areas which act as working electrodes were defined to be about $3 \times 3 \text{ mm}$ by isolation paste in $10 \times 20 \text{ mm}$ area.

Electrochemical determination

All stock solutions were prepared from analytical grade chemicals in 18 M Ωcm deionized water. A three-electrode arrangement was used in all experiments. As a reference, Ag/AgCl (0.3 M KCl) electrode and as a counter electrode, a platinum plate $10 \times 10 \text{ mm}^2$ were used. In all experiments we have used McIlvaine buffer composed of Na_2HPO_4 , citric acid and deionized of water with $\text{pH} = 5$. Before each measurement the electrode was cleaned by 30 cycles of CV (from ESTART = -1.5 V to ESTOP = 1.5 V, scan rate was 100 mVs⁻¹) in pure McIlvainovom solution (MCII) without presence DA or AA. Voltametric experiments were performed with an electrochemical potentiostat/galvanostat PGSTAT128N (Metrohm Autolab B.V.) controlled by a PC.

RESULTS AND DISCUSSION

The oxidation peak for DA was found at $460 \pm 2 \text{ mV}$ ($n=10$), the reduction peak at $85 \pm 0.18 \text{ mV}$ ($n=10$). The anodic peak current increased linearity $R^2 = 0.996$ with the square root of the potential sweep rate for DA, published elsewhere. The current density (Fig. 2) and FWHM (Fig. 3) of all types of electrodes with different B/C ratio from 667 to 10 000 ppm clearly show tendency, highly doped BDD with more than 6 000 ppm gives better results.

All characteristic parameters of BDD electrodes were summarized in Tab. 1. Detection limits LOD for 10 000 ppm B/C ratio with highest sensitivity of 1.88 μM and 7.66 $\mu\text{A.M.cm}^{-2}$ DA calculated from calibration curves of reduction peak (Fig. 4) and for AA 0.34 μM and 11.0 $\mu\text{A.M.cm}^{-2}$ (Fig. 5). All electrodes were measured in extremely wide range of DA (1-300 μM) and AA (10-2300 μM). High stability and linear response of hydrogenated BDD electrodes was observed for 6 000 and 10 000 ppm reduction peaks.

Possible explanation of the detection DA on hydrogenated surfaces BDD is that, valence band edge at hydrogen terminated diamond electrode lies at a greater energy than the aqueous H⁺/H₂ couple, this would result in hydrogen terminated diamond always being in accumulation when in an aqueous electrolyte.

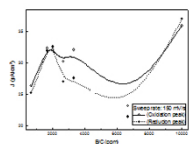


Figure 2: Current density of electrodes from CV measurements with presence of 0.1 mM DA in MCH, for 150 mV sweep rate as a function of B/C ratio.

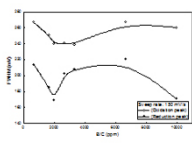


Figure 3: FWHM of electrodes from CV measurements with presence of 0.1 mM DA in MCH, for 150 mV sweep rate as a function of B/C ratio.

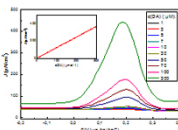


Figure 4: Current density of reduction peak for 10 000 ppm B/C ratio BDD and calibration curve from SWV measurements with presence of 1-300 μM DA.

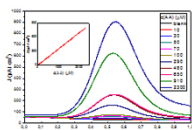


Figure 5: Current density of reduction peak for 10 000 ppm B/C ratio BDD and calibration curve from SWV measurements with presence of 10-2300 μM AA.

Thus any applied potential would be dropped across the Helmholtz layer and reversible electrochemical behavior observed for simple redox couple. Indeed an accumulation of holes at hydrogen terminated diamond surfaces exposed to the atmosphere has been used to explain surface conductivity of the material [6].

CONCLUSION

In conclusion, several functional BDD electrodes have been used for determining various bio-analytes over the past decade or so. We have compared different measurements in presence of biological molecules DA and AA with various BDD electrodes. Excellent properties of BDD substrates, these BDD based amperometric biosensors exhibited good performances in terms of high sensitivity, selectivity, reproducibility and long-term stability. BDD electrodes are interesting candidates for the construction of next generation of biosensors or the direct electrochemical detection of biomolecules.

ACKNOWLEDGEMENT

The authors would like to thank Mr. Král for technical assistance. This work was financially supported by grant of Slovak Research and Development Agency No. APVV-0548-07, LPP-0094-09 and Ministry of Education of Slovak Republic and the Slovak Academy of Sciences No. 1/1102/11 and 1/1103/11 and DAAD 507 552 00.

REFERENCES

- [1] G. Kefala, et al., *Talanta*, 61, (2003), 603-610
- [2] I. Švancara, K. Vytřas, *Chemické Listy*, 100, (2006), 90-113
- [3] V. Řeháček, I. Hotový, M. Vojs, *Sensors and Actuators B. Chemical*, 127, (2007), 193-197
- [4] T. Ižák, et al., *Vacuum*, 82, (2008), 134-137
- [5] V. Řeháček, et al., *Journal of Electrical engineering*, 62, 1, (2011), 52-56
- [6] G. Pastor-Moreno, D.J. Riley, *Electrochimica Acta* 47, (2002), 2589-2595

THE ANTICANCER DRUG ELLIPTICINE INDUCES CYTOCHROME b_5 AND CYTOCHROMES P450 1A1, 1A2 AND 3A IN RAT LIVER, KIDNEY AND LUNG

Iveta VRANOVA¹, Michaela MOSEROVA¹, Petr HODEK¹, Rene KIZEK^{2,3}, Eva FREI⁴, Marie STIBOROVA^{1*}

¹ Department of Biochemistry, Faculty of Science, Charles University, Prague, Albertov 2030, 128 40 Prague 2, Czech Republic

² Department of Chemistry and Biochemistry, Faculty of Agronomy, Mendel University in Brno, Zemedelska 1, 613 00 Brno, Czech Republic

³ Central European Institute of Technology, Brno University of Technology, Technicka 3058/10, 616 00 Brno, Czech Republic

⁴ Division of Preventive Oncology, National Center for Tumor Diseases, German Cancer Research Center (DKFZ), In Neuenheimer Feld 280, 69 120 Heidelberg, Germany,

*stiborov@natur.cuni.cz

ABSTRACT

The antineoplastic alkaloid ellipticine is a prodrug, whose pharmacological efficiency is dependent on its cytochrome P450 (CYP)- and/or peroxidase-mediated activation in target tissues. This compound was found to induce expression of cytochrome b_5 , CYP1A1, 1A2 and 3A proteins determined electrochemically (Western blotting) and their enzymatic activities in livers, lungs and kidneys of rats treated (i.p.) with ellipticine. In addition, induction of these proteins resulted in an increase in ellipticine oxidation to 7-hydroxy-, 9-hydroxy-, 13-hydroxy- and 12-hydroxyellipticine, the metabolites that are both detoxication products (7-hydroxy-, 9-hydroxyellipticine) and metabolites responsible for generation ellipticine-derived DNA adducts (12-hydroxy- and 13-hydroxyellipticine). The results demonstrate that by inducing CYP1A1/2, 3A and cytochrome b_5 , ellipticine increases its own metabolism leading both to an activation of this drug to reactive species forming DNA adducts and to detoxication metabolites, thereby modulating its own pharmacological and/or genotoxic potential.

INTRODUCTION

Ellipticine (5,11-dimethyl-6H-pyrido[4,3-*b*]carbazole) and its derivatives are efficient anticancer compounds that function through multiple mechanisms participating in cell cycle arrest and initiation of apoptosis (for a summary see [1-6]). Ellipticine was found (i) to arrest cell cycle progression due to modulation of levels of cyclinB1 and Cdc2, and phosphorylation of Cdc2 in human mammary adenocarcinoma MCF-7 cells, (ii) to initiate apoptosis due to formation of toxic free radicals, the stimulation of the Fas/Fas ligand system and the modulation of proteins of a Bcl-2 family in several tumor cell lines, (iii) to induce the mitochondrion-dependent apoptotic processes (for a summary see [3,4,7]). These effects and ellipticine-induced cell cycle arrest resulted from multiple DNA damage. The predominant mechanisms of ellipticine biological effects were supposed to be (i) intercalation into DNA [5,6] and (ii) its action as an inhibitor of topoisomerase II [3-6]. Nevertheless, it was also shown that this antitumor agent forms covalent DNA adducts after its enzymatic activation with cytochromes P450 (CYP) and peroxidases [1-

4,7-11], which suggests another DNA-damaging mechanism of ellipticine effects.

Of the CYP enzymes investigated, human CYP3A4 and rat CYP3A1 are the most active enzymes oxidizing ellipticine to 13-hydroxy- and 12-hydroxyellipticine, the reactive metabolites that dissociate to ellipticine-13-ylum and ellipticine-12-ylum which bind to DNA [3,7,8,10], while the CYP1A isoforms preferentially form the other ellipticine metabolites, 9-hydroxy- and 7-hydroxyellipticine, which are the detoxication products. Recently we have found that cytochrome b_5 alters the ratio of ellipticine metabolites formed by CYP1A1, 1A2 and 3A4. While the amounts of the detoxication metabolites (7-hydroxy- and 9-hydroxyellipticine) were either decreased or not changed with added cytochrome b_5 , 12-hydroxy-, 13-hydroxyellipticine and ellipticine N^2 -oxide increased considerably. The change in amounts of metabolites resulted in an increased formation of covalent ellipticine-DNA adducts, one of the DNA-damaging mechanisms of ellipticine antitumor action [10,11].

Because of the important role of cytochrome b_5 and CYP1A and 3A enzymes in ellipticine metabolism, expression levels of their proteins

are crucial for antitumor, cytostatic and/or genotoxic activities of this drug in individual tissues.

Recently we found that ellipticine as a ligand of aryl hydrocarbon receptor (AHR) [12] is a strong inducer of CYP1A1 and 1A2 in rats *in vivo* [13] and in several cancer cell lines *in vitro* [14,15]. In addition, levels of cytochrome b_5 are increased by ellipticine in liver of rats treated with this drug [11]. Moreover, ellipticine also induces expression of *CYP3A4* mRNA and P450 3A4 protein in several cancer cell lines [14,15]. However, in contrast to induction of CYP1A by ellipticine *in vivo* and mechanisms of this induction have already been investigated, the effect of ellipticine on expression of CYP3A and cytochrome b_5 *in vivo* remains to be investigated.

Therefore, the Western-blotting-electrochemical method was used in this work to evaluate the effect of ellipticine on expression of not only of CYP1A1/2, but also of CYP3A and cytochrome b_5 proteins in rats *in vivo*. Real-time (RT) polymerase chain reaction (PCR) was employed to estimated expression levels of mRNA for these proteins.

MATERIAL AND METHODS

Animal Experiments

The study was conducted in accordance with the Regulations for the Care and Use of Laboratory Animals (311/1997, Ministry of Agriculture, Czech Republic), which is in compliance with Declaration of Helsinki. Male and female Wistar rats (~100 g) were treated with a single dose of 4 or 40 mg/kg body weight ($n=3$) of ellipticine by intraperitoneal injection as described previously [13]. Microsomes were isolated from the livers, kidneys and lungs of rats as described [1].

Electrochemical determination of CYP protein levels in microsomes of rat liver, kidney and lung

Immunoquantitation of rat liver, kidney and lung microsomal cytochrome b_5 and CYPs (CYP1A1, 1A2, and 3A) was done by sodium dodecyl sulfate (SDS)-polyacrylamide gel electrophoresis. Samples containing 75 μ g microsomal proteins were subjected to electrophoresis on SDS/10% polyacrylamide gels [16,17]. After migration, proteins were transferred onto a nitrocellulose membrane and incubated with 5% non-fat milk to block non-specific binding. The membranes were then exposed to specific rabbit polyclonal anti-cytochrome b_5 (1:750, AbCam, MA, USA), anti-CYP1A1 (1:1000, Millipore, MA, USA) and anti-CYP3A4 (1:5000, AbD Serotec, Oxford, UK) antibodies overnight at 4 °C. The antigen-antibody complex was visualized with an alkaline phosphatase-conjugated rabbit anti-

-chicken IgG antibody and 5-bromo-4-chloro-3-indolylphosphate/nitrobluetetrazolium as chromogenic substrate [16,17]. Antibody against glyceraldehyde phosphate dehydrogenase (GAPDH) (1:750, Millipore, MA, USA) was used as loading control.

CYP1A and 3A enzyme activity assays

The rat liver, kidney and lung microsomal samples were characterized for CYP1A activity using 7-ethoxyresorufin *O*-deethylation (EROD), CYP1A2 activity using 7-methoxyresorufin *O*-demethylation (MROD) [18], for the oxidation of Sudan I (a marker substrate for CYP1A1) [16,17] and for 6- β -hydroxylation of progesterone (a marker for CYP3A) [19].

CYP1A and 3A mRNA contents in rat livers, kidneys and lungs

The mRNA contents of CYP1A and 3A in rat liver, kidney and lung were carried out as described previously [13].

Oxidation of ellipticine

Oxidation of ellipticine by liver, kidney and lung microsomes of rats either untreated (control) or treated with ellipticine was determined as described previously [7,10,11].

RESULTS AND DISCUSSION

Using electrochemical determination (Western blot analysis with antibodies raised against CYP1A1, 3A4 and cytochrome b_5), the effects of exposure of rats to ellipticine on protein levels of these proteins were analyzed. Rats treated i.p. with 4 and 40 mg/kg body weight were used as a model. An induction potential of ellipticine to increase expression of mRNAs and proteins of CYP1A and 1A2 in hepatic, renal and pulmonaru microsomes found previously [13] was fully confirmed in the present work. A significant dose-dependent increase in CYP1A1 and 1A2 protein expression due to ellipticine correlated with expression of their mRNAs and their enzymatic activities (EROD for CYP1A1/2, MROD for CYP1A2 and oxidation of Sudan I for CYP1A).

Besides CYP1A1 and 1A2, expression of CYP3A and cytochrome b_5 proteins was also increased with treating rats with ellipticine. A dose-dependent increase in levels of CYP3A protein and a marker activity of the CYP3A enzymes, progesterone 6- β -hydroxylation were produced in the studied organs of rats treated with ellipticine. Likewise, the increase in levels of cytochrome b_5 was dose-dependent. Further studies that would explain the mechanisms of the CYP3A and cytochrome b_5 induction by ellipticine, we plan to perform, will be directed on relevance of individual receptors such as

AHR, CAR and PXR on ellipticine potential to induce CYP3A and cytochrome b₅.

We compared oxidation of ellipticine incubated with microsomes from the livers, kidneys and lungs of treated and control rats. Besides an increase in oxidation of ellipticine to 9-hydroxyellipticine and 7-hydroxyellipticine, up to a 2-fold increase in formation of 13-hydroxy- and 12-hydroxyellipticine was found. These results corresponds to induction of both CYP1A1/2 and CYP3A and cytochrome b₅ by treatment of rats with ellipticine.

CONCLUSION

Utilizing the Western-blotting-electrochemical method, expression of CYP1A, 3A and cytochrome b₅ proteins was found to be induced by treating rats with ellipticine. Such an increase resulted in an increase in their marker activities as well as in ellipticine own oxidation.

ACKNOWLEDGEMENT

The work has been supported by Grant Agency of the Czech Republic (grant P301/10/0356) and Charles University in Prague (grant UNCE #42).

REFERENCES

- [1] Stiborová M., Bieler C.A., Wiessler M., et al.: *Biochemical Pharmacology*, 62 (2001), 1675-1684.
- [2] Stiborová M., Rupertová M., Schmeiser H.H., et al.: *Biomedical Papers*, 150 (2006), 13-23.
- [3] Stiborová M., Rupertová M., Frei E.: *Biochimica et Biophysica Acta*, 1814 (2011), 175-185.
- [4] Kízek R., Adam V., Hrabeta J., et al.: *Pharmacology & Therapeutics*, 133 (2012), 26-39.
- [5] Auclair C.: *Archives of Biochemistry and Biophysics*, 259 (1987), 1-14.
- [6] Garbett N.C., Graves D.E.: *Current Medicinal Chemistry. Anti-Cancer Agents*, 4 (2004), 149-172.
- [7] Stiborová M., Sejbál J. Bořek-Dohalská L., et al.: *Cancer Research*, 64 (2004), 8374-8380.
- [8] Stiborová M., Poljaková J., Ryšlavá H., et al.: *International Journal of Cancer*, 120 (2007), 243-251.
- [9] Stiborová M., Rupertová M., Aimová D., et al.: *Toxicology*, 236 (2007), 50-60.
- [10] Stiborová M., Indra R., Moserová M., et al.: *Chemical Research in Toxicology*, (2012), DOI: 10.1021/tx3000335.
- [11] Kotrbová V., Mrázová B., Moserová M., et al.: *Biochemical Pharmacology*, 82 (2011), 669-680.
- [11] Gasiewicz T.A., Kende R.S., Rucci G., et al.: *Biochemical Pharmacology*, 52 (1996), 787-830.
- [12] Aimová D., Svobodová L., Kotrbová V., et al.: *Drug Metabolism and Disposition*. 35 (2007), 1926-1934.
- [13] Martínková E., Döntenwill M., Frei E., et al.: *Neuro Endocrinology Letters*, 30 (Suppl. 1) (2009), 60-66.
- [14] Poljaková J., Hřebáčková J., Dvoraková M., et al.: *Neuro Endocrinology Letters*, 32 (Suppl 1) (2011), 101-116.
- [15] Stiborová M., Martínek V., Rýdlová H., et al.: *Cancer Research*, 62 (2002), 5678-5684.
- [16] Stiborová M., Martínek V., Rýdlová H., et al.: *Cancer Letters*, 220 (2005), 145-154.
- [17] Guengerich F.P., Shimada T.: *Chemical Research in Toxicology*, 4 (1991), 391-407.
- [18] Bořek-Dohalská L., Hodek P., Šulc M., et al.: *Chemico-Biological Interactions*, 138 (2001), 85-106.

REJSTŘÍK

A

Vojtech ADAM.....68, 75, 77, 134, 140, 142,
146, 148, 150, 153, 156, 160, 163, 166, 171,
174, 177, 180, 182, 184, 186, 189, 192, 195,
223, 229, 234, 237, 239, 242, 267, 269, 275,
285, 288, 290, 305, 307, 329, 331, 334
Anton AMBROZY.....119
Tomas ANDRYSEK.....50
Volker M. ARLT.....124

B

Petr BABULA.....68, 77, 174, 177, 192, 223, 307
Marie BALABANOVA.....142
Zdenka BALCAROVA.....64
Jaroslav BALOGH.....14
Jan BALVAN.....307
Zuzana BARBIERIKOVA.....17
Martin BARTOSIK.....351
Marek BEDLEK.....19
Ivana BEDNAROVA.....180, 195
Miroslav BEHUL.....355
Miroslava BEKLOVA.....163, 180, 195, 223
Tomas BERTOK.....21
Andrea BEZDEKOVA.....14, 174, 192, 223
Miroslava BITTOVA.....85
Iva BLAZKOVA.....129
Miroslava BOBENICOVA.....23
Branislav RUTTKAY-NEDECKY.....225
Vlasta BREZOVA.....17
Gabriela BRONCOVA.....32
Jiri BURSIK.....341
Petra BUSINOVA.....25, 73, 251, 325
Eduard BUZETSKI.....256

C

Andrea CAKLOSOVA.....23
Gabriela M. CASTILLO.....28, 216
Olga CELECHOVSKA.....262
Jan CERMAK.....61, 254
Vera CERNA.....100
Natalia CERNEI.....160, 182, 184
Hana CERNOCKA.....351
Andrea CONGRADYOVA.....121

Jan CVENGROS.....256
Zuzana CVENGRISOVA.....256

D

David HYNEK.....134
Jakub DEMKO.....211
Juraj DIAN.....32, 102
Hana DOCEKALOVA.....93
Bohumil DOLENSKY.....293
Helene DORIZON.....30
Dana DOSPIVOVA.....150, 186, 189, 192, 272
Simona DOSTALOVA.....285
Ladislav DRAJNA.....59
Jana DRBOHLAVOVA.....19, 39,
73, 83, 156, 189, 251, 314
Lucie DRTINOVA.....242
Dana DVORANOVA.....23
Jana JAKLOVA DYTTRTOVA.....37
Matej DZURO.....39

E

Tomas ECKSCHLAGER.....150,
182, 184, 244, 269, 290, 296, 331

F

Zdenek FARKA.....43
Antonin FEJFAR.....254
Nuria FERROL.....148
Pavel FIALA.....115
Jaroslav FILIP.....46, 311
Petra FISEROVA.....51
Lukas FOJT.....220
Miroslav FOJTA.....52
Frantisek FORET.....309
Eva FFREI.....357
Eva FREI.....124, 244, 296

G

Imrich GABLECH.....54, 197
Lenka GAJDOVA.....57
Lukas GALA.....59
Pavel GALAR.....61
Peter GEMEINER.....21, 46, 311
Eliska GLOVINOVA.....138
Jakub GRUNT.....87
Jaromir GUMULEC.....68,
77, 184, 269, 305, 307

Libor GURECKY.....64

H

Ken HAENEN.....131

Stanislav HASON.....220

Martin HAVLIK.....293

Josef HEDBAVNÝ.....93

Dominik HEGER.....113, 115

Colin J. HENDERSON.....124

Michael HEYROVSKÝ.....66

Tibor HIANIK.....28, 30

Lenka HLAVATA.....119

Marian HLAVNA.....68, 77, 305, 307

Martin HLOZEK.....104

Petr HODEK.....71, 100, 134, 357

Monika HOLUBOVA.....307

Jiri HOMOLA.....70

Pavel HORKÝ.....225

Jan HRABETA.....41

Ales HRDLICKA.....104

Radim HRDÝ.....19, 39, 73, 209, 251, 303, 314

Ludek HRIVNA.....323

Jaromir HUBALEK.....19, 25, 39, 54, 73, 75, 83,

134, 146, 150, 153, 156, 160, 166, 177, 182, 184,

186, 189, 192, 197, 209, 229, 234, 237, 239, 242,

251, 275, 283, 285, 288, 303, 314, 325, 329, 334

Pavel HUBIK.....254

Kristyna HUDCOVA.....77

Jiri HUDECEK.....100

Lucia HUSARIKOVA.....80, 347

David HYNEK.....146, 150, 153, 156, 160, 163,

166, 177, 180, 186, 189, 195, 234, 242, 272, 275

CH

Jana CHOMOUCKA.....73, 83,

202, 214, 251, 283, 303

Jaromira CHYLKOVA.....337

I

Michal ILCIN.....96

Jan IMRICH.....59

Tibor IZAK.....293

J

Michal JAKL.....37

Jana JAKLOVA DYTRTOVA.....327, 337, 339

Petra JANCIKOVA.....225

Libor JANU.....140, 189, 237,

239, 275, 288, 290

Ondrej JASEK.....251

Tomas JECMEN.....100

František JELEN.....207

Katerina JELINKOVA.....85

Eva JILKOVA.....134

Klaudia JOMOVA.....121

Matej JURAK.....349

Tunde JURIKOVA.....334

K

Magdalena KADLECICOVA.....317

Jozef KAISER.....104, 248

Libor KALHOTKA.....129

Michal KALINA.....87

Tomas KANA.....90

Renata KENSOVA.....57, 146

Rene KIZEK.....14, 68, 75, 77, 134, 140,

142, 146, 148, 156, 160, 163, 166, 169,

171, 174, 177, 180, 182, 184, 186, 189,

223, 229, 234, 237, 239, 242, 244, 262,

267, 269, 272, 275, 280, 283, 285, 288,

290, 296, 305, 307, 329, 331, 334, 357

Andrea KLECKEROVA.....93

Erik KLEIN.....96, 258, 260

Andrea KLEINOVA.....256

Martina KLUCAKOVA.....87

Monika KOBEROVA.....100

Jan KOCKA.....254

Marketa KOMINKOVA.....148, 182, 184, 331

Veronika KONECNA.....104, 248

Martin KONECNY.....32, 102

Pavel KOPEL.....150, 153, 156, 189

Hafsa KORRI-YOUSSOUFI.....30

Tibor HIANIK.....30

Mario KOTLAR.....344

Jan KOURIL.....248

Zuzana KOVACOVA.....107

David KOVAR.....43, 278

Alzbeta KRACMAROVA.....242

Vit KRAJICEK.....278

Marie KRATKA.....110

Jan KRAUSKO.....113

Lubica KRAUSKOVA.....115
Ludmila KREJCOVA.....134,
153, 156, 160, 177
Monika KREMPLOVA.....160, 163, 166, 223
Jitka KRIZKOVA.....71
Sona KRIZKOVA.....169,
195, 267, 269, 272, 288
Alexander KROMKA.....61, 110, 131, 254, 293
Boris KRSKA.....334
Jarmila KRUSEOVA.....269
Kamila KRUZIKOVA.....57, 262
Olga KRYSTOFOVA.....180, 195, 223
Vladimira KUBICOVA.....116
Hana KYNCOVA.....73

L
Jan LABUDA.....119
David LANG.....87
Michael LAWSON.....121
Martin LEDINSKY.....254
Jozef LENGYEL.....96
Katerina LEVOVA.....124
Jozef LIETAVA.....17
Premysl LUBAL.....264
Jiri LUDVIK.....300
Vladimir LUKES.....96, 258, 260

M
Iva MACOVA.....71
Peter MACHATA.....200
Radomir MALINA.....104, 248
Petr MALY.....61
Jiri J. MARES.....254
Petr MARES.....142
Marie STIBOROVA.....357
Marian MARIK.....202, 303
Ladislav MARTISKA.....80
Marian MARTON.....344, 355
Michal MASARIK.....68, 77, 169,
182, 184, 269, 305, 307
Natalie MATIJESEKUKOVA.....288
Milan MAZUR.....80
Miguel-Angel MERLOS.....148
Radovan METELKA.....206, 300
Ana MIHAJLOVIC.....83
Pavol MICHNIAK.....344, 349, 355
Hana MIKULASKOVA.....180, 195
Tomas MIKYSEK.....300
Anna MIODEK.....30
Danica MISLOVICOVA.....21
Helena MODRA.....262
Jan MONCOL.....121
Michaela MOSEROVA.....124, 357

N
Rudolf NAVRATIL.....207
Tomas NAVRATIL.....327, 337, 339
Daniel H. NEBERT.....124
Tomas NECAS.....321
Lukas NEJDL.....171, 275
Barbora NEMCOVA.....180, 195
Neda NEYKOVA.....110
Renata NORKOVA.....37
Katerina NOVAKOVA.....337
Marie NOVAKOVA.....68
Zuzana NOVAKOVA.....209
Jan NOVOTNY.....104, 248
Karel NOVOTNY.....104, 248

O
Andrej ORINAK.....211
Renata ORINAKOVA.....209, 211
Veronika OSTATNA.....319, 351

P
Emil PALECEK.....319, 351
Martina PARISOVA.....327
Pavel PORIZKA.....104
Jan PEKAREK.....202, 214, 251, 303
Michal PETRILAK.....104
David H. PHILLIPS.....124
Lubomir PIKNA.....107
Iveta PILAROVA.....64, 216
Zdenek PILAT.....248
Hana PIVONKOVA.....34
Miroslav POHANKA.....242
Jitka POLJAKOVA.....41, 244, 296
Pavel PORIZKA.....248
Jan POSPICHAL.....138
Jan PRASEK.....25, 54, 73, 197, 214, 251

Jan PRIBYL.....278
David PROCHAZKA.....104, 248
Lubomir PROKES.....104
Ivo PROVAZNIK.....14, 116, 174, 280
Oldrich PYTELA.....353
Zdenek PYTLICEK.....54, 197

R

Peter RAPTA.....200
Martina RAUDENSKA.....77, 305, 307
Robert REDHAMMER.....349
Robert REDHAMMER.....344
Vlastimil REHACEK.....355
Zuzana REPICKA.....80, 347
Bohuslav REZEK.....61, 110, 131, 254, 293
Jan RIMARCIK.....96, 256, 258, 260
Vendula ROBLOVA.....85
Otakar ROP.....334
Michael ROSSBERG.....349
Lenka ROTTMANNOVA.....96, 258
Zdenek ROUBAL.....115
Branislav RUTTKAY-NEDEC-
KY.....142, 171, 174, 223, 334
Marketa RYVOLOVA.....83, 140, 169,
229, 234, 237, 239, 272, 285, 288, 290

S

Ota SAMEK.....248
Imre SARKOZY.....256
Jiri SEDLACEK.....325, 329
Petr SEDLACEK.....87
Jana SEFCOVICOVA.....311
Ludmila SEKERAKOVA.....17
Ivana SESTAKOVA.....327, 339
Marie SEVCIKOVA.....262
Romana SEVCIKOVA.....264
Peter SCHAAF.....349
Heinz H. SCHMEISER.....124
Michal SIDLO.....341
Sylvie SKALICKOVA.....267,
269, 272, 275, 331, 334
Lenka SKANTAROVA.....211
Petr SKLADAL.....43, 278
Matej SKLENAR.....192
Peter SKORNA.....260

Helena SKUTKOVA.....280
Jan SLAVIK.....283
Kristyna SMERKOVA.....285
Mojmir SOB.....90
Pavlina SOBROVA.....229, 234, 237, 239
Jiri SOCHOR.....14, 68, 134, 142, 171,
174, 177, 180, 195, 223, 225, 334
Dmitry SOLOVEI.....325, 329
Sona KRIZKOVA.....134
Jiri SOPOUSEK.....341
Maja STANISAVLJEVIC.....290
Silvia STEFANOVA.....107
Stepan STEHLIK.....293
Olga STEPANKOVA.....229
Marie STIBOROVA.....41, 71, 100, 124,
134, 150, 184, 244, 290, 296, 331
Matej STOCES.....300
Tibor STRACINA.....68
Lenka STRAKOVA.....180
Miroslav SULC.....100
Kvetoslava SUSTOVA.....129
Eva SVABENSKA.....278
Ivan SVANCARA.....204, 300
Vojtech SVATOS.....39, 202, 283, 303
Zdenka SVOBODOVA.....57, 262
Marketa SZTALMACHOVA.....68, 77, 305, 307

T

Veronika TANHÄUSEROVA.....77, 305, 307
Anna TARANTOVA.....309
Jan TKAC.....21, 46, 311
Mojmir TREFULKA.....351
Libuse TRNKOVA.....28, 50, 64, 85, 134, 146,
150, 153, 156, 160, 177, 182, 184, 186, 189, 192,
207, 216, 229, 234, 237, 239, 275, 285, 331
Vladimir TVAROZEK.....355

U

Jiri UHLIK.....41
Egor UKRAINTSEV.....110, 131, 254

V

Adam VAGANEK.....96, 258
Dusan VALIGURA.....80, 347
Marian VALKO.....59, 80, 121
Jirina VALKOVICOVA.....314

Jan VANCO.....177
Lubomir VANCO.....317
Jakub VANEK.....264
Veronika VARGOVA.....319, 351
Marian VESELY.....344, 349, 355
Vladimír VETTERL.....220
Andrej VINCZE.....349
Martin VITEK.....280
Pavlina VLASAKOVA.....204
Marcela VLKOVA.....267
Marian VOJS.....344, 349, 355
Nikola VOLAKOVA.....204
Iveta VRANOVA.....357
Radimir VRBA.....214
Zdenka VYCHODILOVA.....34
Jiri VYSLOUZIL.....321, 323
Lenka VYSLOUZILOVA.....229
Karel VYTRAS.....300

W

C. Roland WOLF.....124

Z

Jaromir ZAK.....329
Josef ZEHNALÉK.....146
Ladislav ZEMAN.....142
Jarmila ZIDKOVA.....275
Ondrej ZITKA.....68, 140, 148, 163, 166, 171,
182, 184, 223, 267, 269, 272, 275, 331, 334
Marko ZIVANOVIC.....319
Svatava ZUPKOVA.....341

Sborník příspěvků

XII. Pracovní setkání fyzikálních chemiků a elektrochemiků

Grafická úprava: Michal Horák

Technická úprava: Michal Horák, Olga Kryštofová, Jiří Sochor

Vydala: Mendelova univerzita v Brně

Tisk: LITERA BRNO, Tábor 43a, BRNO

První vydání, 2012

Náklad: 250 ks

ISBN 978-80-7375-618-5



Metrohm Česká republika s.r.o.

Na Harfě 935/5c

190 00 Praha 9

Telefon: 00420 246 063 433

Fax: 00420 246 063 468

Web: www.metrohm.cz

Titrace, iontová chromatografie, elektrochemie...

Kompletní řada iontových analýz pod jednou střechou

Naše firma se specializuje v oblastech přístrojového vybavení pro:

- iontové analýzy zastoupené produkty firmy Metrohm AG,
- elektrochemie a elektroanalýtyky zastoupené firmou Metrohm Autolab
- aplikované iontové analýzy v průmyslu zastoupené firmou Applikon.



Naše přístroje jsou široce využívány v oblastech chemického průmyslu, petrochemie, farmacie, potravinářství, analýzy vody a vzduchu a v neposlední řadě ve vědě a výzkumu.

Online přístup ke stovkám aplikací

Jen to nejlepší řešení je dost dobré pro Vaše aplikace!

Kvalifikované poradenství, důvěryhodný servis a nejvyšší kvalita nám umožnili získat vedoucí postavení na trhu. Odborníci po celém světě se snaží zajistit, aby tomu tak bylo i nadále.

Aplikace jsou seřazeny do následujících kategorií:

*Průmysl: Automobilový, biochemický, biopaliva...

*Metody: titrace, iontová chromatografie a další

*Standardy jako jsou ASTM, ISO, DIN,...

*Validační pokyny pro Metrohm zařízení

*Aplikační literatura: Metrohm aplikační bulletiny, poznámky, články, monografie a technické postery



Metrohm Quality Service®

Spolehlivé výsledky měření po celou dobu životnosti Vašeho přístroje

Bez ohledu na to zda provádíte analýzu vody s přístrojem 850 Professional IC, prvkovou analýzu s VA, analýzu lázní se systémy ProcessLab nebo určujete obsah vody v léčivech s použitím Karl Fischerovy titrace - Metrohm Quality Service® zajistí, že se můžete na 100% spolehnout na Vaše výsledky, a to po celou dobu životnosti Vašeho přístroje.



Automatický spektrofotometr BS-200

mindray

- 8 fixních vlnových délek: 340, 405, 450, 510, 546, 578, 630, 670 nm
- výkon 200 fotometrických testů za hodinu
- automatické ředění abnormálních vzorků
- metody měření: *endpoint*, *kinetika*, *fixní čas (jedno i dvoureagenční)*
- automatické omývání dávkovacích jehel
- 40 chlazených pozic na reagentie
- vzorkový kruh se 40-ti pozicemi



Reagencie pro průtokovou cytometrii

- jedno-, dvoj- a trojbarevné reagentie (MultiMix™)
- Lyzační roztoky na erythrocyty UtiLyse, EasyLyse
- IntraStain pro nitrobuněčný výzkum
- QIFIKIT pro nepřímou kvantifikaci
- Telomere PNA Kit
- ApopTest pro kvantifikaci apoptotických buněk

 **Dako**

Produkty STARLAB





- vynikající *TipOne* špičky pro pipety - *univerzálně použitelné*
- robotické špičky pro automatické pipetovací stanice
- třepačky a další drobné laboratorní přístroje
- systémy uskladnění vzorků: *stojánky*, *krabičky*, *boxy*
- jednorázové laboratorní rukavice MICROFLEX





• Eppendorf centrifugy



• Elektronická pipeta Eppendorf Xplorer®

• Eppendorf zkumavka Safe-Lock



• Hlubokomrazící boxy New Brunswick

Eppendorf a New Brunswick produkty

S námi do Vašich laboratoří vstoupí: spolehlivost, preciznost, ergonomie a ekologický přístup

- Manuální pipety
- Elektronické pipety
- Dávkováče
- Byrety
- Automatické pipetovací stanice
- Pipetovací špičky, LoRetention
- Zkumavky Safe-Lock, LoBind®
- Combitips
- Kalibrační software

- Hlubokomrazící boxy
- Centrifugy
- Vakuové koncentrátoři
- Thermomixery
- PCR přístroje a spotřební materiál
- Fotometry
- Eppendorf zkumavky a destičky
- Kyvety
- epServices

- CO₂ inkubátory
- Třepačky
- Mikromanipulátory
- Mikroinjektory
- Mikrokapiláry
- Elektroporátory
- Elektroporační kyvety
- Komůrky pro buněčnou fúzi
- Fermentory / bioreaktory

eppendorf

Eppendorf Czech & Slovakia s.r.o. · Kolovratská 1476 · 251 01 Říčany u Prahy
Tel / Fax: +420 323 605 454 · E-mail: eppendorf@eppendorf.cz · Internet: www.eppendorf.cz

yourfavoritegene

PROTILÁTKY NA VYZKOUŠENÍ ZDARMA!

Jak to funguje? Objednáte si nejmenší dostupné balení protilátky z nabídky Sigma-Aldrich obvyklým způsobem a vyzkoušíte si protilátku ve Vaší aplikaci. Pokud protilátka nebude ve Vaší aplikaci fungovat, napište o tom krátkou e-mailovou zprávu na adresu CzeTechSV@sial.com a obdržíte kredit ve 100% hodnotě zakoupené protilátky. Kredit můžete použít k úhradě nákupu jakéhokoliv zboží z nabídky Sigma-Aldrich.

Při nákupu 2 a více protilátek dostanete navíc slevu 20%. Stačí jen poslat poptávku na adresu CzeTechSV@sial.com nebo udělat poptávku po internetu a do poznámky dát text "Sleva 20% - 2 protilátky".

Je z čeho vybírat, v nabídce máme nyní více než

55 000 protilátek!



K vyhledání protilátek použijte software **Your Favorite Gene**, který je umístěn zde www.sigmaaldrich.com/vfg

Stačí pak zadat symbol genu, který studujete (např. EGFR), a zobrazí se Vám **všechny produkty** se vztahem k tomuto genu včetně protilátek. K dispozici jsou kromě protilátek také např. proteiny, shRNA klony, siRNA, esiRNA, konstrukty pro knockout všech lidských genů na bázi ZFN technologie, databáze malých bioaktivních molekul ...

To vše a navíc zobrazení proteinů v signální kaskádě, zobrazení interakcí s ostatními proteiny, či reference týkající se např. expresního profilu, získáte jedním kliknutím.

Sigma-Aldrich spol. s r.o. Česká republika
Slovensko

Tel.: +420 246 003 200
Tel.: +421 02/555 71 562

Fax: +420 246 003 291
Fax: +421 02/555 71 564

SIGMA-ALDRICH®

CENTRIFUGY, ULTRACENTRIFUGY

- multifunkční centrifugy
- vysokootáčkové centrifugy
- velkokapacitní centrifugy
- Ultracentrifugy
- mikrocentrifugy a malé centrifugy
- zkumavky pro centrifugaci



MIKRODEŠTIČKOVÁ INSTRUMENTACE

- spektrofotometry, fotometry
- fluorometry, luminometry
- dávkovače, promývačky
- automatické pipetovací satnice
- magnetické purifikátory KingFisher®



GEL-IMAGING a ANALÝZA

- gelová dokumentace a analýza
- chemiluminiscence, fluorescence
- software pro 1D i 2D analýzu
- transiluminátory
- elektroforézy, zdroje pro elfo



POČÍTAČKY KOLONIÍ

- automatické počítačky kolonií
- poloautomatické počítačky kolonií
- analyzátoru inhibičních zón



MYČKY

- laboratorní myčky
- velkokapacitní myčky
- myčky pro chovné boxy



KONCENTRÁTORY VZORKŮ

- vakuové centrifugační koncentrátory
- stolní lyofilizátory
- velkoobjemové lyofilizátory
- vakuové sušárny



PŘÍPRAVA ČISTÉ VODY

- reverzní osmóza, deionizační systémy
- kompaktní laboratorní systémy
- poloprovodní systémy



AUTOKLÁVY

- stolní laboratorní autoklávy
- velkoobjemové laboratorní autoklávy



BUNĚČNÁ MÉDIA a SÉRA

- média - klasická, s různým obsahem séra
- bioprocessing kontajnery

BIOHAZARDY, IZOLÁTORY LAMINÁRNÍ BOXY

- biohazard boxy
- laminární boxy
- biohazardy tř.III a izolátory
- boxy pro laboratorní zvířata
- bezodtahové digestoře
- dekontaminační systémy



INKUBÁTORY, TERMOSTATY

- CO₂, CO₂/O₂ inkubátory
- termostaty do 80°C, 300°C
- třepací termostaty
- chlazené termostaty
- anaerobní boxy
- Mikroaerofilní boxy
- horkovzdušné sterilizátory
- klimatické a růstové boxy
- systémy pro monitoring teploty



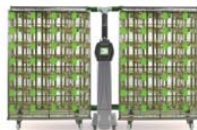
MRAZICÍ A CHLADICÍ BOXY, KRYO BOXY

- mrazič boxy do -86°C a -150°C
- řízené zamrazování LN₂-180°C
- skladovací boxy LN₂-180°C
- mrazič boxy -5°C až -40°C
- chladicí boxy 0°C až +15°C
- transportní boxy
- výrobky ledu, šokové zmrazovače



CHOV LABORATORNÍCH ZVÍŘÁT

- IVC individuálně ventilované boxy
- chovné nádoby, příslušenství
- ochranné a přestýlaci boxy
- komplexní projekty



PIPETY a PLAST

- pipety Finnpiette a Matrix
- kompletní sortiment špiček
- spotřební plast Nalgene, Nunc
- stripy a destičky
- steppery, dávkovače
- pipetovací nástavce



SERVIS

- záruční servis
- pozáruční servis
- validace přístrojů
- ekologické likvidace



www.trigon-plus.cz

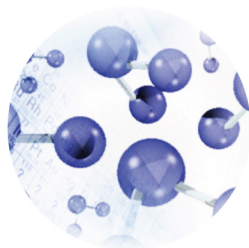
TRIGON PLUS spol. s r. o., Čestlice, Západní 93, 251 01 Říčany u Prahy, ČR
telefon: +420 272 680 190, fax: +420 272 680 914, e-mail: mail@trigon-plus.cz, www.trigon-plus.cz

ZAKÁZKOVÁ SYNTÉZA PEPTIDŮ

- Produkt v závislosti na sekvenci a množství v čistotě od 70 do 98 %
- Kvalitativní analýza (MALDI-TOF,ESI)
- Kvantitativní analýza (HPLC)
- Purifikace peptidu pomocí HPLC
- Možnost modifikace peptidu (fosforylace, biotinylace, acetylace, značení izotopem, FAM)
- Možnost konjugace peptidu na proteiny KLH (BSA) přes glutaraldehyd nebo cystein (vhodné pro přípravu protilátek)
- Dodací lhůty do 3 týdnů

ZAKÁZKOVÁ VÝROBA PROTILÁTEK

- Syntéza peptidu a následná konjugace na nosič (KLH, BSA)
- Produkce polyklonálních protilátek v králících
- Testování protilátek
- Afinitní purifikace až 50 ml séra
- Vzorek 5 -10 mg peptidů zdarma přiloženého k zásilce protilátky
- Standardní dodání za 10-12 týdnů



Clonestar
Peptide Services s. r. o.
Křižíkova 70, 612 00 Brno

Tel.: 549 213 475
GSM: 775 266 192, 775 266 191
E-mail: brno@clonestar.cz

www.clonestar.cz



pragolab

laboratorní přístroje a zařízení

- hmotnostní spektrometrie
- separační techniky
- elementární analýza
- atomová spektroskopie
- UV-VIS spektrometrie
- reologie
- analýza povrchů
- elektrochemie
- laboratorní informatika
- spotřební materiál
- laboratorní vybavení
- **servis**

Thermo
SCIENTIFIC

www.pragolab.eu
pragolab@pragolab.cz
Nad Krocínkou 55, 190 00 Praha
Jamborova 25, 615 00 Brno
Drieňová 34, 821 00 Bratislava

MANEKO

Laboratorní přístroje a technika

autoklávy a parní sterilizátory,
osmometry, hustoměry,
refraktometry a polarimetry,
centrifugy,
mikrovlňné pece,
laboratorní pece,
laboratorní nábytek,
digestoře a bezpečnostní skříně,
laminární boxy,
míchačky, třepačky,
homogenizátory, dispergátory,
mikroskopy, bodotávky,
mlýny, síťovačky,
mrazící boxy, dewarovy nádoby,
myčky, dezinfektory,
pipety a dávkovače kapalin,
spektrofotometry,
kolorimetry, turbidimetry,
sušárny, inkubátory,
testovací komory,
teploměry, vlhkoměry, tlakoměry,
topné desky,
vzorkovače,
váhy a předvážky,
vakuové odparky a pumpy,
viskozimetry, rheometry
vodní lázně a termostaty,
ultrazvukové lázně a homogenizátory,
zdroje čisté vody,
chemikálie

 **BINDER**

Best conditions for your success

salvisLAB

Alfa Aesar[®]

A Johnson Matthey Company

 **Cole-Parmer**[®]
Delivering Solutions You Trust


ILMVAC

TOFF[®]
I N D U S T R I E

VWR [™]

Supplier Partnerships for Customer Solutions

Maneko, spol. s r. o.
Na Pískách 71
160 00 Praha 6

www.maneko.cz

233 335 638-9
233 336 579
Fax: 233 332 656



ILABO spol. s. r. o.

dodavatel laboratorní přístrojové techniky

-FRITSCH (příprava vzorků, granulometrie)

-GERHARDT (analyzační přístroje)

-JULABO (termostaty, kryostaty)

-BANDELIN (ultrazvukové přístroje)

-Kruss (optické přístroje)

-BINDER (sušárny, inkubátory)

CHROMSPEC

SPOL. S R.O.

 *CHROMSERVIS*[®]